RISK FACTORS, MECHANISMS AND THERAPEUTICS FOR RIGHT HEART FAILURE ASSOCIATED WITH PULMONARY HYPERTENSION

by

Jason Gordon Ernest Zelt

uOttawa

Thesis submitted to the University of Ottawa in partial fulfillment of the requirements for a Doctorate in Philosophy degree in Cellular and Molecular Medicine, Department of Cellular and Molecular Medicine, Faculty of Medicine, University of Ottawa.

Department of Cellular and Molecular Medicine

Faculty of Medicine,

University of Ottawa, Ontario, Canada

(May, 2020)

<< O you possessed of sturdy intellect,
observe the teaching that is hidden here
beneath the veil of verses so obscure>>

Durante di Alighiero degli Alighieri

Abstract

Right ventricular function (RV) is one of the most important predictors of prognosis in many cardiovascular disease states. Despite the significance of RV function to survival, there are no therapies that directly nor selectively improve RV function. As well, the basis for RV failure is poorly understood. This is particularly relevant for patients with pulmonary arterial hypertension (PAH), where RV failure in the setting of pressure overload is the leading cause of death. PAH will be introduced in the 2nd chapter of this thesis by comparing and refining contemporary mortality risk assessment strategies. I will then explore 1) RV neurohormonal function and, 2) RV energetics, two molecular pathways thought to be involved in the pathogenesis and progression of maladaptive RV failure. I employed small animal molecular imaging using positron emission tomography (PET) to non-invasively investigate these pathways. The PET imaging techniques employed in this thesis have the unique potential for translation to human studies, to further explore disease mechanisms.

PAH is an insidious disease of the pulmonary vasculature, which, despite recent advancements in treatment, remains an incurable disease with a dismal prognosis. As no single variable yields adequate prognostic information in PAH, a patient's clinical trajectory remains very difficult to predict. A multi-parametric risk assessment strategy has therefore been recommended which incorporates measures of RV function, pulmonary hemodynamics and exercise capacity. If widely adopted, a risk assessment strategy has the potential to better define individual-specific prognosis and standardize treatment goals. In the first section of the thesis I compared contemporary risk assessment tools in a Canadian PAH population. I demonstrated that REVEAL-based risk strategies have superior long-term transplant-free-survival risk discrimination than current European guidelines. I also demonstrate the prognostic importance of

kidney function in PAH risk assessment, which to date has not been incorporated into contemporary guidelines. RV function is one of the most important measures of prognosis for patients with PAH. In this novel Canadian PAH cohort, deteriorating RV function, as assessed by transthoracic echocardiography, was a powerful marker of prognosis. I next created a novel risk tool, 'The Ottawa PAH Risk Score', incorporating measures of kidney and RV function, which we believe will represent a simplified yet robust tool to help clinicians individualize and guide management in PAH. Validation of this new tool is ongoing.

Since in the risk assessment analysis, RV function emerged as a major prognostic factor, I then examined the mechanisms responsible for RV adaption or maladaptation in PAH. Sympathetic nervous system (SNS) activation, which plays an important pathophysiologic role in the development and progression of left-sided heart failure (HF), is thought to be similarly involved in right HF. Non-invasive techniques using radiotracers for PET have been employed clinically to characterize the cardiac sympathetic nervous system (SNS). To date, norepinephrine (NE) analogs such as [^{11}C]hydroxyephedrine (HED) for PET have been the most widely used to characterize presynaptic function. For the first time we also applied SNS PET imaging to an animal model of PAH which demonstrated progressive and selective regional sympathetic denervation within the RV with parasympathetic nerves being largely spared. Treatment with the beta-blocker carvedilol was not able to reverse the pathological changes.

Widespread clinical utility of PET SNS imaging is currently limited because of the short half-life (20min) of ^{11}C-labeled tracers. A new ^{18}F labeled tracer, such as [^{18}F]Flubrobenguane (FBBG) would take advantage of the resolution and quantification advantages of PET as well, due to its longer half-life (110 min), the potential for wide distribution needed for maximum patient

and clinical impact. In the next portion of the thesis I validated this new ^{18}F-labeled tracer, FBBG, against the current PET standard HED in both the left and right ventricle (RV).

There is tremendous interindividual heterogeneity in RV remodeling and progression to RV failure in PAH which is not well explained by differences in the severity of hemodynamic abnormalities, highlighting the importance of genetic influences. This is recapitulated by marked strain differences in RV adaptation between Sprague-Dawley (SD), which exhibit adaptive RV remodeling and excellent survival and inbred Fischer rats which show maladaptive remodeling and very high mortality in response to severe PAH. Using [11C]Acetate for PET, we demonstrated inefficient cardiac energetics and failure of RV adaptation in Fischer rats which is likely due a genetic defect in AK1, and thus impaired shuttling of ATP from the mitochondria to the actin/myosin cross-bridge for muscle contraction.

This journey began with an analysis of risk assessment in patients with PAH. This led to as series of mechanistic studies to better elucidate to the pathogenesis of RV failure in this disease, and then culminated in the discovery of a novel molecular mechanism of genetically determined RV maladaptation that may have important implications for the human disease.

Acknowledgements

Dear Dr. Mielniczuk, Dr. Beanlands, and Dr DeKemp: I would first like to express my sincere appreciation and thanks to my supervisors, Dr. Lisa Mielniczuk, Dr. Rob Beanlands and Dr. Rob Dekemp. In particular, I am extremely grateful for Dr. Mielniczuk and the research environment fostered throughout the course of my degree, full of inspiration, enthusiasm, and particularly important to me, the freedom to try my strengths. You have provided me with numerous research and career opportunities that greatly enriched my experience. I look forward to continued research collaborations as I pursue my medical career and beyond.

Dear Rosemary and Dr. Stewart: My words can't fully express how sincerely grateful I am for your generosity, mentorship and guidance. You both continually push me intellectually and encourage me to strive for my dreams. Your contributions to my learning and my PhD experience have greatly shaped my future scientific ambitions. I would be forever grateful it you would both mentor me throughout my career.

Dear Virgilio: Thankyou for being an incredible scientist and friend. It means so much to me that you shared your scientific passion, I promise to carry it forward throughout my career. I really appreciate your patience and guidance in teaching me so many new and amazing scientific skills. Ps. Thankyou for introducing me to the coffee shot (i.e. espresso), I am sure it will serve me well in the years to come.

To the Stewart Lab and Collaborators: This thesis could not have been possible without the tremendous support of many talented individuals at the University of Ottawa Heart Institute and the Ottawa Hospital Research Institute. I would like to express my sincere appreciation for the help of everyone in Dr. Stewarts lab, in particular Nicholas Cober, Rafael Godoy, Katelynn Rowe and Yupu Deng who were always willing to lend a helping hand. I would also like to thank Julia Petryk who helped me perform small animal PET imaging, and Richard Seymour who helped perform some animal surgeries. I would also like to thank our collaborators in Dr. Megeney's lab who helped us with the proteomic analysis.

Dear Jordan Hutson: Typing the last words of this thesis was incredibly emotional because I would not have crossed this proverbial 'finish-line' without you. Thankyou for your unconditional love and support throughout my degree. You always put a smile on my face when experiments failed, and inspired me to try again.

Dear Mom and Dad: Lastly, I would like to thank my parents who sacrificed so much in life so that I could pursue my dreams. Mom and Dad, none of my accomplishments could have been achieved without your guidance, inspiration and love.

Table of Contents

List of Figures

List of Tables

List of Abbreviations

^{11}C	Carbon-11
^{18}F	Fluorine-18
^{64}Co	Cobalt-64
ACE	Angiotensin Converting Enzyme
ACh	Acetylcholine
AChE	Acetylcholinesterase
ADMIRE HF	AdreView Myocardial Imaging for Risk Evaluation in Heart Failure
AK1	Adenylate Kinase 1
AKI	Acute Kidney Injury
AMP	Adenosine Monophosphate
ANG	Angiotensin
Ang 1	Angiopoitin-1
ARB	AT_1 Receptor Antagonists
ARs	Adrenergic receptors
ATP	Adenosinetriphosphate
BMPR2	Bone Morphogenetic Protein Receptor 2
BNP	Brain Natriuretic Peptide
CAD	Coronary artery disease
CK	Creatine Kinase
CO	Cardiac Output
COMT	Catecholamine-O-methyl-transferase
CPAP	Continuous positive airway pressure
CRT	Cardiac resynchronization therapy
CT1	Cardiotrophin 1
DCA	Dichloroacetate
dP/dt	Change in pressure over time
DV	Distribution Volume
Ea	Arterial Elastance
Ees	End Systolic Elastance
eNOS	Endothelial nitric oxide synthase

EPI	Epinephrine
ERA	Endothelin Receptor Antagonists
ERS	European Respirology Society
ESC	European Society of Cardiology
FAC	Fractional Area Change
FAOx	Fatty Acid Oxidation
FBBG	Flubrobengaune (LMI1195)
FDG	Fluorodeoxyglucose
FTHA	Fluoro-6-thioheptadecanoic acid
GAPDH	Glyceraldehyde 3-phosphate dehydrogenase
GLUT1	Glucose Transporter 1
HED	Hydroxyephedrine
HFpEF	Heart Failure preserved Ejection Fraction
HFrEF	Heart Failure reduced Ejection Fraction
ICD	Implantable cardioverter defibrillator
k_{mono}	Monoexponential washout rate
LHF	Left Heart Failure
LV	Left Ventricle
MAO	Monoamine oxidase
MCT	Monocrotaline
mFBG	*Meta*-fluorobenzylguanidine
MHC	Myosin heavy chain
MI	Myocardial Infarction
mIBG	*Meta*-iodobenzylguanidine
MMP	Matrix Metalloproteinases
MRA	Mineralocorticoid Receptor Antagonists
mRNA	Messenger ribonucleic acid
NE	Norepinephrine
NET	NE Transporter
NOS	Nitric Oxide Synthase
NYHA	New York Heart Association
OSEM3D/MAP	Ordered subset expectation maximization 3 dimensional maximum a posteriori

PAB	Pulmonary Artery Banding
PAH	Pulmonary Arterial Hypertension
PAP	Pulmonary Artery Pressure
PAREPET	
PCH	pulmonary capillary haemangiomatosis
PDE5	Phosphodiesterase-5
PDH	Pyruvate Dehydrogenase
PDK	Pyruvate Dehydrogenase Kinase
PET	Positron Emission Tomography
PH	Pulmonary Hypertension
PHEN	Phenylephrine
PNS	Parasympathetic Nervous System
PVOD	Pulmonary Veno-occlusive disease
PVR	Pulmonary Vascular Resistance
RAAS	Renin-Angiotensin-Aldosterone System
REVEAL	Registry to Evaluate Early and Long-term PAH Disease Management
RHC	Right Heart Catheterization
RHF	Right Heart Failure
RI	Retention Index
ROS	Reactive Oxygen Species
RV	Right Ventricle
RVEF	Right Ventricular Ejection Fraction
RVF	Right Ventricular Failure
RVH	Right Ventricle Hypertrophy
RVSP	Right Ventricular Systolic Pressure
SCD	Sudden Cardiac Death
SD	Sprague-Dawley
sGC	Soluble guanylate cyclase
SNS	Sympathetic Nervous System
SPECT	Single photon emission computed tomography
SScPAH	Scleroderma associated PAH
SU	Sugen

SUHx	Sugen + Chronic Hypoxia
SV	Stroke Volume
TAPSE	Tricuspid Annular Plane Systolic Excursion
VEGF	Vascular endothelial growth factor
VMAT2	Vesicular monoamine transporter 2

Chapter 1

Introduction

Portions of this chapter have been published in the following review articles:

1. **Zelt J.G.E**., Chaudhary K., Cadete V., Mielniczuk L.M., Stewart D.J. (2019). Medical Therapy for Heart Failure Associated with Pulmonary Hypertension. *Circulation Research* 124(11):1551-1567.

Author Contributions:
Jason Zelt: Develop review outline and wrote the manuscript.
Duncan Stewart: Develop review outline, wrote and critical review of the final manuscript.
Other authors: Content experts and edited the final manuscript.

2. **Zelt J.G.E**., deKemp R.A., Rotstein B.H., Nair G.M., Narula J., Ahmadi A., Beanlands R.S, Mielniczuk LM. (2019). Nuclear Imaging of the Cardiac Sympathetic Nervous System: A Disease Specific Interpretation. *JACC: Cardiovascular Imaging* 2020 Apr;13(4):1036-1054. doi: 10.1016/j.jcmg.2019.01.042.

Author Contributions:
Jason Zelt: Conception of review outline, and wrote the manuscript.
Lisa Mielniczuk: Develop review outline and critical review of the final manuscript.
Other authors: Content experts and edited the final manuscript.

3. Farber, G., Boczar K., Wiefels C., **Zelt JGE**., Celiker E., DeKemp R., Beanlands R., Rotstein B. (2020) The Future of Cardiac Molecular Imaging. *Seminars in Nuclear Medicine*

Author Contributions:
Jason Zelt: Wrote two main sections for the review 1) neurohormonal imaging, 2) metabolic imaging.

1.1 Introduction

The past two decades have witnessed more than 40% improvement in mortality for patients with heart failure and left ventricular (LV) systolic dysfunction.[1] This success has coincided with the stepwise availability of drugs that target neurohormonal activation: beta adrenergic receptor blockers (β-blockers), angiotensin converting enzyme (ACE) inhibitors and angiotensin (ANG) II blockers, neprolysin inhibitors and aldosterone antagonists. Our understanding of right heart failure (RHF) has lagged behind and many proven targeted therapies for left heart failure (LHF) do not appear to provide similar benefits for RHF. Until recently, the right ventricle (RV) has often been viewed as less important than the LV and in contemporary literature received the moniker 'The Forgotten Ventricle'. Recent advances in echocardiography, nuclear imaging and magnetic resonance imaging (MRI) have enabled detailed assessments of RV anatomy and physiology in both health and disease allowing us to more accurately describe the clinical sequelae and end-organ manifestations of RHF. RV function is now recognized as one of the most important predictors of prognosis in many cardiovascular disease states.[2] Despite the significance of RV function to survival, there are no clinically approved therapies that directly nor selectively improve RV function. As well, relative to our understanding of LHF, the basis for RHF remains poorly understood.

1.2 RV Developmental Considerations

The right ventricle (RV) is not just a diminutive version of the left ventricle, but in many ways, it is very different structurally, embryologically, anatomically and functionally. The LV develops first, originating from splanchnic mesoderm within the primary heart field with key transcriptional regulation from MEF2C, Nkx2.5, eHAND and TBX5.[3,4] In contrast, the RV

develops from extracardiac mesoderm (pharyngeal) within the secondary heart field with myocyte differentiation regulated by dHAND and MEF2C.[3–5] The fetal circulation is utterly unique, with gas exchange occurring across the placenta and not the lungs. The *in utero* circulation is characterized by high-resistance pulmonary circulation (hypoxemia induced vasoconstriction in lung), low-resistance systemic circulation and equal pulmonary and aortic pressures (patent ductus arteriousus and foramen ovale). Experiencing equivalent afterloads, the fetal RV and LV wall thickness increase *pari passu* throughout fetal life with the capacity for equal force generation.[6,7] With low resistance to flow through the foramen ovale and ductus arteriousus, the fetal RV is the dominant ventricle contributing ~50% of the total cardiac output.[8] Lung aeration at birth initiates a cascade of events transitioning fetal circulation to the separate and parallel pulmonary and systemic circulations fit for extrauterine life.[9] The substantial drop in pulmonary vascular resistance (PVR) after birth decreases pulmonary artery pressure (normal mean pulmonary pressures ~10-15 mm Hg). The RV adapts to the reduced afterload with a relative regression in hypertrophy. That is, the RV wall thickness remains ~3.5-4mm, while the LV experiencing systemic pressures (>100 mm Hg) increases its wall thickness 3-4 fold.[7,10] The ventricular remodeling soon after birth yields the typical postnatal heart with a thin-walled crescent-shaped RV and bullet shaped LV. This early embryologic divergence in the origin of the LV and RV not only underlies the chamber-specific responses to pressure and volume overload, but may also foreshadow a differential response to treatment.

1.3 Diagnosing Right-Sided Heart Failure

RHF is a clinical syndrome that results from a compromised ability of the right heart to accommodate the cardiac output while maintaining the normally low venous pressures.[11] The etiology of RHF can be stratified into three broad categories: 1) pulmonary hypertension (PH); 2)

RV/ valve pathology; and 3) diseases of the pericardium. The contents of this thesis will predominantly focus on pulmonary hypertension , the most prevalent cause of RHF. Studies incorporated into this thesis will i) implement mortality risk assessment in patients with PAH; ii) examine the efficacy of neurohormonal modulation in preclinical PAH models; and iii) elucidate novel molecular mechanisms involved in the progression from adaptive to maladaptive RHF.

1.3.1 Clinical Assessment

Patients in RHF generally exhibit elevated right-sided filling pressures (right atrial pressure >8 mm Hg) and reduced cardiac index (<2.5 L/min/m^2). The symptoms of RVF include exertional dyspnea, fatigue, peripheral edema, and abdominal fullness/ascites. Patients with severe PH and RVF can also complain of exertional chest pain (angina) and exhibit presyncope and syncope resulting from a critical reduction in cardiac output. On physical examination, elevated jugular venous pressure (JVP) is a common sign of RHF, reflecting an increase in right atrial pressure. Other signs include a right sided 3rd heart sound, Carvallo sign (increase tricuspid regurgitation on inspiration), and a RV lift/heave. While the physical exam remains an invaluable tool for the prudent clinician, the sensitivity and specificity of the signs and symptoms for diagnosing heart failure are limited,[12] and cardiac imaging plays an increasingly important role in the diagnosis, management and prognostication of patients with PH and RHF.

1.3.2 Clinical Imaging of the Right Ventricle

MRI is considered the 'gold standard' for assessment of RV function, volumes, and mass.[13] A comprehensive RV assessment by MRI includes a concomitant evaluation of fibrosis with late gadolinium enhancement. However, in many countries imaging costs and accessibility

currently limit its widespread application. Cardiac echocardiography is relatively inexpensive, widely accessible and enables a rapid assessment of RV size and function, and therefore often constitutes first-line imaging in patients with suspected RHF. Due to the complex geometric shape and bellows-like motion of the RV, volume estimates that are commonly used for assessing LV function are inaccurate for the RV, limiting 2D echocardiography to a more qualitative assessment of RV function. Septal flattening, RV dilation and kinetics are often assessed, but in the absence of any single reliable quantitative measure of RV systolic function, several surrogate echocardiography parameters have been proposed for use in the clinical setting. It is important to keep in mind that all of these parameters are load dependent, each with their own inherent limitations and thus a multimodal imaging approach is recommended.

Two common assessments of global RV systolic dysfunction are fractional area change (FAC) and tricuspid annular plane systolic excursion (TAPSE). FAC is defined as the percentage change in RV chamber area between systole and diastole and assesses both longitudinal and radial components of RV contraction, yielding a global estimate of RV systolic function.[14] A FAC of <35% is indicative of RV systolic dysfunction.[14] While FAC does correlate well with MRI measures of RVEF, this parameter is limited by the position of the imaging plane, image quality, and operator tracing. TAPSE reflects the longitudinal shortening of the RV and can be assessed in M-Mode.[15] A TAPSE of <18mm suggests RV dysfunction.[15] TAPSE is biased by alignment, and ignores contributions of the septum and transversal displacement of the RV free wall.

Evaluation of PH is also critical in the imaging assessment of RHF. PASP can be estimated by measuring the velocity of the tricuspid regurgitation (Bernoilli equation). Other signs of elevated ventricular pressures include septal flattening (D-sign), a dilated PA and

distended inferior vena cava. The presence of a pericardial effusion is important to note as it carries prognostic significance. Although not as widely available, recent advancements in 3D echocardiography and speckle tracking/strain imaging may yield more reliable estimates of RVEF/RV systolic function, and is thought to be less operator dependent.[14] A description of these techniques is beyond the scope of this review but has been previously reviewed.[14]

1.3.3 Right Ventricle Biomarkers

While the list of potential biomarkers for the diagnosis and prognostication of RVF continues to grow, most lack specificity and for the most part can be elevated in almost any form of heart disease. Brain Natriuretic Peptide (BNP) is the only biomarker included in 2015 ESC/ERS guidelines for risk assessment in PAH. BNP is released from the ventricle in response to increased pressure or volume overload and has become an established tool in the diagnostic and prognostic assessment of patients with heart failure. [16] Importantly, BNP levels correlated with hemodynamic parameters, echocardiographic indices of RV overload, NYHA functional class, and mortality in patients with PH and RVF.[16] BNP is also the only biomarker widely used in routine practice of PH centers and clinical trials to monitor response to therapy, with reductions often paralleling improvements in exercise capacity, RV function and hemodynamics.[16] A number of novel biomarkers are being evaluated, including circulating levels of microRNAs,[17] proteins[18] and metabolites,[19] but these are only in very early stages of development.

1.4 Pulmonary Hypertension

Pulmonary hypertension is the most common cause of RHF, with a global prevalence estimate of 1%, increasing up to 10% in individuals aged more than 65 years.[20] PH was traditionally defined by a mean pulmonary artery pressure (mPAP) ≥25 mm Hg at rest, measured during a right-heart catheterization (RHC).[21] Although somewhat contentious, this definition was recently revised at the 2018 World Health Symposium on PH to recognize i) the traditional 25 mm Hg cutoff was arbitrarily chosen; ii) in health, mPAP is 14±3.3 mm Hg with an upper limit of normal of 20 mm Hg and not 25 mm Hg; and iii) a mPAP of 21-24 mm Hg is associated with a poor prognosis.[22] PH is now defined as a mPAP>20 mm Hg at rest, as assessed by a RHC.

At the 2nd World Symposium on Pulmonary Hypertension, held in 1998 in Evian, France, causes of PH were grouped into five categories to reflect shared pathologic and clinical manifestations as well as available treatment options: pulmonary arterial hypertension (PAH; Group 1); PH due to left heart disease (LHD; Group 2); PH due to chronic lung disease/hypoxia (Group 3); chronic thromboembolic PH (Group 4); and PH due to unclear multifactorial mechanisms (Group 5).[23] This classification was since updated at the 4th World Symposium in 2013 in Nice, France, to incorporate the advancing knowledge, particularly with regards to genetic causes of PAH (Table 1.1).[24]

Table 1.1 Clinical Classification of Pulmonary Hypertension.

Group 1: Pulmonary Arterial Hypertension (PAH)
1.1 Idiopathic PAH 1.2 Heritable PAH 1.3 Drug – and - Toxin Induced PAH 1.4 PAH Associated with: 1.4.1 Connective Tissue Disease (eg. Scleroderma) 1.4.2 HIV infection 1.4.3 Portal Hypertension 1.4.4 Congenital Heart Disease 1.4.5 Schistosomiasis 1.5 PAH long-term responders to Calcium Channel Blockers 1.6 PAH with overt features of venous/capillaries (PVOD/PCH) involvement 1.7 Persistent PH of the newborn syndrome
Group 2: Pulmonary Hypertension due to left heart disease
2.1 PH due to HFpEF 2.2 PH due to HFrEF 2.3 Valvular heart disease 2.4 Congenital/acquired cardiovascular conditions causing post-capillary PH
Group 3: Pulmonary Hypertension due to lung diseases and/or hypoxia
3.1 Obstructive lung disease 3.2 Restrictive lung disease 3.3 Mixed restrictive/obstructive pattern 3.4 Hypoxia 3.5 Developmental lung diseases
Group 4: Pulmonary Hypertension due to pulmonary artery obstructions
4.1 Chronic thromboembolic PH 4.2 Other pulmonary artery obstructions
Group 5: Pulmonary Hypertension with unclear/multifactorial mechanisms
5.1 Haematological disorders 5.2 Systemic/metabolic disorders 5.3 Others 5.4 Complex congenital heart disease

PH: Pulmonary Hypertension PAH: pulmonary arterial hypertension; PVOD: pulmonary veno-occlusive disease; PCH: pulmonary capillary haemangiomatosis; HFpEF: Heart failure with preserved ejection fraction; HFrEF: Heart failure with reduced ejection fraction. Table adapted from Simonneau et al.[25]

1.5 Group 1 Pulmonary Arterial Hypertension

PAH (Group 1 PH) is a rare but devastating pulmonary vasculopathy. In addition to a mPAP ≥20mm Hg, a pulmonary capillary wedge pressure (≤15 mm Hg) is required for diagnosis of PAH and the US guidelines also requires a pulmonary vascular resistance (PVR) >3 Woods units.[26] The incidence of PAH is estimated to range from 2.0-7.6 cases per million per year, with a prevalence of 11-26 cases per million. The disease has a female preponderance (4:1 female to male); however, males typically have a more progressive phenotype with a malignant clinical trajectory. Clinically, PAH is a heterogenous disease of multifactorial origin. Nearly half of patients have idiopathic PAH (~50%), with the next largest subgroup consisting of patients with connective tissue diseases (~25%, eg. scleroderma).[27] Before the advent of PAH-vasoactive medications in the 1980s, median survival was grim at 2.8 years.[28] Despite recent advances in therapeutics, current median survival is estimated at only 7 years.[29] Due to the insidious nature of increasing pulmonary arterial pressure and resistance, patients with PH often present to hospital late in the disease progression once RV dysfunction has developed.

1.5.1 Pathophysiology of PAH

PAH is a heterogenous disease of multifactorial origin (Table 1.1). Irrespective of the etiology, the lungs of patients with end-stage PAH are characterized by extensive remodeling of the small pulmonary arterioles. Pathological examination of these small arterioles reveals intimal hyperplasia, medial hypertrophy and fibrosis, infiltration of inflammatory mediators and *in situ* thrombi.[30] In advanced disease, neointimal formation and plexiform lesions often (but not always[31]) emerge and obliterate of the vascular lumen. These neointimal and plexiform vascular lesions are widely considered a hallmark pathological feature of PAH. It is important to note that

many of these observations are restricted to a cohort of patients with end-stage-disease, which may not reflect the true pathogenesis of patients with early-stage-disease. The extent to which the vascular plexiform lesions contribute to the progression of the disease is the subject of much debate and ongoing research. Specifically, it is currently unknown whether the plexiform lesions engender the elevated PAP, or whether elevated pressures precede the development of these lesions, but nevertheless, provide the necessary substrates for plexiform lesion formation. This chicken or the egg causality debate may seem pedantic, but elucidating the exact cause of the perturbed hemodynamics carries important therapeutic implications.

Endothelial Injury/Dysfunction

Early Dysfunction: In health, the endothelium of the pulmonary vasculature functions to regulate vascular tone, permeability and coagulation. However, in PAH, endothelial cell homeostasis shifts towards increased vasoconstrictor production, such as thromboxane and endothelin-1 and decreased vasodilator release such as prostacyclin and nitric oxide.[32,33] These vasodilators and vasoconstrictors exert anti-mitogenic and induces pro-proliferative effects on smooth muscle cells, respectively. Thus, all of these processes converge to produce a pro-proliferative, vasoconstriction and apoptosis-resistant milieu. In this respect, early endothelial injury may represent an early pathogenic feature in PAH whereby there is a perpetual cycle of endothelial cell dysfunction, aberrant proliferation of smooth muscle cells and further vasoconstriction and pulmonary vascular remodeling. Current therapies for PAH predominantly aim to reset endothelial homeostasis and therefore restoring vascular tone (discussed in section 1.5.3).

Early Injury: accumulating evidence now implicates endothelial cell apoptosis, at the level of the distal intra-acinar arterioles, in the early development of PAH.[34,35] Comprising of only one or two endothelial cells with scant supporting matrix, this microvasculature may be uniquely susceptible to degenerative processes. This level of lung microvasculature also constitutes the majority of the pulmonary vascular resistance (PVR), the loss of which clearly engenders elevations in pulmonary artery pressures. As previously eluded to, it remains highly contested whether the loss of lung microvasculature is due to a decrease in lumen cross-sectional area via proliferative processes, or due to endothelial cell injury via degenerative processes. In preclinical models of PAH, enhancing expression of pro endothelial survival factors, vascular endothelial growth factor (VEGF), endothelial nitric oxide synthase (eNOS) or angiopoitin-1 (Ang 1), all abrogate the pathogenesis of PAH.[35–37] In contrast, factors that induce endothelial cell apoptosis such as SU5416, a VEGF receptor-2 antagonist, combined with chronic hypoxia (i.e. Sugen + Chronic hypoxia model of PAH; Section 1.5.2) induce PAH and lead to hyperproliferative lesions that resemble the human PAH phenotype.[38] In this sugen hypoxia model of PAH, inhibiting endothelial cell apoptosis also prevents the hemodynamic alterations and hyperproliferative phenotype.[38,39] Together these data suggest that endothelial cell apoptosis and dysfunction is an early feature in the pathogenesis of PAH, which heralds subsequent proliferative vascular remodeling.

Distal Pulmonary Artery Muscularization

Muscularization of the distal small peripheral, normally non-muscular, pulmonary arteries is a shared feature in all causes PH. While the exact cellular mechanisms remain to be fully elucidated, the appearance of these smooth muscle-like cells is thought to appear from the

transdifferentiation of pericytes and/or fibroblasts.[40,41] These vascular changes likely emerge from a reactive process due to cellular injury and increased shear stress.

Neointimal and Plexiform Lesions

A hallmark feature of PAH is the formation of a layer of cells and extracellular matrix between the endothelium and the internal elastic lamina, termed 'neointimal'.[41] The cells comprising the neointimal are predominantly myofibroblasts that seem to appear as a result of increased shear stress such as conditions of increased blood flow.[42] Importantly, these lesions contribute significantly to the increased PVR seen in PAH. Plexiform lesions are also a common (but not always[31]) pathological feature in PAH, that result from disorganized proliferation of endothelial cells. These lesions typically appear in arteries of diameter 200-400 μm, and are often observed at branch points. In a recent report, Westoo *et al.* used synchrotron-based phase contrast micro-CT to study the 3D structure of plexiform lesions.[43] In this preliminary report, authors identified 4 distinct types of plexiform lesions in lung tissue from PAH patients. Two of these lesion types were localized to bronchopulmonary and vasa vasorum anastomoses and would theoretically function as 'safety-valves' to effectively relieve pressures. Indeed, this recent evidence seems to challenge the prevailing dogma of the relationship between the appearance of these complex lesions altered hemodynamics. Only one intravascular lesion subtype, which was observed as completely occluded pulmonary arteries with re-canalization could contribute to increased PVR and pulmonary pressures.

1.5.2 Animal Models of PAH

The in-depth study of any disease process often relies on animal models that faithfully recapitulate the human disease phenotype. As previously illustrated, PAH is a disease of multifactorial origin likely involving a complex interplay between underlying genetic and environmental factors. As such, the induction of many PAH animal models may not reliably simulate the pathogenesis of the human disease, but rather simply recapitulate some of the pathological features, such as vascular remodeling of the distal lung vasculature and right ventricular hypertrophy.

Small animals, such as mice and rats are frequently used in the evaluation of experimental PAH and right heart failure (RHF); their similarities to humans in cardiovascular physiology, relatively fast reproductive rate and ease of animal handling make them ideal models for research. Although mice are more amenable to transgenic modifications, their lung vasculature seems highly regenerative and are resistant to the development of PAH. In contrast, rats are highly susceptible to the development of PH. The monocrotaline (MCT) and the combined SU5416 + chronic hypoxia (SUHx) rat models are most commonly employed to study PAH.

Chronic Hypoxia Model of PH

The murine chronic hypoxia PH model is probably the most extensively studied model of PH. Although very useful for studying the pathophysiology of altitude induced PH, it fails to reproduce the severity of pulmonary pressure elevations and right heart remodeling that is evident in humans patients with PAH.[44] Unlike the Sugen + chronic hypoxia model of PAH

(discussed below), in the chronic hypoxia pulmonary phenotype usually regresses upon return to nonmoxic conditions.

Rodent Monocrotaline Model

The MCT model is the most frequently used model given its technical advantages in being easy to initiate (a single i.p. injection 60-100mg/kg) with a severe PAH phenotype emerging by 3 weeks. MCT is a plant alkaloid that requires hepatic bioactivation to the active metabolite MCT pyrrole (MCTP) to induce PH.[45,46] MCTP induces PH through i) endothelial cell apoptosis through capsase-3 activation ii) inducing a robust inflammatory response within the lung microenvironment and iii) inhibiting cell proliferation by forming of DNA cross-linkages.[47–50] Impaired eNOS and BMPR2 (Bone Morphogenetic Protein Receptor Type 2) signaling have also been implicated in the remodeling process.[48] RV hypertrophy and dysfunction are also commonly observed by 3 weeks in this model. This model is often criticized for not fully recapitulating the human condition. Medial hypertrophy, elevated PAPs and RV hypertrophy are common features of the model, but not others such as the complex plexiform lesions. Off target toxicity also greatly limits its relevance to studying pressure induced RHF, as myocarditis induced by MCTP has been documented.[51]

Rodent Sugen (SU5416)-Hypoxia Model

The Sugen-5416 + chronic hypoxia (SUHx) model of PAH is widely considered the most representative model of human PAH, based on its ability to recapitulate many of the PAH features, including elevated PAPs, RV hypertrophy and complex plexiform-like lesions. Sugen-5416 (SU) is a receptor tyrosine kinase inhibitor that antagonizes the VEGF receptor 2. In a

seminal report, Taravsaveciene-Stewart *et al*. demonstrated the SU induces widespread pulmonary artery endothelial cell apoptosis, with the emergence of a hyperproliferative, apoptosis-resistant vascular cells that contribute to the formation of plexiform-like lesions. [38] Combining SU with 3 weeks of hypoxia engenders persistently elevated pulmonary artery pressures. [38] One crisitism of this model is the lack of perivascular inflammation that is observed in the human disease and the MCT model.[41,52]

1.5.3 Pharmacological Therapies for PAH

Currently, there are 5 main classes of agents approved for the treatment of PAH. PAH therapies include prostacyclin analogs, phosphodiesterase-5 (PDE5) inhibitors/activators of soluble guanylate cyclase and endothelin receptor antagonists (ERAs) which target the prostacyclin, nitric oxide and endothelial pathways, respectively. These therapies are all predominantly vasodilators that have been shown to ameliorate symptoms, and improve functional capacity, but do little to stymie disease progression. A recent meta-analysis of major PAH trials demonstrated an increase in stroke volume is always accompanied by a decrease in pulmonary artery pressure, suggesting reductions in PVR without an accompanying increase in cardiac contractility.[53] These data suggest that current PAH medications predominantly target the pulmonary vasculature, with only limited cardiac-specific benefit.[54]

Prostacyclin Analogs

Prostacyclin is a metabolite of arachidonic acid and produced within the vascular endothelium. Prostacyclin is a potent vasodilator and inhibits the growth of vascular smooth-muscle cells and platelet aggregation.[55] Prostacyclin expression is reduced in the lungs of

patients with PAH.[56] Epoprostenol (Flolan) was the first FDA approved therapy for patients with PAH, and remains one of the most efficacious therapies for patients with advanced disease.[57] Importantly, beyond symptom relief and functional improvement, epoprostenol is the only therapy with a proven survival benefit in randomized-control trials.[57] The short half-life (~3min) in the circulation precludes oral delivery and must be administered only by continuous intravenous delivery. Given the substantial fiscal and administrative burden to patients, this therapy is often reserved for patients with NYHA class III-IV. New formulations, such as Treprostinil, have been introduced to improve the half-life, stability and mitigate the administrative burden. Various formulations of Treprostinil have been approved to treat PAH (i.e. subcutaneous, intravenous, inhalational and oral).[58,59] Selexipag is a new orally available, non-prostanoid activator of IP receptors. In the GRIPHON trial[60], Selexipag significantly reduced time to composite endpoint of death, PAH hospitalization, lung transplantation, atrial septostomy or initiation of IV/SC prostanoid therapy.

Endothelin-Receptor Antagonists

Endothelin-1 (ET1) is one of the most potent endogenous vascular smooth muscle cell (VSMC) constrictors produced by the vascular endothelium. In addition to its vasoconstrictor effects, ET1 is also a powerful mitogen and exerts a powerful inflammatory and profibrotic response.[33,61] The effects of ET1 are mediated through ET_A and ET_B receptors. Both ET_A and ET_B receptors are located on VSMC, whereby activation leads to vasoconstriction and proliferation. In contrast, ET_B receptors are predominantly expressed on the surface of vascular endothelial cells and can also influence vasoconstriction. Interestingly, ET1 is a secretagogue of NO and prostacyclin through ET_B activation on endothelial cells, and thus can also contribute

some vasodilatory properties.[33,61] There is a robust upregulation of ET1 expression in plasma and lungs tissue of patients with PAH.[33] Three ET receptor antagonists are currently approved with varying specificities for ET_A and ET_B receptors. Bosentan and Macitentan are both dual ERAs that improve pulmonary hemodynamics and exercise capacity in PAH patients.[62,63] The SERAPHIN trial, for Macitentan reached its time to composite endpoint, an effect driven largely by reductions in worsening PAH.[63] In contrast, Ambrisentan is a selective ET_A receptor antagonist and has shown a similar efficacy in improving pulmonary hemodynamics and functional capacity when given as a monotherapy.[64]

Drugs Targeting the Nitric Oxide Pathway

Nitric oxide is potent pulmonary vasodilator that is secreted by pulmonary endothelial cells. Within pulmonary VSMCs, nitric oxide activates soluble guanylate cyclase (sGC) to generate cGMP. However, patients with PAH have reduced expression of eNOS which synthesizes nitric oxide and increased expression of phosphodiesterase 5 (PDE5), which degrades cGMP.[32] Three drugs, Sildenafil, Tadalafil, and Riociguat have been approved for the treatment of PAH, all of which aim to restore nitric oxide signaling. Sildenafil and Tadalafil are both PDE5 inhibitors that have demonstrated efficacy in improving exercise capacity, functional class and pulmonary pressures.[65,66] A newer agent, Riociguat is a direct sGC stimulator, that also improves exercise capcacity, pulmonary hemodynamics, NT-proBNP and time to clinical worsening.[67] There is some evidence that transition to Riociguat from PDE5 inhibitors improves exercise capacity and hemodynamics in patients with an inadequate response to the PDE5 inhibitors.[68]

Combination Therapy

There has been a recent paradigm shift towards aggressive upfront management of patients with PAH. This came is the wake of accumulating clinical evidence that patients on combination therapy reduces risk of clinical worsening.[69] This idea was formally tested in the AMBITION trial, which evaluated the effect of initial combination therapy (ambresentan + Tadalafil) compared to monotherapy in WHO class II or III PAH patients. Key findings of this trial demonstrated that upfront dual therapy in treatment naïve patients significantly lowered risk of clinical-failure events (composite of death, hospitalization, disease progression, unsatisfactory long-term clinical response).[70] The new 2019 CHEST guidelines incorporated this evidence, which now advocates for upfront dual therapy for patients with at least WHO Class II symptoms.[71] The advent of oral prostacyclin analogues (i.e. Selexipag) now facilitates a management strategy that targets all three pathways, particularly at a much early stage of disease progression. Indeed, preliminary pilot studies have signaled a potential survival benefit of upfront triple therapy.[72] The TRITON trial (NCT02558231) is currently comparing the efficacy and safety of initial triple oral therapy (macitentan, tadalafil, selexipag) versus initial dual therapy (macitentan + tadalafil + placebo). Results of the trial were recently presented at ATS, which demonstrate no difference in pulmonary hemodynamics of NT-proBNP at 26 weeks.[73] It is important to note that while significant therapeutic advancements have been made, these therapies do little to stymie disease progression, and patients will unfortunately succumb to their disease. Disease progression in many patients is very difficult to predict. There is tremendous interest in whether risk assessment algorithms can aid clinicians in guiding therapeutic management.

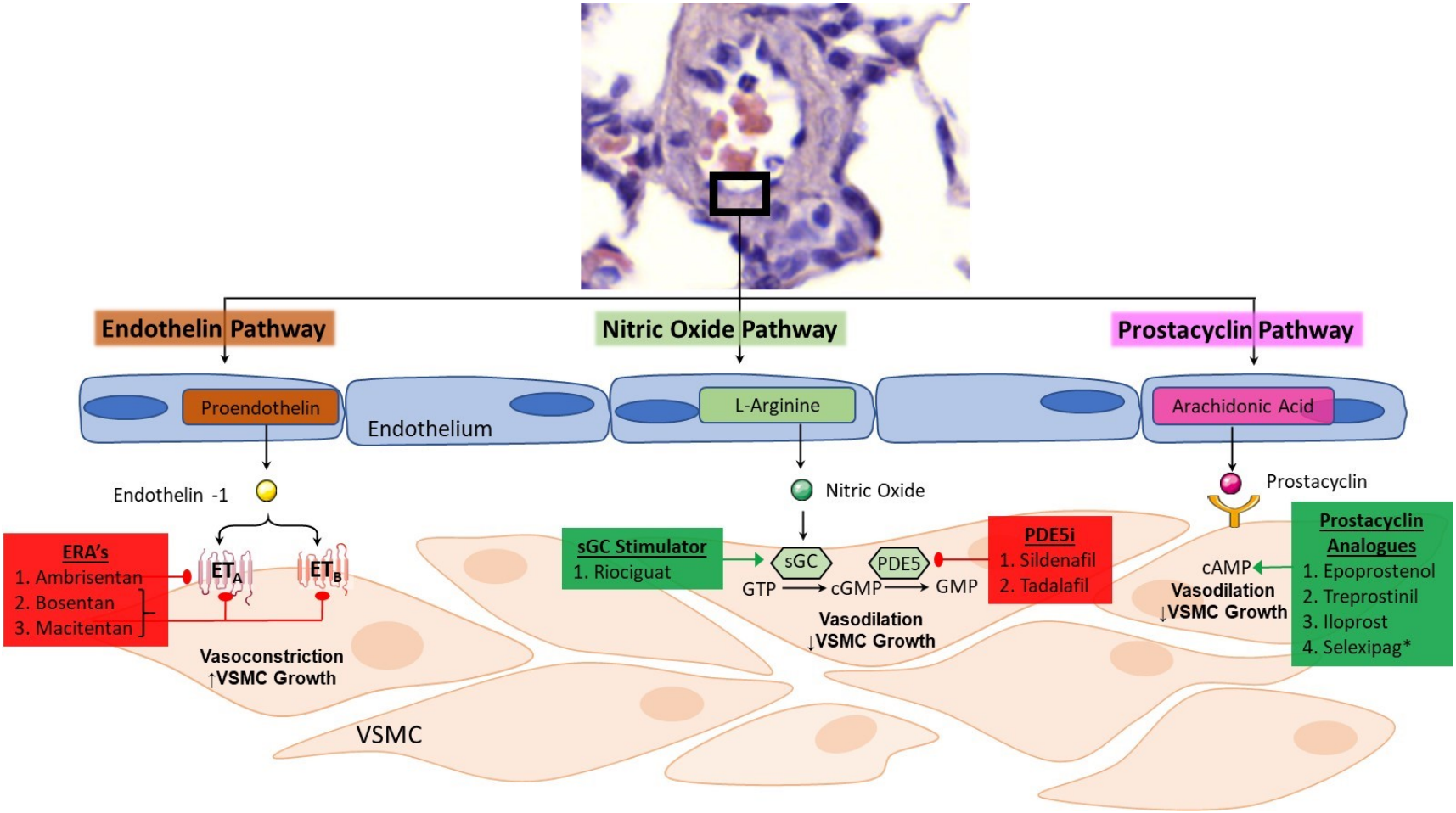

Figure 1.1 Pharmacotherapy for PAH. Currently, there are 5 main classes of agents that are approved for the treatment of PAH. These agents target three main pathways: 1. The Endothelin Pathway, 2. The Nitric Oxide Pathway, and 3. The Prostacyclin Pathway. ERA, Endothelin Receptor Antagonist; sCG, soluble guanylate cyclase; cGMP, cyclic GMP, PDE5, phosphodiesterase 5. *Selexipeg is a synthetic prostacyclin receptor antagonist

1.6 Risk Assessment in PAH:

Epidemiological studies suggest that the hemodynamic severity of PAH, as measured by pulmonary vascular resistance (PVR) and mean pulmonary artery pressure (mPAP), does not reliably predict mortality.[54] Rather, the response of the right ventricle (RV) to the elevated afterload has emerged as a powerful predictor of prognosis in these patients.[54,74] As no single variable yields adequate prognostic information, a patient's clinical trajectory remains very difficult to predict. A multiparametric risk assessment strategy has therefore been recommended, which incorporates measures of PAH disease severity, exercise tolerance, and right ventricular (RV) function.[75,76] If widely adopted, a risk assessment strategy has the potential to better define individual-specific prognosis and standardize treatment goals.

Much of what we now know about the epidemiology of PAH has been gleaned from large PAH registries. These large databases have yielding valuable information on prognostic risk factors enabling an increasing refined ability to assess risk for individual patients. The National Institute of Health (NIH) registry was established in the 1980s and was the first large PAH cohort to systematically and prospectively evaluate survival.[77] From the final cohort of 194 PAH patients, the NIH derived a predictive equation to estimate survival using baseline hemodynamic from the right heart catheterization. The NIH risk equation has fallen out of favor for tools derived from more contemporary PAH registries. The REVEAL score and the European Society of Cardiology (ESC)/European Respirology Society (ERS) risk table are both multidimensional approaches and yield a more comprehensive assessment of risk.

1.6.1 REVEAL-based Risk Assessment

"Registry to Evaluate Early and Long-term PAH Disease Management" or REVEAL is a multicenter, prospective registry that enrolled patients with incident and prevalent WHO group 1 PAH at 55 centers across the United States from 2006-2009. A total of 2716 patients were recruited, of whom, 78% were women with predominantly idiopathic PAH (47%).

REVEAL 1.0 Score

The REVEAL 1.0 risk calculator uses up to 12 clinically relevant variables and was derived from the REVEAL registry data (Table 1.2).[29,78] The REVEAL 1.0 score calculator assigned patients a score from 0 to 22, with higher scores reflecting worse 1-year survival. REVEAL 1.0 scores were also stratified into Low (score ≤7), Average (8), Moderately High (9), High (10-11) and Very High (≥12) risk strata. The derivation of the REVEAL score was statistically rigorous, which included both modifiable and non-modifiable variables, and weighted these variables to be commensurate with their prognostic importance. The final risk model has since been externally validated in both incident and prevalent PAH patients.[27,29,79] Studies evaluating serial assessment of REVEAL risk demonstrate that, irrespective of a patients baseline risk, achieving a lower risk profile (likely due to introduction of PAH therapies), confers substantial prognostic benefit.[80] Interestingly, follow-up risk assessment seems to be stronger predictor of survival than baseline assessment. Together, this indicates that a patients response to therapy foreshadows future risk. Since the REVEAL score's inception, the clinical utilization has been hindered, likely by the perceived complexity, the number of incorporated variables and the perception that some variables (i.e. PVR>32 Wood units) are infrequently encountered, even in patients with advanced disease.

REVEAL 2.0

The REVEAL Registry PAH risk score calculator was recently updated in 2019 recognizing the importance of periodic refinements to the risk score (Table 1.2).[81] Cut-points for 5 of the variables, including PVR, in the original score were refined to optimize clinical relevance. A new variable, 'all-cause hospitalization', and a revised variable, renal function as measured by estimated glomerular filtration rate (eGFR), were also incorporated into the REVEAL 2.0 to further enhance risk prediction. Importantly, the REVEAL 2.0 is the first PAH risk score to incorporate quantitative indices of renal function. The updated calculator assigns patients a score from 0 (lowest risk) to 23 (highest risk). REVEAL 2.0 scores can also be stratified into Low (≤6), Intermediate (7-8), and High (≥9) risk strata.[81]

1.6.2 ESC/ERS-Based Risk Assessment

In 2015, the ESC/ERS were the first to formally incorporate risk assessment into contemporary guidelines. Periodic risk assessment was recommended using a table of variables with cut-points associating with low, intermediate and high risk features. The low, intermediate and high risk variables were to correspond with an estimated 1-year mortality of <5%, 5-10%, and >10%, respectively (Table 1.3). Appreciating the need for serial assessment, only modifiable risk factors were incorporated into the table. However, this decision ignores the prognostic impact of PAH etiology, age, sex, and other comorbidities that are routinely considered in clinical practice. The ESC/ERS did not establish a method to calculate a patient's cumulative risk. Indeed, the optimal method of implementing the tool in clinical practice remains to be determined, but two methods have recently been proposed.

Mean ESC/ERS Score

In two separate studies from the Swedish[82] and COMPERA[83] PAH registries, patients were classified as low, intermediate or high risk by assigning a score between 1-3 (1=low risk; 3=high risk) for each available variable, using the ESC/ERS tool (table 1.3).[75] The sum of the scores across all variables is then divided by the number of variables available for each patient, and rounded this number to the nearest integer to arrive at a mean risk score for that patient. In both studies, patient were successfully stratified into three discrete risk strata (low, intermediate and high) corresponding with a one-year mortality of <5%, 5-10% and >10%, respectively. These studies also corroborated the results of Nickel *et al.*[84] which demonstrated that patients who improve to a low-risk status at follow-up (after the initiation of PAH therapy) have the same prognosis as low-risk patients at baseline.[82,83] The clear mortality difference between an intermediate and low risk patient that is maintained at follow-up also implies that clinical stability is an unacceptable treatment goal, and clinicians should be striving to reach a low risk profile.

Number of Low Risk Criteria

Boucly *et al.* used a different approach to validated the ESC/ERS tool, acknowledging the importance of reaching a low-risk status.[85] Using data from the French Pulmonary Hypertension Registry (FPHR; n=1017), only four modifiable variables were considered and the number of low-risk criteria from each patient were summed (score 0-4; 0, highest risk; 4, lowest risk). The number of low-risk criteria were defined as 1) NYHA functional class I or II, 2) 6MWD >440 m, 3) RAP <8 mmHg and 4) cardiac index ≥ 2.5 $L \cdot min^{-1} \cdot m^{-2}$. Importantly, patients

who had 3 or 4 of these low risk criteria had a 0-1% risk of death at 1 year and a 5-year TFS of 81-94%.

1.6.3 Implementing Risk Stratification in Clinical Practice

As reviewed above, the ESC/ERS-based and REVEAL-based strategies have taken dramatically different approaches to risk assessment with respect to, i) methods for variable selection, 2) the variables incorporated (only 5 of 21 variables in common), and iii) methods to calculate individual risk. The theoretical utility and benefit of using these tools is thus evident, yet a recent international survey suggests the uptake and compliance amongst pulmonary hypertension centers remains poor.[86] Risk assessment, in its current form, is likely challenging for clinicians to implement in practice given their overall complexity and the number of incorporated variables. This is further complicated by the availability of several contemporary algorithms without a clear indication as to which strategy yields the most robust discrimination. This is discouraging given that the ESC/ERS has endorsed the utilization of risk assessment strategies and the 2018 World Symposium has more recently incorporated risk assessment into a theoretical treatment algorithm. [75,76,87] This is in contrast to current USA (Chest 2019) and Europe (ESC/ERS) guidelines which still rely exclusively on NYHA functional class to guide therapeutic management. This lack on uptake into guidelines likely stems from a lack of evidence on whether a risk-based treatment strategy is superior to the standard treatment algorithm, which bases decisions on NYHA functional class alone.

Table 1.2 USA REVEAL and updated REVEAL 2.0 Risk Strategies.

	REVEAL			REVEAL 2.0		
WHO Group 1	APAH-CTD 1+	APAH-PoPH 2+	FPAH 2+	CTD-PAH 1+	PoPAH 3+	FPAH 2+
Demographics	Males >60yrs 2+			Males >60yrs 2+		
Comorbidities	Renal Insufficiency 1+			eGFR <60 mL/min/1.73 m2, OR Renal Insufficiency +1		
WHO Functional Class	FC I -2	FC III 1+	FC IV 2+	FC I -1	FC III 1+	FC IV 2+
Vital Signs	SBP<110mmHg 1+		HR>92 BPM 1+	SBP<110mmHg 1+		HR>96 BPM 1+
All Cause Hospitalizations				Hospitalization ≤6 Months 1+		
6-Minute Walk Test	≥440m -1		<165m 1+	≥440m -2	320-440m -1	<165m 1+
BNP	<50pg/mL -1		>180pg/mL 1+	<50pg/mL -2	200-800pg/mL 1+	≥800pg/mL 2+
Echocardiogram	Pericardial Effusion 1+			Pericardial Effusion 1+		
Pulmonary Function Test	%Pred. DLCO ≥80% -1		%Pred. DLCO ≤32% 1+	%Pred. DLCO <40% 1+		
Right Heart Catheterization	mRAP≥20mmHg 1+		PVR>32 Wood 2+	mRAP≥20mmHg 1+		PVR<5 Wood -1
Sum of Above +6						
Risk Score	Low ≤8	Intermediate 9	High ≥10	Low ≤6	Intermediate 7-8	High ≥9

APAH-CTD, Connective Tissue Disease Associated Pulmonary Arterial Hypertension; APAH-PoPH, Portopulmonary Hypertension associated Pulmonary Arterial Hypertension; FPAH, Familial/Hereditary Pulmonary Arterial Hypertension; eGFR, estimated glomerular filtration rate; FC- Functional Class; SBP, Systolic Blood Prressure, HR, Heart Rate; DLCO, Diffusion Capacity for Carbon Monoxide; mRAP, Mean Right Atrial Pressure; PVR, Pulmonary Vascular Resistance.

Table 1.3 ESC/ERS-Based Risk Assessment

	ESC/ERS Risk Assessment (European Guidelines			FPHR		
	Low (1 point each)	**Intermediate (2 points each)**	**High (3 points each)**	**1 Point Each for ESC/ERS Low Risk**		
WHO Functional Class	FC I – FC II	FC III	FC IV	FC 1 – FC II 1+		
6MWD	>440m	165 – 440m	<165m	>440M 1+		
Hemodynamics	RAP <8mmHg CI≥2.5 L/min/m^2 SVO_2>65%	RAP 8-14mmHg CI 2-2.4 L/min/m^2 SVO_2>65%	RAP >15mmHg CI<2.0 L/min/m^2 SVO_2>65%	RAP <8mmHg 1+ CI≥2.5 1+		
Heart Failure Sy.	Absent	Absent	Present			
Progression of Symptoms	No	Slow	Rapid			
Syncope	No	Occasional	Repeat			
BNP, OR NT-proBNP	BNP<50ng/L proBNP<300 ng/L	BNP 50-300ng/L proBNP 300-1400	BNP>300ng/L proBNP >1400			
Imaging (Echo or cMRI)	RA area <18cm^2 No pericardial effusion	RA area18-26cm^2 No/minimal pericardial effusion	RA >26cm^2 pericardial effusion			
Cardiopulmonary Exercise Testing	Peak VO2 >15 ml/min/kg (>65% pred.) VE/VCO2 slope <36	Peak VO2 11–15 ml/min/kg (35–65% pred.) VE/VCO2 slope 36–44.9	Peak VO2 <11 ml/min/kg (<35% pred.) VE/VCO2 slope ≥45			
Average Score	Average Score					
Sum				Sum Score		
Risk Score	Low 1 to <1.5	Intermediate 1.5 to <2.5	High ≥2.5	Low 3-4	Inter. 1-2	High 0

ESC, European Society of Cardiology; ERS, European Respirology Society; FPHR, French Pulmonary Hypertension Registry ; FC, Functional Class; 6MWD, Six Minute Walk Distance; RAP, Right Atrial Pressure; CI, Cardiac Index; SVO_2, Mixed Venous O_2 Saturation;

1.7 Importance of RV Function

RV function is one of the most important predictors of symptoms and prognosis in both PAH[2] and PH associated with LHD, including HFpEF.[88] In PAH, the 5-year survival for patients with stable or improving RV function is >90%; whereas, survival for patients with decreasing RV function is <30%, independent of changes in PVR, with right HF being the most common cause of death.[2] Epidemiological studies have demonstrated that survival is significantly associated with changes in right ventricle ejection fraction (RVEF), and much less with changes in pulmonary vascular resistance or pressures.[54] However, there are currently no therapies that directly target the right ventricle.

1.8 Mechanisms of RV Adaptation and Maladaptation

As pulmonary artery pressure (PAP) and RV afterload progressively increase, the RV goes through a transition of adaptive remodeling before succumbing to RVF. To appreciate the hemodynamic alterations involved in the development of RVF, RV function must be expressed relative to its load, referred to as 'coupling'. Coupling is a measure of energy transfer and can be assessed from the ratio of end-systolic elastance (E_{es}) and arterial elastance (E_a), variables both derived from pressure-volume loop analysis of multiple cardiac cycles under varying pre- and after-load conditions (Figure 1.2). E_{es} is the slope of the end-systolic pressure/volume relationship and is a load-independent measure of RV contractility.[89] This contrasts with more traditional measures, such as stroke volume and cardiac output, which are both load and contractility dependent. E_a is a ventricular-independent measure of the load on the RV, and reflects PVR x heart rate.[89] A ratio of E_{es}/E_a of ~2 is consistent with coupling of the RV to its load and represents optimal flow output at minimal energy cost.

Increases in PVR with progressive PH result in increases in E_a and RV wall stress, and is a key driver of both adaptive remodeling and progression to RVF. Wall stress can be estimated with LaPlace's law, in relation to pressure (RVSP), the radius of the cavity; and wall thickness. The RV hypertrophies in response to increased RV afterload, an initial adaptive response which decreases wall stress to restore 'coupling' despite increased afterload (i.e. ventriculoarterial coupling). Sustained and progressive pressure overload will eventually cause the RV to dilate to maintain stroke volume and cardiac output, by means of the Frank-Starling mechanism. Heart rate (HR) also increases as SV declines to maintain CO further increasing E_a. The combined increase in HR and RV wall thinning increases wall stress, and RVF ensues as the RV becomes 'uncoupled' from the load (E_{es}/E_a=~1.3).[89] Treatments aimed at restoring RV function work to restore ventriculoarterial coupling.

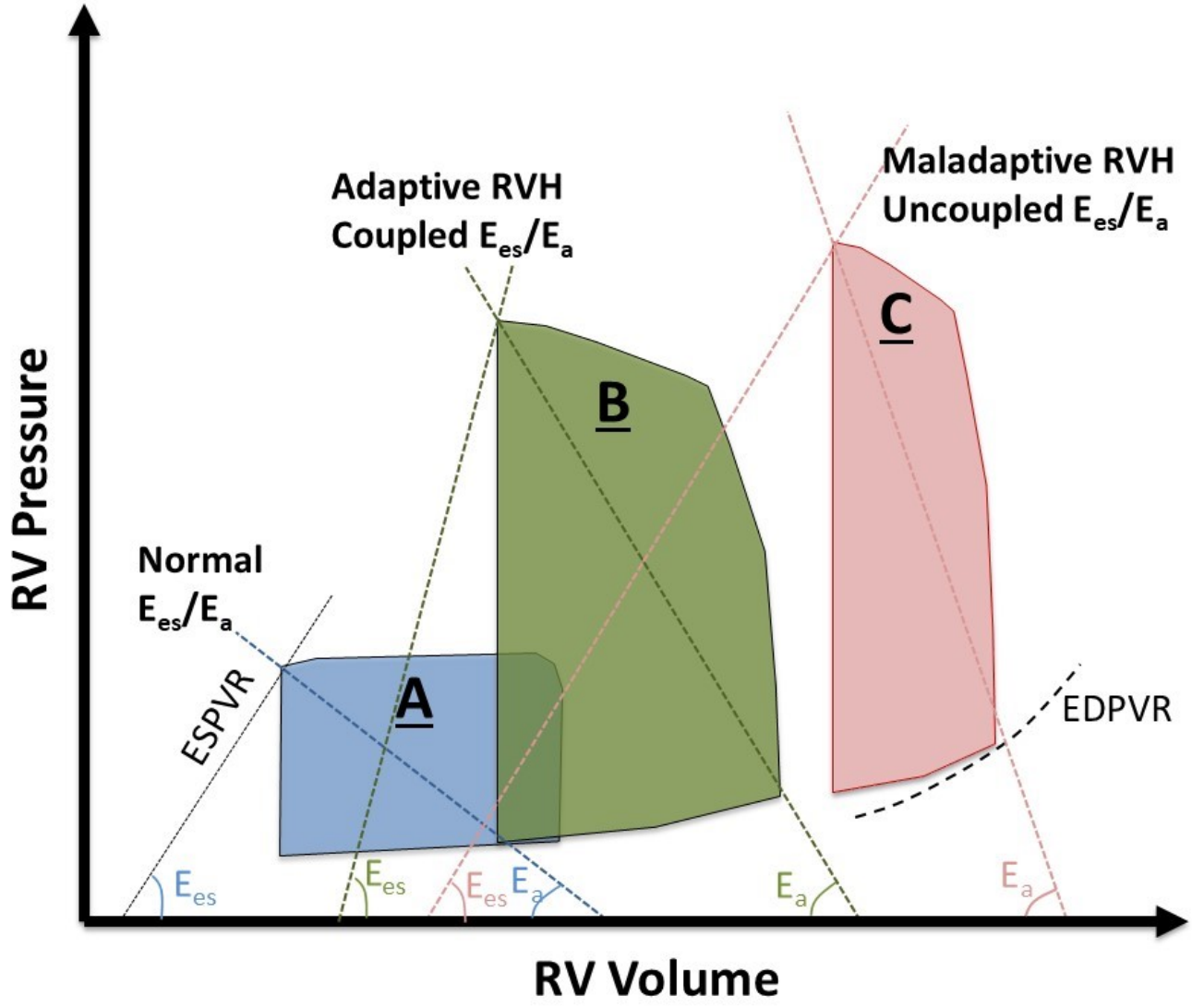

Figure 1.2. RV pressure-volume loops from RVH to failure. Representative pressure-volume loop relationships in health (A), PH with maintained coupling (i.e. adaptive remodeling; B), and PH with uncoupling (i.e. maladaptive RHF; C). E_{es} is the slope of the end-systolic pressure volume relationship and is considered a load independent measure of RV function. E_a is a ventricular independent measure of arterial load. E_{es}/E_a ratio is a measure of energy transfer. In adaptive remodeling, the RV is able to increase wall thickness (decrease wall stress) and contractility to remain coupled to its load (i.e. maintain efficient energy transfer). In maladaptive remodeling (C), the RV dilates and becomes uncoupled from the load, making energy transfer inefficient and RHF ensues. Figure adapted from Noordegraaf et al. [90]

1.9 Adaptive and Maladaptive RV Remodeling

There is tremendous heterogeneity in the RV response to chronic pressure overload, including the degree of hypertrophy, its effects on cardiac output and the likelihood of progression to RVF, that is not explained by differences in RV mass or degree of afterload.[91] While the remodeling process is best viewed as a continuum, studies often dichotomize these processes into adaptive or maladaptive phenotypes (Figure 1.3). *Adaptive RV remodeling* is defined by preservation of normal cardiac output, RV ejection fraction (RVEF) and exercise capacity. It is usually characterized by concentric RV hypertrophy (RVH) with minimal RV dilatation and fibrosis (i.e. compensated RV function).[92] In contrast, *maladaptive RV remodeling* refers to pathologic remodeling of the RV. It is characterized by myocardial apoptosis, fibrosis, progressive dilatation, decreased RV capillary density and results in RV failure, reduced exercise capacity and low cardiac output.[91,92] It is associated with progressive RV failure and portends a worsening prognosis (i.e. decompensated RV function).

Clinically some patients tolerate increased RV afterload without developing features of RHF (adaptive remodeling), while others with similar elevation in RV pressures exhibit rapid decompensation (maladaptive remodeling).[93] Eisenmenger syndrome, a state in which persistent left-to-right shunting leads to progressive increases in PVR and reversal of the shunt direction, represents one end of the spectrum of adaptive RV remodeling. In Eisenmenger syndrome, patients can maintain compensated RV function for many years despite supra-systemic pulmonary arterial pressures, whereas patients who develop PAH in adulthood are far more likely to progress to RVF even with more modest elevation in pressures.[94] Hopkins and Waggoner (2002) studied RV and LV wall thickness of patients with Eisenmenger syndrome in infancy, adolescence and into adulthood.[94] Cross-sectional morphology of RV and LV revealed

equal wall thickness, independent of age and RV function. With defects such as ventricular septal defect and patent ductus arteriosus, the RV is exposed to nearly systemic pressures since birth, and the normal prenatal hypertrophy never undergoes the regression that occurs in the transition from the fetal to post-natal circulations, maintaining a morphology closely resembling the fetal heart. Although speculative, the more favorable prognosis in these patients may be related to the RV being 'primed' for a lifetime of functioning at systemic pressures.[94]

1.9.1 Animal models of adaptive and maladaptive remodeling

Animal models of PAH have been used to study the transition from RV adaptation to failure. Historically, the monocrotaline (MCT) model of PAH has been used extensively to study RV failure, but off target toxic effects greatly limits its relevance. Studies often use the pulmonary artery banding (PAB) model to represent adaptive remodeling; however, PAB typically results in far less RV decompensation and RVF than would be seen in the context of similar degrees of pressure overload from PH. The recent introduction of a new PH model, the SU54126 (SU) and chronic hypoxia (CH) model that more closely resembles human PAH, has opened further possibilities for the study of RV adaptation. SU is an antagonist of VEGFR2 and a single SC injection together with a 3-week exposure to CH results in a severe and progressive PAH phenotype which exhibits many of the typical lung pathological features of human PAH, including complex arterial remodeling producing occlusive plexiform-like lesions.

Strain-dependent differences in survival have been reported in the SUHx model of severe PAH.[95,96] While Sprague-Dawley (SD) rats from one major supplier (Harlan Laboratories/ Envigo) showed excellent survival for over 14 weeks, Fischer rats exhibited nearly 100%

mortality by 7 weeks in the same model,[95] despite having comparable abnormalities in pulmonary hemodynamics at 7 weeks. The increased mortality in Fischer rats was foreshadowed by progressive dilation of the RV, which was associated with reduced RVEF and cardiac output. In contrast, SD rats showed a recovery and stabilization in RV diameters and function over the same period.[97] These findings suggest that differences in survival in the severe PAH model between the two strains is dependent on genetically determined differences in the respective abilities of their RVs to adapt to pressure overload; with the SD strain exhibiting an adaptive remodeling response and the Fischer rats showing maladaptation. This recapitulates the heterogeneity in RV remodeling phenotypes observed in human patients, and provides an ideal model to explore mechanisms underlying maladaptive remodeling.

1.10 Mechanisms of Adaptive vs. Maladaptive RV Remodeling

Recent clinical and experimental studies have identified several key structural and molecular determinants that are associated with either adaptive or maladaptive remodeling. These include capillary rarefaction[98], metabolic shift from oxidative metabolism towards glycolysis [93], sympathetic hyperactivity, and upregulation of profibrotic pathways.[91,99] There is increasing interest in novel therapies which directly target these adverse profiles, some of which are currently in development or in clinical trials, and will be discussed later in the review.

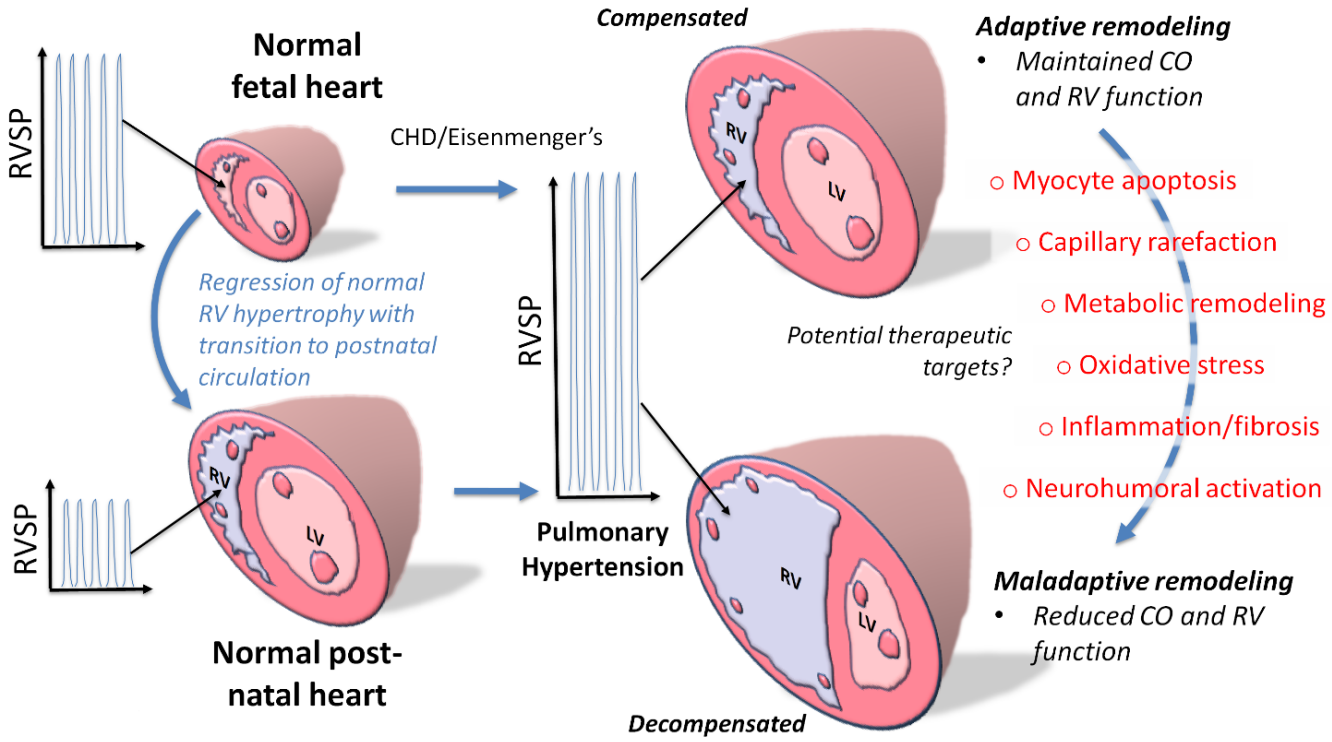

Figure 1.3. Adaptive vs. maladaptive RV remodeling. In the fetal circulation, the RV is exposed to systemic arterial pressures and, like the LV, is a muscular ventricle (upper left). After birth, the two circulations are separated, and the pulmonary arterial pressures become much lower. The RV then remodels to become the thin-walled chamber that is typical of the normal adult RV (lower left). In PH, the RV responds to chronic pressure overload by hypertrophic remodeling which can be compensated (upper right) or decompensated (lower right), which is not explained solely by differences in RV mass or the degree of pressure overload. A number of mechanisms have been proposed to explain whether RV remodelling is adaptive or maladaptive, which include: capillary rarefaction, metabolic remodelling, oxidative stress, inflammation and fibrosis, and neurohormonal activation.

1.10.1 Inadequate Vascularization

Elevated ventricular wall stress increases oxygen demand which requires an appropriate increase in vascularization to match the blood supply to the demand[89] and thus, inadequate oxygen delivery to the RV may contribute to the transition from adaptive RVH to RHF.[100] In health, the low RV systolic pressure permits flow through the right coronary artery during both diastole and systole. However, in PH increased wall stress compresses intramural arteries during systole, causing a biphasic flow pattern which limits blood flow to diastole, analogous to the normal LV.[101] Nuclear studies with PET/SPECT support these concepts and demonstrate progressive RCA flow impairments and reduced RV perfusion in patients with PH.[101] Reduced microvascular density can also contribute to relative RV ischemia, and is considered a *sine qua non* of maladaptive remodeling.[98] Previous studies have found a relative decrease in capillary density in RV samples from PAH patients and in animals models of PH (Figure 3). RV biopsies from IPAH patients with decompensated and RVF show reduced microvascular density, as well as downregulation of angiogenic and vasculoprotective genes such as, VEGF, Ang-1 and apelin, and angiogenic microRNAs such as, miR-126, compared to patients with compensated RVH.[102,103] Similar findings have been reported in animal models of compensated and decompensated RVH.[104] Recently, our lab has reported strain-dependent differences in angiogenic gene expression between the Fischer and SD rats. The former exhibited poor RV adaptation compared to SD rats which show fully adaptive RV remodeling,[97] supporting the idea that lack of proportional increase in the myocardial microvasculature may contribute to the RV maladaptive response. Whether a "rarefaction" of capillaries in RVH results from microvascular loss was assessed by Graham *et al.* using designed-based stereology.[105] They did not observe evidence of endothelial cell apoptosis in the SUHx model, rather they demonstrated that reduced

capillary density occurred as a result of the lack of proportional increase in the microvasculature to maintain the optimal ratio of capillaries to myocyte cross-sectional area (Figure 1.4). Krogh's Cylinder model has long served as a mathematical basis for understanding oxygen supply to muscle. Myocyte hypertrophy without accompanying angiogenesis creates a cylinder too large for adequate oxygenation of tissues surrounding the distal capillary. The result is an area of anoxic tissue called 'lethal corners' near the distal periphery of the cylinder. Therefore, this relative reduction in numbers of capillary in relation to the increase in myocyte mass could still result in significant ischemia contributing to RV dysfunction. While Graham *et al.* were unable to confirm the presence of ischemia in their model, they only studied SD rats which we have shown represent a model mainly of adaptive RV remodeling. Moreover, Sutendra *et al*. have suggested that there may be a link between mitochondrial metabolism, ischemia and maladaptive RV remodeling,[106] in which marked increases in mitochondrial reactive oxygen species (ROS) production inhibits HIF1α and suppresses angiogenesis.[106]

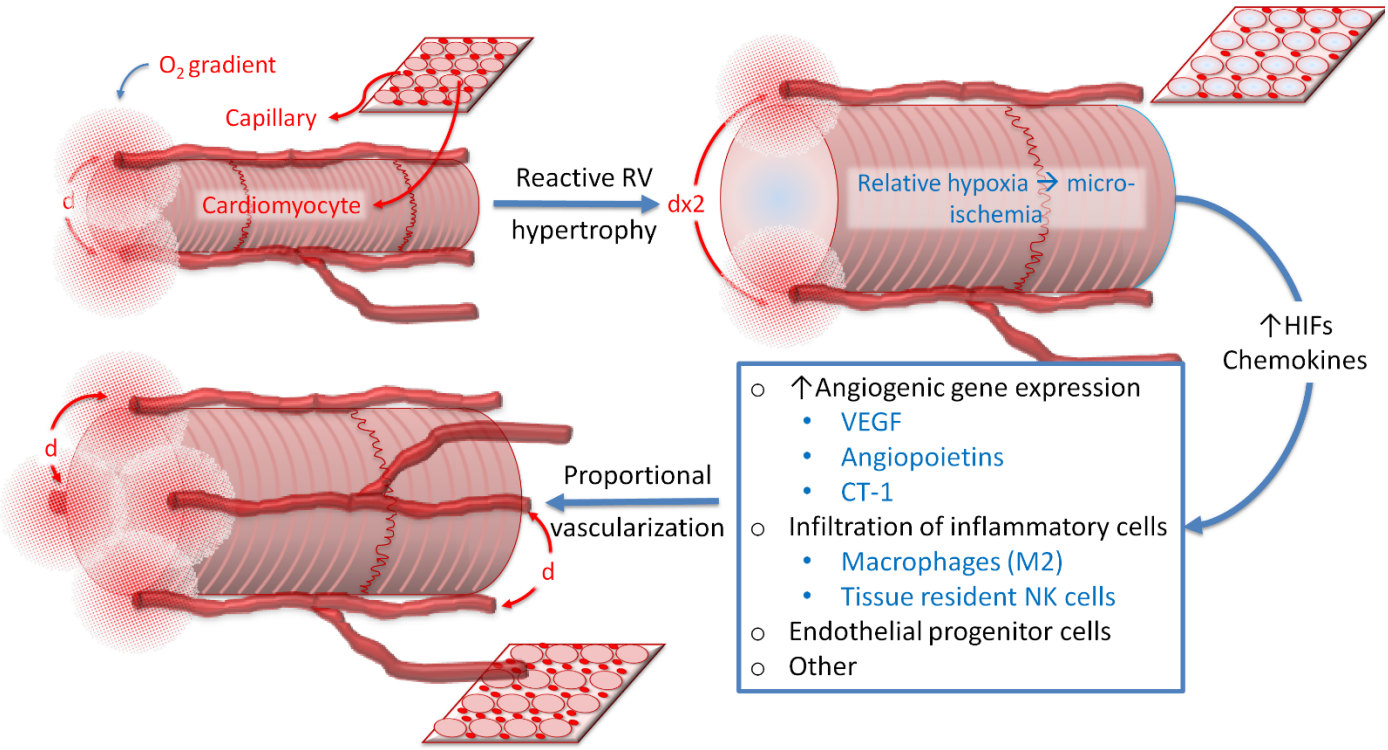

Figure 1.4. Capillary rarefaction and RHF. Elevated ventricular wall stress results in the RV cardiomyocyte hypertrophy and increases oxygen demand which requires a proportionate increase in vascularization to match the blood supply to the demand. A relative reduction in the number of capillaries in relation to myoctye cross-sectional area can result in relative ischemia and contribute to decreased contractile function and RVF. A number of angiogenic mechanisms may be involved in matching vascularization to increasing RV myocyte mass and demands, which include: increase angiogenic gene expression, angiogenic cytokines and chemokines released by inflammatory cells, and homing of circulating progenitor cells.

1.10.2 Metabolism

Important differences in cardiac energy metabolism have been observed between adaptive and maladaptive RVH phenotypes, and may relate to the predisposition to progressive RHF. As with the left ventricle, RVH is associated with reactivation of the fetal gene expression program, with a shift in ventricular myosin heavy chain (MHC) isoform composition in favour of the slower/less active but more efficient beta-isoform.[107] This is thought to be an adaptive response to reduce the overall ATP demand of RV myocytes. In the healthy adult heart, more than 95% of ATP is derived from mitochondrial oxidative phosphorylation (i.e. fatty acid oxidation (FAOx) and to a lesser extent glucose oxidation), which provides the highest energy yield per substrate molecule and is the predominant energy source (40-60%)[108], with the remainder from uncoupled glycolysis (without glucose oxidation).[109] However, in the progression from adaptive remodeling to RHF, glucose becomes a major substrate for energy production, and pyruvate dehydrogenase (PDH) kinase (PDK), the gatekeeper of glucose oxidation, is markedly elevated in humans with RVF, effectively diverting pyruvate from entering the mitochondrial Krebs cycle, thereby uncoupling glycolysis from oxidative pathways (Figure 1.5).[93] This well characterized shift away from oxidative metabolism and towards glycolytic metabolism is known as the Warburg effect. Glutaminolysis is also associated with Warburg metabolism and is an alternative metabolic pathway commonly upregulated in cancer cells. The monocrotaline model of decompensated RV remodeling demonstrates increased glutaminolysis and increased expression of glutamine transporters, which was not seen in the more adaptive PAB model.[103] Glutamine transporters are also upregulated in the RV of patients with PAH with RVF,[110] consistent with metabolic remodeling.

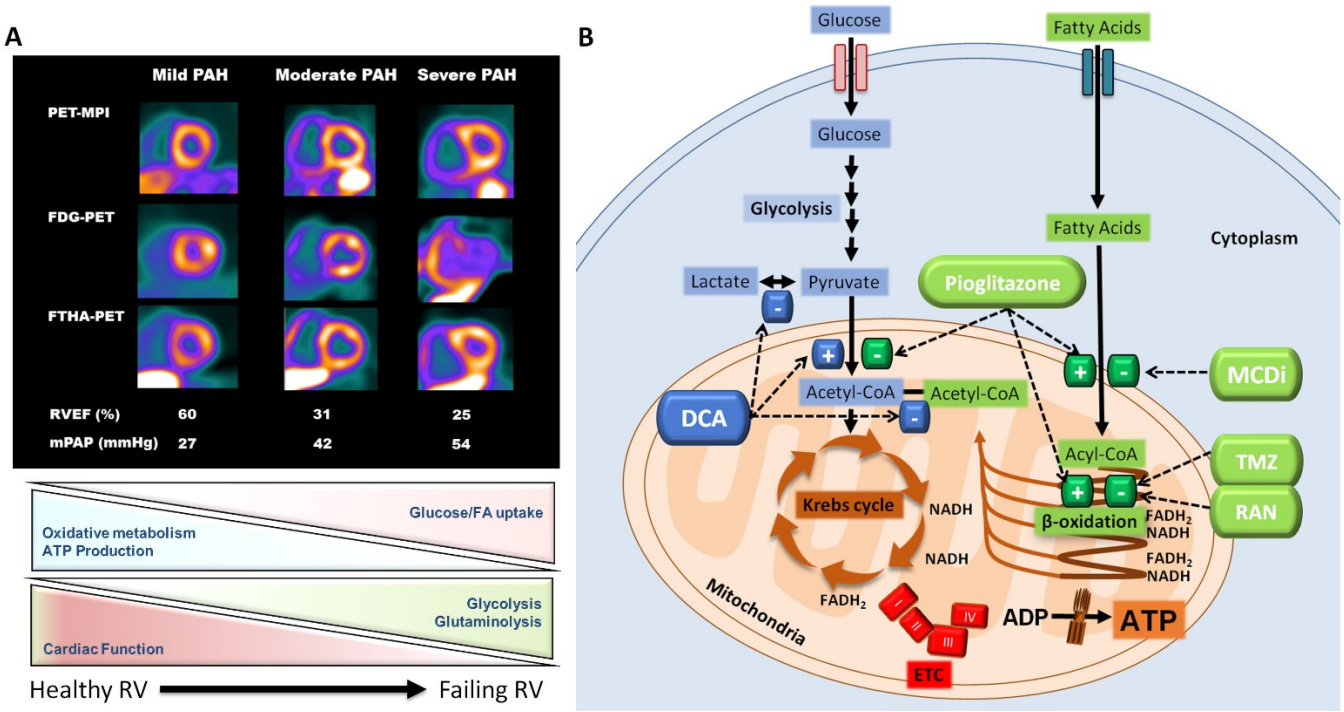

Figure 1.5. Metabolic remodeling in PH-induced RHF. (A) Representative examples of positron emission tomography (PET) for myocardial perfusion imaging (MPI; top panel), 18 flurodeoxyglucose (FDG) uptake (middle panel), and 18fluro-thia-hepadecanoic acid (FTHA) for FFA uptake (lower panel) in three patients with PAH of mild, moderate or severe degree (uptake relative to maximal signal). PET images were previously published by our group[111], and reprinted with permission of the publisher. The transition from adaptive to maladaptive RV failure is characterized by a shift from oxidative and towards glycolytic metabolism with increases in myocardial substrate (glucose and FFA) uptake to drive ATP production. **(B)** Metabolic modulation therapies predominantly aim to decrease glycoysis and increase oxidative metabolism. Dichloroacetate (DCA) inhibits PDK thus re-coupling glycolysis and glucose oxidation. Inhibition of FFA oxidation by trimetazidine (TMZ) and ranolzine (RAN) increases PDH activity and increases glucose oxidation. Malonyl-CoA decarboxylase inhibitors (MCDi) decreases mitochondrial FFA transport. Conversely, Pioglitazone increases FFA oxidation, increasing ATP production and decreasing intramyocardial lipids.

Although oxygen sparing, glycolysis only generates 2 ATP per glucose molecule compared to 31 from oxidation and leads to the production of lactic acid, which together with reduced ATP production, could contribute to contractile dysfunction and RHF. A marked upregulation of the Glucose Transporter 1(GLUT-1) and glucose uptake is required to maintain ATP production, which can be detected by PET scan using [^{18}F]Fluorodeoxyglucose (FDG), a glucose analog and marker for the tissue uptake of glucose.[112] Our group has recently demonstrated that in patients with PAH, the degree of mismatch between RV glucose (FDG) uptake and perfusion measured using PET (nitrogen-13 ammonia or rubidium-82) is proportional to the severity of PA pressure elevation.[111] This supports the concept that relative ischemia of RV, due to a lack of proportional vascularization during RV remodeling, may be driving the glycolytic switch by limiting oxygen availability for oxidative metabolism. Together, these data suggest the transition from adaptive to maladaptive RV remodeling may be initiated by a vicious cycle of microvascular myocardial micro-ischemia, inefficient ATP generation and impaired cardiac function.

The importance of the role of fatty acid metabolism in RV adaptive and maladaptive remodeling is unclear. Glucose uptake and metabolism are known to inhibit FAOx by means of the Randle Cycle, and increased reliance on glucose may promote glycolysis in RVF.[113] However, our group has demonstrated that fatty acid uptake is increased in the failing RV proportional to both the decline in RVEF and increase in pulmonary artery pressures using cardiac [^{18}F]Fluoro-6-thioheptadecanoic acid (FTHA) PET imaging.[111] This is consistent with experimental PH models of maladaptive remodeling, demonstrating reduced FAOx but increased free fatty acid uptake (↑CD36 transporter).[114,115] It is possible that incomplete lipid metabolism may result in the accumulation of lipotoxic compounds such as ceramides, and may also contribute to ventricular failure.[116] The shift away from FAOx towards glucose oxidation is often

interpreted as oxygen sparing consuming 12% less oxygen; however, recent evidence suggests that therapeutically augmenting FAOx may be cardioprotective.[116] The progression to RV dysfunction in humans and rodents is associated with a reduction in peroxisome proliferator-activated receptor gamma coactivator 1-alpha (PGC-1α), and its receptors PPAR-α and estrogen-related receptor (ERRα).[117] PGC-1α is a transcriptional coactivator that regulates several genes involved in glucose and fatty acid metabolism, as well as a key regulator of mitochondrial biogenesis. Targeted deletion of PGC-1α or PPARγ has previously been shown to induce cardiac dysfunction, decrease FAOx, enhance intramyocellular lipid deposition, and increase glucose oxidation, all common features of maladaptive remodeling.[116,118] Interestingly, we have recently demonstrated marked reduction in PGC-1α in the RVF-prone Fischer rat strain compared SD rats in the SUHx model of severe PAH using an unbiased transcriptomic approach, which again supports a protective role of FAOx in adaptive RV remodeling in response to pressure overload.[97]

1.10.3 Oxidative Stress

Oxidative stress is an important mechanism of vascular and cardiac injury. While there has be considerable interest about its role in LHF, relatively little is known about the importance of oxidative stress specifically in RV remodeling and failure. Oxidative stress, defined as an excess production of reactive oxygen species (ROS) relative to antioxidant defense mechanisms, is enhanced in both animal models and patients with PH. [119,120] In the LV, ROS can directly impair contractile function, induce myocyte apoptosis and activate pathological remodeling signaling pathways through stimulation cardiac myofibroblast activation and proliferation as well matrix metalloproteinases (MMPs), all contributing to the development and progression of maladaptive remodeling.[121] Studies in experimental RHF have demonstrated diminished cellular

antioxidant activity,[122] but few studies have investigated the sites of ROS production. There are several important sources of ROS generation within cardiomyoctes including mitochondria, NADPH oxidase, xanthine oxidase and uncoupled nitric oxide synthase (NOS).[121] The major source of ROS production in RHF is subject to debate, but in the MCT model both NADPH and mitochondria seem to be significant sources of ROS production.[123] ROS production within the mitochondria is also increased under ischemic conditions, suggesting a link between mitochondrial function, ischemia, metabolism and oxidative stress. In a direct comparison of models of adaptive (i.e. PAB and maladaptive remodeling (i.e. SUHx)), Bogaard and co-workers demonstrate evidence of greater oxidative stress within the RV of SUHx animals as compared to the PAB model, [104] which was accompanied by a downregulation in key antioxidant enzymes, superoxide dismutase (SOD) and heme-oxygenase-1(HO-1). As well, increased oxidative stress was associated with increased RV apoptosis, fibrosis and worsening RV function.[104]

1.10.4 Fibrosis

Late gadolinium enhancement on MRI is frequently observed at the RV insertion points in PH patients, which is associated with indices of RV dysfunction and mortaltiy.[124] These findings are consistent with localized fibrosis and is thought to be due to increase mechanical stretch at these areas. Interestingly, a postmortem morphometric analysis of RVs from patients with Eisenmenger physiology had less cardiac fibrosis compared to PAH patients, possibly contributing to the better diastolic function and prognosis in the former phenotype.[125] Interstitial and perivascular fibrosis within the RV is also commonly observed in the SUHx and MCT models of PAH, but is relatively spared in the PAB model which is characterized by adaptive RV remodeling.[104,126] Perivascular fibrosis can also directly increase coronary resistance which

reduces coronary flow reserve and increases susceptibility to ischemia.[127] The RV has a tremendous ability to reverse remodel and recover contractile function after normalization of afterload, as observed after lung transplant.[128] As compared to the LV, the RV's greater capacity to reverse model may be related to the overall lower fibrotic burden[129] in addition to the developmental differences discussed above. Nonetheless, the innate plasticity of the RV could make it an attractive target for anti-fibrotic therapies.

1.10.5 Inflammation

Inflammation and cytokine release has long been accepted as a fundamental mechanism for the progression of LHF through exacerbating hemodynamic abnormalities as well as exerting direct toxic effects on the myocardium. [130] Mounting evidence also highlights the role of inflammation in pulmonary vascular remodeling and the pathogenesis of PAH.[131] However, less is known about the role of inflammation in the transition from RV adaptation to failure.[132] Scleroderma is a systemic tissue disease characterized by marked inflammation, fibrosis and immune dysfunction. Patients with scleroderma associated PAH (SScPAH) exhibit worse RV function and survival as compared to those with IPAH, despite similar increases in RV afterload.[133] At autopsy, there is greater RV infiltration of inflammatory cells in SScPAH (neutrophilic granulocytes, macrophages and lymphocytes) localized to the myocardial interstitium, implicated inflammation in maladaptive remodeling.[134] Anti-endothelial cell antibodies have been detected in serum of patients with PAH, and may play a role in the pathogenesis of endothelial cell damage.[135]

Moreover, plasma levels of inflammatory chemokines and cytokines are also elevated in PAH patients, many of which (i.e. CXCL10, CXCL12, CXCL16, IL-6, TNF-α) correlate with echo and MRI derived parameters of RV function and represent independent markers of prognosis.[136,137] Indeed, it has been recently suggested that proinflammatory mediators released by the PAH lung into pulmonary circulation might be transported through the coronary bed and contribute to inflammation and other detrimental processes in the RV, i.e. the "sick lung circulation", thereby promoting maladaptive remodeling.[138]

In experimental studies on LHF, mechanical stress, ischemia[139], and neurohormonal activation (RAAS + SNS activity)[140] are all triggers for expression of inflammatory cytokines in the myocardium. The extent to which these processes contribute to RVF remains to being elucidated, but inflammation is known to directly impair myocardial contractility and induce hypertrophy, apoptosis and fibrosis.[141] Although there is some variability across animal models, immune cell infiltration, as well as increased RV expression of TNF-α, IL-1, IL-6 and CCL-2, have been suggested to contribute to progression to RVF.[142] This inflammatory signature is particularly robust in models with a propensity for maladaption;[142,143] whereas, no inflammatory changes have been found in models of stable PH.[144,145]

We have recently found marked differences in the expression of genes related to natural killer (NK) T-cells between the Fischer and SD rat strains in the severe PAH model, with a marked reduction in the RHF-prone Fischer rats.[97] This was associated with a profound deficiency in NK cells in the myocardium of Fischer rats, whereas these cells were abundant in the remodeled RV of SD rats. NK cells have previously been implicated in orchestrating angiogenesis and the growth of spiral arteries during vascularization of the placenta.[146] Interestingly, impaired function of circulating NK cells has recently been correlated with the

severity of PAH,[147] consistent with a beneficial effect of these cells on lung vascular remodeling. Moreover, it has been recently reported that transgenic mice deficient in genes essential for NK cell development exhibit spontaneous PH with aging.[148] Together, this suggests a potential role for NK cells in adaptive RV remodeling, possibly mediating proportional vascularization as the RV hypertrophies.

1.10.6 Neurohormonal Dysfunction

Preliminary studies have demonstrated sympathetic nervous system (SNS) hyperactivity in patients with right HF and PAH, which was found to be an independent predictor of clinical deterioration.[149] Sympathetic activity also results in activation of the renin-angiotensin-aldosterone system (RAAS) through renin secretion.[150] The compensatory increases in SNS activity and RAAS is beneficial during the early stages of heart failure, providing inotropic support, peripheral vasoconstriction, and salt and water retention to maintain forward flow. Although these mechanisms help to acutely preserve cardiac output, chronic overactivation of the SNS and RAAS can generate a malignant profile characterized by decreased β_1-receptor density and function, pathological ventricular remodeling, shifts in energy metabolism and apoptosis/necrosis of myocytes.[151] Adrenergic remodeling is more extensive in animal models of maladaptive remodeling (Sugen/hypoxia or monocrotaline) than adaptive remodeling (PAB), with a broad downregulation of β_1, α_1, dopamine-1 receptors.[152] These changes were also associated with an impaired inotropic reserve in the RV, a feature commonly observed in PAH patients with RVF.[152,153]

With increasing focus on the SNS, the parasympethic nervous system (PNS) has been relatively neglected in the study of RHF. Da Silva *et al.* recently characterized PNS in the RV of

patients with PAH.[154] PNS dysfunction, characterized by reduced heart rate recovery, was greater in patients with lower RVEF and was associated with reduced RV acetlycholinesterase and increased α-7-nicotinic acetylcholine receptor. [154] These findings are consistent with an adaptive, albeit inadequate, response to reduced PNS signaling in RHF (Figure 1.6).

There has been increasing interest in the role of renin angiotensin aldosterone system (RAAS) in RV adaptation and maladaptation to long-term pressure overload. Plasma aldosterone levels are elevated in patients with PAH and correlate with indices of disease severity and RV function.[155] RAAS activation has also been directly implicated in the pathogenesis of vascular remodeling[156] and RV dysfunction in experimental PAH.[157,158] Aldosterone synthase gene is expressed in the failing left heart and is a potent inducer of myocyte hypertrophy and fibrosis.[159] However, whether local aldosterone production similarly contributes to maladaptive RV remodeling remains to be demonstrated.

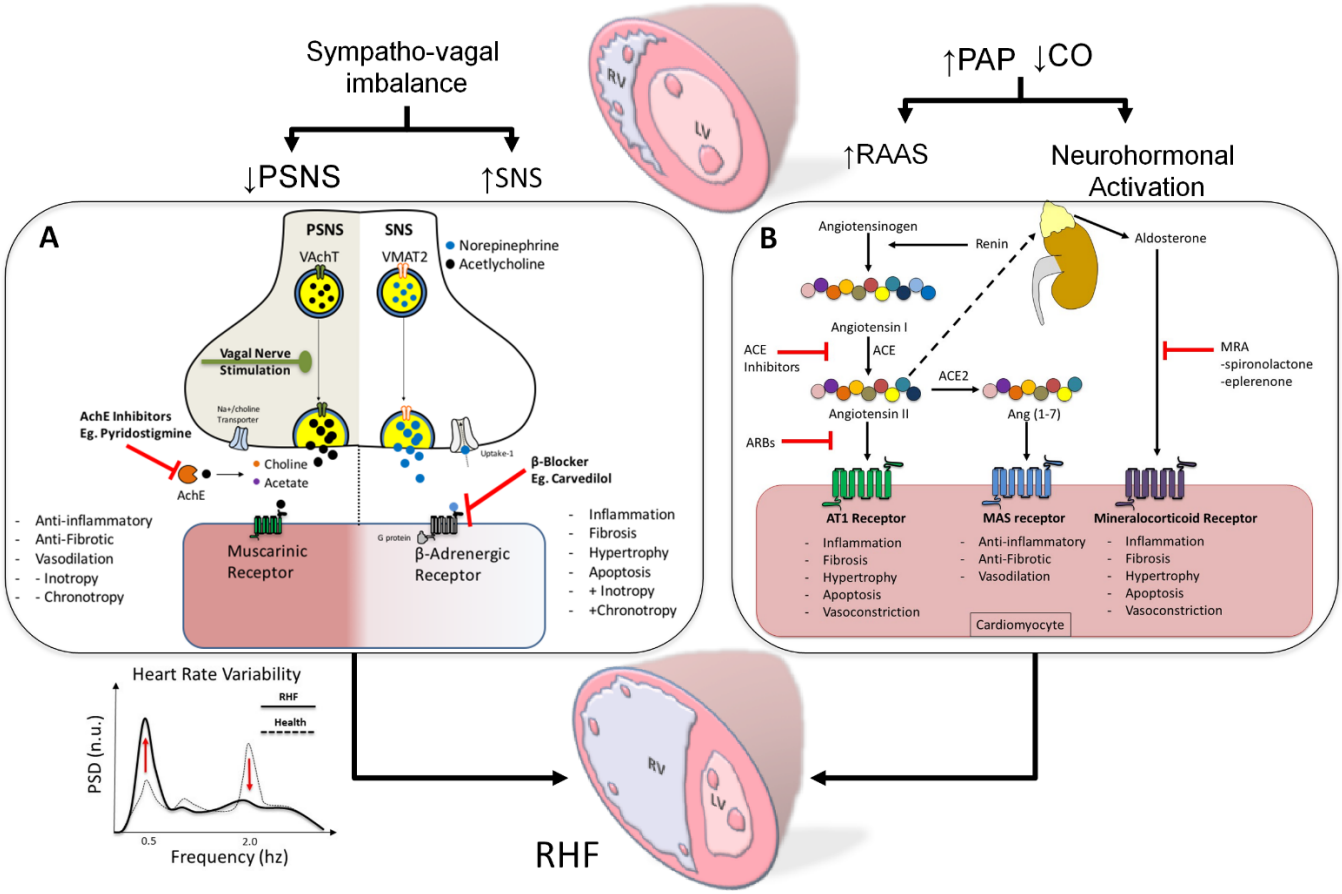

Figure 1.6. Neurohormonal mechanisms of RHF. (A) As in LHF, sympatho-vagal imbalance occurs in patients with RHF, as reflected by reduced heart rate variability (HRV). This occurs as a result of an increased sympathetic nervous system (SNS) activity (low frequency domain on HRV) and decreased parasympathetic (PSNS) activity (high frequency domain). Therapies targeting the imbalance in sympatho-vagal include β-blockers and acetocholine estrerase (AchE) inhibitors. **(B)** As HF progresses, there is progressive activation of the renin-angiotensin-aldosterone system (RAAS) activation in order to maintain cardiac output. However, chronic RAAS activation is thought to contribute to maladaptive remodeling. Angiotensin converting enzyme (ACE) inhibitors, angiotensin II receptor blockers (ARBs) and mineralocorticoid receptor antagonists (MRAs) are all well established therapies for patients with LV systolic dysfunction. These therapies are currently being investigated for the treatment of patients with RHF.

1.11 Cardiac Autonomic Nervous System

The autonomic nervous system plays an integral role in cardiac function, including regulating blood flow, heart rate and contractility. The sympathetic branch of the autonomic nervous system (SNS) exerts positive chronotropic (heart rate), bathmotropic (excitability), inotropic (contractility) and dromotropic (conduction) effects on the heart, whereas parasympathetic stimulation has the opposite effects. At rest, the heart is predominantly under parasympathetic nervous system control by the vagus nerve. However, the SNS is robustly activated in both left and right HF and has been directly implicated in their pathogenesis and disease progression. The contents of this thesis will predominantly focus characterizing SNS function in health and disease.

1.11.1 Sympathetic Neuronal Biology

Sympathetic innervation works in conjunction with epinephrine (EPI), norepinephrine (NE), and components of the renin-angiotensin-aldosterone-system (RAAS), as a part of neurohormonal regulation. Preganglionic sympathetic neurons originate from the intermediolateral horn of the spinal cord at levels T1-T5 and synapse with postganglionic neurons within the sympathetic nerve chain. These postganglionic neurons give rise to cardiac sympathetic efferent nerves which are located in the subepicardium. They follow the course of the major coronary arteries and penetrate the myocardium with the vasculature [160].

The peripheral effects of the SNS are primarily mediated by the release of the chemical neurotransmitter norepinephrine (NE) from presynaptic nerve terminals. NE targets adrenergic receptors (ARs) on the myocardium and represents the mechanistic link between SNS activation and modulation of cardiac function. The human heart contains two main categories of ARs,

beta and alpha receptors. The release of NE from presynaptic nerve terminals is regulated by $alpha_{2A}$ and $alpha_{2C}$ ARs, with stimulation inhibiting release. Whereas, NE stimulation of $beta_1$ and $beta_2$ receptors exert a positive inotropic, chronotropic and dromotropic effect on the heart. The cumulative effects of $beta_3$ receptor stimulation are still being elucidated, but they seem to exert the opposite action of the $beta_1$ and $beta_2$ receptors during excessive adrenergic stimulation[161]. While $alpha_{1A}$ and $alpha_{1B}$ receptors are expressed at much lower concentrations in the heart, they are heavily populated in major vessels such as the coronary arteries and primarily function to regulate blood flow.

Approximately 80-90% of the NE released by sympathetic nerve terminals is taken back up into presynaptic nerve terminals via the NE transporter (NET) Uptake1 (Figure 1.7)[162]. Uptake1/NET is a sodium-dependent transport protein expressed at the cell surface of sympathetic neurons. Once inside the nerve terminal, NE is transported into vesicles through vesicular monoamine transporter 2 (VMAT2) or is metabolized by monoamine oxidase (MAO). The remainder of NE can either be cleared into the circulation or on the post-synaptic side via uptake-2 [163] which transports NE into extra-neuronal tissues such as the heart where it is metabolized by catecholamine-O-methyl-transferase (COMT).

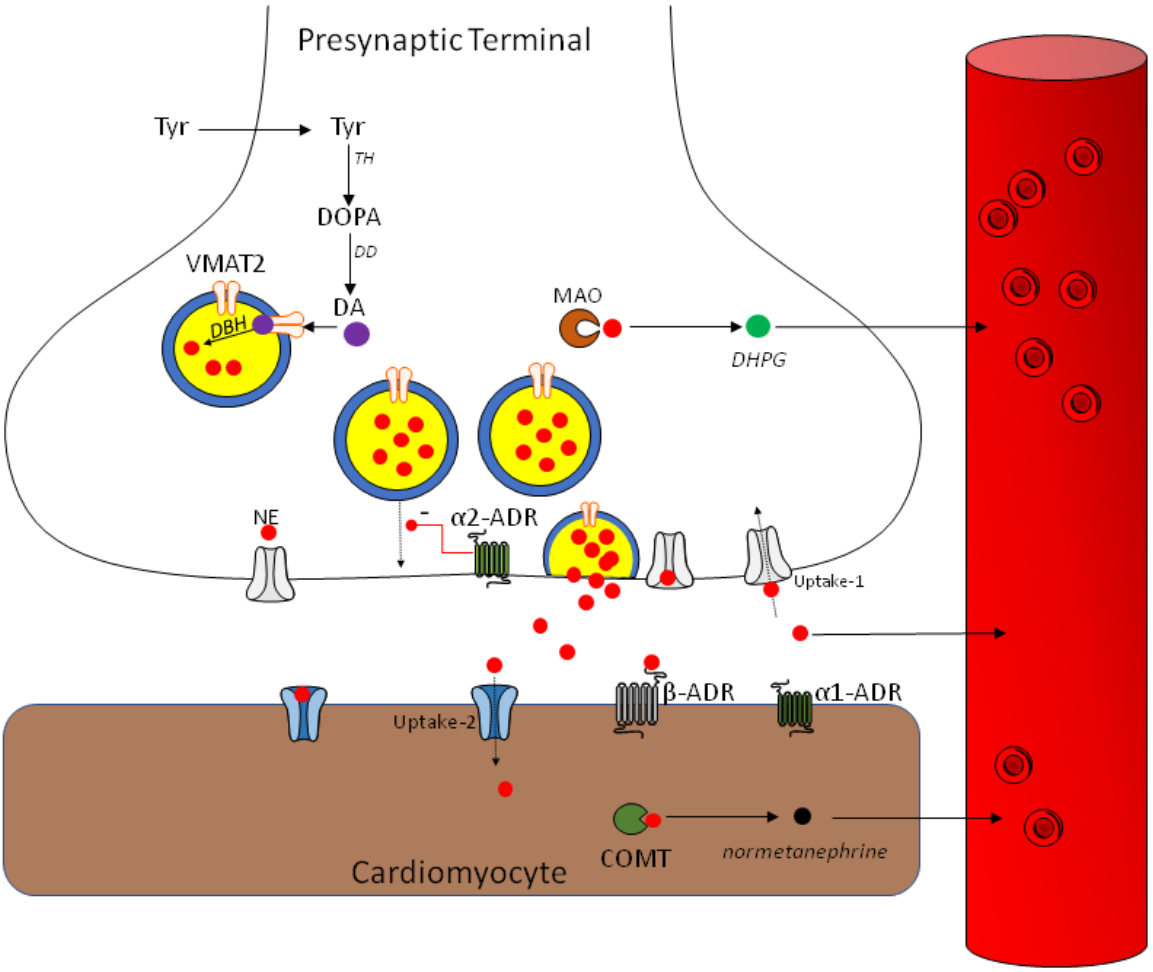

Figure 1.7 Presynaptic Neuronal Biology. The main pathways in the formation, metabolism, and release of norepinephrine from sympathetic nerve terminals as well as post-synaptic modulation. In the presynaptic nerve terminal, tyrosine (Tyr), is converted to dihydroxyphenylalanine (DOPA) by tyrosine hydroxylase (TH). DOPA is then converted via DOPA decarboxylase (DD) into dopamine (DA). Dopamine is then transported into synaptic vesicles via vesicular monoamine transporter 2 (VMAT2) and then converted into norepinephrine (NE) by dopamine B-hydroxylase (DBH). Nerve impulses release NE into the synaptic cleft by exocytosis. NE acts on alpha and beta adrenergic receptors on cardiomyocytes. NE also acts on presynaptic alpha2 adrenergic receptors (α2-ADR) that inhibits further NE release. 80-90% of NE is taken up by NE transporter Uptake1 into the cytosol of the presynaptic neuron, where is may be repackaged into storage vesicles via VMAT2 or metabolized by monoamine oxidase (MAO) into dihydroxyphenylglycol (DHPG).

1.11.2 Sympathetic Function

'Sympathetic function' is an overarching term that encompasses: 'sympathetic nerve density', 'neuronal integrity', 'sympathetic nerve activity/outflow', 'sympathetic tone' and all of their individual components[164]. The most basic of these is 'nerve density', which is the number of functional nerve terminals per gram of tissue. The other components represent functional terms. 'Neuronal integrity' describes the ability of the presynaptic nerve terminal to recycle, store and metabolize NE, and the coordination and function of Uptake1 transporter, VMAT2, and MAO enzyme. 'Sympathetic outflow' describes the rate of nerve impulses sent to the nerve terminal resulting in NE release, whereas sympathetic tone includes both sympathetic outflow and postsynaptic receptor modulation.

1.11.3 Assessing Cardiac Sympathetic Function

Various techniques have been developed to assess autonomic nervous system function and activity. A summary of popular techniques is summarized in Table 1.4. Although technical improvements have allowed for a more precise assessment of human adrenergic function, no available technique can be viewed as the "gold standard" for cardiac SNS assessment. [165,166] [^{11}C]HED uptake on PET imaging however, is widely considered the best standard for non-invasive assessment of the myocardial SN function.[167–169]

Table 1.4 Measures of Sympathetic Function

Technique	Autonomic Parameter	Description	Advantages	Disadvantages
Heart Rate Variability[170]	Sympathovagal Balance	- Beat-to-beat analysis of HVR is a marker of autonomic input to the heart. - Power spectral analysis separates i) low-frequency domains (0.04-0.15Hz), representing vagal and sympathetic influences and ii) high frequency domains (0.15-0.40Hz), representing vagal tone.	- Non-invasive cardiac assessment - Inexpensive - Easy to Perform	- No regional analysis - Data is variable and highly dependent of the ECG signal.
Plasma and Urine NE[171]	Adrenergic drive	-Plasma levels are increased in patients with heart failure. - Plasma levels reflect NE spillover + release from adrenal cortex.	- Non-invasive	-limited sensitivity and reproducibility -only a minor amount (5-10%) of NE released from Sympathetic Nerves -A global index and not specific to changes in the heart (not a regional evaluation
NE Spillover[172]	Sympathetic Outflow	-A small amount of NE escapes neuronal reuptake and 'spills over' into the blood vessels,. -NE measured as an assessment of sympathetic outflow	Most accurate quantification of regional sympathetic drive.	- Requires use of radiolabeled NE - Requires catheterization of coronary sinus for assessment of cardiac NE spillover. - No regional data
Microneurography (MSNS) [172]	Peripheral Sympathetic Activity	- Intraneuronal microneurographic recordings of postganglionic efferent sympathetic nerve activity in skeletal muscle or cutaneous tissue.	- Direct measure of sympathetic nerve activity	-Does not provide direct evidence of sympathetic nervous system function in the heart.
Cardiac Nuclear Imaging	Sympathetic Neuronal Integrity	-PET and SPECT nuclear tracers have been developed that have a high affinity for the NE transporter Uptake1 on sympathetic nerve terminals	- Non-invasive cardiac assessment - Regional quantification capabilities - Accurate cardiac tracer quantification	- Expensive - Requires Technical Expertise - Radiation Exposure

NE, norephinephrine

1.12.4 Radiolabeled Tracers for Imaging the Cardiac SNS

Although not a comprehensive list, below is a brief description of the neuronal handling of popular tracers to image the cardiac sympathetic nervous system. The following tracers are either labeled catecholamines or labeled catecholamine analogs. Catecholamine analogs are derived from norepinephrine or from the antihypertensive drug guanethidine. To date, the tracers used most extensively, [^{123}I]*meta*-iodobenzylguanidine (mIBG) and [^{11}C]*meta*-hydroxyephedrine (HED), target the presynaptic nerve terminal. Much of the literature for [^{123}I]mIBG has described the use of planar scintigraphy and demonstrated its prognostic value[173]. While this is a straightforward method to provide whole myocardium measures of the state of the cardiac SNS, regional evaluation is extremely limited. Though regional analysis is possible with SPECT [174], PET may have some advantages in this regard. These include increased spatiotemporal resolution and well-validated attenuation correction for accurate quantification of tissue radiotracer concentrations, translating to superior quantitative capabilities to assess regional abnormalities. In addition to [^{11}C]HED, other presynaptic PET tracers such as [^{18}F]*meta*-fluorobenzylguanidine (mFBG), [^{18}F]bromo-fluorobenzylguanidine (LMI1195 or flurobrobenguane)[175,176], [^{11}C]EPI (epinephrine), and [^{11}C]PHEN (phenylephrine) are included to discuss their potential utility. The neuronal handling of these tracers is represented in Figure 1.8.

SPECT Tracer

a. **[^{123}I]mIBG** is the most widely used agent to image the sympathetic nervous system. MIBG is a false neurotransmitter, and an analog of the antihypertensive drug guanethidine. MIBG has a high affinity for both uptake1 and uptake2, but neuronal retention through uptake1 predominates given the low contribution of

uptake2 to catecholamine clearance in humans[177,178]. MIBG has a relatively higher affinity for VMAT2 than HED, resulting in efficient packaging into storage vesicles. Neuronal activation leads to vesicular docking and release of MIBG and endogenous catecholamine into the synaptic cleft. MIBG SPECT imaging is usually quantified using early and late myocardial contrast as heart-to-mediastinal (H/M) ratio[179]. SPECT imaging (>4hrs) appears to primarily reflect retention, whereas the rate of washout (from early to late images) from the myocardium is related to sympathetic tone/activity in the heart[179].

PET Tracers

Advantages of PET over SPECT imaging are increased spatiotemporal resolution and well validated attenuation corrections for quantification of tissue radiotracer concentrations. These technical aspects translate to superior quantitative capabilities to assess regional abnormalities of the cardiac autonomic nervous system.

b. **[^{11}C]HED**, an analog of norepinephrine, is the most popular PET tracer to map the cardiac sympathetic nervous system. HED has a high affinity for Uptake1 at the presynaptic nerve terminal, and is resistant to degradation by MAO and COMT[180,181]. Vesicular storage via VMAT2 seems to occur within the nerve terminal, but because of its relatively higher lipophilicity, HED diffuses out of vesicles as well as across the nerve terminal[182]. The addition of a desipramine chase (uptake1 inhibitor) to isolated perfused rat hearts demonstrated accelerated HED washout[181,183]. These data suggest that HED retention is dependent on

continuous recycling, release and reuptake of the tracer into the sympathetic nerve terminal.

c. **[^{18}F]Flubrobenguance (FBBG, *LMI1195)*.** Flubrobengaune (N-[3-Bromo-4-(3-[^{18}F]fluro-propoxy)-benzyl]-guandidine) was designed similar to [^{123}I]mIBG but incorporated ^{18}F to overcome the limitations of ^{11}C labeled compounds with a shorter half-life. The kinetic properties seem to be similar to MIBG[183].

d. **[^{11}C]Epinephrine (EPI)** is an endogenous neurotransmitter synthesized from norepinephrine. Being structurally identical to the endogenous neurotransmitter, it's physiological neuronal handling is similar to the native neurotransmitter. That is, EPI has a high affinity for uptake1, is effectively stored in nerve terminals and is susceptible to metabolism by MAO and COMT[184]. EPI is often referred to as a marker of vesicular storage[185].

e. **[^{11}C]Phenylephrine (PHEN)** is structurally similar to HED with the absence of the a methyl group, making PHEN susceptible to metabolism by MAO[186]. Mechanistic studies on isolated rat hearts suggests that PHEN is a marker of vesicular storage function and MAO activity[184].

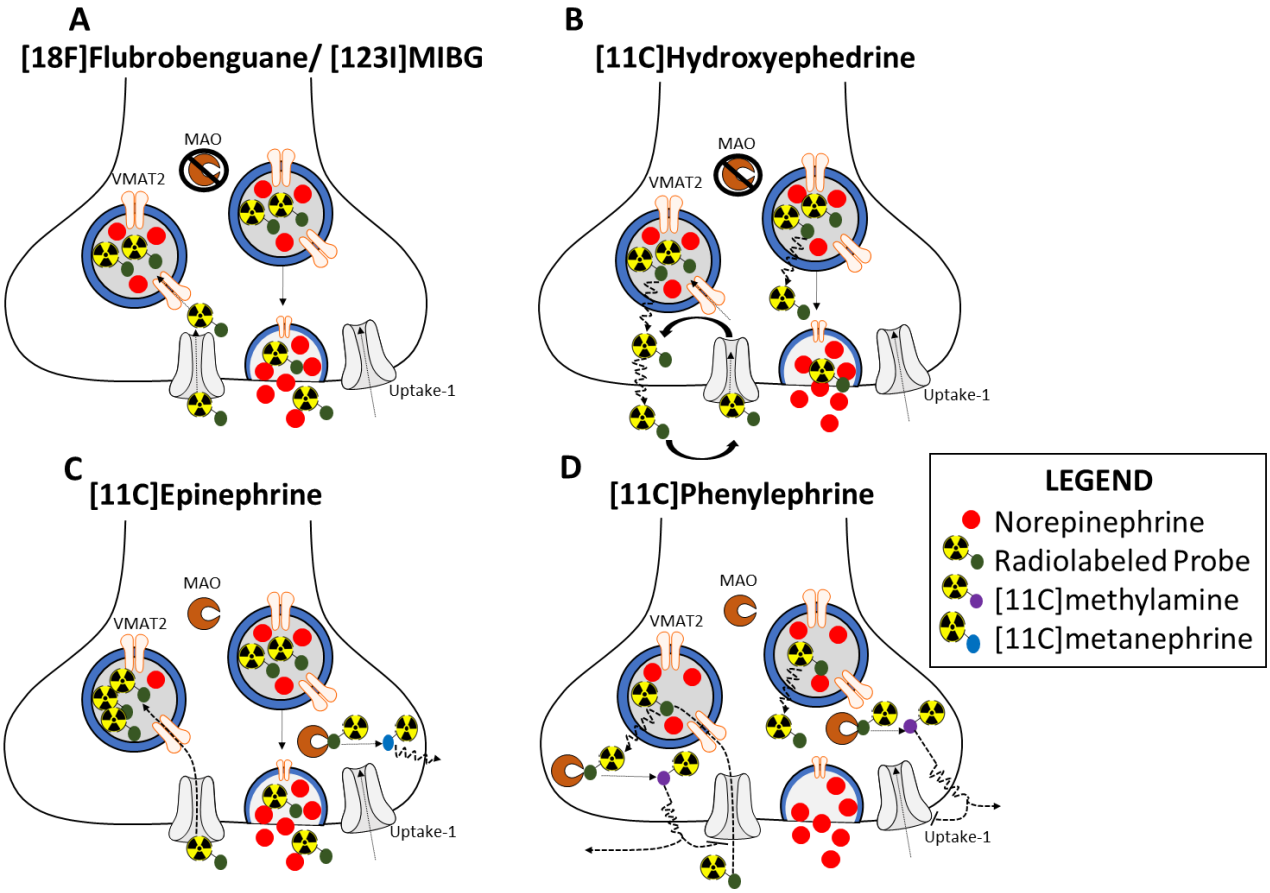

Figure 1.8 Summary of neuronal handling of popular tracers available for SPECT and PET. These tracers are all substrates for the NE transporter Uptake1. [123I]mIBG, [18F]Flurobenguan and [^{11}C]HED are all resistant to degradation by MAO and COMT; whereas [^{11}C]EPI and [^{11}C]PHEN being similar in structure to endogenous neurotransmitters are susceptible to metabolism by MAO and COMT. [^{11}C]EPI is an excellent substrate for VMAT2 and is effectively stored in vesicles protecting it from degradation by MAO. Some [^{11}C]EPI is metabolized by MAO into [^{11}C]metanephrine, which is not retained by the heart. In contrast, [^{11}C]PHEN is less efficiently stored in vesicles and, being lipophilic, leaks across vesicle membranes where it is metabolized by MAO into methylamine. Methylamine leaks across neuronal membranes and is not a substrate for Uptake1 so it is washed into the circulation.

1.12.5 SNS imaging in Ischemic Cardiomyopathy

There is some controversy regarding the mechanistic cause of [^{11}C]HED or [^{123}I]mIBG imaging defects in patients with ischemic heart disease. This can be attributed to a combination of factors: a) the etiology of ischemia (micro vs macro vascular disease); b) the type of ischemic injury (transmural vs subepicardial); and c) the timing of ischemia (acute vs chronic).

The rate of tracer extraction from plasma is a function of its extraction fraction (Uptake1 dependent) and blood flow. Imaging with [^{11}C]HED/[^{123}I]mIBG in patients with ICM should be interpreted cautiously as both exhibit rapid neuronal uptake through Uptake1 transporters, and are considered to be flow dependent.

a) Ischemic myocardium:

Ischemically mediated sympathetic nerve damage has been documented in patients with early CAD, without myocardial infarction[187,188]. Neuronal uptake of NE through Uptake1 is an energy-dependent process that requires oxygen for proper function. These mechanisms have been found to be more sensitive to ischemia than the myocardium. Sympathetic dysfunction in the setting of CAD may be inappropriately interpreted as denervation; however, investigations suggest varying contributions of neuronal stunning[189], decreased cellular function (i.e. decreased Uptake1)[190], and/or anatomical denervation. The conflicting reports are likely attributable to the extent and duration of ischemia, as brief coronary-occlusion-reperfusion injury (with no evidence of necrosis) causes temporary neuronal stunning[189,191], whereas chronic ischemia in hibernating myocardium models cause a combination of neuronal cellular dysfunction and denervation[188,190,192].

Sympathetic innervation imaging data also support this concept. Dae et al. induced brief (30

minutes) coronary occlusion-reperfusion injury in dogs and assessed sympathetic nerve function with [^{123}I]mIBG immediately and 1-2 weeks after the ischemic injury[193]. Persistent [^{123}I]mIBG defects were identified in 5 of 11 dogs on follow-up imaging (~1-2 wks) and were associated with sympathetic denervation (immunohistochemical evidence) and subendocardial necrosis. In contrast, 6 of the 11 dogs with no necrosis had accelerated mIBG washout immediately after coronary occlusion, but had normal innervation patterns with preserved NE content on follow-up imaging (1-2 wks). This suggests that brief periods of ischemia may induce neuronal stunning. Studies by Fallavollita *et al.* in dogs have consistently demonstrated that reperfusion therapies that restore flow to hibernating myocardium fail to improve SNS function assessed by [^{11}C]HED PET[190,194]. In subsequent studies, sympathetic nerve dysfunction in hibernating myocardium was found to be due to a combination of neuronal stunning, sympathetic denervation and regional nerve sprouting[190]. Sympathetic nerve sprouting occurs following neuronal damage and has significant arrhythmogenic risk[195]. The distinction between neuronal stunning and denervation may be clinically important, as the former may be reversible and less likely to induce nerve sprouting as compared to denervated myocardium. Together these data indicate that neuronal stunning represents a transient neuronal dysfunction, and ischemic duration is likely an important factor for both functional and neuronal parameters.

b) Infarcted myocardium

i) *Infarction Zone:* Sympathetic neurons travel with the coronary vasculature in the subepicardium (upper 0.20-0.5mm) and dive transmurally with the blood vessels to innervate the endocardium. Therefore, it is possible that both nerve terminals and nerve fibers within an ischemic zone become damaged during coronary occlusion.

Using a canine model, Dae et al. demonstrated that transmural infarction causes sympathetic anatomical denervation beyond the infarction zone, particularly in areas distal, but not proximal to the infarcted territory. In contrast, in non-transmural infarctions sympathetic denervation more closely matches the infarction zone, with no denervation in areas distal to the infarcted area[193,196]. These results have been replicated[197], and together elegantly display the pathological link between imaging defects and basic neuronal anatomy.

ii) *Viable Peri-Infarct Zone:* The extent of sympathetic neuronal damage closely matches the ischemia area, extending beyond the infarct area[188,197,198]. This effect is often interpreted as sympathetic neurons being more sensitive to ischemia than cardiomyocytes. The viable peri-infarct zone is more heterogeneous and harder to interpret on innervation imaging than the infarct zone, with varying contributions of both denervated and dysinnervated/stunned myocardium, depending on the type and duration of ischemia. In a porcine model of acute myocardial infarction (MI), Lautamaki *et al.* conducted PET studies using [^{11}C]epinephrine, [^{11}C]phenylephrine, and [^{11}C]HED to assess neuronal integrity and [^{13}N]ammonia to quantify perfusion[198]. Their results suggested that in the viable infarct border zone, neuronal vesicular catecholamine storage is more severely impaired than catecholamine uptake. These results raise important questions about whether neuronal dysinnervation is a transition state towards complete denervation. In the border zone, immunohistologic analysis revealed intact sympathetic nerve terminals and increased nerve sprouting. The latter results are consistent with previous work[195,198,199] and

suggests a causal link between sympathetic remodeling following MI and the development of malignant ventricular arrhythmias.

1.12.6 SNS imaging in Non-Ischemic/Dilated Cardiomyopathy

In patients with non-ischemic HF, the defect pattern is usually more heterogenous with smaller focal defects[200] or homogeneous[201] with no defects at all. There are many theories regarding the mechanistic cause of reduced tracer retention in these patients. Early stages of HF are often characterized by hyperactivity of sympathetic neurons. Elevated NE may decrease [^{11}C]HED uptake by increasing competition for neuronal reuptake. Although previous clinical studies have failed to demonstrate a correlation between plasma norepinephrine levels and [^{11}C]HED uptake in patients with dilated cardiomyopathy and left ventricular dysfunction[202,203], controlled pre-clinical studies in rats demonstrate a dose-dependent decrease in [^{11}C]HED retention by infusing NE[204]. This link remains speculative, as the pattern of reduction in these animal studies is more homogenous, and is less reflective of the heterogenous pattern of reduction seen in patients with NICM[204]. Decreased expression of the NE transporter Uptake1 has been documented in both humans and animals with HF. Rats receiving a continuous infusion of NE for 5 days had a 35% decrease in [^{123}I]mIBG uptake and a corresponding 29% decrease in Uptake1 density in the LV[205]. This suggests that decreased radiolabeled NE analog uptake is related to the functional mechanism of NE-induced downregulation of Uptake1 density, and may represent the missing link between systemic NE levels and radiotracer uptake.

Ungerer *et al.* investigated the relationship between [^{11}C]HED PET images and analysis from tissue samples of patients with dilated cardiomyopathy[206]. [^{11}C]HED uptake was assessed in 8 patients with dilated cardiomyopathy before heart transplantation. Regional [^{11}C]HED retention was significantly correlated to the density of Uptake1 ($r=0.63$). These results suggest either a loss

of neurons or downregulation of Uptake1 could be contributing to imaging defects (or tracer uptake reduction), but this may depend on the specific etiology of the NICM and warrants further investigation. Immunohistochemical studies of the density of tyrosine hydroxylase (a marker of sympathetic nerves), demonstrate anatomical denervation within left and right ventricle of patients with dilated cardiomyopathy[207]. One study found a correlation between sympathetic nerve density and LV ejection fraction, suggesting that denervation is more extensive in patients with severe disease[207]. Because most of the histological evidence in humans is limited to patients undergoing heart transplant, this body of evidence is limited to patients with end-stage disease, and may not reflect the neuronal state of patients with stable or early disease and/or milder impairments in ventricular function.

Backs *et al.* used an aortic banding model of chronic HF showed a 37% reduction in NE uptake within the LV, and an associated 41% reduction of Uptake1 expression[208]. The density of sympathetic nerve fibers within the heart was unchanged. These data suggest a functional transition state of impaired neuronal integrity (decreased Uptake1) that precedes anatomical denervation.

1.12.7 Clinical Utility of SNS imaging in patients with Left-Sided HF

Patients with HF and reduced ejection fraction (HFrEF) are at high risk of mortality from sudden death and progressive CHF[209]. Automatic implantable cardioverter defibrillator (ICD) and cardiac resynchronization therapy (CRT) have reduced the risk of sudden cardiac death and heart failure-related mortality[210].

***Sudden Arrhythmic Death Risk in Post Myocardial Infarction Subjects**:*

Survivors of myocardial infarction (MI) have a four-fold higher risk of sudden death compared to persons without a history of MI[211]. While patients with ejection fractions below 35% are at highest risk of sudden death, the majority of arrhythmic deaths occur in patients with mild to moderately reduced LV function (EF 35-50%) since there are many more patients at risk in this subgroup [212]. Given the lethality of the condition, screening should be able to identify most individuals at risk (sensitive) and correctly classify those at high risk compared to those at lower risk of SCD (accurate). Abnormalities of the electrical architecture of the myocardium resulting from MI facilitate arrhythmia initiation, while modulating conditions such as the autonomic tone are responsible for the maintenance of ventricular arrhythmias[195].

Potential Utility of Cardiac Sympathetic Nervous System Function Evaluation:

Current risk assessment approaches fail to identify the majority of subjects with myocardial infarction and HFrEF at risk of sudden cardiac death (SCD) furthermore not all patients with HF may be at the same risk for SCD[213]. Tomographic imaging of the cardiac SNS offers the potential for improving the prediction of SCD risk in post MI subjects. The addition of cardiac SNS imaging to current risk stratification strategies in subjects with prior MI has the potential to identify subjects at a higher risk of SCD and guide therapy to improve survival.

The ADMIRE-HF trial evaluated [^{123}I]mIBG imaging to identify HF patients (ICM and NICM) most likely to experience cardiac events[173]. The cumulative primary endpoint (time to first occurrence of NYHA functional class progression, life-threatening arrhythmic event or cardiac death) was compared with [^{123}I]mIBG heart-to-mediastinum (H/M) ratio on planar imaging. The cumulative cardiac event risk was lower for patients with H/M ≥1.60; hazard ratio

was 0.40 ($p<0.001$). The 2-year event rates were 38% vs. 15% for H/M ratio ≥1.60 and <1.60 respectively. The ADMIRE-HF extension (ADMIRE-HFX) confirmed H/M ratio as a significant predictor of all-cause mortality over a median of 24 months [214]. In a separate study, a late mIBG H/M cutoff of 1.82 was identified for both ischemic and nonischemic patients. However, in patients with LVEF <40%, ischemic and nonischemic patients had an optimal late H/M cutoff of 1.50 and 2.02, respectively[215].

Further investigation is warranted to optimize these thresholds. As well, ranges may be even better as uptake is continuous rather than a dichotomous variable. This may become particularly relevant if it becomes useful clinically to guide cardiac defibrillator (ICD) implantation. These results confirm the conclusions of several previous observational studies and meta-analysis, that [^{123}I]mIBG imaging is an effective and independent prognosticator in patients with HF[216,217]. Currently mIBG imaging is approved for use in heart failure prognosis. Its use for identifying arrhythmic risk, and predicting need for an ICD remains investigational.

A second seminal trial was PAREPET, evaluating [^{11}C]HED PET to identify ischemic cardiomyopathy patients at highest risk of sudden cardiac death (SCD). Patients with LVEF ≤35% eligible for ICD therapy were enrolled. Innervation defects at baseline were greater in patients who developed SCD (33% vs 11% of LV). SNS denervation on [^{11}C]HED PET was associated with SCD, independent of LVEF and infarct volume. PET sympathetic denervation, ventricular end-diastolic volume index, creatine and not being on angiotensin inhibition (no ACE/ARB therapy) were included in the multivariate model to predict time to SCD. This model successfully identified a cohort of patients with low (none of the 4 variables; <1% SCD/year) and high (≥2 variables; 12% SCD/year) risk of SCD. Similar results have also been demonstrated

by groups investigating the relationship between [^{123}I]mIBG results and either late ventricular potentials[218,219] or appropriate ICD therapy[220,221].

Cost-effective decision making for primary prevention ICD therapy requires methods to discriminate patients at high risk of SCD from other cardiac causes (i.e pump failure). In a post-hoc analysis of the PARPET data, denervation volume (assessed by [^{11}C]HED PET) was associated with cause specific cardiac mortality[222]. Specifically, in the competing risk model, denervated myocardium was associated with SCD (HR: 1.45 (95%CI: 1.00-2.10); p=0.05), but not non-SCD (0.93 (0.70-1.24; p=0.62). Whether innervation imaging can guide these types of therapy in patients with HF is the subject of ongoing trials such as MISTIC (ClinicalTrials.gov ID#: NCT01185756). Other trials are also planned using the new tracer flurbrobenguane.

Another potential clinical application of nuclear innervation imaging is monitoring the impact of various treatment strategies on sympathetic function in patients with HF. Beta-blockers[223], continuous positive airway pressure (CPAP)[224], and aldosterone[225] have been shown to increase retention of [^{11}C]HED or uptake of [^{123}I]mIBG. Although basic investigations are lacking, the mechanism is thought to be related to a combination of decreased sympathetic tone, improved Uptake-1 function and/or improved subcellular function (packaging of storage vesicles).

1.12.8 SNS imaging of the Right Ventricle

There is a paucity of data on the sequelae of chronic SNS activation in patients with pulmonary hypertension and right HF. There is even less available nuclear imaging data with only a few SPECT [^{123}I]MIBG studies evaluating sympathetic function in this population[226]. To date, studies evaluating SNS dysfunction using PET in patients with PH and right HF have not been conducted, but is an avenue of current investigation.

Studies have demonstrated sympathetic hyperactivity in patients with right HF and pulmonary hypertension, and SNS overactivation in these patients is an independent predictor of clinical deterioration[149,227,228]. [^{123}I]MIBG imaging has been used to demonstrate sympathetic dysfunction within the RV free wall and interventricular septum in both RV failure and PH patients. [229–231] Preliminary studies in patients with PH suggest that [^{123}I]MIBG SPECT imaging may be beneficial to non-invasively assess the severity, as well as predict survival in these patients. Morimitsu *et al* demonstrated a negative and significant correlation between MIBG uptake in the interventricular septum relative to the LV (IVR:LV ratio) and pulmonary arterial pressure[229,230]. These findings were corroborated by Sakamaki *et al,* who demonstrated that MIBG uptake, as assessed by the H/M ratio, correlated with the severity of pulmonary hypertension[231]. These investigators also found that PH patients with a [^{123}I]MIBG H/M ratio <2.0 had worse survival than patients with a H/M ratio >2.0. Work is ongoing to investigate the relationship between sympathetic denervation and PH/right HF using [^{11}C]HED PET, as well as response to spironolactone therapy (STAR-HF ID: NCT03344159).

1.12.9 Imaging the Parasympathetic Nervous System

Compared to recent progress on SNS imaging, research and development of tracers targeting the parasympathetic component of the autonomic nervous system are lacking. Research in this area is challenging given 1) a higher density of PNS terminals within the thin-walled atria as compared to the sparsely innervated ventricles, and 2) the rapid degradation of ACh by AChE within the synaptic cleft. Abnormalities in PNS function have similarly been implicated in HF and various cardiomyopathies, suggesting these studies may yield valuable mechanistic information. It is important to note that while this represents an important area of mechanistic

research, any direct clinical application in cardiology remains to be elucidated. Much of the research in presynaptic cholinergic imaging stems from applications in brain imaging. To our knowledge no tracer has been well validated for cardiac imaging. Potential targets include the AChE ([^{11}C]donepezil), and VAChT ([^{18}F]FEOBV and other labeled vesamicol analogs). Postsynaptic cholinergic muscarinic type 2 (M2) receptors are highly expressed in the heart, and represent a viable imaging target. Several studies have used the M2 receptor antagonist [^{11}C]methylquinuclidinyl benzylate (MQNB) to non-invasively quantify receptor density in the heart.[232,233] These studies have consistently demonstrated an upregulation of the M2 receptor in idiopathic dilated cardiomyopathy and in patients with ischemic cardiomyopathy.[232,233] Although speculative, it is possible that the upregulated M2 receptor represents a protective mechanism to attenuate heterogenous sympathetic activity, and arrhythmogenicity.

1.12 Current Therapy for Right Heart Failure

Management of RHF still remains supportive and symptom-based, and there are no therapies which directly and selectively target the right ventricle (RV). The American Heart Association recently released their 2018 scientific statement on the evaluation and management of right-sided heart failure.[234] The current treatment paradigm remains centered around reducing afterload, optimizing preload, and increasing RV contractility.

1.12.1 Afterload Reduction

Compared to the LV, RV systolic function is highly sensitive to changes in afterload, with only small increases in PAP engendering large reductions in stroke volume (SV). Accordingly, therapies aimed at reducing RV afterload are the cornerstone of management of

patients with RVF due to PH, regardless of the underlying etiology. For patients with Group 1 PAH these therapies include prostacyclin analogs, phosphodiesterase-5 (PDE-5) inhibitors/activators of soluble guanylate cyclase and endothelin receptor antagonists (ERAs) which target the prostacyclin, nitric oxide and endothelial pathways, respectively. A recent meta-analysis of major PAH trials demonstrated an increase in SV is always accompanied by a decrease in PAP, suggesting reductions in PVR without an accompanying increase in cardiac contractility.[53] These data suggest that current PAH medications predominantly target the pulmonary vasculature, with only limited cardiac-specific benefit.[54]

Unfortunately, there are no approved therapies (beyond treating the underlying heart disease) for groups 2, 3 and 5 PH. This is particularly a concern for Group 2 PH, resulting from left heart disease and elevations in left ventricular filling pressures, which is the most common cause of PH and RHF. In light of the substantial symptomatic and functional benefits of PAH-specific vasoactive drugs in patients with group 1 PH, these agents have been studied in patients with PH due to LHF. While a number of small single center trials indicated a potential benefit, larger randomized clinical trials have produced at best mixed results, with some even suggesting potential harm (i.e. FIRST trial).[235] RCTs evaluating ERAs (NCT00840463, NCT00820352) or PDE5 inhibitors for patients with HFpEF have either failed to meet recruit targets or have reported no benefit for patients with LHF.[236,237] These mixed results may stem from overly broad inclusion criteria and do not necessarily preclude benefit in specific subpopulations i.e. HFpEF or HFrEF with mixed pre- and post-capillary PH disease. As it stands, these agents are not indicated for PH patients with HFrEF or HFpEF until more definitive trials are completed.

1.12.2 Optimizing Preload

RHF can lead to fluid retention often manifesting as ascites and peripheral edema. Diuretics remain the cornerstone of management for patients with RHF; however, the benefits beyond symptomatic relief in reducing ventricular wall stress are not well studied. Optimizing diuretic strategies in patients with RHF is largely empiric with no clear guidelines, but there is interest in using novel approaches such as invasive hemodynamic monitoring (CardioMEMS HF system) or biomarkers (i.e. BNP) to guide dieresis in patients with RHF. The importance of optimizing preload was established in CHAMPION trial in which CardioMEMS invasive hemodynamic monitoring of LHF patients resulted in a 37% reduction in HF related hospitalization, an effect attributable to more diuretic adjustments.[238] When optimizing volume status in patients with RHF it is also important to obtain serial assessments of renal function and electrolytes. Acute kidney injury (AKI) is a common sequela of RVF, which further complicates the management of RVF. The cause of AKI is often believed to be primarily due to renal hypoperfusion (pre-renal), and thus in a patient with RHF and reduced CO our tendency is to administer fluids. However, an increasing body of evidence implicates venous congestion as a primary contributor to AKI in the setting of RHF[239] which may be accentuated with fluid administration. Augmenting RV contractility can also reduce filling pressures; however, few studies have evaluated the long-term effects of digoxin treatment on RV function.[240]

1.13 Evolving Therapies for Right Heart Failure

1.13.1 Neurohormonal Modulation

There is little doubt that neurohormonal activation plays a central role myocardial remodeling in the LV, however the role of similar mechanisms in the progression from adaptive to maladaptive

RV remodeling is less well understood. To the extent that this is the case, the same well-established therapies that have proven benefit for LV systolic dysfunction might also be useful in the treatment of RHF. The following paragraphs will summarize the preclinical and clinical experience to date with this approach for RHF.

β-Adrenergic Receptor Blockers (β-blockers)

Despite proven efficacy of β-blockers for treatment LHF,[241] their utility in RHF is uncertain. Patients with severe PH and RV dysfunction rely heavily on changes in heart rate to maintain cardiac output, and thus β-blockers are generally believed to be contraindicated in these patients unless required to treat a comorbidity.[242] However, whether these short-term hemodynamic risks might be offset by the potential positive neurohormonal, vascular and cardiac remodeling benefits during long-term β-blocker therapy in RHF is a subject of much debate and ongoing research. In aggregate, pre-clinical studies have consistently demonstrated direct RV benefit for β-blocker therapy in the SUHx and the MCT experimental models of PAH.[99,243] In these models, carvedilol, bisoprolol and nebivolol all directly improve RV function, exercise capacity and reduce fibrosis and capillary rarefaction.[244] However, these agents have contrasting effects on the pulmonary vasculature that may be related to the class of β-blockers; for example, nebivolol (but not carvedilol) reduces PAP, consistent with differences in their selectivity for adrenergic receptors and adjunctive effects on oxidative stress and inflammation. Human studies with β-blockers in PAH have produced conflicting results with studies suggesting benefit[245], no effect or even harm[246]. While the safety of carvedilol in PAH patients was recently demonstrated recently in a randomized clinical trial, there was no improvement in 6 minute walk test, hemodynamics (CO, PAP), and echocardiography assessment of RV function.[247] Moreover, bisoprolol was

shown to have detrimental effects on cardiac index and exercise capacity in patients with PAH.[246] Given that HFpEF is emerging as the most common cause of PH and RHF in developed nations, it should be noted that the beneficial effect of β-blocker therapy that has been so well established for HFrEF has not been demonstrated in clinical trials for patients HFpEF, again pointing to the need for a better understanding of the underlying mechanism of disease.[248]

Arterial Sympathetic Denervation

Hyperactivity of the SNS is intricately involved in the pathogenesis of PAH and left and right heart failure. The efficacy of both renal artery and pulmonary artery denervation therapy using catheter ablation based approaches have recently been elevated. Pulmonary sympathetic afferents may directly contribute to the elevated vasoconstriction and pulmonary artery remodeling in patients with PAH. Recent clinical studies in a small group of PAH patients have demonstrated that pulmonary artery denervation can significantly improve pulmonary artery remodeling, reduce pulmonary pressures, improve function capacity and improve RV function.[249,250]

Renal afferent and efferent sympathetic nerves responding to renal hypoxemia or ischemic in heart failure may also contribute to increased central sympathetic neural outflow. In preclinical models of heart failure, renal artery denervation decreased renal norepinephrine spillover, which was associated with improvements in LVEF, myocardial contractility and BNP.[251]

Increasing Parasympathetic Signaling

Autonomic dysfunction in RHF is characterized by marked increases in SNS activity and PNS withdrawal. Treatments targeting the autonomic nervous system aim to restore sympatho-vagal balance. Da Silva *et al.* recently tested pyridostigmine, a drug that increases PNS activity through acetylcholinesterase inhibition, in experimental PAH (SUHx). Using pressure-volume loop analysis this group demonstrated direct improvements in RV function, which was associated with reduced RV inflammation, hypertrophy, fibrosis, stiffness, and mortality.[154] Emerging evidence suggests that electrical vagal nerve stimulation may improve RV function in the Fischer rat model of maladaptive remodeling.[252] Remarkably, this group also demonstrated improved survival past 10 weeks post SU injection in the Fischer rat SUHx model, whereas others have reported to near 100% mortality by week 7 using this model.[95] While interesting, it remains to be determined whether these therapeutic approaches have any value in clinical populations.

ACE/ERBs

As is the case with β-blockers, the use of angiotensin-converting enzyme (ACE) inhibitors and AT_1 receptor antagonists (ARBs) in PH has not been thoroughly evaluated and their use for the treatment of RHF remains controversial. The RAAS is clearly activated in RHF and while preclinical studies have demonstrated marked improvements in RV function and remodeling with its inhibition, ACE inhibitors and ARBs showed no clear hemodynamic benefit in small PAH cohorts.[253,254] Moreover, there are concerns about possible adverse events resulting from reducing systemic arterial pressures in patients who may have comprised cardiac output and are already predisposed to presyncope and syncope. More recently, research has focused on targeting

the ACE2-angiotensin-(1-7)-Mas axis of the renin-angiotensin system. ACE2 converts angiotensin II to angiotensin-(1-7), which binds to the Mas receptor and exerts vasodilatation, antiapoptotic and antiproliferation actions.[255] Shenoy et al. pioneered methods to generate human ACE2 and angiotensin-(1-7) within plant chloroplasts. Oral delivery markedly improved pulmonary hemodynamics and RV function in both prevention and reversal MCT model of PAH.[256] However, it is currently unclear whether these benefits on RV remodeling and fibrotic burden are independent of afterload reduction.[256] This innovative therapy is currently being tested in a phase-1 trial evaluating the safety, efficacy and mechanisms of ACE2 treatment in PAH (NCT01884051).

Mineralocorticoid receptor antagonists (MRA)

As in LHF, aldosterone levels are elevated in patients with RHF. Levels are also increased in some patients receiving ACE inhibitor or ARB therapy, suggesting that aldosterone escape from RAAS blockade could represent an important target for therapy. In experimental models of PAH, spironolactone improves pulmonary vascular remodeling and reduces PAP. Beneficial effects on RV remodeling, hypertrophy, fibrosis and function were also noted.[156,257] However, in a PAB model of PH, eplerenone failed to improve RV function.[258] While this suggests the beneficial effects on RV remodeling may be attributable to afterload reduction, it does not necessary preclude direct effects on the RV in models that exhibit more maladaptive remodeling such as the SUHx or MCT models.

In a retrospective analysis of data from the ARIES-1 and ARIES-2 trials, improvements in exercise capacity, BNP levels and NYHA functional class were seen in PAH patients treated with spironolactone,[259] and prospective clinical trials are currently ongoing to confirm these

findings (NCT01712620). Our research team is also performing a trial evaluating the effect spironolactone on RV SNS activity, as well as RV function and remodeling in patients with chronic RHF (STAR-HF trial; NCT03344159). This clinical trial is using serial MRI and cardiac PET imaging with [^{11}C]hydroxyephedrine to evaluate the neurohormonal and remodeling effects of spironolactone in RHF, assessing both the safety and efficacy of spironolactone in this patient population.

1.13.2 Antioxidant Therapy

Therapeutic strategies aimed at reducing oxidative stress and restoring redox balance fall into one of three categories: 1) decreasing ROS production; 2) restoring endogenous antioxidant capacity; or 3) supplementation with endogenous antioxidants. The latter category has been the most thoroughly tested treatment strategy in experimental PH and RHF, with mixed results.[260] Some of the first evidence implicating oxidative stress in RHF came from studies demonstrating that hemoxygenase-oxygenase (HO-1) deficient mice progress to RVF when exposed to chronic hypoxia.[261] Whereas, treatment of SUHx rats with Protandim, a plant extract which is thought to increase antioxidant enzymes such as HO-1 and SOD, improves RV function with no effect on pulmonary vascular remodeling. [104] Together these data suggest that increasing antioxidant defenses can prevent maladaptive remodeling and preserve RV function.[104] In the MCT model, the synthetic antioxidant EUK-134, which is a SOD mimetic that is capable of scavenging ROS, was effective at reducing RV oxidative stress,[262] associated with improved RV systolic function, and decreased hypertrophy and fibrosis. The RAAS has also been implicated in increasing ROS production in LHF. Both AT1 and mineralocorticoid receptor signaling activates NADP oxidase to increase ROS formation.[263] Although not thoroughly tested in RHF, any benefit of

ACE/ARB/MR antagonism (discussed above) may, in part, work through reducing oxidative stress.

1.13.3 Metabolic Modulation

Metabolic remodeling has been proposed as a major mechanism driving the progression from adaptive RVH to maladaptive RHF. Thus, reversing these metabolic changes with a focus on recoupling glycolysis with oxidative pathways and/ improving metabolic efficiency, may have beneficial effects on RV remodeling and function. A number of therapeutic strategies using metabolic modulators in PH and RHF have been studied in preclinical models and even clinical trials.

PDK Inhibitors

PDH converts pyruvate into acetyl-coA which is subsequently oxidized in the mitochondria to produce ATP. PDK, an inhibitor of PDH, is elevated in patients with RVF and is thought to be responsible for the well characterized metabolic shift from glucose oxidation to glycolysis.[93] Preclinical studies have yielded promising results using the PDK inhibitor dichloroacetate (DCA), which has long been used as a clinical therapy for lactic acidosis, to restore oxidative metabolism in PH and RHF models. Beyond the marked reductions in pulmonary pressures, DCA also improved RV electrical remodeling (through restoration of voltage gated K^+ channels) and RV function in PAB and MCT models.[264] DCA was also shown to be effective in both treatment and reversal studies using the rat chronic hypoxia and MCT models[264] providing compelling evidence to support translation to clinical studies. The results of the phase-1 trial investigating the safety and tolerability of DCA in PAH patients (NYHA class III-IV) on optimal

medical therapy were recently published[265]. Compared to baseline measures, DCA increased glucose oxidation, decreased MAP and PVR on RHC, and improved functional capacity (6-minute walk test). Interestingly, there was marked variability in the response to DCA therapy between individual patients, which authors suggest was related to functional variants in SIRT3 and UCP2 (PDK-independent mitochondrial suppression). Interestingly, improvement in pulmonary hemodynamics and RV function was seen mainly in patients without SIRT3/UCP2 variants, suggesting that in future studies genotyping may be able to predict who will respond (or not) to DCA.

FAOx Inhibitors

As reviewed above, FFA are the major substrate for cardiac metabolism and FAOx may promote glycolysis through the mutually competitive relationship with glucose oxidation (Randle Cycle), thus representing an important therapeutic target. In PAB and PAH models, FAOx inhibitors trimetazidine and ranolazine have both been able to reverse the metabolic changes in RV hypertrophy, increasing glucose oxidation and improving RV function.[113] Improvements in RV remodeling and function with 3 months of ranolazine was confirmed in a phase III trial in PAH patients.[266] There is also an ongoing investigation on the effects of the effect of ranolazine on RV function in patients with PAH and RV dysfunction (NCT02829034). There was initial promise for ranolazine in preclinical HFpEF studies, but a recent phase IV trial failed to demonstrate any improvements in diastolic function.[267] A phase II trial studying the effects of trimetazidine on RV function in PAH is currently on-going (NCT02102672).

PPARγ Agonists

Although somewhat paradoxical, there is preliminary evidence suggesting that promoting FAO may confer benefit in LHF. Heart failure is a state of energy deprivation, and thus upregulation in FFA uptake and metabolism (highest energy yield per substrate) may be an adaptive mechanism to drive ATP production. In a recent study using the SUHx model, oral treatment with the PPARγ agonist pioglitazone completely normalized PAP, vascular remodeling and prevented progression to RHF.[116] Authors further demonstrated that pioglitazone increased FAOx and decreased accumulation of lipotoxic compounds in the myocardium. Given the dramatic improvements in PH and lung vascular remodeling, the degree to which these results are due to direct effects on RV function, rather than the indirect effect due to improved pulmonary hemodynamics, remains to be determined. Unfortunately, a phase II trial using polyglitazone in PAH was recently terminated because of poor enrolment (NCT00825266).

1.13.4 Angiogenic Therapy

Dysregulated angiogenesis in the lung is pathognomonic of PAH. More recent evidence links impaired angiogenesis to maladaptive RHF, and modulating angiogenic pathways may represent a novel approach to maintain RV function, or even reestablish the adaptive phenotype.[268] miR-126 has emerged as a critical regulator of angiogenesis by suppressing SPRED-1 and PIK3R2, two negative regulators of VEGF signaling pathways. Expression of miR-126 is reduced in patients and animal models of maladaptive RHF and restoring expression levels with a miR-126 mimic in increased RV capillary density and improved RV function and exercise capacity in the monocrotaline PH model. In the LHF, delivery of a variety of proangiogenic growth factors including, VEGF-A, VEGF-B, FGF-2, FGF-5 and Angpt-2, have

been investigated with some success, but to our knowledge similar studies have not yet been conducted in experimental RHF.[269] While there may be some concerns about possible detrimental effects of angiogenic growth factors on pulmonary arterial remodeling in PAH, angiogenic gene therapy has been shown to be effective in preventing and reversing PH in experimental models.[270]

Cardiotrophin-1 (CT1)

CT1 is a cytokine member of the interleukin-6 superfamily, known to bind to gp130 receptor complexes, activating prosurvival, antiapoptosis and hypertrophic signaling pathways.[271] CT-1 levels are elevated in many cardiovascular disease states including hypertension, valvular heart disease, and LHF. [271] Although plasma levels correlate with disease severity and are associated with a worse prognosis, it has been suggested that elevated CT-1 levels may reflect an adaptive response to increasing ventricular wall stress.[96] Indeed, cardiomyoctye-restricted knockout of pg130 predisposes mice to the development of LHF when subjected to pressure overload.[272] Similarly, our research group recently evaluated the ability of exogenous CT1 delivery to rescue the maladaptive RV phenotype of the Fischer rats in the SUHx model of severe PAH.[96] In this model, CT1 ameliorated RV contractile function (cardiac output, fractional area change), improved structural remodeling (RVID:LVID ratio), and increased capillary density. These changes were observed in the absence of any effects on RVSP, consistent with a direct effect of CT-1 on RV remodeling.

1.13.5 Stem Cell Therapy

Although cell based therapies have produced mixed results in clinical trials for LHF, overall they were reported as safe and feasible, which holds promise for future innovation to

hone therapeutic efficacy (e.g. molecular homing signals, microencapsulation to increase engraftment and cell viability).[273] There has been tremendous interest in the molecular mechanisms by which stem cells support a regenerative milieu. This has led to a recent paradigm-shift away from a direct cell-mediated regeneration towards indirect paracrine effects mediated by the release of factors (storage vesicles, cytokines, growth factors) to trigger regenerative pathways within the diseased myocardium.

Several stem cell-based therapies have been evaluated in experimental PAH but these therapies primarily targeted the pulmonary circulation, although there may be ancillary effects on the RV. Mesenchymal stem cells (MSC), endothelial progenitor cells (EPC), and cardiac progenitor cells (CPC) have all demonstrated efficacy in reducing RVSP and RVH in animal models of PAH.[274] However, it is difficult to know whether any concomitant improvements in RV function with pulmonary cell therapy care related by direct effects or just secondary to RV afterload reduction. Oommen and coworkers delivered umbilical cord blood (UBC)-derived mononuclear cells via intramyocardial RV injection in a rodent PAB model.[275] Using cMRI analysis, they demonstrated improvements in RV volumes and function that were associated with increased capillary density and angiogenic markers as well as decreased RV fibrosis. Interestingly, these changes were not associated with a regression in RVH, suggesting UBC-MNCs can induce an adaptive form of remodeling, whereby cardiomyocyte growth increases *pari passu* with capillary density. Similar findings were recently reported in the PAB model using aggregated CPCs.[276]

We have previously demonstrated reductions in RVH and RVSP with central venous delivery of EPCs engineered to overexpress endothelial nitric oxide synthase (eNOS) in the rat MCT-induced PH.[277] The efficacy and safety of repeated monthly dosing of autologous eNOS-

enhanced EPCs is currently being studied in patients with severe PAH (SAPPHIRE trial; NCT03001414). The primary endpoint of this trial is a change in 6-minute walk test, but secondary endpoints capture echocardiography and MRI indices of RV function.

1.14 Objectives and Hypotheses

Thesis Objectives: The overall goal of my doctoral research curriculum is to compare and refine contemporary PAH risk assessment strategies and explore the pathogenic mechanisms contributing to the development of maladaptive right HF and, given this insight, explore therapeutic strategies that target this adverse profile. Validating a new methodology to assess cardiac sympathetic innervation and function in left and right HF is also an important goal of the encompassing studies.

Thesis Hypotheses: It is hypothesized that impairments in RV i) sympathetic function and ii) energetics are important pathological mechanisms in the transition from adaptive to maladaptive RHF. It is further hypothesized that the novel ^{18}F-labeled PET tracer flubrobengaune, with its favorable imaging characteristics and capacity for site distribution will be a preferred approach to assess SNS function in the myocardium.

<u>Introduction to Manuscripts: Objectives and Hypotheses</u>

1.14.1 Manuscript #1 (Chapter 2)

Objectives: To compare contemporary risk assessment tools, and to determine the prognostic significance of risk parameters of kidney and RV function and whether they can the further improve risk prediction for patients with PAH.

Hypotheses: RV systolic function (on echo) and eGFR (kidney function) will emerge as important prognostic factors that can further refine contemporary risk assessment.

1.14.2 Manuscript #2 (Chapter 3)

Objectives: In an animal model of PAH-induced RHF, the primary goals are to a) validate the use of clinically applicable neurohormonal imaging using cardiac positron emission tomography (PET) to evaluating changes in cardiac SNS integrity and response to treatment, and b) evaluate whether beta-adrenergic receptor blockade (β-blockers) can preserve myocardial SNS function and reverse pathogenic right heart remodeling.

Hypotheses: It is hypothesized that carvedilol treatment will improve RV function in experimental PAH. These improvements will be associated with favorable effects on cardiac sympathetic activity, as assessed by increased RV HED retention by cardiac PET imaging. We also hypothesize that HED PET will correlate with immunohistochemical measures of sympathetic innervation, and thus validating its use for measuring RV denervation burden.

1.14.3 Manuscript #3 (Chapter 4)

Objectives: The primary objective of the study is to validate the new PET tracer [^{18}F]Flubrobengaune as a marker of presynaptic neuronal function in humans with and without left heart failure by correlating myocardial [^{18}F]Flubrobengaune retention against the current PET standard [^{11}C]HED retention.

Hypotheses: It is hypothesized that there will be a moderate-to-strong correlation (r>0.6) between myocardial [^{11}C]HED and [^{18}F]flubrobengaune retention in both LV and RV. These data will support that [^{18}F]flubrobengaune with its favorable imaging characteristics and capacity for site distribution will be a preferred approach to assess SNS function in the myocardium.

1.14.4 Manuscript #4 (Chapter 5)

Objectives: To explore the molecular determinants and metabolic mechanisms underlying maladaptive remodeling in Fisher rats in an experimental of severe PAH.

Hypotheses: We hypothesize that Fischer rats have impaired RV energetics that predisposes to the development of RHF. The impaired RV energetics will have a genetic basis and may explain the marked heterogeneity in adaptive and maladaptive RV phenotypes.

1.14.5 Manuscript #5 Appendix B

Objectives: The objectives were two-fold: 1) in a competing-risk analysis compare the robustness of regional and global [^{11}C]HED quantification parameters for predicting cause-specific mortality from SCA and 2) determine whether the global RI and DV assessments yield any independent and additive prognostic value over the regional defects alone.

Hypotheses: It is hypothesized that HED assessment of global innervation will further refine SCA risk. That is, global RI or DV will predict SCA independent of regional denervation scores.

1.14.6 Manuscript #6 Appendix C

Objectives: The purpose of this study was to characterize the reproducibility and repeatability of [^{11}C]-meta-hydroxyephedrine (HED) positron emission tomography (PET) imaging of cardiac SNS innervation, regional denervation, and blood flow.

Hypotheses: It is hypothesized that there will be excellent reproducibility of both measures of regional denervation and global innervation. HED will have favorable kinetics and will validate to enable a parallel assessment of myocardial blood flow.

1.14.7 Manuscript #7 Appendix D

Objectives: The objectives of this study are to assess the relationship and interaction of the biomarkers NT-proBNP (N-Terminal Prohormone of Brain Natriuretic Peptide) and hs-cTnT (High Sensitivity Cardiac Troponin T) with myocardial scar and hibernation in patients with chronic ischemic HF.

Hypotheses: We hypothesize that NT-proBNP and hs-cTnT will be elevated in patients with ischemic cardiomyopathy and will correlate with the severity of hibernating myocardium, but not scar. We hypothesize that scar tissue may lack the molecular machinery required for peptide synthesis.

1.14.8 Manuscript #8 Appendix E

Objectives: The objective of this study was to evaluate the utility of NT-proBNP, hs-cTnT, and NGAL (neutrophil gelatinase-associated lipocalin) for prediction and early detection of congestive acute kidney injury following cardiac surgery.

Hypotheses: We hypothesize that these cardiac and renal biomarkers will facilitate early identification of congestive type acute kidney injury in the setting of right heart failure.

**Note: Supplemental figures for Chapters 2-5 of this thesis are displayed in Appendix A of the thesis.

Chapter 2

Incorporation of Renal Function in Mortality Risk Assessment for Pulmonary Arterial Hypertension

Zelt et al. 2020 Journal of Heart and Lung Transplantation (*in press*)
DIO: 10.1016/j.healun.2020.03.026

Running Title: Kidney Function Refines Mortality Risk in PAH

Authors: **Jason G.E. Zelt MSc[a,b]**, Alomgir Hossain PhD[c], Louise Y. Sun MD SM[c,d], Sanjay Mehta, MD[e], George Chandy MD, MSc[b,f], Ross A. Davies MD[b], Vladimir Contreras-Dominguez MD[f], Rosemary Dunne[b], Caroyln Doyle-Cox[b], George Wells PhD, Duncan J. Stewart MD[a,b,g], and Lisa M Mielniczuk MD,MSc[a,b]

[a]Department of Cellular and Molecular Medicine, Faculty of Medicine, University of Ottawa, Ottawa, Canada.
[b]Division of Cardiology, University of Ottawa Heart Institute and University of Ottawa;
[c]School of Epidemiology and Public Health, University of Ottawa, Ottawa, ON, Canada [d]Division of Cardiac Anesthesiology, Department of Anesthesiology and Pain Medicine, University of Ottawa Heart Institute, Ottawa, ON, Canada.
[e]Division of Respirology, Department of Medicine, London Health Sciences Centre, Schulich School of Medicine and Dentistry, Western University, London ON
[f]Division of Respirology and Internal Medicine, University of Ottawa;
[g]Sinclair Centre for Regenerative Medicine, Ottawa Hospital Research Institute, Ottawa, Canada;

Authorship Contributions:
JGEZ: Created the retrospective cohort of PAH patients. With PI, conceived the study design and research question. He performed the statistical analysis, graphical representation and wrote the manuscript.
AG and GW: Oversaw the statistical analysis
SM, GC, RAD, VCD, DJS and LM are PAH specialists at The Ottawa Heart Institute
LMM: PI on the project, helped conceive the study design and provided a critical review of the manuscript.

Key Words: Pulmonary Arterial Hypertension, Risk Assessment, Renal Disease

2.1 Abstract

Background: Risk assessment is important for prognostication and individualized treatment decisions for patients with pulmonary arterial hypertension (PAH). The purpose was to 1) compare contemporary risk assessment tools, and 2) to determine the prognostic significance of risk parameters of kidney function and whether they can the further improve risk prediction for patients with PAH.

Methods: We identified a cohort of treatment naïve patients (n=211) who received an incident diagnosis of PAH at the University of Ottawa Heart Institute. Using demographics, disease characteristics and hemodynamic data at diagnosis, patients were categorized as low, intermediate or high risk according to current European guidelines (ESC) and REVEAL risk scores. The primary endpoint was transplant-free survival (TFS).

Results: Patients were predominantly women (64.6%) with WHO function class III symptoms (66.5%). The median TFS was 7.09 years. There was little agreement between ESC and REVEAL-based risk estimates (weighted kappa=0.21-0.34). Although both the ESC (Log-Rank,p=0.0002) and REVEAL algorithms stratified TFS risk ($p<0.0001$), the REVEAL score provided superior dicrimination (C-statistic=0.70 vs 0.59,p=0.004). Renal function at diagnosis ($p<0.0001$) and Δrenal function at 6 months ($p<0.0001$) were identified as novel risk parameters, and served to reclassify some patients in the 'intermediate risk' category to a 'lower or higher risk' strata ($p<0.0001$).

Conclusion: REVEAL-based strategies provide superior TFS risk discrimination to ESC/ERS-based approaches. However the classification of "intermediate" risk patients varied significantly across tools. We demonstrate the importance of renal function, which further improved the stratification of risk in PAH patients, particularly in patients who are considered "intermediate risk".

2.2 Introduction

Pulmonary arterial hypertension (PAH) is an insidious disease of the pulmonary vasculature, which, despite recent advancements in treatment, remains an incurable disease with a dismal prognosis. Epidemiological studies suggest that the hemodynamic severity of PAH, as measured by pulmonary vascular resistance (PVR) and mean pulmonary artery pressure (mPAP), does not reliably predict mortality.[54] Rather, the response of the right ventricle (RV) to the elevated afterload has emerged as a powerful predictor of prognosis in these patients.[54,74] Indeed, it is no surprise that the disease trajectory and clinical course remain difficult to predict. A more comprehensive risk assessment strategy has therefore been recommended, which incorporates measures of PAH disease severity, exercise tolerance, and right ventricular (RV) function.[75,76] If widely adopted, a mortality risk assessment strategy would guide treatment decisions, thus maximizing clinical impact and patient outcomes in a cost-effective approach in this contemporary fiscal climate.

Data from large PAH registries have been used to derive algorithms to estimate survival. The REVEAL risk calculator uses up to 12 clinically relevant variables and was derived from a large US registry collected between 2006-2009.[29,78] Since then, the European Society of Cardiology (ESC) and the European Respiratory Society (ERS) released a comprehensive PAH risk assessment strategy in 2015 (current ESC/ERS guidelines). More recently, the Swedish, COMPERA (Comparative, Prospective Registry of Newly Initiated Therapies for Pulmonary Hypertension) and French registries have each derived their own risk assessment strategies using 4-8 variables, selected for clinical relevance, all of which used individual parameter thresholds from the 2015 ESC/ERS guidelines. To date, none of the existing risk tools have been universally adopted, possibly due to perceived complexity, the number of variables required to

calculate risk and/or the experience of the PH center. This has important therapeutic implications, given that both the ESC/ERS 2015 guidelines and the 2018 World Symposium treatment algorithms endorse the use of risk assessment at diagnosis to guide treatment decisions.[75,76,87] While the importance of identification of low or high-risk is intuitive, the clinical utility of stratification into the intermediate-risk category is less certain. Indeed, more refined risk assessment in this intermediate-risk category is highly relevant, since the majority of PAH patients often fall into this risk category and the specific treatment recommendations for "intermediate risk patients" are not well defined.

Renal disease is a critical prognostic marker across many cardiovascular disease states. It is prevalent in up to 36-47% of patients with PAH, is associated with impaired hemodynamics, and portends a poor prognosis.[278,279] Renal dysfunction is also a common sequela of right heart failure (RHF), which is common in patients with PAH. Despite the importance of renal function in the PAH population, it has not been formally incorporated into many of the contemporary PAH risk tools, including current guidelines. The REVEAL 2.0 is a recent update of the original risk calculator and the first to incorporate estimated glomerular filtration rate (eGFR) as a measure of renal function.[81]

Given these important and unanswered questions in the risk assessment and management of PAH patients, we conducted the current study to 1) compare the contemporary risk assessment tools in a real-world PAH population and 2) determine the prognostic significance of risk parameters of kidney function and whether they can the further improve risk prediction, especially in the intermediate risk category.

2.3 Methods:

This study was approved by the Research Ethics Review Board at the University of Ottawa Heart Institute (20180423-01H).

2.3.1 Patients

Included in this retrospective study was a cohort of treatment naïve WHO (World Health Organization) Group 1 PAH patients who received their incident diagnosis at the University of Ottawa Heart Institute between January 2007 - October 30, 2017. Group 1 PAH was ascertained by right heart catheterization in accordance with clinical guidelines.[75] At diagnosis, patient demographics, disease characteristics, and hemodynamic data were recorded for risk assessment. Using this information, patients were categorized as low, intermediate or high risk according to guidelines and contemporary risk assessment tools.

2.3.2 Risk Stratification Strategy:

Patients were categorized as 'Low', 'Intermediate', or 'High' risk according to the ESC/ERS 2015 guidelines, the FPHR (French Pulmonary Hypertension Registry) 2015 strategy and the REVEAL 1.0 and REVEAL 2.0 Risk Calculators. The variables used in stratifying patients according to these risk scores appear in Figure 2.1. The variables captured in the risk scores are color coded for increasing overlap between stratification strategies. New York Heart Association (NYHA) / WHO functional class, six minute walk test distance (6MWD), and right atrial pressure (RAP) were the only variables shared across all risk scores. Variables not captured in

our database are italicized. For instance, cardiopulmonary exercise testing is not routinely assessed at our institution, and also was not incorporated into the ESC/ERS 2015 risk assessment. Data available for risk stratification are indicated in brackets in Figure 2.1.

a) ESC/ERS-Based Risk Assessment

i) ***ESC/ERS 2015 Guidelines:*** We assigned a score between 1-3 (1=low risk; 3=high risk) for each variable, using published cutoffs.[75] We then divided the sum of the scores across all variables by the number of variables available for each patient, and rounded this number to the nearest integer to arrive at a mean risk score for that patient. This scoring strategy has been previously been used with the SPAHR (Swedish PAH Registry)[82] and COMPERA,[83] which used truncated versions of the ESC/ERS 2015 guidelines (6-8 variables). To our knowledge, the present study is the most comprehensive assessment of the guidelines, incorporating up to 10 of the 12 variables.

ii) FPHR (French Registry): The FPHR 2015 model uses cutoffs from the 2015 ESC/ERS risk assessment criteria.[85] The number of low-risk criteria were defined as 1) NYHA functional class I or II, 2) 6MWD >440 m, 3) RAP <8 mmHg and 4) cardiac index ≥ 2.5 $L \cdot min^{-1} \cdot m^{-2}$. The number of low risk criteria for each patient were summed (score 0-4; 0, highest risk; 4, lowest risk). For comparison to 2015 guidelines, the FHPR score was further stratified into Low (FHPR Score 3-4), Intermediate (1-2) and High (0) risk groups, as previously published.[280] The FPHR 2015 model was originally validated in idiopathic, heritable or drug-induced PAH; however, it has been also been subsequently validated for use in patients with

CTD.[281] In the present study, we apply this risk score to a mixed group I PAH population.

b) REVEAL-Based Risk Assessment

iii) REVEAL 1.0 Score (USA Registry): The REVEAL Registry PAH risk score calculator assigned patients a score from 0 (lowest risk) to 22 (highest risk). REVEAL 1.0 scores were stratified into Low (score ≤7), Average (8), Moderately High (9), High (10-11) and Very High (≥12). For comparison to guidelines, the 5 risk strata were further collapsed into Low (≤8), Intermediate (9), and High (≥10) risk strata, as previously published.[280,282]

iv) REVEAL 2.0 Score (USA Registry): The REVEAL Registry PAH risk score calculator was recently updated in March 2019. The updated calculator assigns patients a score from 0 (lowest risk) to 23 (highest risk). As previously published, REVEAL 2.0 scores were stratified into Low (≤6), Intermediate (7-8), and High (≥9) risk strata.[81] Although REVEAL 2.0 was originally intended to be used at follow-up (given the hospitalization variable at 6 months), its discrimination for TFS was also previously assessed at baseline. We used the REVEAL 2.0 on baseline data with the hospitalization variable set to 0, as was done by previously.

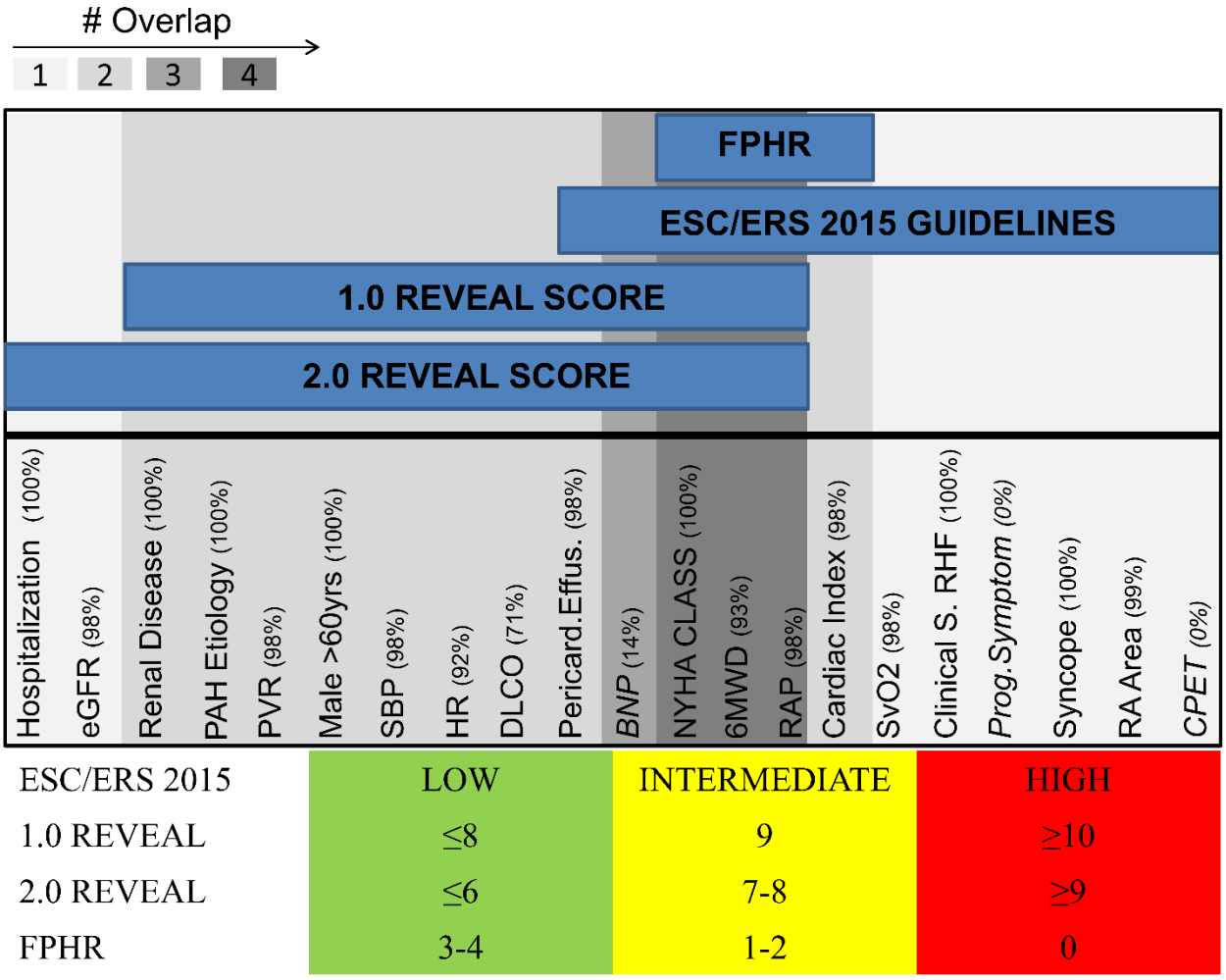

Figure 2.1. Summary of contemporary risk stratification algorithms and variables incorporated into the risk assessment scores. The bars capture the variables below on the x-axis, with the length of the bar proportional to the number of variables incorporated in the risk algorithms. The degree of variable overlap (shades of grey), reflects a variables prevalence in contemporary risk assessment. Risk stratification scores are then further stratified into Low, Intermediate and High-risk groups for comparison with the ESC/ERS 2015 Guidelines. The % of data available for each variable in our Ottawa PAH Cohort appears in brackets.

2.3.3 Renal Function

In all patients, creatinine was measured in the University of Ottawa outpatient PH clinic. At baseline, creatinine was assessed before the initiation of PAH-specific medications. eGFR was calculated for each patient using the CKD-EPI equation. [283,284] CKD severity was classified based on baseline and 6 month ± 2 weeks eGFR: Stages 1 and 2 eGFR≥60 mL/min/1.73m^2; Stages 3 eGFR 30-60 mL/min/1.73m^2; and Stages 4 and 5 eGFR<30 mL/min/1.73m^2.[285] Patients were also divided into 3 groups based on the percent change in eGFR between baseline (diagnosis) and 6 months (+/- 2 weeks): i) ≥10% ↑eGFR; ii) ≤10% ↓eGFR and iii) <10% ↑ or ↓ in eGFR (stratification previously published in REVEAL database).[284]

2.3.4 Statistical Analysis

The primary endpoint was transplant free survival. All patients were followed for at least 12 months until death, cardiac transplant, or October 30, 2018; whichever occurred first. Patients were censored at the end of the follow-up period. For the risk algorithms, transplant-free survival was analyzed using the Kaplan-Meier method and differences between risk strata were assessed by the Log-Rank Trend Test or Log-Rand test when appropriate. Risk algorithms were compared using the Uno's concordance statistic. For the impact of eGFR on transplant-free survival, we used a multivariable Cox proportional hazards model to assess for the HR associated with an increase and decrease in eGFR, as compared to patients whose eGFR stayed constant during the follow-up period. We reported the crude hazard ratios, as well as those adjusted for 1) baseline eGFR and 2) baselines eGFR, 6MWD and NYHA functional class. These variables were selected and modeled as previously published in the REVEAL registry.[284] P<0.05 was considered statistically significant. Statistical analysis were performed using SAS 9.4 (SAS

Institute, NC), and graphics were created using Graphpad Prism 6.0 (GraphPad, La Jolla, CA, USA).

2.4 Results

2.4.1 Characteristics at Diagnosis:

We identified a cohort of 211 incident and treatment naïve WHO Group 1 PAH patients (70% iPAH, 24% APAH-CTD, and 6% APAH-CHD). Patients included in this Ottawa PAH Cohort had a mean age of 63.2±16.3 years at the time of diagnosis, with the majority (66.5%) experiencing NYHA/WHO function class III symptoms (Table 2.1). Comorbid renal disease was prevalent, with 42.1% of the patients having at least stage 3 CKD (eGFR<60mL/min/1.73m^2) at baseline. At diagnosis, 41.6% of the patients also had at least moderate RV systolic dysfunction by echocardiography. PAH specific therapies within three months after diagnosis appear in Table 1; of note, 83% of these patients were on monotherapy.

2.4.2 Survival

The median follow-up time was 3.8 years (IQR: 1.7-6.0). Maximum follow-up duration was 12.3 years. 88 deaths and 2 transplants occurred during follow-up with a median TFS of 7.09 years. While the cohort was predominantly female (64.6%), mortality rate was greater in men (HR 1.55; 95% CI:1.02-2.37). In addition, connective tissue disease, diabetes, CKD, atrial fibrillation and system hypertension were also independently associated with death or lung transplant (Supplemental Figure 1). Patients with higher NYHA/WHO functional class, and lower exercise tolerance, cardiac index, and SvO_2 at diagnosis had an increased mortality rates (Supplemental Figure 2.2).

Table 2.1: **Patient Demographics and Clinical Characteristics at Diagnosis**

Characteristics (n=211)	% or Mean (SD)
Age (years)	63.2 (16.3)
Women	64.6%
BMI (kg/m^2)	28.9 (8.1)
WHO Group 1 PAH Subgroups	
Idiopathic	69.8%
Connective Tissue Disease	23.7%
Congenital Heart Disease	6.6%
NYHA/WHO Functional Class	
I	1.0%
II	27.3%
III	66.5%
IV	5.2%
6MWD (m)	272 (130.2)
NT-proBNP	3152.4 (3916)
Diabetes	27.9%
Systemic Hypertension	45.7%
Ischemic Heart Disease	17.9%
Atrial Fibrillation	22.2%
Creatinine (umol/L)	105.9 (66.7)
eGFR ($mL/min/1.73m^2$)	76.9 (40.7)
CKD Stage	
1-2 (eGFR>60)	57.9%
3 (eGFR 30-60)	34.8%
4-5 (eGFR<30)	7.3%
Echocardiography	
RV Systolic Dysf. (≥moderate)	41.6%
RV Dilation (≥moderate)	62.8%
Tricuspid Regurg (>mild)	19.8%
Pericardial Effusion (yes)	13.7%
Right Heart Catheterization	
mRAP (mm Hg)	7.9 (4.9)
mPAP (mm Hg)	44.9 (12.7)
PAWP (mm Hg)	10.2 (5.4)
Cardiac Index ($L\cdot min^{-1}\cdot/m^2$)	2.17 (0.6)
SVO_2 (%)	60.7 (11.3)
PVR (Woods Units)	9.8 (5.1)
Therapy (within 3 months after diagnosis)	
Monotherapy	83%
ERA	69%

PDE-5i/sGC	30.1%
PCA	0.6%
CCB	5 %
Combination Therapy	11.8%
Anticoagulation	38.2%

BMI= body mass index; 6MWD= 6-minute walk distance; NYHA= New York Heart Association; WHO= World Health Organization; Association; PAH= pulmonary arterial hypertension; eGFR= estimated glomerular filtration rate; CKD= chronic kidney disease; RV= right ventricle; mRAP= mean right atrial pressure; mPAP= mean pulmonary artery pressure; PAWP= pulmonary artery wedge pressure; SVO_2= mixed venous oxygen saturation; PVR= pulmonary vascular resistance; ERA= endothelin receptor antagonists; PDE-5= phosphodiesterase type 5 inhibitor; sGC= soluble guanylate cyclase; PCA= Prostacyclin analogues; CCB=calcium channel blockers.

2.4.3 Risk Stratification

a) Reclassification between risk algorithms

We implemented the four risk assessment algorithms (two REVEAL strategies and two ESC/ERS-based strategies) in our Ottawa cohort to externally validate and compare their performance. As the FPHR 2015 algorithm does not accept any missing variables, our validation cohort was reduced to the 189 patients without missing data. Patient stratification appears in Figure 2.2A. ESC/ERS-based assessment stratified a higher proportion of patients to intermediate risk than REVEAL-based assessment ($p<0.0001$), while REVEAL resulted in a greater number stratified to low risk. Specifically, using the ESC/ERS 2015 risk stratification algorithm (current international guidelines), 24%, 71% and 5% of patients were categorized as low, intermediate and high-risk, respectively (Figure 2.2B). To investigate reclassification between risk assessment strategies, patients in each of the ESC/ERS 2015 risk groups were re-stratified to the low, intermediate and high-risk categories according to the FPHR 2015, REVEAL and REVEAL 2.0 algorithms. There was little agreement between the risk scores with the weighted kappa ranging from 0.21-0.34 (Table 2.2). The REVEAL and REVEAL 2.0 had an excellent intraclass correlation coefficient (ICC) of 0.84 with their raw scores, but had a poor weighted kappa when grouped into three strata (Table 2.2). Each of the 4 risk strategies consistently identified high-risk patients; however, there was tremendous variability in how the risk tools identified low and intermediate risk patients (Figure 2.2B, Supplemental Table 2.1). Compared to the ESC/ERS guidelines, the REVEAL score tended to underestimate risk in intermediate and high-risk patients; whereas, both the REVEAL 2.0, and the FPHR 2015 models tended to overestimate risk in low and intermediate risk patients (Figure 2.2). However, these differences were not statistically significant.

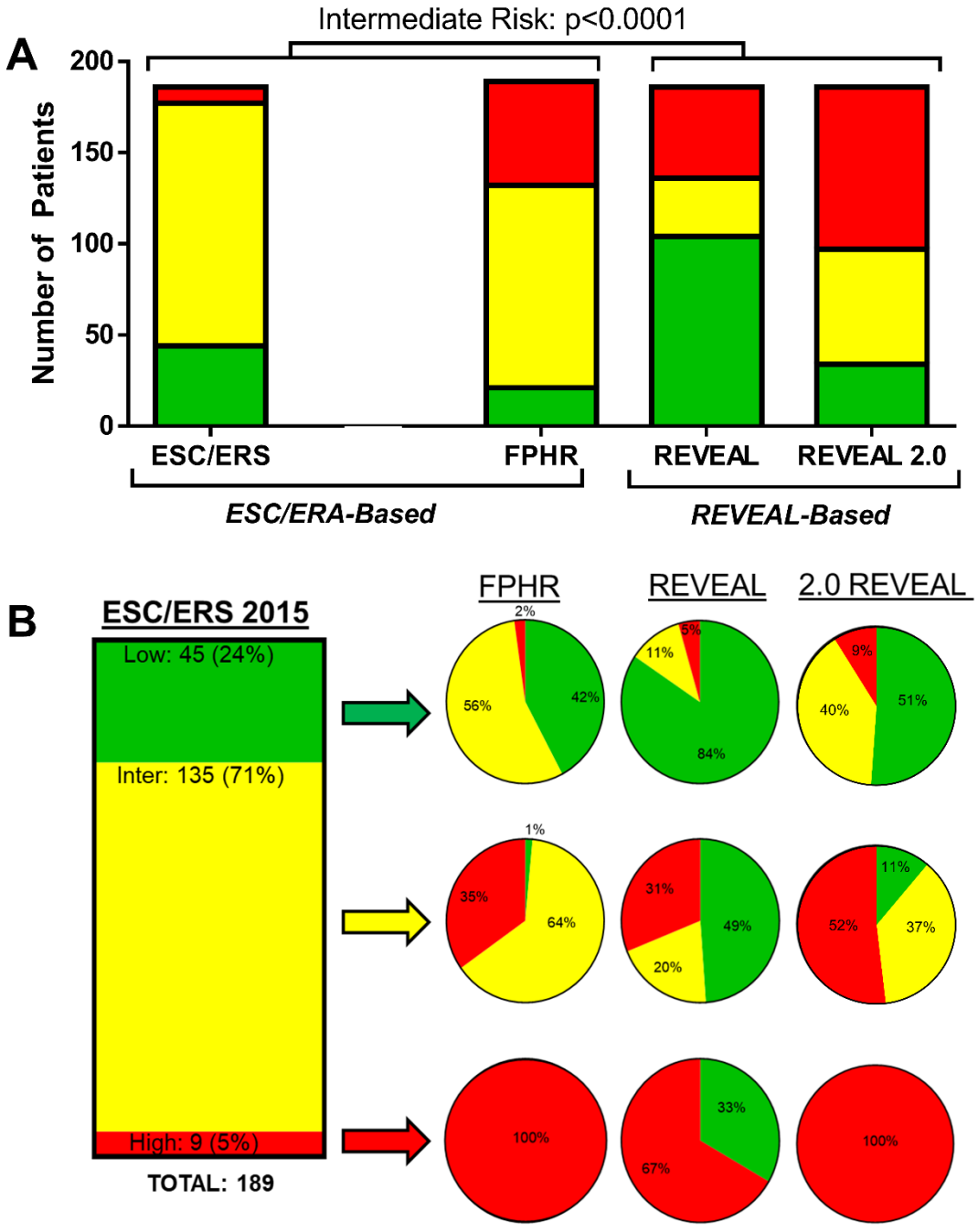

Figure 2.2 Number of patients stratified into Low, Intermediate and High Risk strata in accordance with ESC/ERS and REVEAL-Based strategies (A). Percent reclassification of ESC/ERS guidelines between FPHR and REVEAL risk assessment strategies (B).

Table 2.2: Agreement between risk stratification tools.

		Three Strata	Raw Scores
Comparison		***Weighted Kappa (95% CI)***	***ICC (95%CI)***
ESC/ERS	FPHR	0.35 (0.25-0.45)	-
	REVEAL 1.0	0.22 (0.14-0.29)	0.49 (0.37-0.58)
	REVEAL 2.0	0.25 (0.17-0.32)	0.61 (0.51-0.69)
FPHR	REVEAL 1.0	0.21 (0.13-0.29)	-
	REVEAL 2.0	0.34 (0.23-0.45)	-
REVEAL 1.0	REVEAL 2.0	0.43 (0.36-0.50)	0.84 (0.79-0.87)

ICC, intra-class correlation coeffient

b) Predicting Transplant-Free Survival: Baseline Assessment

Using baseline characteristics, the ESC/ERS 2015 guidelines (p=0.0002), REVEAL (p<0.0001) and REVEAL 2.0 (p<0.0001) algorithms were each able to stratified TFS into low, intermediate and high-risk groups (Figure 2.3); however, the observed TFS rates were quite variable for the 'intermediate' category across these tools. The parent FPHR 2015 model (5 categories) was also able to significantly stratify risk (5+yr Uno C-Statistic=0.58, 95%CI 0.52, 0.60; p=0.01; Supplemental Figure 2.3), but not when collapsed into three risk categories (p=0.07) (Figure 2.3B). In a sensitivity analysis of only iPAH patients (n=128), the three category FPHR 2015 model was not able to significantly stratify risk (p=0.15).

c) Risk Model Comparison:

Time-dependent ROC analysis and differences in Uno's concordance statistic was used to compare stratification strategies (Figure 2.4, Table 2.3). The REVEAL (5 yr Uno C-Statistic 0.70; 95%CI 0.64, 0.75) and REVEAL 2.0 (5 yr Uno C-Statistic 0.70; 95%CI 0.65, 0.74) risk stratification algorithms significantly outperformed the ESC/ERS 2015 guidelines (5 yr Uno C-Statistic 0.60; 95%CI 0.56, 0.65) and the FPHR 2015 strategies (5 yr Uno C-Statistic 0.56; 95%CI 0.47, 0.65) (both the 5 and 3 category score) for predicting 5-year TFS (Figure 2.4) and 5+-year TFS (Table 2.3). 5-year and 5+ year TFS risk discrimination was not different between the original REVEAL score and the updated REVEAL 2.0 (5 yr Uno C-Statistic 0.70, p=0.96). The 5 category FPHR 2015 and REVEAL 1.0 were compared to the other risk tools, but results were not different from their respective 3 category strategies.

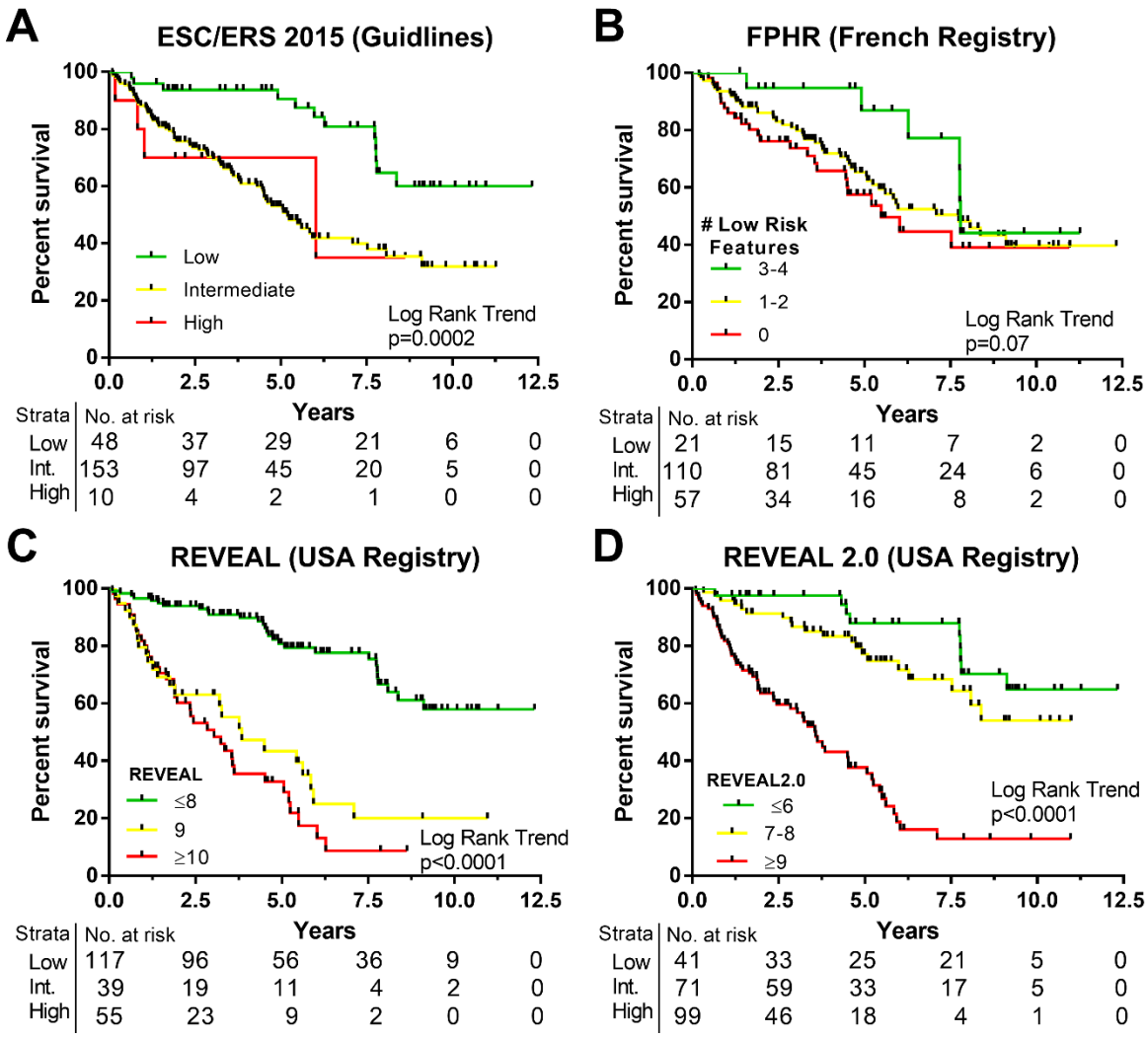

Figure 2.3. Contemporary Risk Tools and Survival. Kaplan-Meier curve analysis for long-term transplant free survival using contemporary risk models with baseline characteristics (at diagnosis).

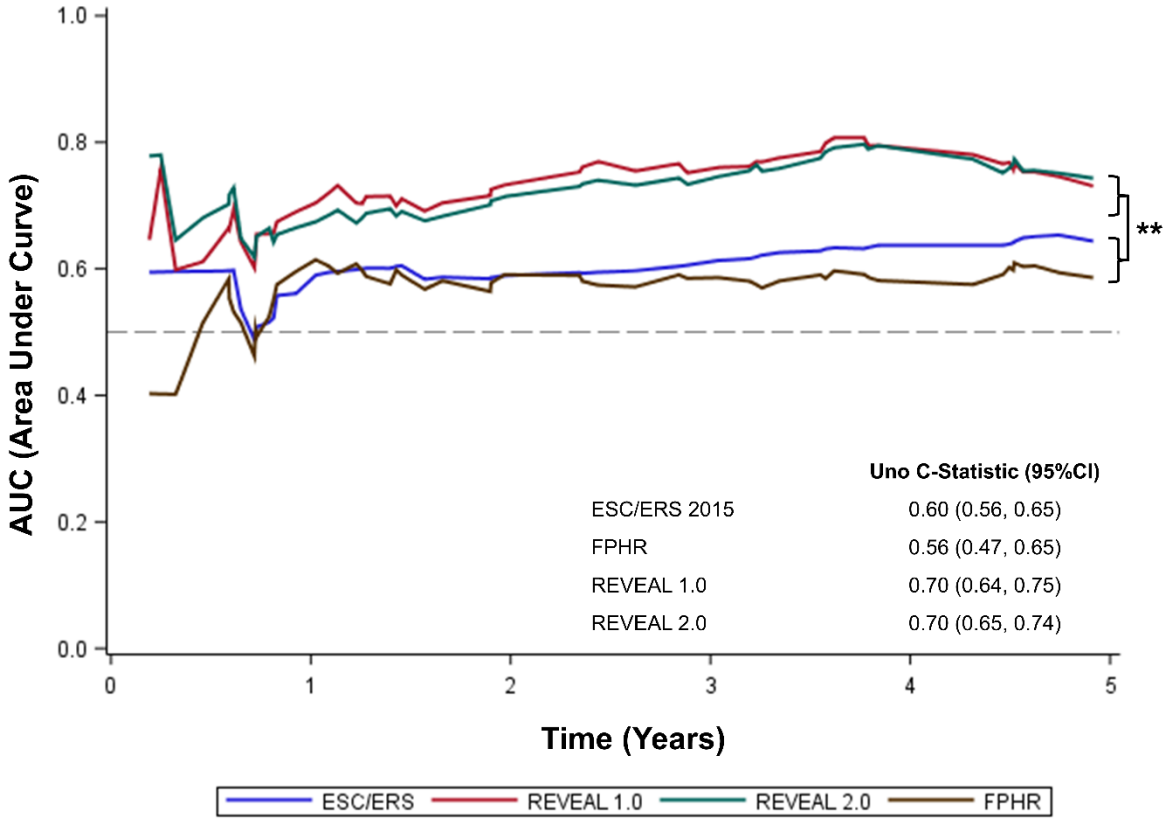

Figure 2.4. Contemporary risk model comparison for transplant free survival over 5 years from diagnosis. Models were compared using the time-dependent AUC. REVEAL-based risk assessment provided supervisor long-term TFS risk discrimination, as compared to ESC/ERS-based assessment. **p<0.01.

Table 2.3 Model Comparison: Time-Dependent Area Under the Curve (Differences in Uno C-Statistic). Three Strata Models.

Comparison		5-Year Transplant Free Survival			5+ Year Transplant Free Survival		
		Δ C-Statistic	**Standard Error**	**p-value**	**Δ C-Statistic**	**Standard Error**	**p-value**
ESC/ERS	REVEAL 1.0	-0.0913	0.0382	0.0169	-0.0971	0.0338	0.0041
ESC/ERS	REVEAL 2.0	-0.0847	0.0293	0.0039	-0.0961	0.0287	0.0008
ESC/ERS	FPHR	0.0382	0.0411	0.3518	0.0471	0.0328	0.1510
REVEAL 1.0	REVEAL 2.0	0.0066	0.0211	0.7529	0.0010	0.0199	0.9591
REVEAL 1.0	FPHR	0.1296	0.0525	0.0136	0.1442	0.0455	0.0015
REVEAL 2.0	FPHR	0.1229	0.0492	0.0125	0.1432	0.0363	<0.0001

2.4.4 Kidney Function and Likelihood of Transplant-Free Survival

At diagnosis, patients with normal or stage 1-2 CKD (eGFR≥60 mL/min/1.73m^2) had a more favorable prognosis (Figure 2.5A). In contrast, the risk of death or transplantation increased with higher CKD staging at diagnosis and at 6 months (Figure 2.5A/B). In REVEAL 1.0, renal function was included as a "loosely defined qualitative item according to physician's discretion".[284] In our Ottawa cohort, patients identified as having CKD had a mean eGFR of 29 ± 3 mL/min/1.73m^2 (Supplemental Figure 4). ROC analysis for physician assessment revealed an optimal eGFR cutoff of 46.3 mL/min/1.73m^2, which is discrepant from the 60 mL/min/1.73m^2 cutoff now incorporated into REVEAL 2.0 (Supplemental Figure 2.4B).

In our population, 35% of patients had deteriorating renal function over 6 months of follow up (>10% decrease in eGFR); whereas, 41% and 24% of patients had stable or improved renal function, respectively. Overall, deteriorating renal function was associated with a nearly 2-fold increase in mortality rate as compared to no change in renal function ($p<0.001$; Figure 2.5C). Changes in eGFR of less than 10% did not change survival (Figure 2.5C). Deteriorating renal function was also associated with a worse prognosis after multivariate adjustment (Table 2.4). The addition of baseline eGFR and the change in eGFR (during the first 6 months after diagnosis) to the 2015 guidelines (ΔC-statistic=0.063 SE=0.026, p=0.01) and the REVEAL 1.0 score (ΔC-statistic=0.029 SE=0.013, p=0.03) was associated with significantly improved discrimination for both models (Table 2.5). The addition of baseline kidney function also improved the discrimination of the FPHR 2015 strategy, albeit not reaching statistical significance (ΔC-statistic=0.064 SE=0.034, p=0.057).

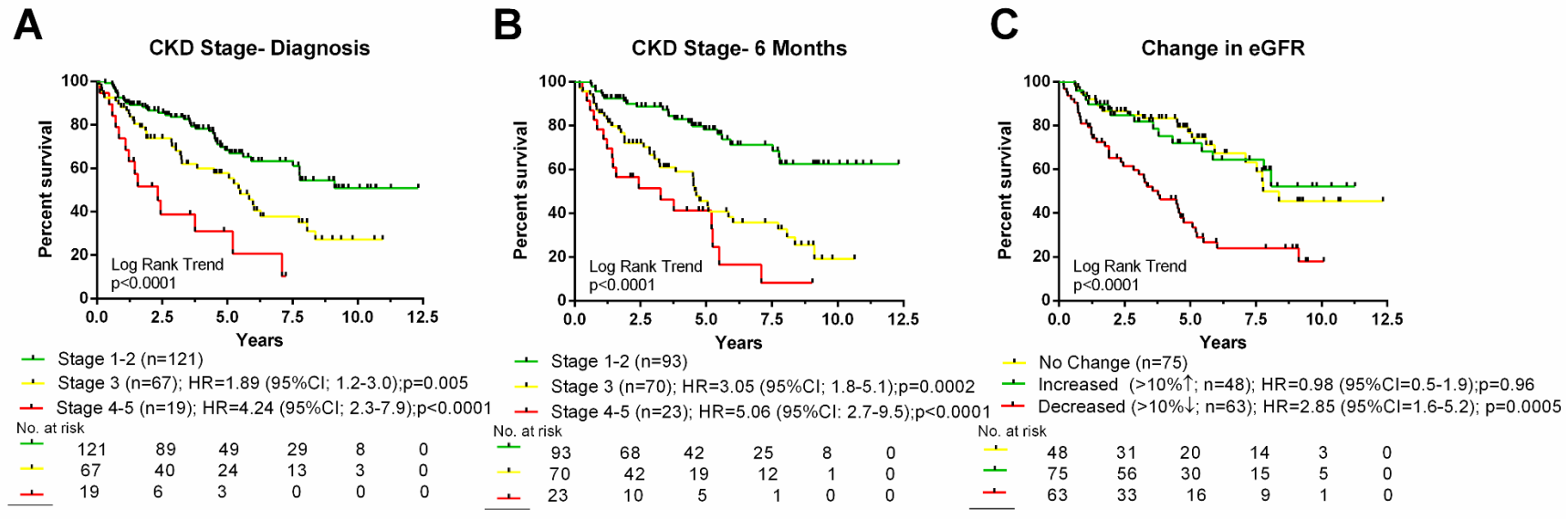

Figure 2.5. Kidney Function and Survival. Kaplan-Meier curve analysis for Transplant free survival. Patients were stratified according to CKD stage at diagnosis (A), at 6 months (B), and change in kidney function from diagnosis to 6 months (C).

2.4.5 Re-Stratifying ESC/ERS-Based "Intermediate Risk'

ESC/ERS-based risk assessment categorized the majority of our PAH cohort as intermediate risk. Importantly, inclusion of presence or absence of renal dysfunction (eGFR<60 mL/min/1.73m^2) at diagnosis or deteriorating renal function (>10%↓ in eGFR) re-stratified many intermediate-risk patients into higher and lower-risk groups, respectively (Figure 2.6 A/B and C/D).

Table 2.4: Models of Survival for change in Kidney Function (diagnosis to 6 months).

Model and Risk Factor	Hazard Ratio (95%CI)	p-value
Survival		
Adjusted for:		
-baseline eGFR		
Increased vs no change	0.83 (0.43-1.59)	0.57
Decreased vs no change	2.47 (1.48-4.12)	0.0006
Adjusted for:		
-baseline eGFR		
-baseline NYHA Class		
-baseline 6MWD		
Increased vs no change	0.75 (0.37-1.52)	0.42
Decreased vs no change	2.24 (1.30-3.85)	0.0037
Adjusted for:		
-baseline eGFR		
-Etiology at enrollment (i.e. CTD vs all others)		
Increased vs no change	1.19 (0.62-2.30)	0.59
Decreased vs no change	3.02 (1.67-5.47)	0.0003

Table 2.5 Addition of kidney dysfunction to model algorithm improves risk discrimination.

	Addition of CKD Staging at Diagnosis			**Addition of ΔeGFR (6 month–diagnosis)**		
	Δ C-Statistic	Standard Error	p-value	Δ C-Statistic	Standard Error	p-value
ESC/ERS 2015	0.0632	0.0257	0.0138	0.0901	0.0357	0.0116
REVEAL 1.0	0.0286	0.0134	0.0330	0.0496	0.0233	0.0332
REVEAL 2.0*	-	-	-	-	-	-
FPHR	0.0641	0.0337	0.0569	0.0730	0.0414	0.0776

*REVEAL 2.0 already incorporates eGFR into the risk score.

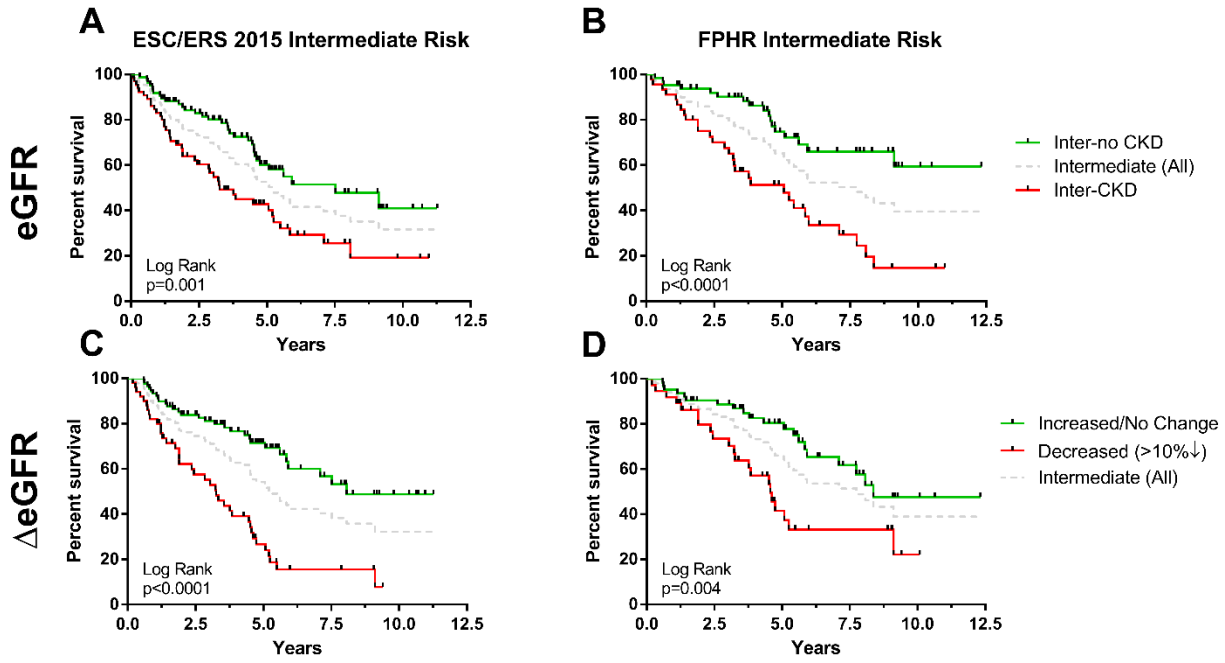

Figure 2.6. Kidney Function Refines Risk Assessment. ESC/ERS-based Intermediate risk groups (in grey) re-stratified based on the presence of Kidney disease (A,B), the change in kidney function from diagnosis to 6 months (C,D).

2.5 Discussion

Clinical practice guidelines endorse risk assessment for each patient with PAH to better define individual-specific prognosis and treatment goals.[75,76] The utility of the available risk assessment tools is evident, yet the uptake and compliance amongst pulmonary hypertension centers remains uneven. Uptake is further impeded by the number of different risk tools available to clinicians without a clear indication as to which provides the most robust risk discrimination. The perceived complexity of these tools and number of variables required to calculate risk may also limit their utility, making it more likely that clinicians will rely solely on their clinical judgement to guide therapeutic management. However, a recent study by Simons et al. (2019) showed clinical gestalt resulted in significant discordance in risk assessment compared to ESC/ERS calculated risk.[86] In this study, 80% of the patients judged to be at low-risk by physicians were actually at a higher-calculated risk. Nonetheless, in the present analysis of the Ottawa cohort, we demonstrate substantial heterogeneity in the prognostic accuracy across contemporary PAH risk assessment tools, and describe three major findings: 1) REVEAL-based risk strategies have superior long-term TFS risk discrimination than ESC/ERS-based assessments, including current guidelines and the FPHR 2015 strategy; 2) significant risk reclassification across the risk tools which is particularly evident for the intermediate-risk group which often comprises >70% of a PAH population; 3) the prognostic importance of kidney function in PAH risk assessment, which to date has not been incorporated into contemporary guidelines. We also provide novel data that kidney function can independently re-stratify ESC/ERS intermediate-risk patients into ‘low’ and ‘high’ risk-like portfolios.

The present study is the first to implement contemporary risk assessment strategies in a Canadian PAH population. An important finding of our study was that the REVEAL 1.0 and REVEAL 2.0 discriminated long-term TFS risk in our cohort more accurately than the ESC/ERS 2015 guidelines and the FPHR 2015 strategy. These results corroborate recent evidence demonstrating superior risk discrimination with the REVEAL 2.0 as compared to the COMPERA and FPHR 2015 risk strategies (both derivatives of the ESC/ERS 2015 guidelines).[81] Benza et al. suggested that the superior performance may be attributable, in part, to the number of variables captured in these risk tools (i.e. 13 vs 6 variables; REVEAL 2.0 and COMPERA, respectively). [81,83] In our Ottawa cohort, we provide the most comprehensive risk assessment to date, incorporating up to 10 of the 12 variables mandated in the ESC/ERS 2015 guidelines. Interestingly, incorporating more variables did not translate to superior prognostication. Overall, ESC/ERS guidelines and the REVEAL strategies have taken markedly different approaches to risk assessment with respect to, i) methods for variable selection, 2) the variables incorporated (only 5 of 21 variables in common), and iii) methods to calculate individual risk. The REVEAL models are statistically derived, whereas ESC/ERS models are generated from expert consensus. Although speculative, it is plausible that REVEAL's superior prognostication may be attributable to incorporating both modifiable and nonmodifiable risk factors and the weighting of important prognostic variables, whereas risk tools derived from the ESC/ERS guidelines do not weight variables and do not include non-modifiable risk factors.[75,83,87,280] In our Ottawa cohort, the majority of patients were categorized as intermediate risk (>70%) by the ESC/ERS and FPHR tools; however, with the addition of baseline renal function, intermediate-risk patients can be further segregated into low and high-risk groups. Interestingly, intermediate-risk patients with

CKD had a prognosis similar-worse than patients stratified as high-risk at baseline. The dichotomy between statistically (REVEAL) versus clinically derived (ESC/ERS) variables may also be important, particularly in a population that is so heterogeneous. Taken together these results suggest that the use of ESC/ERS-based risk strategies may incompletely discriminate long-term TFS.

A key finding of our study was the ability of baseline eGFR to robustly re-stratify ESC/ERS-based risk strategies. The prognostic importance of kidney function was recently demonstrated in the REVEAL registry by Chakinala et al., in which a ≥10% decrease in eGFR was associated with a 66% increase in risk of 1-year mortality.[284] Measures of kidney function were subsequently incorporated into the REVEAL 2.0, which represents the first PAH risk tool to include this potentially modifiable risk factor.[81] Our results meaningfully extend this finding by demonstrating for the first time that eGFR can better stratify patients identified by ESC/ERS-based strategies as intermediate-risk into 'low' and 'high' risk-like strata. While the pathophysiology of kidney dysfunction in PAH remains to be fully elucidated, reduced cardiac output and systemic venous congestion (Type 2 cardiorenal syndrome) have been implicated.[279,286–288] Thus, from a risk standpoint, renal dysfunction may simply represent an end organ manifestation of PAH and related RV failure, and thus yield greater prognostic value (downstream risk factor). Unlike other types of kidney injury, Type 2 cardiorenal syndrome is potentially preventable with early diuretic therapy and by supporting the failing RV with inotropes.[289] We further demonstrate that a decline in eGFR at 6 months was associated with worsening long-term survival. Kidney dysfunction stimulates neurohormonal and RAAS system activation engendering worsening fluid balance and RV function (Type 4 cardiorenal syndrome).[279,284,287] A decrease in renal function may be a harbinger of both RV dysfunction and

further PAH disease progression. However, further research is needed to confirm whether declining eGFR is a sentinel biomarker in prospective cohorts.

2.6 Limitations

We recognize that the retrospective design of the present study represents a limitation. Although our database is relatively complete, missing data is inevitable; for example baseline BNP was only available in 14% of patients since these were not routinely measured at our institution until 2015. While we recognize the prognostic value of BNP, our results are likely more generalizable to many PH centers where natriuretic peptide values are still not commonly accessible. There is a general consensus that serial assessment of risk provides additional prognostic information, with treatment goals aimed at achieving a low-risk profile, whereas we present data only on baseline risk assessment in incident PAH patients. Nonetheless, serial data is not usually available at the time that crucial treatment decisions are made for new PAH patients making incident risk assessment germane for this group, and particularly relevant as we evolve towards more aggressive upfront medical management. Understanding long-term survival in the various risk categories is critically important, when early upfront management is being considered, from a clinical management and a patient prognosis perspective. Similar to REVEAL[284], our study reports only on serial assessment of renal function at 1 year and 6 months, respectively, and future research needs to ascertain the importance of longer-term renal assessments. Finally, our cohort includes patients that were entered over a long period in time over which management for PAH has changed; however, this is a limitation for any study of long-term data that spans more than a decade.

2.7 Conclusion

In our cohort of mixed group 1 PAH patients, the updated REVEAL 2.0 had similar long-term TFS risk discrimination as the original calculator but superior discrimination as compared to the current ESC/ERS guidelines and the FPHR strategies. Our study highlights potential limitations of ESC/ERS-based risk assessment strategies, namely a lack of weighting which dilutes the importance of high-risk features. The lack of risk stratification agreement across contemporary risk strategies identifies the need for consistency across tools, especially in the cohort of intermediate risk patients. An important finding of our study was validating the importance of renal function to prognosis, as originally described in REVEAL. This has the potential to re-stratify ESC/ERS intermediate risk into lower and high risk strata. Our work highlights key limitations of the ESC/ERS-based risk assessment, and suggests that incorporating measures of kidney function are important strategies moving forward. We have recently developed a simplified and robust risk algorithm that incorporates this important modifiable risk factor. Validating this model is the subject of our current work.

2.8 Acknowledgments

Sources of Funding: Jason Zelt is an MD/PhD student at the University of Ottawa Funded, in part, by Vanier Canada Graduate Scholarship and the University of Ottawa. Dr. Mielniczuk is supported by an award from the Heart and Stroke Foundation of Ontario, and is a Tier 2 Chair in HF Research at the University of Ottawa.

Disclosures:

Dr. George Chandy: Advisory Board, Consultant, Travel grants, Speakers Bureau for Actelion Pharmaceuticals and Bayer Pharmaceuticals. Institutional Research: Actelion Pharmaceuticals, Bayer Pharmaceuticals, Northern Therapeutics.

Dr. Lisa Mielniczuk: Advisory Board member, Consultant, Travel grants, Speakers Bureau for Actelion Pharmaceuticals and Bayer Pharmaceuticals. Institutional Research: Actelion Pharmaceuticals, Bayer Pharmaceuticals, Northern Therapeutics

Dr. Sanjay Mehta: Advisory Board member, Consultant, Travel grants, Speakers Bureau for Actelion Pharmaceuticals and Bayer Pharmaceuticals. Institutional Research: Actelion Pharmaceuticals, Bayer Pharmaceuticals, Northern Therapeutics.

Other authors have no disclosures.

2.9 Chapter 2 Extension

i) Ottawa PAH Risk Score

Development of the Ottawa PAH Risk Score:

Clinically relevant variables previously identified in the REVEAL registry and European ESC/ERS 2015 guidelines and thought to yield prognostic value were entered into a stepwise multivariable Cox regression model. NYHA class was removed because of co-linearity with 6-minute walk distance (6MWD). 6MWD was judged to be more clinically useful, given that it is a continuous variable and an objective measure, in contrast to NYHA which is more subjective. An α level of 0.05 was used for model entry, and an α level of 0.10 was selected for variable removal. The final model identified a patients: i) sex, ii) 6-minute walk distance (6MWD), iii) eGFR, and iv) mixed venous oxygen saturation (SVO_2). The 6MWD and SVO_2 variables were dichotomized for ease of use in the subsequent risk score development. The Cox proportional

hazard statistic was used to estimate the influence of these 4 risk factors on time (years from PAH diagnosis) to reaching the primary endpoint of transplant or death. To develop a practical prognostic score, we assigned these four risk factors weighted points proportional to the β regression coefficient values, and rounded to the nearest integer.

Table 2.6. Cox proportional-hazards model for the Ottawa PAH Risk Score.

Parameter	Parameter Estimate	Standard Error	Chi-Square	P-value
Gender (male)	0.51712	0.23928	4.6705	0.0307
Renal Dysf. (<60)	0.66391	0.23853	7.7467	0.0054
6MWD (<330m)	1.10156	0.31728	12.0539	0.0005
SVO2 (<60%)	0.76007	0.24660	9.4995	0.0021

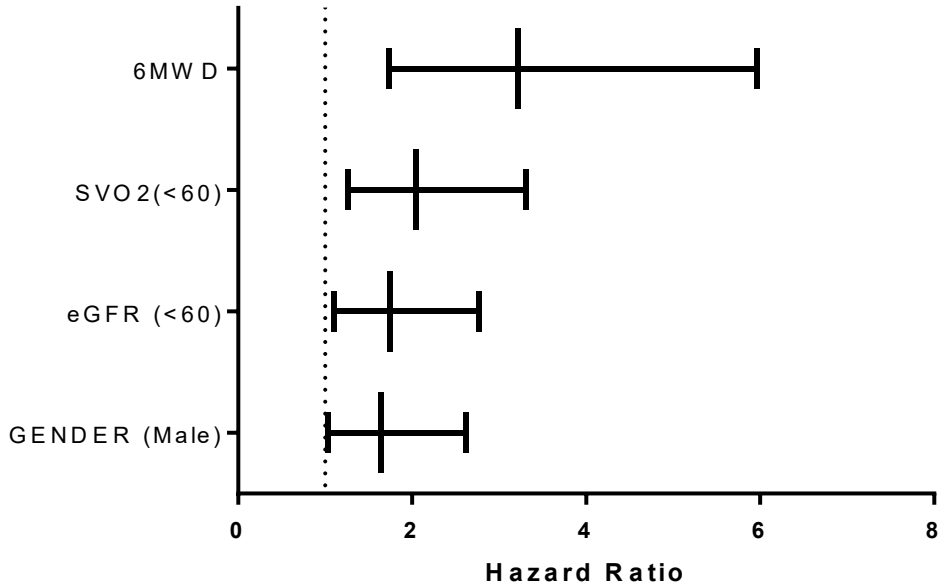

Figure 2.7. Adjusted forest plot for variables in the Ottawa PAH Risk Score.

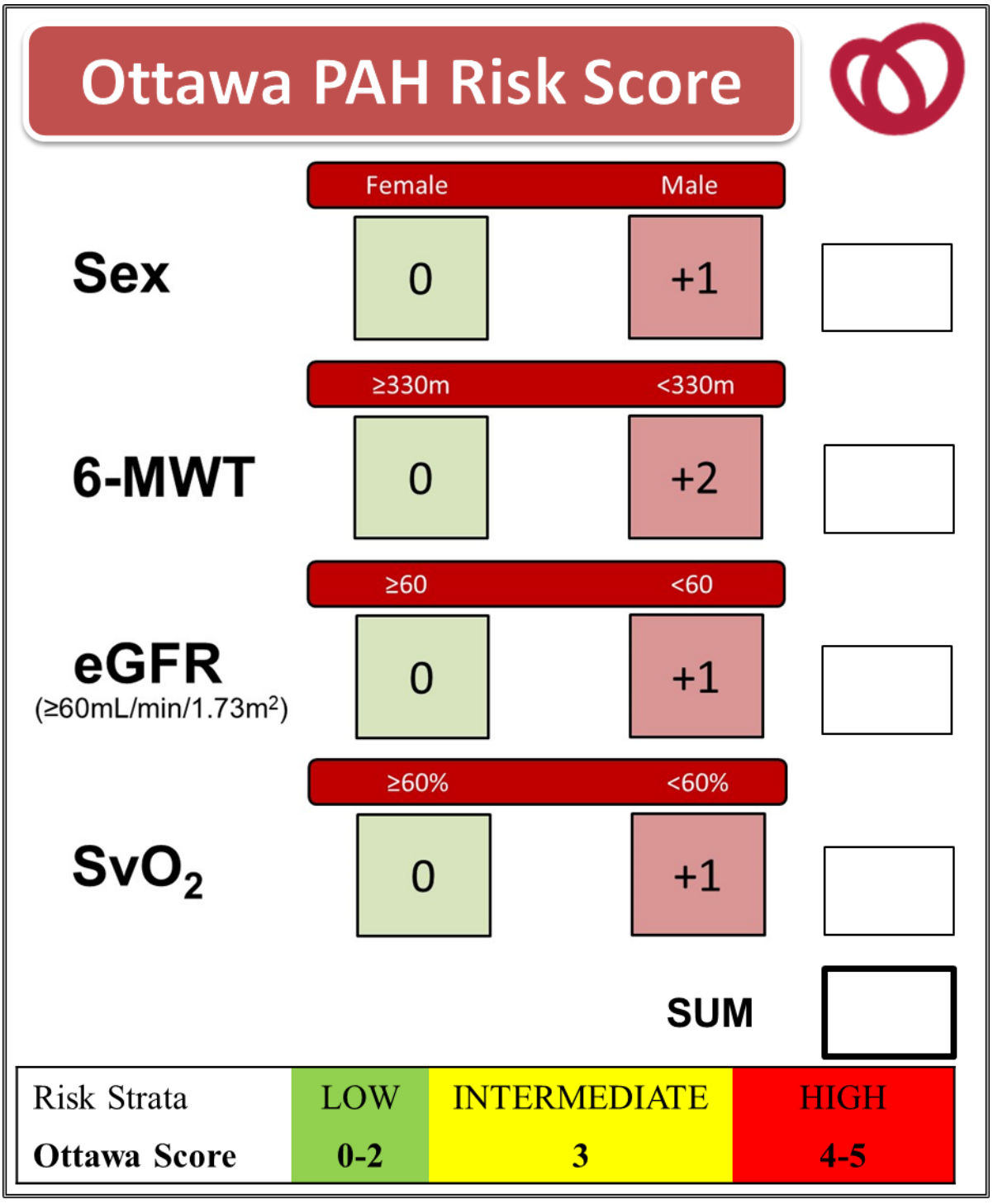

Figure 2.8. The Ottawa PAH Risk Algorithm.

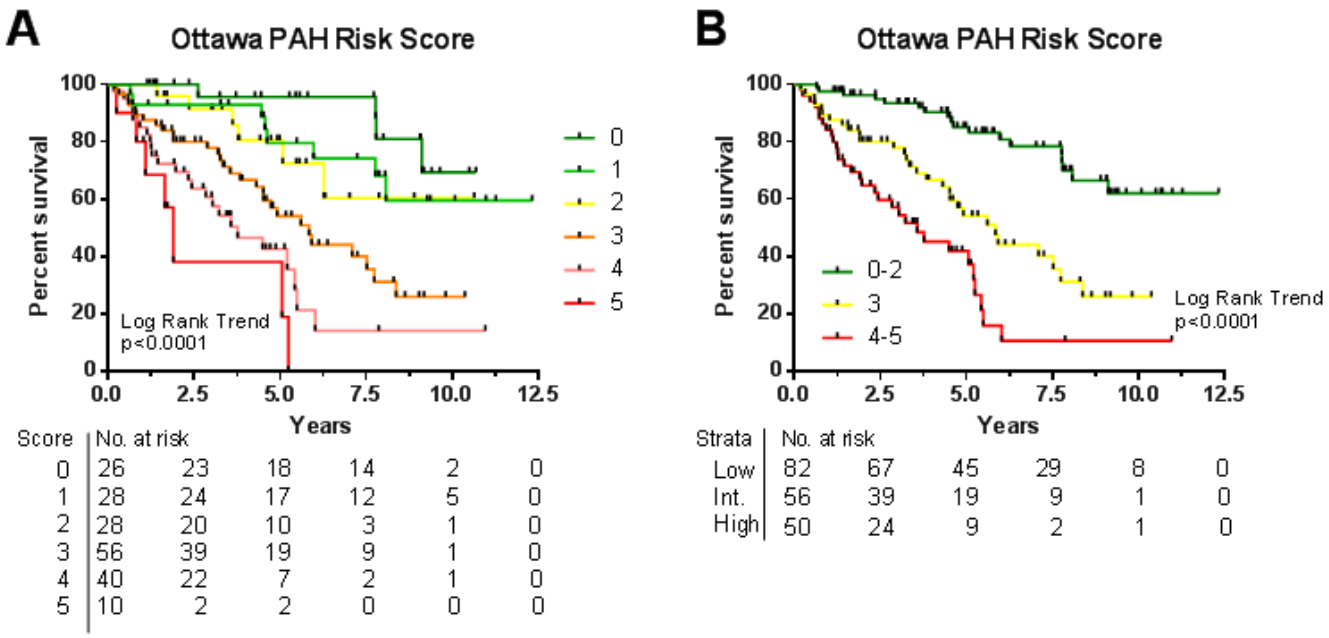

Figure 2.9. Ottawa Risk Score and long-term survival. Kaplan-Meier curve analysis for Transplant free survival stratified by risk in accordance with the Ottawa PAH Risk score (A). The Ottawa Risk Score three category score (three strata). Data is from the derivation cohort. Validation of the risk score is pending.

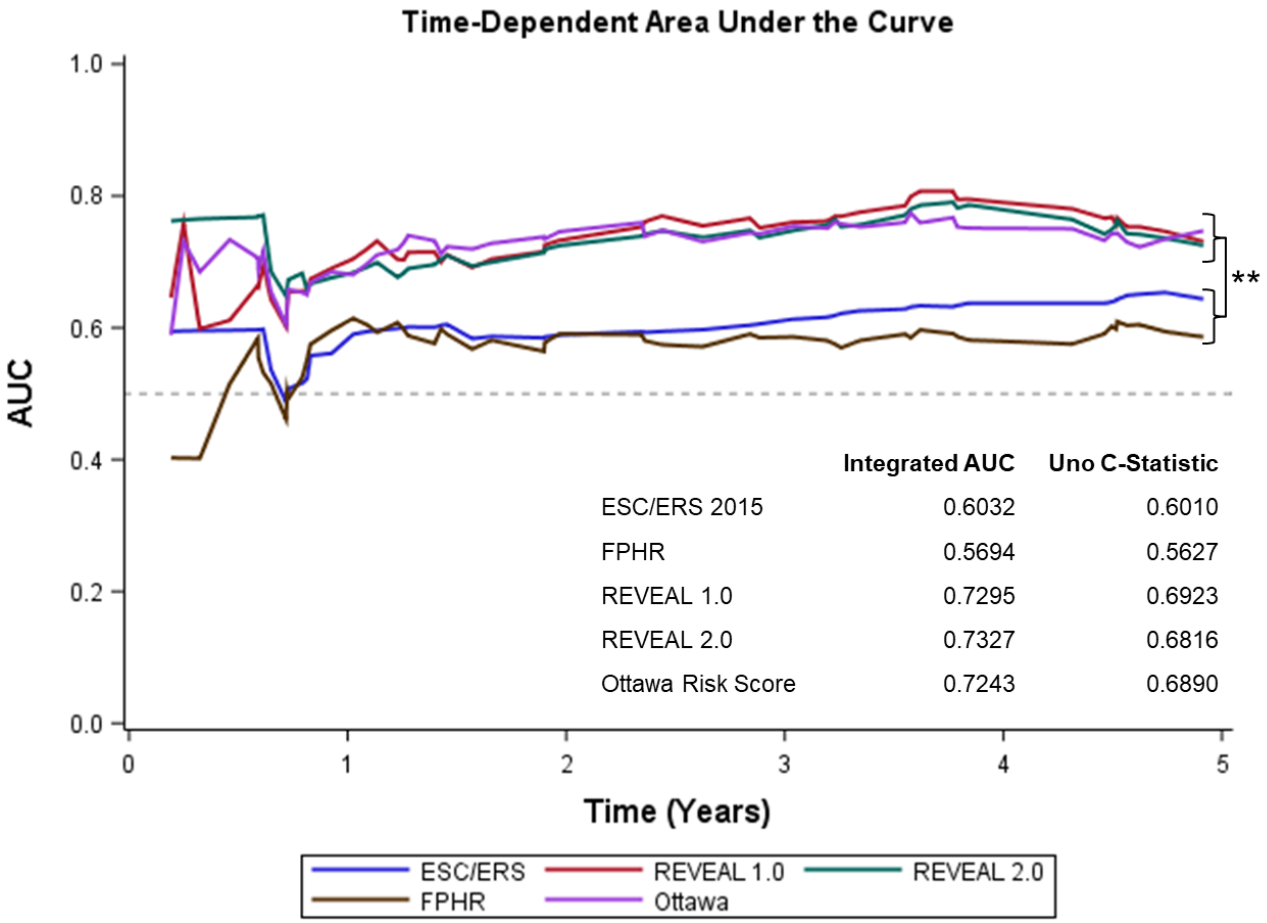

Figure 2.10. Model Comparison: Performance of the Ottawa Risk Score. Model compared using the time-dependent AUC. The Ottawa Risk Score had similar discrimination as the REVEAL-based strategies, but superior to the ESC-ERS-based assessment. **p<0.01.

ii) RV Function

Qualitative assessment of RV systolic function and morphology on transthoracic echocardiography was documented at diagnosis. RV function at the 6month-1year follow-up assessment emerged as a powerful marker of prognosis. We further demonstrate that patients whose RV function fails to improve or decreases have a worse prognosis. This adds to the growing body of literature that how the RV responds to PAH-specific therapy is a critical marker of prognosis.

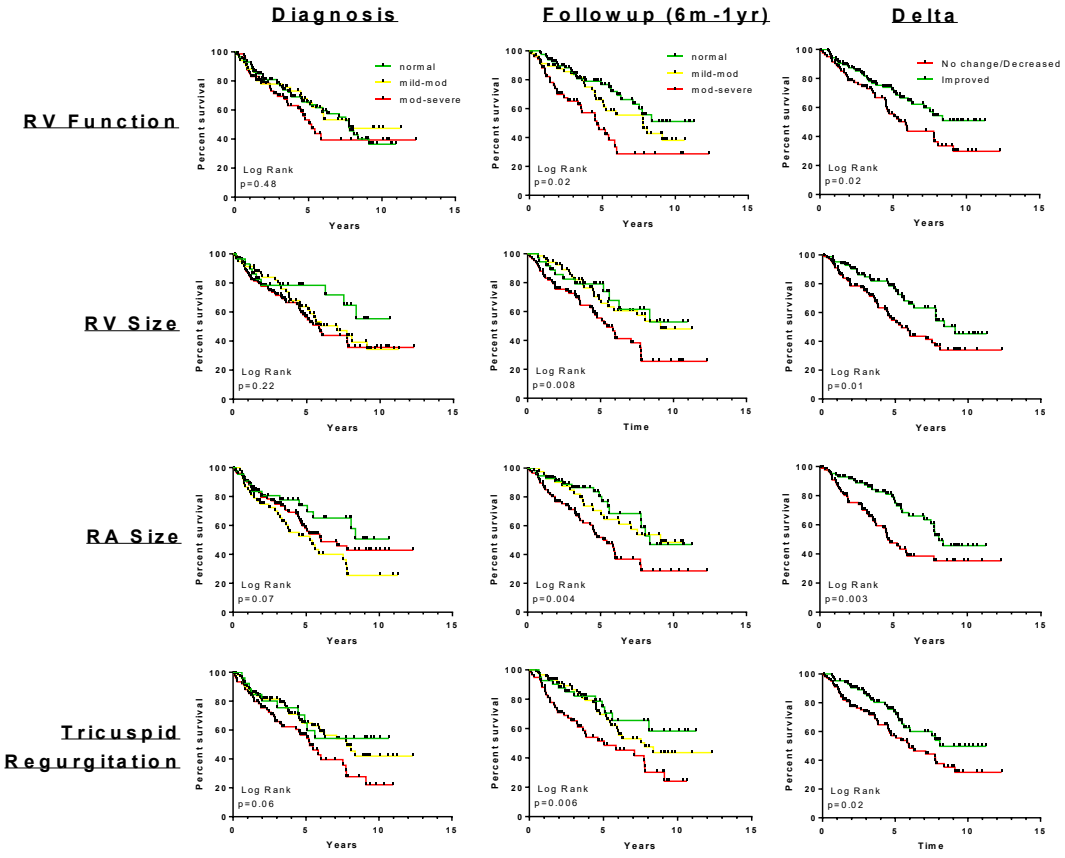

Figure 2.11. RV function assessed on echo and survival. Kaplan-Meier curve analysis for Transplant free survival. Patients were stratified according to qualitative echocardiography assessment of RV function, RV Size, Right atrial size, and tricuspid regurgitation (D), at diagnosis and follow-up.

RV ejection fraction is one of the most important predictors of prognosis in many cardiovascular disease states, including PAH[2,290,291], moderate left HF[292] , HF with preserved ejection fraction[88] and advanced left heart failure.[293] Despite the significance of RV function to survival, there are no therapies that directly nor selectively improve RV function. As well, the basis for RV failure is poorly understood. The RV hypertrophies in response to increased RV afterload, an initial adaptive response. However, there is heterogeneity in RV hypertrophy—its effects on cardiac output and the likelihood of progression to RVF—that is not explained by differences in RV mass or degree of afterload.[91] While the remodeling process is best viewed as a continuum, studies often dichotomize these processes into adaptive or maladaptive phenotypes, the latter being associated with reduced RV function, RVF and poor outcomes (i.e., decompensated RV remodeling).[294] ***The subsequent thesis chapters will explore two potential driving mechanisms of maladaptive RV remodeling in PAH, 1) neurohormonal/sympathetic influences and 2) impaired RV energetics. Molecular imaging using radiotracers for PET will be employed in small animal models of PAH and RHF. Applying clinically available imaging techniques to preclinical models have the unique potential for translational studies in human subjects for further explore disease mechanisms.***

Chapter 3

[11C]meta-Hydroxyephedrine PET Evaluation in Experimental Pulmonary Arterial Hypertension: Effects of Carvedilol on Right Ventricular Sympathetic Function.

Zelt et al. 2020, *Journal of Nuclear Cardiology (In Press)*

Running Title**:** SNS imaging and β-Blockade in PAH

Authors: **Jason G.E. Zelt MSc**[a,b,c], Sarah Schock PhD[d], Robert A.deKemp PhD[a] , Duncan J. Stewart MD[b,c,e], William A. Staines PhD[d], Ali Ahmadi MD[a], PhD, Rob Beanlands MD[a,b,c], and Lisa M Mielniczuk MD,MSc[a,b,c]

[a]Molecular Function and Imaging Program, The National Cardiac PET Centre, Division of Cardiology, Department of Medicine and the Cardiac Research Methods Centre, University of Ottawa Heart Institute and University of Ottawa, Ottawa, Canada.
[b]Department of Cellular and Molecular Medicine, Faculty of Medicine, University of Ottawa, Ottawa, Canada.
[c]Division of Cardiology, University of Ottawa Heart Institute and University of Ottawa, Ottawa, Canada.
[d]Department of Biochemistry Microbiology and Immunology, Faculty of Medicine, University of Ottawa, Ottawa, Canada.
Ottawa, Canada.
[e]Sinclair Centre for Regenerative Medicine, Ottawa Hospital Research Institute, Ottawa, Canada.

Author Contributions:
JGEZ: Conception of study design, performed the experiments and wrote the manuscript
AA: Technical assistance
SS, WAS: Technical assistance with immunohistochemical techniques
RAD. RB" Technical assistance with PET analysis
DJS: PAH content expert and critical review of the manuscript
LM: PI on the project. Conception of study design, wrote and critical review of the manuscript.

Key Words: Sympathetic Nervous System, Positron Emissions Tomography, Beta adrenergic blockade, Pulmonary Arterial Hypertension, Right Heart Failure.

3.1 Abstract

Background: Little is known about the sequelae of chronic sympathetic nervous system (SNS) activation in patients with pulmonary arterial hypertension (PAH) and right heart failure (RHF). We aimed to, 1) validate the use of [^{11}C]-*meta*-hydroxyephedrine(HED) for assessing right ventricular (RV) SNS integrity, and 2) determine the effects of β-receptor blockade on ventricular function and myocardial SNS activity in a PAH rat model.

Methods: PAH was induced in male Sprague-Dawley rats (n=36) using the Sugen+chronic hypoxia model. At week 5 post-injection, PAH rats were randomized to carvedilol (15 mg/kg/day oral;n=16) or vehicle (n=15) for 4-weeks. Myocardial SNS function was assessed with HED positron emission tomography(PET).

Results: With increasing PAH disease severity, immunohistochemistry confirmed selective sympathetic denervation within the RV and sparing of parasympathetic nerves. These findings were confirmed on PET with a significant negative relationship between HED volume of distribution(DV) and right ventricular systolic pressure (RVSP) in the RV ($r=-0.90$, $p=0.0003$). Carvedilol did not reduce hemodynamic severity compared to vehicle. RV ejection fraction (EF) was lower in both PAH groups compared to control ($p<0.05$), and was not further reduced by carvedilol. Carvedilol improved SNS function in the LV with significant increases in the HED DV, and decreased tracer washout in the LV ($p<0.05$) but not RV.

Conclusions:

PAH disease severity correlated with a reduction in HED DV in the RV. This was associated with selective sympathetic denervation. Late carvedilol treatment did not lead to recovery of RV function. These results support the role of HED imaging in assessing SNS innervation in a failing right ventricle.

3.2 Introduction

Drugs that target neurohormonal activation, once thought to be contraindicated, are now a cornerstone of management for patients with left ventricular (LV) systolic dysfunction. Our understanding of right heart failure (RHF) has lagged behind and its management remains largely symptomatic and often palliative. Many proven targeted therapies for left heart failure (LHF) either do not appear to provide similar benefits or have not been rigorously tested in RHF. Indeed, this is particularly relevant for patients with pulmonary arterial hypertension (PAH), where chronic pressure overload heralds RHF and represents the leading cause of morbidity and mortality.[295]

There is little doubt that LHF is a state of chronic sympathetic nervous system (SNS) activation, perpetuating the cycle of pathological remodeling and further LV dysfunction.[160] SNS hyperactivation is also thought to be implicated in PAH[149]; however, the role of similar mechanisms in progression of RV failure is not well understood. Pharmacologic blockade of the SNS with β-adrenergic receptor blockers (β-blockers) remains one of the most efficacious therapies for patients with LV systolic dysfunction.[241] There is interest in whether any similar efficacy exists for the failing RV, but β-blocker therapy is generally believed to be contraindicated unless required to treat a comorbidity.[242] Results from experimental models of PAH have suggested that if given early in disease progression prior to development of RV dysfunction, β-blocker therapy can prevent pathological RV remodeling and preserve systolic

function.[99,296] However, given the insidious nature of progressive pulmonary remodeling, patients often present late in the disease once RV dysfunction has developed. It remains to be determined whether these therapies can reverse established RV dysfunction later in disease progression, at a time that is clinically relevant. Several early-phase clinical studies using β-blockers in patients with PAH have produced conflicting findings suggesting no improvement in RV function or even harm.[246,297,298] These disparate results necessitate further rigorous preclinical studies to shed light on this important clinical question. Furthermore, no previous study has evaluated the effects of beta blocker on RV sympathetic integrity and function.

The objectives of the present study were to evaluate whether [^{11}C]HED PET imaging can be used to non-invasively assess RV sympathetic function and to correlate RV [^{11}C]HED imaging with histochemical evaluation of RV sympathetic and parasympathetic nerve density. We also aimed to determine if chronic β-blocker therapy can 1) reverse RV dysfunction and pathological remodeling and 2) improve RV SNS integrity in the Sugen chronic hypoxia (SuHx) model of PAH using PET imaging. The present study is the first to comprehensively assess sympathetic function within the failing RV using non-invasive PET imaging, which has the unique ability to be translated from preclinical studies to clinical patients.

3.3 Methods

All animal received humane care and procedures conformed to the guiding principles of the National Institute of Health's Guide for the Care and Use of Laboratory Animals, and were approved by the University of Ottawa Heart Institute Animal Care Committee.

3.3.1 Animal Model of Severe PAH

The Sugen Hypoxia animal model (SuHx) of severe PAH and RHF was used as previously described.[99] Briefly, severe angioproliferative PAH and RHF was induced in 7-week old male Sprague-Dawley rats (n= 36; Charles River Laboratories, Montreal, QC; body weight ~150-175g) by a single subcutaneous injection of Sugen5416 (20 mg/kg; Tocris/R&D Biosystems, MN) combined with 3 weeks of exposure to chronic hypoxia (10% O_2). This was followed by 2 weeks of re-exposure to normoxia (21% O_2). At 5-weeks post Sugen5416 injection, rats were randomly stratified into two groups. For the next 4 weeks, rats received either (i) vehicle control or (ii) carvedilol (15mg/kg/day orally). An age-matched healthy group of control rats, under normoxic conditions (n=4) were run in parallel. After 4 weeks of treatment, rats underwent right heart catheterization for pressure measurements. Rats were then sacrificed under a high level of general anesthetic (5% isoflurane). The heart was excised and the ventricles were dissected from the atria, aorta and pulmonary trunk. All tissues were collected and snap frozen in liquid nitrogen and stored at -80^{o}C for further analysis. The timeline of treatment and experimental procedures are displayed in Figure 3.1.

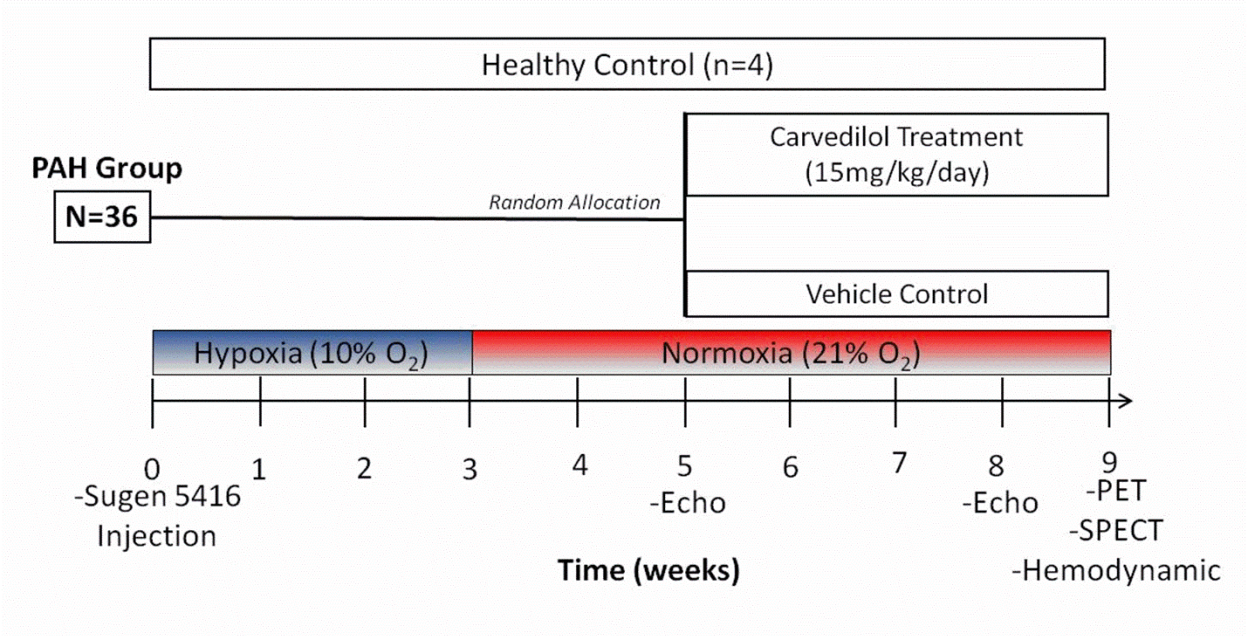

Figure 3.1. Schematic of study design for carvedilol treatment.

3.3.2 β-blocker Treatment

Carvedilol is a nonselective $\alpha_1/\beta_1/\beta_2$ blocker. The dose (15 mg/kg/day orally) was selected based on previous titration studies using telemetry to provide a 20%↓ in heart rate.[99] Carvedilol was selected because, 1) the drug does not affect pulmonary vascular remodeling and RV systolic pressures[99], 2) clinical evidence suggesting effects are superior to metoprolol[99,299], 3) recent preclinical studies suggesting mechanistic benefits in PAH.[99,247] Carvedilol was prepared in 50% DMSO (total volume <200uL) then mixed with 50:50 peanut butter and honey. Vehicle was prepared the same way minus the carvedilol. To mitigate any acute hemodynamic effects of β-blockers on functional outcomes, therapy was held for 24-36 hours prior to echocardiography and SPECT/PET imaging, and 48 hours prior to right heart catheterization. In rats, the half-life ($t_{1/2}$) of carvedilol is ~8-10hrs.[300]

3.3.3 Echocardiography

Transthoracic Pulsed-Wave Doppler Imaging was performed in rats at 5 weeks and 8 weeks post Sugen5416 injection using Vevo 770 high-resolution imaging system (VisualSonics, Toronto, ON) with a 7MHz transducer. After induction of isoflurane anesthesia (1.5-2%), the transducer was aligned with good visualization of the pulmonary artery in the parasternal view. The sample volume was placed at a $10\text{-}12^0$ angle aligned with laminar flow. Pulmonary artery acceleration time (PAAT) was measured using pulmonary artery waveforms from the onset of systolic flow to

peak outflow velocity. The induction and severity of PAH was confirmed by PAAT at 5 weeks. The operator acquiring and analyzing the echocardiographic images was blinded to treatment status. An average of 10 waveforms from each rat was measured and averaged.

3.3.4 Single-Photon Emission Computed Tomography (SPECT) Scan

A multi-gated acquisition scan (MUGA) was performed on all rats at 9 weeks post Sugen 5416 injection for assessment of RV and LV volumes and stroke volume. For each scan, a CT scan was performed first with a tube current of 110 kV to visualize the anatomic structures of heart and adjacent lung tissues. Subsequently, rats were injected via tail vein with stannous gluceptate (16 lg/kg in 0.5 mL of normal saline; IV) followed by a 30-minute incubation period. 70-80 MBq of Tc99m-NaTcO4 (0.5 mL; IV) was injected via tail vein and the animals were immediately imaged. Two sequential 30-minute scans were acquired using a BioScan nanoSPECT-CT scanner. Images were reconstructed using 24 iterations with 45% smoothing, 100% resolution, and summing all projections together to produce a 1-hour blood-pool scan. Images were processed using 4DM- SPECT on a Hermes workstation (Hermes Medical Solutions, Montreal, QC). The operator acquiring and analyzing the SPECT images was blinded to treatment status.

3.3.5 PET Imaging

[^{11}C]Hydroxyephedrine:

[^{11}C]HED was produced by N-methylation of metaraminol freebase by [^{11}C]methyl iodide, as described previously. A subset of rats (CNT, n=1; carvedilol SuHx, n=6; vehicle SuHx, n=5) were imaged at 9 weeks post Sugen 5416 injection. Anaesthetized rats were placed in Siemens Inveon^{TM} small animal PET scanner (Siemens, Knoxville, TN; 12.7 cm axial field-of-view, spatial resolution <1.4mm^3) with heart and lungs centered in the field of view. Following a ^{57}Co attenuation transmission scan, rats were injected with 1.24±0.04mCi (0.5mL) of [^{11}C]HED tracer via a lateral tail vein catheter and dynamic images acquired for 40 minutes. Dynamic images were reconstructed in 26 frames using OSEM3D+MAP with 2+18 iterations. Dynamic PET images were processed and analyzed using in-house software FlowQuant©. Sympathetic innervation and function were assessed by measuring [^{11}C]HED volume of distribution (D_v) using Logan graphical modeling of reversible binding kinetics.[301] Explicit partial volume correction was not performed (i.e. recovery coefficient = 1) as the RV and LV wall thickness was too small for reliable data-driven correction. SNS function describes the ability of presynaptic nerve terminals to uptake, recycle, store and metabolize norepinephrine (NE). Harms *et al* found D_v was less dependent on myocardial blood flow than the Retention Index (RI) and has been shown to be a more sensitive index to early changes in sympathetic function.[302] [^{123}I]-metaiodobenzylguanidine (MIBG, an NE analog for SPECT imaging) washout rate is a well validated parameter of SNS activation.[303] Although MIBG and HED have slightly different kinetic properties, a similar washout parameter for HED has previously been derived. [184,304,305] The washout of [^{11}C]HED was also calculated by fitting a mono-exponential clearance curve (Kmono) to the myocardial data from 5 minutes to 40 minutes as performed previously.[304] The

use of HED washout rate as an index of sympathetic tone remains experimental as validation studies have yet to be performed. Yet, HED washout has been previously correlated MIBG washout rate, and is accelerated by NE administration.[306,307]

Myocardial Blood Flow [^{11}C]Acetate:

On the same subset of rats, anaesthetized rats were injected with 1.28±0.03 mCi (0.5mL) of [^{11}C]acetate tracer via a lateral tail vein catheter and dynamic images acquired for 20 minutes. Myocardial blood flow (MBF) values were measured using a one tissue compartment model (1TCM) and an established tracer extraction function derived in rats.[308]

3.3.6 Right Heart Catheterization

A small incision was made in the right jugular vein. A Millar Mikro-Tip® pressure catheter was advanced through the superior vena cava and right atrium in the RV. The signals were continuously recorded with LabChart software. Hemodynamic data was analyzed using LabChart software. The operator was blinded to treatment allocation.

3.3.7 Histological Analyses

Heart ventricles were preserved in Tissue-Tek® O.C.T compound flash frozen in liquid nitrogen and stored at -80°C.

a) Heart Morphometry

Tissue blocks were sectioned (10µm thickness in the axial plane) at the mid papillary level on a cryostat and mounted on gelatin-coated slides. Fresh frozen sections were stained with

hematoxylin and eosin (according to standard protocol) for assessment of morphology and hypertrophy (wall thickness and cross-sectional area). H&E images were acquired on a Zeiss AxioImager M2 microscope under the 10x objective. LV, RV and septum wall thicknesses were quantified using ImageJ software. Total LV (LV+Septum) and RV cross-sectional area was also quantified. An average of 4 measurements on each of two successive tissue sections were taken as the final measurement for each rat.

b) Immunofluorescence:

Tissue blocks were sectioned (10μm thickness in the axial plane) at the mid papillary level on a cryostat and mounted on gelatin-coated slides. Slides were immediately post-fixed in 4% paraformaldehyde containing picric acid for 30 minutes at room temperature then washed 3x in 1x PBS. To quantify autonomic nerve fiber density, heart sections were incubated with single antibodies against dopamine-β-hydroxylase (DBH; 1:1000; END Millipore Corp MA,USA) and vesicular acetylcholine transporter (VaChT; 1:100; Synaptic Systems; Goettingen, Germany), for SNS and parasympathetic fibers, respectively at 4ºC overnight. The next day slides were washed with 1x PBS and then secondary 488- or 594- AlexaFluor antibodies (Invitrogen) were added (1:400) and sections were incubated at 37ºC for 35 min. Sections were then washed with 1x PBS. DAPI fluoromount (SouthernBiotech) was used to coverslip the slides prior to imaging. Images were acquired using a Ziess Axioplan microscope in gray scale (16 bit) with a fixed exposure

and intensity. Two random fields of view from two successive heart sections (total 4 fields of view) from RV, and LV septum and lateral wall were quantified for nerve area and averaged. Nerve area was quantified using ImageJ software and measured as percent area of immunoreactive nerve fibers of the total selected area.

3.3.8 Statistical Analysis

In the same model, Bogaard *et al.* demonstrated that 4 weeks of carvedilol treatment significantly improved RV function compared to vehicle (Stroke volume: 126±30 vs. 197±71μL, respectively, $p<0.05$). Assuming a similar distribution, approximately 11 rats are needed in each treatment arm for a power of 80% at an alpha of 0.05, to detect a meaningful difference in RV function. Our sample size of 16 rats per treatment arm was selected to 1) account for any attrition and 2) be adequately powered to detect a difference in RV function.

Statistical analysis and graphical presentation were performed using GraphPad Prism 6.0 (Graphpad Software, Inc. Ca, USA). Data are represented as mean±SEM unless otherwise stated. For statistical comparisons, a One-Way ANOVA or Two-Way ANOVA were performed followed by Dunn's multiple comparison test. P-values <0.05 were considered statistically significant.

3.4 Results

3.4.1 Development of PAH

Pulmonary artery acceleration time (PAAT), an echocardiographic index of pulmonary artery pressure, was significantly decreased in PAH rats compared to healthy controls at week 5 prior to treatment randomization ($p<0.0001$, Figure 3.2C). Representative doppler waveforms demonstrate decreased PAAT and reveal a mid-systolic notch in PAH rats compared to healthy control (Figure 3.2D). There was no difference in PAAT between rats subsequently assigned to vehicle and carvedilol treatment at 5 weeks, confirming equivalent PAH severity prior to randomization. Five SuHx rats died prior to randomization (Week 5), leaving a final sample size of 31 rats, of which, 16 were randomized to receive carvedilol and 15 vehicle treatments for the next four weeks. Overall survival was not different between carvedilol and vehicle treated SuHx rats, but two deaths were noted early after β-blocker initiation (Figure 3.2A).

3.4.2 Effect of β-Bocker Therapy on PAH Severity, Cardiac Remodeling and Function

Four weeks of carvedilol treatment had no effect on PAH hemodynamic severity compared to untreated rats. This was demonstrated by equivalent PAAT at 8 weeks and confirmed by invasive hemodynamics (RVSP) at sacrifice (week 9; Figure 3.2E). There was also no treatment effect on the maximum first derivation of right ventricular pressure (Figure 3.2F). Heart rate suppression was still evident 24hrs post treatment at week 8 (Figure 3.2B, Table 3.1), but this effect was lost by 48hrs at the time of right heart catheterization at week 9 (Table 3.1). Chronic RV pressure overload induced significant RV hypertrophy (Figure 3.3). Positive correlations were found between both RV wall thickness ($r=0.72$, $p<0.0001$) and RV area ($r=0.74$, $p<0.0001$) and RVSP. β-blocker treatment had no effect on measures of RV or LV hypertrophy and remodeling. Ventricular weight (LV+RV) normalized to body weight was significantly increased in the carvedilol, but not vehicle, treatment group relative to healthy control (Figure 3.3B).

Tables 3.1: Rat characteristics and Hemodynamics

	Control	SuHx/Veh	SuHx/Carv
Body Weight (g)	665.9±43.9	600.3±7.6	577.7.3±12.4
Ventricle Weight (VW/BW)	0.0023±7.9E-5	0.030±2.8E-4	0.037±2.9E-4*
RV Thickness (mm)	1.24±0.03	1.77±0.09	2.04±0.09*
LV Septum Thickness (mm)	2.56±0.02	2.32±0.07	2.52±0.09
LV Lateral Thickness (mm)	3.20±0.11	3.06±0.07	3.19±0.08
!Heart Rate 24hr Washout	335±15	335±8	309±6.2ϕ
!Heart Rate 48hr Washout	313±19	329±23	315±38

*p<0.05 versus control

Φp<0.05 versus SuHx/Veh

! Heart rate was measured in anesthetized animals (1.5% isoflurane) after a 24 or 48 hour drug washout period, measured at weeks 8 and 9, respectively.

Increased remodeling of the RV was confirmed by morphometric analysis showing that RV wall thickness and RV cross sectional area were significantly elevated in the carvedilol, but not vehicle, treatment group compared to healthy controls ($p<0.05$). There was no effect of carvedilol treatment nor RV pressure overload on LV remodeling (Figure 3.3).

To assess the effects of chronic carvedilol therapy on ventricular function, RV and LV ejection fractions were measured on SPECT imaging (Figure 3.4). RV ejection fraction was significantly lower in both PAH groups compared to healthy control (59.1±7% vs 73.0±5; $p<0.05$; Figure 3.4B). Although no differences in RV function were noted between vehicle and carvedilol, the carvedilol group did trend towards worsening function (Figure 3.4B). We also observed that carvedilol, but not vehicle, increased RV end systolic volume (ESV) and reduced LV function compared to healthy control (LVEF: 72.8±8.1% vs. 82.4±2.4%, respectively; $p<0.05$).

The marked increase in RV ESV together with a decreased LV end diastolic volume (EDV) suggests an effect of ventricular interdependence. Eccentricity index was calculated at end diastole and systole on SPECT images (Figure 3.5). LV eccentricity index at end diastole was elevated in carvedilol, but not vehicle treated rats, compared to control ($p<0.01$). We also examined the relationship between increasing RVSP and LV volumes and function. RVSP correlated highly with LV eccentricity index, LV ejection fraction, and LV EDV (Figure 3.5 C-F).

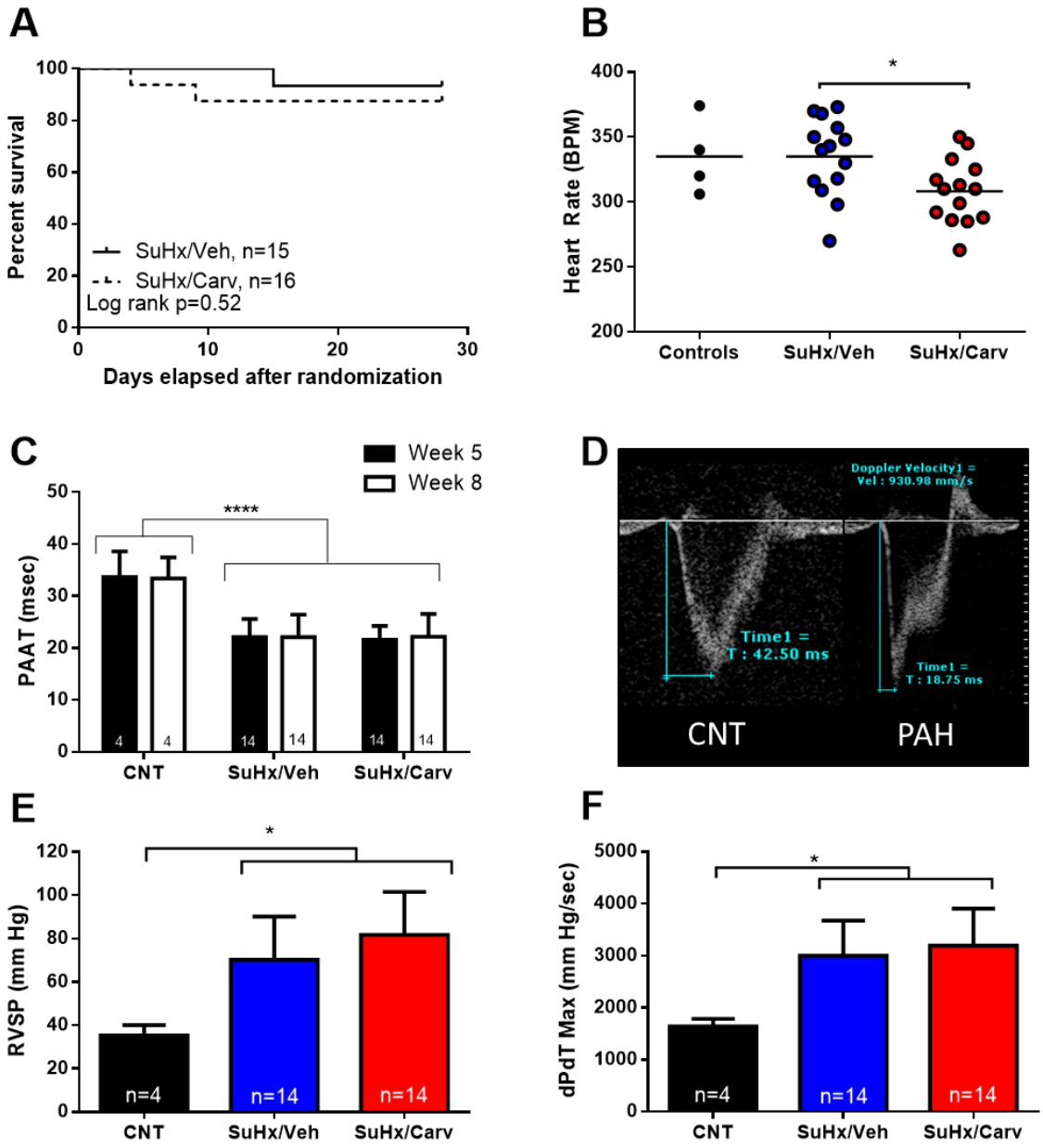

Figure 3.2. Development of PAH over the course of the study. Survival was not different between carvedilol and vehicle treated PAH rats (A). Heart rate was depressed with β-blocker after a 24 hr washout period (B). Pulsewave Doppler confirmed equivalent PAH severity in treatment groups prior to randomization (C). Decreased PAAT and a mid-systolic notch demonstrating severe PAH (D). No effect of carvedilol on pulmonary pressures (E). There was also no effect of carvedilol on the first derivation of right ventricular pressure (F). * P<0.05, ****p<0.0001. PAAT, pulmonary artery acceleration time; RVSP, right ventricular systolic pressure.

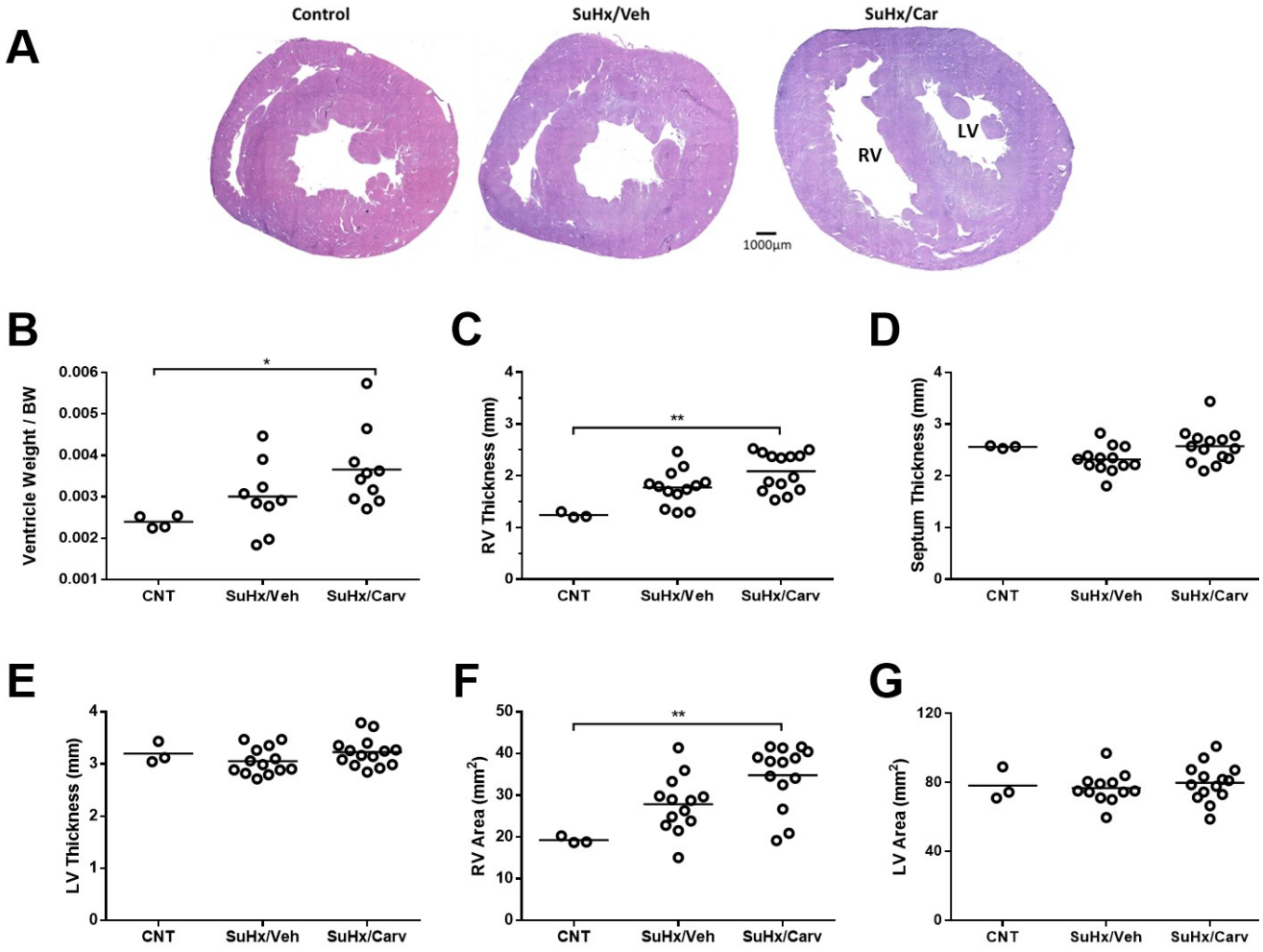

Figure 3.3. Carvedilol fails to reverse RV remodeling in PAH. Representative H&E stain cross sections of RV and LV in healthy control, and PAH rats treated with vehicle or carvedilol (A). Ventricular (LV+RV) to body weight ratio was elevated in carvedilol treated rats, but not vehicle as compared to healthy control (B). This effect was driven by dramatic RV remodeling, as evidence by RV wall thickness (C), RV cross sectional area (F), but not by LV remodeling. PAH nor treatment effected remodeling in the LV, as septum wall thickness (D), LV lateral wall thickness (E) and total LV cross sectional area (G) did not change. *$p<0.05$, ** $p<0.01$.

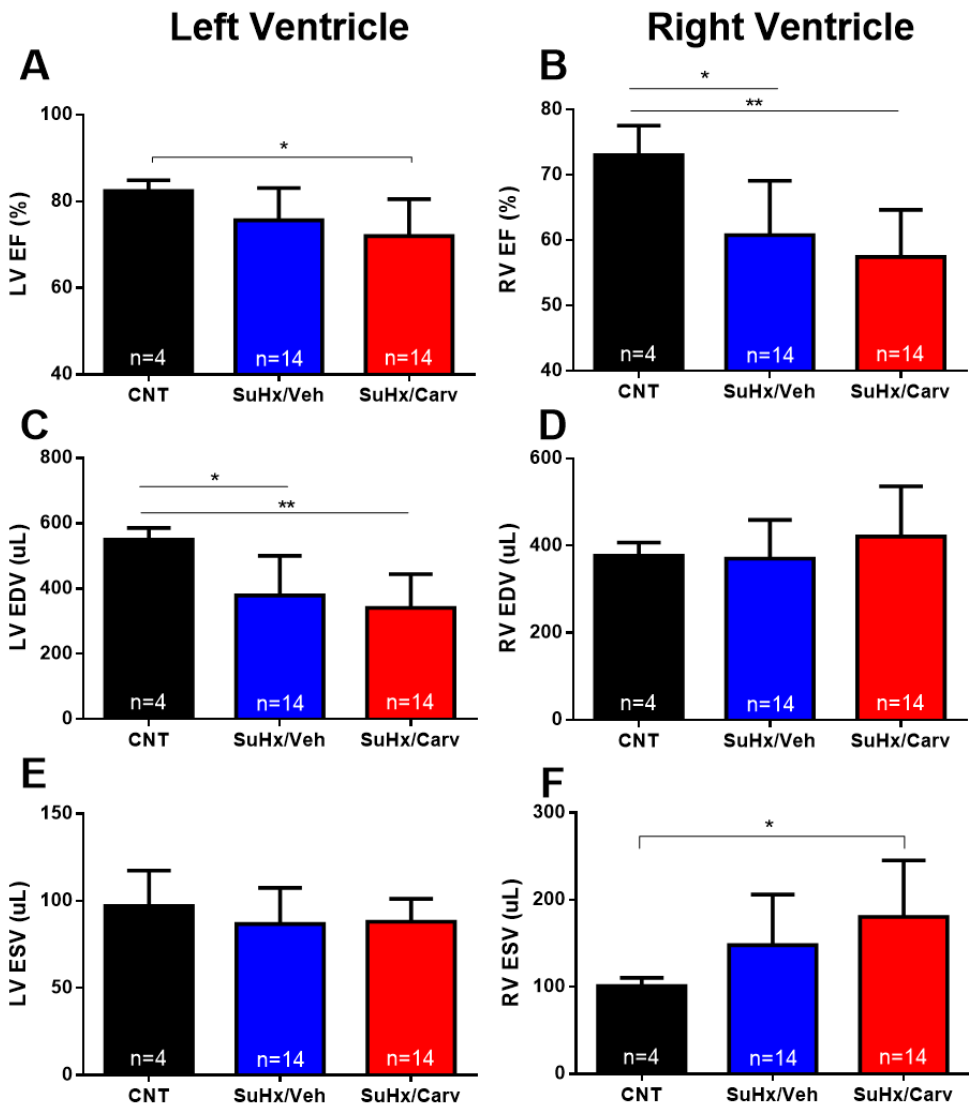

Figure 3.4. Carvedilol fails to recover RV function as assessed by SPECT imaging. Carvedilol, but not vehicle significantly decreased LVEF compared to control (A). LV EDV (C) but not ESV (E) was decreased in PAH animals. RV function was also reduced PAH rats, no differences were observed between vehicle and carvedilol groups, but trended towards worsening function with treatment (B). RV end systolic volume (ESV) was increased in the carvedilol treatment group, but not vehicle, compared to healthy control. No differences were noted in RV EDV (D). EF, ejection fraction; EDV, end diastolic volume; ESV, end systolic volume. *p<0.05, **p<0.01

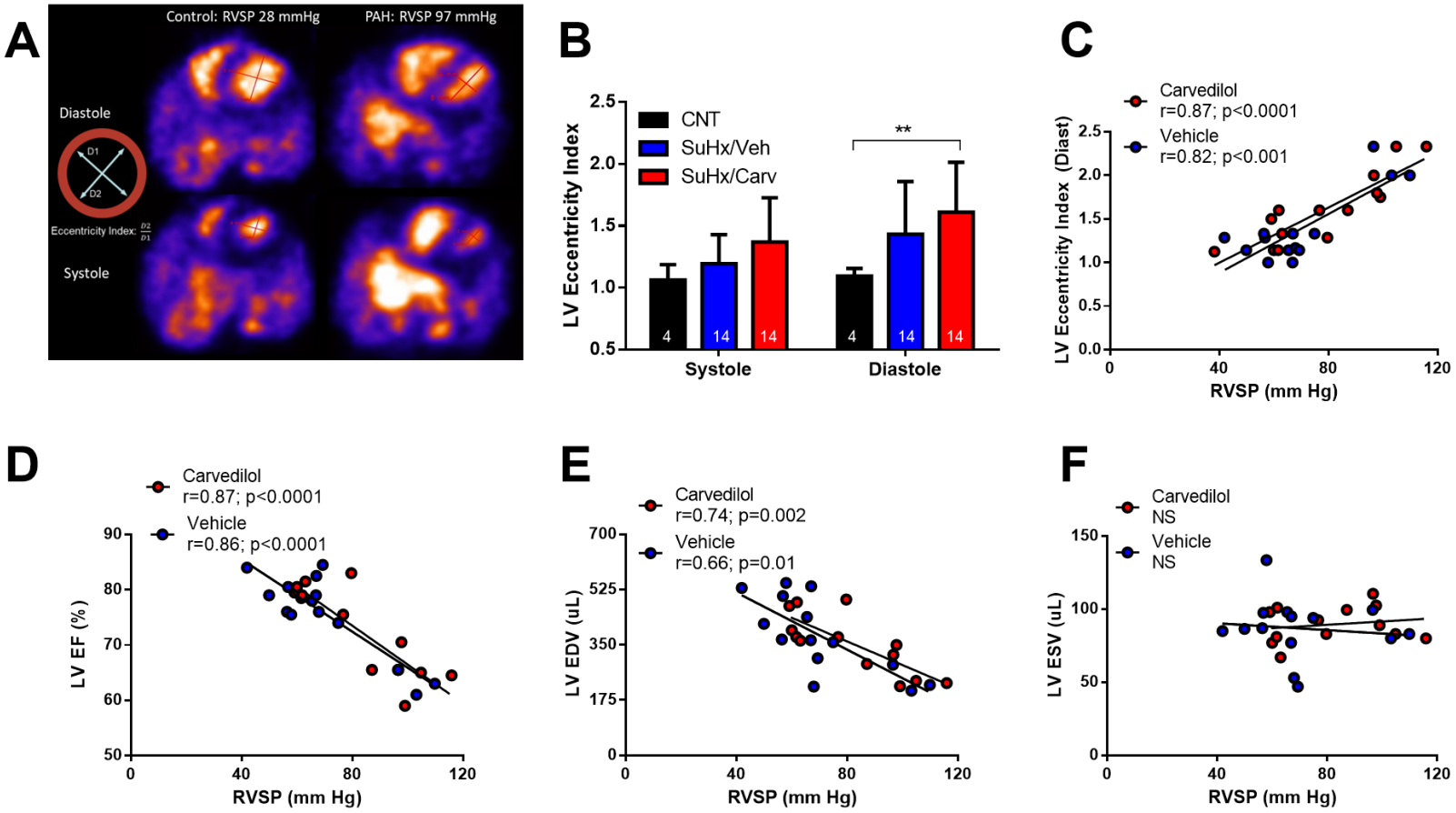

Figure 3.5. LV dysfunction and ventricular interdependence. Representative MUGA images demonstrating eccentricity index (A). In PAH, the RV is dilated which shifts leftward septum into the LV cavity. LV eccentricity index in carvedilol treated rats was not different than vehicle, but was significantly elevated compared to healthy control (B). LV eccentricity index (C), LV EF (D), and LV EDV (E) were all highly correlated with RVSP. No correlation was noted between LV ESV and RVSP (F). **p<0.01. EF, ejection fraction; EDV, end diastolic volume; ESV, end systolic volume. **p<0.01

3.4.3 Carvedilol Effect on Autonomic Function

Carvedilol significantly increased [^{11}C]HED volume of distribution within the LV but not RV (Figure 3.6A/B). Representative polar maps demonstrated improved LV sympathetic function in a rat treated with carvedilol as compared to vehicle control (Figure 3.6 C/D). To elucidate the mechanism of improved LV sympathetic function with carvedilol, HED kinetic data was fitted to a mono exponential function (Kmono) to determine tracer washout rate. Although this parameter is experimental, it is thought to yield some information related to sympathetic activation (Figure 3.6E). Tracer washout rate was markedly reduced with chronic carvedilol treatment in the LV, but not RV (Figure 3.6 E-G). Representative LV [^{11}C]HED tracer kinetics are displayed in Figure 3.6E. Sympathetic and parasympathetic nerve endings within the LV septum, LV lateral wall and RV were imaged with dopamine-β-hydroxylase (DBH)-positive (Figure 3.6H) and vesicular acetylcholine transporter (VAChT)-positive (Supplemental Figure 3.1), respectively. Quantitative analysis did not reveal any difference in sympathetic nor parasympathetic innervation between carvedilol and vehicle-treated rats.

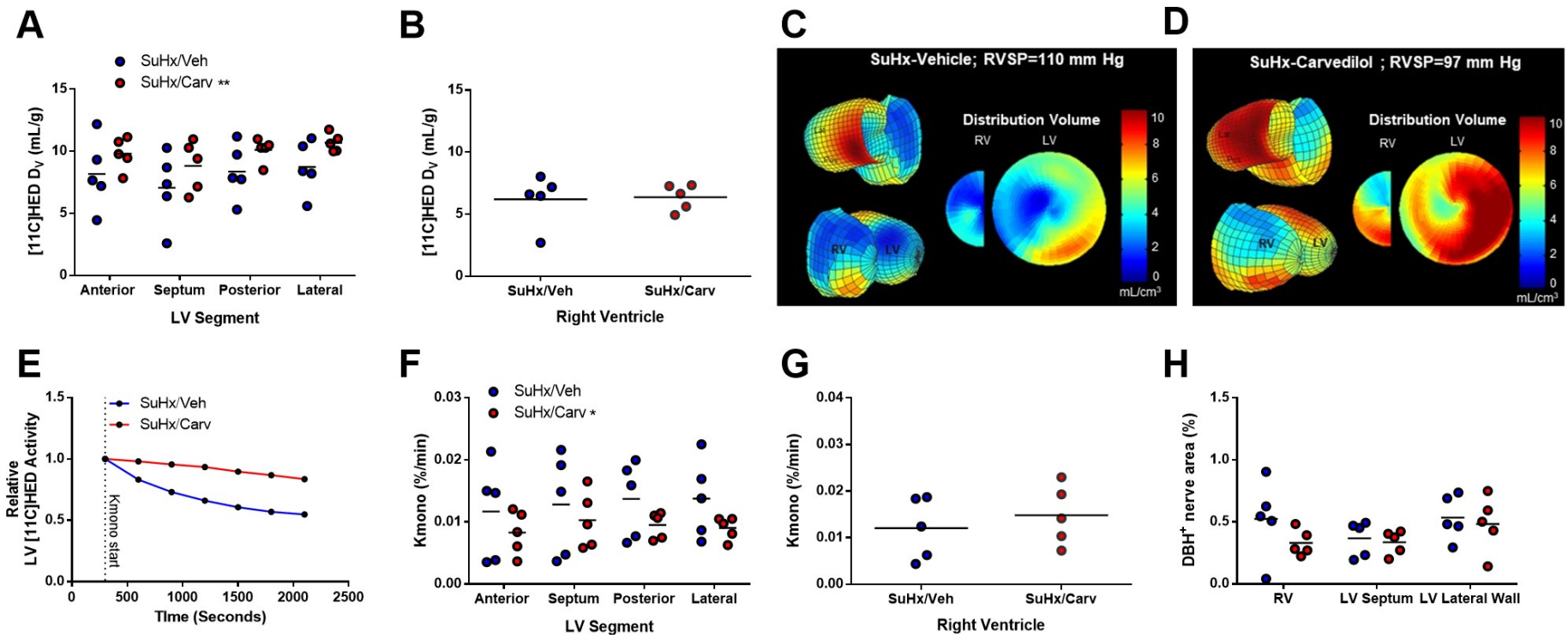

Figure 3.6. Carvedilol improves SNS function in PAH. A treatment effect was observed such that [^{11}C]HED volume of distribution was elevated in the LV (A) but not RV (B). Representative polar maps demonstrating improved [^{11}C]HED DV in the LV of rats treated with carvedilol (C and D). A treatment effect was also observed on [^{11}C]HED kmono in the LV (F) but not the RV (G) with carvedilol treatment. A representative plot of tracer kinetics within the LV demonstrating decreased washout in a rat treated with carvedilol compared to vehicle (E). DBH^{+} nerve density was not effected by treatment status (H). *P<0.05, **p<0.01. D_v distribution volume; kmono, tracer washout rate; DBH, dopamine β-hydroxylase (sympathetic stain). (Carvedilol n=5 vs Vehicle n=5).

3.4.4 PAH Severity and Autonomic Innervation

DBH-positive nerve area within the RV decreased proportional to increasing RVSP (Figure 3.7F). A moderate correlation was observed for the LV septum that approached statistical significance (Figure 3.7D). LV lateral wall DBH^+ nerve area was unaffected by increasing RV pressure (Figure 3.7B). A significant negative correlation was also found between increasing RVSP and [^{11}C]HED V_D in the LV septum and RV, but not the LV lateral wall by PET imaging (Figure 3.7A,C,E). Importantly, DBH-positive nerve density was also highly correlated with [^{11}C]HED D_v (Figure 3.8), but there was also no relationship between increasing RVSP and HED washout rate (Supplemental Figure 3.2). To exclude any effect of HED tracer availability, MBF was found to be homogenous within the LV and RV, and did not change with increasing RVSP (p values range p=0.22 to p=0.60, Supplemental Figure 3.3). Interestingly, no correlation was observed between VAChT-positive nerve density and RVSP (Figure 3.9).

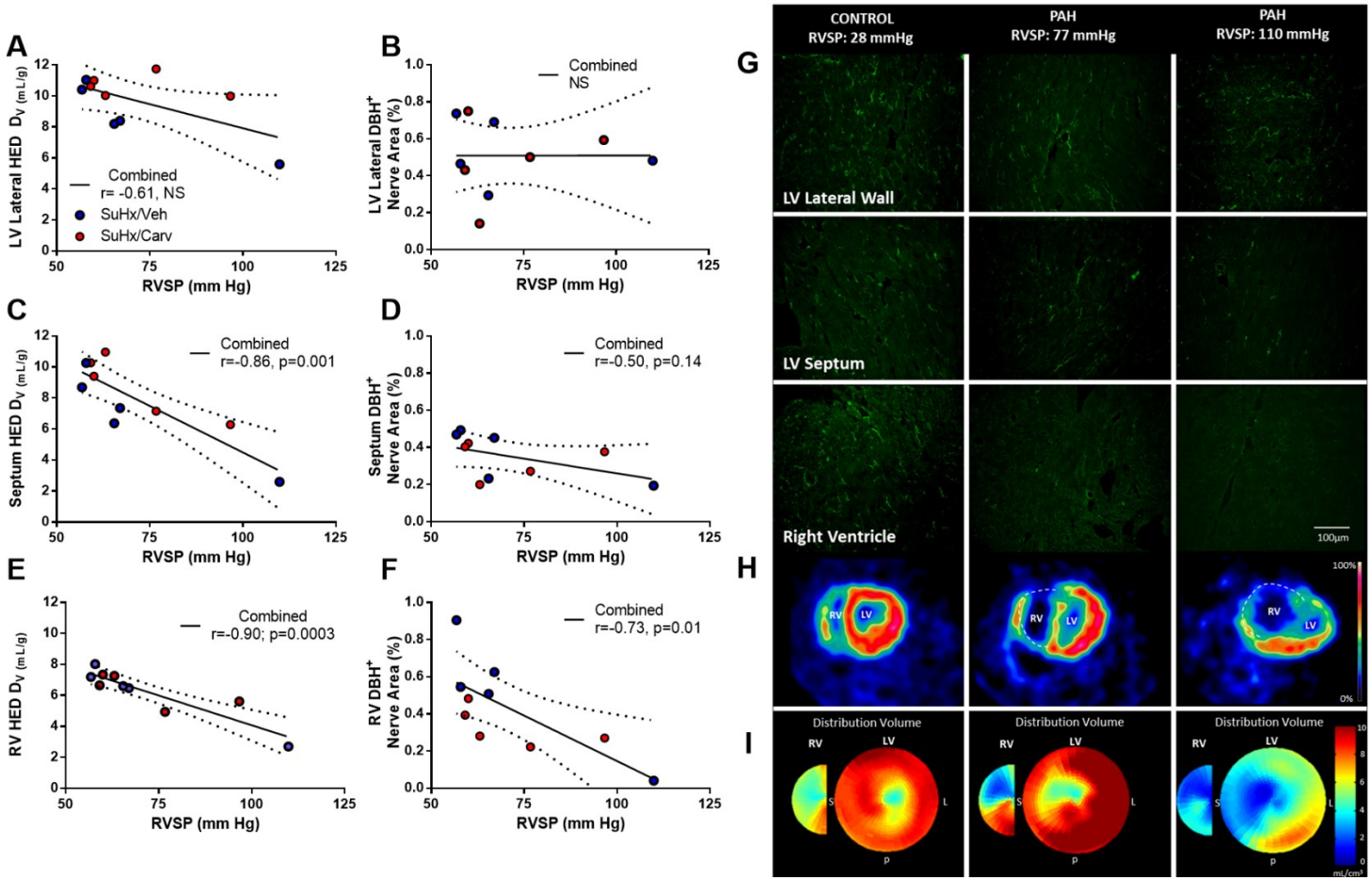

Figure 3.7. Progressive sympathetic denervation within the RV in rats with PAH. Negative correlations between increase RVSP and [^{11}C]HED D_v in the septum (C) and RV (E), but not the LV later wall (A). Representative axial slices of [^{11}C]HED uptake (H) and polar maps of D_v (I) display this concept. Corresponding DBH immunohistochemistry in the same rats demonstrates progressive and selective denervation within the right ventricle with little involvement of the LV free wall. Negative correlations between RVSP and RV DBH+ nerve area (F), but not LV lateral wall (B) and septum (D). Representative DBH immunohistochemestry (G) in the LV lateral wall, LV septum and RV, with progressive PAH disease severity. (Carvedilol n=5 vs. Vehicle n=5)

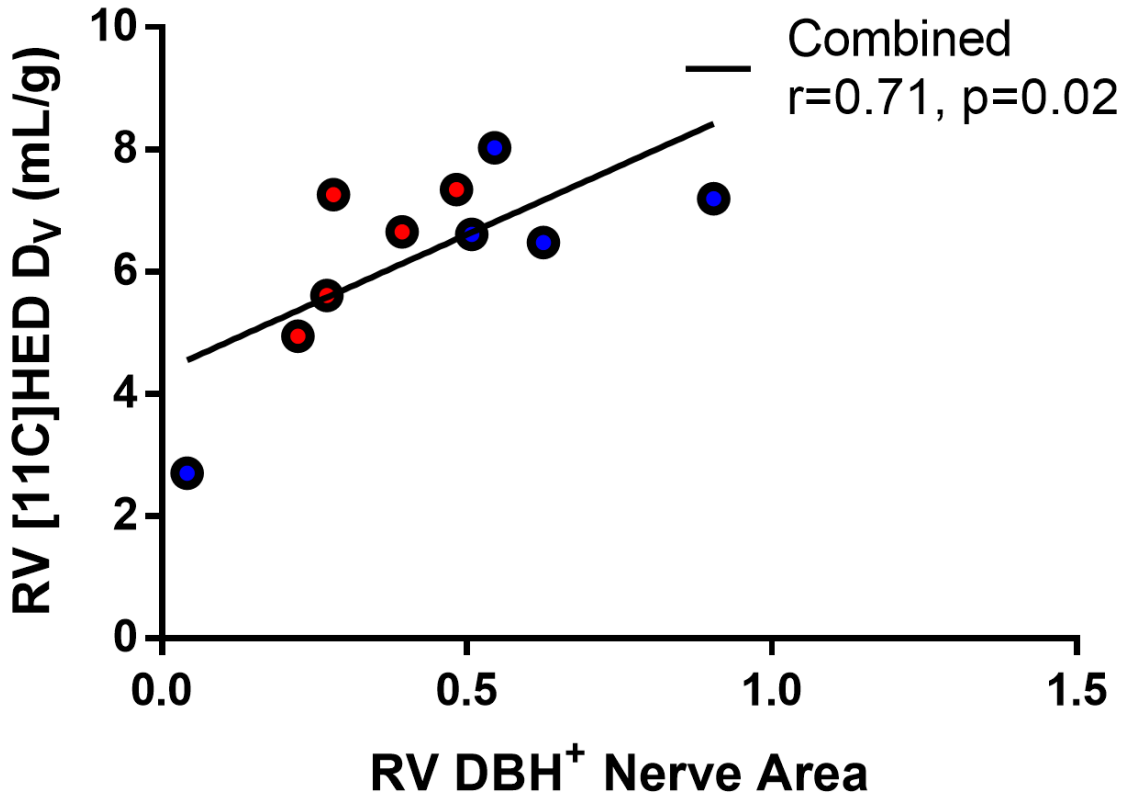

Figure 3.8. Relationship between PET and immunohistochemical evidence of sympathetic innervation. (Carvedilol n=5 vs Vehicle n=5)

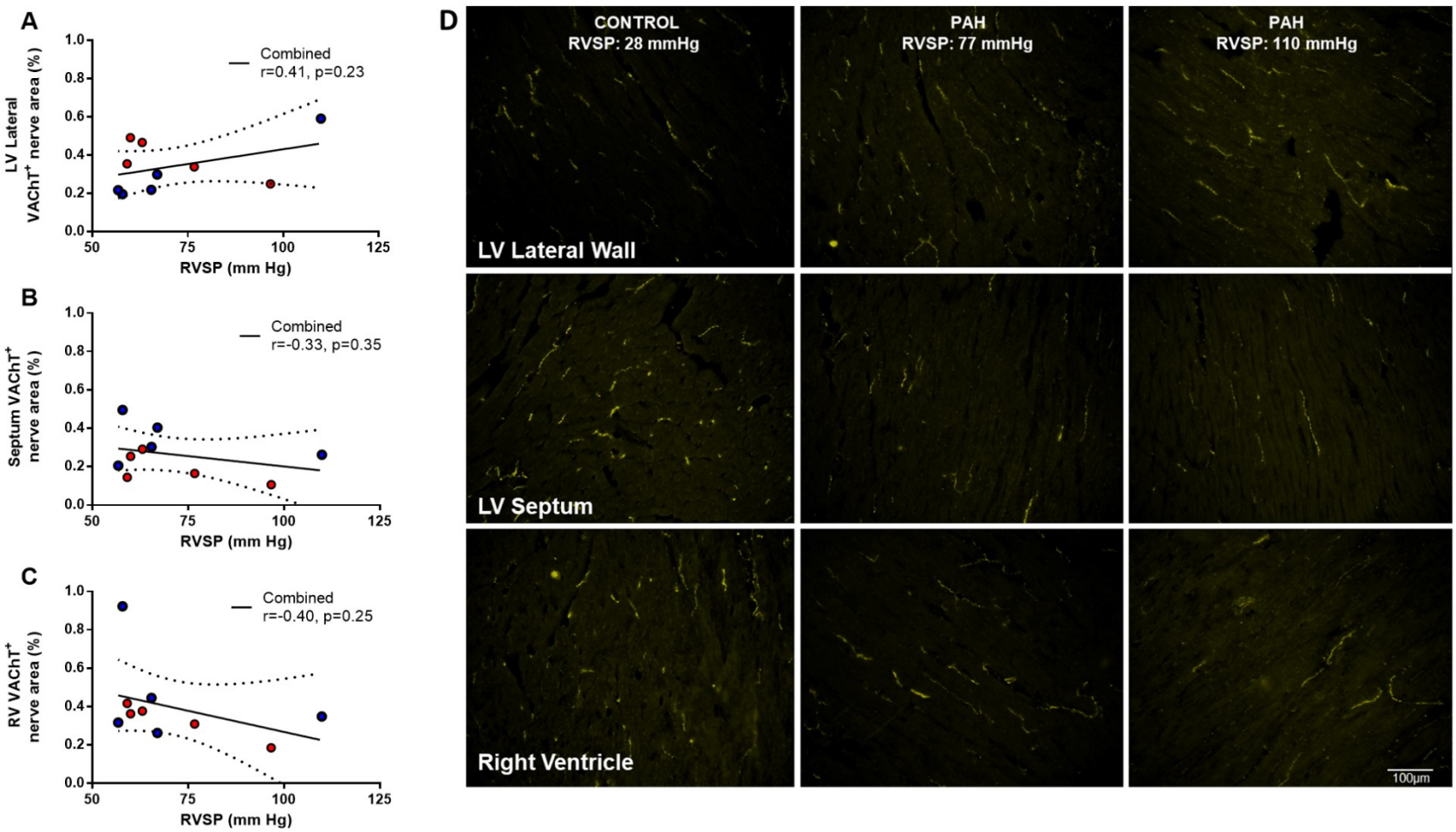

Figure 3.9. Parasympathetic nerve density preserved in animals with PAH. There was no significant correlation between RVSP and VaChT+ nerve area in the LV or RV (A-C). Representative VaChT immunohistochemestry (same representative animals as figure 7) in the LV and RV demonstrate preserved nerve density with increasing disease severity (D). (Carvedilol n=5 vs Vehicle n=5).

3.5 Discussion

This study investigated the effects of long-term carvedilol administration on ventricular and cardiac SNS function in an animal model of PAH and RHF (Supplemental Figure 3.4). Major findings reveal: 1) carvedilol did not demonstrate any beneficial effects on RV remodeling or function; 2) carvedilol increased sympathetic function in the LV but not the RV, an effect that may be due to chronically suppressing sympathetic activation; 3) increasing PAH severity resulted in selective regional sympathetic denervation within the RV, with parasympathetic nerves being largely spared; and 4) a significant correlation between immunohistochemical and [^{11}C]HED PET assessments of sympathetic denervation within the RV. For the first time, these data validates the use of non-invasive neurohormonal imaging to quantify the burden of denervated myocardium in the RV. This has unique potential to be translated to clinical studies for further evaluation of sympathetic integrity as a potential treatment target in patients with RHF. Together, this body of work provides new mechanistic data on the state of autonomic dysregulation within the failing RV extending the paradigm of maladaptive remodeling to include important neuronal influences.

Our study corroborates previous studies in the field demonstrating that the nonselective $\alpha_1/\beta_1/\beta_2$ blocker carvedilol has no effect on pulmonary vascular remodeling and pulmonary pressures.[99,309] However, in contrast to the previous reports, we failed to demonstrate any beneficial effect of carvedilol on RV function or remodeling despite having adequate power based on assumptions from these studies. We further demonstrated that the LV dysfunction in this model of severe PAH is consistent with the reverse Bernheim phenomenon or 'ventricular interdependence'. Also, a few deaths were noted early after β-blocker treatment initiation suggesting a possible adverse effect on RV compensation in this model. Previous studies using

the monocrotaline model have demonstrated that β-blocker therapy initiated early in disease progression (i.e. prevention model) can prevent RV remodeling and dysfunction.[99,243] To our knowledge, only one previous study has investigated the effects of β-blocker therapy in the SuHx model of PAH, which better reflects human PAH.[99] In this study, Bogaard *et al*. investigated the effects of 4-weeks of carvedilol therapy (15 mg/kg/day, initiated on return to normoxia, Week 4,; Figure 3.1). Carvedilol increased exercise endurance and improved RV function without improving pulmonary arterial remodeling in Sugen-hypoxia rats. In contrast, our study used the same dose and duration of treatment, but initiated treatment five weeks after SU5416, at a time point when the PAH phenotype was fully established (i.e. reversal model). In the context of previously published work, our data suggests the timing of therapy is critically important, and β-blocker therapy may only be beneficial prior to development of RV dysfunction. Indeed, our findings are consistent with recent clinical reports demonstrating no direct RV benefit or even harm with carvedilol and bisoprolol, respectively.[246,247,297,298]

There is a paucity of data on the sequelae of chronic SNS activation in patients with PAH and RHF. Studies using muscle sympathetic nerve activity (MSNA) have demonstrated sympathetic hyperactivity in patients with pulmonary hypertension, with SNS overactivation in these patients being an independent predictor of clinical deterioration.[149,227] However, the state of autonomic function directly within the myocardium in patients with PAH remains largely unknown. This has important implications as assessment of SNS function within the myocardium is more sensitive to early changes in HF than systemic measurements.[310] Myocardial indices of SNS function have also demonstrated prognostic value in patients with LHF.[167] [^{11}C]HED PET imaging is widely considered a standard for non-invasive assessment of the myocardial SNS function.[167] [^{11}C]HED is taken up by cardiac sympathetic nerve endings in a

similar manner as norepinephrine.[311] [^{11}C]HED retention is thought to reflect overall sympathetic function (a term that encompasses anatomic innervation, neuronal integrity and activation), whereas tracer washout is an experimental parameter that may yield some information on the state of sympathetic activity.[184,303,304,306] Our study is the first to comprehensively quantify sympathetic function within the RV using [^{11}C]HED PET imaging. These novel results demonstrate that β-blocker therapy significantly improves sympathetic function in the LV but interestingly not RV, possibly by suppressing sympathetic activity. Although not assessed in our system, circulating NE which is released from sympathetic nerves due to increased activation may also increase HED washout.[307] Using [^{123}I]-metaiodobenzylguanidine (MIBG), a similar sympathetic tracer for SPECT, studies have also demonstrated a dose dependent relationship between β-blocker dose and MIBG washout within the LV in patients with LHF; however, the RV was not assessed in these studies.[312] We speculate that the divergent LV and RV findings can be explained by one of two hypotheses. First, we demonstrated progressive regional sympathetic denervation within the RV, but not the LV. Although speculative, drugs targeting SNS activation may need to target the stage of dysfunction before sympathetic denervation occurs.[313] Alternatively, the RV and LV have distinct embryological origins, and unique structural and functional properties, that could account for the different responses to therapy.[3]

The present study also provides mechanistic insight into the state of autonomic plasticity within the failing RV, which may have important therapeutic implications. The finding of selective and progressive sympathetic denervation within the failing RV, with parasympathetic nerves being largely spared is novel and may explain, in part, the autonomic imbalance in these patients. While previous studies in humans have also noted sympathetic denervation using

similar immunohistochemical approaches, these analyses were restricted to patients with end-stage disease.[207,314] Although we did not establish a temporal relationship, we did identify a relationship between neural remodeling, PAH disease severity, and the functional consequences of RV remodeling. The preservation of a healthy population of parasympathetic nerves suggests that this branch of the autonomic nervous system may be a more viable approach to target autonomic dysfunction in RHF. This concept is supported by recent preclinical studies that have demonstrated dramatic RV benefit from augmenting parasympathetic activity with pyridostigmine and vagal nerve stimulation.[154,315]

Additional key findings of our work include the correlation between the PET imaging and immunohistochemical evidence of sympathetic innervation (Figure 3.7 & Figure 3.8). This helps validate the use of neurohormonal imaging to quantify the burden of denervated myocardium in the RV. Knowledge derived from the left-ventricle has taught us that β-blockers are not efficacious in all patient populations and disease states.[248] MIBG imaging has been shown to be an excellent predictor to response to bisoprolol in a cohort of patients with non-ischemic cardiomyopathy, with a direct relation between clinical benefit and improvements in MIBG uptake (i.e. cardiac SNS function).[316] Based on the present results, we hypothesize that once anatomic denervation is established, therapies that target SNS activation may confer no benefit, and potentially even increase risk. This requires prospective clinical determination and validation. As well, it remains to be determined whether SNS imaging with PET can identify RV myocardium with preserved sympathetic innervation, more likely to respond to target treatments, thus enabling a precision-targeted patient selection process.

Limitations

We did not titrate carvedilol to the desired dose, as is mandated in clinical practice. It is likely that titrating the β-blocker may have increased tolerability; but, to date, this dosing regime has not been adopted in the preclinical field. While our data, in the context of previously published studies, suggests the timing of therapy is critically important, the present study was not intended to compare a prevention versus reversal model. Future studies should also aim to explore the temporal relationship between autonomic remodeling the RV and the consequences on pathological remodeling. Our results may not be generalized to the entire class of β-blocker agents, as differences in their selectivity for adrenergic receptors as well as any ancillary properties on oxidative stress may have differing effects on RV remodeling. Another important limitation was the RV function was not serially assessed in the course of the experiment, and we did not perform MUGA imaging prior to the initiation of carvedilol. Another limitation of the present was study was the use of only male rats, future studies should assess any sex-specific differences in treatment efficacy. Although the number of rats in the healthy controls (n=4) was low, the study was powered to detect differences in PAH rats treated with vehicle versus carvedilol. We feel this is reasonable as there is little heterogeneity in healthy rats RV function and pulmonary pressures. The lack of a baseline/healthy control group for the PET imaging was an important limitation. The RV wall thickness in controls is only 1-1.2mm, and thus a data driven partial volume correction is technically challenging. We imaged one control animal to assess regional uptake patterns only, and to have a comparison for DBH^+ nerve area on histology. A partial volume correction was not applied for the PAH rats, which may underestimate the actual DV values. However, there was a similar degree of RV hypertrophy in both vehicle and carvedilol treated animals and thus the correction would be similarly applied between these two comparison groups.

Conclusion

The use of β-blockers to selectively target SNS activation in patients with PAH and RHF remains widely contested. Our study suggests that when given at a clinically relevant time-point, carvedilol fails to recover RV function, and in fact tended to worsen RV and LV function. The potential deleterious effects of carvedilol in our study illustrates the potential dangers of administering therapy later in the progression to maladaptive RV remodeling when the negative inotropic and chronotropic effects of therapy may overwhelm any positive effects on sympathetic function and/or RV remodeling. We further demonstrated that carvedilol was effective at suppressing sympathetic activity in the LV but not the RV, potentially due to extensive sympathetic denervation within the failing RV. Importantly, for the first time we show that non-invasive imaging with PET can quantify this denervation burden in the RV. These imaging findings have the unique ability to be directly translated from our animal model to clinical patients. The finding of selective SNS nerve denervation may suggest that targeting the parasympathetic nervous system is an untapped therapeutic avenue

New Knowledge Gained:

Our study is the first to use [^{11}C]hydroxyephedrine PET to non-invasively characterize the RV's sympathetic nervous system (SNS) in PAH. Using complimentary immunohistochemistry, we validate the use of HED to quantify the burden of sympathetic denervation within the failing RV. These imaging findings have the unique ability to be directly translated from our animal model to clinical patients.

Compliance with Ethical Standards:

Funding: Jason Zelt is an MD/PhD student co-supervised by Drs Lisa Mielniczuk, Rob Beanlands and Rob deKemp and supported in part by the Vanier Canada Graduate Scholarship and The University of Ottawa. Rob Beanlands is a Career Investigator supported by the Heart

and Stroke Foundation of Ontario (HSFO) and is a Tier 1 Chair in Cardiac Imaging Research at the University of Ottawa and the Vered Chair in Cardiology at the University of Ottawa Heart Institute. Lisa Mielniczuk is a Mid-career Clinician Scientist supported by HSFO and a Tier 2 Chair in HF Research at the University of Ottawa. This work was supported in part by a grant the Heart and Stroke Foundation of Canada (G-17-0018315).

Disclosures: RdK is a consultant for- and has received grant funding from Jubilant DraxImage. RdK receives revenues from Rubidium-82 generator technology licensed to Jubilant DraxImage, and from sales of FlowQuant software. RSB is or has been a consultant for- and has received grant funding from GE Healthcare, Lantheus Medical Imaging, and Jubilant DraxImage. The remaining authors have nothing to disclose.

Ethics Approval: All animal received humane care and procedures conformed to the guiding principles of the National Institute of Health's Guide for the Care and Use of Laboratory Animals, and were approved by the University of Ottawa Heart Institute Animal Care Committee.

Acknowledgments: We would like to thank Julia Petryk and Richard Seymour for their technical assistance with the nuclear imaging, hemodynamic assessments, respectively.

Disclosures: RdK is a consultant for- and has received grant funding from Jubilant DraxImage. RdK receives revenues from Rubidium-82 generator technology licensed to Jubilant DraxImage, and from sales of FlowQuant software. RSB is or has been a consultant for- and has received grant funding from GE Healthcare, Lantheus Medical Imaging, and Jubilant DraxImage. The remaining authors have nothing to disclose.

3.6 Chapter 5 Extension: HED Imaging in Adaptive and Maladaptive Animal Model

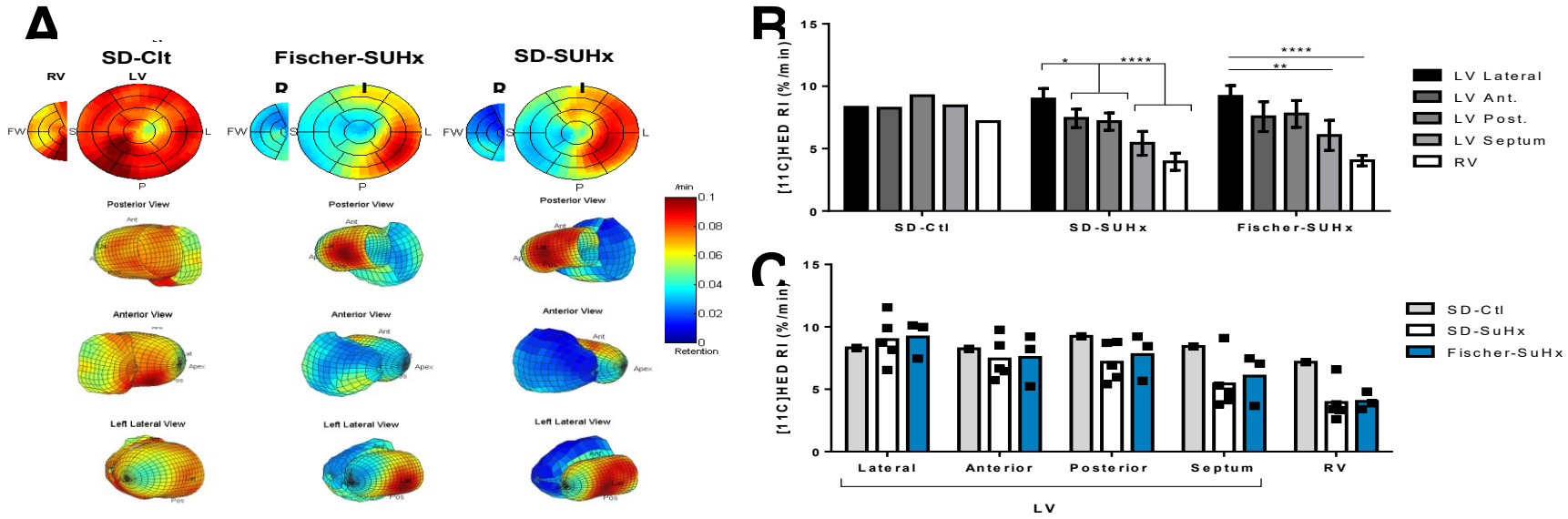

Figure 3.10. **HED imaging in adaptive and maladaptive models of RHF.** HED imaging is SD and Fischer SuHx rats at 4-weeks post SU. There were no strain differences in the degree of RV denervation. Compared to the LV laterwall, there is significant denervation in both Fischer and SD SuHx rats in the LV septum and RV.

Chapter 4

Equivalent Regional Distribution of Fluorine-18-Flubrobengaune and Carbon-11-Hydroxyephedrine for Cardiac PET Imaging of Sympathetic Innervation.

Zelt *et al.* 2020 Submission to Journal Pending

Authors: **Jason G.E. Zelt MSc**[1,2,3], Deron Britt BSc[1], Braeden Mair BSc[2], Benjamin Rotstein PhD[2], Sarah Quigley RN[3], Linda Garrard RN[3], Lisa M. Mielniczuk MD[1,2,3], Robert A. deKemp PhD[1,2,3]* and Rob S. Beanlands MD [1,2,3]*

*Co-Principal Investigator

[1] Division of Cardiology, University of Ottawa Heart Institute and University of Ottawa, Ottawa, Canada
[2] Department of Cellular and Molecular Medicine, Faculty of Medicine, University of Ottawa, Ottawa, Canada.
[3]Molecular Function and Imaging Program, The National Cardiac PET Centre, University of Ottawa Heart Institute and University of Ottawa, Ottawa, Canada

Authorship:

JGEZ: Conducted the clinical imaging, performed the PET image analysis an statistical approach, and wrote the manuscript.
DB: Performed image analysis
BM and BR: HPLC for FBBG metabolites
SQ and LG: Research coordinators
LMM: Content expert and critical review of the manuscript
RAD and RSB: PIs on the project.

Key words: Flubrobenguane, Sympathetic Nervous System, Ischemic Cardiomyopathy, Sudden Cardiac Death.

4.1 Abstract

Background: To date, [^{123}I]*meta*-iodobenzylguanidine (mIBG) for planar scintigraphy and SPECT is the most extensively studied tracer for imaging cardiac presynaptic nerve terminals. Yet, these measures remain crude, with assessment predominantly restricted to a global assessment of sympathetic function using the planar heart-to-mediastinum ratio. PET tracers have been developed with superior quantitative capabilities to assess regional abnormalities of the cardiac sympathetic nervous system (SNS). [^{11}C]*meta*-hydroxyephedrine (HED) is the most commonly used PET tracer in humans, but widespread clinical utility is limited because of the short half-life of ^{11}C. The aim of this study was to investigate the regional distribution of novel ^{18}F-labeled PET tracer, Flubrobenguane (FBBG), to assess myocardial presynaptic sympathetic nerve function in humans.

Methods: Twenty-five participants (healthy n=6; ischemic cardiomyopathy n=14, left ventricular (LV) ejection fraction (EF)=34±5%; and non-ischemic cardiomyopathy n=5, EF=33±3%) underwent two separate PET imaging visits within one week. On visit [a] participants underwent dynamic HED PET imaging. On visit [b], participants underwent dynamic FBBG PET imaging. The order of testing was random. HED and FBBG global innervation (retention index (RI) and distribution volume (DV)) and regional denervation (% non-uniformity) were quantified to assess regional presynaptic sympathetic innervations.

Results: FBBG RI (r^2=0.87; ICC=0.83; p<0.0001), DV (r^2=0.62; ICC=0.77; p<0.0001), and regional denervation (r^2=0.97; ICC=0.98; p<0.0001) correlated highly with HED. Average LV RI values were equivalent between HED (7.3±2.4%/min) and FBBG (7.2±1.8%/min p=0.56). A post-hoc analysis also did not reveal between-tracer differences on a segmental level (17-segment), suggesting equivalent regional distributions in both patients with and without ischemic cardiomyopathy.

Conclusions: [^{18}F] FBBG and [^{11}C]HED yields equivalent global and regional distributions in both patients with and without ischemic cardiomyopathy. ^{18}F-labeled PET tracers, such as FBBG, are critical for widespread distribution necessary for multi-center clinical trials and to maximize patient impact.

4.2 Introduction

Heart failure (HF) is the final common pathway for myriad diseases that affect the heart. Affecting up to 5.7 million people in the United States, HF is a staggering clinical and public health problem associated with significant mortality, morbidity and healthcare costs [317]. The sympathetic nervous system (SNS) is integral to proper cardiac function, but when perturbed contributes to the pathogenesis and progression of various disease states. Cardiac sympathetic nerves are thought to be exquisitely sensitive to ischemia with the zones of denervation often extending beyond the ischemic penumbra [318–320]. Within the neuronal microenvironment, abnormalities of the electrical architecture and heterogenous innervation within the infarct border zones may provide an important nidus for arrhythmogenesis. Indeed, survivors of myocardial infarction (MI) have a 4-fold elevated risk of sudden cardiac death (SCD)[211].

Measurements of SNS function within the myocardium have been shown to be more sensitive to early changes in HF than systemic measurements and may yield greater prognostic value [310]. Non-invasive techniques using radiotracers for positron emission tomographic (PET) and single photon emission computed tomography (SPECT) have been employed clinically to characterize the cardiac sympathetic nervous system (SNS). To date, norepinephrine (NE) analogs with a high affinity for the norepinephrine transporter (NET), such as [^{123}I]*meta*-iodobenzylguanidine (mIBG) for SPECT and [^{11}C]hydroxyephedrine (HED) for PET, have been the most widely used radiopharmaceuticals to characterize presynaptic SNS function. Beyond prognostication, these tracers also have demonstrated utility in predicting life-threatening arrhythmias [173,203,320,321]. The PAREPET trial (Prediction of ARrhythmic Events With Positron Emission Tomography; NCT01400334), recently evaluated [^{11}C]HED for identifying ischemic cardiomyopathy patients at highest risk of sudden cardiac death. In these patients, the degree of

denervation, assessed with quantitative PET, was the strongest predictor of SCD, more so than traditional risk factors such as LVEF[320]. The potential utility of noninvasively measuring myocardial SNS function is thus evident yet current methods have important limitations. Limitations in mIBG availability and quantification methods have discouraged widespread clinical utility. Clinical utility of PET SNS imaging is also currently limited because of the short half-life (20 min) of ^{11}C-labeled tracers. A novel ^{18}F-labeled tracer, such as [^{18}F]flubrobengaune (LMI1195 or *N*-[3-bromo-4-(3-[^{18}F]fluoropropoxy)-benzyl]-guanidine), with its longer half-life (110 min) has the potential for wide distribution needed for maximum patient and clinical impact.

Flubrobenguane (FBBG) and mIBG are both benzylguanidine analogs with similar kinetic properties in preclinical animal models [183,322–324]. This presents an opportunity to build on the longstanding safety and efficacy portfolio of mIBG, while capitalizing on the superior resolution and quantification capabilities of PET. Sinusas *et al.* recently completed the first-in-human study evaluating the dosimetry, biodistribution, and safety of FBBG PET imaging in 12 healthy subjects[176]. Results suggest favorable kinetics for cardiac imaging with radiation doses comparable to other PET tracers. The primary objective of this study is to validate the new ^{18}F labeled PET tracer FBBG as a marker of presynaptic neuronal function in humans with and without left heart failure by correlating myocardial FBBG uptake and retention against HED.

4.3 Methods

The study was approved by the University of Ottawa Heart Institute Human Research Ethics Board. All patients provided informed consent.

4.3.1 Study Design

Inclusion Criteria

14 patients with ***ICM*** were recruited with the following inclusion criteria: 1) LV systolic dysfunction (LVEF< 45% by echocardiography, cMRI, radionuclide or contrast ventriculography); and 2) confirmed history of coronary artery disease (CAD) on optimal medical therapy. 5 patients with ***NICM*** were recruited with an LVEF<45% without a history of CAD. A group of ***healthy volunteers*** (n=6) were recruited with a low likelihood of CAD (<5%) as defined by Diamond and Forester standard criteria. Healthy participants had no known comorbidities and a normal ECG and lipid profile.

Exclusion Criteria

Exclusion criteria were patients with the following: 1) use of tricyclic antidepressants, cocaine, or drugs which may alter catecholamine uptake; 2) a requirement for revascularization within three months prior to enrollment; 3) unstable angina or myocardial infarction within 4 weeks before study enrollment; 4) HF/LV dysfunction due to severe valvular disease; 5) decompensated HF 3 months prior to enrollment defined as: i) an emergency room visit and/or admission for HF, or ii) received IV furosemide, and a change in the following drugs: beta blockers, ACE inhibitors, and mineralocorticoid receptor antagonists; and 6) Any cardiac event of clinical instability requiring changes in medical treatment between the 2 imaging visits.

Study Protocol:

All patients underwent two separate PET imaging visits within one week. On visit [A] participants underwent rest perfusion PET imaging according to standard protocols using [^{13}N]ammonia[325–328], followed by 40-60 minute dynamic [^{11}C]HED PET imaging. On visit [B], participants underwent 40-60 minute dynamic [^{18}F]FBBG PET imaging. In a subset of patients, an additional 20 minute scan was done 3 hours post injection of [^{18}F]FBBG to measure tracer retention. The order of testing days [A] and [B] were random. The chemical structures of FBBG and HED appear in Figure 4.1.

4.3.2 PET Imaging

1) Imaging Preparation

Participants reported to the University of Ottawa Heart Institute PET imaging department after an overnight fast. All participants were asked to refrain from consuming any caffeinated beverages for 24 hours prior to both imaging visits. Patients with ischemic cardiomyopathy and NICM were instructed to take their medications as clinically indicated.

2) Rest [^{13}N]ammonia PET Protocol

All PET imaging was performed on patients in a supine position in a quiet and awake state in a GE Discovery 690 PET-CT (Waukesha, WI) scanner. A low-dose transmission scan was performed using x-ray computed tomography to correct for photon attenuation. Immediately after the transmission scan, 3 MBq/Kg [^{13}N]ammonia was administered intravenously, and a 20-minute dynamic PET scan was initiated (10 frames x 10 seconds; 3 frames x 30 seconds; 1 frame x 60 seconds; 1 frame x 120 seconds; 1 frame x 240 seconds; 2 frames x 300 seconds).

3) [11C]HED PET Protocol

[^{11}C]HED was produced from [^{11}C]methyl iodide and metaraminol free base, as previously described.[329] Two-hours after [^{13}N]ammonia injection (allowing for decay of ^{13}N; $t_{1/2}$=2.84 minutes), patients were then repositioned in the scanner and underwent a repeat transmission scan (for attenuation correction) followed by the intravenous bolus administration of 3 MBq/kg of [^{11}C]HED (followed by a 10mL saline push) and a 40-60 minute dynamic PET acquisition (9 frames x 10 seconds; 3 frames x 30 seconds; 2 frame x 60 seconds; 7 frames x 300 seconds).

4) [^{18}F]Flubrobenguane PET Protocol

[^{18}F]FBBG was synthesized from a brosylate precursor using a single-step ^{18}F displacement reaction, as previously described [176,322,330]. Following a transmission scan, a bolus of 3 MBq/kg [^{18}F]FBBG (followed by a 10 mL saline push)) was administered intravenously, and a 40-60 minute dynamic acquisition was initiated (9 frames x 10 seconds; 3 frames x 30 seconds; 2 frame x 60 seconds; 7 frames x 300 seconds). A subset of patients (3 patients per group) returned 3 hours after injection, for an additional 20-minute scan.

5) Image Reconstruction

PET images were reconstructed with all physical corrections applied, using the vendor iterative algorithm (VuePoint HD) and 8 mm Hann post-filter. Dynamic Images were analyzed using FlowQuant® v2.4 (University of Ottawa Heart Institute, Ottawa, Canada).

6) Sympathetic Innervation and Denervation PET Parameters

a) Global innervation

The tracer distribution volume (DV) and retention index (RI) were estimated in 496 polar-map sectors, and the LV-mean values were computed as measures of global SNS innervation.

4.4 i) Retention Index

Net uptake of HED and FBBG at early (5-10min) and late (30-40min) scan times were estimated using the retention index (RI) as [331]:

$$RI = \frac{C_m(T_R)}{\int_0^{T_R} C_p(t)dt} \times 100\%$$

where C_m is the activity concentration in myocardial tissue, C_p is the unchanged tracer activity in plasma, and T_R is the function evaluation end-time (10min or 40 min). Since the blood spillover into the myocardial region is not estimated using the retention model, only global partial-volume correction was applied assuming full recovery of C_m as reported previously.[332,333]

ii) Distribution Volume

The distribution volume is defined as the ratio of tracer concentration in the myocardium to arterial plasma, at equilibrium. For receptor ligands, the DV physiologically reflects tracer binding affinity (i.e. B_{max}/K_d), where B_{max} is density of the Uptake1-transporter and $1/K_d$ is the affinity of HED or FBBG for the transporter. [334] Volumes of distribution were calculated using a one-tissue compartment model as previously described.[333] This method can be expressed by the following equation, where C_m is myocardial tracer concentration, C_p is arterial plasma tracer concentration, and T_E is the time to equilibrium:

$$DV = \frac{K_1}{k_2} = \frac{C_m(T_E)}{C_p(T_E)}.$$

Quantitative analysis requires subtraction of radiolabeled blood metabolites accumulating in the blood stream to ensure accurate computation. The arterial whole-blood time-activity curve was

obtained from a 20 mm^3 region in the LV cavity. The following equation was used to correct for blood metabolites is as follows: $C_p(t) = C_{WB}(t) \times pfp(t)$, where $C_p(t)$ is the unchanged parent tracer concentration in plasma, $C_{WB}(t)$ is the arterial whole-blood tracer concentration, and pfp(t) is the parent fraction in plasma function.[335,336] For FBBG, the plasma metabolite correction was taken from Sinusas *et al.*[176]

The same partial volume recovery coefficient (RC = 1) was applied as well as the fraction of blood volume within myocardial tissue f_B as part of the one-tissue compartment model: $C_p(t) = RC \times C_m(t) + f_B \times C_p(t)$.

b) Regional Denervation

iii) Denervation Score

The regional denervation score reflects the extent x severity of the relative defects, expressed as a percent of the left ventricle.[332] The denervation (defect) score was calculated by quantifying tracer uptake in 496 myocardial sectors at early (5-10min) and late (30-40min) scan times; those with ≥75% relative to the peak tracer activity were defined as normal and set to equal 100%. The LV non-uniformity is then calculated as 100% minus the average polar-map value. Test-retest repeatability of this method has been reported as 5.5%.[332,333]

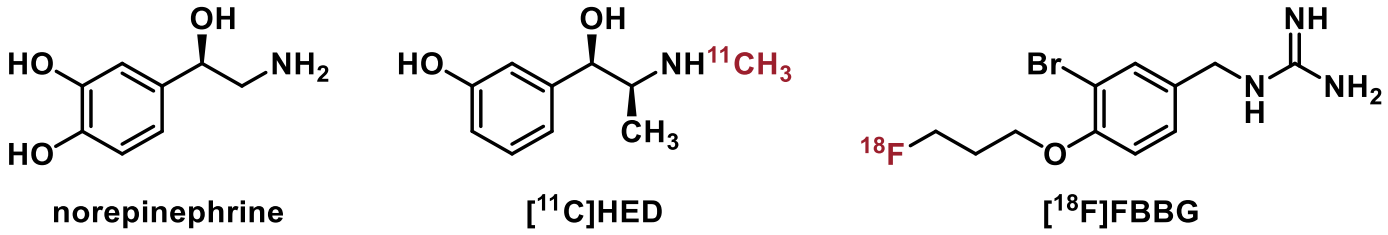

Figure 4.1. Chemical structures of PET tracers. Chemical structures of norepinephrine, [^{11}C]*meta*-hydroxyephedrine and [^{18}F]flubrobenguane.

Evaluation of Patient Safety

Safety was assessed at during both imaging visits by monitoring adverse events (AEs), clinical laboratory tests, electrocardiograms, physical examination, and vital signs. Heart rate, blood pressure and laboratory assessments were obtained before and at various time points during imaging. We reported no major AEs in response to tracer HED or FBBG administration or imaging.

4.4.1 Statistical Methods

Statistical analysis and graphical representation were performed using GraphPad Prism 6.0 (GraphPad, La Jolla, CA, USA). Continuous variables were represented as mean±SD. Correlations between HED and FBBG regional and global scale parameters were performed using a Pearson's Correlation coefficient and intraclass correlation coefficient (ICC). Mean differences in global innervation and regional denervation between three participant groups (healthy, NICM and Ischemic) were compared with a one-way analysis of variance (ANOVA). Mean differences between tracers were compared using a paired t-test (two-tails), or a repeat-measure two-way ANOVA where appropriate

4.5 Results

27 participants (14 ischemic cardiomyopathy, 6 NICM, and 7 healthy volunteers) were enrolled into the trial and gave informed consent. 1 healthy volunteer and 1 NICM participant dropped out after the first imaging visit, due to claustrophobia/discomfort. Only participants who completed both HED and FBBG scans were included in the final analysis (n=25). No major

adverse events were reported during the study proceedings. The average time interval between imaging visits [A] and [B] was 8.7 ±7.6 days (range 2-35 days; 22 of 25 participants completed both visits within 2 weeks). Patients clinical status and medication regimens remained unchanged in all patients during the study period. Participant characteristics appear in Table 4.1.

4.5.1 FBBG Global Innervation

As expected, measures of global LV innervation, RI and DV, as assessed by both [^{11}C]HED and [^{18}F]FBBG were markedly lower in patients with ischemic cardiomyopathy, as compared to healthy participants ($p<0.05$, Supplemental Figure 4.1). This difference was noted at both early (5-10min) and late (30-40min) imaging timepoints. In contrast, global LV RI and DV for both tracers were not lower in patients with NICM as compared to healthy participants.

FBBG RI ($r^2=0.87$; ICC=0.83; $p<0.0001$) and DV ($r^2=0.62$; ICC=0.77; $p<0.0001$) correlated highly with HED (Figure 4.2, Table 4.2). At the late imaging timepoint, average innervation parameters of global RI and DV were not significantly different between FBBG and HED (table 4.2, Figure 4.2). These similarities in global innervation were also independent of disease status (Figure 4.2A). There was also no difference in RI on a segmental level (17-segment) between tracers or disease groups, suggesting that HED and FBBG yield equivalent regional distributions in both patients with and without ischemic cardiomyopathy (Figure 4.2B). Representative retention polar maps are displayed in figure 4.2D.

Table 4.1 Patient Demographics and Characteristics

Variable	Healthy Control (n=6)	Ischemic Cardiomyopathy (n=14)	Nonischemic Cardiomyopathy (n=5)
Demographics			
Sex (Male)	3 (50%)	12 (86%)	5 (100%)
Age (yrs)	54.5 ± 10.9	72.3 ± 7.5	61.8 ± 6.2
BMI (kg/m^2)	27.4 ± 3.3	28.1 ± 4.5	29.7. 8.0
Diabetes	0 (0%)	4 (29%)	2 (40%)
LVEF (%)	-	34.1 ± 5.0	32.9 ± 3.4
NT-ProBNP (pg/mL)			
HED	35.5 ± 29.4	812.9 ± 502.9	729.2 ± 809.3
FBBG	39.5 ± 27.5	847.3 ± 711.6	1086.8 ± 1271.7
NYHA Functional Class	-		
Class I	-	4 (29%)	0
Class II	-	9 (64%)	5 (100%)
Class III	-	1 (7%)	0 (0%)
Class IV	-	0 (0%)	0 (0%)
CAD	0 (0%)	100 (100%)	0 (0%)
Previous MI	0 (0%)	12 (86%)	0 (0%)
Previous ACS	0 (0%)	1 (7%)	0 (0%)
Previous CABG	0 (0%)	4 (29%)	0 (0%)
Previous PCI	0 (0%)	11 (79%)	0 (0%)
Medications			
β-blocker	0 (0%)	14 (100%)	5 (100%)
ACE/ARB	0 (0%)	14 (100%)	5 (100%)
MRA	0 (0%)	9 (64%)	5 (100%)
Diuretic	0 (0%)	8 (57%)	2 (40%)
Ca^{2+} Channel Blockers	0 (0%)	0 (0%)	0 (0%)
Statin	0 (0%)	13 (93%)	3 (60%)
Antiplatelets	0 (0%)	12 (86%)	0 (0%)
Rate Pressure Product			
HED	7680 ± 2943	6428 ± 1518	8700 ± 3946
FBBG	7679 ± 1676	6624 ± 1250	8724 ± 3122

BMI, Body mass index; LVEF, left ventriclular ejection fraction; NT-proBNP, N-terminal pro-B-type natriuretic peptide; NYHA, New York Heart Association; MI, myocardial infarction; ACS, acute coronary syndrome; CABG, coronary artery bypass gaft; PCI, percutaneuous coronary intervention; ACE, angiotensin-converting enzyme; ARB, angiotensin receptor blocker; MRA, mineralocorticoid receptor antagonist.

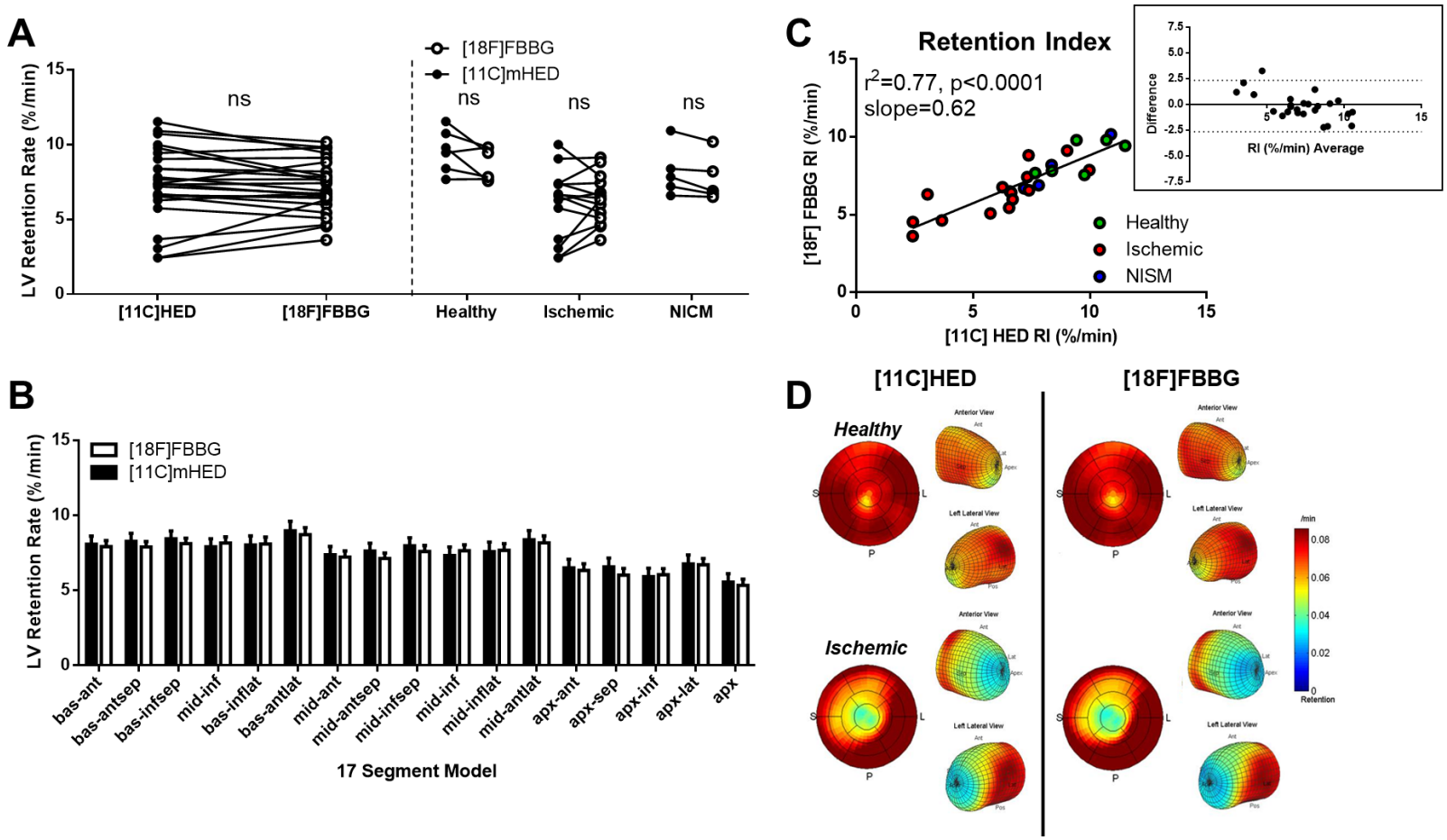

Figure 4.2. **HED and FBBG global (A) and regional (B) retention.** Correlation between LV global retention (1 segment model) illustrated (C). Representative retention polar maps in a healthy participant and a patient with ischemic cardiomyopathy (D).

Table 4.2. Tracer regional denervation and global innervation. Regional denervation and global innervation parameters compared between FBBG and HED in health participants and patients with ischemic and non-ischemic cardiomyopathy.

	[^{18}F] FBBG		[^{11}C]HED		p-Value (b/t tracer)	
Tracer S.A (mCi/μmol)	21044.3 ± 11447.7		750.1 ± 388.6		-	-
	Early	***Late***	***Early***	***Late***	***Early***	***Late***
LV Non-Uniformity (%LV)	19.0 ± 14.8	20.5 ± 15.8	19.5 ± 15.4	21.6 ± 16.8	0.28	0.06
Healthy	3.5 ± 2.9	3.2 ± 2.3	3.5 ± 3.4	3.5 ± 2.4	0.99	0.99
Ischemic	28.0 ± 12.6*	30.4 ± 12.5*	28.4 ± 13.3*	31.6 ± 13.4*	0.83	0.36
NICM	12.6 ± 9.9	13.6 ± 11.9	13.6 ± 11.1	15.6 ± 14.7	0.64	0.37
LV Global RI (%/min)	15.9 ± 3.6	7.2 ± 1.8	15.0 ± 4.3	7.3 ± 2.4	0.007	0.56
Healthy	20.1 ± 1.2	8.7 ± 1.1	20.1 2.1	9.6 ± 1.4	0.99	0.23
Ischemic	13.5 ± 2.4*	6.3 ± 1.6*	12.2 ± 3.2*	6.0 ± 2.3*	0.01	0.77
NICM	17.7 ± 2.6	7.7 ± 1.5	16.7 ± 2..4	8.2 ± 1.7	0.40	0.77
LV Global DV (mL/g)	5.7 ± 2.8	12.8 ± 4.3	5.3 ± 2.1	13.0 ± 5.5	0.29	0.76
Healthy	7.1 ± 1.5	16.3 ± 3.3	7.0 ± 1.3	16.7 ± 3.6	0.99	0.98
Ischemic	4.5 ± 2.7	10.5 ± 3.5*	4.1 ± 1.8*	10.4 ± 5.3*	0.87	0.99
NICM	7.5 ± 2.9	15.2 ± 3.7	6.6 ± 1.7	15.9 ± 4.2	0.72	0.96

FBBG, flubrobenguane; HED, hydroxyephedrine; NICM, non-ischemic cardiomyopathy; LV, Left Ventricle; S.A., Specific Activity; RI, Retention Index; DV, Distribution volume.*Significantly different than healthy control, $p<0.05$. RI, Retention Index; DV, Distribution Volume.

4.5.2 HED and FBBG Regional Denervation

The LV non-uniformity (size x severity of defect) defect size was greater in patients with ischemic cardiomyopathy than both healthy participants and NICM patients (Supplemental Figure 4.1). The mean regional defect size was equivalent between [^{11}C]HED and [^{18}F]FBBG (21.6±16.8, vs 20.5±15.8, %LV). Denervation volume was also equivalent between tracers irrespective of disease status (Figure 4.3A, Table 4.2). FBBG regional denervation score (r^2=0.97; ICC=0.98; $p<0.0001$) correlated highly with [^{11}C]HED (Figure 4.2, Table 4.3). LV regional denervation was also equivalent at the early and late imaging timepoints for both HED (ICC=0.97) and FBBG (ICC=0.98) (Figure 4.3C). Representative LV uptake polar maps are displayed in Figure 4.3D.

4.5.3 Organ Contrast Ratio

FBBG demonstrated favorable heart-to-lung and heart-to-liver contrast ratios over the course of imaging (Figure 4.4). FBBG heart-to-blood contrast was significantly greater than HED given the faster clearance kinetics. Overall, contrast ratios for HED and FBBG were similar in patients with ischemic and non-ischemic cardiomyopathy (Supplemental Figure 4.2).

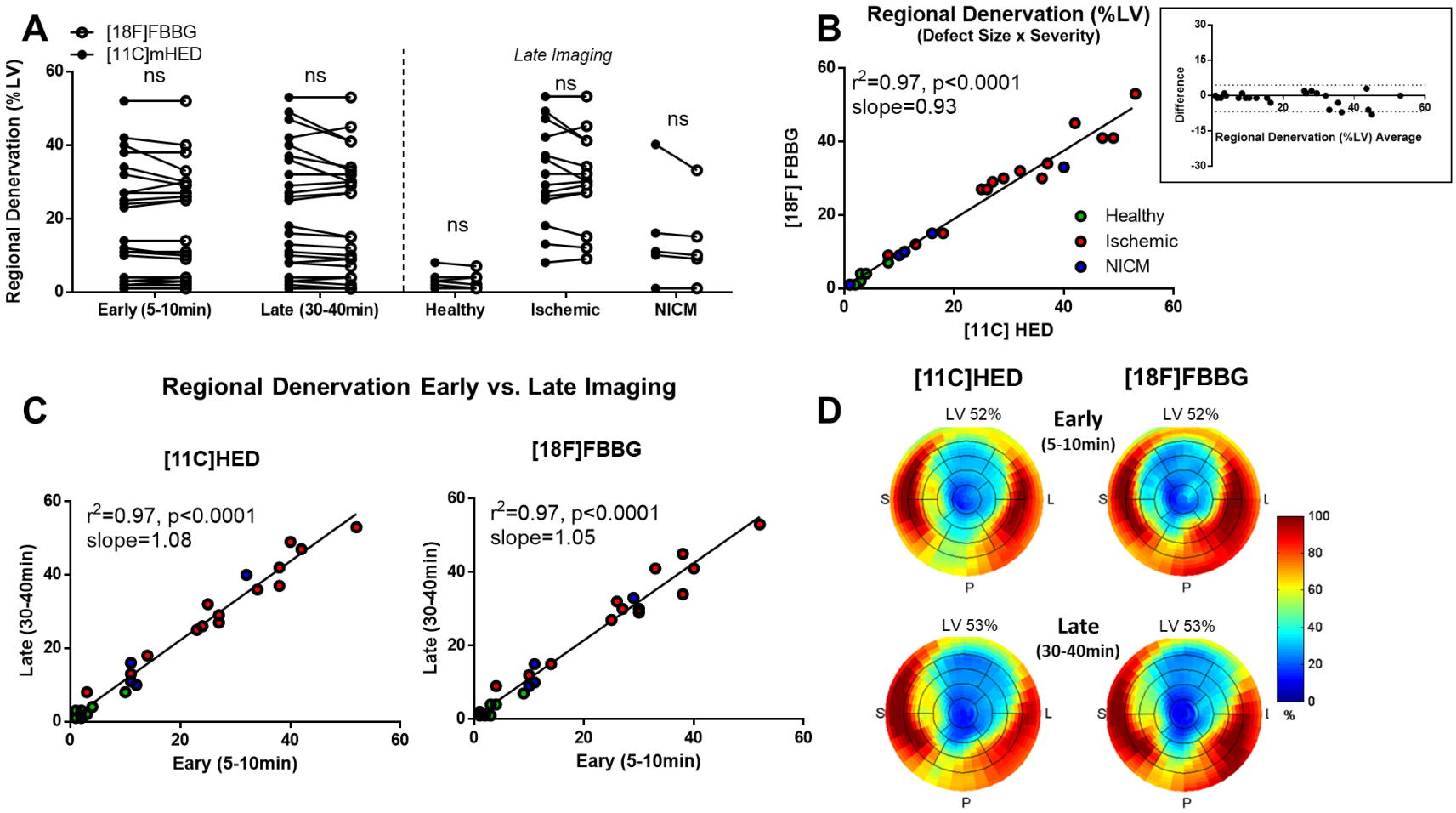

Figure 4.3. HED and FBBG regional denervation score (%LV non-uniformity) is equivalent between tracers (A). Correlations between tracers (B) and imaging time points (C) are displayed. Representative uptake polar maps in a patient with ischemic cardiomyopathy at a early (5-10min) and late (30-40min) time point (D).

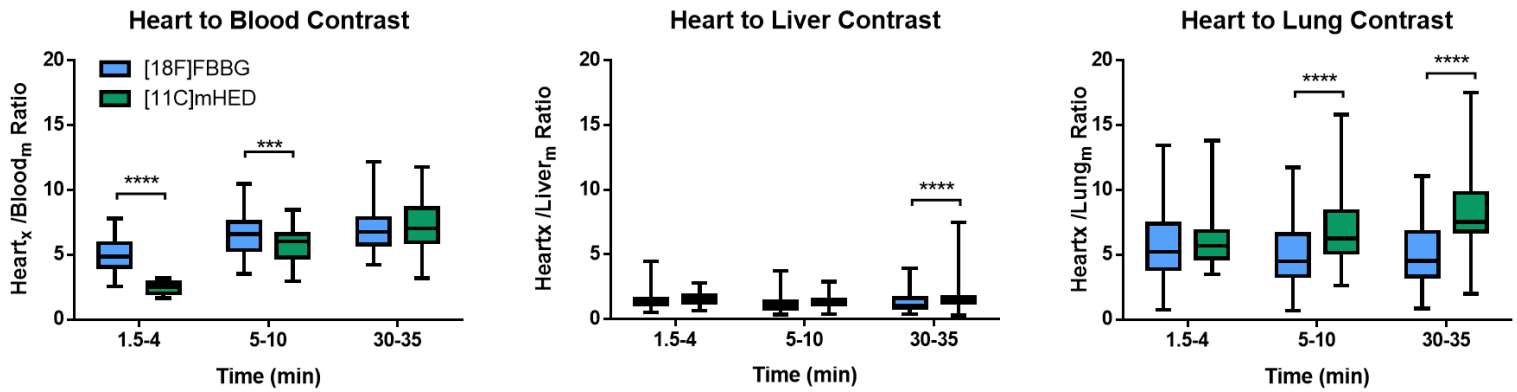

Figure 4.4. HED and FBBG Heart contrast ratio (Calculated as tissue (SUV heart max / background tissue or blood) assessed over time in the LV (A), liver (B) and Lung (C). Max and Mean SUVs were assessed from VOI in the LV blood pool, lung and liver and LV.

Table 4.3: Correlations between i) FBBG and HED and ii) Early and Late imaging.

Parameter	Linear Regression		ICC (95%CI)
	R^2	Slope (95%CI)	
i) [^{11}C]HED vs [^{18}F]FBBG			
LV Non-Uniformity			
Early Imaging	0.98	0.96 (0.90, 1.01)	0.99 (0.98, 0.99)
Late Imaging	0.97	0.93 (0.86, 1.00)	0.98 (0.96, 0.99)
Global Retention Index			
Early Imaging	0.89	0.78 (0.66, 0.90)	0.91 (0.73, 0.96)
Late Imaging	0.77	0.62 (0.47, 0.76)	0.83 (0.66, 0.92)
Global Distribution Volume			
Early Imaging	0.47	0.89 (0.48, 1.30)	0.66 (0.37, 0.83)
Late Imaging	0.62	0.62 (0.41, 0.84)	0.77 (0.55, 0.89)
ii) Early vs Late Imaging			
[^{11}C]HED			
LV Non-Uniformity	0.97	1.08 (0.99, 1.16)	0.97 (0.89, 0.99)
Global Retention Index	0.85	0.53 (0.44, 0.63)	0.24 (-0.04, 0.66)
Global Distribution Volume	0.82	2.34 (1.87, 2.80)	0.23 (-0.07,0.57)
[^{18}F]FBBG			
LV Non-Uniformity	0.97	1.05 (0.97, 1.13)	0.98 (0.94, 0.99)
Global Retention Index	0.78	0.43 (0.34, 0.53)	0.12 (-0.03, 0.41)
Global Distribution Volume	0.42	1.02 (0.51, 1.53)	0.21 (-0.06, 0.55)

ICC, Intraclass correlation coefficient; FBBG, flubrobenguane; HED, hydroxyephedrine;

4.6 Discussion

Quantifying the burden of sympathetic denervation can help predict life-threatening arrythmias, thus offering the potential to guide advanced therapies such as prophylactic implantable cardiac defibrillators (ICD). This phase II, single center clinical trial aimed to validate a novel ^{18}F labeled norepinephrine analog, flubrobengaune, against the current SNS imaging PET standard [^{11}C]*meta*-hydroxyephedrine. The present study represents the first use of FBBG to non-invasively image the cardiac SNS in patients with ischemic and non-ischemic cardiomyopathy. Major finds reveal that FBBG and HED yield equivalent global and regional distribution in both patients with and without ischemic cardiomyopathy. The faster blood pool clearance of FBBG yields greater contrast, which may offer more favorable kinetics for early imaging. ^{18}F-Labeled tracers such as FBBG offer the potential for the wide distribution needed for maximum patient and clinical impact.

mIBG and HED are the most well characterized tracers to non-invasively image and characterize cardiac sympathetic innervation and function. The ADMIRE-HF and PAREPET trials revitalized interest in the field of sympathetic imaging which demonstrated the utility in mortality prognostication and SCA risk prediction.[173,320] Although exciting, the widespread utility of these tracers are limited with respect to crude quantification methods and short tracer half-life. The new ^{18}F tracer flubrobenguane was created to overcome these limitations while taking advantage of the superior quantification methods of PET. HED is a structural analog of norepinephrine (NE); whereas, mIBG and FBBG analogs of guanethidine and are considered false neurotransmitters.[311,337] These tracers all have a high affinity for the NE transporter, but within the neuronal microenvironment are resistant to degradation by monoamine oxidase.

Although these tracers all exhibit similar uptake mechanisms, their intra-neuronal kinetics are markedly different. HED is believed to have some vesicular packaging, but its high lipophilicity makes it susceptible to 'leakage' across lipid membranes.[305,183] HED kinetics are therefore reliant on a continuous recycling process of uptake and leak/release. In contrast, FBBG and mIBG are packaged and efficiently stored in neuronal vesicles and are thought to be released in to synaptic cleft upon neuronal activation.[183]

In a recent retrospective analysis of the PAREPET trial, we aimed to compare global innervation and regional denervation parameters for SCA risk prediction (in review). Key findings suggest that global innervation parameters (RI and RV) offer no independent or additive prognostic value to regional denervation. This suggests the quantification method utilized in the PAREPET trial (analogous to non-uniformity score) yield the most robust SCA risk prediction. In the present study, the regional defect sizes were equivalent between the two tracers in patients with and without ischemic disease. We further demonstrate stable defect scores between early and late imaging for both tracers. Taken together, these data will greatly simplify both the quantification and imaging protocols for SNS imaging with FBBG, which opens a large imaging window (i.e. 5 minutes to 3-4hrs).

In summary, the novel ^{18}F tracer FBBG yields a reliable estimate of cardiac sympathetic innervation as compared to HED. Having a similar molecular structure as mIBG (for SPECT) enables an opportunity build on mIBG's longstanding efficacy portfolio while capitalizing of the superior resolution and quantification capabilities of PET. Studies completed to date demonstrate that SNS imaging yields clinically useful data to quantify arrhythmogenic/sudden death risk, possibly guiding the selection of appropriate device therapies for a cohort of patients at risk for what remains a lethal and unpredictable disease. The present study suggests the FBBG is an

excellent candidate for future randomized trials investigating whether SNS imaging can better predict outcome benefits in patients with ischemic cardiomyopathy after ICD placement, and thus enabling a more precision targeted patient selection process. Whether an imaging-guided strategy alone can yield outcome-driven cost-effective therapy selection represents an important goal of the field.

Funding

Jason Zelt is an MD/PhD student supported in part by the Vanier CIHR graduate scholarship, and the University of Ottawa. Rob Beanlands is a Career Investigator supported by the Heart and Stroke Foundation of Ontario (HSFO) and is a Tier 1 Chair in Cardiac Imaging Research at the University of Ottawa. Lisa Mielniczuk is a Mid-career Clinician Scientist supported by HSFO and a Tier 2 Chair in HF Research at the University of Ottawa. This project is funded under an Ontario Research Fund Grant ORF-RE-07-021 and Lantheus Medical Imaging.

Disclosures:

RdK is a consultant for- and has received grant funding from Jubilant DraxImage. RdK receives revenues from Rubidium-82 generator technology licensed to Jubilant DraxImage, and from sales of FlowQuant software. RSB is or has been a consultant for- and has received grant funding from GE Healthcare, Lantheus Medical Imaging, and Jubilant DraxImage. Roche Diagnostics Global is a partner with the Genome Canada grant to PPL.

4.7 Chapter 4 Extension: FBBG in the RV

Preliminary results suggest equivalent global RV retention rate between HED and FBBG.

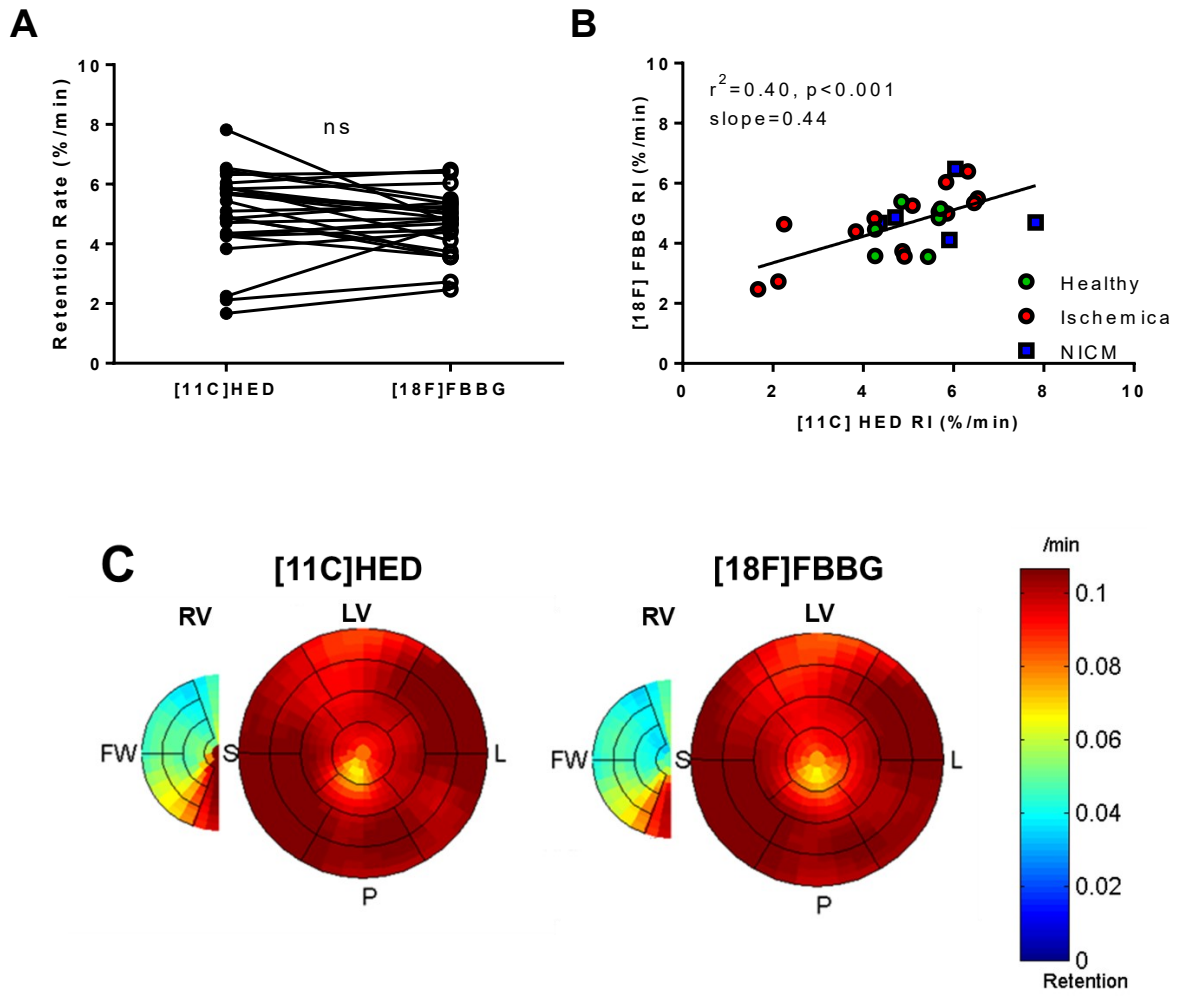

Figure 4.5 FBBG vs HED in the Right Ventricle. HED and FBBG global (A) RV retention (A). Correlation between RV global retention (1 segment model) illustrated (B). Representative retention polar maps are displayed (C).

Chapter 5

Failure of Right Ventricular Adaptation in Response to Pressure Overload Related to a Profound Deficiency in Adenylate Kinase 1 and Impaired Ventricular Energetics

Zelt *et al.* 2020. Submitting to *Circulation*

Running Title: *Right Heart Metabolic Maladaptation in PAH*

**Authors: *Jason G.E. Zelt[1,2] PhD; ***Virgilio Cadete[3] PhD; Yupu Deng[3]; Alexanne Cuillerier MSc; Katelynn Rowe[3] MSc; Mohammad Abdul-Ghani[3] PhD; Lynn Megeney[3] PhD, Yan Burelle[4] PhD; Antonio Giulivi[5] MD; Robert deKemp PhD[1]; Rob Beanlands[1,2] MD; Lisa M Mielniczuk[1,2] MD, MSc; and Duncan J. Stewart[1,2,3,6] MD

* These authors contributed equally

[1] Molecular Function and Imaging Program, The National Cardiac PET Centre, and Advanced Heart Disease Program, Division of Cardiology, Department of Medicine, University of Ottawa Heart Institute,, Ottawa, Canada
[2] Department of Cellular and Molecular Medicine, Faculty of Medicine, University of Ottawa, Ottawa, Canada.
[3] Sinclair Centre for Regenerative Medicine, Ottawa Hospital Research Institute, Ottawa, Canada
[4] Faculty of Health Sciences, University of Ottawa
[5] Eastern Ontario Regional Laboratory Association

Authorship Contributions:
JGEZ: Performed experiments, statistical analysis, graphical representation and wrote the manuscript.
VC: Performed experiments, statistical analysis, graphical representation
YD: Technical assistance with cardiac echocardiography and right heart catheterization.
MAG and LM: Proteomic Analysis
AG: Hematologist
RD and RSB: PET technical expertise
AG and GW: Oversaw the statistical analysis
DJS and LM: Supervision and PIs on the project. Helped conceive experimental design and content experts.

Key words: Adenylate Kinase, Metabolism, Pulmonary Hypertension, Right Ventricle, Heart Failure

5.1 Abstract

Background: Interindividual heterogeneity in right ventricular (RV) remodeling and progression to RV failure in pulmonary arterial hypertension (PAH) is not well explained by differences in the degree of afterload, highlighting the importance of genetic factors. This is recapitulated by marked strain differences in RV adaptation between Sprague-Dawley (SD) and inbred Fischer rats, which exhibit adaptive and maladaptive remodeling, respectively.

Methods: PAH was induced by a single subcutaneous injection of the VEGFR antagonist, SU5416, followed by a 3-week exposure to hypoxia (SUHx). *In vivo* oxidative metabolism, assessed by the RV/LV ratio of [^{11}C]acetate PET clearance (kmono).

Results: Fischer rats exhibited RV failure and 100% mortality at 5-weeks, whereas SD rats showed preserved RV function and excellent survival beyond 9-weeks (88%; $p<0.0001$). *In vivo* oxidative metabolism (RV/LV ratio[^{11}C]acetate kmono), was increased in Fischer rats compared to SD at 4 weeks in SUHx (0.82±0.09 vs 1.0±0.11min-1, respectively; $p<0.05$). Interestingly, the higher oxidative metabolism in Fischer rats was associated with impaired RV efficiency compared to SD (work metabolic index: 58.4±12.4, 102.2±20.0 mmHg·mL/cm^2 respectively; $p<0.001$). In contrast, no baseline differences were observed in mitochondrial oxidative phosphorylation complex activity, measured in permeabilized RV cardiac fibers. Unbiased, global transcriptional profiling was preformed to compare background RV gene expression in Fischer and SD rats at baseline and after SuHx. Ten genes were differentially expressed in controls, of which 6 demonstrated consistent expression patterns in SuHx rats ($p<0.05$). In particular, adenylate Kinase 1 (AK1) mRNA expression was markedly lower in Fischer rats (FC: 3.36, $P<0.05$) and SuHx rats (FC: 2.7,

p<0.x05), as compared to SDs. As well, label-free proteomic analysis confirmed near complete absence of AK1 protein expression in Fischer rats, which was validated by Western blotting (>10-fold, P<0.001). Similarly, in human RV samples, AK1 protein levels were significantly reduced only in PAH patients who exhibited decompensated RV function and right heart failure.

Conclusion: For the first time, we have demonstrated inefficient cardiac energetics in the maladapted RV of Fischer rats with severe PAH which is due to a strain-dependent deficiency in AK1. Under conditions of stress the AK1 pathway plays a dominant role in shuttling ATP from the mitochondria to the actin/myocin cross-bridge for muscle contraction, and thus AK1 deficiency represents a novel mechanism for RV failure in response to chronic increases in afterload.

5.2 Introduction

Right ventricular (RV) function is a critical determinant of prognosis for patients with pulmonary arterial hypertension (PAH).[2] Interindividual heterogeneity in RV remodeling and progression to RV failure in PAH is not well explained by differences in the degree of afterload, highlighting the importance of inter-individual heterogeneity, largely due to genetic factors.[91] Clinically, the remodeling process is often dichotomized into adaptive or maladaptive phenotypes, the latter being associated with reduced RV function, RV failure and poor outcomes (i.e., decompensated RV remodeling).[74,294] The 5-year survival for PAH patients with stable or improving RV function is >90%; whereas, survival for patients with decreasing RV function, independent of changes in PVR, is documented <30%, with right HF being the most common cause of death.[2]

The molecular mechanisms responsible for these divergent phenotypes remain to be fully elucidated, but underlying genetic differences in RV energetics may, in part, explain this heterogeneity and the propensity for progressive RV failure in some patients. To maintain cardiac output during sustained RV afterload, sufficient power output must be generated, but at the cost of increased oxygen utilization. This increased oxygen requirement is essential to maintain a constant flux of ATP for contraction. Patients with PAH often have severely limited perfusion reserve, and thus the RV must increase mechanical efficiency to meet energy requirements or risk succumbing to RV failure. Indeed, some PAH patients can increase RV mechanical efficiency[338], an initial adaptive response; whereas patients who display an impaired RV efficiency, progress to RV failure.[339,340] This suggests an intrinsic link between RV energetics and pathologic RV remodeling that may drive the progression of RV failure.

The marked heterogeneity in response to pressure overload is recapitulated by strain differences in RV adaption between Sprague-Dawley (SD) and Fischer (CDF) rats. While SD rats exhibit adaptive RV remodeling, in-bred Fischer rats show progressive RV decompensation in the Sugen and chronic hypoxia (SuHx) model of severe PAH, [95,96] which was associated with RV dilatation and reduced contractile function, and near universal mortality by 6 weeks. Detailed characterization of the maladaptive RV phenotype in Fischer rats revealed greater RV dilatation, reduced myocardial vascularization and excessive fibrosis and suggested that this genetically determined, RV failure-prone model was ideally suited for the further exploration of molecular mechanisms underlying maladaptive remodeling.[97] Therefore, in the present study we used this unique model to explore the underlying molecular determinants and metabolic mechanisms of maladaptive remodeling in severe PAH.

5.3 Methods

All animals received humane care and procedures conformed to the guiding principles of the Canadian Council on Animal Care (CCAC) , and were approved by the animal ethics and research committee (University of Ottawa, Ontario, Canada).

5.3.1 SUHx Model of Severe PAH

The Sugen Hypoxia animal model (SuHx) of severe PAH was used as previously described.[99] Briefly, severe angioproliferative PAH was induced in male Sprague-Dawley (SD, Harlan laboratories, Indianapolis, IN, USA) and Fischer (CDF, Charles River, Montreal, Quebec, Canada) rats weighing 125-200 g by a single subcutaneous injection of Sugen5416 (SU: 3-(3,5-dimethyl-1H-pyrrol-2- ylmethylene)-1,3-dihydroindol-2-one) (Tocris, Bristol, UK) combined with 3 weeks of exposure to chronic hypoxia (10% O_2).

5.3.2 Non-Invasive Echocardiography

Non-invasive transthoracic echocardiographic Imaging was performed in rats at 4 weeks post Sugen5416 injection using Vevo2100 ultrasonography system (VisualSonics, Toronto, ON, Canada). Animals were anesthetized using isoflurane anesthesia (1.5-2%). RV chamber size was assessed on short-axis Mmode echocardiography and was expressed as the ratio of end-diastolic RV to LV internal diameter (RVID-d/LVID-d). The transducer was then aligned with good visualization of the pulmonary artery in the parasternal long axis view. The sample volume was placed at a $10\text{-}12^0$ angle aligned with laminar flow. Pulmonary artery acceleration time (PAAT) was measured using pulmonary artery waveforms from the onset of systolic flow to peak outflow velocity. Cardiac output was calculated using the pulmonary artery velocity time integral PA-VTI method as previously described.[49] The operator acquiring and analyzing the echocardiographic images was blinded to treatment status.

5.3.3 RV Microarray Gene Expression

We re-analyzed our previously published RV gene expression data to investigate base-line strain gene expression differences.[97] RNA was isolated from RV tissues in Fischer and SD rats 4 weeks post SU injection and aged matched controls using miRCURY RNA isolation kit (Exiqon, Woburn, MA, USA) according to manufacturer's protocol. Total RNA was measured using Affymetrix Rat Gene 2.0ST and Affymetrix miRNA 4.0 gene chip. Fold change analyses were performed using the R Bioiconductor limma package, according to gene expression changes in Fischer vs SD controls and SuHx animals with cutoff values of adjusted p-value <0.05.

5.3.4 Proteomics

RV proteomic quantification was performed using label-free LC-MS/MS (as adapted from Schechter et al). Briefly, RV tissue samples were subject to methanol protein extraction, then treated with RapiGEST in 50mM ammonium bicarbonate. Protein pellets (5mg total) were then treated at 90C for 5 min to solubilize hydrophobic and proteolytic resistant proteins, followed by standard tryptic digestion. Digested samples were then subject to sequential reduction (100mM DTT), alkylation (20mM iodoacetamide) and overnight tryptic proteolysis (1:50 w/w sequencing grade trypsin). Digestion was terminated with 1% TFA. Centrifuged, cleared digested protein samples (25mg) were then spiked with 1.25 pmol of yeast ADH1 protein (as the internal peptide standard for quantitation) and heated to 60C for 2 hours. Samples w stored at -80C until use for LC-MS/MS on a system comprised of an UltiMate 3000 RSLC nano, LTQ Orbitrap XL hybrid mass spectrometer, and nanospray ionization source (Thermo Fisher Scientific, MA, USA). (Thermo Fisher Scientific, MA, USA). Appropriate software was utilized for peptide identification and DDA (Data-Dependent quantitative Analysis; Scaffold DIA from Proteome Software Inc).

5.3.5 Western Blotting

Western blotting RV and LV lysates were prepared in RIPA lysis buffer (MilliporeSigma, ON, Canada) using the TissueLyser (Qiagen, ON, Canada) two cycles of 25hz for 3 min. The tissue lysate was then centrifuged at 10000xg for 10 min and supernatant was collected. Protein concentration were determined colorimetrically using the DC Protein Assay kit (Bio-rad, ON, Canada). SDS-polyacrylamide gel electrophoresis of RV and LV protein extract (20 µg) was performed with NuPAGE® Novex® 4-12% Tris-glycine Protein Gels (ThermoFisher Scientific, ON, Canada). Following transfer of these separated proteins to nitrocellulose membranes

(NOVEX iBLOT Gel transfer Stacks, ThermoFisher Scientific, ON, Canada), blots were incubated with primary antibodies to Adenylate Kinase 1 (Abcam, 1:1000 dilution) GAPDH (NEB/CST;1:1000 dilution), and a total mitochondrial cocktail (Abcam; 1:1000 dilution), in 5% BSA in TBS-T (TBS containing 0.1% tween 20, pH 7.4) for overnight at 4° C. Then the blots were washed for three times for 10 min with TBS-T, then for onetime for 10 min with TBS and then incubated with appropriate IR Dye® anti-rabbit or anti-mouse secondary antibodies (LI-COR Biotechnology, NE, USA) in 5% BSA/TBS. Blots were then washed for twice for 5 min with TBS and imaged with Odyssey® imaging system (LI-COR Biotechnology, NE, USA).

***Western blotting analysis of human RV tissue*:**

Total proteins were extracted from human right ventricle using a 2% Chaps protein extraction buffer supplemented with a protease-inhibitor cocktail (Roche). Protein concentration was determined using the Bradford method. Equal amounts of protein were loaded on SDS page, electrophoresed, and transferred onto polyvinylidene fluoride membranes using a liquid blotting system (Bio-Rad). After blocking with either 5% non-fat dry milk or 5% goat serum in TBS-T buffer for 1 hour, membranes were incubated overnight at 4°C with indicated primary antibodies (Table 7). Membranes were then incubated with appropriate HRP-conjugated secondary antibodies for 2 hours. Antibodies were revealed using ECL reagents (Perkin–Elmer) and using the imaging Chemidoc MP system (Bio-Rad Laboratories). Protein expression was quantified using the Image lab software (Bio-Rad Laboratories) and normalized to Amido black, as previously reported[65,66].

5.3.6 Mitochondrial Respiration in Isolated RV Fibers

Right ventricle free walls were used for dissection and fiber permeabilization. RV fiber bundles were permeabilized with saponin and kept on ice until use, as described previously.[341] All mitochondrial functional parameters were expressed relative to wet fiber weight. Mitochondrial respiration was measured using Clark-type electrodes in permeabilized RV fibers (< 2 mg wet weight) at 23°C, with constant stirring, in a respiration buffer [in mM: 2.77 CaK EGTA, 7.23 K EGTA (100 nM free Ca2+), 6.56 MgCl2 (1 mM free Mg2+), 20 taurine, 0.5 DTT, 50 potassium methane sulfonate (160 mM ionic strength), 20 imidazole, pH 7.1]. Oxygen consumption rate (nmol O2 min–1) was determined using the following sequence[341]: complex I substrates glutamate–malate (5:2.5 mM); ADP (2 mM); the complex I blocker amytal (2 mM); the complex II substrate succinate (5 mM); the complex III blocker antimycin-A (8 μM); and the complex IV substrates N,N ,N -tetramethyl-p-phenylenediamine dihydrochloride (TMPD)–ascorbate (0.9:9 mM).

5.3.7 Citrate Synthase Activity

Citrate synthase (CS) activity was measured spectrophotometrically in RV lysates with a plate reading using standard coupled enzyme assays as previously described. [341]

5.3.8 [^{11}C]Acetate Positron Emission Tomography (PET)

[11C]Acetate PET imaging was performed to assess myocardial oxidative metabolism and RV energetics. Anaesthetized rats were placed in Siemens Inveon^{TM} small animal PET scanner (Siemens, Knoxville, TN; 12.7 cm axial field-of-view, spatial resolution <1.4mm^3) with heart and lungs centered in the field of view. Following a ^{57}Co attenuation transmission scan for attenuation correction, rats were injected with 0.9-1.0 mCi (0.5mL) of [11C]acetate via a lateral tail vein catheter and dynamic images acquired for 20 minutes. Images were reconstructed using

OSEM3D+MAP with 2+18 iterations. Dynamic PET images were processed and analyzed using in-house software FlowQuant© to measure 11-C clearance reflecting tricarboxylic acid cycle (TCA) flux which is linearly related to myocardial oxygen consumption.[342] The clearance rate-constant, k_{mono}, was determined regionally in the LV and RV by fitting a mono-exponential function to the [11C]acetate time-activity data. Explicit partial volume correction was not performed (i.e. recovery coefficient = 1) as the RV and LV wall thickness was too small for reliable data-driven correction. Only one control Fischer and SD rat were imaged because the RV wall thickness in controls is ~1mm, and thus a data driven partial volume correction is technically challenging. A single Fischer and SD control animal was imaged to visualize the regional uptake patterns of [11C]acetate.

RV efficiency/ Work Metabolic Index: A fraction of the energy generated via oxidative metabolism is converted to external contractile work by the heart. Therefore, work metabolic index (WMI) can be used to estimate cardiac efficiency.[342–344]

Work Metabolic Index (WMI): is a simplified estimate of cardiac efficiency calculated as[343–345],

$$\text{WMI} = \frac{\text{SVI x HR x RVSP}}{\text{RV K}_{\text{mono}}}$$

Where SVI is the rat RV stroke volume indexed to the rat body surface-area; HR is heart rate; RVSP is right ventricular systolic pressure; k_{mono} is the RV [11C]Acetate mono-exponential clearance rate function applied to the RV [11C] acetate kinetics time- activity data .

RV power: the power output of the RV was calculated using the following equation,

$$\text{RV power} = \text{HR x RVSP x SV x } 2.22\text{x}10^{-6}$$

5.3.9 Metabolomics

To investigate the metabolic processes altered in Fischer and SD rats in response to SuHx (n=6 per group), we performed a metabolomic screen at the University of Ottawa metabolomics Core Facility. Aqueous metabolites were extracted via biphasic liquid-liquid extraction (methanol, water, acetonitrile, dichloromethane). Samples were run on a 6470 Triple Quadruple MS (Agilent) equipped with a 1290 Infinity ultraperformance LC system (Agilent), utilizing the Metabolimics Dynamic MRM Database and Method (Agilent), which uses an ion-pairing reverse phase chromatography.[346] Relative metabolite quantiifcations were calculated by interpolating compound calibration curves in Mass Hunter Quantification (Agilent).

5.3.10 Hematological Assessment

Hematological assessment was performed on a subset of control rats (n=3/ strain), and rats exposed to 3 weeks of hypoxia (n=5/strain). In hypoxia alone rats, blood was sampled immediately out of hypoxia. Blood was sampled from the left ventricle by cardiac puncture under anesthesia. Complete blood count analyses and blood films were performed at The Ottawa Hospital laboratory. Blood films were reviewed by a hematologist at the Ottawa Hospital.

5.3.11 Human RV Tissue

Experimental procedures using human tissues conformed to the principles outlined in the Declaration of Helsinki and were performed with the approval of Laval University and the IUCPQ Biosafety and Ethics Committees (CER#20773, CER#20735 and CER#21747). Tissues were obtained from patients who had previously given written informed consent. RV samples were categorized as control RV, compensated RV or decompensated RV based on clinical history and cardiac index (CI) (Table 1). Briefly, control RV was obtained from patients with

normal RV function who underwent aortic valve surgery or early autopsy following sudden death for which the previous medical history and the autopsy did not reveal cardiac or respiratory diseases. Compensated RV was obtained from cardiac biopsy or autopsy of patients with RV hypertrophy and preserved CI (>2.2 L/min/m^2) measured by echocardiography. Decompensated RV was obtained from early autopsy of patients with end-stage PAH.

5.3.12 AK1 Gene Expression in Human HFpEF

Given the known link between nucleotide homeostasis and muscle relaxation, we accessed a publicly available RNA-seq database of patients with HFpEF.[347] AK1 expression was compared in patients undergoing elective coronary bypass surgery (CABG) with heart failure with preserved ejection fraction (HFpEF) and patients with normal LV physiology. LV myocardial biopsies were obtained from 16 patients (n=5 HFpEF) with LVEF≥45%. AK1 expression was also correlated with indices of diastolic dysfunction, i.e. E/e' ratio and left atrial volume index (LAVI).

5.3.13 Statistical Analysis:

Statistical analysis and graphical presentation were performed using GraphPad Prism 6.0 (Graphpad Software, Inc. Ca, USA). Data are represented as mean±SD unless otherwise stated. For statistical comparisons, a One-Way ANOVA or Two-Way ANOVA were performed followed by Dunn's multiple comparison test. P-values <0.05 were considered statistically significant.

5.4 Results

5.4.1 Marked strain differences in mortality not due to hemodynamics or hypertrophy

In agreement with previous reports,[95–97] Fischer rats exhibited very poor survival in the SUHx model with >90% mortality by 42 days after SU injection; whereas, SD rats demonstrated excellent survival (Figure 5.1A, $p<0.0001$) despite similar elevations in RVSP (Figure 5.1B) and RV hypertrophy (Fulton Index, Figure 5.1C) at 4 weeks. By 4 weeks post SU-injection, both SD and Fischer rats showed severe pulmonary arteriolar remodeling with evidence of plexiform-like lesions (Figure 5.1D, representative image). Despite a similar hemodynamic burden on the RV, Fischer SuHx rats exhibited hallmark features of progressive right heart failure (RHF), namely, reduced cardiac output (E) and increased RV dilation (F), as compared with SD-SuHx ($p<0.05$). No hemodynamic or functional differences were noted between strains in healthy control rats. Although the RV free wall diameter is comparable between rats strains, control Fischer rats heart size was found to be smaller, proportional to their lower body weight (Supplemental Figure 5.1).

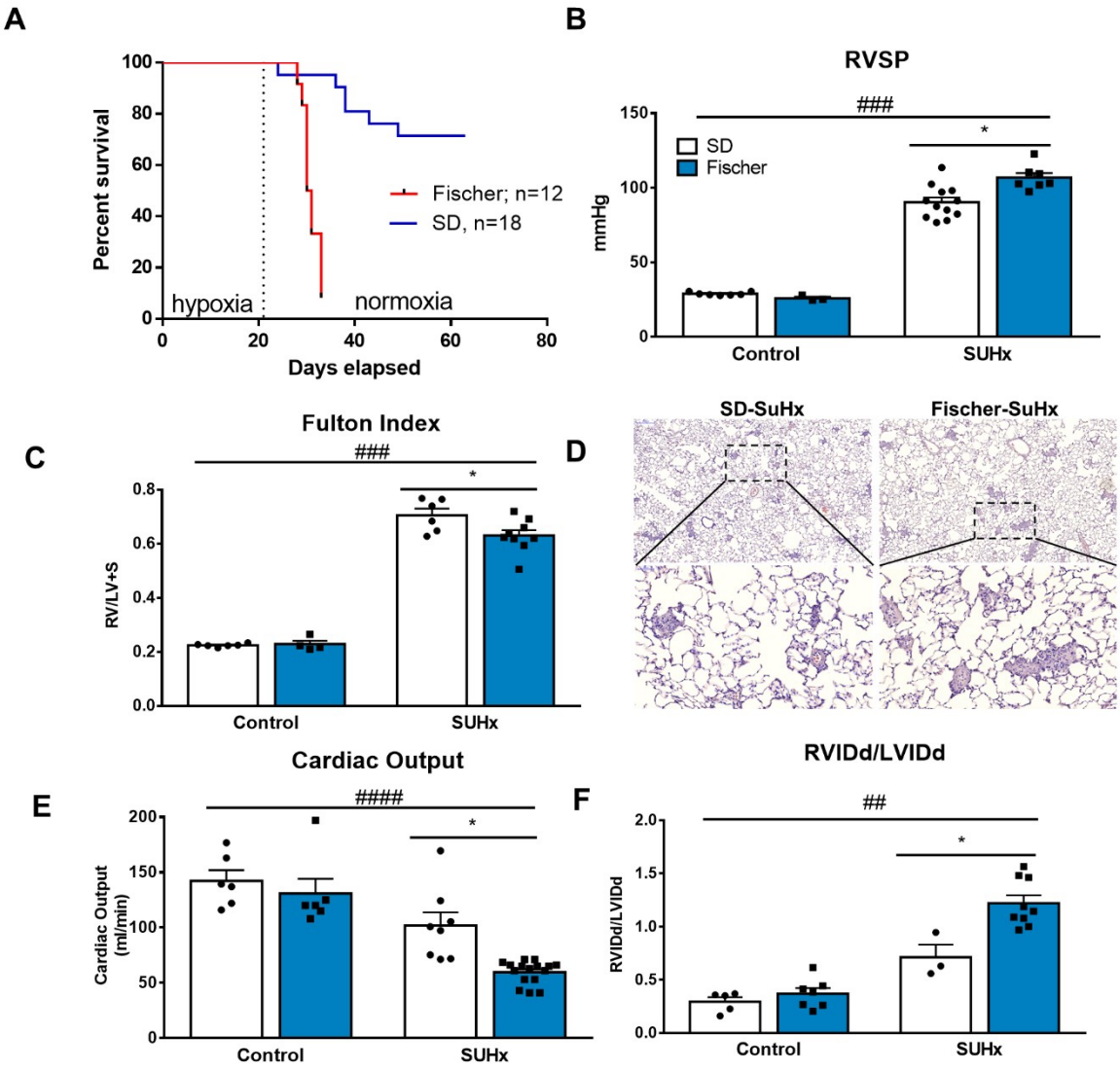

Figure 5.1 Strain differences in mortality and hemodynamics. Strain-dependent differences in severe PAH phenotype in rats exposed to SU5416 and 3-weeks of chronic hypoxia. Marked differences in survival with 100% mortality in Fischer rats by 5-6 weeks, whereas Sprague-Dawley (SD) rats show excellent survival up to 10 weeks (A). At 4-weeks, both strains exhibit plexiform-like lesions on lung histopathology (B). In this model, at 4-weeks, both rat stains display similar elevations in RVSP (C), hypertrophy (D). Despite a similar hemodynamic burden, Fischer rats exhibit characteristics of right heart failure, namely, reduced cardiac output (E) and greater RV dilation (F), compared to SD rats. Statistically significant difference between rat strains * $p<0.05$. Statistically significant difference between controls and SuHx ##$p<0.01$; ###$p<0.001$; #### $p<0.0001$

5.4.2 Impaired RV energetics in Fischer rats

RV TCA flux (i.e. oxidative metabolism) was assessed using [11C]acetate PET 4 weeks post SU-injection. Representative polar k_{mono} polar maps appear in Figure 5.2A. There were no significant differences in RV or LV k_{mono} between Fischer-SuHx and SD rats (Figure 5.2B and C). However, when normalized to the LV, the RV/LV oxidative metabolism ratio was significantly elevated in Fischer-SuHx rats as compared to SDs ($p<0.05$; Figure D). Nonetheless, Fischer SuHx rats had reduced RV power (Figure 5.2E, Figure 5.1E), and thus displayed a profound mechanical inefficiency (Figure 5.2F). Consistent with these findings was an elevated citrate synthase activity (a key TCA enzyme) in isolated permeabilized RV fibers in naïve Fischer rats compared to SDs (Figure 5.2G). The marked elevation in citrate synthase activity, even in control Fischer rats, is a consistent indicator of metabolic compensation for an inherent defect in a metabolic pathway.

Mitochondrial function was assessed in isolated permeabilized RV fibers in SuHx rats and matched controls. Although mitochondrial complex IV activity was reduced in response to SuHx ($p<0.05$), no strain differences were observed (Supplemental Figure 5.2). Mitochondrial complex protein expression was remarkably preserved up to 5 weeks at the time of RV failure in Fischer SuHx rats (Supplemental figure 5.2 and 5.33). The preserved TCA (Acetate PET) and electron transport chain (ETC) function in Fischer SuHx rats suggests an RV energetic defect extrinsic the mitochondria in Fischer rats.

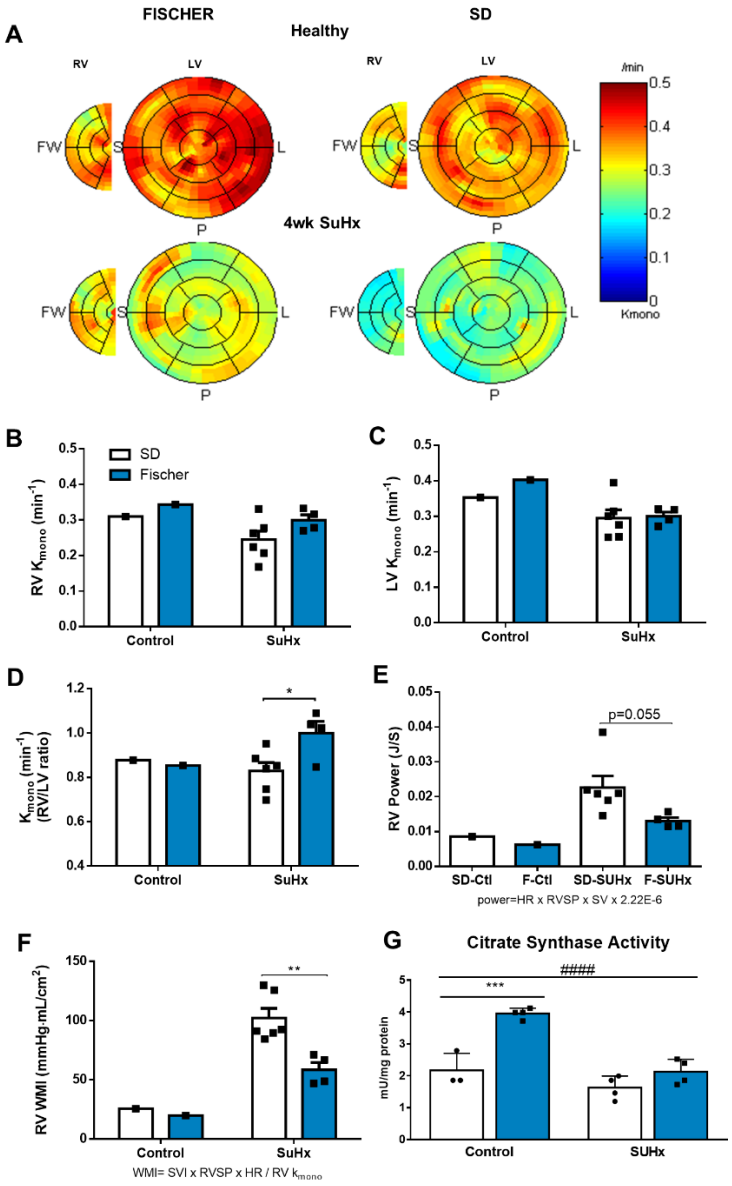

Figure 5.2. Oxidative metabolism in Fischer and SD SuHx rats, as assessed by [^{11}C]Acetate clearance on PET. Oxidative metabolism in Fischer and SD SuHx rats, as assessed by [11C]Acetate clearance on PET. Representative [11C]Acetate kmono (myocardial clearance) polor maps in Fischer and SD rats are displayed (A). Myocardial clearance of [11C] from [11C]acetate (kmono) is proportion to oxidative metabolism, therefore a greater clearance, suggests a higher rate of oxidative metabolism. RV kmono (B) trended towards being elevated in Fischer SuHx rats compared to SDs, but no differences were observed in the LV (C). RV normalized to LV clearance (RV/LV ratio) was elevated Fischer SuHx rats compared to SDs (D), but had lower RV power (E). This indicates a marked impairment in RV efficiency (F) in Fischer SuHx rats. Citrate synthase activity (key enzyme in TCA) was supressed in SuHx rats, but strain differences were observed at baseline (G). Statistically significant difference between rat strains *** $p<0.001$; ** $p<0.01$. Statistically significant difference between controls and SuHx #### $p<0.0001$.

5.4.3 RV global transcriptomic profiling reveals a deficiency in AK1 in Fischer rats

We had previously reported on the changes in gene expression profile in the severe PAH model in Fischer and SD rats.[97] However, in the present report, we were interested in contrasting differences in baseline RV gene expression profiles that might better reflect genetically determined differences between these two strains. Unbiased, global transcriptional profiling of the 20 000 genes, revealed only 10 differentially expressed genes that reached an adjusted p-value of <0.05 in Fischer control rats (Figure 5.3A), six of which (spta1, LOC100910934, cyp4v3, AK1, Car4 and AKr1b10) were also differential expressed in Fischer vs. SD rats exposed to SuHx (Figure 5.3B). Of these six genes, only adenylate kinase 1 (AK1) has been previously implicated in energetics and metabolism. The AK1 mRNA expression was significantly lower in Fischer control rats (FC: 3.36-times, P<0.05) and SuHx rats (FC: 2.7-times, p<0.05) compared to SD rats. Of note, of the AK family of genes, only AK1 was reduced in Fischer compared with SD rats with minimal, if any, compensatory increase in the other isoforms in SuHx (Figure 5.3C).

5.4.4 RV proteomic expression profiling

Unbiased RV proteomic quantification at baseline and after SuHx in Fischer compared with SD rats was performed using label-free LC-MS/MS. In the principal component analysis (PCA), a unique proteomic profile for Fischer rats was identified in controls, but not after treatment with SuHx (Figure 5.4A). In control rats, 642 unique proteins were identified, of which 71 were differentially expressed in Fischer compared with SD rats. In SuHx rats, 566 unique proteins were identified, and 105 were differentially expressed in Fischer compared with SD rats (Figure 5.4 B - C). Of interest, a profound reduction in AK1 protein expression was seen by unbiased proteomic analysis in Fischer rats (Figure 5.4D) and this was confirmed by Western blot analysis

(Figure 5.4 F-G). The dramatic decrease in AK1 expression in the LV and RV was similarly observed under control and SuHx conditions (Figure 5.4 F-G). AK1 protein expression did not change from control to SuHx (Supplemental Figure 5.4) Of interest, Creatine Kinase- Muscle (CK-MM), which has a complementary function to AK1 was found to be markedly reduced in PH animals in both strains in the proteomic analysis (Figure 5.4E); however, no strain differences were identified in CK protein expression.

A

Control (Relative Gene Expression)

Gene	LogFC	Adj. p value
Spta1	4.43	0.0021
LOC100910934	-4.78	0.0093
LOC502907	1.67	0.013
Rab3b	2.20	0.013
Ak1	-1.75	0.025
LOC287167	-3.24	0.025
Cyp4v3	-1.64	0.032
Ddah1	-1.29	0.035
Car4	-1.57	0.035
Akr1b10	1.98	0.048

B

SuHx (Relative Gene Expression)

Gene	LogFC	Adj. p value
LOC100910934	-5.16	7.28E-05
Spta1	4.02	0.00042
Ano5	3.10	0.0022
Cyp4v3	-2.08	0.0079
Lcn2	-1.85	0.022
Ephx2	1.74	0.028
Ak1	-1.44	0.028
Car4	-1.98	0.029
Akr1b10	2.23	0.048

C

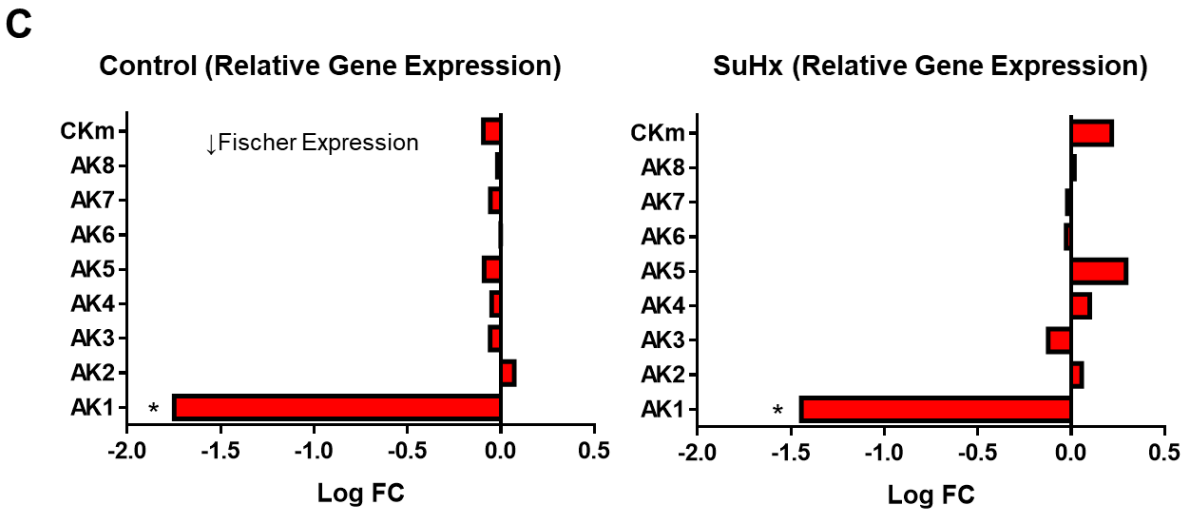

Figure 5.3 Microarray analysis of differentially expressed genes in the right ventricle of controls (A) and SuHx (B) Fischer and SD rats. Expression is expressed as a relative change LogFC (Fischer/SD). Of the AK isoforms, only AK1 was depressed in Fischer rats (C). Statistically significant relative change in gene expression, * adj. p value <0.05.

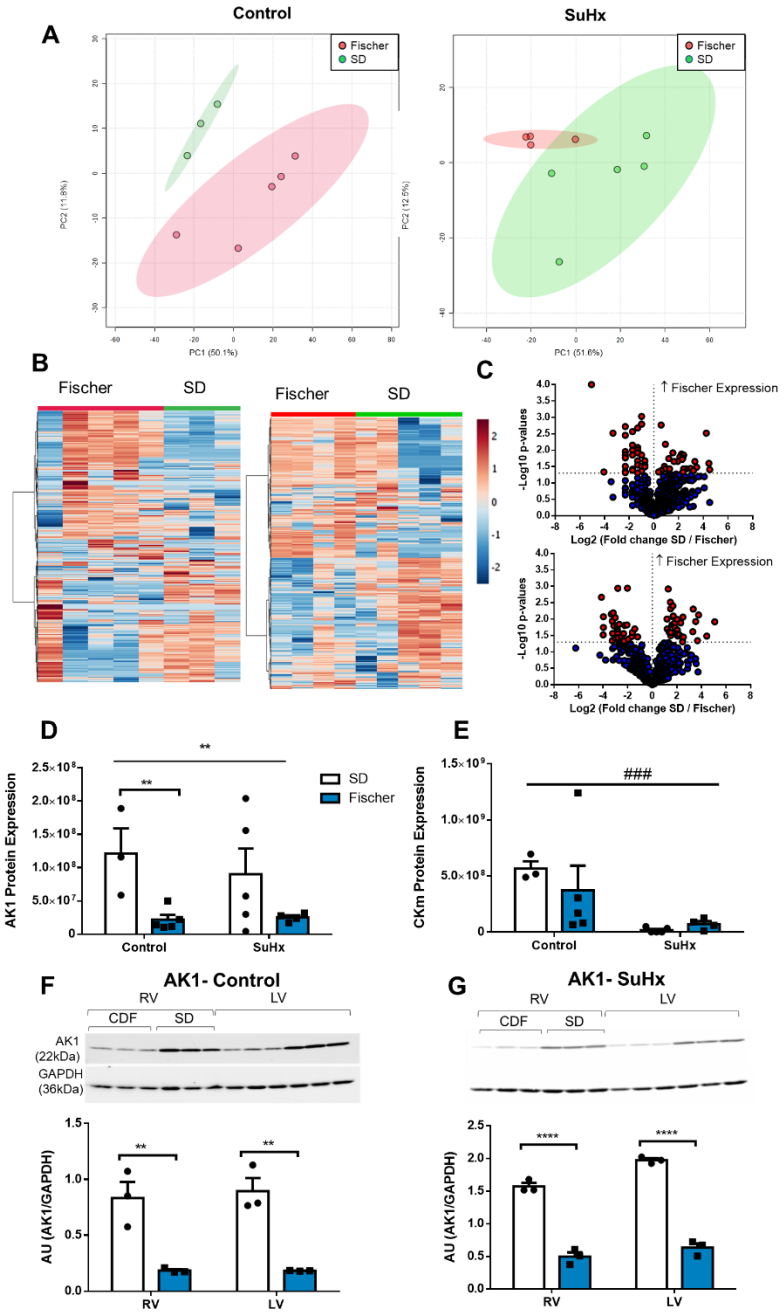

Figure 5.4 Proteomic analysis of protein expression in the right ventricle in controls and SuHx (5 wk Fischer, 9 wk SD). Principal component analysis of RV protein expression changes in SD and Fischer controls and SuHx rats (A). Heatmaps of differentially expressed proteins in the SD and Fischer RVs in controls an SuHx induced PAH (B). Volcano plots of RV protein expression changes in SD and Fischer controls and SuHx rats (C). Select proteins related to Phosphoryl-transfer are displayed, AK1(D) and Creatine kinase (CK) (F). AK1 results were confirmed by western blot in RV tissue of Fischer and SD rats (E). Statistically significant difference between rat strains ** $p<0.01$; **** $p<0.001$;. Statistically significant difference between controls and SuHx ###$p<0.001$; #### $p<0.0001$.

5.4.5 RV nucleotides in AK1 deficient Fischer rats

Adenylate kinase catalyzes the reversible phosphotransfer reaction, $2ADP \leftrightarrow ATP + AMP$. Although the unsupervised PCA did not separate strain differences in metabolites (Figure 5.5A), there were strain-dependent differences in nucleotide levels in response to SuHx, consistent with a marked deficiency in AK1 in Fischer rats. Of note, there was an increase in both ADP (3-fold, $P<0.05$) and AMP ($P<0.05$) nucleotides in Fischer rats relative to control (Figure 5.5C and D, and while the relative change in ATP levels in response to SuHx was slightly lower, this was not significant (Figure 5.5E). Creatine levels, an important substrate for CK, were significantly lower in Fischer rats than SDs SuHx rats relative to control levels (Figure 5.5F).

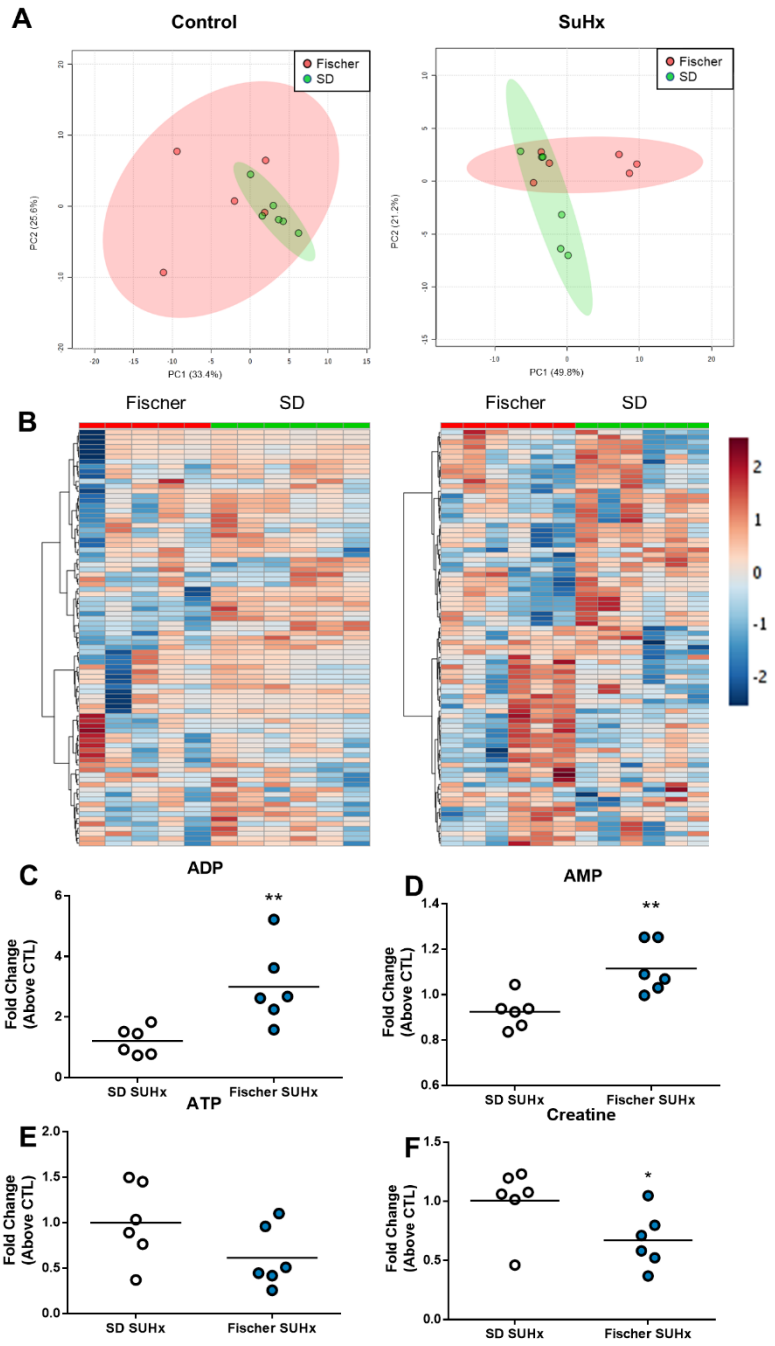

Figure 5.5. Metabolomic analysis in the right ventricle of controls and SuHx rats. PCA and heat map analysis are displayed (A,B). Relative changes in adenosine nucleotides (C-E) and creatine (F). Statistically significant difference between rat strains ** $p<0.01$.

5.4.6 Hematological phenotype in Fischer rats exposed to metabolic stress

Erythrocytes express only the AK1 isoform of this family, which is essential for maintenance of red blood cell shape and deformability. Rare loss-of-function single nucleotide mutations have been described in humans associated with nonspherocytic hemolytic anemia. Therefore, we investigated whether Fischer rats exhibited abnormalities in hematological parameters compared to SD rats at baseline or in response to metabolic stress (hypoxia). Although red blood cell (RBC) number were similar between strains under normoxia (Figure 5.6A), naïve fischer rats evidence of mildly increased polychromasia and shows spherocytosis (Figure 5.6B representative blood smears). As expected, hypoxia increased RBC number and hematocrit in both rat strains. Hypoxia also induced macrocytosis, resulting in an elevated mean corpuscular volume in both strains; however, RBC distribution width was only elevated in Fischer rats. These findings are consistent with an increase in immature red blood cells in the circulation, which typically have high cell volumes, in metabolically stressed Fischer rats. This was confirmed on blood films which revealed markedly elevated levels of polychromatic RBCs and spherocytes in response to hypoxia exclusively in Fischer rats (Figure 5.6A, $P<0.0001$). Interestingly, naïve Fischer rats also exhibited marked lympho- and monocytopenia compared to SD rats (Supplemental Figure 5; $p<0.0001$) which was not altered by exposure to hypoxia. In contrast, hypoxia induced a relative thrombocytopenia in both rat strains (27% reduction), although this was more pronounced in Fischer rats (68% reduction, Supplemental Figure 5B $p<0.0001$). Together these results reveal a unique hematological phenotype in Fischer AK1-deficient rats characterized by RBC macrocytosis, normoblastemia and spherocytosis in response to metabolic stress, consistent with increased RBC destruction and a concomitant increased production of RBCs in Fischer rats.

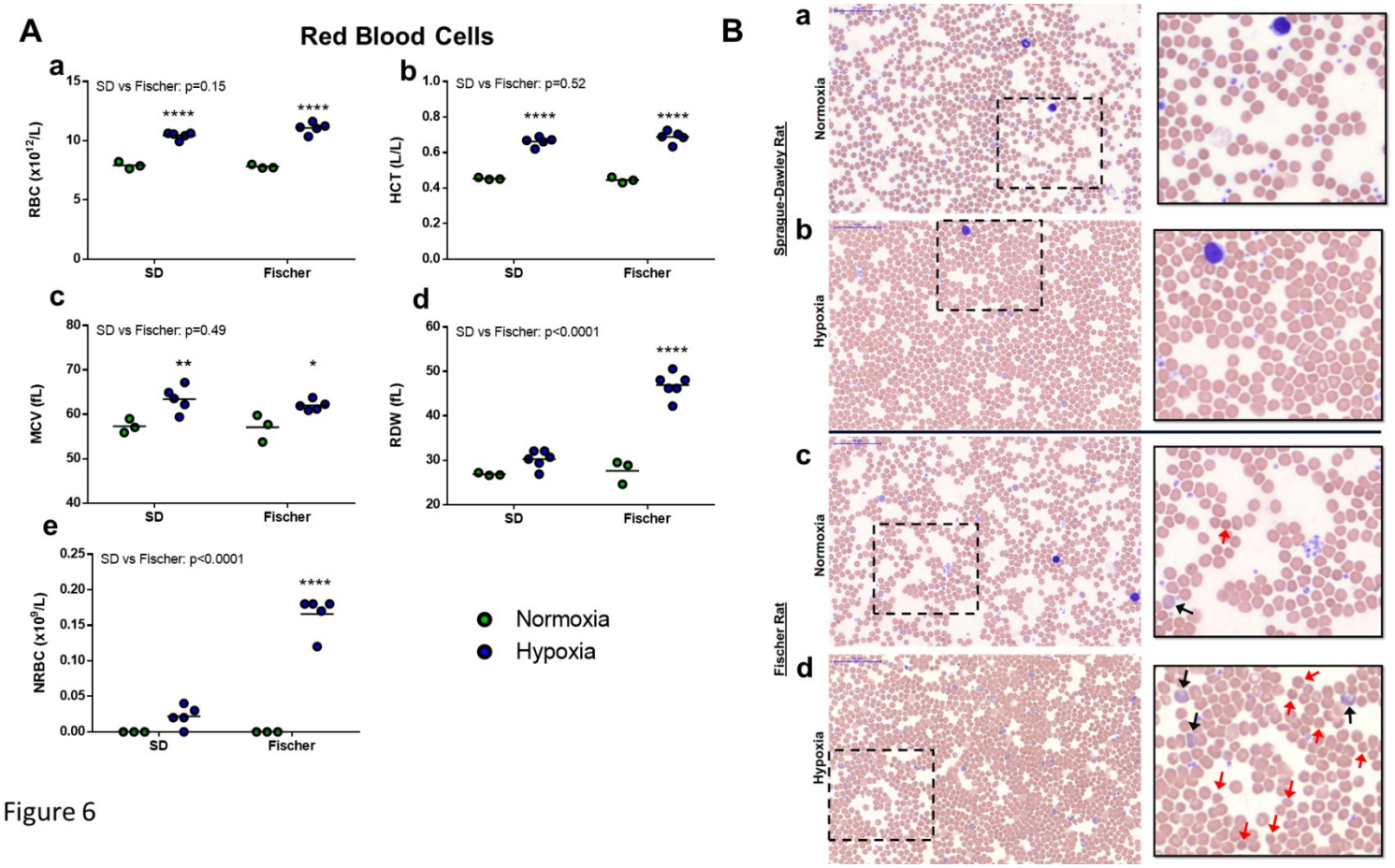

Figure 6

Figure 5.6. RBC count and morphology. Complete blood count (A) in Fischer and SD rats at baseline, and in response to hypoxia alone. Representative blood smears in Fischer and SD rats under control and hypoxic conditions are displayed (B). Peripheral blood smear from SD (a,b) and Fischer rats (c,d) under Normoxia (control) and hypoxic conditions (10% O2). SD control blood smear demonstrates normal lymphocytes and neutrophils, normal polychromatic RBC and normal RBC morphology. SD hypoxic rats demonstrate mildly increased polychromasia but RBC morphology is normal. Fischer control blood smear (c) demonstrates mildly increased polychromasia and shows spherocytosis (red arrow). In Fischer hypoxic rats (d) there is an increased spherocytosis (red arrow) and increased polychromasia of RBC. Red arrow, spherocytes; black arrow, polychromatic RBC. *p<0.05; **p<0.01; ***p<0.001; ****p<0.0001. Main effect of strain is displayed at the top of each graph.

5.4.7 AK1 Expression in human patients with maladaptive RV remodeling and right heart failure

To assess whether reduced AK1 levels may contribute to RV decompensation, we studied the protein expression in the myocardium of patients with preserved RV function compared those with RHF. AK1 protein expression was reduced selectively in the RV of PAH patients with maladaptive RV remodeling and poor RV function compared to patients exhibiting compensated RV adaption (Figure 5.7A, $p<0.05$). In contrast, patients with preserved RV function appeared to show a trend toward a compensatory increase in AK1 expression compared to controls ($p=0.10$). Similarly, in PAH patients with RV decompensation, expression of creatine kinase muscle (CK-MM), the major phosphoryl transfer pathway in the normal heart, was significantly reduced compared to controls, whereas CK expression in patients with compensated RV function, while qualitatively reduced, was not significantly different from the levels in control or RHF patients (Figure 5.7A,c, $p<0.05$). Together, these data implicate a deficiency in ATP turnover and phosphoryl transfer, caused by a relative reduction in RV myocardial AK1 expression, as a novel mechanism contributing to RV decompensation in patients chronic pressure overload and RVF.

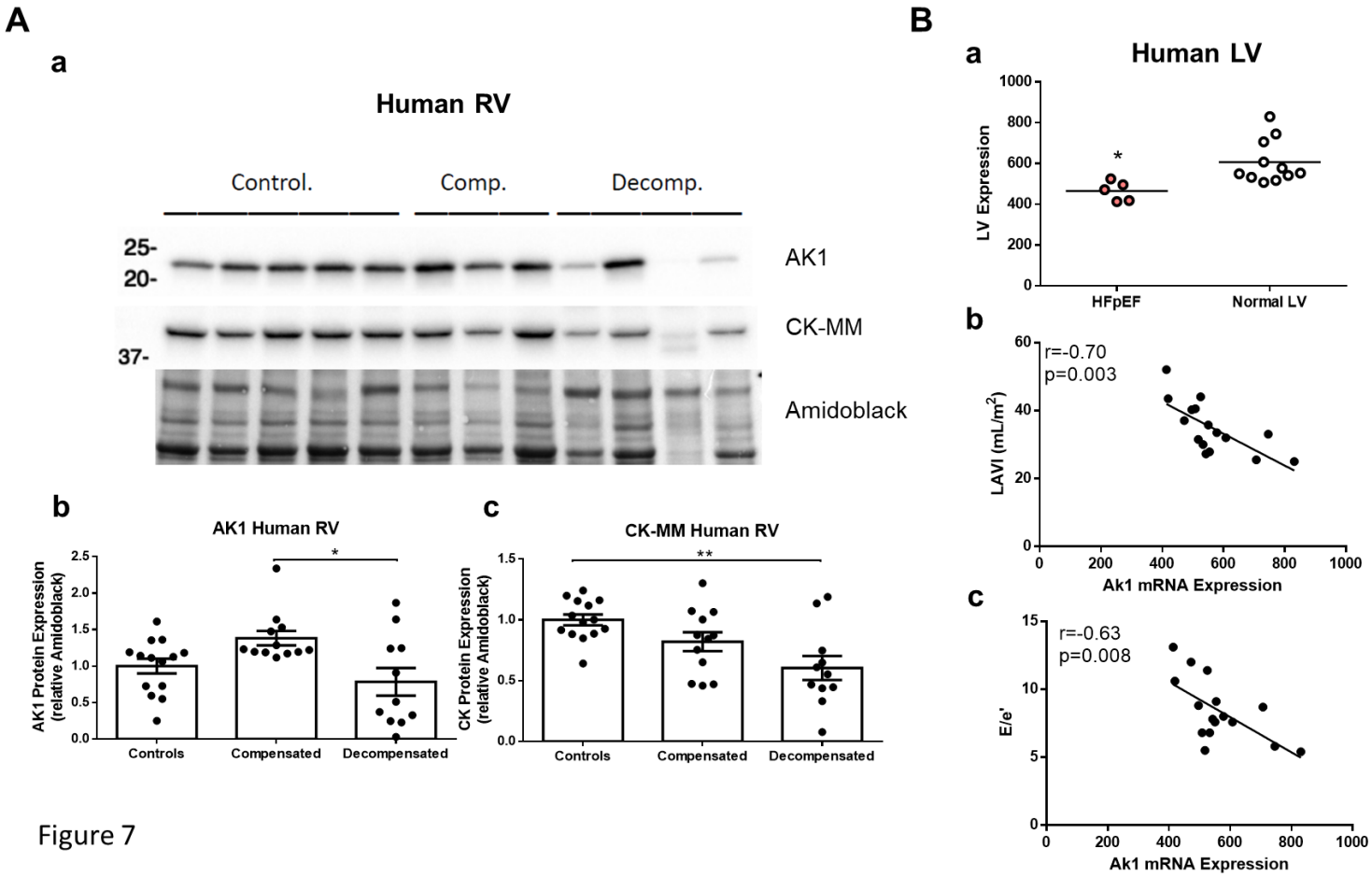

Figure 7

Figure 7. AK1 expression in human RV of patients with adaptive and malaptive RHF (A) and human LV of patients with HFpEF (B). PAH patients with decompensated RHF have lower AK1 protein expression compared to patients with compensated RVH (A). CK-M expression was also lower in decompensated patients (A,c). Patients with HFpEF also have mildly lower LV AK1 mRNA expression than patients with normal function (B). AK1 expression correlated with LAVI (B,b) and E/e' ratio (B,c), both measures of diastolic dysfunction. LV, left ventricle; LAVI, left atrial volume index. *p<0.05

5.4.8 Reduced LV AK1 expression in human patients with HFpEF

Since AK1 was equally reduced in the LV compared to the RV in the Fischer rat model, we analyzed a public database of LV transcriptomic data from patients undergoing elective CABG surgery accessed through ArrayExpress (E-MTAB-7454).[347] Levels of AK1 transcripts were found to be lower in patients with HFpEF as compared to patients with normal LV function ($p<0.05$, Figure 5.7B). AK1 levels also negatively correlated with left atrial volume index (LAVI; $r=-0.70$, $p=0.003$; Figure 5.7B) and the ratio between early mitral inflow velocity and mitral annular early diastolic velocity (E/e'; $r=-0.63$, $p=0.008$; Figure 5.7B,c), both indices of diastolic dysfunction. These data suggest that reduced expression of AK1 may be relevant to clinical heart failure in humans by contributing to LV, as well as RV, dysfunction under conditions of metabolic stress.

5.5 Discussion

This is the first demonstration that RV maladaptation and right heart failure in Fischer rats exposed to chronic pressure overload is due to a specific deficiency in AK1, and thus impaired ATP recycling and shuttling from the mitochondria to the actin/myocin cross-bridge for muscle contraction. Moreover, we have shown that this AK1-dependent mechanism of impaired myocardial energetics may also be implicated in in patients with pulmonary hypertension and right heart failure and in other cardiac disorders as well.[338–340]

In tissues with high energy demand, such as the brain and heart, creatine kinase (CK) and adenylate kinase (AK) catalyzed reactions facilitate thermodynamically efficient coupling between ATP generating and consuming sites.[348–351] Therefore, CK and AK phospho-relay networks in the cytoplasm work to effectively shuttle ATP from the mitochondria to the actomyosin ATPase. These enzymes also have a prominent role in transferring high energy phosphoryl groups to regenerate ATP within the local microenvironment, thus supporting efficient cardiomyocyte contraction and protecting against energy deprivation during periods of sustained energy demands. In healthy myocardium, the CK-mediated reactions predominate contributing ~90% of local ATP turnover rates, whereas AK1 only contributes 10%.[351] This likely explains why Fischer rats exhibited normal cardiac function and hemodynamic parameters under baseline conditions despite a profound reduction in AK1 expression. However, in response to heart failure or hypoxic stress[352], there is a substantial rearrangement in phosphotransfer signaling such that the contribution of CK is reduced by >50%, with a compensatory increase in AK-catalyzed phosphotransfer by 134%. [351,353] The increase in AK flux plays a major role in supporting myocardial energetics during periods of metabolic stress in the failing heart. The marked reduction in CK expression in the RVs of SD and Fischer rats in response to severe PH is

consistent with this phenomenon. SD rats with preserved AK1 expression have the capacity to redistribute phosphotransfer flux, thus allowing the RV to robustly adapt to increase RV power. In contrast, in AK1-deficient Fischer rats, ATP supply through diffusional nucleotide exchange is inefficient, particularly under conditions of prolonged increases in RV afterload in which CK is downregulated. This results in inefficient RV energetics and a maladaptive response to increase afterload, with an inability to sufficiently increase RV power. Indeed, AK1 and CK double knockout mice demonstrate profound energetic defects with compromised contractile performance.[350]

AK1 deficiency may also contribute to other pathologies in Fisher rats in response to hypoxic or ischemic insults. For example Fischer rats have been reported to sustain larger infarct volumes than SD rats in response to middle cerebral artery occlusion.[354] To the best of our knowledge, no such strain comparison has been reported for hypoxic damage induced by myocardial ischemia, however AK1 knockout mice have been shown to have an accelerated loss of contractile force compared to wildtype controls at the onset of myocardial ischemia, consistent with reduced tolerance to ischemic stress.[349] AK1 deficiency may also contribute to decreased cardiac mass in Fischer rats. In a previous study, Sebkhi *et al.* investigated the genetic contribution to total heart weight variation in Fischer and Wistar rats,[355] and identified a significant quantitative trait loci (QTL) on chromosome 3 which explained the variation in cardiac mass. Four genes were located within this QTL on chromosome 3 (Gsg, Scn2a1, Ptgs1 and AK1). [355] More recent evidence implicates an essential role of AK1 in cardiac stem cell differentiation and cardiac development.[348] AK1 also has also been shown to play an important role in maintaining nucleotide homeostasis, particularly in buffering an increase ADP levels

during exercise (or increased workloads) which can have deleterious effects on skeletal muscle contraction.[356,357]

Mutations in the AK1 gene in humans are exceedingly rare; however, when present the major phenotype is hematological and to the best of our knowledge, no studies have yet investigated the effects on the heart. Point mutations in AK1 are associated with a disease characterized by nonspherocytic hemolytic anemia. Erythrocytes express only one member of the AK family, AK1, and do not express CK. AK1 is therefore essential for the maintenance of RBC shape and its deficiency predisposes to hemolysis. While anemia was not present in Fischer rats at baseline, a hematological dyscrasia was unmasked when these animals were exposed to hypoxia, closely resembling the human phenotype. Macrocytosis and an elevated RBC distribution width with a marked increase in immature RBCs were observed, features consistent with increased production of immature RBCs in response to RBC loss by a destructive process. As well, marked lymphopenia and monocytopenia were seen at baseline which might explain differences in innate and adaptive in Fischer compared to other rat strains.[358,359] Hypoxia also led to thrombocytopenia in both rat strains, although this was more profound in Fischer rats, which is consistent with a recent report describing severe thrombocytopenia in Fischer SuHx rats.[360]

The relevance of AK1 deficiency may extend well beyond a rare genetic disease and may also represent a general mechanism involved in RV decompensation in the context of chronic pressure overload. In a series of patients with PAH we found the level of AK1 expression was associated with the degree of RV compensation. While patients with overt right heart failure had significantly lower AK1 protein levels in the RV myocardium, patients with compensated RV function demonstrated, if anything, and tendency towards increased levels. Thus, the maintenance of AK1 expression and activity may be a critical determinant of the ability of the

RV to compensate energetically and maintain contractility in the face of sustained increases in afterload. This would also suggest that strategies to bolster the levels of AK1 may represent a novel therapy for RV failure.

Inefficient myocardial energetics in AK1 deficient Fisher rats may also have implications for the left heart since the deficiency of AK1 in Fischer rats was not limited to the RV but was also evident in the left ventricle LV as well. Interestingly, biventricular diastolic dysfunction was described in Fischer rats exposed to SuHx,[360] although no comparison was made to other rat strains. This compliments previous studies in AK1 null mice demonstrating elevated ADP levels and impaired relaxation kinetics during conditions of high-energy demand.[357] While AK1 mutations are very rare in humans, it is likely that there is interindividual variability in expression levels in the general population that may contribute to differences in cardiac adaptation to stress in the LV as well as the RV. Indeed, an analysis of online transcriptomic data revealed that expression of AK1 was lower in patients with heart failure and preserved ejection fraction (HFpEF) and this correlated inversely with echocardiographic indices of diastolic dysfunction.

In summary, we now demonstrate that inefficient cardiac energetics underlies the inability of Fischer rats to adapt to chronic RV pressure overload, due to a profound deficiency in AK1. Moreover, AK1 levels were found to be lower in PAH patients with RV failure suggesting that defects in AK1-dependent bioenergetic pathways may represent an unrecognized cause of RV maladaptation and dysfunction in PH and may also contribute to other cardiac disorders as well.

Chapter 6

General Discussion and Perspectives

6.1 Summary

The investigations in chapters 2 through 5 comprise 4 independent, but related studies aimed at 1) comparing contemporary mortality risk assessment strategies in PAH; 2) elucidating the neurohormonal and metabolic mechanisms underlying maladaptive remodeling in experimental PAH; and 3) validating a new 18-labeled tracer to maximize wide-spread clinical impact for SCA risk prediction, as well as extending the paradigm of neurohormonal imaging to the right ventricle.

6.1.1. Refining Contemporary PAH Mortality Risk Assessment

If widely adopted, a risk assessment strategy has the potential to better define individual-specific prognosis and standardize treatment goals. Several contemporary algorithms are available without a clear indication as to which strategy yields the most robust discrimination. In chapter 2 of this thesis we compared contemporary risk assessment approaches in a Canadian PAH population which demonstrated that REVEAL-based strategies have superior long-term mortality risk discrimination than ESC/ERS-based assessments. We further demonstrated the prognostic importance of kidney function, which to date has not been incorporated into contemporary guidelines. Measures of kidney function had the potential to re-stratify ESC/ERS intermediate risk into lower and high risk strata. Our work highlights key limitations of the ESC/ERS-based risk assessment, and suggests that incorporating measures of kidney function are important strategies moving forward.

Ottawa PAH Risk Score:

Risk assessment, in its current form, is likely challenging for clinicians to implement in practice given their overall complexity and the number of incorporated variables. This is further complicated by the availability of several contemporary algorithms without a clear indication as to which strategy yields the most robust discrimination. This is discouraging given that the ESC/ERS and the 2018 World Symposium endorse the utilization of risk assessment strategies and is incorporated into the treatment algorithms.

Building on the knowledge derived from the European and USA registries we aimed to develop a simplified risk strategy that includes only variables that yield the most important information. In an extension of Chapter 2, statistical modeling identified four independent prognostic variables (renal dysfunction, 6 minute walk distance, SVO_2, and sex), which provided equivalent risk prediction to the current US standard REVEAL. Work is ongoing to validate our algorithm in prospective PAH cohorts for PH Centers in Alberta and Vancouver.

Future Studies:

1. **Ottawa Risk Score Validation.** Before clinical implementation, validation is an important step. Work is currently ongoing to validate our PAH risk algorithm in prospective PAH cohorts from PH centres in Alberta and Vancouver.
2. **Ottawa Risk Score Clinical Implementation:** Although the theoretical utility of risk assessment tools are evident, uptake by practicing clinicians is currently limited by robust data to support its efficacy. Our group, in collaboration with PH centers in Canada are in works to start a pragmatic trial to see whether risk assessment approaches translates to improved patient outcomes.

6.1.2. Imaging of the Sympathetic Nervous System with PET

In chapters 3-4 (and Appendix B-C), we present 4 independent studies aimed at validating cardiac SNS imaging for application in the left and right ventricles. The PAREPET trial revitalized interest in the field of sympathetic imaging which demonstrated its utility in SCA risk prediction. Various methods of quantification have been proposed to assess the burden of sympathetic denervation and dysfunction. While these methods may require varying degrees of quantitative sophistication and imaging time, it remains to be determined which method yields the most robust SCA risk discrimination. In Appendix B we performed a competing-risk analysis compare the robustness of regional and global [^{11}C]HED quantification parameters for predicting cause-specific mortality from SCA. A key finding of our study was that absolute global scale values such as RI and DV yield no independent or additive benefit clinical use in distinguishing SCA risk. Further, in Appendix C, we demonstrate that HED regional defect parameters also have better reproducibility than global scale parameters. These results have widespread implications for future cardiac sympathetic HED analysis and imaging protocols. Taken together we demonstrate that SCA risk stratification is sufficiently predicted with HED activity defect scores and other more sophisticated quantification measures of DV, DV defect score, and RI may not be required for clinical prognostication.

The clinical utility in SCA risk prediction are thus evident, yet current PET approaches are greatly limited by the short half-life of 11C-labeled tracers. In Chapter 4, we aimed to validate a novel 18F-labeled tracer Flubrobengaune for assessment of sympathetic innervation. We discovered that the 18F labeled tracer Flubrobengaune yields equivalent regional and global distribution in both patients with and without ischemic cardiomyopathy. 18F-labeled tracers such as FBBG offer the potential for the wide distribution needed for maximum patient and clinical

impact. In an extension to Chapter 4, we also demonstrated equivalent RV retention between both tracers. We are planning on comparing the tracers in a small population of patients with pulmonary hypertension.

There is a paucity of data on the sequelae of chronic SNS activation in patients with PAH and RHF. Although some studies have used surrogate markers such as plasma NE, heart rate variability or muscle sympathetic nerve activity to assess sympathetic function in patients with PH, the state of autonomic function directly within the myocardium in patients with PAH remains largely unknown. In Chapter 3, we performed the first comprehensive quantification of sympathetic function within the RV using [^{11}C]HED PET imaging in animals with SuHx induced PAH. We discovered that with increasing PAH disease severity, there is selective regional sympathetic denervation within the RV, with parasympathetic nerves being largely spared. We also demonstrated a significant correlation between immunohistochemical and [^{11}C]HED PET assessments of sympathetic denervation within the RV. For the first time, these data validates the use of non-invasive neurohormonal imaging to quantify the burden of denervated myocardium in the RV.

Future Studies:

1) Expand the use of SNS imaging to novel CVD populations, i.e. atrial fibrillation, Parkinson's disease, right heart failure and pulmonary arterial hypertension, Takosubo cardiomyopathy.
    a. To explore the utility of SNS probes in these disease populations to stratify risk, monitor neurohormonal benefits of therapies and link this to improved outcomes.
2) Integrating these probes with high-resolution PET/MR imaging will for the first time enable accurate characterization of neurohormonal function in the RV and atria.

3) In RCTs, investigate whether SNS imaging can better predict outcome benefits in patients with HF with mild to moderate LV dysfunction (see below) or LV dysfunction after ICD placement, and thus enable a more precision targeted patient selection process.
    a. Determine whether an imaging-guided strategy alone can yield outcome-driven cost-effective therapy selection.

6.1.3. Metabolic Mechanisms underlying maladaptive remodeling in PAH

Interindividual heterogeneity in RV remodeling and progression to RV failure in PAH is not well explained by differences in the degree of afterload, highlighting the importance of inter-individual heterogeneity, largely due to genetic factors. This observation is recapitulated by strain differences in RV adaption between Sprague-Dawley and Fischer rats. In chapter 5, we corroborate previous findings which demonstrates poor survival and progressive right heart failure in Fisher rats in response to severe PAH. We significantly extend these findings by demonstrated inefficient cardiac energetics and RV maladaptation in response to chronic pressure overload in Fischer rats, likely due to a genetic defect in AK1. Although a human AK1 mutations in humans are rare, heterogenous myocardial expression was present in patients undergoing elective CABG with an inverse relationship between AK1 expression and diastolic dysfunction in patients with HFpEF. While future studies are needed to confirm overexpression of AK1 can rescue of the right heat failure phenotype in Fischer rats, together these results suggest that strategies to increase AK1 may represent an unrecognized therapeutic avenue, which may yield pleiotropic effects in improving both myocardial energetics and actin/myosin cross-bridge dynamics.

Future Studies

1) **Confirming Importance of AK1 in Heart Failure.** Using unbiased global transcriptional and proteomic profiling we identified AK1 as the most likely genetic defect explaining the impaired RV energetics and propensity for maladaptation in Fischer rats. Future studies are warranted to confirm the importance of AK1 in the setting of pressure overload. We recently formed a collaboration with Dr. Xu Chen at UCLA who is sharing AK1 knockout nice. We plan to elucidate the importance of AK1 in the progression of heart failure by banding the aorta or main pulmonary artery in AK1 knockout and wildtype mice, to induce left and right heart failure, respectively.
2) **AK1 Targeted Therapy:** Future studies will need to confirm whether overexpression of AK1 can rescue the right heart failure phenotype in Fischer rats. Our finds of an inverse relationship between AK1 expression and diastolic dysfunction in patients with HFpEF is exciting and may suggest that augmenting AK1 may improve mechanical efficiency and cardiomyocyte relaxation. We have studies planned using an adeno-associated viral (AAV) vector (serotype 9), to drive myocardial expression of AK1 in Fischer rats. This has unique potential for clinical translation, as these vectors appear safe in humans and do not incorporate in to the human genome.

Appendix A

Supplemental Figures and Tables

Chapter 2 Supplement

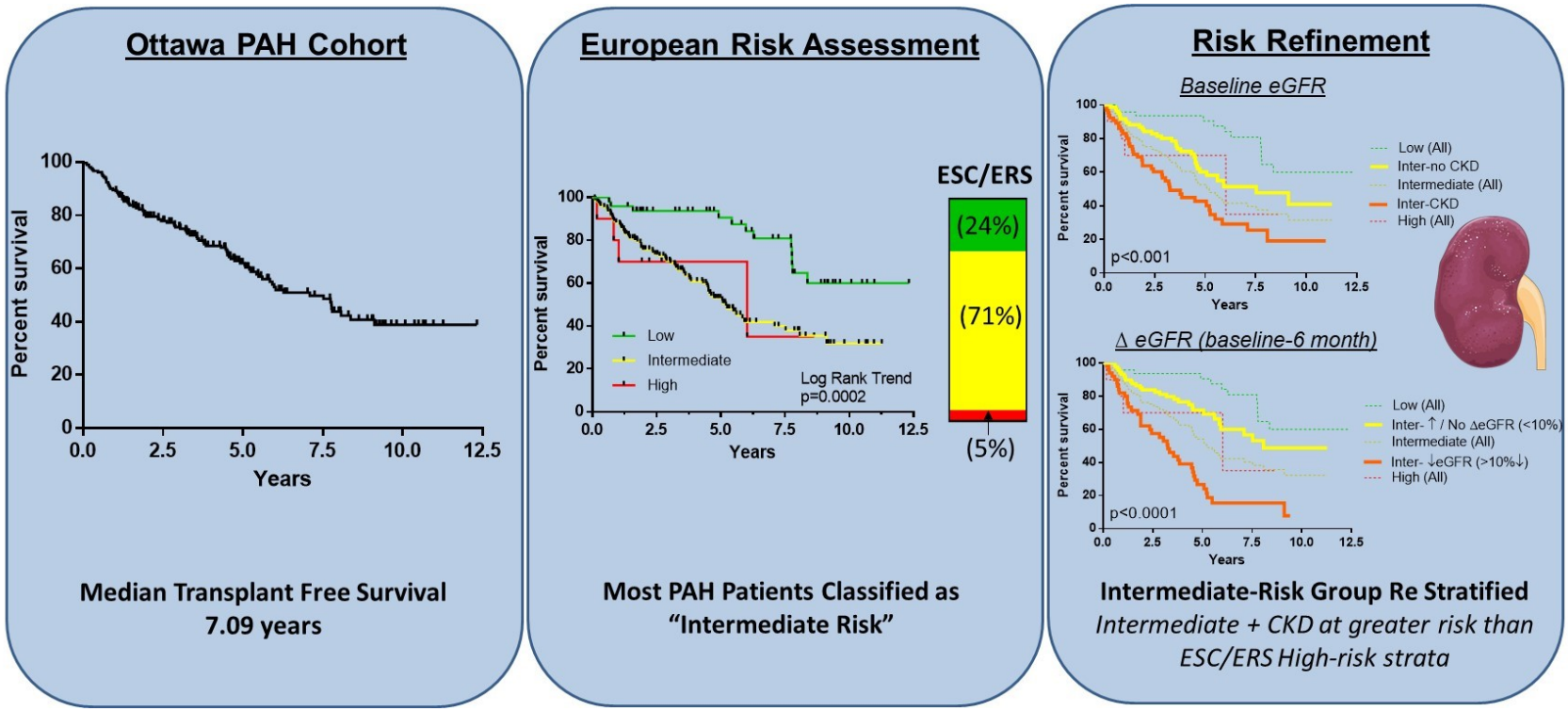

Supplemental Figure 2.0. Graphical Abstract for Risk Assessment. The present study is the first implementation of contemporary risk assessment in a Canadian PAH population. Using the European Guidelines, most PAH patients get stratified into the intermediate risk group (71%). Indeed, the specific treatment recommendations for "intermediate risk patients" are not well defined. Baseline eGFR and change in eGFR can significantly stratify intermediate-risk patients into a higher and lower like group. Parts of the figure were created using Servier Medical Art

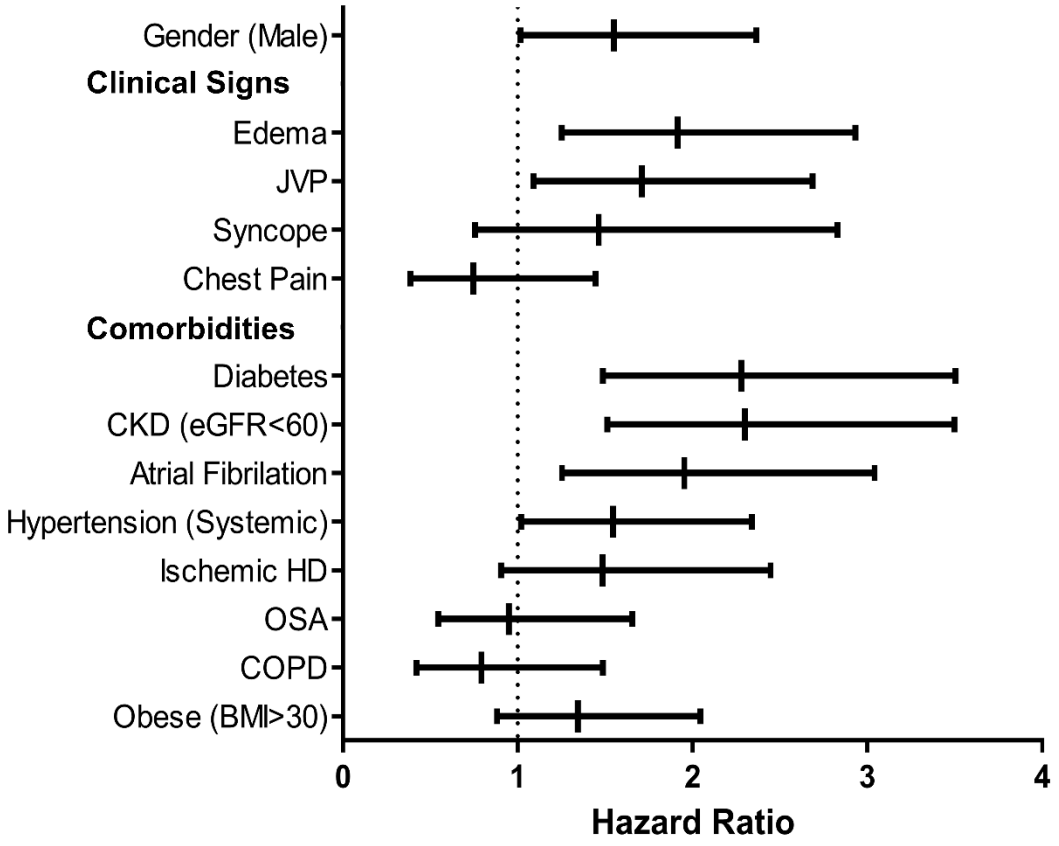

Supplemental Figure 2.1: Risk Factors and Mortality in PAH. Unadjusted Forest Plot of Hazard ratio (95% CI) for comorbidities and clinical signs in WHO group 1 patients.

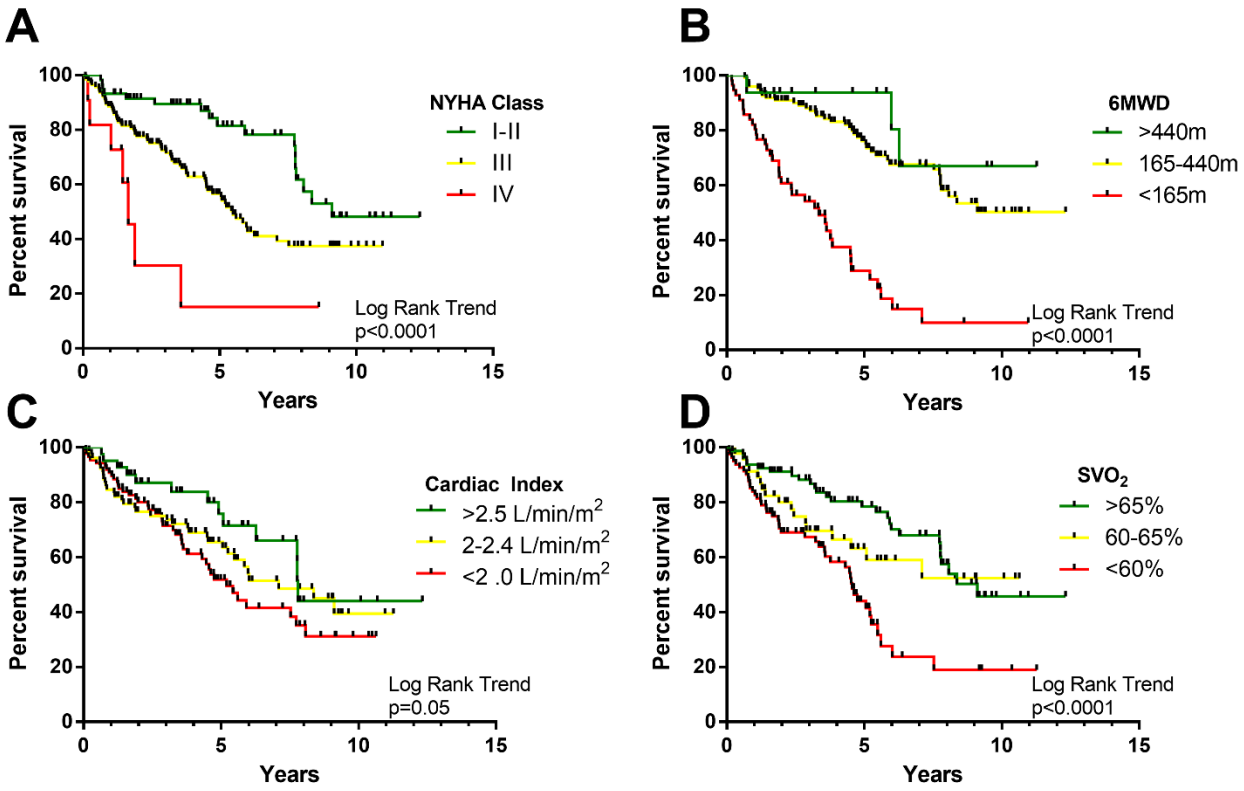

Supplemental Figure 2.2 Functional and Hemodynamic risk factors for survival. Kaplan-Meier curve analysis for Transplant free survival. Patients stratified according to baseline NYHA functional class (A), Six minute walk distance (B), and Cardiac index (C) and SVO2 (D) on right-heart catheterization.

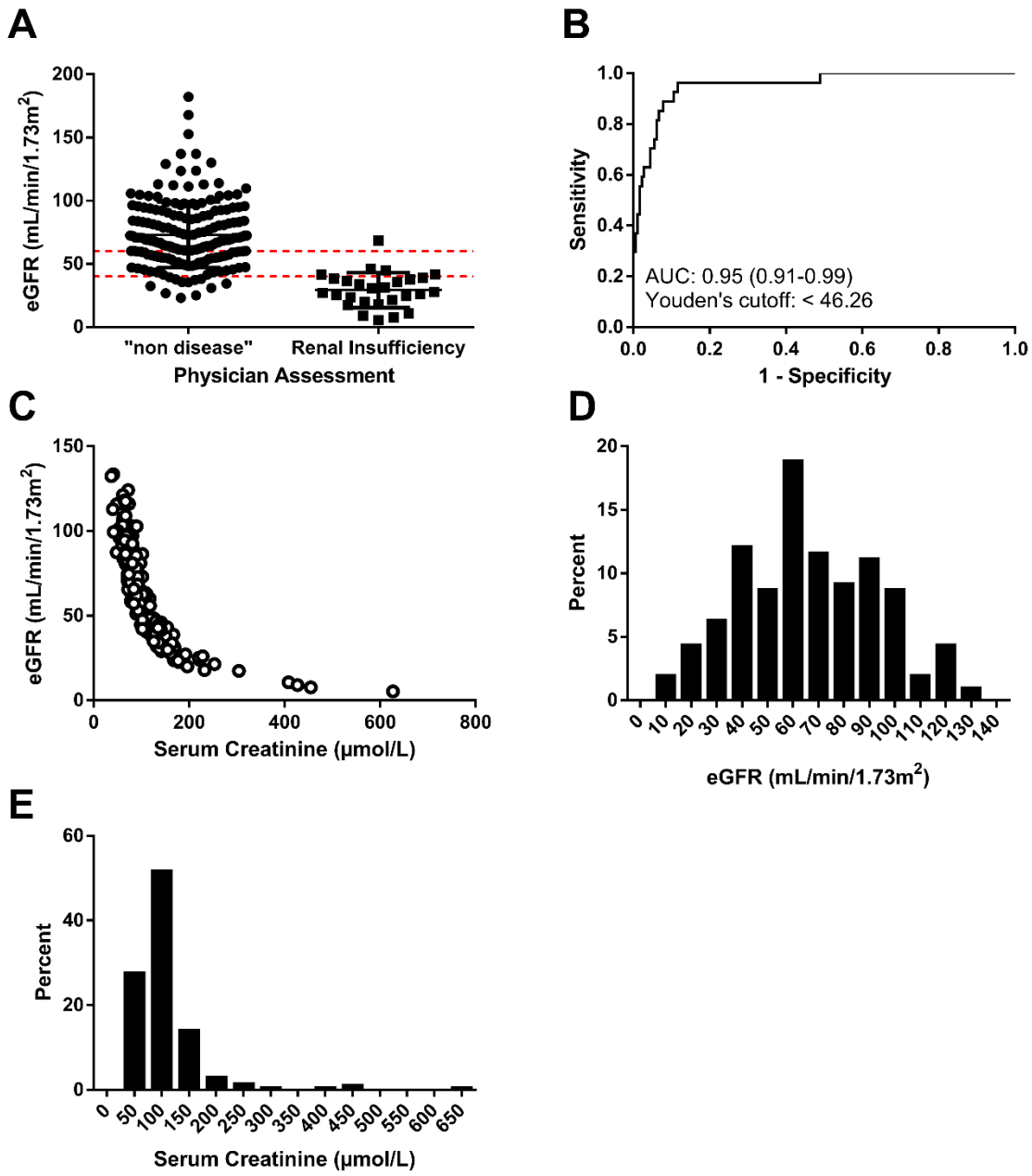

Supplemental Figure 2.3 Distribution of creatinine and eGFR. REVEAL 1.0 includes a physician's assessment of renal insufficiency, whereas REVEAL 2.0 includes eGFR. Physician's assessment of renal insufficiency fails to capture patients in the 40-60mL/min/1.73m^2 range (A). In ROC analysis, the physician's assessment of renal dysfunction (<60) had excellent predictive power with an AUC of 0.95, but the optimal cutoff markedly lower at 46.26 mL/min/1.73m^2 (B). eGFR detects renal impairment more accurately and at an earlier stage than serum creatinine (C). Distribution of eGFR (D) and serum creatinine (E) in our population.

Chapter 3 Supplement

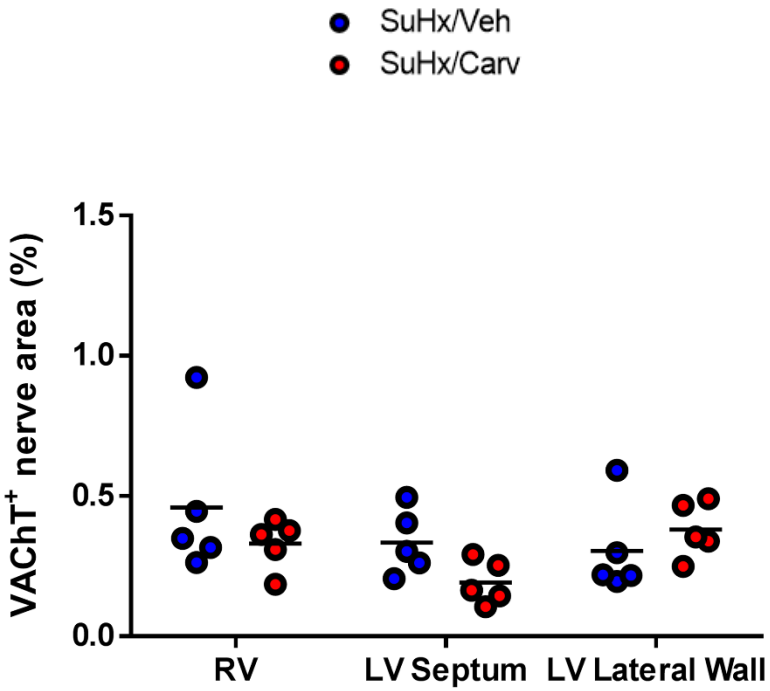

Supplemental Figure 3.1. Carvedilol does not effect parasympathetic nerve density. Immunohistochemical analysis demonstrates no impact of carvedilol treatment on VaChT+ nerve density. (Carvedilol n=5 vs Vehicle n=5)

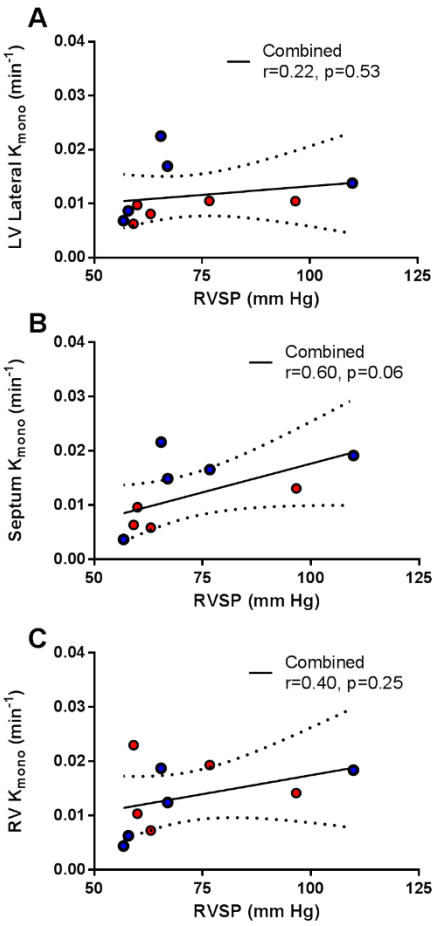

Supplemental Figure 3.2. Sympathetic activity does not increase with increasing PAH disease severity. No relationship was observed between HED Kmono, tracer washout, and RVSP in the LV lateral wall (A), LV septum (B) and RV (C). (Carvedilol, red, n=5; vs Vehicle, blue, n=5)

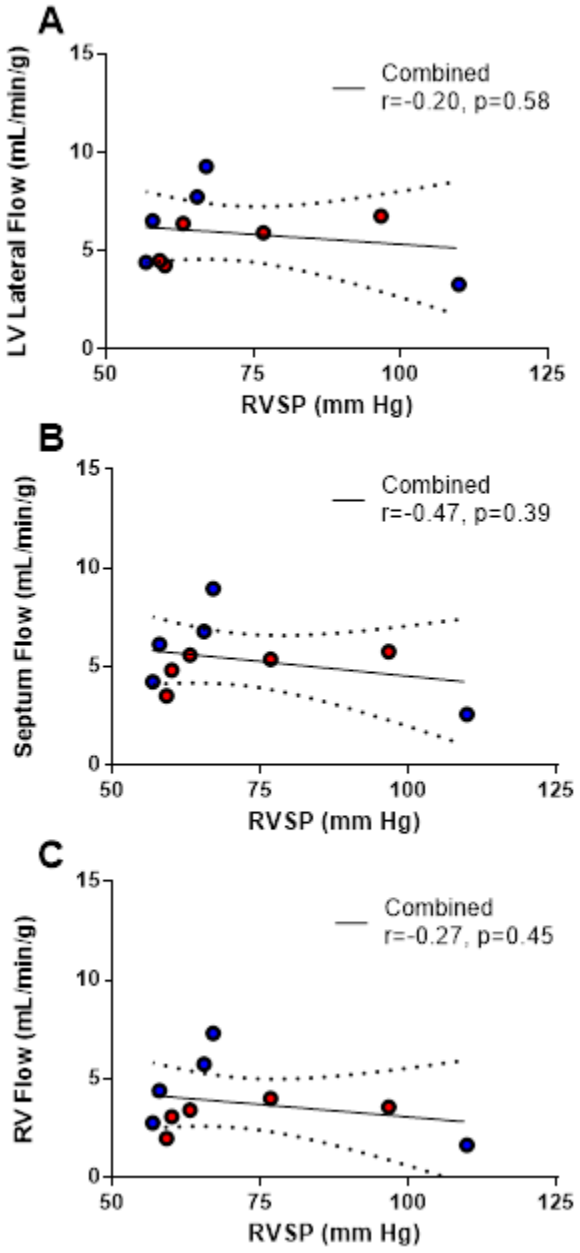

Supplemental Figure 3.3. Myocardial blood flow does not decrease with increasing PAH disease severity. No relationship was observed between MBF and RVSP in the LV lateral wall (A), LV septum (B) and RV (C). (Carvedilol, red, n=5; vs Vehicle, blue, n=5)

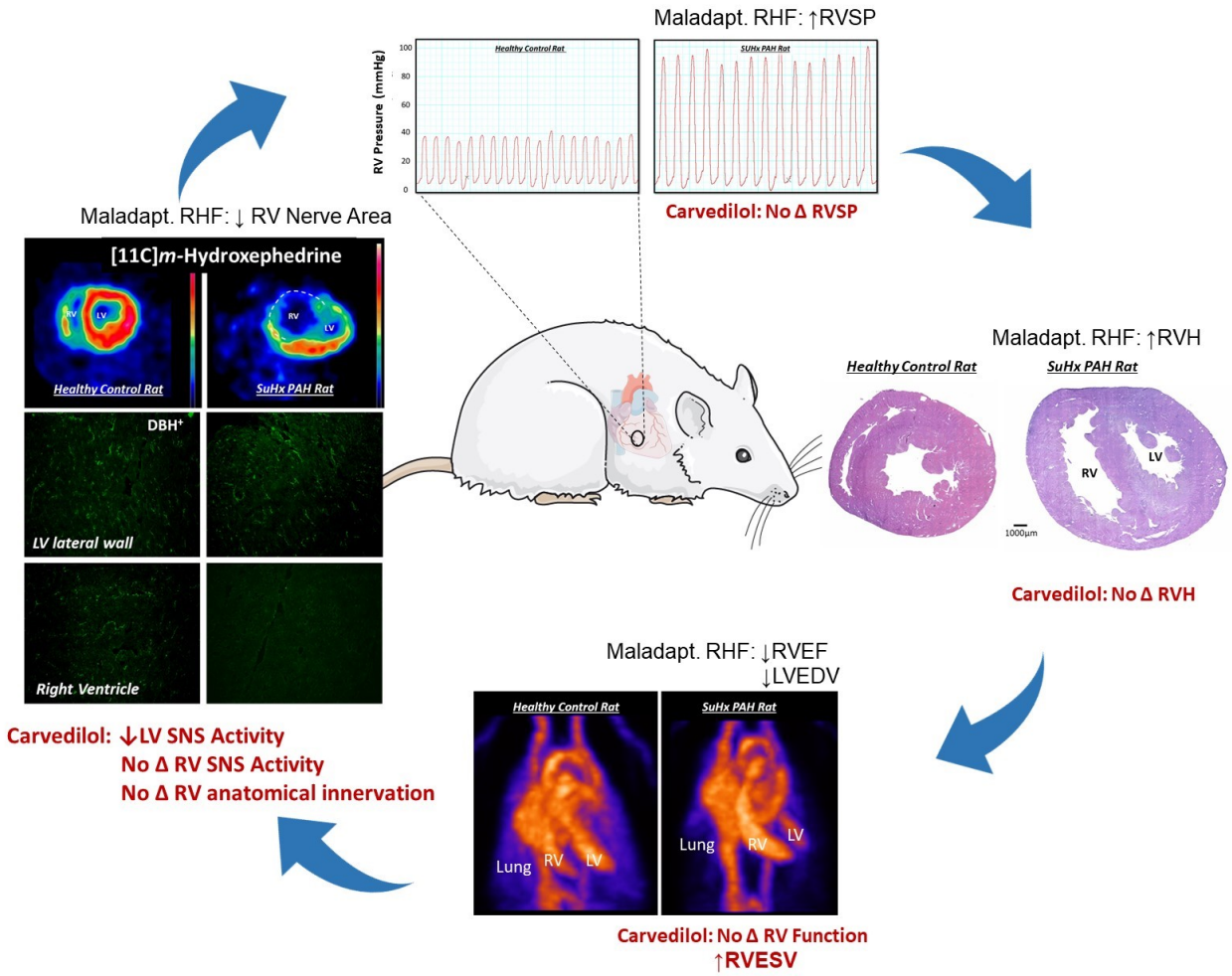

Supplemental Figure 3.4. Summary Figure. Effects of β-Blocker Carvedilol in Maladaptive Right Heart Failure Induced By PAH. The Sugen Hypoxia (SuHx) model induced severe PAH by 5 weeks and induced right heart failure. Carvedilol had no effect on pulmonary hemodynamics, RV remodeling or function. [^{11}C] HED PET was used to assess the cardiac sympathetic nervous system. Progressive sympathetic denervation was noted in the RV of PAH rats, but carvedilol had no effect of RV innervation or sympathetic activation. Parts of the figure were created using Servier Medical Art.

Chapter 4 Supplement

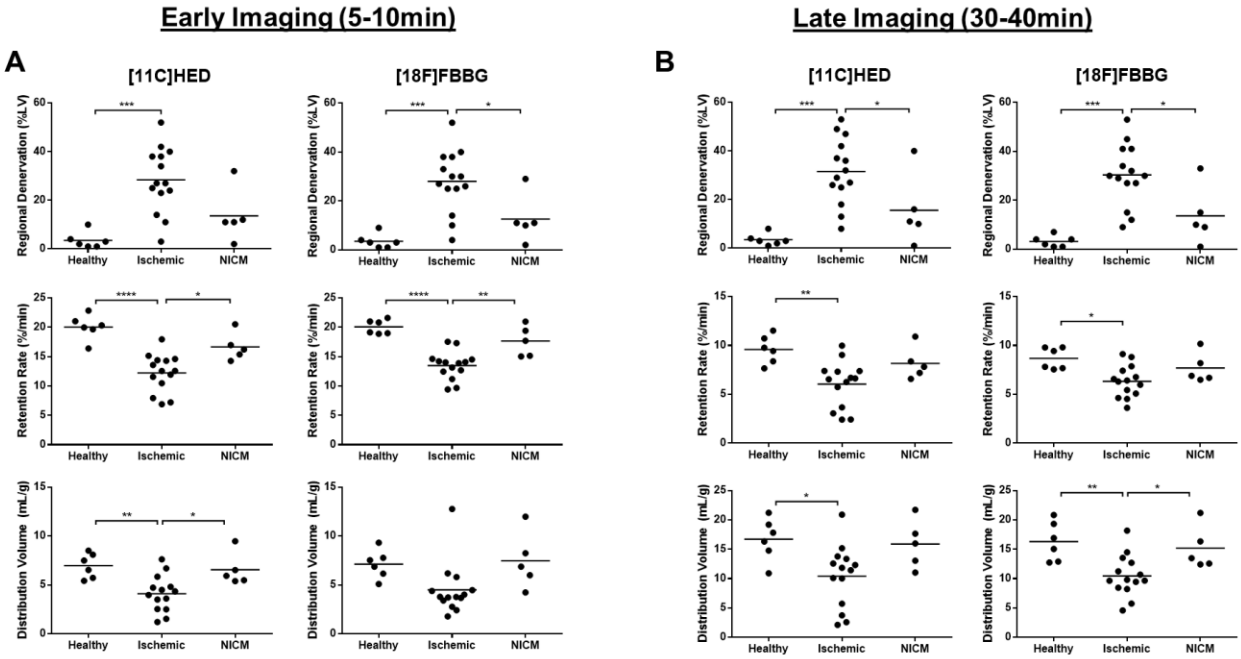

Supplemental Figure 4.1. HED and FBBG and LV global innervation in patient populations. HED and FBBG measures of LV global innervation (RI and DV) and regional denervation (%LV) in healthy participants and patients with ischemic and non-ischemic cardiomyopathy. Quantification parameters are displayed at early (A) (5-10min) and late (B) (30-40min) time post-injection.

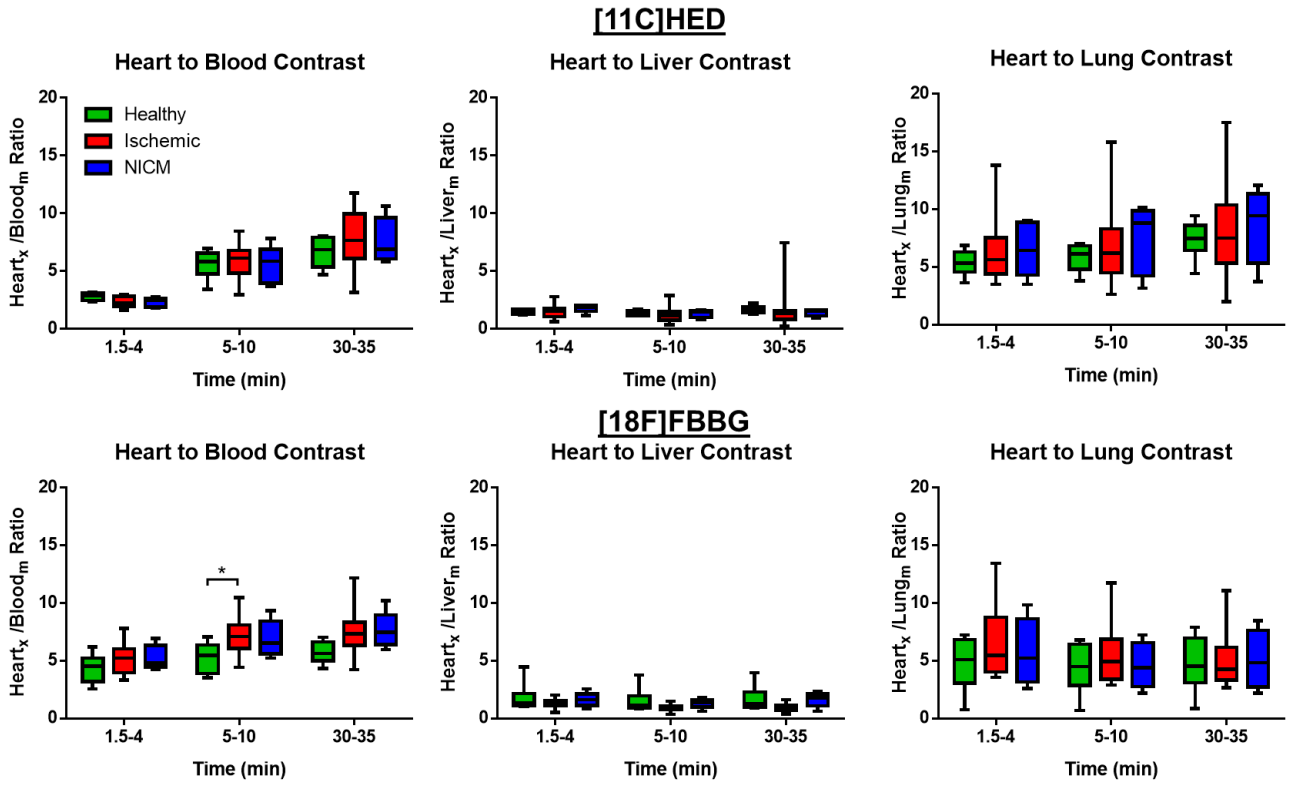

Supplemental Figure 4.2. Contrast ratios in patient populations. HED and FBBG Heart contrast ratio (Calculated as tissue (SUV heart max / background tissue or blood) assessed over time in the LV (A), liver (B) and Lung (C) in healthy participants and patients with ischemic and non-ischemic cardiomyopathy. Max and Mean SUVs were assessed from VOI in the LV blood pool, lung and liver and LV.

Chapter 5 Supplement

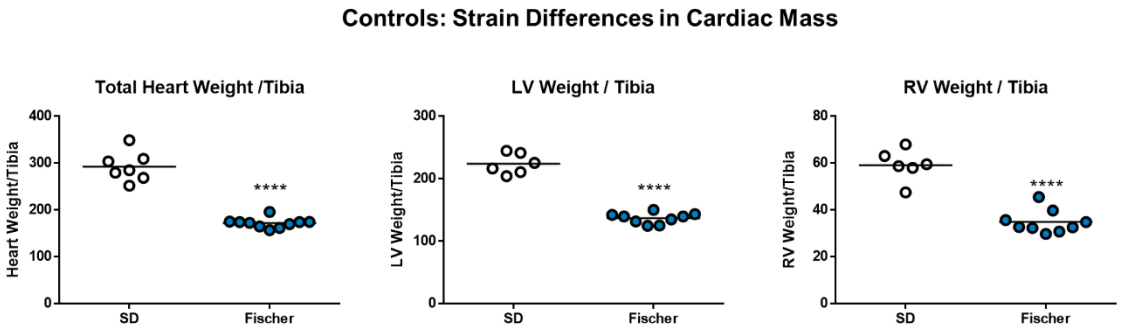

Supplemental Figure 5.1. Strain differences in heart mass. Heart mass in naïve Fischer and SD rats, normalized to tibia length. Total heart weight. ****p<0.0001

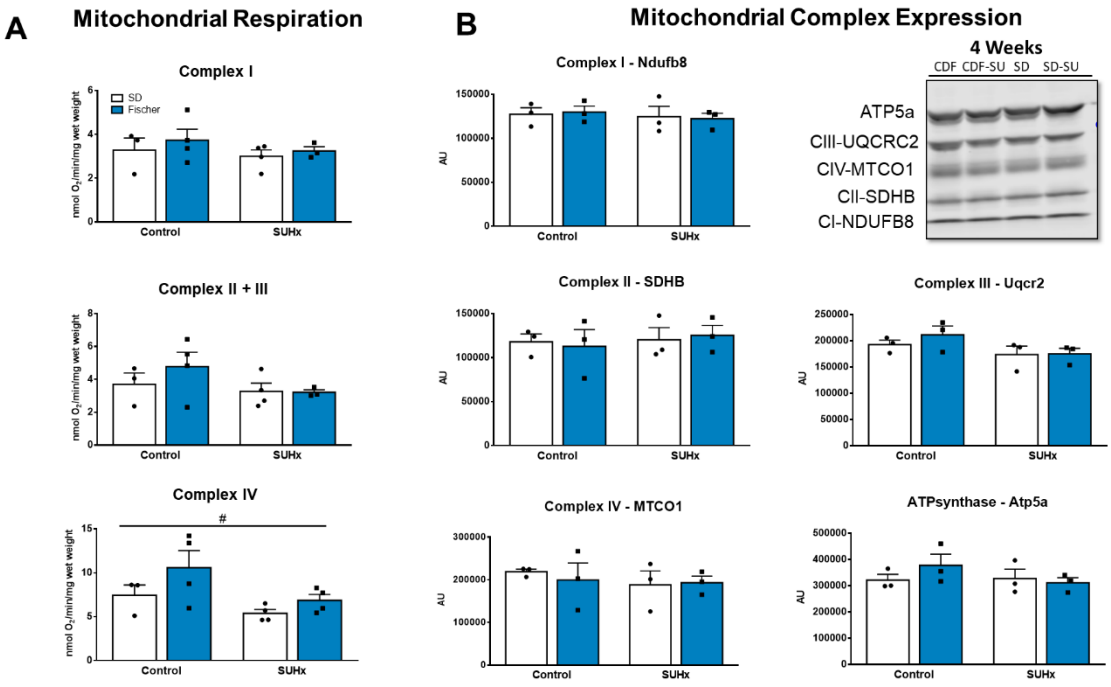

Supplemental Figure 5.2. Mitochondrial Electron Transport Chain complex function (respiration) and protein expression in Fischer and SD rats after 4 weeks of SuHx. Mitochondrial respiration (A) and protein expression (B) were remarkably preserved in both Fischer and SD SuHx rats. Only complex IV (A) respiration was similarly impaired in both SD and Fischer SuHx rats. Statistically significant difference between controls and SuHx #p<0.05

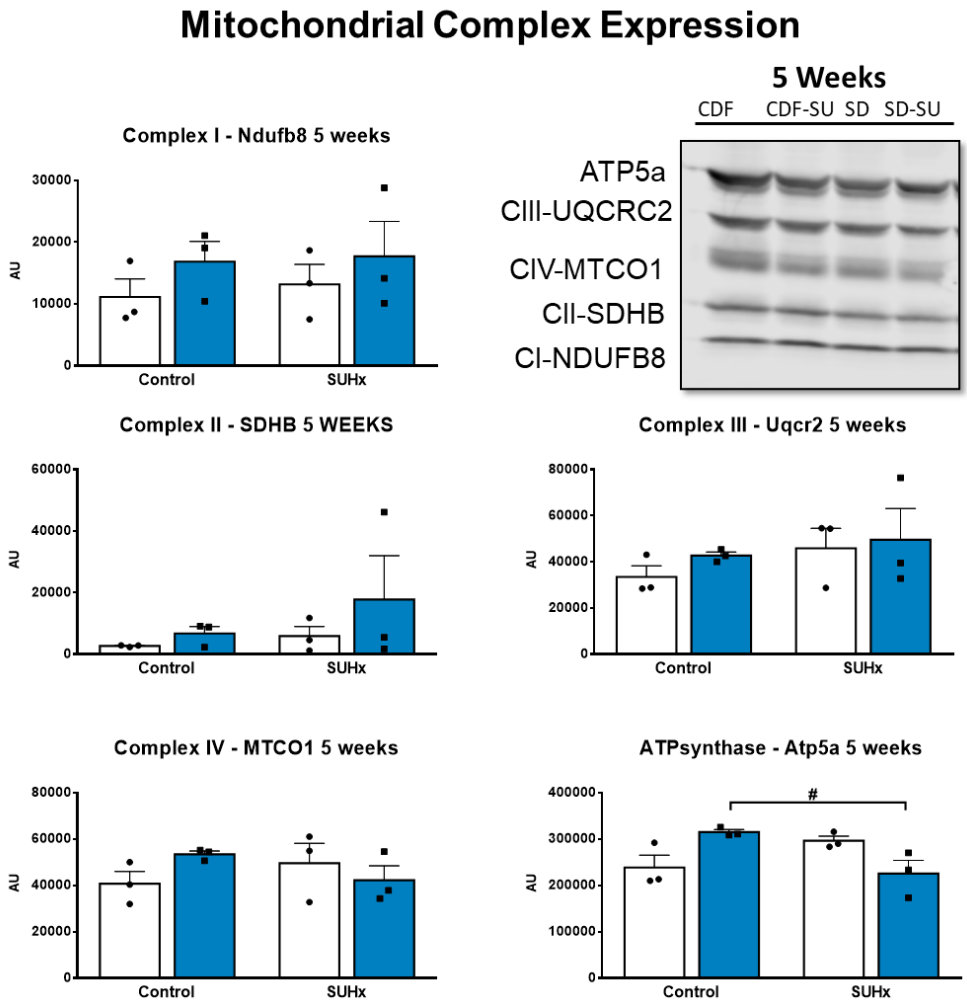

Supplemental Figure 5.3. Mitochondrial Electron Transport Chain complex expression in Fischer and SD rats after 5 weeks of SuHx. Statistically significant difference between controls and SuHx #p<0.05

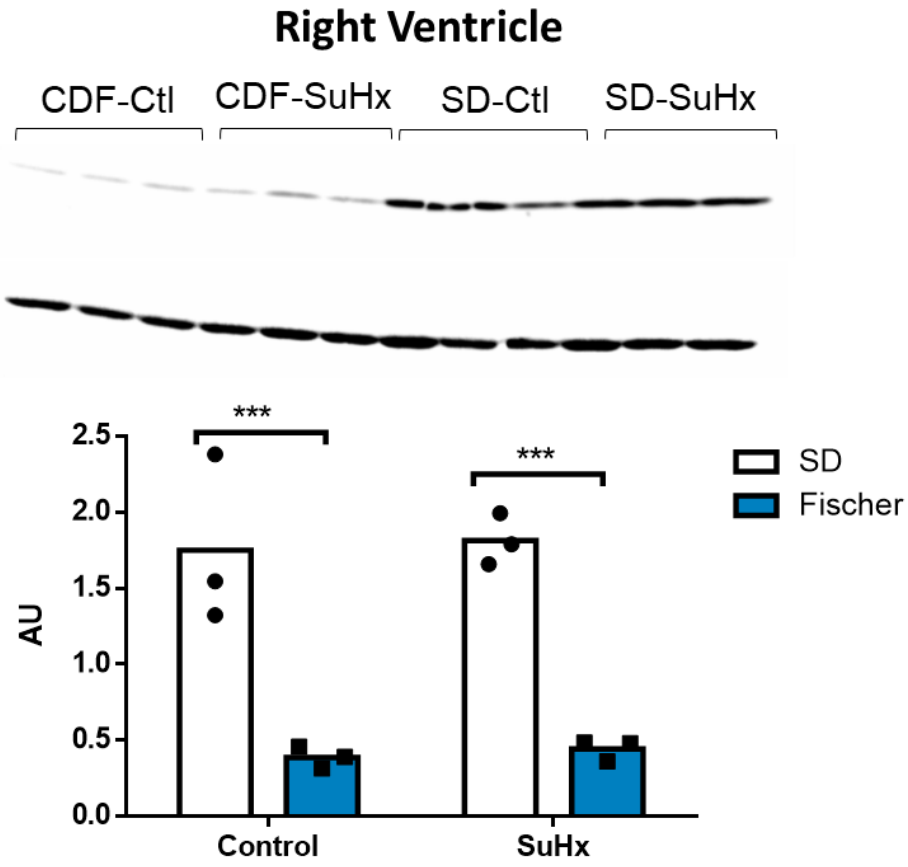

Supplemental figure 5.4. AK1 protein expression normalized to GAPDH in the RV of SD and Fischer rats. AK1 expression does not change in response to SuHx. ***p<0.001.

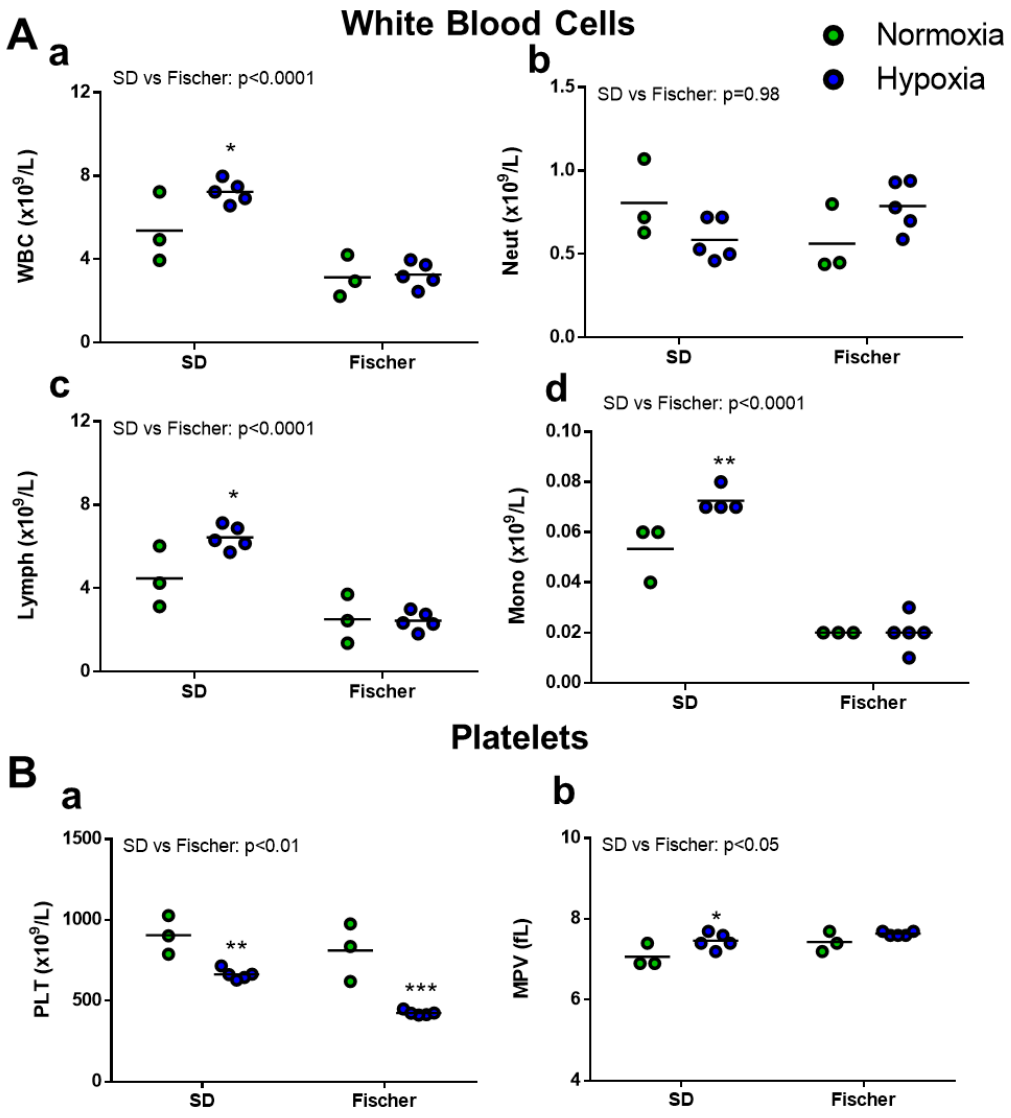

Supplemental figure 5.5. Complete blood count in Fischer and SD rats at baseline, and in response to hypoxia alone. WBC (A) and platelet (B) counts and morphological parameters are displayed. *p<0.05; **p<0.01; ***p<0.001; ****p<0.0001. Main effect of strain is displayed at the top of each graph.

Appendix B

Regional Denervation Improves Risk Stratification Compared to Global Sympathetic Innervation in Patients with Ischemic Cardiomyopathy

Zelt *et al.* 2020 Submitted to JACC: Cardiovascular Imaging

Running Title: Global HED Quantification and SCA Risk

Authors: Jason G. E. Zelt, MSc[1,2,3]*; Jean Zhuo Wang, BHSc[1,2]*; Lisa M. Mielniczuk MD, MSc [1,2,3]; Rob S.B. Beanlands, MD[1,2]; James A. Fallavollita, MD[4,5]; John M. Canty Jr., MD[4,5]; Robert A. deKemp, PhD[1,2].

*Equal Contribution by authors

[1]Department of Medicine (Cardiology), University of Ottawa Heart Institute, Ottawa, Canada

[2]Faculty of Medicine, University of Ottawa, Ottawa, Canada

[3]Department of Cellular and Molecular Medicine, University of Ottawa, Ottawa, Canada

[4]VA Western New York Healthcare System, Buffalo, NY, USA.

[5]Division of Cardiovascular Medicine, University of Buffalo, Buffalo, NY, USA

Author Contribution:

JGEZ: Performed Statistical Analysis and graphical representation and wrote the manuscript
JZW: Performed image analysis and helped write the manuscript
RSB and LMM: PET Content expert, and critical appraisal of manuscript
JAF and JMC: Conducted the PAREPET Trial
RAD: Wrote manuscript and critical appraisal of the manuscript

Key Words: Sudden Cardiac Arrest; Sympathetic Innervation: Sympathetic Denervation;

Hydroxyephedrine; Positron Emissions Tomography

B.1.0 Abstract

Introduction: Current risk assessment approaches fail to identify the majority of patients at risk of sudden cardiac arrest (SCA). Non-invasive imaging of the cardiac sympathetic nervous system (SNS) using SPECT and PET offers the potential for refining SCA risk assessment. While various [^{11}C]meta-hydroxyephedrine (HED) quantification parameters have been proposed, it is currently unknown whether regional denervation or global innervation yields greater SCA risk discrimination. The aim of the study was to determine whether the global innervation parameters yield any independent and additive prognostic value over the regional denervation alone.

Methods: In a retrospective competing risks analysis of the PAREPET trial, we compared global innervation and regional denervation parameters using the norephinephrine analog HED for SCA risk discrimination. Patients with ischemic cardiomyopathy (n=174) eligible for an implantable cardiac defibrillator (ICD) for the primary prevention of SCA were recruited into the trial. HED uptake and clearance rates were measured to assess global (LV mean) retention index (RI) and volume of distribution (DV). Regional defects were quantified as the percentage of the LV having values <75% of the maximum.

Results: During a median follow-up of 4.2 years, there were 56 cardiac related deaths, of which 26 were SCAs. For any given regional denervation volume there was substantial heterogeneity in global innervation scores. Global RI and DV did not decrease until regional defects exceeded 40% LV. Global scale parameters, RI and DV (AUC=0.61), yielded inferior SCA risk discrimination compared to regional parameters (AUC=0.74).

Conclusion: Regional denervation volume has superior cause-specific mortality prediction for SCA vs. global parameters of sympathetic innervation. These results have widespread implications for future cardiac sympathetic imaging, which we predict will greatly simply innervation analysis.

B.2.0 Introduction

Sudden cardiac arrest (SCA) remains a lethal and unpredictable event, accounting for half of all heart related deaths.[361] Survivors of myocardial infarction (MI) have a four-fold elevated risk of arrhythmic death compared to persons without a history of MI.[211] Clinically, ejection fraction (EF) is the main parameter used to delineate risk and guide the need for primary prevention ICD therapy (EF≤35%).[362] Yet, the long-term appropriate discharge rate among these patients is only 11-35% over a 3-4 year period.[212,363,364] Non-invasive imaging of the cardiac sympathetic nervous system (SNS) has been proposed to compliment SCA risk assessment. This may not only enable more cost-effective patient selection and improved outcomes but also provide a way to identify the large number of patients that develop SCA with an EF >35%.

Alterations in the sympathetic nervous system have been implicated in the development of lethal ventricular arrhythmias.[218–222,365,366] These can arise from global alterations in myocardial sympathetic tone without structural alterations in sympathetic nerve density. In addition, since sympathetic nerves are exquisitely sensitive to ischemia and infarction, regional defects can develop with the zone of denervation often extending beyond the ischemic penumbra.[367]

Various methods of [^{11}C]*meta*-hydroxyephedrine (HED) quantification for positron emissions tomography (PET) have been proposed to assess the burden of sympathetic denervation and dysfunction. While these methods may require varying degrees of quantitative sophistication and imaging time, it remains to be determined which method yields the most robust SCA risk discrimination. Quantification of both global (i.e. total tracer uptake and retention) and regional (i.e. defect volume) sympathetic innervation have been reported in the literature. The PAREPET (Prediction of Arrhythmic Events with Positron Emission

Tomography) trial calculated a regional normalized uptake defect, defined as the fraction of polar-map sectors <75% of the maximum normalized uptake value and expressed as percentage of the total left ventricle (LV).[367] In contrast, other studies report global parameters with HED quantification of tracer retention index (RI) and/or volume of distribution (DV). While there is some debate as to which better reflects global cardiac sympathetic innervation[335,368–371], initial reports suggest DV may be less flow-dependent and thus may be a more relevant parameter, particularly for patients with ischemic cardiomyopathy.[371] Conceptually, patients with a given defect size may have varying degrees of global LV uptake. Mechanistically, this may be due to differing defect severities, heterogenous uptake in remote regions or a global reduction in tracer uptake. It remains to be determined the prognostic significance of global tracer uptake parameters, independent of defect size and whether they offer any additive value in SCA risk prediction. The objectives of the present analysis were two-fold: 1) in a competing-risk analysis compare the robustness of regional and global [^{11}C]HED quantification parameters for predicting cause-specific mortality from SCA and 2) determine whether the global RI and DV assessments yield any independent and additive prognostic value over the regional defects alone.

B.3.0 Methods

B.3.1 Study Population

The PAREPET trial (NCT01400334) enrolled 204 subjects with ischemic cardiomyopathy, eligible for an ICD for primary prevention of SCA. [367] The University of Buffalo Institutional Review Board approved the study protocol and all subjects signed an informed consent form. Of the 204 participants, 190 patients underwent HED PET scans. N=16 were excluded from the present study due to reasons listed in Figure B.1, leaving n=174 included for analysis.

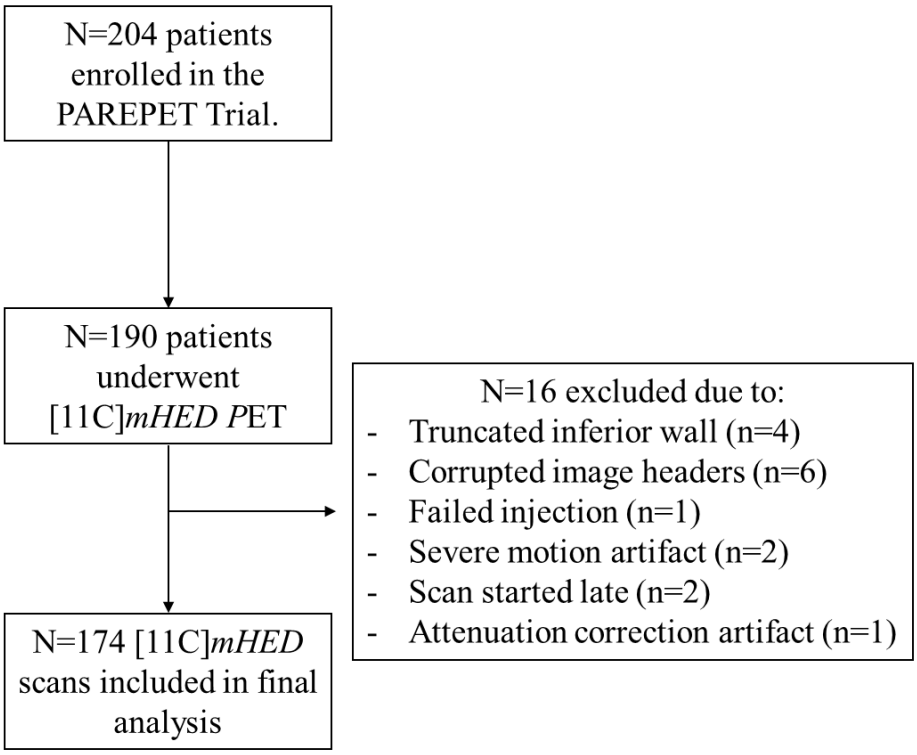

Figure B.1. Flow diagram of patient inclusion/exclusion.

B.3.2 PET Imaging

PET imaging was performed as described in prior methods.[367,372] An intravenous bolus of 740 MBq (20 mCi) of HED was administered, followed by dynamic cardiac PET imaging for 60 minutes (6×30 sec, 2×60 sec, 2×150 sec, 2×300 sec, 2×600 sec, 1×1200 sec frames). The images were reconstructed with all corrections enabled using filtered back-projection and a Hann window of the Ramp filter, resulting in ~10mm isotropic resolution. Dynamic Images were analyzed using FlowQuant® v2.4 (University of Ottawa Heart Institute, Ottawa, Canada).

B.3.3 HED Parameters

Retention Index

Retention index is a measure utilized to estimate the net uptake of HED at scan end-time, calculated using the following equation which relates the activity in myocardial tissue (C_m) to the unchanged tracer activity in plasma (C_p) and the function evaluation time (T_R):

$$RI_{(RC)} = \frac{C_m(T_R)}{\int_0^{T_R} C_p(t)dt} \times 100\%$$

No partial-volume recovery correction (RC=1) was applied as fractional blood volume is not estimated using the retention model.

Distribution Volume

The distribution volume is defined as the ratio of tracer concentration in the myocardium to arterial plasma, at equilibrium. For receptor ligands, the DV physiologically reflects tracer binding affinity (i.e. B_{max}/K_d), where B_{max} is Uptake1 density and $1/K_d$ is the affinity of HED for

the Uptake1 transporter. [334] Volumes of distribution were calculated using a one-tissue compartment model as previously described.[333] This method can be expressed by the following equation, where C_m is myocardial tracer concentration,C_p is arterial plasma tracer concentration, and T_E is the time to equilibrium: $DV = \frac{K_1}{k_2} = \frac{C_m(T_E)}{C_p(T_E)}$.

Quantitative analysis requires subtraction of radiolabeled blood metabolites accumulating in the blood stream to ensure accurate computation. The arterial whole-blood time-activity curve was obtained from a 20 mm^3 region in the LV cavity. The following equation was used to correct for blood metabolites is as follows: $C_p(t) = C_{WB}(t) \times pfp(t)$, where $C_p(t)$ is the unchanged parent tracer concentration in plasma, $C_{WB}(t)$ is the arterial whole-blood tracer concentration, and pfp(t) is the parent fraction in plasma function.[335,336]

The same partial volume recovery correction (RC = 1) was applied as well as the fraction of blood volume within myocardial tissue. The following equation was incorporated in the one-tissue compartment model: $C_p(t) = RC \times C_m(t) + f_B \times C_p(t)$.

Regional Defects

Regional defect scores for tracer normalized uptake (NU) and DV reflect the extent × severity of relative defects, expressed as a percent of the left ventricle.[332] The defect scores were calculated by quantifying tracer uptake or DV in 496 myocardial sectors; those with ≥75% relative to the peak tracer activity were defined as normal and set to equal 100%. The defect score then calculated as 100% minus the average polar-map value.

B.3.4 Clinical Endpoint

The primary PAREPET endpoint was SCA, including ICD discharge for fast ventricular tachycardia (>240 bpm) or ventricular fibrillation as an equivalent. The secondary endpoint in the competing risks analysis was total cardiac mortality, including both SCA and non-sudden cardiac arrest. Events were arbitrated blindly by 3 board-certified cardiologists.[367]

B.3.5 Statistical Analysis

Continuous variables were represented as mean±SD. Correlations between regional and global scale parameters were performed using a Pearson's Correlation coefficient. In Figure B.2, we used a one-way analysis of variance (ANOVA) to assess statistical differences in global parameters at a range of regional NU defect values. Time-to-endpoint was analyzed using the Kaplan-Meier method and differences between tertiles were assessed by the Log-Rank test. A cox-proportional hazards regression was also used to assess the association between the HED PET parameters and SCA. A competing risks analysis was performed to simultaneously assess the HED PET parameters associated with SCA and NSCD. A multivariate analysis was performed with both global and regional parameters entered into the model to identify any independent value of global quantification. Area under (AUC) the receiver operator characteristic (ROC) curve was used to assess the ability of the individual HED PET parameters to discriminate between patients who developed SCA vs. those who did not. For this analysis, discrimination was compared at the median follow-up time of 4.2 years. We also evaluate the incremental value of global scale parameters when added to regional defect parameters using the methods of Delong, Delong, and Clarke-Pearson [373]. In the original PAREPET trial, a 4 variable clinical model was created consisting of i) the normalized uptake defect score, ii) creatinine, iii)

indexed LVEDV, and iv) no ACE/ARB therapy. [367] From this model, optimized cut points were derived (NU defect score >37% of LV, creatinine >1.49 mg/dL, LVEDVI >99 mL/m^2, and no ACE/ARB therapy). Patients with none of these risk factors had a SCA risk of <1%/year, whereas patients with ≥2 risk factors had a SCA event rate of 11.7%/year. In this clinical model, we scrutinized the ability of the global scale HED parameters to re-classify patients across these event thresholds. The incremental additive value of the global parameters were assessed using the net reclassification index (NRI) and the integrate discrimination improvement (IDI).[374] The IDI evaluates reclassification as a continuous outcome across the spectrum of risk, whereas NRI is defined by prespecified thresholds, chosen apriori. $P<0.05$ was considered statistically significant. Statistical analysis and graphical representation were performed using SAS 9.4 (SAS Institute, NC), and GraphPad Prism 6.0 (GraphPad, La Jolla, CA, USA).

B.4.0 Results

Patient demographics and characteristics appear in Table B.1. Overall patients were optimally treated with 97% on β-blocker therapy, 90% on an ACE or ARB, and 99% receiving either warfarin or antiplatelet therapy. After a median follow-up of 4.2 years (IQR: 2.7-5.3 years) there were 56 cardiac related deaths (n=26 SCA, n=30 non-sudden cardiac death (NSCD)), and 25 non-cardiac related deaths (NCD).

Table B.1. Patient Characteristics

Variables (n=174)	Average
Demographics	
Age (years)	67.6 ±11.6
Sex (male)	156 (90%)
BMI (kg/m^2)	28.7 ± 5.1
Diabetes mellitus	82 (47%)
Resting Heart Rate (bpm)	65 ± 12
Rate/Pressure Product (per 100 bpm/ mm Hg)	8473 ± 2294
No ACE/ARB Therapy	18 (10%)
β-blocker Therapy	168 (97%)
Warfarin	69 (40%)
Antiplatelet (ASA or Clopidogrel)	153 (89%)
Digoxin	67 (39%)
Echocardiographic and Electrocardiographic Variables	
Ejection Fraction (%)	27.6 ± 8.9
LV End Diastolic Volume Index (mL/m^2)	87.1 ± 29.1
LV End Systolic Volume Index (mL/m^2)	63.9 ± 25.5
LA Volume Index (mL/m^2)	41.9 ± 15.7
LV Mass Index (g/m^2)	152.1 ± 47.5
QRS Duration (ms)	136.7 ± 35.5
Laboratory Values	
Creatinine (mg/dL)	1.43 ± 0.9
B-type natriuretic peptide, ng/L	423.1 ±455.8
Hematocrit (%)	40.6 ± 4.9
[^{11}C]HED PET Quantification	
Global Scale Parameters	
Retention Index (%/min)	4.6 ± 1.7
Distribution Volume (mL/g)	10.5 ± 4.0
Regional Defect Parameters (%LV)	
Normalized Uptake	27.5 ± 11.1
Distribution Volume	38.0 ±11.4

B.4.1 Agreement Between HED Quantification

Four HED quantification methods were performed, two regional defect parameters (NU and DV) and two global scale parameters (RI and DV). To investigate the agreement between the quantification methods, patients were stratified into tertiles based on their respective regional defect and global scale parameters. There was good to excellent agreement within the global (weighted kappa=0.53) and regional defect (weighted kappa=0.71) quantification values (Table B.2). In contrast, there was poor agreement between regional defect and global scale parameters tertiles (weighted kappa 0.16-0.34). Similarly, there were weak linear correlations between the global scale and regional defect parameters (RI: r^2=0.049; DV: r^2=0.082; Figure B.2 C,D). Interestingly, for a given regional defect size, there was substantial heterogeneity in global HED DV (Figure B.2A) and RI (Figure B.2B) values, with no consistent reductions in these parameters until the regional defect size increased above 40% LV ($p<0.05$). Representative polar maps (Figure B.3) illustrate this concept. We aimed to investigate whether the global parameters offer any independent, or additive prognostic value.

Table B.2: Agreement Between PET Parameter Tertiles

Comparison			Weighted Kappa	95% CI
Normalized Uptake	vs	DV Regional	0.71	0.63, 0.79
	vs	DV Global	0.24	0.12, 0.35
	vs	RI Global	0.16	0.04, 0.28
DV Regional	vs	DV Global	0.34	0.22, 0.45
	vs	RI Global	0.21	0.09, 0.33
DV Global	vs	RI Global	0.53	0.43, 0.64

Tertiles were aligned according to theoretical risk, i.e. Tertile 1 for regional variables we compared to Tertile 3 for global parameters.

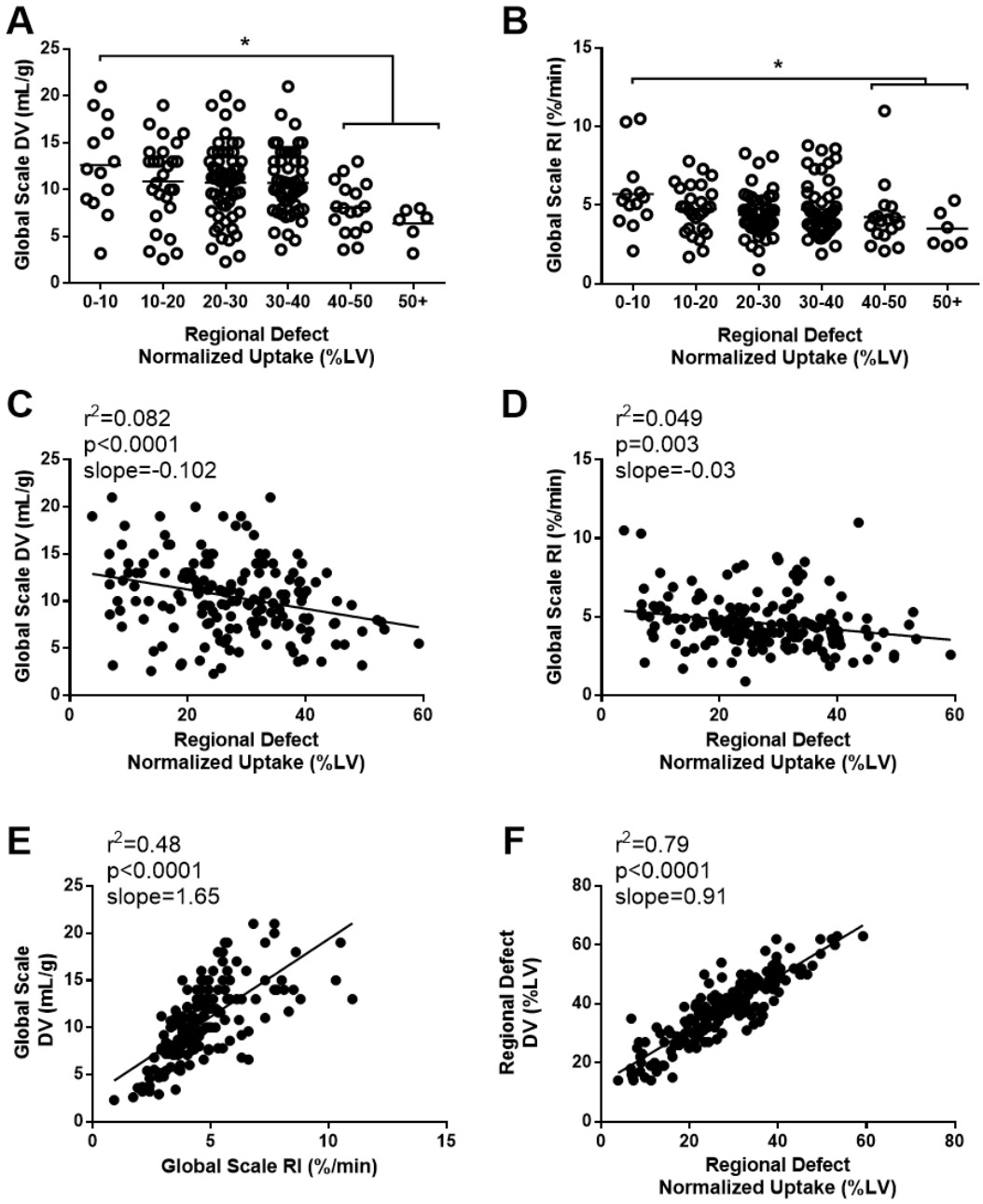

Figure B.2. Relationship between regional defect and global scale [^{11}C]HED PET parameters. For a given regional defect, patients display a range of global DV (A) and global RI (B) values. Correlations between the regional defect normalized uptake (used in the PARREPET trial) and global scale parameters displayed (C,D). Excellent correlations were observed within global scale (E) and regional defect (F) [^{11}C]HED PET parameters. DV, distribution volume; RI, retention index; LV, left ventricle.

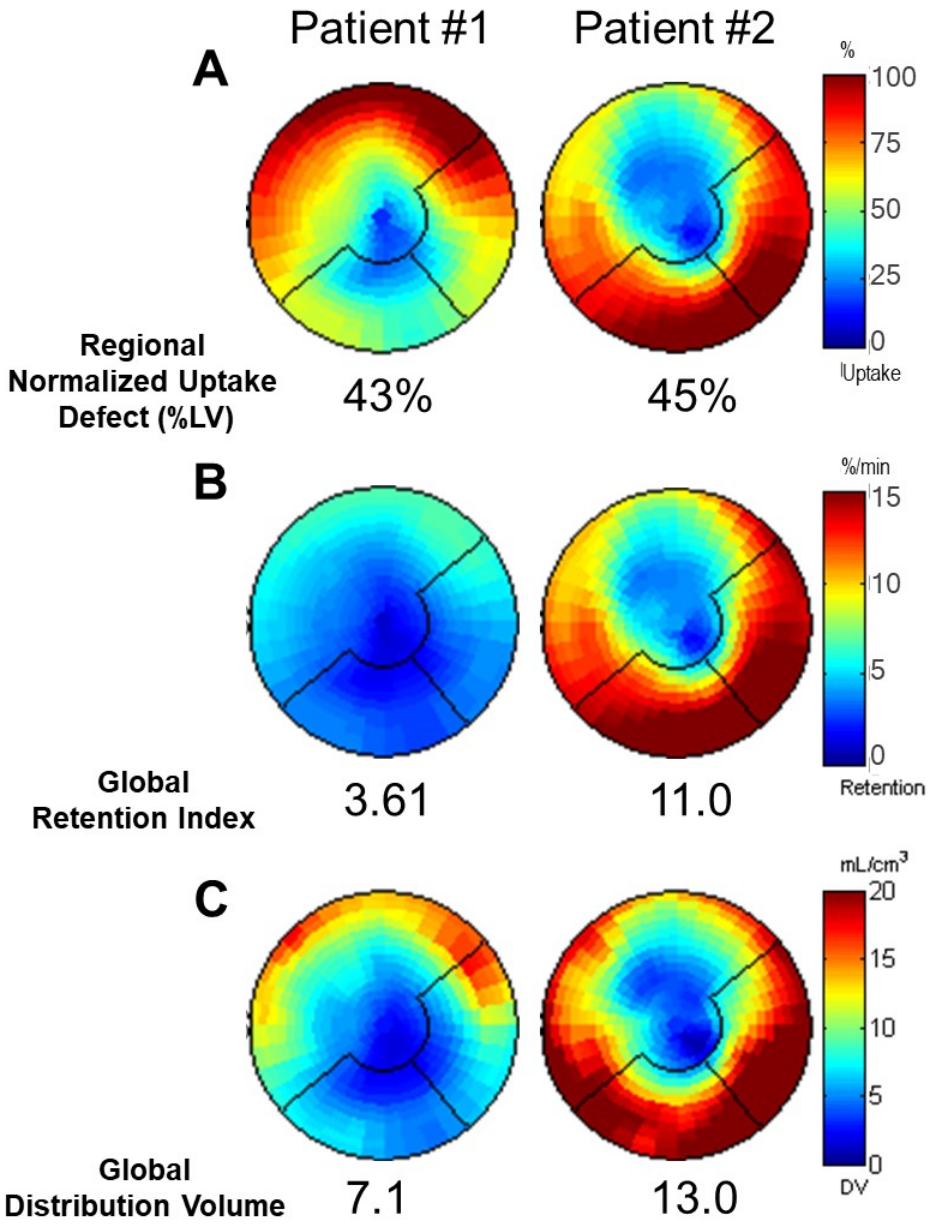

Figure B.3 Representative polar maps. Polar maps of regional normalized uptake (A), and global scale retention (B) and distribution volume (C) for two patients with similar regional defect scores but differing global RI and DV scores.

B.4.2 HED Parameters and Survival

The HED regional defect and global scale parameters association with time to the cardiac end points are summarized in Table B.3. Only the regional defect parameters were associated with total cardiac mortality ($p<0.05$), whereas both regional defect and global scale parameters were associated with SCA ($p<0.05$). None of the HED parameters were associated with non-sudden cardiac death. Kaplan-Meier functions summarize this data (Figure B.4). After adjusting for competing risks, SCA was associated with increased regional defect size, NU ($p=0.0025$) and DV ($p=0.0005$), and decreased global scale parameters, DV ($p=0.04$), RI ($p=0.02$) as shown in Table B.4. However, after statistically controlling for regional defect size (NU), these global scale parameters were no longer significantly associated with SCA in the competing-risk model (Table B.4). In the unadjusted competing risk analysis, the effect of each of these HED quantification parameters on probability of SCA, NSCD and non-cardiac death is illustrated in Figure B.5.

Table B.3. Univariate Associates with Cardiac Endpoints

PET Variable	Total Cardiac		Sudden Cardiac Arrest		Non-Sudden Cardiac Death		Non-Cardiac Death	
	Hazard Ratio	*p*-Value	Hazard Ratio	*p*-Value	Hazard Ratio	*p*-Value	Hazard Ratio	*p*-Value
Regional Defect (per 1% of LV)								
Normalized Uptake	1.035	0.0053*	1.055	0.0024*	1.016	0.34	0.98	0.35
Distribution Volume	1.035	0.0057*	1.066	0.0008*	1.010	0.54	0.98	0.33
Global Scale (per 1 unit)								
Distribution Volume	0.93	0.057	0.90	0.047*	0.97	0.46	1.02	0.69
Retention Index	0.86	0.12	0.72	0.033*	0.98	0.86	0.99	0.98

*significant at $p<0.05$.

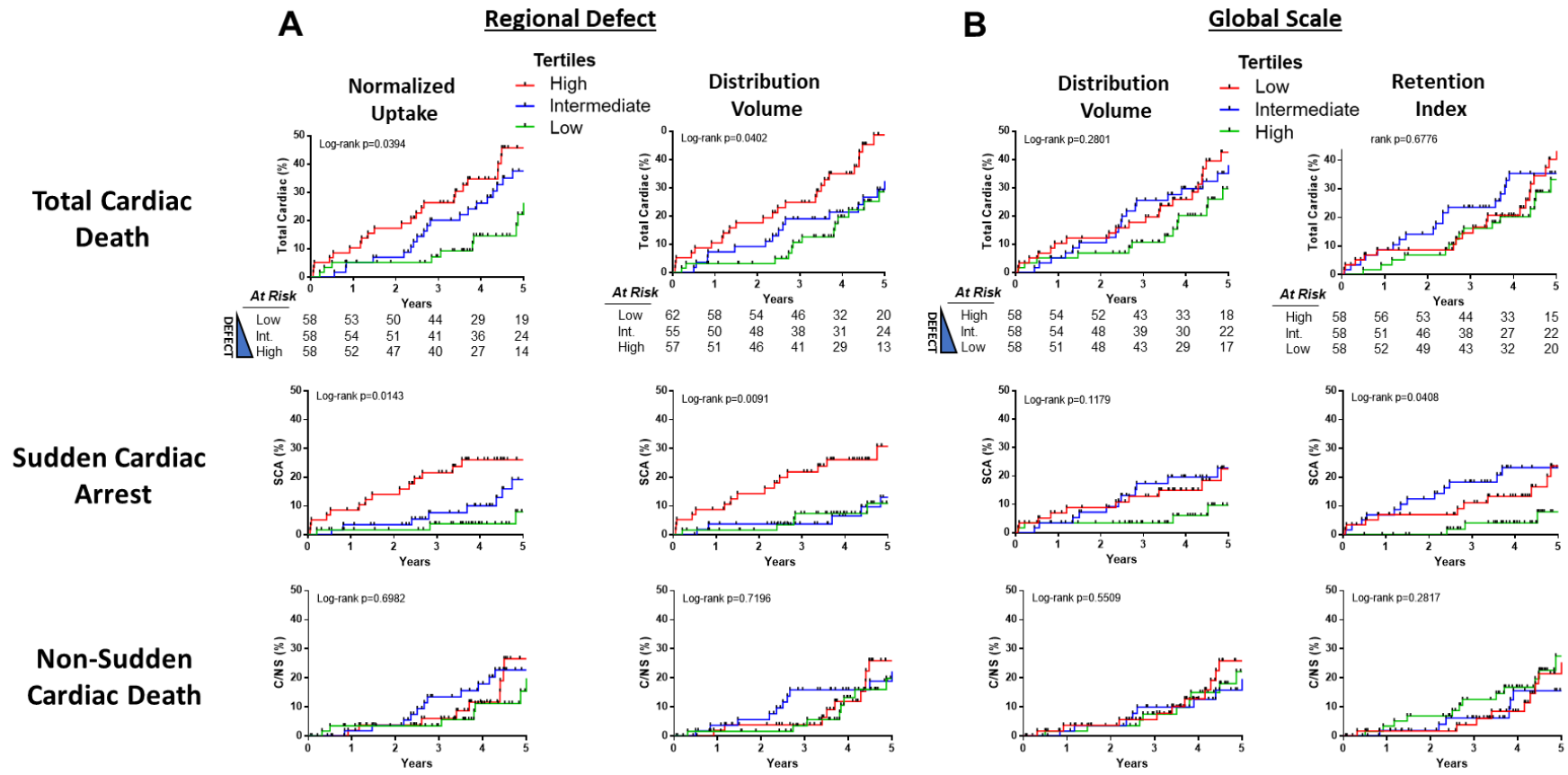

Figure B.4. Kaplan-Meier curves show the incidence of cardiac endpoints for tertiles of regional defect (A) and global scale (B) [^{11}C]HED quantification methods. Note that the coloring of the tertiles for the global scale parameters (B) is reversed to correspond with the theoretical risk. For the regional defect parameters, the low (green) and high (red) tertiles for Normalized Uptake (low: <22.87%, high ≥32.6%) and DV (low: <35%, high ≥43%) are shown. Similarly, for the global scale parameters, the low (red) and high (green) tertiles for DV (Low: <8.7mL/g, High: ≥12.2 mL/g) and RI (Low: <3.84 %/min, High: ≥4.85%/min). Corresponding P values for the univariate analysis using continuous variables are in Table B.3. SCA, sudden cardiac arrest; C/NS, non-sudden cardiac death.

Table B.4. Competing Risk Model for SCA vs Non-Sudden Cardiac Death and Non-Cardiac Death.

Variable	Sudden Cardiac Arrest			Non-Sudden Cardiac Death			Non-Cardiac Death		
	Hazard Ratio	95%CI	*p*-Value	Hazard Ratio	95%CI	*p*-Value	Hazard Ratio	95%CI	*p*-Value
Regional Defect (per 1% LV)									
Normalized Uptake	1.055	1.019, 1.092	0.0025*	1.016	0.983, 1.051	0.3398	0.982	0.946, 1.019	0.3451
Distribution Volume	1.066	1.027, 1.106	0.0005*	1.010	0.978, 1.044	0.5421	0.983	0.948, 1.018	0.3347
Global Scale (per 1 unit)									
Distribution Volume	0.897	0.806, 0.998	0.041*	0.964	0.875, 1.063	0.4620	1.022	0.919, 1.136	0.6922
Retention Index	0.713	0.524, 0.972	0.021*	0.980	0.783, 1.228	0.8624	0.997	0.773, 1.286	0.9823
Multivariable Model									
Model A									
NU	1.048	1.011, 1.086	0.010*	-	-	-	-	-	-
Global Scale RI	0.788	0.578, 0.788	0.134	-	-	-	-	-	-
Model B									
NU	1.047	1.010, 1.086	0.013*	-	-	-	-	-	-
Global Scale DV	0.935	0.832, 1.052	0.264	-	-	-	-	-	-

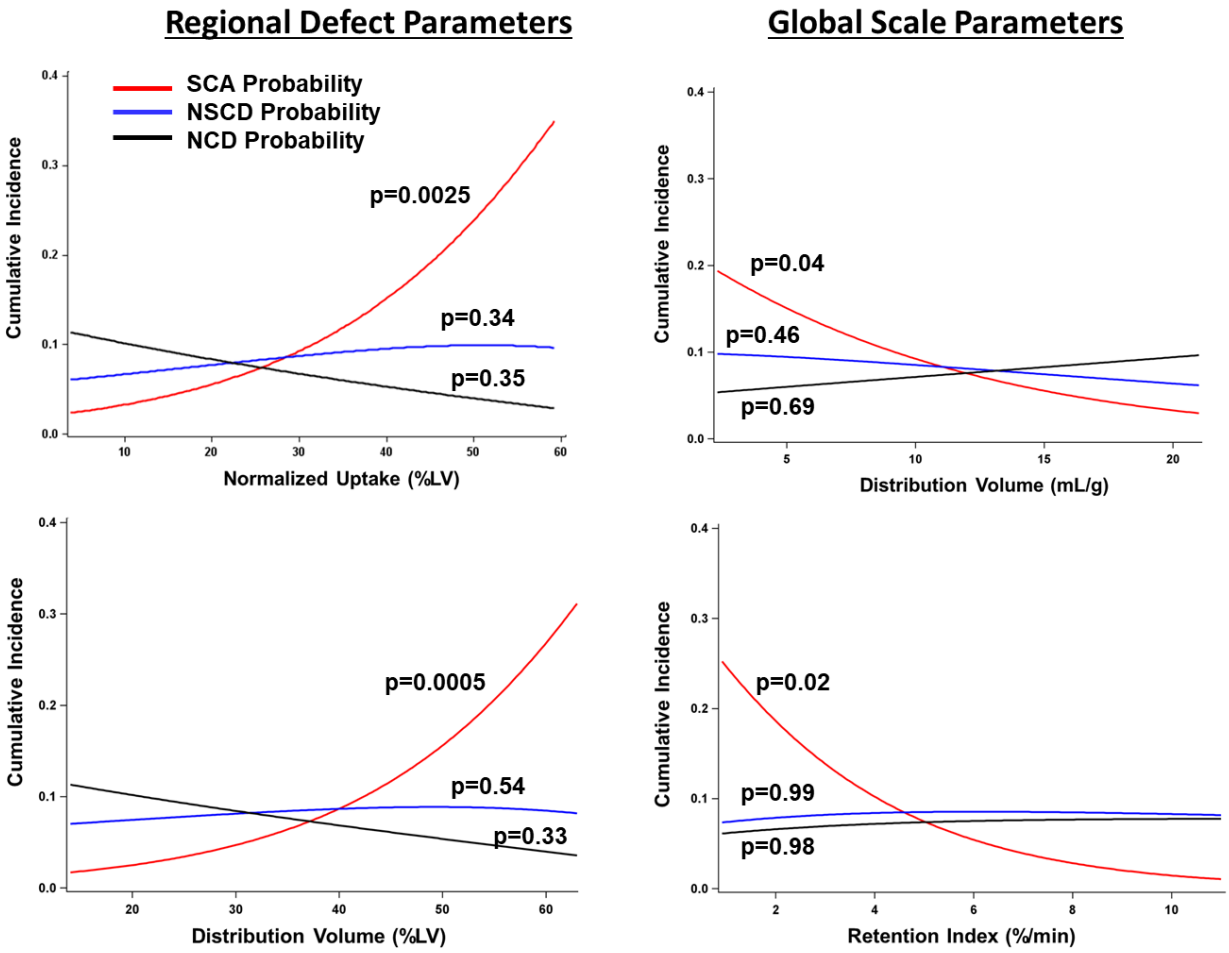

Figure B.5. Estimated event rates from the competing risk analysis for HED PET regional defect and global scale quantification. P values are derived from the competing-risk analysis in Table 3.4. Figure illustrates the anticipated effect of each HED quantification parameter on SCA (red line), non-sudden cardiac arrest (blue line) and non-cardiac death (black line) within the follow-up period. All HED quantification parameters were associated with SCA after adjusting for competing risks. The effect of each PET parameter was assessed individually. LV, left ventricle; SCA, sudden cardiac arrest; NSCD, non-sudden cardiac death; NCD, non-cardiac death.

B.4.3 HED Parameters and SCA Risk Prediction

Table B.5 and Figure B.6 summarize the AUCs for the individual HED quantification methods for predicting SCA. Of these parameters, the regional normalized uptake defect score had the best SCA risk discrimination (AUC 0.74) and had a significantly higher AUC than both global RI (ΔAUC=0.13, p=0.03) and global DV (ΔAUC=0.12, p=0.04). The addition of either global parameters to the regional normalized uptake defect score did not significantly improve the AUC (Table B.5). In the original PAREPET trial, a 4 variable clinical model was created consisting of i) the normalized uptake defect score, ii) creatinine, iii) indexed LVEDV, and iv) no ACE/ARB therapy (Table B.6). [367] From this model, optimized cut points were derived (NU defect score >37% of LV, creatinine >1.49 mg/dL, LVEDVI >99 mL/m^2, and no ACE/ARB therapy). Patients with none of these risk factors had a SCA risk of <1%/year, whereas patients with ≥2 risk factors had a SCA event rate of 11.7%/year. In this clinical model, we scrutinized the ability of the global scale HED parameters to re-classify patients across these event thresholds. Global Scale RI and DV did not significantly improve the model and appropriately reclassify patients in accordance with their SCA risk (NRI and IDI not significant, Table B.7).

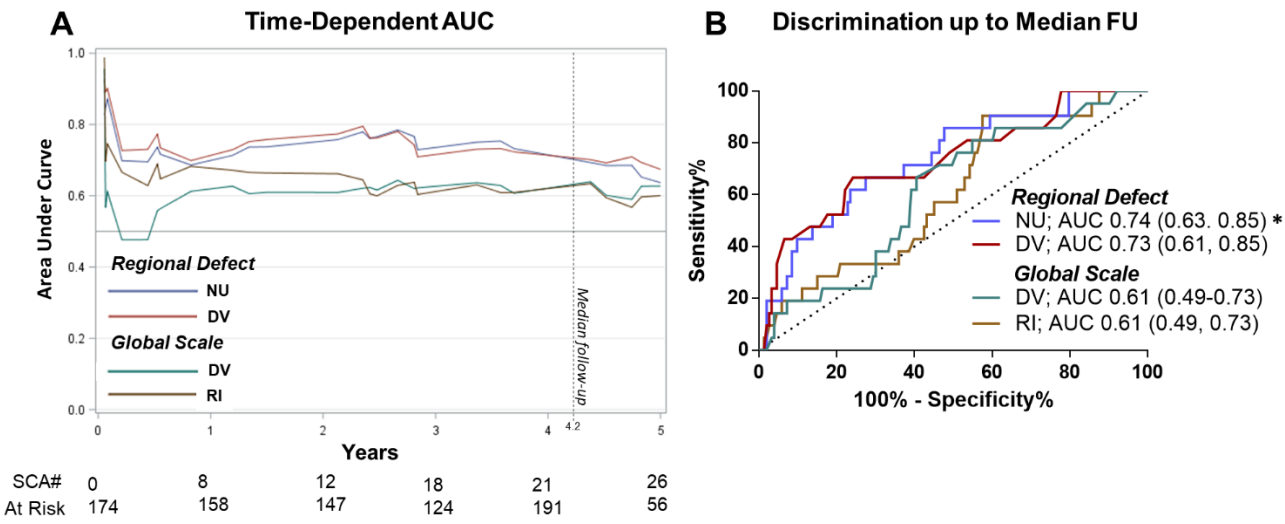

Figure B.6. Comparison of Regional Defect and Global Scale [^{11}C[HED PET parameters for SCA risk discrimination. Time-dependent AUC illustrate discrimination over time (A). PET parameters were compared up to the median follow-up (4.2years). ROC curve comparison for regional defect and global scale parameters up to median follow-up (B). Corresponding P values are displayed in Table B.5. * AUC superior than both global scale parameters, $p<0.05$.

Table B.5: Comparison of PET Parameter AUC for Predicting SCA up to the median follow-up (4.2 yrs)

Comparison			ΔAUC	95% CI		*p*-Value
Regional Normalized Uptake	vs	Regional Distribution Volume	0.00669	-0.0398	0.0532	0.7779
	vs	Global Scale Distribution Volume	0.1256	0.00234	0.2488	0.0458*
	vs	Global Scale Retention Index	0.1310	0.00934	0.2527	0.0348*
Regional Distribution Volume	vs	Global Scale Distribution Volume	0.1189	-0.0111	0.2488	0.0729
	vs	Global Scale Retention Index	0.1243	-0.00372	0.2524	0.0570
Global Scale Retention Index	vs	Global Scale Distribution Volume	-0.00545	-0.1139	0.1030	0.9216
Combined Model						
Regional Normalized Uptake	vs	+ Global Scale Retention	-0.00187	-0.0359	0.0322	0.9143
	vs	+ Global Scale Distribution Volume	-0.00156	0.0240	0.0209	0.8920

Table B.6. PAREPET Multivariate Model for Time to SCA

Parameter	Hazard Ratio	95% CI	*p*-Value
Per 1 Unit Increase			
Normalized Uptake Defect Score (%LV)	1.045	1.009,1.082	0.0135*
Creatinine (mg/dL)	1.386	1.064, 1.804	0.0153*
Indexed LVEDV (mL/m^2)	1.025	1.010, 1.040	0.0012*
No ACE/ARB	5.770	2.131, 15.623	0.0006*

Table B.7. Net Reclassification Improvement and Integrated Discrimination Improvement for Global PET Parameters to the PAREPET Multivariate Model.

PET Parameter	NRI	*p*-Value	Individuals with event		Individuals without event		IDI	*p*-Value	R^2 Difference
			Up	Down	Up	Down			
Global Scale RI	0.0092	0.8515	0	1	3	9	0.021	0.089	3.17
Global Scale DV	-0.024	0.6204	0	1	4	6	0.0079	0.2961	1.03

*Risk Thresholds for NRI set at 0.9%, 3.9% 11.7% for low, intermediate and high risk, respectively. These are the event rates that correspond to patients with 0 ,1 or >2 high risk parameters (in table 5).

B.5.0 Discussion

This study represents the first assessment of both regional and global HED PET imaging quantification methods for predicting cause-specific mortality from SCA. In this retrospective analysis of the PAREPET trial, two regional defect (NU and DV) and two global scale (RI and DV) parameters were investigated. Four major findings were derived this study. 1) For a given regional defect size, there is substantial heterogeneity in global scale quantification values. We further assessed whether there was any independent and additive prognostic value in these global scale parameters. 2) In a competing-risk analysis, both global scale and regional defect parameters were associated with SCA risk, but not non-sudden cardiac death and non-cardiac death. 3) Global scale parameters have inferior SCA risk discrimination as compared to regional parameters and yield no additive or independent prognostic value. 4) Overall, there were no differences between normalized uptake and DV regional defects with respect to SCA risk prediction. These results have widespread implications for future cardiac sympathetic HED analysis and imaging protocols. Taken together we demonstrate that SCA risk stratification is sufficiently predicted with HED activity defect scores and other more sophisticated quantification measures of DV, DV defect score, and RI may not be required for risk stratification.

Relationship Between Global and Regional HED Quantification Parameters

Our results corroborate previous findings of a strong correlation between global scale RI and DV parameters.[333] The poor correlation between global and regional parameters is novel and arises from substantial heterogeneity in global tracer uptake and retention. As a result, for a given regional defect size, there can be either global preservation or downregulation of tracer

uptake. Alterations in HED uptake can arise from both anatomical and functional properties of the cardiac SNS.[311] Indeed, it is not possible to differentiate the relative contribution of dysinnervation or neuronal stunning from denervation (true loss of sympathetic nerves) using a single tracer approach.[311] Preclinical studies indicate that sympathetic nerve function is particularly susceptible to ischemia, whereas denervation and a loss of sympathetic nerves arise in the infarct and peri-infarct risk region. In addition, sympathetic nerve sprouting occurs at the border between infarcted and normal tissue and this hyperinnervation carries significant arrhythmogenic risk[195]. All of these contribute to inhomogeneity in sympathetic innervation and the resulting substrate for lethal ventricular arrhythmias.[375,376] In contrast, global reductions in tracer uptake are affected by these regional alterations as well as elevated SNS tone, high systemic norephinephrine (NE) or a global reduction in Uptake1 (NE transporter).[305,311,377] Mechanistically, the distinction between neuronal stunning and denervation may be clinically important, as the former may be reversible and less likely to induce nerve sprouting as compared to denervated myocardium.

Competing Risks Analysis

A recent competing risk analysis of the PAREPET trial identified PET and clinical variables associated with cause-specific cardiac mortality. In this analysis, SCA was correlated with greater regional HED defect score, lack of ACE/ARC therapy, elevated BNP and larger LVEDV index. [378] The denervation volume was not associated with non-sudden cardiac death. [378] The present analysis extends these findings by comparing regional defect and global scale HED parameters in the competing risk analysis. This analysis enables the assessment of the independent components of cardiac mortality, namely SCA and NSCD. In our analysis both

regional and global HED parameters were associated with cause-specific mortality from SCA, but not NSCD or NCD. However, after adjusting for regional defect size, the global RI and DV were not associated with SCA, indicating that global scale parameters offer no independent prognostic information.

SCA Risk Discrimination

In the original PAREPET trial, global RI values were not statistically different in patients that had an arrhythmic event or ICD equivalent.[367] These results were corroborated in a separate HED imaging study of ischemic cardiomyopathy patients (EF<35%).[364] In the latter study, patients underwent an electrophysiological study (EPS) after ICD implantation. Patients with inducible ventricular arrhythmias had comparable global RI values (RI EPS positive 2.41 vs EPS negative 2.81, p=0.07). However, in both of these analysis regional and global HED quantification SCA risk prediction were not formally compared. We demonstrated that the global scale parameters have inferior SCA risk discrimination as compared to the regional normalized uptake defect score used in the PAREPET trial. The global scale parameters also offered no incremental discrimination as compared to the regional defect parameters alone. In a recent test-retest analysis, we demonstrated that HED regional defect parameters also have better reproducibility than global scale parameters.[333] Together, these results suggest regional defect parameters may be the optimal approach for routine clinical SCA risk prediction.

Comparison to Previous Studies

The present study is the first to directly compare the SCA discrimination of various HED PET imaging parameter. A number of studies have examined global cardiac sympathetic

innervation using the tracer ^{123}I-meta-iodobenzylguanidine (MIBG) to predict cardiovascular outcomes in heart failure patients but there also remains equipoise regarding the optimal parameters to predict cardiovascular risk. While global indices of tracer quantification including the heart-to-mediastinum ratio and MIBG washout rate have been studied, quantitative analysis of regional defect size with SPECT has been challenging.[365] The ADMIRE-HF trial enrolled 961 participants with an LVEF ≤ 35% and NYHA Class II/III symptoms and examined a composite outcome of heart failure progression, potentially life-threatening arrhythmias and cardiac death.[365] This large study included ischemic and nonischemic cardiomyopathy patients and found the H/M ratio (similar to the global scale RI in our study) to be predictive of the composite primary endpoint. Another study (n=116) examined the MIBG H/M ratio, washout rate, and defect score, and found only the defect score by SPECT was predictive of ventricular arrhythmias.[379] This is consistent with our analysis of quantifying regional defect score and the primary endpoint of SCA. While quantifying defect volume with SPECT is challenging, technical advances such as CZT cameras may allow this in the future.

Study Limitations

While appropriate ICD therapy for VF or VT at rates of 240 BPM and faster were used as a surrogate for aborted arrhythmic death, ventricular arrhythmias at slower rates were not considered as a primary end-point. Currently there is no consensus regarding which classification of ICD discharge represents the most appropriate definition. Available evidence suggests that using the definition of the present study, the rate of ICD discharge is approximately similar to the difference in mortality rate in clinical trials comparing patients receiving a primary prevention ICD with coronary artery disease vs. a medically treated population. [380] A broader analysis of

ventricular arrhythmias in the PAREPET trial demonstrated that the HED defect size did not predict slower ventricular arrhythmias and the prognostic impact of HED for VF and fast VT remained.[381]

Clinical Implications

The findings of this study may have implications for broader implementation of imaging myocardial sympathetic innervation. Current HED quantification methods have varying degrees of sophistication. Regional HED activity uptake quantification capabilities are likely available with most commercial PET software. In contrast, parametric imaging of distribution volume, which also requires kinetic modeling and long image acquisition times, may only be available to academic institutions that have access to compartmental analysis. A key finding of our study was that absolute global scale values such as RI and DV yield no independent or additive benefit clinical use in distinguishing SCA risk. This greatly simplifies future PET innervation imaging for predicting clinically meaningful outcomes and should facilitate translation into clinical care as fluorinated norepinephrine analogs become available to assess regional inhomogeneity in sympathetic innervation with PET.

Funding: This study was supported in part by research grants-in-aid (Heart and Stroke Foundation of Ontario T6426 and NA7158), by the IMAGE–Heart Failure team grant (Canadian Institutes of Health Research CIF99470), the National Heart and Blood Institute (HL-76252 and HL-130266) and the Advanced Imaging in Heart Failure grant (Ontario Research Fund ORF-RE-07-029). RSB holds a Tier 1 uOttawa Research Chair in Cardiovascular Research and is

supported by the Ottawa Heart Institute Vered Chair in Cardiology. JGEZ is an MD/PhD student supported in part by the Vanier Graduate Scholarship and the University of Ottawa.

Disclosures: RSB is a consultant for- and has received grant funding from GE Healthcare, Lantheus Medical Imaging and Jubilant DraxImage (JDI). RAdK is a consultant for JDI and receives royalties from Rubidium PET technologies licensed to JDI and to INVIA Medical Solutions. JMC is a consultant for Lantheus Medical Imaging. The other authors, JGEZ, JZW, and JAF have no disclosures.

Appendix C
Reliable Quantification of Myocardial Sympathetic Innervation and Regional Denervation using [11C]meta-Hydroxyephedrine PET

Wu and Zelt *et al.* 2019 Eur J Nucl Med Mol I
DOI: 10.1007/s00259-019-04629-5

Kai Yi Wu*, MD[a,b]; **Jason G.E. Zelt*, MSc[b,c]**; Tong Wang[d]; Vincent Dinculescu, MD[e]; Robert Miner, MSc[b]; Catherine Lapierre[b]; Nicole Kaps[b], Aaryn Lavallee[b], Jennifer M. Renaud, MSc[b]; James Thackeray, PhD[f], Lisa M. Mielniczuk, MSc, MD[b]; Shin-Yee Chen, MD[b]; Ian G. Burwash, MD[b]; Jean N. DaSilva PhD[g], Rob S.B. Beanlands, MD[b,c]; Robert A. deKemp, PhD[b]

*equal contribution by these authors

[a.]Department of Medicine, University of Alberta Faculty of Medicine & Dentistry, Edmonton, Alberta, Canada
[b.]National Cardiac PET Centre, Department of Medicine (Cardiology), University of Ottawa Heart Institute, Ottawa, Canada
[c]Department of Cellular and Molecular Medicine, Faculty of Medicine, University of Ottawa, Ottawa, Canada.
[d]Department of Physiology, University of Toronto, Toronto, Canada
[e]Department of Radiology, University of Calgary, Calgary, Alberta, Canada
[f]Department of Nuclear Medicine, Hannover Medical School, Hannover, Germany
[g]Centre de Recherche du Centre Hospitalier de l'Université de Montréal, Montréal, Québec, Canada

Address for Correspondence:
Dr. Robert deKemp
40 Ruskin Street, Ottawa
Ontario, Canada, K1Y 4W7
Email; RAdeKemp@ottawaheart.ca
Fax 613-696-7104; Phone 613-696-7347

Keywords: Sympathetic nervous system . [11C]meta-Hydroxyephedrine . Myocardial blood

flow

C.1.0 Abstract

Purpose: Cardiac sympathetic nervous system (SNS) dysfunction is associated with poor prognosis in chronic heart failure patients. This study characterized the reproducibility and repeatability of [^{11}C]meta-hydroxyephedrine (HED) positron emission tomography (PET) quantification of cardiac SNS innervation, regional denervation, and myocardial blood flow (MBF).

Methods: Dynamic HED PET-CT scans were performed 47±22 days apart in 20 patients with stable heart failure and reduced ejection fraction. Three observers, blinded to clinical data, used FlowQuant® to evaluate the test-retest repeatability, inter- and intra-observer reproducibility of HED tracer uptake and clearance rates to measure global (LV-mean) retention index (RI), volume of distribution (V_T) and MBF. Values were also compared with and without regional partial-volume correction. Regional denervation was quantified as %LV defect size of values <75% of the LV-maximum. Test-retest repeatability and observer reproducibility were evaluated using intra-class-correlation (ICC) and Bland-Altman coefficient-of-repeatability (NPC).

Results: Intra- and inter- observer correlations for both V_T and RI were excellent (ICC=0.93-0.99). Observer reproducibility (NPC=3-13%) was lower than test-retest repeatability (NPC=12-61%). Both regional (%LV defect size) and global (LV-mean) measures of sympathetic innervation were more repeatable using the simple RI model compared to V_T (NPC=12% vs. 19% and 30% vs 54%). Using either model, quantification of regional denervation (defect size) was consistently more reliable than the global LV-mean values of RI or V_T. Regional partial-volume correction degraded repeatability of both the global and regional V_T measures by 2-12%.

Test-retest repeatability of MBF estimation was relatively poor (NPC=30-61%) compared to the RI.

Conclusions Quantitative measures of global and regional SNS innervation were most repeatable using the simple RI method of analysis compared to the more complex V_T. Observer variability was significantly lower than the test-retest repeatability using a highly-automated analysis program. These results support the use of the simple RI method for reliable analysis of HED PET images in clinical research studies for future evaluation of new therapies and for risk stratification in patients with heart failure.

C.2.0 Introduction

Cardiac sympathetic nervous system (SNS) dysfunction is implicated in the pathogenesis of various cardiac disease states, such as congestive heart failure, arrhythmia, as well as ischemic and non-ischemic cardiomyopathy [382–384]. Non-invasive imaging techniques using radiotracers for positron emission tomography (PET) have been used to characterize cardiac SNS function. The majority of these tracers are norepinephrine (NE) analogs with a high specificity for NE transporters within cardiac sympathetic nerve terminals [385]. To date, [^{11}C]meta-hydroxyephedrine (HED) is the most commonly used PET tracer to evaluate SNS dysfunction in humans. HED can accurately evaluate regional neuronal defects and provide valuable insight on SNS pathologies as we and others have reviewed [382,386].

Sympathetic nerves appear to be more sensitive to ischemia than cardiomyocytes, with the zone of denervation often extending beyond that of reduced myocardial blood flow (MBF) [367,387,388]. This MBF-vs-innervation mismatch zone is thought to be an important substrate for inducible ventricular tachycardia [367,389]. Building on this knowledge, the recent PAREPET trial employed HED PET to demonstrate that ischemic HF patients with larger regions of denervated myocardium were more susceptible to sudden cardiac arrest SCA [367]. Recent evidence suggests that the kinetic properties of HED may also allow for the parallel estimation of MBF [390,391], expanding its repertoire from solely an innervation-based tracer to one that may also yield information on regional MBF-vs-innervation mismatch. Although a single scanning session to derive both parameters is appealing, further validation is needed in heart failure patients.

Characterization of HED kinetics has typically been performed with quantification of the tracer retention index (RI) and/or volume of distribution (V_T). There is some debate as to which of these two parameters better reflects cardiac sympathetic innervation [335,368–371]. Our group has

previously reported the test-retest repeatability of HED PET in preclinical animal models [392] and in humans using compartmental and graphical modeling [393]. However, studies in humans have not been performed to determine the most reliable methods for evaluation of global innervation and regional denervation with PET.

The purpose of this study was to evaluate cardiac sympathetic nervous system function, as evaluated using HED RI and V_T, as well as the potential to estimate MBF from the same scan. We sought to characterize the reliability of HED PET imaging by evaluating the test-retest repeatability and observer variability of the measured parameters in patients with stable heart failure and reduced ejection fraction (HFrEF) at baseline and followup 6-8 weeks later.

C.3.0 Materials and Methods

C.3.1 Study Design

Twenty-three patients with stable heart failure (NYHA class ≥ II) and reduced left ventricular ejection fraction (LVEF <40%) were enrolled as control subjects for a prospective study (NCT00756366) that evaluated the effects of continuous positive airway pressure (CPAP) on cardiac energetics in patients with heart failure and obstructive sleep apnea (OSA). These subjects had the same inclusion and exclusion criteria as the patients reported in the main study [331], but did not have OSA. Twenty of the 23 patients had complete baseline and followup HED PET imaging data available and were included in the current cohort. All subjects provided written informed consent to participate in the study, as approved by the institutional Human Research Ethics Board. Patient demographics were collected at baseline, and PET measurements were obtained at baseline and followup (47±22 days apart) including ECG, heart rate, and blood pressure monitored at regular intervals during the scan [394].

C.3.2 PET Imaging

As described previously, HED was synthesized from ^{11}C-methyl-iodide and metaraminol-free base using standard methods for high purity and specific activity for patient injection [331,395]. Patient scans were acquired in equal number on the ECAT-ART PET (Siemens/CTI, Knoxville, TN) or Discovery RX (DRX) PET-VCT (GEHC, Waukesha, WI) scanners. Transmission scans for photon attenuation correction were performed using x-ray computed tomography (DRX) or ^{137}Cs isotope sources (ART) [396]. 10-15 mCi (370-550 MBq) of HED was then injected (with 10 mL saline push) and a 40-minute dynamic PET acquisition (9×10 s; 3×30 s; 2×1 min; 7×5 min) was performed [331]. Dynamic images of tracer activity concentration (Bq/mL) were reconstructed with all physical corrections applied, using the PET vendor standard algorithms and 12 mm isotropic Hann filter [393].

Images were analyzed in randomized order; twice by observer 1 (V.D.), once by observer 2 (R.M.), and once by observer 3 (K.Y.W.) using FlowQuant® automated software (University of Ottawa Heart Institute, Ottawa, ON) [397]. Observers were blinded to the subject's clinical data and all previous analysis results.

C.3.3 Volume of Distribution

The kinetics of HED in the myocardium were analyzed using a reversible one-tissue compartment model (1TCM) which has been previously shown to provide more robust estimates of V_T than the reversible two-tissue-compartment model (2TCM) [371]. While the 2TCM is more physiologically complete than the 1TCM, it requires estimation of 2 additional rate constants reflecting neuronal uptake (k_3) and clearance (k_4) which may not be reliable in practice. Instead, the macro-parameter $V_T = K_1/k_2 \times (1 + k_3/k_4)$ is commonly used as a more reliable index of receptor

binding or transporter function. When the value of k_3 is high (enough) relative to K_1, then the tracer kinetics, i.e. the shape of the tissue time-activity curves, may still be accurately described by a simpler 1TCM, where the 'apparent' rate constants K_1' and k_2' are estimated to characterize the effects of tracer exchange between plasma and the combined tissue compartments. V_T in myocardial tissue is defined as the ratio of tracer concentrations in the tissue to arterial plasma under conditions of equilibrium. However in practice, equilibrium between plasma and tissue is rarely achieved during PET imaging, but can be estimated using the simplified 1TCM rate constants as [393]:

$$V_T \sim \frac{K_1'}{k_2'} \quad (1)$$

V_T (mL/g) is an index of tracer binding affinity (i.e. B_{max}/K_d), where B_{max} is the density of NE uptake transporter and $1/K_d$ is the affinity of HED for the NE reuptake transporter [334]. K_1' is the apparent tracer uptake rate which is (for all tracers) a product of the unidirectional plasma-to-tissue extraction fraction E(MBF) × MBF (mL/min/g), and k_2' is the apparent washout rate (1/min). Furthermore, the values of K_1' from the ITCM are monotonically related to the values of K_1 from the 2TCM and can therefore be used to estimate MBF using the appropriate extraction function. LV-mean values of V_T were estimated using the simplified 1TCM and validated against the 2TCM values to confirm accuracy. *By definition, V_T should be independent of tissue perfusion.* While K_1' and k_2' are both dependent on tissue perfusion, their ratio used to calculate V_T has been confirmed in previous receptor binding studies (in the brain) to be independent of changes in perfusion up to 2-fold [398–400].

Corrections for red blood cell binding and radiolabeled metabolites in the blood were performed by calculating the parent fraction in plasma as a function of time (previously defined in heart failure patients) to estimate the unchanged tracer available for exchange with the myocardial

tissue [335,336]. Partial volume correction (PVC) was integrated into the 1TCM to account for underestimation of myocardial tissue concentrations caused by blurring of the acquired PET images. The PVC model was employed according to the following equation, as reported previously by our lab and others [371,393,397]:

$$C_p(t) = RC \times C_m(t) + FBV \times C_p(t) \quad (2)$$

$C_p(t)$ is the concentration of unchanged tracer in the arterial plasma, $C_m(t)$ is the concentration of tracer in the myocardial tissue. The fractional blood volume (FBV) represents the component of blood signal measured in the myocardium region of interest (ROI). The PVC factor RC (Recovery Coefficient) accounts for the underestimation of tracer activity in the myocardium (affecting RI, V_T and K_1) due to the blurring effects of wall-motion and finite spatial resolution of the PET scanner. Kinetic modeling parameters were partial-volume-corrected using the RC value as [393]:

$$K'_{1\,(RC)} = \frac{K'_1}{RC} \quad (3)$$

and

$$V_{T\,(RC)} = \frac{V_T}{RC} \quad (4)$$

Values of K_1' and V_T were computed using both global (RC=1) and regional (RC=1−FBV) partial-volume corrections to enable comparison with previously published results [371,393].

C.3.4 Retention Index

Net HED uptake (or tracer deposition) at the scan end-time was also estimated using the retention index (RI) as [331]:

$$RI_{(RC)} = \frac{C_m(T_R)}{\int_0^{T_R} C_p(t)dt} \times 100\% \quad (5)$$

where C_m is the activity in myocardial tissue, C_p is the unchanged tracer activity in plasma, and T_R is the function evaluation time (40 min). Since the FBV is not estimated using the retention model, only global partial-volume correction (RC=1) was applied.

C.3.5 Myocardial Blood Flow

The HED uptake rate K_1' was used to estimate myocardial blood flow (MBF) according to the standard relationship describing the unidirectional extraction of tracer from plasma to tissue:

$$K'_1 = (1 - e^{-PS/MBF}) \times MBF \quad (6)$$

where the permeability × surface-area (PS) product for HED was estimated using MBF-standard measurements in the same patients (Supplement Figure C.S1).

C.3.6 Global Values and Regional Defects

The values of V_T and RI were estimated in 460 polar-map sectors (Figure C.1), and the LV-mean values were computed as indices of global SNS innervation. The extent of regional denervation was analyzed using similar methods as reported previously in the PAREPET trial [367]. Briefly, for each measured parameter a regional defect score was calculated as the fraction of polar-map sectors <75% of the LV-maximum value and expressed as percentage of the total area (%LV). A homogenous 'normal' polar-map with all values ≥75% of the maximum would have a defect score of zero. The same methods were used to quantify global perfusion and corresponding regional defects using the estimated parameters K_1 and MBF.

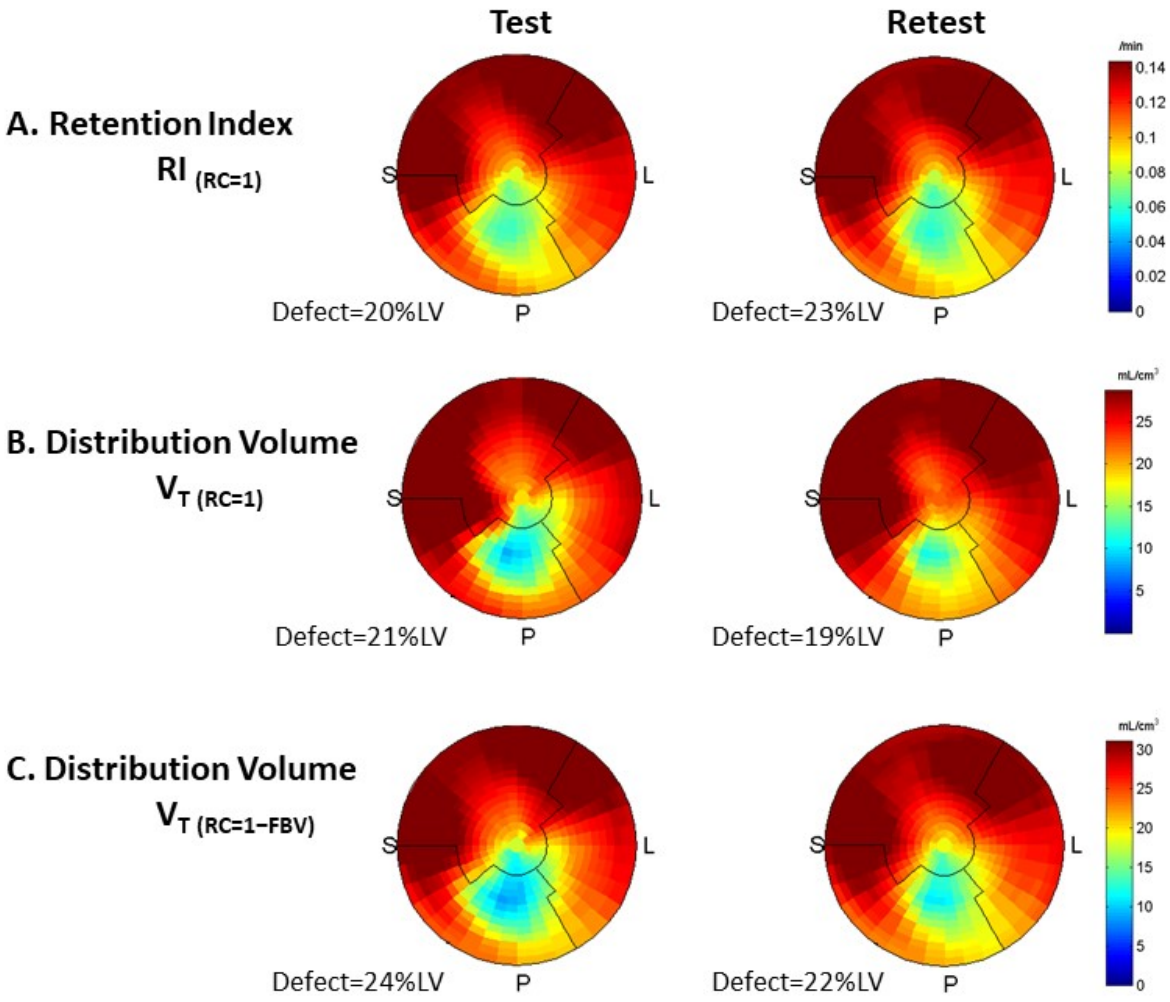

Figure C.1: Representative test-re-test polar maps. PET images of global sympathetic innervation (LV-mean) and regional denervation (defect %LV) shown as left ventricle polar-maps of [^{11}C]HED tracer retention index (**a**) and distribution volume with global (**b**) and regional (**c**) partial-volume corrections. S = interventricular septum, P = posterior wall, L = lateral wall, RC = recovery coefficient, FBV = fractional blood volume

C.3.7 Echocardiography

Echocardiography methodology for this study was described previously [394]. LVEF was derived from the modified Simpson's rule using the biplane method [401]. Forward stroke-volume (SV) was calculated from the velocity-time-integral of the pulsed Doppler left ventricle outflow tract (LVOT) velocity signal and the LVOT diameter [402]. Stroke volume index (SVi) was computed by dividing SV by the body surface area [331].

C.3.8 Statistical Analysis

Patient hemodynamics and characteristics were compared using the Wilcoxon Signed Rank test. LV-mean (global) values and regional defect scores of $RI_{(RC=1)}$, $V_{T\,(RC=1\text{-}FBV)}$, $V_{T\,(RC=1)}$, $K_{1\,(RC=1\text{-}FBV)}$, $K_{1\,(RC=1)}$, and $MBF_{(RC=1\text{-}FBV)}$ were compiled. Intra-observer, inter-observer, and test-retest mean effects were evaluated using two-way repeated measures ANOVA. Absolute-agreement intra-class correlation coefficient (ICC) with two-way mixed effects model and Bland-Altman analysis were employed to evaluate the intra-observer, inter-observer, and test-retest reproducibility and repeatability [403,404]. Intra-observer reproducibility was evaluated by comparing observer 1A vs 1B values. Inter-observer reproducibility was evaluated between observers 1A vs 2, 1A vs 3, and observer 2 vs 3, and then pooled to obtain final ICC and 95% limits-of-agreement. ICC values were categorized as: ICC>0.90 excellent, 0.75-0.90 very good, 0.40-0.75 good, and <0.4 poor [403]. The limits-of-agreement of repeated measures were estimated using: i) median difference ± non-parametric repeatability coefficient (NPC=1.45×IQR) to account for the variable effect of outliers, and ii) mean difference ± coefficient-of-repeatability ($RPC=1.96\times SD_{difference}$). The NPC was also reported as it is a more robust measure of repeatability for non-gaussian distributed data [405]. The 95% confidence intervals on the limits-of-agreement were calculated as

$\sqrt{(3/N)} \times SD_{difference}(t_{95\%,\ n-1})$, where N is the number of pairs being analyzed [406]. The variance between the intra- and inter-observer differences, and between test-retest and observer differences was evaluated using the non-parametric Levene's test [407]. A 2-tailed p-value<0.05 was considered statistically significant for all tests. Statistical analyses were performed using Excel 2016 (Microsoft) and SPSS 20.0 (IBM).

C.4.0 Results

C.4.1 Patient Characteristics

Baseline characteristics are listed in Table C.1. 70% of the patients were male with a mean age of 67±10 years and BMI of 27±5 kg/m^2. Most patients were taking one or more cardiac medications. There was no change in heart failure status (NYHA class or symptoms) between imaging visits. There were no significant changes in resting heart rate (65±17 vs 63±11 bpm) or systolic blood pressure (113±23 vs 110±22 mmHg) between baseline and followup PET scans (Table C.2). Echocardiography parameters were stable as well (Table C.2).

Table C.1. Patient Characteristics at Baseline (n=20)

Description	Value
Age (years)	67.4 ± 9.5
Body Mass Index	27.2 ± 4.8
Males	14 (70%)
Smoking Status	
Current	2 (10%)
Former	10 (50%)
Never	8 (40%)
Diabetes Mellitus	6 (30%)
Hypertension	14 (70%)
Dyslipidemia	13 (65%)
Family History of Heart Disease	9 (45%)
Medications	
ACE Inhibitor	18 (90%)
Beta Blocker	8 (40%)
Digoxin	7 (35%)
Diuretics	12 (60%)
Statin	15 (75%)
Acetylsalicylic acid	15 (75%)
Plavix	6 (30%)
Coumadin	5 (25%)
New York Heart Association Class	
Class II	17 (85%)
Class III	3 (15%)
Congestive Heart Failure	20 (100%)
Left Ventricular Ejection Fraction	31.2 ± 6.2%
Ischemic Cardiomyopathy	
Previous Revascularization	14 (70%)
Previous Myocardial Infarction	13 (65%)

Table C.2. Hemodynamic Parameters at baseline and follow-up (n=20)

Parameter	Baseline	Follow-up	p-value*
Left Ventricular outflow tract (cm)	2.1 ± 0.3	2.1 ± 0.3	0.61
Left ventricular outflow tract velocity x time integral (cm)	163 ± 3.1	16.5 ± 2.9	0.48
Stroke Volume (mL/beat)	55.1 ± 16.7	57.4 ± 19.5	0.97
Left ventricular ejection fraction (%/beat)	33.2 ± 6.4	35.2 ± 9.5	0.07
Heart rate (bpm)	64.5 ± 17.0	63.2 ± 11.2	0.50
Systolic blood pressure (mmHg)	113.2 ± 23.7	110.1 ± 21.7	0.48
Diastolic blood pressure (mmHg)	65.5 ± 12.2	63.7 ± 9.3	0.32
Rate-pressure product (heart rate x systolic blood pressure) (beats/min x mmHg) thousands	6.8 ± 3.2	7.0 ± 1.8	0.65

*Significance assessed by the Wilcoxon signed-rank test.

C.4.2 1TCM and 2TCM values of V_T and K_1

The estimated values of V_T using the 1TCM were validated against the 2TCM values in the same patients (Figure C.2A) with a median slope=0.96 close to unity (p=0.29 vs 1.0). The variability in 2TCM values was much higher than the corresponding 1TCM values (40% vs 23%, p<0.001) with 6 of 40 patients having regional SD>500% due to instability of the 2TCM (Supplement Figure C.S2A). In contrast, the regional variability of V_T values from the 1TCM all had SD<50%. The 1TCM values of K_1' were monotonically related to the 2TCM K_1 values (Figure C.2B) with a median slope = 0.5 (p<0.001 vs 1.0). There were no outliers in the 1TCM K_1' values compared to 3 outliers using the 2TCM, again due to model instability. As with V_T, the variability of 2TCM K_1 was significantly higher than 1TCM K_1' (SD = 71% vs 20%, p<0.001) as shown in Supplement Figure C.S2B, supporting use of the 1TCM parameters for all subsequent analyses.

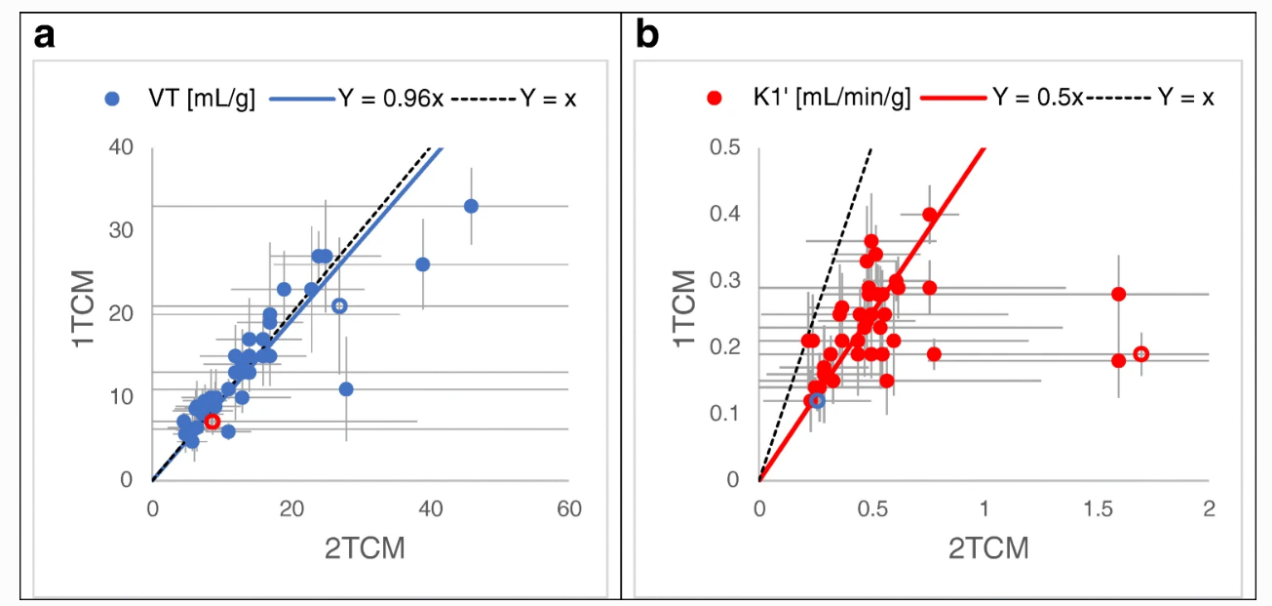

Figure C.2. Comparison of 1TCM vs. 2TCM estimates of V_T (a) and K_1 (b). V_T estimates are close to the line-of-identity (dashed line). Error bars are standard deviation (SD) of the regional polar-map values, which are significantly higher for both parameters using the 2TCM vs. 1TCM ($p < 0.001$). Open circles represent outlier values illustrated in Supplemental Figure S2

C.4.3 Repeatability and Reproducibility Measurements

The HED PET parameter values at baseline and followup are shown in Table C.3. There was no significant bias between observers ($p>0.13$) or test-retest measurements ($p>0.06$) for any parameter values at baseline or followup (two-way repeated measures ANOVA). The reliability statistics are shown in Table C.4, with the test-retest and observer results illustrated in Figures C.3 and C.4 respectively. All intra- and inter-observer correlations were excellent (ICC≥0.93) and observer reproducibility values were significantly lower than the corresponding test-retest values (NPC=3-13% vs. 12-61%, $p<0.001$), as shown in Figure C.5. Repeatability of the global LV-mean values tended to improve using the RI vs V_T model with global PVC (NPC=30% vs. 54%; $p=0.11$) and were significantly improved with regional PVC (NPC=30% vs. 60%; $p<0.03$). The regional defect sizes (%LV) were consistently less variable using the RI model compared to V_T with global or regional PVC (NPC=12% vs 19% or 25%; both $p<0.01$).

There were no changes in the mean baseline vs followup MBF values, as expected in this clinically stable cohort. Similar to the results observed for measures of sympathetic innervation, repeatability of the regional MBF defect size was significantly better than the LV-mean values (NPC=30% vs. 61%, $p<0.001$) because it only depends on the relative polar-map uniformity and is not affected by variability in the absolute scale of the measurements (Table C.4). The values of K_1' defect size (before partial-volume or extraction corrections) were more repeatable as an index of MBF uniformity (NPC=13% vs. 30%, $p<0.001$).

Table C.3 Measures of global sympathetic innervation and regional denervation (n=20) using [11C]HED PET

Parameters[a]	Observer 1A		Observer 1B		Observer 2		Observer 3	
	Baseline	**Follow-up**	**Baseline**	**Follow-up**	**Baseline**	**Follow-up**	**Baseline**	**Follow-up**
Global values (LV-mean ± SD)								
RI $_{(RC = 1)}$ (%/min)	6.9 ± 2.3	7.5 ± 3.1	6.9 ± 2.3	7.5 ± 3.0	7.1 ± 2.5	7.6 ± 3.1	7.0 ± 2.4	7.6 ± 3.1
$V_{T\,(RC = 1)}$ (mL/g)	11 ± 5	13 ± 8	11 ± 5	13 ± 8	11 ± 5	13 ± 8	11 ± 6	14 ± 8
$V_{T\,(RC = 1 - FBV)}$ (mL/g)	19 ± 8	21 ± 11	19 ± 9	20 ± 11	19 ± 9	21 ± 11	19 ± 8	20 ± 9
$K_{1\,(RC = 1)}$ (mL/g/min)	0.21 ± 0.06	0.22 ± 0.07	0.22 ± 0.06	0.22 ± 0.07	0.22 ± 0.06	0.23 ± 0.07	0.21 ± 0.06	0.22 ± 0.07
$K_{1\,(RC = 1 - FBV)}$ (mL/g/min)	0.37 ± 0.10	0.35 ± 0.11	0.37 ± 0.11	0.34 ± 0.10	0.37 ± 0.10	0.35 ± 0.10	0.36 ± 0.10	0.34 ± 0.10
$MBF_{(RC = 1 - FBV)}$ (mL/g/min)	0.74 ± 0.37	0.69 ± 0.28	0.74 ± 0.35	0.70 ± 0.28	0.74 ± 0.35	0.71 ± 0.29	0.74 ± 0.36	0.68 ± 0.29
Regional defects (%LV ± SD)								
RI $_{(RC = 1)}$ (%/min)	25 ± 18	23 ± 17	25 ± 17	25 ± 19	26 ± 18	24 ± 18	25 ± 18	24 ± 18
$V_{T\,(RC = 1)}$ (mL/g)	36 ± 17	32 ± 16	37 ± 16	35 ± 17	37 ± 18	35 ± 17	37 ± 18	34 ± 18
$V_{T\,(RC = 1 - FBV)}$ (mL/g)	29 ± 17	28 ± 19	30 ± 18	31 ± 18	32 ± 20	29 ± 17	30 ± 19	29 ± 16
$K_{1\,(RC = 1)}$ (mL/g/min)	27 ± 17	26 ± 17	28 ± 18	27 ± 18	27 ± 17	25 ± 19	28 ± 19	25 ± 19
$K_{1\,(RC = 1 - FBV)}$ (mL/g/min)	27 ± 19	27 ± 15	27 ± 19	28 ± 17	27 ± 19	28 ± 16	28 ± 19	27 ± 16
$MBF_{(RC = 1 - FBV)}$ (mL/g/min)	38 ± 17	38 ± 18	40 ± 17	38 ± 18	38 ± 17	38 ± 18	38 ± 18	39 ± 18

LV, left ventricle; *RI*, retention index; V_T, volume of distribution; K_1, tracer uptake rate; *RC*, recovery coefficient; *MBF*, myocardial blood flow

[a]No significant observer ($p > 0.13$) or baseline-follow-up ($p > 0.06$) effects using two-way repeated-measures ANOVA

Table C.4. Observer and test-retest correlations (ICC) and relative differences (mean and median) of [11C]HED PET measurements

Parameters[a]	Intra-observer (n = 40 pairs)			Inter-observer (n = 120 pairs)			Test-retest (n = 80 pairs)		
	ICC	Mean ± RPC	Median ± NPC	ICC	Mean ± RPC	Median ± NPC	ICC	Mean ± RPC	Median ± NPC
Global values (LV-mean)									
RI $_{(RC = 1)}$ (%/min)	0.99	− 0.2 ± 9%	− 0.9 ± 4%	0.97	1.7 ± 17%	0.0 ± 6%	0.75	6.3 ± 41%	1.0 ± 30%
$V_{T\,(RC = 1)}$ (mL/g)	0.99	− 0.1 ± 18%	− 0.5 ± 7%	0.99	0.0 ± 21%	− 0.3 ± 10%	0.67	14 ± 59%	4.3 ± 54%
$V_{T\,(RC = 1 - FBV)}$ (mL/g)	0.98	− 0.7 ± 19%	− 1.1 ± 13%	0.96	− 0.4 ± 23%	− 0.5 ± 13%	0.68	5.1 ± 65%	− 6.2 ± 60%
$K_{1\,(RC = 1)}$ (mL/g/min)	0.98	1.0 ± 7%	0.0 ± 5%	0.98	− 0.3 ± 6%	0.0 ± 3%	0.82	2.8 ± 35%	6.4 ± 37%
$K_{1\,(RC = 1 - FBV)}$ (mL/g/min)	0.94	− 0.2 ± 19%	− 0.1 ± 9%	0.93	1.2 ± 19%	0.3 ± 9%	0.71	− 5.6 ± 43%	− 4.5 ± 39%
MBF$_{(RC = 1 - FBV)}$ (mL/g/min)	0.98	1.5 ± 20%	0.4 ± 9%	0.98	3.2 ± 23%	1.1 ± 10%	0.80	− 4.5 ± 59%	− 8.6 ± 61%
Regional defects (%LV)									
RI $_{(RC = 1)}$ (%/min)	0.98	1.3 ± 7%	0.1 ± 3%	0.98	0.6 ± 7%	0.0 ± 3%	0.89	− 1.3 ± 16%	− 0.4 ± 12%
$V_{T\,(RC = 1)}$ (mL/g)	0.94	1.6 ± 11%	0.2 ± 5%	0.94	1.2 ± 12%	0.4 ± 9%	0.85	− 1.0 ± 19%	− 0.8 ± 19%
$V_{T\,(RC = 1 - FBV)}$ (mL/g)	0.93	2.1 ± 11%	1.5 ± 6%	0.94	1.2 ± 12%	0.0 ± 5%	0.58	− 2.9 ± 30%	− 3.9 ± 25%
$K_{1\,(RC = 1)}$ (mL/g/min)	0.96	0.4 ± 10%	0.3 ± 6%	0.95	0.6 ± 2%	0.0 ± 4%	0.86	− 1.7 ± 18%	− 0.8 ± 13%
$K_{1\,(RC = 1 - FBV)}$ (mL/g/min)	0.98	0.5 ± 11%	0.0 ± 5%	0.99	1.6 ± 14%	0.5 ± 7%	0.48	0.3 ± 34%	− 3.4 ± 25%
MBF$_{(RC = 1 - FBV)}$ (mL/g/min)	0.97	1.1 ± 9%	0.5 ± 4%	0.97	0.0 ± 8%	0.0 ± 4%	0.54	0.1 ± 33%	2.5 ± 30%

LV, left ventricle; *RI*, retention index; V_T, volume of distribution; K_1, tracer uptake rate; *RC*, recovery coefficient; *MBF*, myocardial blood flow[a]No significant bias vs. zero. Lowest test-retest repeatability values are shown in bold font

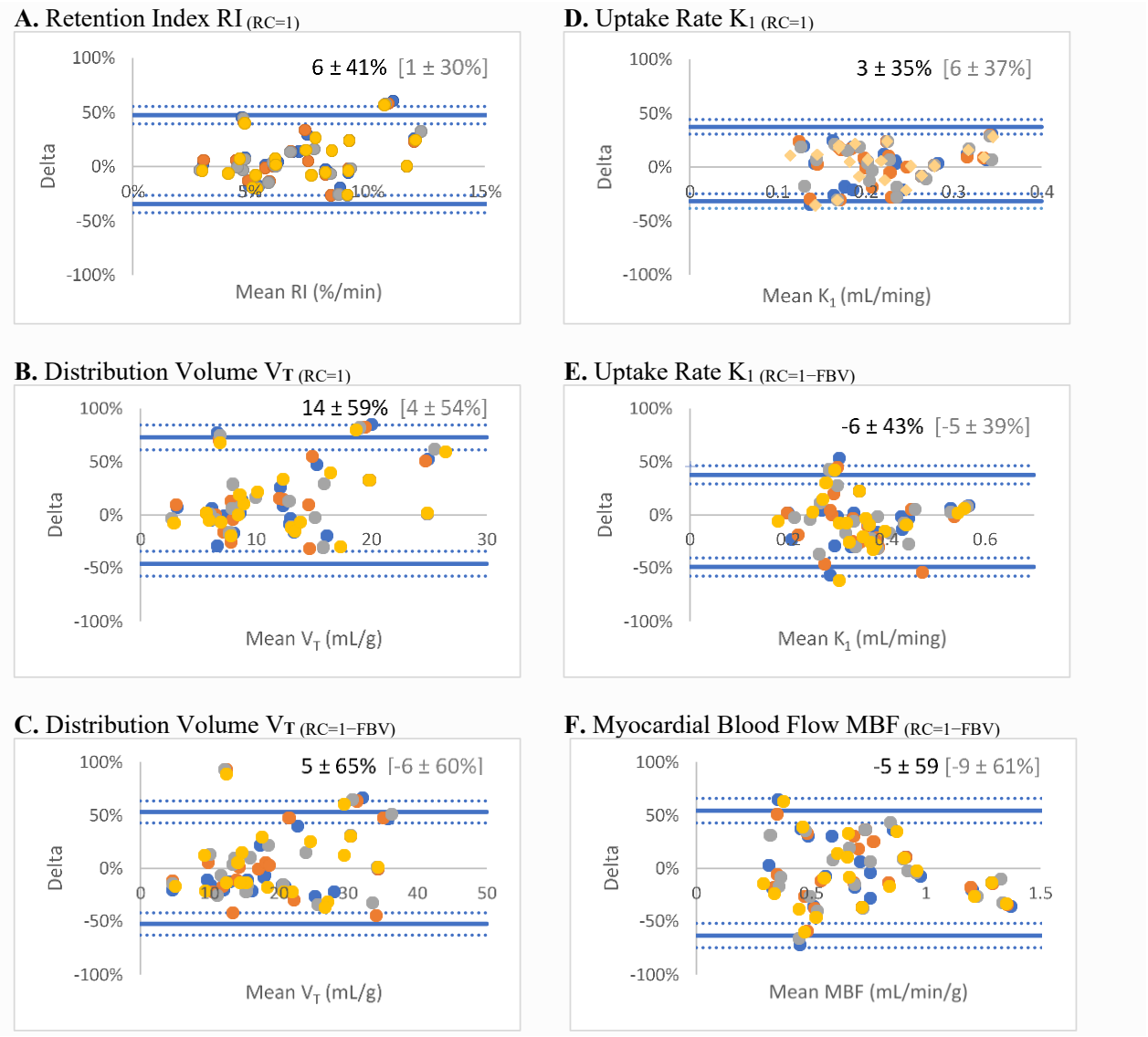

Figure C.3. Test-retest repeatability of [^{11}C]HED PET measurements ($N = 20$ scans × 4 observations) **of global (LV-mean) values** of sympathetic nerve function (**a**–**c**) and blood flow (**d**–**f**). Ninety-five percent limits-of-agreement (blue lines) and confidence intervals (dotted lines) are shown at delta = mean ± 1.96 × SD (median ± 1.45 × IQR). RC, recovery coefficient; FBV, fractional blood volume. **a** Retention index RI (RC = 1). **b** Distribution volume V_T (RC = 1). **c** Distribution volume V_T (RC = 1 − FBV). **d** Uptake rate K_1 (RC = 1). **e** Uptake rate K_1 (RC = 1 − FBV). **f** Myocardial blood flow MBF (RC = 1 − FBV)

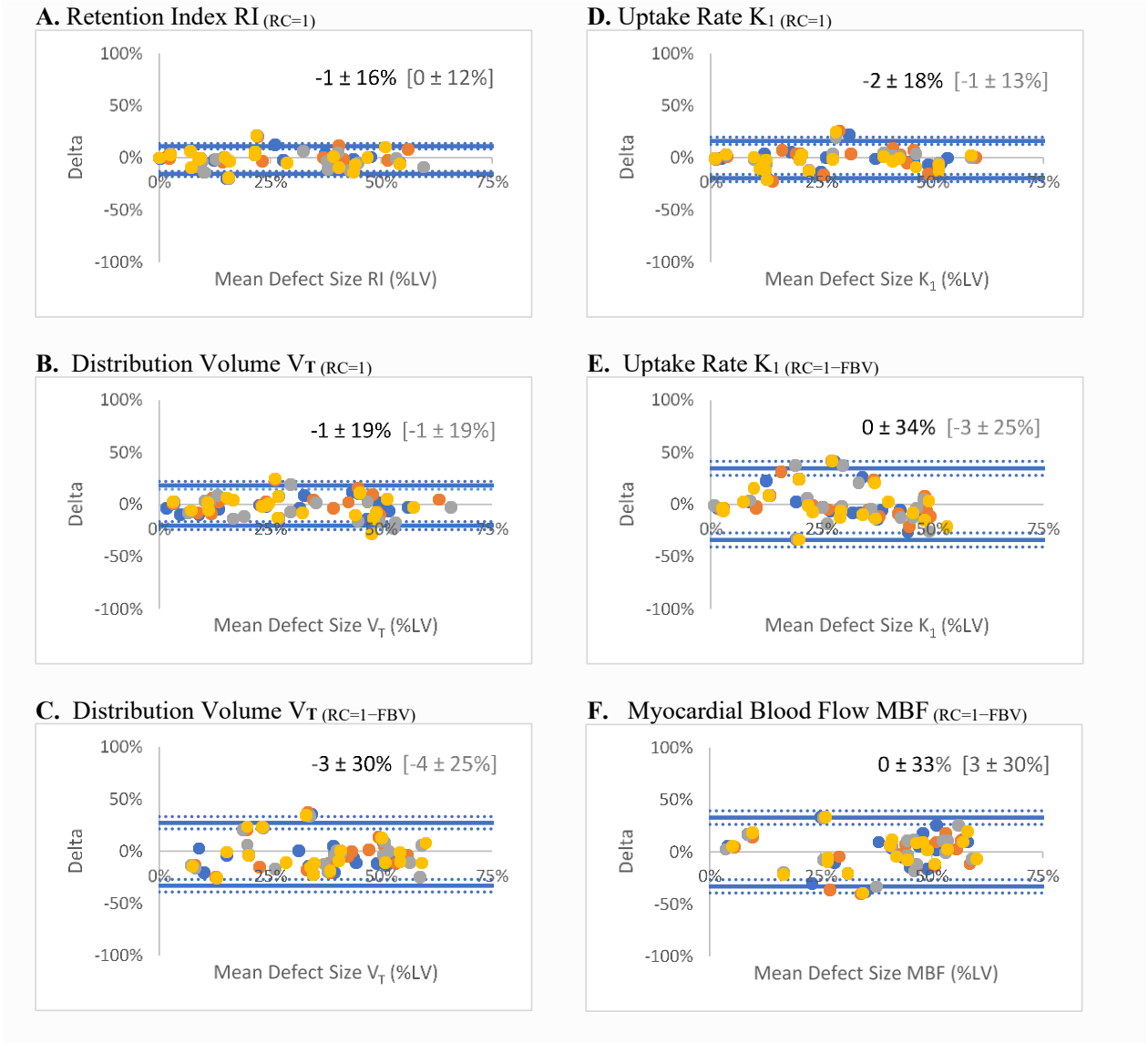

Figure C.4. Test-retest repeatability of [^{11}C]HED PET measurements ($N = 20$ scans × 4 observations) **of regional (%LV) defect sizes** in sympathetic nerve function (**a**–**c**) and blood flow (**d**–**f**). Ninety-five percent limits-of-agreement (blue lines) and confidence intervals (dotted lines) are shown at delta = mean ± 1.96 × SD (median ± 1.45 × IQR). RC, recovery coefficient; FBV, fractional blood volume; LV, left ventricle. **a** Retention index RI $_{(RC = 1)}$. **b** Distribution volume V_T $_{(RC = 1)}$. **c** Distribution volume V_T $_{(RC = 1 - FBV)}$. **d** Uptake rate K_1 $_{(RC = 1)}$. **e** Uptake rate K_1 $_{(RC = 1 - FBV)}$. **f** Myocardial blood flow MBF $_{(RC = 1 - FBV)}$

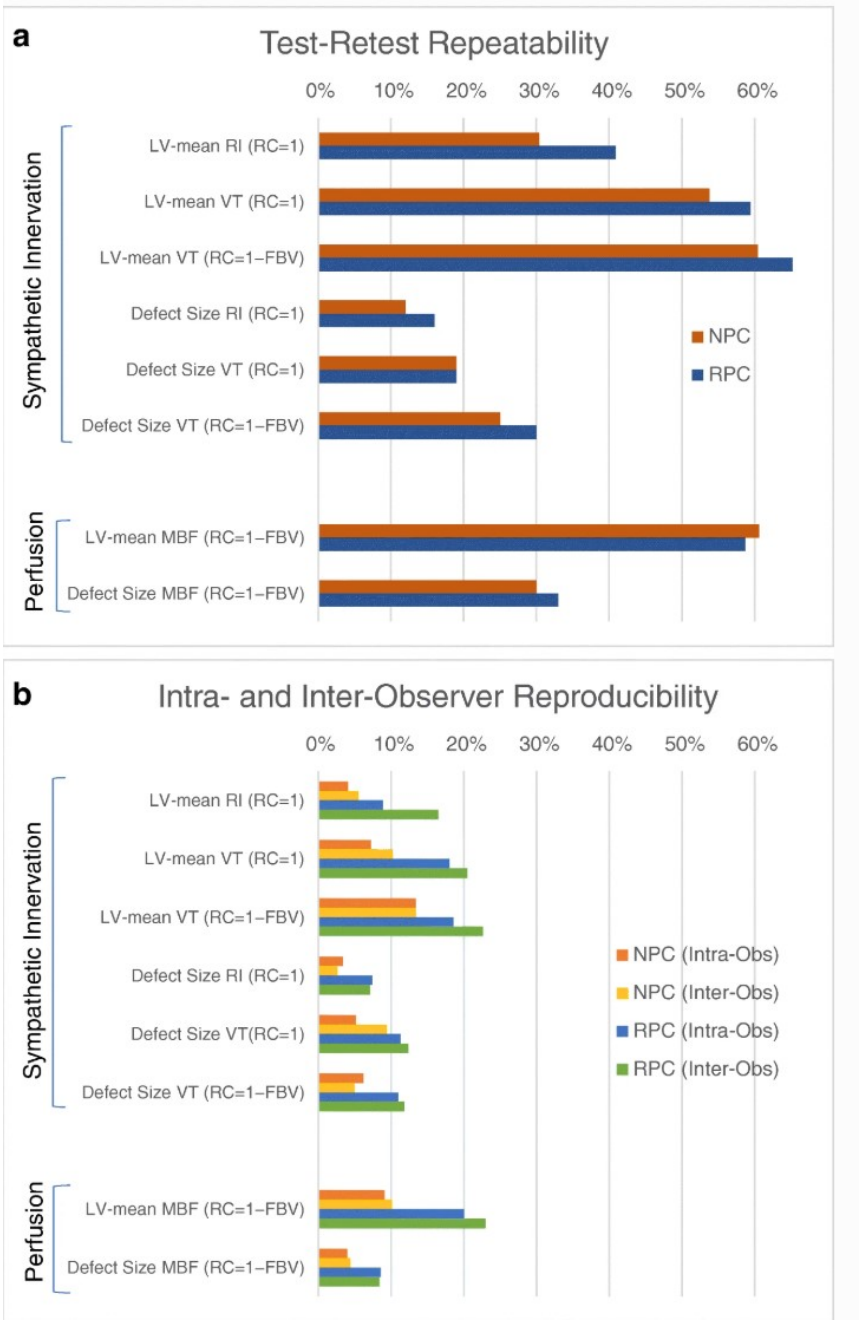

Figure C.5. Test-retest (a) and observer (b) variability of global (LV-mean) values and regional (%LV) defect size measurements of sympathetic innervation and myocardial blood flow (MBF). RPC, coefficient of repeatability; NPC, nonparametric coefficient of repeatability; LV, left ventricle; RI, retention index; V_T, volume of distribution; K_1, tracer uptake rate; RC, recovery coefficient; FBV, fractional blood volume

C.5.0 Discussion

To our knowledge, this is the first study to characterize the test-retest repeatability and operator reproducibility of HED PET imaging for quantitative assessment of global and regional cardiac SNS innervation in patients with impaired ventricular systolic function. This study builds on our previous work that compared the performance of graphical models against the established one-tissue-compartment model for the evaluation of HED volume of distribution [393]. Several novel findings were derived from this study: (1) The dominant source of variability in serial measurements is the physiological day-to-day variation. This information will be critical for sample size calculations when designing future clinical trials to evaluate SNS innervation in similar HFrEF populations. (2) HED PET analysis can be performed reliably by different operators using a highly-automated program. (3) Measures of global innervation and regional denervation of the LV were more repeatable using the simple retention index compared to the volume of distribution obtained by kinetic modeling. (4) Regional denervation defect scores were more repeatable than the global measures of innervation. (5) Regional denervation (defect size) estimated without partial-volume correction (RC=1) as in the PAREPET trial [367], had good test-retest repeatability for both distribution volume and retention index parameters (ICC=0.85 and 0.89; NPC=12 and 19%). (6) Repeatability of MBF using HED PET was relatively poor compared to the uptake rate K1' (NPC=60% vs 37%) and compared to the Retention Index of SNS innervation (NPC=30%).

C.5.1 Test-Retest Repeatability

This is the first study to evaluate the reliability of longitudinal HED PET measurements in humans. The test-retest variation (methodological + physiological variation) for all PET

parameters (NPC=12-61%) were significantly higher than the intra- and inter-observer (NPC=3-13%) reproducibility (methodological variation). This variation was unlikely due to changes in patients' clinical status, as the measured hemodynamic and echocardiographic parameters remained stable between imaging visits [331,394]. Although not measured in the present study, circulating catecholamines have been shown to decrease HED myocardial retention in preclinical models [392]. Plasma norepinephrine is chronically elevated in patients with HF, and the acute increases in circulating levels are well characterized in response to both physiological and psychological stressors. The test-retest variation observed is not likely due to changes in physiologic stressors given the stable clinical status; however, any change in psychological stress may increase systemic norepinephrine and contribute as a source of variation. Changes in medications were also an unlikely source of variation given that: 1) there were no changes in medications between visits, 2) patients were instructed to take medications at the same time of day, and 3) medications known to inhibit NET function (e.g. Tricyclic anti-depressants or cocaine) were listed as exclusion criteria for study enrollment. Taken together, these results suggest that the variation likely reflects either the normal day-to-day or month-to-month changes in basal sympathetic tone (i.e. physiological variation) in this HFrEF population, or other methodological variations such as patient position during scans.

These data will be critical for power calculations to estimate sample size requirements for future research studies using serial HED PET imaging in similar heart failure populations. For example, the RPC values for regional denervation (%LV) using RI and V_T were 16% and 19% (Table 4), corresponding to measured standard deviations (SD) of 8% and 9.5%, respectively. If using the RI model, then N=7 subjects would be needed to detect a clinically relevant baseline-to-followup improvement of Δ=10%LV, whereas N=10-24 subjects would be needed to detect the

same difference using V_T (with $\alpha_1 = \beta = 0.05$). Additional sample size estimates can be found in Table 5, demonstrating that more subjects are required to measure significant changes in global values compared to regional defects, for all reported parameters.

Bateman et al. recently published on the test-retest reproducibility of the Heart-to-Mediastinum (H/M) ratio derived from [^{123}I]meta-iodobenzylguanidine (mIBG) planar scintigraphy in patients with heart failure (LVEF≤35%) [408]. They concluded that the H/M ratio was a highly consistent and reproducible measurement of innervation in patients with stable heart failure. The study reported the limits-of-agreement of ±13% for the mIBG H/M ratio, which is much lower than the ±30% limits-of-agreement for the global values of HED RI in our study (Table 4). However, when we used HED RI to assess regional denervation (%LV defect size), the limits-of-agreement were ±12%, similar to the mIBG H/M ratio. It is important to note that the H/M ratio is a relative-scale index of global LV-mean innervation, as regional analysis has not been explored with mIBG due to the poor image quality of ^{123}I-based single-photon emission computed tomography images compared to PET. Although a similar relative-scale index for HED PET (e.g. Heart-to-Lung or Heart-to-Liver ratio) has not been explored for global innervation, we would expect one to yield similar or better reproducibility than demonstrated in this study.

C.5.2 Observer Reproducibility

Intra- and inter-observer comparisons of global innervation and regional sympathetic denervation did not reveal any significant differences between repeated measurements by the same or different operators (ICC≥0.93 and NPC=3-13%). The use of this highly automated program required minimal operator interaction, producing very similar results between and within operators, even when used by novice operators without extensive training.

C.5.3 Comparison of RI and V_T

To date, analysis of HED data in clinical research has been performed predominantly using the RI method. The RI model has been criticized by some as a relatively simple semi-quantitative measure of sympathetic innervation. It may be sensitive to intravascular activity and variable partial-volume (blood and tissue spill-over) effects of cardiac motion and PET scanner resolution, potentially complicating its absolute accuracy and reproducibility between centers [371]. Relatively few studies have reported quantitative results using compartment modeling, however our measurements of V_T were highly correlated with the RI. As an index of sympathetic innervation, the simpler RI appears to be more repeatable than the more physiologically relevant but also more mathematically complex measurement of V_T. The interpretation of HED PET measurements as reflecting sympathetic innervation is complicated due to the fact that the tracer uptake may be, at least partially, MBF-limited. Harms et al. proposed to ameliorate some of these concerns by demonstrating that HED kinetics could be assessed reliably with 1TCM and 2TCM models in validation studies [371]. These compartmental model analysis methods can yield separate parameters reflecting innervation and blood flow, providing the potential to separate these two effects by studying MBF together with V_T. Similar methods have been used and validated in the past with dynamic [^{11}C]acetate PET for example, to measure MBF using a simplified 1TCM (from K1') as well as a metabolic parameter - myocardial oxygen consumption (MVO_2 from k2')[409]. Both the past and present studies take advantage of the compartmental modeling approach to separate the *scale parameter* (K1') related to MBF, from the *shape parameters* (k_2 or V_T) related to the biological function of interest (MVO_2 or SNS function respectively).

In the studies by Harms et al., V_T appeared to less dependent on MBF than RI, and has been proposed to be a more sensitive index to early changes in sympathetic function [371,410]. Contrary to Harms et al. [371], our data suggest that measurements of V_T are more variable and potentially less repeatable than RI, whereas both values displayed similar relative changes with MBF (**Supplement Figures S3 and S4**). Thackeray et al. demonstrated that the RI was sensitive to detect early changes in sympathetic innervation in an animal model of diabetic neuropathy [411,412]. In separate preclinical studies, Thackeray et al. also demonstrated a low test-retest variability of 15% (SD) using the RI, thereby supporting its use in longitudinal experimental animal studies [392]. Results of the present study corroborate these findings by demonstrating that RI model was a more repeatable measure compared to the 1TCM V_T with or without regional partial volume correction, likely because of the simpler implementation of the RI calculation. Together these results add to the body of literature by suggesting a trade-off, with V_T possibly being a more physiologic measure of sympathetic innervation than RI but associated with greater variability for serial imaging.

C.5.4 Regional Defects

Publication of the PAREPET trial has stimulated significant interest in the field of regional non-invasive innervation imaging, with results demonstrating that HED PET can identify patients with ischemic cardiomyopathy at highest risk of sudden cardiac arrest (SCA) [367]. This risk was highly dependent on the total volume of denervated myocardium (%LV), and independent of more traditional risk factors such as LV ejection fraction. The lower test-retest repeatability values (Table 4) suggests that RI may be a more repeatable measure than V_T to evaluate sympathetic innervation and to track the progression of disease or monitor treatment response over time. It is also important to note that measurements of the regional defect scores were generally much more

repeatable than the global LV-mean values, as shown in Figure 5. This is not surprising as the defect scores are measured *relative* to the LV maximum value, whereas the LV-mean values are *absolute scale* measurements that also include variability in the LV maxima. Similar observations have been reported using relative myocardial perfusion imaging for example, compared to quantification of absolute myocardial blood flow which has higher test-retest variability [397].

This information will be instrumental in designing subsequent clinical trials (Table 5) to assess the utility of PET innervation imaging in selecting patients at highest risk of SCA who are most likely to benefit from primary prevention implantable cardioverter-defibrillator (ICD) therapies.

C.5.5 Comparison of V_T with and without PVC

A comparison between the repeatability of V_T with and without regional partial volume correction (PVC) was performed in our study. Accounting for the partial volume correction via the recovery coefficient RC allows for the calculation of V_T and K_1 based on the actual fraction of blood in the myocardium ROI [413] and may provide more accurate estimates of V_T and K_1. Despite the statistically significant increase in NPC values using V_T with vs. without PVC, the difference in repeatability was marginal for the LV-mean value (60% vs 54%, p=0.028) and defect size (25% vs 19%, p=0.025), as shown in Table 4. The increased variability likely comes from the added FBV parameter estimates used in the PVC, which had a test-retest NPC of 27%. Although the regional PVC should account for the underestimation of V_T by partial-volume effects to improve accuracy (on average), there is a small but statistically significant degradation in measurement precision (repeatability) of the values that should be considered as a trade-off.

C.5.6 Myocardial Blood Flow

The test-retest repeatability for LV-mean resting MBF was relatively poor (RPC=59% and NPC =61%) compared to other PET flow tracers, e.g. ~20% for ^{15}O-water, 20%-40% for ^{13}N-ammonia and ^{82}Rb-chloride, and 40% for ^{11}C-acetate [394,405]. Adjusting for changes in the rate-pressure-product between baseline and followup scans did not improve the MBF repeatability (RPC=63%). The relatively high variability of the MBF estimates is likely a result of the low tracer extraction (<50%) at rest as shown in **Supplement Figure S1**. Our estimated extraction function is similar to that of Harms et al. [391] measured in 17 ischemic cardiomyopathy patients with heart failure (LVEF<35%), but about 2-fold higher compared to that of Hiroshima et al. [390] measured in 10 healthy subjects and 13 suspected-CAD patients. These conflicting results suggest that further standardization and validation of methodologies may be required before this method can be considered robust for use in future clinical or research studies. The present work only evaluated repeatability of the LV-mean MBF values, whereas further validation studies are needed to determine the accuracy and repeatability of regional MBF estimates in heart failure patients with significant perfusion defects.

C.5.7 Clinical Relevance

Sympathetic denervation of the myocardium plays a key role in the genesis of life-threatening ventricular arrhythmias in patients with prior myocardial infarction [367,414]. It remains to be determined whether HED PET can guide the selection of appropriate ICD therapy for these patients at risk of SCD, but recent evidence suggests HED imaging can predict cause-specific cardiac mortality in primary-prevention candidates. In a competing risk analysis of the PAREPET trial, a 10% increase in denervated myocardium was associated with a 94% increase in SCD [415].

Aikawa et al. found ~40% difference in global RI between controls and patients with heart failure with preserved ejection fraction. The present study identified a test-retest variability for regional defects in RI or V_T equal to 12-19% [416]. Taken together, these results suggest that HED PET has the needed reliability to detect clinically relevant changes in regional denervation in many patient populations. These data will be critical for the design of future clinical trials aimed as assessing whether neurohormonal imaging can guide ICD selection for patients at risk for what remains a lethal and unpredictable disease.

To date, mIBG SPECT and HED PET have been the most widely used tracers to characterize sympathetic innervation in humans. However, quantification using mIBG has been limited to the assessment of sympathetic innervation using whole-heart to mediastinum ratios (H/M). PET imaging has superior spatiotemporal resolution and well-validated attenuation correction as compared to SPECT imaging, which allows for accurate quantification of regional abnormalities of sympathetic innervation. While the widespread clinical utility of SNS imaging with PET is currently limited by the short half-life (~20min) of ^{11}C-labeled tracers such as [^{11}C]HED, studies are currently underway to validate the utility of a new ^{18}F-labeled tracer, [^{18}F]flubrobenguane (also known as LMI-1195) to quantify sympathetic innervation [417]. Such tracers, with a longer isotope half-life (110 minutes) have the potential for wide distribution to maximize clinical impact.

C.5.8 Limitations

There was some variability in the time interval between baseline and followup imaging of the patients, potentially adding physiological variability to the test-retest results, although the patient's heart failure symptoms were stable during the test-retest interval. The findings in this

study apply to clinically stable HFrEF patients with moderate LV dysfunction, whereas results may vary in healthy volunteers and other patient populations depending on the etiology and severity of disease [418]. Test-retest HED data were not available in healthy volunteers for comparison to the heart failure patients.

C.5.9 Conclusion

Quantification of global and regional sympathetic innervation can be performed reliably using HED PET imaging by different operators using a highly automated analysis program. Relative measures of regional denervation (%LV defect) were more repeatable than absolute values of global innervation (LV-mean), and both were more repeatable using the simple RI compared to V_T, thereby supporting the use of RI over V_T for clinical trials using serial measurements of sympathetic innervation. These test-retest repeatability values help to inform statistical power calculations for study sample sizes that will be required to demonstrate significant baseline-to-followup changes using PET measurements of sympathetic innervation in heart failure populations. Both RI and V_T parameters demonstrated excellent reliability in general, supporting their use to predict cause-specific mortality from sudden cardiac arrest in patients with heart failure and ischemic cardiomyopathy.

C.5.10 Disclosures: JMR is consultant for Jubilant DraxImage Inc. and receives revenues from the sales of FlowQuant software. RdK is consultant for- and received grant funding from Jubilant DraxImage Inc. RSB is consultant for- and received grant funding from GE Healthcare, Lantheus Medical Imaging, and Jubilant DraxImage Inc. RdK receives revenues from Rubidium-82 generator technology licensed to Jubilant DraxImage Inc., and from sales of FlowQuant software.

C.5.11 Ethics Approval: All research subjects provided written informed consent, as approved by the Human Research Ethics Board at the University of Ottawa Heart Institute. The study has been performed in accordance with the ethical standards as laid down in the 1964 Declaration of Helsinki and its later amendments or comparable ethical standards.

Acknowledgments/Funding: KYW was a MD candidate supported by the University of Ottawa. JZ is an MD/PhD candidate supported in part by a Vanier Canada Graduate Scholarship. RSB is a Career Investigator supported by the Heart and Stroke Foundation of Ontario (HSFO), Tier 1 Chair in Cardiac Imaging Research and Vered Chair in Cardiology at the University of Ottawa Heart Institute. LM is a Mid-Career Clinician Scientist supported by HSFO and Tier 2 Chair in Heart Failure Research. This study was funded by HSFO (T-6426, NA-7158) and Canadian Institutes of Health Research (CIF-99470) Grants.

C.6.0 Supplemental Material

HED Extraction Fraction

In addition to HED PET imaging, patients also underwent a [^{11}C]acetate PET scan at baseline and followup, from which $MBF_{Acetate}$ values were measured using a 1TCM model and an established tracer extraction function derived in humans.[331,394] The reproducibility and test-retest repeatability of the $MBF_{Acetate}$ values from these patients were reported previously.[394] [^{11}C]acetate MBF values were adjusted for differences in the heart rate × systolic blood pressure product (RPP) to account for hemodynamic changes between the Acetate and HED scans:

$$MBF = \frac{MBF_{Acetate}}{RPP_{Acetate}} \times RPP_{HED} \quad \text{(S1)}$$

To obtain flow estimates from the HED uptake rate constant K_1', the HED-specific parameters of a modified Renkin-Crone extraction function [419,420] were estimated as:

$$E_{HED}(MBF) = 1 - e^{-PS/MBF} \quad \text{(S2)}$$

$$PS(MBF) = \mathrm{a} + \mathrm{b} \times MBF \quad \text{(S3)}$$

The permeability surface-area (PS) function coefficients (a,b) were estimated by curve fitting to the values of:

$$K_1' = E_{HED}(MBF) \times MBF \quad \text{(S4)}$$

The Renkin-Crone function describing the HED extraction fraction was determined to be:

$$E_{HED}(MBF) = 1 - 0.74 \times e^{\left(-\frac{0.35}{MBF}\right)} \quad \text{(S5)}$$

The extraction function derived in this study to obtain estimates of MBF from the 1TCM uptake rate constant (K_1') (Equation S5) is illustrated in Figure C.S1. This function is in good agreement with that determined previously by Harms et al.[391], with both curves demonstrating average tracer

extraction of approximately 50% (45-50%) at resting flows of 1 mL/min/g. The function from Harms was determined using MBF measurements from [^{15}O]water PET scans as the reference standard, and a similar 1TCM to the version presented in this study with regional PVC (RC=1−FBV) to obtain 17-segment HED K_1 estimates. However, it included an extra myocardium-to-blood spillover factor and a right ventricular activity and spillover component. Additionally, they fit a linear rather than an exponential equation to the K_1 vs. MBF data. Both of these factors likely account for the small discrepancies observed between our curve and that of Harms. Conversely, both our function and that from Harms demonstrate higher HED extraction than the relationship published recently by Hiroshima et al.[421] The relationship reported by Hiroshima was determined using MBF from [^{15}O]water as the reference standard; however, they used a different 1TCM formulation and PVC method compared to Harms, resulting in lower HED K_1 estimates and therefore a lower apparent extraction fraction. Their particular formulation of the 1TCM has also been previously shown to produce lower estimates of the extraction fraction for another tracer, ^{82}Rb.[422] The HED extraction function derived with their 1TCM implementation is similar to that found for the data in the present study when global PVC (RC=1) was applied, again suggesting that the differences are likely due to the particular compartment model formulations.

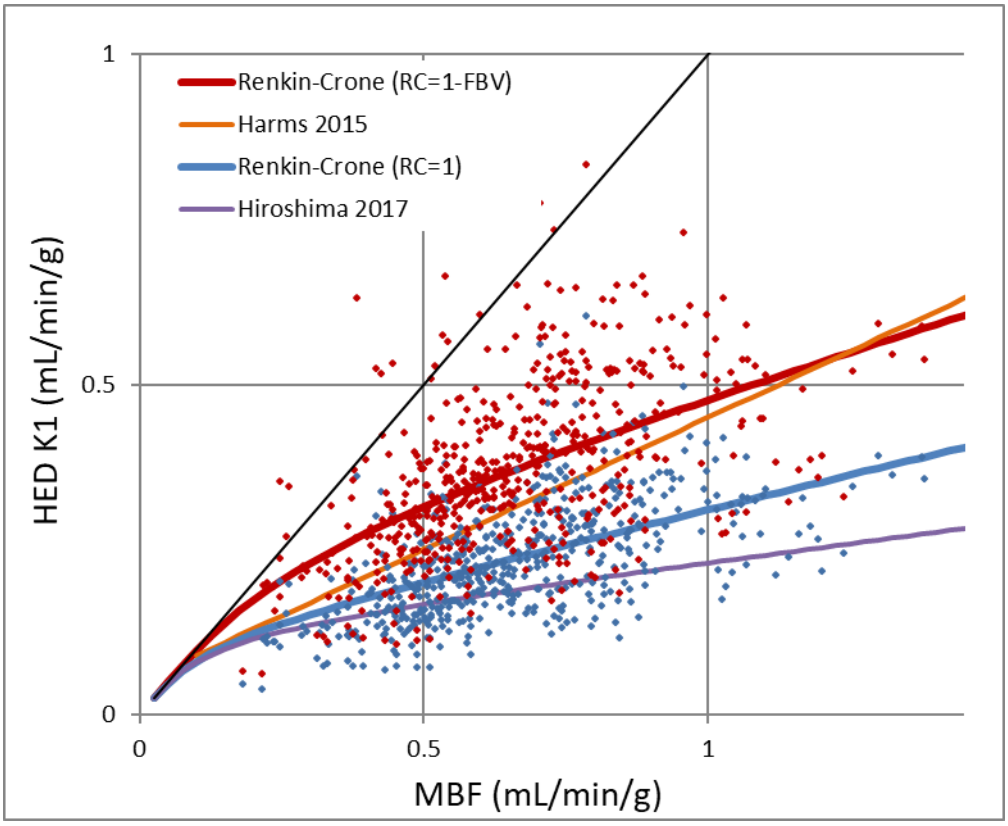

Figure C.S1: Comparison of HED extraction functions from the present study (red and blue) with previous studies from Harms et al. (orange) and Hiroshima et al. (purple).

Similar curves were obtained by Harms: $K_1 = 0.05 + 0.4 \times MBF$, and by the present study using regional PVC (RC = 1 − FBV): $K_1 = (1 - 0.74 \times e^{(-0.35/MBF)}) \times MBF$ (red). Both these curves were derived by curve-fitting of 17-segment HED K_1 values vs. MBF (using [^{15}O]water and [^{11}C]acetate, respectively).

Hiroshima used a different 1TC model formulation to fit 3-segment HED K_1 values vs. [^{15}O]water MBF, resulting in lower estimated extraction values: $K_1 = (1 - 0.89 \times e^{(-0.146/MBF)}) \times MBF$. This curve was more similar to that in the present study using global PVC (RC=1): $K_1 = (1 - 0.80 \times e^{(-0.14/MBF)}) \times MBF$ (blue).

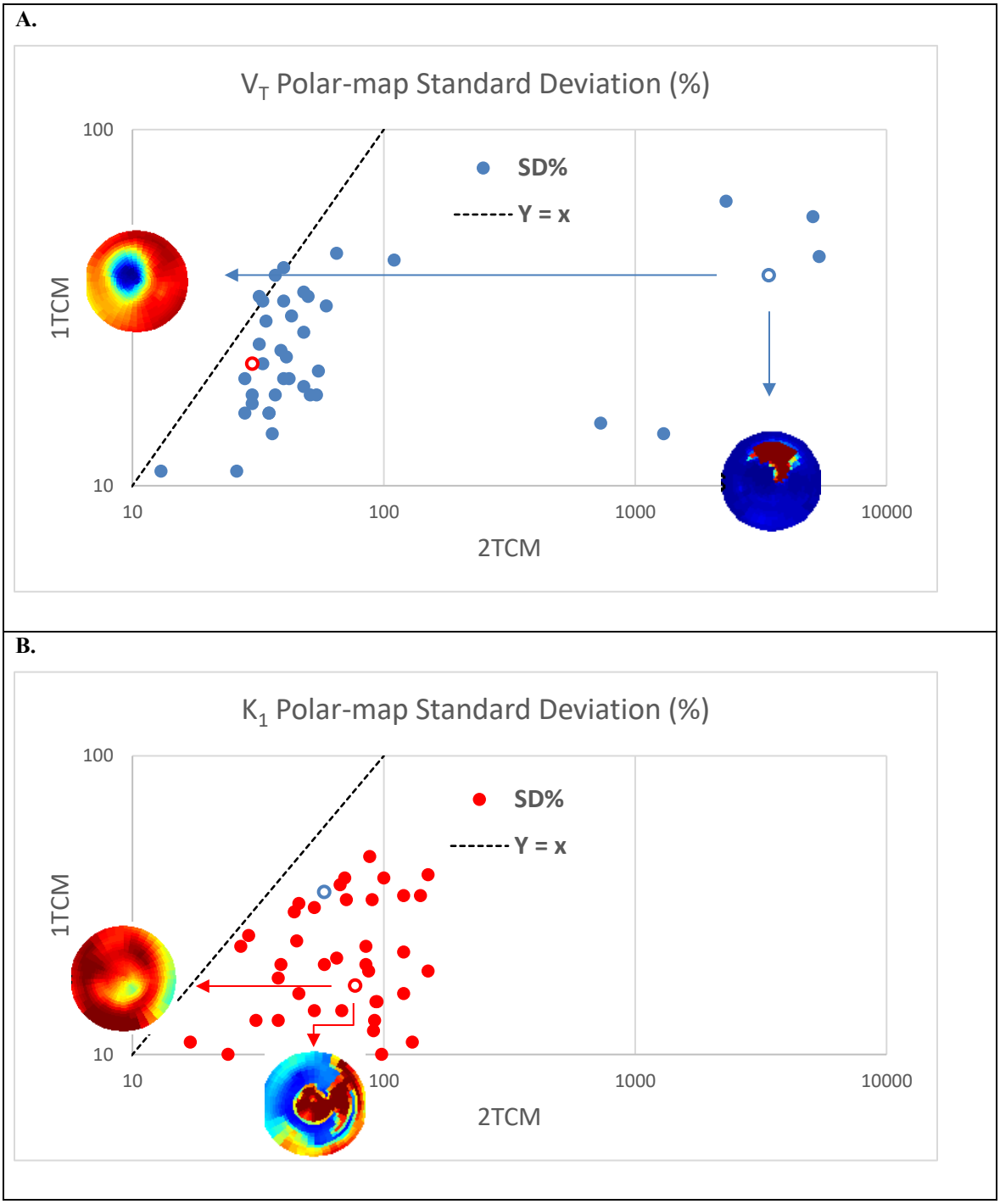

Figure C.S2: Comparison of 1TCM vs 2TCM variability (SD%) in the polar-map estimates of V_T (A) and K_1 (B). Open circles correspond to the polar-maps shown for V_T (blue) and K_1 (red). Model instability of the 2TCM is evident as disjoint polar-map regions that have reached the upper-bounds of the allowed parameter values (shown in deep red colour). In contrast, the 1TCM polar-maps are robust and free of any model-fitting or parameter-estimation artifacts.

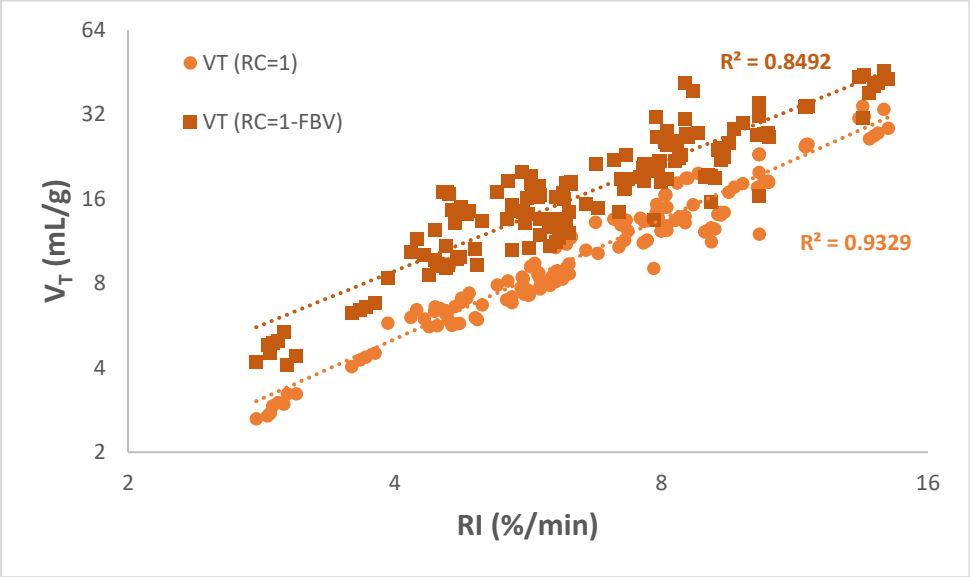

Figure C.S3: HED PET Measurements of V_T are highly correlated with RI using either global (RC=1) or regional (RC=1−FBV) partial-volume correction.

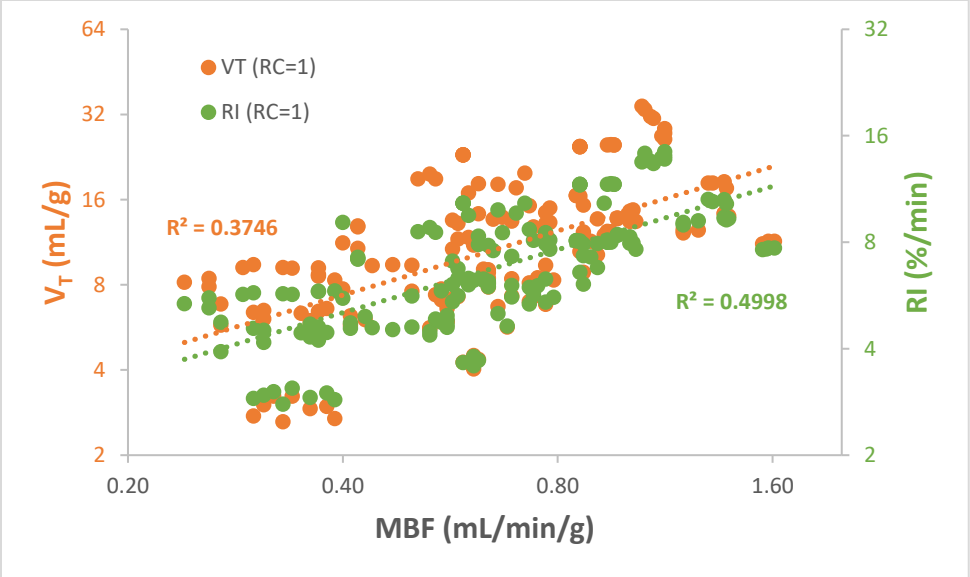

Figure C.S4: Flow dependence of HED PET parameters. HED PET V_T has significantly lower correlation with MBF compared to RI correlation with MBF ($p<0.05$) but the flow-dependence (slope) is very similar over the range of measured values.

Table C.S1: Comparison of variances in test-retest delta/mean values from Table 4

Parameters Compared	**NPC (%)**	**Non-Parametric Levene's Test (P-Value)**
$V_{T\ (RC=1)}$ vs $V_{T\ (RC=1\text{-}FBV)}$	54 vs 60	0.028
$V_{T\ (RC=1)}$ vs **RI**	54 vs **30**	0.114
$V_{T\ (RC=1\text{-}FBV)}$ vs **RI**	60 vs **30**	<0.001
%LV Defect: $V_{T\ (RC=1)}$ vs $V_{T\ (RC=1\text{-}FBV)}$	19 vs 25	0.025
%LV Defect: $V_{T\ (RC=1)}$ vs **RI**	19 vs **12**	0.008
%LV Defect: $V_{T\ (RC=1\text{-}FBV)}$ vs **RI**	25 vs **12**	<0.001
%LV Defect: MBF vs $K_{1(RC=1)}$	30 vs 30	0.436
%LV Defect: MBF vs $\mathbf{K_{1(RC=1\text{-}FBV)}}$	30 vs **13**	<0.001

Lowest values shown in bold

Appendix D
N-Terminal Pro B-Type Natruiretic Peptide and High-Sensitivity Cardiac Troponin T Levels are Related to the Extend of Hibernating Myocardium in Patients with Ischemic Heart Failure

Zelt *et al*. Can J Cardiol. 2017;33(11):1478–1488.
doi:10.1016/j.cjca.2017.06.012

Authors: Jason G.E. Zelt MSc[a,b], Peter P. Liu MD[a,b,c], Fernanda Erthal MD[a], Robert A. deKemp PhD[a], George Wells PhD[a], Eileen O'Meara MD[d], Linda Garrard BScN[b], Rob S.B. Beanlands* MD[a,b] and Lisa M Mielniczuk* MD[a,b]

[a]Molecular Function and Imaging Program, The National Cardiac PET Centre, and the Advanced Heart Disease Program, Division of Cardiology, Department of Medicine and the Cardiac Research Methods Centre, University of Ottawa Heart Institute and University of Ottawa, Ottawa, Canada
[b]Department of Cellular and Molecular Medicine, Faculty of Medicine, University of Ottawa, Ottawa, Canada.
[c]Departments of Medicine and Physiology, University of Toronto
[d]Division of Cardiology, Montréal Heart Institute, Montréal, Canada
*Co-Senior Authors

Author Contributions:

JGEZ: Performed statistical analysis and graphical representation. Wrote the manuscript for publication.
PPL. Performed biomarker assays
GW: Oversaw statistical analysis
RSB and LMM: PI on the project. Conceived study design and critical review of the manuscript.

D.1.0 Abstract

Background: Increased brain natriuretic peptide (NT-proBNP) and cardiac troponin (hs-cTnT) can identify heart failure (HF) patients at increased risk of cardiac events. The relationship of these biomarkers to the extent of hibernating myocardium and scar has not been previously characterized in patients with ischemic LV dysfunction and HF.

Methods: Patients with ischemic HF meeting recruitment criteria and undergoing perfusion and 18F-fluoro-2-deoxyglucose (FDG) positron emission tomography (PET) imaging to define myocardial hibernation and scar were included in the study. A total of thirty-nine patients (mean age 67±8 years) with NYHA class II-IV HF and ischemic cardiomyopathy (ejection fraction (EF) = 27.9±8.5%) were enrolled in the study.

Results Serum NT-proBNP and high sensitivity cardiac troponin T (hs-cTnT) levels were elevated in patients with ≥10% hibernating myocardium, compared to those with <10% (NT-pro-BNP: 7419.10±7169.5 vs 2894.6±2967.4 pg/ml; hs-cTnT: 789.3±1835.3 vs 44.8±78.9 ($p<0.05$)). The overall ROC-AUC value for NT-proBNP and hs-cTnT to predict hibernating myocardium were 0.76 and 0.78, respectively ($p<0.05$). The NT-proBNP ($p=0.02$) and hs-cTnT ($p<0.0001$) levels also correlated with hibernation, particularly in patients with ≥10% scar, independently of EF, age and eGFR. No differences were noted in biomarker levels for patients with- versus without ≥10% scar.

Conclusions:

NT-proBNP and hs-cTnT levels are elevated in ischemic HF patients with hibernation, and correlated with the degree of hibernation, but not with the presence or extent of scar. Taken together, these data support the novel concept that NT-proBNP and hs-cTNT release in patients with ischemic HF reflects the presence and extent of hibernating myocardium.

Abbreviated Abstract:

In 39 patients with ischemic HF, NT-proBNP and hs-cTnT levels were elevated in patients with ≥10% hibernating myocardium, compared to those with <10%. Levels also correlated with hibernation, particularly in patients with ≥10% scar, independent of EF, age and eGFR. No differences were noted in biomarker levels for patients with- versus without ≥10% scar. These data suggest that NT-proBNP and hs-cTNT release in patients with ischemic HF reflect the presence and extent of hibernating myocardium.

D.2.0 Introduction

Coronary artery disease (CAD) is the leading cause of heart failure (HF)[423]. Although there is increased risk, revascularization is often considered in patients with ischemic HF but the selection of patients most likely to benefit remains a challenge[424–426].

In patients with ischemic HF, recurrent myocardial ischemia may lead to scar formation, hibernation or a combination of both. Although these entities contribute to left ventricular (LV) dysfunction, only viable dysfunctional myocardium (hibernation) is potentially recoverable with restoration of adequate perfusion[325,424,427–432]. Cardiac imaging modalities have emerged with the ability to differentiate between myocardial scar and viable myocardium and are now often used to direct therapy decisions including revascularization[325,424,425,427–437]. Among these, cardiac PET using ^{18}F-flurodeoxyglucose (FDG) is widely considered a "gold standard" and the most sensitive modality for detecting hibernating viable myocardium[425,428,435]. However, the evidence is conflicting as to whether viability imaging guided strategies alone can yield significant clinical benefit upon revascularization. Some studies do suggest benefits[325,427–432,434–437], while others suggest no significant role[438,439]. Hence there remains a need to improve approaches to better identify patients with ischemic HF likely to benefit from revascularization.

Cardiac specific biomarkers, such as BNP and cTnT are excellent prognosticators in patients with HF[440–443]. They may offer an additional approach to compliment current image-guided strategies for patient selection. However, it is largely unknown how cardiac specific biomarkers are released in relation the presence and extent of myocardial scar and hibernation in patients with ischemic HF. This relationship may provide additional insights as to the underlying pathophysiology of biomarker dynamics in ischemic HF.

The objectives of this study are to assess the relationship and interaction of the biomarkers NT-proBNP and hs-cTnT with myocardial scar and hibernation in patients with chronic ischemic HF.

D.3.0 Methods

Patients with suspected ischemic cardiomyopathy were prospectively recruited into an imaging study using cardiac PET to determine perfusion deficit, scar or hibernation. The patients also had blood sampling at baseline to determine biomarkers.

The patients are part of the overall IMAGE HF (Imaging Modalities to Assist with Guiding Therapy in The Evaluation of Patients with HF) program and its subproject Alternative Imaging Modalities in Ischemic HF (AIMI-HF)(www.ClincalTrials.gov; NCT01288560)[326]. Full details on the AIMI-HF study design and methods have been published separately[326].

This study was approved by the University of Ottawa Heart Institute (UOHI) Human Research Ethics Board (protocol #2010620-01H). This study was conducted in accordance with the Declaration of Helsinki, Good Clinical Practice and the TriCouncil Policy.

Patients:

Patients in this study met the AIMI-HF enrollment criteria[326]. Briefly, patients with clinical HF or severe LV systolic dysfunction who needed further definition of viability or scar were enrolled. Eligible patients were included if they were 18 years of age or older; had known

or highly suspected coronary artery disease documented by coronary angiography or by history of previous MI or evidence of moderate ischemia or scar based on prior imaging. Patients were being treated with optimal medical therapy and their LV dysfunction was primarily attributable to ischemic heart disease with i) EF ≤45% as documented by echocardiography, radionuclide angiography, LV angiography, PET or SPECT, or CMR within the previous 6 months and NYHA class II to IV symptoms or ii) EF ≤30% within the previous 6 months and NYHA class I to IV symptoms. Patients on renal replacement therapy were excluded from this biomarker study.

Imaging

Patients underwent routine assessment of LV function with commonly accepted methods. In this study, this included echocardiography (n=38), radionuclide angiography (n=3), MRI (n=1) or SPECT perfusion (n=1).

The PET imaging methods are detailed in previous reports and are in accordance with guidelines[325–328]. All PET images were acquired using either GE Discovery 690 PET/VCT or GE Discovery 600 PET/CT (Waukesha, WI) scanners. PET perfusion imaging was acquired at rest with a standard protocol using ^{82}Rb or ^{13}N-ammonia as described previously[325–328]. For ^{18}F-FDG imaging, nondiabetic patients were studied after an oral glucose load, whereas an insulin-euglycemic clamp was used for those with diabetes[325–328,444].

PET Data Analysis and Interpretation

An automated method of image analysis[445] (FlowQuant©; UOHI) was applied to the perfusion/^{18}F-FDG PET data to yield quantified measures of the extent and severity of perfusion/FDG mismatch as a measure of myocardial hibernation and perfusion/FDG match as a measure of scar as previously described[325,430]. Match (scar) and mismatch (hibernation) are

expressed as percentage of the LV as previously described and as illustrated in Figure D.1and D.2 [325,430]. In addition, all scans are reviewed by an imaging expert. The expert considers the qualitative images along with the quantitative polar map data and assigns a semi-qauntitative category for scar and hibernation to be none (0-5%); mild (5-10%); moderate (10-20%); or severe (>20%) that is included in the pre-defined image case report form and also the clinical report (available at http://www.image-hf.ca/PDFs/HF12_ViabiltyPETSPECT.pdf)[326]. For purposes of this study moderate-severe was combined to represent ≥10% as mid semi-quantitative category. This was pre-defined for this analysis and considered reasonable considering prior published literature applying this clinically significant cut-point for definition of hibernation and scar[429,433].

Blood Biochemistry

Prior to PET imaging, blood samples were procured from all patients and stored at -80^{0}C for later analysis. Serum hs-TnT (Roche Diagnostics) and NT-proBNP (Roche Diagnostics) were measured using commercially available FDA approved electrochemiluminescence immunoassays with a Roche Cobas e411 analyzer. The normal limit for the hs-cTn is below the ninety-ninth percentile (<14ng/L)[446,447]. This discriminatory 99th percentile is designated as the decision level for the diagnosis of myocardial infarction[448]. NT-proBNP cutoffs have been validated to diagnose acute HF. An age-independent cut-point of 300 pg/mL had a 98% negative predictive value to exclude acute HF[449].

Statistical Analysis

Statistical analyses and graphical representations were performed using Stata 14 and Graphpad Prism 6.0. The log-transformed hs-cTnT and NT-proBNP levels were used, as their distributions were not normal. A Student's-*t*-test was used to detect statistical differences between <10% and ≥10% scar and hibernation. Pearson correlation coefficients were used to determine the degree of association between variables. The diagnostic performance (i.e. the detection of ≥10% hibernation) of each biomarker was represented with receiver operator characteristic (ROC) curves, and the area under the curve (AUC). The Youden's index was used to identify the ROC optimal cutoff. We performed a secondary post-hoc analyses evaluating hibernation in patients with ≥10% scar (n=29). This cutoff was selected based on being the midpoint of the predefined semi-quantitative categories and based on previous literature which used 10% to define extensive scar[433].

Multivariable analyses using a logistical and multiple regression were used to evaluate the relationship of NT-proBNP or hs-cTnT and hibernation/scar adjusting for age, EF and eGFR as these are known to be parameters that may affect NT-proBNP and/or hs-cTnT[450–454]. P-values <0.05 were considered statistically significant.

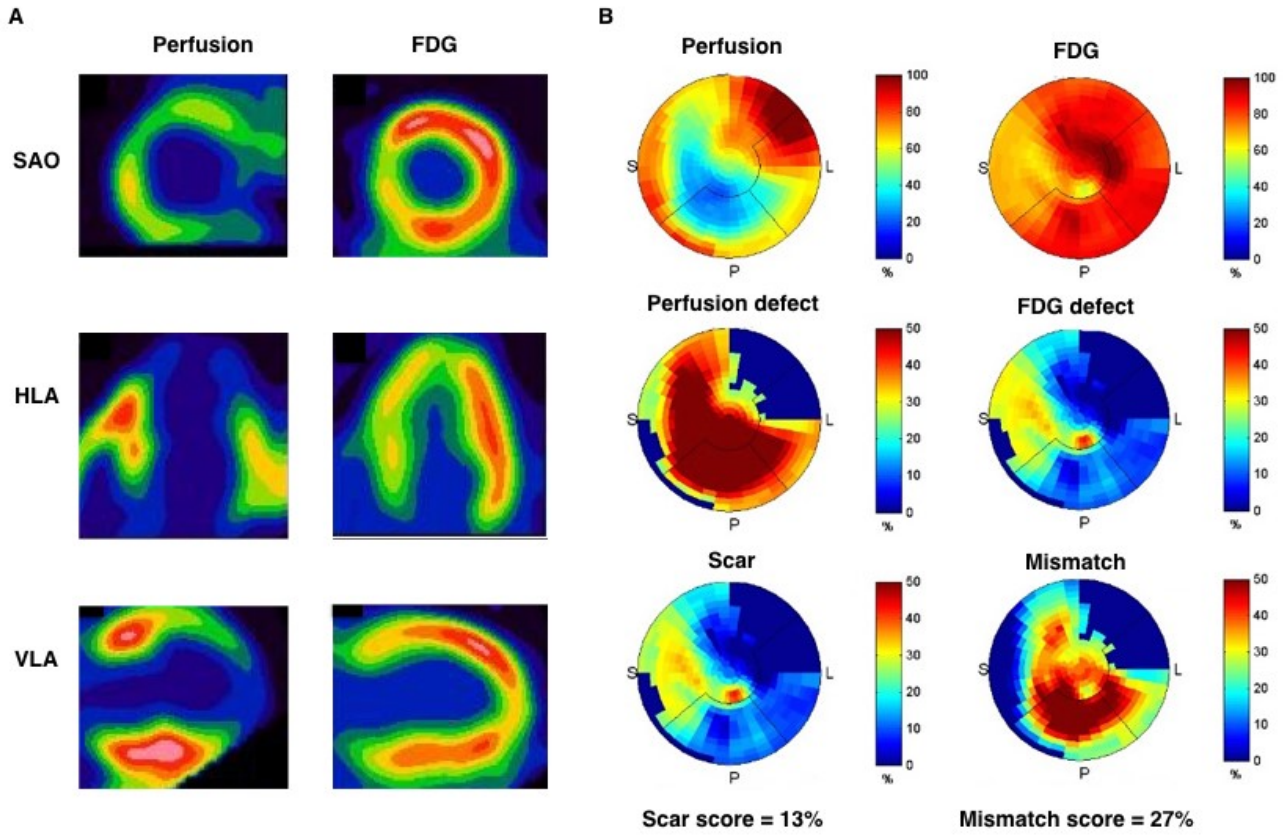

Figure D.1. Example of perfusion and fluorodeoxyglucoseepositron emission tomography images in a patient with moderate scar (13% of left ventricle) and significant mismatch (27% of left ventricle) in the inferior, inferolateral, anterior, anteroseptal, and apical walls. The patient's high sensitivity cardiac troponin and N-terminal pro b-type natriuretic peptide levels were high (489.7 pg/mL and 32,032 pg/mL, respectively). Left: Perfusion; Right: FDG. HLA, horizontal long-axis planes; SOA, short axis; VLA, vertical long axis.

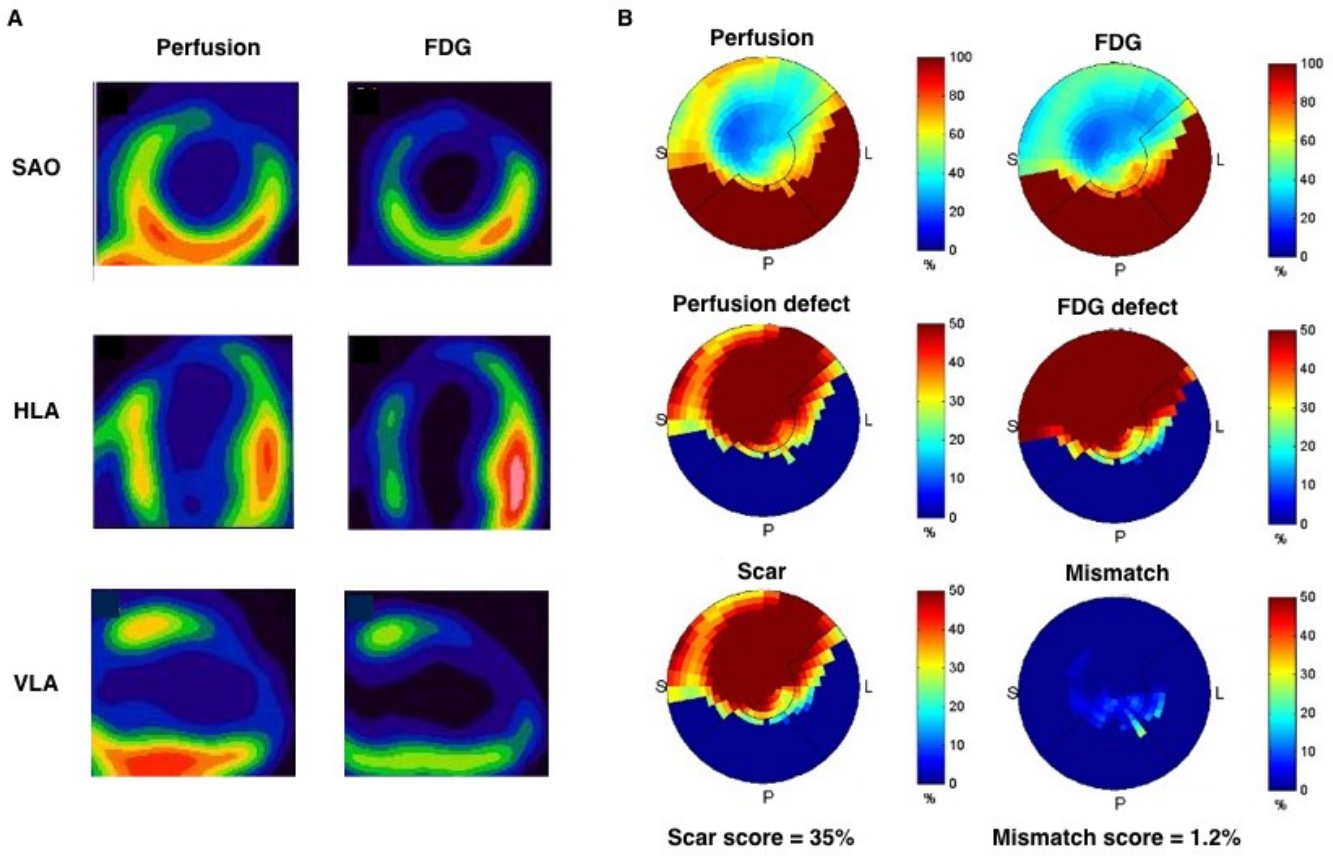

Figure D.2. Example of perfusion and fluorodeoxyglucoseepositron emission tomography images in a patient with predominant scar (35%) in the anterior, septal, anterolateral, and apical walls of the left ventricle and nonsignificant mismatch (1.2%). The patient's high-sensitivity cardiac troponin and N-terminal pro b-type natriuretic peptide levels were low (8.34 pg/mL and 1997 pg/mL, respectively). HLA, horizontal long-axis planes; SOA, short axis; VLA, vertical long axis

B.4.0 Results

Baseline Characteristics

There were 43 consecutive eligible patients who underwent FDG PET imaging and had blood sampling for biomarkers for the study. Two patients could not complete the imaging due to claustrophobia and were excluded. Two patients were noted to be on dialysis and were thus excluded, giving a final sample of 39 patients with complete analyzable data who were included in this study. Baseline characteristics appear in Table D.1. The NT-proBNP levels ranged from 151.3-22823 pg/mL with a mean of 3706.7 ± 4288.7 pg/mL (median with inter quartile range (IQR)=1997 pg/mL (1024.5-5359.5)). Hs-cTnT levels ranged from 4.17 to 4947 mg/mL with a mean of 178.4 ± 787.7 pg/mL (median (IQR)=34.48 pg/mL (18.12-43.02). Overall on the FDG PET study, 29 patients had significant (≥10%) scar, 7 patients had significant (≥10%) hibernation. There were 8 patients who had no significant (≥10%) scar or hibernation, and 5 patients who had both.

Table D.1 Patient Characteristics

Clinical Characteristics (n=39)	
Age, Y	67.2 ± 7.9
Sex (male)	33 (85%)
Diabetes mellitus	25 (64%)
Hypertension	28 (72%)
Systolic Blood Pressure (mm Hg)	120.3 ± 18.6
Diastolic Blood Pressure (mm Hg)	68.8 ± 12.4
Hyperlipidemia	28 (72%)
Smoking	24 (62%)
Family History Premature CAD	15 (38%)
Chronic Renal Dysfunction (eGFR <60)	10 (26%)
eGFR (mL/min/1.73m^2)	78.8 ± 34.2
Creatinine (uM)	107.1 ± 41.9
Peripheral Vascular Disease	4 (10%)
Pulmonary Disease	12 (31%)
Cerebrovascular Disease	5 (13%)
Body Mass index, kg/m^2	28.2 ± 4.5
Previous Myocardial Infarction	27 (69%)
Previous PCI	12 (31%)
Previous CABG	2 (5%)
Ejection Fraction	27.9 ± 8.5%
NYHA Class	
I	0 (0%)
II	20 (50%)
III	18 (45%)
IV	1 (2.5%)
Medications	
β Blocker	35 (90%)
ACE Inhibitor or ARB	36 (92%)
Aldosterone antagonist	10 (26%)
Statin	35 (90%)
Digoxin	4 (10%)
Antiplatelet or Anticoagulant	37 (95%)
Biomarkers	
NT-proBNP (pg/mL)	
Mean ± SD	3706.7 ± 4288.7
Median (IQR)	1997 (1024.5- 5359.5)
Hs-cTnT (pg/mL)	
Mean ± SD	178.4 ± 787.7
Median (IQR)	34.48 (18.12-43.02).

Data expressed as mean ± SD or mean (%). CAD=Coronary Artery Disease, eGFR= estimate Glomerular Filtration Rate, PCI=Percutaneous Coronary Intervention, CABG=Coronary Artery Bypass Graft, ACE=Angiotensin Converting Enzyme, ARB=Angiotensin Receptor Blocker.

Relationships of Biomarkers to LV Hibernation

Both NT-proBNP and hs-cTNT levels were significantly elevated in patients with >10% hibernation (≥10% hibernation; mean ± SD: 7419.1 ± 7169.5 pg/mL; vs. <10% hibernation; mean ± SD: 2894.6 ± 2967.4; for NT-proBNP; $p<0.05$) and (≥10% hibernation; mean ± SD: 789.3 ± 1835.3 pg/mL; vs. <10% hibernation; mean ± SD: 44.8 ± 78.9 pg/mL; for hs-cTnT $p<0.01$) (Figure D.3 A/B). NT-proBNP was significantly related to the presence of ≥10% hibernation after adjustment for age, eGFR and EF ($p<0.05$). In this model, hs-cTnT approached statistical significance ($p=0.06$; Table D.2).

The ROC curve analysis for the detection of >10% hibernation myocardium for NT-proBNP and hs-cTnT is described in Figure D.3. The ROC-AUC value for NT-proBNP and hs-cTnT was 0.75 (95%CI: 0.54-0.97; $p=0.03$) and 0.78 (95%CI: 0.56-1.01; $p=0.02$), respectively. The analysis showed an optimal cutoff of NT-proBNP of >3066 pg/mL (sensitivity: 86%, specificity: 72%) and of hs-cTnT of >66 pg/mL (sensitivity: 71%, specificity: 94%) (Figure D.4).

There was a continuous relationship between increasing degrees of hibernation and increasing NT-proBNP and hs-cTnT levels. (Figure D.3C/D) Hs-cTnT levels increased with the degree of LV hibernation. There was a statistically significant relationship between Log hs-cTnT and % hibernation ($r=0.57$, $p<0.001$, CI=3.15 – 9.01) (Figure D.3D). Furthermore, the multivariable regression analysis confirmed that hs-cTnT (regression coefficient (coef.)=5.55, $p<0.001$, CI=2.48 – 8.61) and age (coef=-0.22, $p<0.05$, CI= -0.44 – -0.0036) were independently correlated with hibernation after adjusting for eGFR and EF (Table D.3).

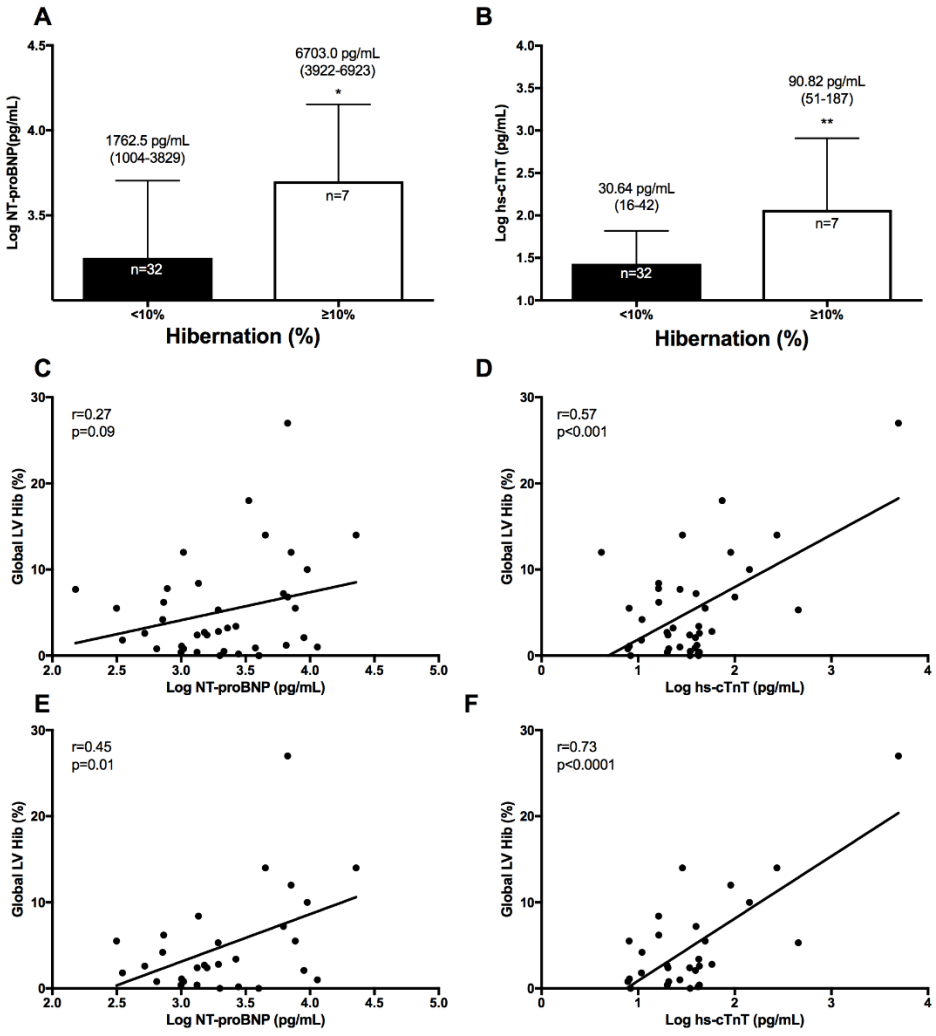

Figure D.3: Log of the Serum NT-proBNP (A,C,E) and hs-cTnT (B,D,F) concentrations in patients with varying LV hibernation severity. A and B compare patients with- and without significant (>10%) hibernation. Median (IQR) values of serum NT-proBNP (A) and hs-cTnT (C) levels are shown at the top of each corresponding bar. C and D plot the relationship of the Log serum NT-proBNP (B) and hs-cTnT (D) versus the % LV hibernation on quantitative analysis. E and F plot the relationships between Log serum NT-proBNP (E) and hs-cTnT (F) and levels with % LV hibernation in a subgroup of patients (n=29) with the presence of significant (≥10%) scar. Data is expressed mean ± SD. * $p<0.05$, ** $p<0.01$.

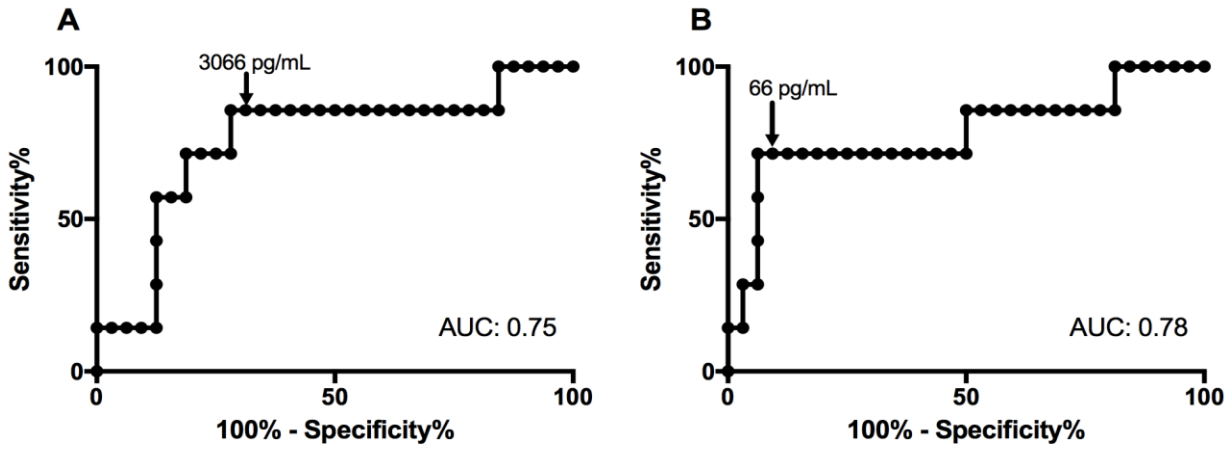

Figure D.4: Receiver operator characteristic curve analysis for both NT-proBNP (A) and hs-cTnT (B). The optimal cutoff for the detection of >10% hibernation was 3066 pg/mL for NT-proBNP and 66 pg/mL for hs-cTnT.

Table D.2: Logistic regression analysis between the presence of hibernation and clinical variables including Log NT-proBNP and Log hs-cTnT.

	Odds Ratio	Std. Err.	z	P- Value	[95% Conf. Interval]
>10% Hibernation					
Log hs-cTnT	8.57	9.87	1.86	0.062	0.90 - 82.00
Age	0.86	0.06	-2.06	0.039	0.74 - 0.99
eGFR	0.98	0.019	-0.86	0.390	0.94 - 1.02
EF	1.03	0.074	0.41	0.681	0.89 - 1.19
>10% Hibernation					
Log NT-proBNP	8.83	18.33	2.16	0.031	0.15 – 515.59
Age	0.82	0.076	-2.12	0.034	0.69 - 0.98
eGFR	0.98	0.02	-1.03	0.305	0.93 - 1.02
EF	1.23	0.16	1.66	0.097	0.96 - 1.58

eGFR= estimate Glomerular Filtration Rate, EF=ejection fraction. Age (per one year increase), eGFR (per 1 mL/min/1.73m^2 increase), EF (per 1% increase). Log hs-cTnT (per 1 increase in logged values), Log NT-pro-BNP (per 0.1 increase in logged values)

Table D.3: Multivariable regression analysis between LV hibernation (%) and clinical variables including Log NT-proBNP and Log hs-cTnT.

	Coef.	Std. Err.	t	P-Value	[95% Conf. Interval]
Model 1: NT-proBNP					
Log NT-proBNP	3.61	2.20	1.64	0.110	-0.86 – 8.08
Age	-0.23	0.12	-1.92	0.064	-0.48 – 0.014
eGFR	-0.054	0.031	-1.75	0.089	-0.12 – 0.0088
EF	0.22	0.12	1.88	0.068	-0.017 – 0.45
Model 2: hs-cTnT					
Log hs-cTnT	5.55	1.51	3.68	0.001	2.48 - 8.61
AGE	-0.22	.11	-2.07	0.047	-0.44 - -0.0036
eGFR	-0.040	.027	-1.49	0.146	-0.094 - 0.015
EF	.11	.094	1.12	0.269	-0.085 - 0.30

eGFR= estimate Glomerular Filtration Rate, EF=ejection fraction.

Relationships of Biomarkers to LV Scar

NT-proBNP and hs-cTnT levels were similar in patients with moderate-severe scar (≥10%) compared to patients with scar <10% (Figure D.5A/C). There was also no statistically significant correlation between LV scar and either NT-proBNP (r= -0.05, p=0.78, CI= -8.14 – 6.12) or hs-cTnT (r= -0.10, p=0.54, CI= -8.19 – 4.36) (Figure D.5B/D).

Biomarker relationships to hibernating myocardium in patients with scar

To elucidate whether the relationships between hs-cTnT and NT-proBNP levels with hibernation were affected in the presence of significant (≥10%) scar, a post-hoc analysis was conducted in this patient subgroup (n=29). In patients with significant scar, both hs-cTnT and NT-proBNP levels increased as the degree of LV hibernation increased. Log NT-proBNP (r=0.45,p=0.01, CI=1.21–9.82) and Log hs-cTnT (r=0.73,p<0.0001,CI= 4.56 – 9.91) significantly correlated with LV hibernation (%) (Figure D.3E/F). Furthermore, the multivariable regression analysis revealed that NT-proBNP (coef=6.39, p=0.02, CI=1.01 – 11.77) and hs-cTnT (coef=7.27, p<0.0001, CI=4.19 – 10.35) were independently correlated with LV hibernation, and not scar. The adjusted model in Table D.4 summarizes that the interaction between LV hibernation and either NT-proBNP or hs-cTnT is still statistically significant after adjusting for eGFR, EF and age.

Relationships of biomarkers to GFR and EF

Linear regression analyses were performed between serum NT-proBNP or hs-cTNT and renal and LV function, evaluated with eGFR and EF respectively. Both NT-proBNP (r= -0.42, p<0.01, 95% confidence interval (CI)= -50.58 - -8.89) and hs-cTnT (r= -0.35, p<0.05, CI= -41.03 – -2.31) were negatively correlated with eGFR. There was a significant negative correlation between NT-proBNP and EF (r= -0.42, p<0.01, CI= -12.54 – -2.15); however hs-cTnT was not correlated with EF (r=0.04, p=0.82, CI= -4.54 – 5.72).

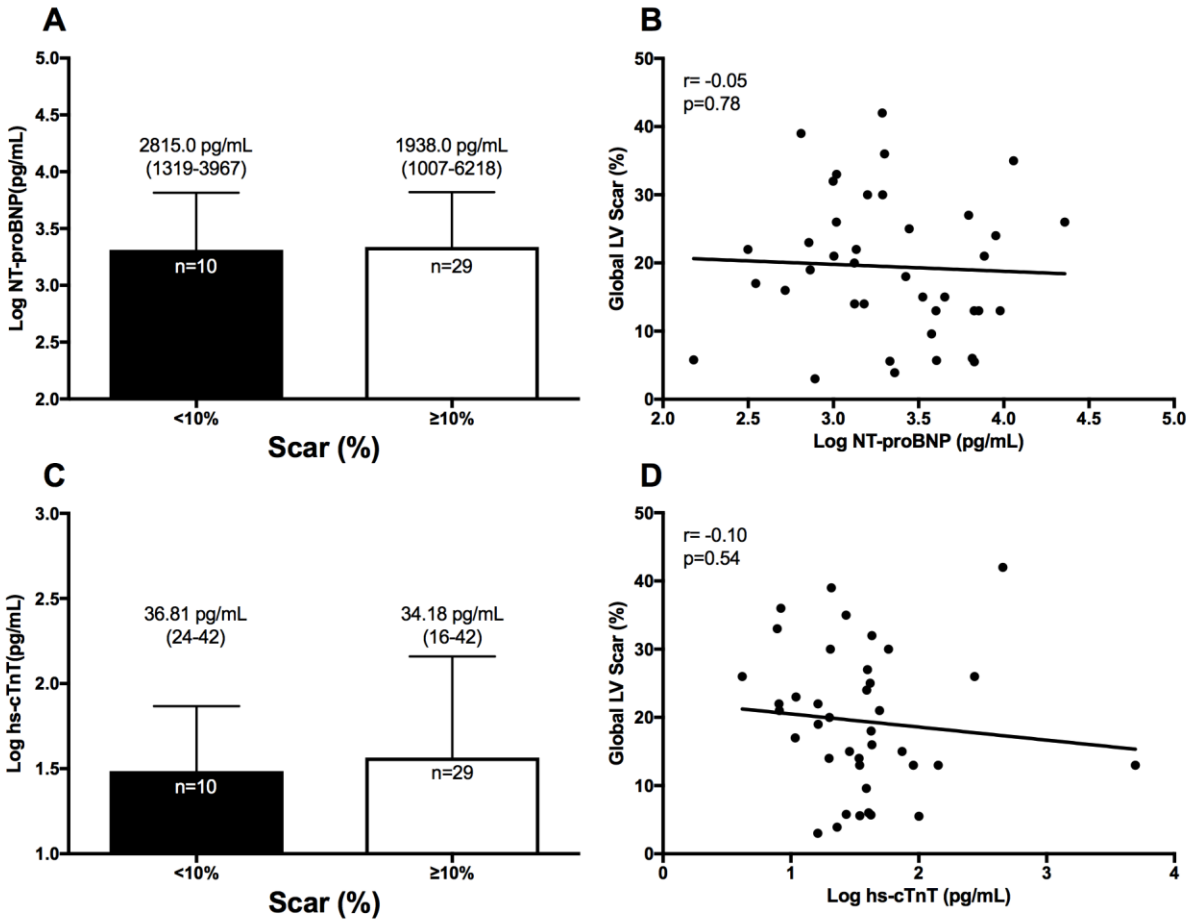

Figure D.5: Log of the Serum NT-proBNP (A,B) and hs-cTnT (C,D) concentrations in patients with varying LV scar severity. A and C compare patients with and without significant (>10%) scar. Median (IQR) values of serum NT-proBNP (A) and hs-cTnT (C) levels are shown at the top of each corresponding bar. C and D plot the relationship of the Log Serum NT-proBNP (B) and hs-cTnT (D) versus the % LV scar on quantitative analysis. Data is expressed mean ± SD.

Table D.4: Multivariate regression analysis between LV hibernation (%) and clinical variables including Log NT-proBNP and Log hs-cTnT in patients with significant scar (>10%).

	Coef.	Std. Err.	t	P- Value	[95% Conf. Interval]
Model 1: NT-proBNP					
Log NT-proBNP	6.39	2.61	2.45	0.022	1.01 - 11.77
Age	-0.14	0.18	-0.80	0.429	-0.50 - 0.22
eGFR	-0.022	0.038	-0.58	0.567	-0.099 - 0.056
EF	0.19	0.13	1.49	0.149	-0.073 - 0.45
Model 2: hs-cTnT					
Log hs-cTnT	7.27	1.49	4.87	<0.0001	4.19 - 10.35
Age	-0.12	0.14	-0.86	0.400	-0.41 - 0.17
eGFR	-0.0084	0.029	-0.29	0.774	-0.068 - 0.051
EF	0.016	0.098	0.16	0.871	-0.19 - 0.22

eGFR= estimate Glomerular Filtration Rate, EF=ejection fraction.

4.0 Discussion:

This study demonstrates that serum levels of NT-proBNP and hs-cTnT are elevated in stable patients with moderate-severe levels of hibernating myocardium and LV dysfunction or HF. The biomarker levels correlated with the extent of hibernation independent of EF, age and eGFR in ischemic cardiomyopathy, (in particular in patients with ≥10% scar). Furthermore, a level of NT-proBNP >3066 pg/mL or hs-cTnT >66 pg/mL had reasonable diagnostic value for the detection of significant hibernation. NT-proBNP and hs-cTnT levels were not correlated with the extent of the scar in these patients. Taken together, these data support the novel concept that both the severity and extent of LV hibernation are determinants of serum NT-proBNP and hs-cTNT elevation in patients with ischemic HF, rather than extent of pre-existing myocardial damage or scar extending the traditional variables related to EF and the severity of LV dysfunction.

Patients with ischemic HF are often considered for revascularization therapy[424–426]. Evidence exists that supports the notion that revascularization yields clinical benefit in patients with viable myocardium as defined by imaging techniques such as FDG PET[328,427–432,435–437]. However, controversy remains as other studies suggest image guided strategies may not yield definitive clinical benefit in this population[424,438,439]. The current study is the first step towards understanding the unique information content of NT-proBNP and cTnT in the context of viability imaging and ischemic HF. This will help to determine whether a biomarker-guided approach can complement the current image-guided strategy for clinical decision making in ischemic HF patients. Future studies are needed to determine whether NT-proBNP and cTnT levels preceding or in combination with viability imaging, can better predict outcome benefits in ischemic HF patients following revascularization, and thus enable a more precision targeted

patient selection process.

It is now well established that BNP levels are chronically elevated in patients with ischemic HF[450,455,456]. NT-proBNP is a prohormone secreted in response to elevated volume and pressure load in the atria and ventricles, as well as stress and hypoxia[450,457]. To our knowledge, only one previous study has suggested a correlation between BNP and hibernation as measured with cMRI and dobutamine echocardiography. In this study, the BNP levels were assessed in patients with recent myocardial infarction, NYHA functional class I-II dyspnea and mild reductions in LVEF (48 ± 15%)[458]. They observed a moderate correlation between LogBNP levels and indices of viable myocardium and scar. Differences in patient selection (recent MI and mild LV dysfunction) may explain the heterogeneity in results when compared to this study. In contrast, our study included patients with much more significant LV dysfunction (mean 27.8%), and thus greater dynamic range of both biomarkers and extent of scar or hibernation as well as being a potentially more relevant population for defining viability where revascularization decisions are more difficult[425].

There is no consensus in the literature on the relationship between BNP or TnT and scar in this patient population. Studies have reported that BNP levels either decrease[459], do not change[460] or increase[458,461] in patients with stable scar. The heterogeneity of the results in the literature may be explained by the differences in patient populations, as well as timing post MI. Aktas *et al.* found decreased BNP levels in patients with large scar (>33%), as evaluated in a relatively homogenous population of patients with ischemic HF with EF <35%, similar to our study[459]. Our data showed that there was no difference in NT-proBNP and hs-cTn levels between patients with- versus those without moderate-severe scar. Together these data support the

suggestion by Atkas et al that areas with significant scar "may lack the cellular biomachinery required" for this peptide[459].

The current study also demonstrated that the relationship between NT-proBNP or hs-TnT and hibernation remains in patients with significant scar. That is, patients with significant scar and hibernation had markedly elevated BNP and TnT levels. Further, in patients with moderate-severe scar, both BNP and TnT levels were independently correlated with the degree of hibernation, after adjusting for EF, eGFR and age. Although speculative, it is plausible that hs-cTnT elevation in patients with hibernation, rather than scar, is due to continued cell death, raising the need for early revascularization in this patient population. The improved relationship between BNP or TnT levels and hibernation severity in patients with scar (≥10%) may be due to the increased tension and stress on the remaining myocardium in the presence of a significant scar, inducing further production and release of cardiac stress peptides such as BNP and cTnT especially from the hibernating myocardium. One may speculate that the ischemic but viable hibernating myocardium is thus doubly stressed with additional hemodynamic stimulus, thus further increasing the biomarker levels in the circulation. Further studies are required to support this hypothesis.

The release of hs-cTnT in HF, when acute coronary syndromes have been excluded, has been attributed to supply-demand mismatch, increased myocyte turnover with progressive myocardial dysfunction and/or subendocardial ischemic injury due to wall stress, myocardial apoptosis and oxidative injury[462–466]. Given the proposed mechanism for hibernation as metabolic and functional down-regulation secondary to repeated ischemia, it is logical to surmise that hs-cTnT release would relate to the degree of hibernation. However, in spite of the known

pathophysiological mechanisms for troponin elevations, studies evaluating its relationship to myocardial hibernation have been limited to date. The current study, may represent one of the first reports that hs-cTn levels in patients with ischemic HF relate to the degree of hibernation.

Regarding natriuretic peptides, recent evidence indicates they are secreted in hypoxic, ischemic and/or hibernating myocardium in addition to known responses to volume and pressure load[441,450,467,468]. Goetze *et al.* demonstrated that plasma BNP and proBNP were markedly increased in patients with CAD undergoing revascularization even without LV dysfunction and were strongly associated with left ventricle tissue BNP mRNA expression[467]. May et al, using a transgenic model of myocardial hibernation, showed that BNP expression was strongly induced in LV cardiomyocytes coinciding with regions of cellular hypoxemia and hibernation. The authors further demonstrated that reversal of hibernation was accompanied by downregulation of myocardial BNP expression to control levels[468].

Based on this prior research and the current results, one may speculate that the ischemic but viable hibernating myocardium is doubly stressed with additional hemodynamic stimulus, thus further increasing the biomarker levels in the circulation. Further research is required to support this hypothesis and to further understand the mechanisms for BNP and troponin release in patients with hibernating myocardium.

Study Limitations

The modest sample size is a limitation of the present study. However, our sample size is similar to other related studies in the field to date[458] and can alert the readers to further investigation in this field. A small sample size can pose a risk of overfitting of a logistic regression model. To address this potential limitation we also analyzed and displayed the data as

continuous variables.

The differences in hs-TnT and NT-proBNP levels for hibernating myocardium were significant and yielded promising AUC values in ROC analysis. The correlation between the level of hibernation with the level of hs-cTnT was significant with a reasonable r value of 0.57 and with the level of NT-proBNP showed a trend that did not reach statistical significance with a modest r value of 0.27 (Figure 2). These relationships were numerically better and statistically significant when patients with scar ≥10% were consider (r values of 0.73 and 0.45 respectively). However, as a post-hoc analysis, this should be interpreted with caution. Further studies are required to support these findings and are ongoing.

Another study limitation was the lack of direct patient outcomes, especially related to revascularization. This will be followed up separately in the future as part of an ongoing prospective trial[326] and is beyond of the scope of the current study.

Conclusion:

These data support the novel concept that both the presence and extent of LV hibernation influence NT-proBNP and hs-cTnT release in patients with ischemic HF and LV dysfunction, without influence from the extent of scar. This new insight puts these biomarkers in a new light in the setting of suspected ischemic HF. Future studies are needed to confirm these findings and to devise means to evaluate new strategies to complement current imaging approaches to identify patients who are most likely to benefit from revascularization.

Acknowledgments:

The authors express their gratitude to the patients who have enrolled in the study and to the hard

work of the research co-ordinator who has recruited the patients, Ermina Moga CCRP, Debra Williams RPN, the imaging and data analysis team: Jennifer Renaud, MSc, My-Linh Tran MSc and PET imaging team: May Aung CNMT, Kim Gardner CNMT, Pat Grant RN, Laurie Camrass RN and the biomarker analysis team.

Sources of Funding

Jason Zelt is an MD/PhD student supported in part by the Vanier Canada Graduate Scholarship, The University of Ottawa, and by a government/industry grant from the Ontario Research Fund (ORF RE07-021); (industry partners Lantheus Medical Imaging and Jubilant DraxImage).

Rob Beanlands is a Career Investigator supported by the Heart and Stroke Foundation of Ontario (HSFO) and is a Tier 1 Chair in Cardiac Imaging Research at the University of Ottawa and the Vered Chair in Cardiology at the University of Ottawa Heart Institute. Lisa Mielniczuk is a Mid-career Clinician Scientist supported by HSFO and a Tier 2 Chair in HF Research at the University of Ottawa.

This study was supported in part by Canadian Institute for Health Research (CIHR) Team Grant (IMAGE-HF; grant # CIF 99470), Genome Canada Grant (GAPP Program on Biomarker Discovery to PPL) and CIHR Project Grant on Novel Biomarkers and Target in HF (PPL).

Disclosures

RdK is a consultant for- and has received grant funding from Jubilant DraxImage. RdK receives revenues from Rubidium-82 generator technology licensed to Jubilant DraxImage, and from sales of FlowQuant software. RSB is or has been a consultant for- and has received grant funding

from GE Healthcare, Lantheus Medical Imaging, and Jubilant DraxImage. Roche Diagnostics Global is a partner with the Genome Canada grant to PPL.

Appendix E
Utility of Novel Cardiorenal Biomarkers in the Prediction and Early Detection of Congestive Kidney Injury Following Cardiac Surgery

Zelt *et al.* J Clin Med. 2018;7(12):540
doi:10.3390/jcm7120540

Authors: Jason G.E. Zelt MSc[a], Lisa M. Mielniczuk MD MSc[a,b], Peter P. Liu MD[b], Jean-Yves Dupuis MD[d], Sharon Chih MD PhD[b], Ayub Akbari MD MSc[c], Louise Y. Sun MD SM[d,e]

[a]Department of Cellular and Molecular Medicine, Faculty of Medicine, University of Ottawa, Ottawa, ON, Canada.
[b]Division of Cardiology, Department of Medicine, University of Ottawa Heart Institute, Ottawa, ON, Canada.
[c]Division of Nephrology, Department of Medicine, The Ottawa Hospital, Ottawa, ON, Canada.
[d]Division of Cardiac Anesthesiology, Department of Anesthesiology and Pain Medicine, University of Ottawa Heart Institute, Ottawa, ON, Canada.
[e]School of Epidemiology and Public Health, University of Ottawa, Ottawa, ON, Canada

Author Contributions

JGEZ: Performed statistical analysis and graphical representation, and wrote the manuscript.
LYS and LMM: Designed the study
All authors participated in data interpretation, critical revisions and approval of the manuscript.

Key words: cardiac surgery; biomarkers; right heart failure; congestive acute kidney injury; venous congestion

E.1.0 Abstract

Acute Kidney Injury (AKI) in the context of right ventricular failure (RVF) is thought to be largely congestive in nature. This study assessed the utility of biomarkers hs-cTnT, NT-proBNP and NGAL for prediction and early detection of congestive AKI (c-AKI) following cardiac surgery. This prospective nested case-control study, recruited 350 consecutive patients undergoing elective cardiac surgery requiring cardiopulmonary bypass. Cases were patients who developed 1) AKI 2) new or worsening RVF or 3) c-AKI. Controls were patients free of these complications. Biomarker levels were measured at baseline after anesthesia induction and immediately postoperatively. Patients with c-AKI had increased mean durations of mechanical ventilation, length of stay in hospital and in the intensive care unit ($p<0.01$). For prediction of c-AKI, baseline NT-proBNP yielded an AUC of 0.74 (95% CI, 0.60-0.89). For early detection of c-AKI, postoperative NT-proBNP yielded an AUC of 0.78 (0.66-0.91), postoperative hs-cTnT yielded an AUC of 0.75 (0.58-0.92), and Δhs-cTnT yielded an AUC of 0.80 (0.64-0.96). The addition of baseline creatinine to Δhs-cTnT improved the AUC to 0.87 (0.76-0.99), and addition of diabetes improved the AUC to 0.93 (0.88-0.99). Δhs-cTnT alone, or in combination with baseline creatinine or diabetes, detects c-AKI with high accuracy following cardiac surgery.

E.2.0 Introduction

Right ventricular failure (RVF) is associated with significant morbidity and mortality following cardiac surgery[469,470]. Acute RVF is present in up to 50% of patients with postoperative hemodynamic instability[471] and is associated with difficult separation from cardiopulmonary bypass (CPB)[472], up to 75% increase in operative mortality as well as poor late survival[473,474]. Acute kidney injury (AKI) is a common sequela of RVF, which further complicates the management of RVF and portends a worsening prognosis. AKI occurs in up to 30% of cardiac surgical patients, of whom 1-2% require renal replacement therapy[475,476]. Management of perioperative AKI is primarily focused on maintenance of renal perfusion pressure and treatment of hypovolemia[477,478]. However, in the presence of RVF, AKI worsens with fluid administration and improves only with fluid removal[470]. This congestive form of AKI (c-AKI) is both difficult to diagnose and treat, especially as the cause of c-AKI is often not readily apparent and it is difficult to diagnose using current clinical criteria. Current diagnosis of AKI relies on measures of glomerular filtration such as serum creatinine, which is insensitive and lags behind actual renal injury; leading to delayed diagnosis and unfavourable outcomes[479,480]. The paucity of early predictive biomarkers is one purported reason for the failure of recent prevention and treatment clinical trials for cardiac surgery induced AKI[481].

The pathogenesis of cardiac surgery induced AKI is multifactorial including many interrelated, and largely non-modifiable, injury pathways. However, venous congestion-induced AKI may potentially be reversed through diuretic and vasodilator based preventative and early treatment strategies. Contrary to popular belief, central venous pressure (CVP) is a poor indicator of circulating blood volume and fluid responsiveness[482,483]. Hence, there remains a need for better identification of patients who are most likely to benefit from early decongestive therapy.

Cardiac and renal biomarkers such as high sensitivity cardiac troponin T (hs-cTnT), N-Terminal Pro-B-Type Natriuretic Peptide (NT-proBNP), and neutrophil gelatinase-associated lipocalcin (NGAL) are excellent prognosticators in patients with RVF and/or AKI[449,484–490]. These biomarkers provide direct cellular insight into cardiorenal physiology and may enable early identification of patients who are already in a congestive state prior to development of clinical consequences of venous congestion. However, the timing and pattern of release of these biomarkers are unknown in the setting of c-AKI with an acutely failing right ventricle (RV). An in-depth understanding of these biomarker patterns may enable identification of high-risk patients for intensive monitoring and early treatment. The objective of this study was to evaluate the utility of NT-proBNP, hs-cTnT, and NGAL for prediction and early detection of c-AKI following cardiac surgery.

E.3.0 Methods

The research ethics board of the University of Ottawa Heart Institute (UOHI) approved this prospective nested case-control study. Written informed consent was obtained from all participants prior to enrolment.

E.3.1 Patients

We recruited 350 consecutive consenting patients aged 18 years or older, who underwent major elective cardiac surgery requiring CPB at UOHI between September 29, 2015 and February 21, 2017. Exclusion criteria included end stage renal disease (glomerular filtration rate [GFR] <15mL/min or dialysis dependence), history of renal transplantation, solitary kidney, emergent operative status, off pump procedures, procedures involving circulatory arrest, heart transplantation, and left ventricular assist device implantation.

E.3.2 Outcomes

The primary outcome was c-AKI, defined by AKI in the presence of postoperative RVF (Supplemental Table 1). The secondary outcomes were non-congestive AKI, RVF, duration of mechanical ventilation, intensive care unit (ICU) and hospital lengths of stay and in-hospital mortality. AKI was defined by the Acute Kidney Injury Network (AKIN) criteria[491] as >50% relative or >26 μmol/L absolute rise in serum creatinine above preoperative value within 48 hours of surgery, or new onset dialysis. Postoperative RVF was defined as new or worsening RVF satisfying published criteria A and/or B[492,493] post separation from CPB and until postoperative day 2 (Supplemental Table 1). Pulmonary artery catheterization is practiced routinely for patients undergoing cardiac surgery at our institution.

A. Combined Clinical and Echocardiographic:[493,494]

i. Difficult separation from CPB, characterized by

1. Concurrent use of ≥1 vasopressor and ≥1 inotrope or ≥1 pulmonary vasodilator (i.e. nitric oxide or epoprostenol); or
2. More than one CPB weaning attempt; or
3. Mechanical support device (i.e., RV assist device); and

ii. >20% relative reduction in RV fractional area change measured by two-dimensional echocardiography.

B. Hemodynamic criteria:

i. CVP >18 mmHg or cardiac index < 1.8 L/min/m^2, in the absence of elevated left atrial and pulmonary capillary wedge pressure >18 mmHg, tamponade, ventricular arrhythmias or pneumothorax; and

ii. RV stroke work index <4 g.min^{-1}.m^2. RVSWI = 0.136 x SVI x (mPAP – RAP); where SVI = stroke volume index = stroke volume/body surface area, mPAP = mean pulmonary artery pressure, and RAP = right atrial pressure.

E.3.3 Cases and Controls

Cases were defined as patients with postoperative RVF, c-AKI or non-congestive AKI. Controls were patients who were free of these complications during the follow up period. Controls were 1:1 matched to the cases based on age and sex. All patients received routine standard of care during the study period.

E.3.4 Study Procedures

All patients were followed prospectively until hospital discharge. Baseline patient characteristics, operative data and postoperative outcomes were recorded by trained research staff. The attending anesthesiologist recorded baseline RV function, and whether difficulty was encountered with CPB separation. Baseline RV function was recorded from the most recent echocardiogram within 90 days of surgery in patients with stable cardiac disease, and during the index surgical admission or intraoperatively prior to CPB in patients who presented acutely.

Biomarkers

Biomarkers were sampled at baseline immediately following anesthesia induction and postoperatively within 1 hour of arrival to the ICU. In addition, serum creatinine was measured at least daily during the first 2 postoperative days. Biomarker samples were centrifuged and plasma supernatants stored at -80°C until analysis. Plasma hs-cTnT (Roche Diagnostics, Indianapolis, IN) and NT-proBNP (Roche Diagnostics) were measured using commercially available US food and Drug Administration-approved electrochemiluminescence immunoassays with a Roche Cobas e411 anaylzer. Manufacturer's normal reference value for hs-cTnT and NT-proBNP are <13.5 pg/mL (99th percentile) and <300 pg/mL, respectively[449,495]. NGAL levels were measured using a commercially available ELISA kit (Bioporto) and using a mean reference value in healthy volunteers of 35.4 (95% CI, 18.9-46.5) ng/mL[496].

E.3.5 Statistical Analysis

Statistical analyses and graphic representation were performed using SAS 9.4 (SAS Institute, Cary, NC) and Graphpad Prism 6.0 (Graphpad Software, San Diego, CA). Categorical characteristics were compared using X^2 or Fisher's exact test for categorical variables where

appropriate. Continuous variables were compared using Student's *t* test or Wilcoxon rank sum test depending on normality of distribution. An analysis of variance (ANOVA) was used to compare hospital and ICU stay and ventilation duration between groups. Log transformed NGAL, NT-proBNP and hs-cTnT were used because their distributions were not normal. A two-way, repeated measure ANOVA was used to compare the effects of time (pre-versus post surgery) and AKI/RVF status for all variables. A Bonferroni correction was used for post hoc pairwise comparison of means. We used conditional logistic regression to assess the association between individual biomarker levels and c-AKI, with and without adjustment for baseline estimated GFR (eGFR), diabetes, and surgery type. These covariates were selected *a priori* based on the strength of their known association with AKI and RVF in cardiac surgical patients[487,497]. As cases were already matched to controls based on age and sex, these covariates were not included in the model. Measure of association was odds ratio (OR) with associated 95% confidence interval (CI). In addition, linear regression was used to assess the association between biomarker levels and continuous outcomes such as length of hospital/ICU stay and duration of mechanical ventilation. The Pearson correlation coefficient was reported as measure of correlation. Area under (AUC) the receiver operator characteristic (ROC) curve was used to assess the ability of individual biomarkers to discriminate between patients who developed each of the outcomes vs. those who did not. Youden's index was used to identify the optimal ROC cutoff. We also evaluated the incremental value of these biomarkers when added to the clinical model using the method of Delong, Delong, and Clarke-Pearson[373]. $P < 0.05$ was considered statistically significant.

E.4.0 Results

Patient Characteristics

A total of 350 patients were enrolled in the study, from whom 89 cases were identified and age-sex matched to 89 controls (Supplemental Table E.2). Of the cases, 36 (40.5%) developed postoperative RVF, 35 (39.3%) developed non-congestive AKI, and 18 (20.2%) developed c-AKI. Baseline characteristics of c-AKI cases and controls are shown in Table E.1. Compared to matched controls, c-AKI patients were more likely to have pre-existing renal insufficiency, diabetes, and to undergo more complex surgery with longer CPB and aortic crossclamp durations. In addition, there was a trend towards higher baseline CVP and lower cardiac index in c-AKI patients. There were no differences in baseline left ventricle ejection fraction (LVEF) between c-AKI and controls.

Biomarker Analysis Pre And Post Cardiac Surgery

Patients who developed c-AKI had significantly higher baseline NT-proBNP levels compared to controls (Figure E.1A). In patients who developed non-congestive AKI, baseline NT-proBNP, NGAL and hs-cTnT were significantly higher than controls (Figure E.1A-C). Following surgery, NT-proBNP remained relatively unchanged while hs-cTnT and NGAL increased 2-2.5 fold in all groups (Figure E.1B and C). The magnitude of postoperative increase in hs-cTnT was highest in the c-AKI group. Postoperatively, NGAL increased in those who developed RVF but remained relatively unchanged in the AKI, c-AKI and control groups.

Table E.1: Characteristics of patients with congestive acute kidney injury (c-AKI) vs. controls.

	Control (n=89)	C-AKI (n=18)	P-value
Baseline Characteristics			
Male	61 (68.5%)	11 (61.1%)	0.54
Age (years)	66.0 (63.8-68.2)	67.1 (61.1-73.2)	0.57
Body Mass Index (kg/m^2)	28.5 (27.4-29.7)	30.5 (27.3-33.6)	0.35
eGFR (mL/min/1.73m^2)	89.8 (83.4-96.1)	75.2 (60.6-89.7)	0.03
Serum Creatinine (µmol/L)	84.3 (79.5-89.1)	100.7 (87.3-114.1)	0.009
Cardiac Index (L/min/m^2)	2.18 (2.03-2.33)	1.93 (1.66- 2.19)	0.08
Central Venous Pressure (mmHg)	13.9 (12.9-14.9)	16.6 (14.1-19.1)	0.06
Left Ventricle Ejection Fraction (%)	53.1 (51.4-54.9)	49.6 (44.3-54.8)	0.14
Comorbidities			
Hypertension	57 (64%)	12 (67%)	0.83
Diabetes	20 (22%)	12 (67%)	0.0002
COPD	8 (9%)	1 (6%)	1.0
Pre-existing Right Heart Dysfunction	1 (1.1%)	1 (6%)	0.31
Coronary Artery Disease	57 (64%)	11 (61%)	0.81
Medications			
ASA	54 (61%)	11 (62%)	0.97
Beta Blocker	59 (66%)	11 (62%)	0.67
ACE Inhibitor	50 (56%)	8 (44%)	0.36
Lipid Lowering agents	55 (62%)	11 (62%)	0.96
Intraoperative Characteristics			
Surgery Type			0.0006
CABG	43 (48%)	5 (28%)	
Single Valve	33 (37%)	3 (17%)	
Combined CABG/Valve/Other	13 (15%)	10 (56%)	
Cardiopulmonary Bypass Duration (min)	89.1 (82.1-96.0)	141.1 (114.5-167.7)	0.0002
Aortic Cross Clamp Duration (min)	64.6 (58.4-70.8)	102.1 (78.8-125.4)	0.003
Postoperative characteristics			
Length of Hospital Stay (days)	11.8 (9.5-14.1)	23.3 (14.2-32.4)	0.0001
Length of Intensive Care Unit Stay (days)	2.1 (1.3-2.8)	6.1 (3.4- 8.8)	<0.0001
Mechanical Ventilation Duration (hours)	9.7 (3.6-15.7)	63.0 (1.23-124.7)	<0.0001

eGFR, estimated glomerular filtration rate; CABG, coronary artery bypass graft; COPD, chronic obstructive pulmonary disease; ASA, Acetysalicylic acid; ACE, angiotensin-converting-enzyme
Data presented are expressed as n (%) or mean (95% confidence interval).

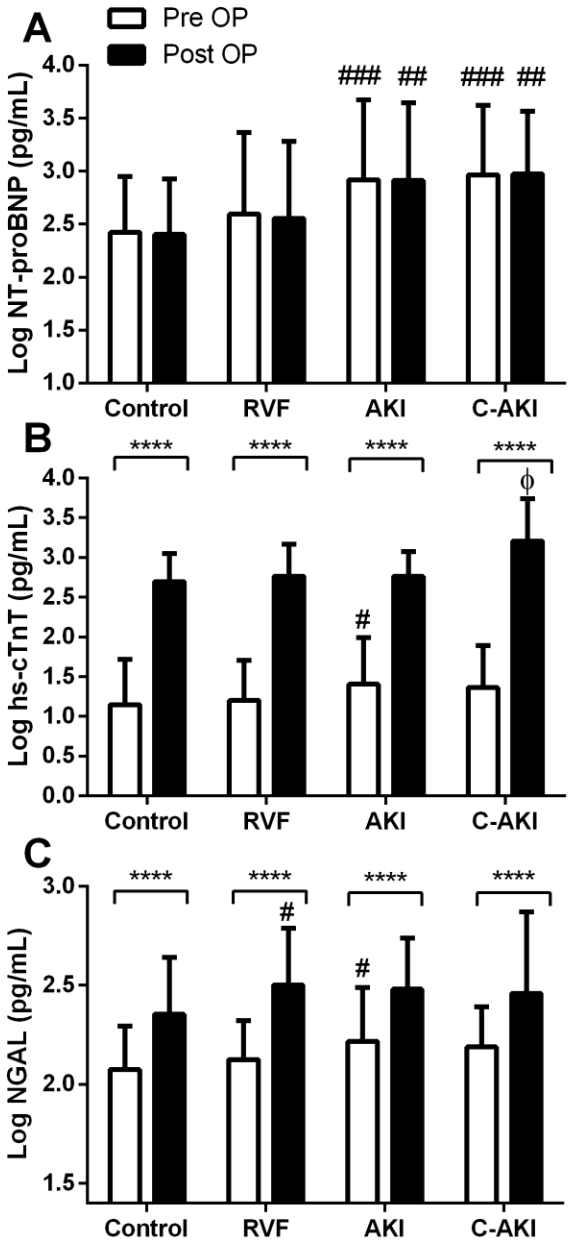

Figure E.1. Baseline and postoperative biomarker levels in patients who developed congestive acute kidney injury (c-AKI) vs. controls. *Within group differences (baseline vs postoperative) ****p<0.0001. #Significantly different than control p<0.05, ## p<0.01. Φ Significantly different than control, right ventricular failure (RVF) and AKI, P<0.05.

Hemodynamics Pre And Post Cardiac Surgery

Compared to controls, patients who developed c-AKI had significantly lower cardiac index at all time points (Figure E.2A). Conversely, CVP decreased postoperatively from baseline in both c-AKI and control groups but remained higher in c-AKI patients throughout the postoperative period (Figure 2B). This trend was particularly evident on postoperative day 2 where CVP in c-AKI patients remained >1.5 fold higher than in the controls ($p<0.001$).

In patients with non-congestive AKI, a similar trend was observed where CVP was significantly elevated compared to controls throughout the follow up period (Supplemental Figure 1A). No significant differences in hemodynamic profiles were observed for patients who developed RVF vs. controls (Supplemental figure E.1 B and D).

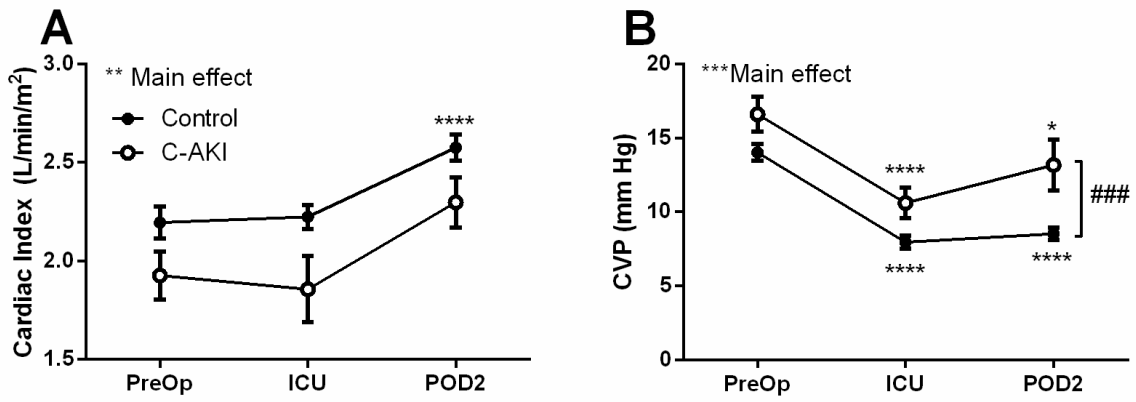

Figure E.2. **Cardiac index (A) and central venous pressure (B) in patients who developed congestive acute kidney injury (c-AKI) vs. controls**. Hemodynamic variables were assessed preoperatively, upon admission to the intensive care unit and on postoperative day two.
* Significantly different than baseline levels, P<0.05; **P<0.01; ***P<0.001; **** P<0.0001. ### Significant difference between c-AKI and control, P<0.001.

Biomarker and Hemodynamic Correlation

A weak positive relationship was observed between baseline log hs-cTnT and CVP (r=0.21, p=0.006). However, log NT-proBNP and log NGAL levels did not correlate with CVP at baseline. At baseline, cardiac index was inversely correlated with log NT-proBNP (r=-0.2, p=0.01) and log hs-cTnT (r=-0.19, p=0.01). In addition, there were weak-moderate inverse correlations between baseline eGFR and log hs-cTnT (r=-0.27, p=0.0002), log NT-proBNP (r=-0.37, p<0.0001), and log NGAL (r=-0.28, p<0.0001). Postoperatively, a positive correlation was observed between log NT-proBNP and CVP (r=0.20, p=0.007), but no correlations were found between cardiac index and biomarkers.

Performance of Biomarkers vs. Traditional Parameters for c-AKI Prediction and Detection

Prediction of c-AKI

Higher baseline CVP was associated with c-AKI after multivariable adjustment (adjusted OR 1.20, 95% CI 1.04-1.38 for each 1mmHg increase in CVP) (Table E.2).

Table E.3 and Figure E.3 summarize the AUCs for individual biomarkers and traditional parameters for prediction of c-AKI. Of the baseline biomarkers, NT-proBNP had the highest AUC for predicting c-AKI (0.74, 95% CI 0.60-0.89). However, the clinical model alone (based on baseline eGFR, diabetes and surgery type) had an AUC of 0.83 (0.72-0.94), and the addition of NT-proBNP to the clinical model did not significantly improve the AUC (p=0.39, Table E.3). The optimal cut-off of baseline NT-proBNP for c-AKI prediction was > 476 pg/mL (sensitivity 77%, specificity 72%) (Table E.4).

Table E.2: Association between cardiorenal biomarkers and congestive acute kidney injury

	Unadjusted		Adjusted[a]	
	OR (95% CI)	P value	OR (95% CI)	P value
Baseline				
NGAL	1.37 (1.05-1.78)	0.02	1.19 (0.88-1.61)	0.25
NT-proBNP	1.17 (1.06-1.29)	0.001	1.10 (0.97-1.24)	0.12
hs-cTnT	1.06 (0.98-1.15)	0.15	0.99 (0.87-1.11)	0.81
CVP	1.12 (1.01-1.25)	0.03	1.20 (1.04-1.38)	0.01
Postoperative				
NGAL	1.11 (0.93-1.33)	0.25	1.02 (0.83-1.26)	0.86
NT-proBNP	1.21 (1.09-1.34)	0.0005	1.13 (1.00-1.29)	0.05
hs-cTnT	1.26 (1.10-1.45)	0.0009	1.22 (1.05-1.42)	0.008
CVP	1.17 (1.03-1.32)	0.01	1.15 (0.98-1.35)	0.09
Change (Postoperative - Baseline)				
ΔNGAL	1.23 (0.96-1.57)	0.09	1.26 (0.93-1.71)	0.13
ΔNT-proBNP	0.99 (0.96-1.03)	0.85	0.99 (0.94-1.05)	0.84
Δhs-cTnT	1.15 (1.07-1.24)	0.0002	1.25 (1.09-1.44)	0.001
ΔCVP	1.00 (0.91-1.10)	0.94	0.93 (0.83-1.04)	0.20

eGFR, estimated glomerular filtration rate; NGAL, neutrophil gelatinase-associated lipocalcin; NT-proBNP, N-Terminal Pro-B-Type Natriuretic Peptide; hs-cTNT, high sensitivity cardiac troponin T; CVP, central venous pressure; OR, odds ratio; CI, confidence interval.

[a]Biomarker models were adjusted for eGFR, diabetes and type of cardiac surgery.
Baseline and postoperative biomarker levels were log transformed. Odds ratios were expressed per 0.1 unit increase in log-transformed baseline and postoperative biomarker levels and per 100 pg/mL increase for Δbiomarker levels.

Table E.3 Areas under the Receiver-Operating Curve for the prediction of congestive acute kidney injury

	Unadjusted AUC (95% CI) Biomarker Only	[a]**Adjusted AUC (95%CI)** Biomarker + Clinical Model
Clinical Model	-	0.83 (0.72, 0.94)
Baseline		
NGAL	0.67 (0.51-0.82)	0.84 (0.73-0.95)
NT-proBNP	0.74 (0.60-0.89)	0.84 (0.75-0.94)
hs-cTnT	0.67 (0.53-0.81)	0.82 (0.71-0.94)
CVP	0.64 (0.50-0.78)	0.88 (0.80-0.96)
Postoperative		
NGAL	0.60 (0.43-0.77)	0.83 (0.72-0.94)
NT-proBNP	0.78 (0.66-0.91)	0.86 (0.76-0.96)
hs-cTnT	0.75 (0.58-0.92)	0.88 (0.80-0.96)
CVP	0.68 (0.55-0.81)	0.87 (0.80-0.95)
Change (Postoperative – Baseline)		
ΔNGAL	0.61 (0.42-0.79)	0.82 (0.72-0.93)
ΔNT-proBNP	0.69 (0.54-0.85)	0.83 (0.71-0.94)
Δhs-cTnT	0.80 (0.64-0.96)	*0.94 (0.89-0.99)
ΔCVP	0.49 (0.34-0.63)	0.84 (0.72-0.96)
Combined Model		
ΔHs-cTnT + Preoperative Creatinine	0.87 (0.76- 0.99)	-
ΔHs-cTnT + Diabetes	0.93 (0.88- 0.99)	-

eGFR, estimated glomerular filtration rate; NGAL, neutrophil gelatinase-associated lipocalcin; NT-proBNP, N-Terminal Pro-B-Type Natriuretic Peptide; hs-cTNT, high sensitivity cardiac troponin T; CVP, central venous pressure; AUC, area under the receiver operative characteristic curve; CI, confidence interval.

*Significantly improves AUC of the clinical model $p<0.05$.

[a]Biomarker models were adjusted for eGFR, type of cardiac surgery and diabetes.

Table E.4 Cutoff values for predicting congestive acute kidney injury

	Cutoff	Sensitivity	Specificity
Baseline			
NGAL (pg/mL)	140.2	64.7	69.7
NT-proBNP (pg/mL)	476.0	76.5	71.9
hs-cTnT (pg/mL)	25.0	47.1	84.3
CVP	15.5	61.1	67.8
Postoperative			
NGAL (pg/mL)	440.9	41.2	84.3
NT-proBNP (pg/mL)	599.5	72.2	79.5
hs-cTnT (pg/mL)	1089.0	66.7	84.1
CVP	10.5	44.4	84.3
Change (Postoperative-Baseline)			
ΔNGAL (pg/mL)	181.7	50.0	77.5
ΔNT-proBNP (pg/mL)	-38.8	76.5	62.5
Δhs-cTnT (pg/mL)	730.9	82.4	75.0
ΔCVP	-9.5	88.9	26.4

NGAL, neutrophil gelatinase-associated lipocalcin; NT-proBNP, N-Terminal Pro-B-Type Natriuretic Peptide; hs-cTNT, high sensitivity cardiac troponin T; CVP, central venous pressure.

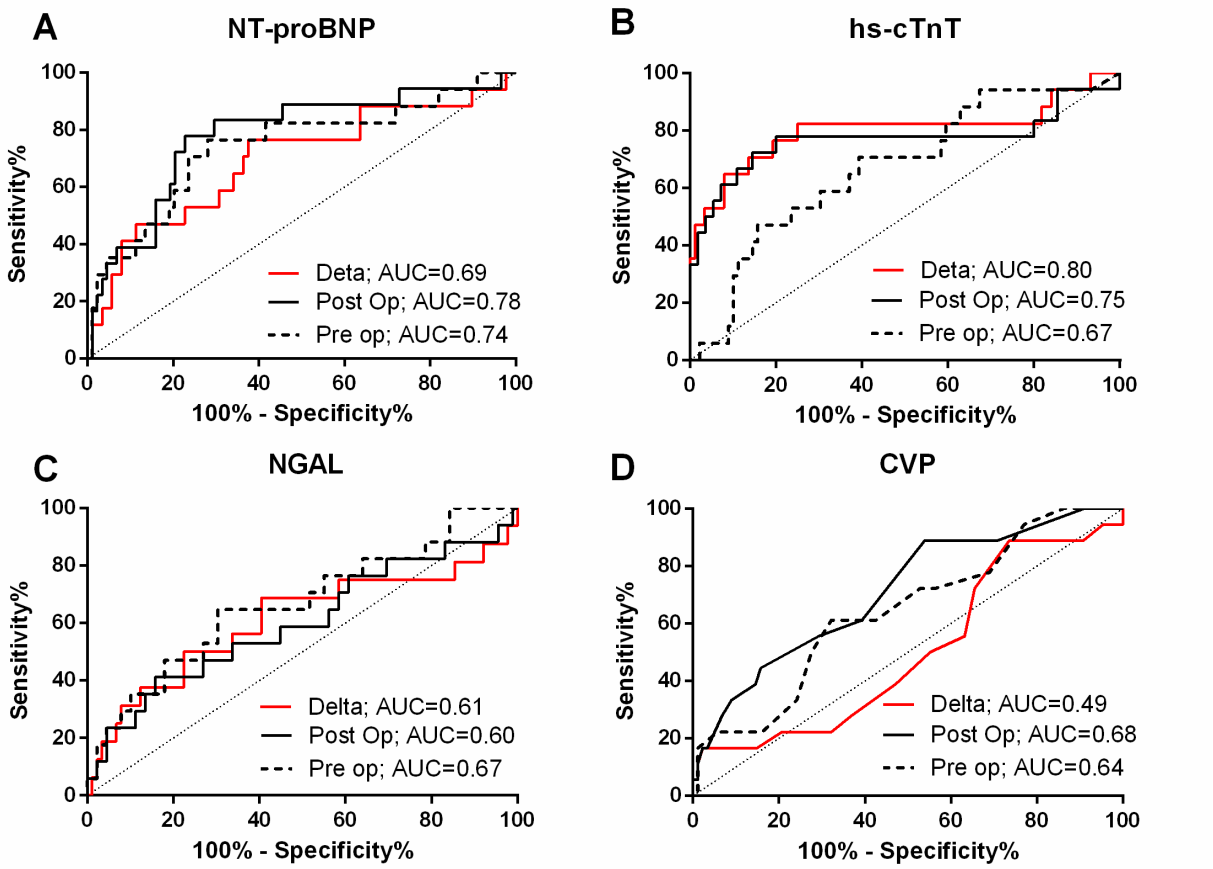

Figure E.3. Receiver operating characteristic curves for NT-proBNP (A) hs-cTnT (B), NGAL (C) and central venous pressure (D). Dotted lines are for baseline assessments, black lines are for postoperative assessments, and red lines are for change in levels (post-preoperative). AUC, area under the curve.

Early Detection of c-AKI

After adjusting for eGFR, diabetes and type of surgery, postoperative NT-proBNP and hs-cTnT remained robust in detecting c-AKI (Table E.2). Of note, postoperative CVP was not associated with c-AKI after risk adjustment.

ROC analysis (Table E.3, Figure E.3) revealed postoperative NT-proBNP and hs-cTnT as parameters with the highest AUCs for early detection of c-AKI after multivariable adjustment. Specifically, AUC for postoperative NT-proBNP was 0.78 (0.66-0.91) alone (optimal cutoff 599.5 pg/mL, sensitivity 72.2%, specificity 79.5%) and 0.86 (0.76-0.96) after risk adjustment (Table E.3). AUC for postoperative hs-cTnT was 0.75 (0.58-0.92) alone (optimal cutoff 1089.0 pg/mL, sensitivity 66.7%, specificity 84.1%) and 0.88 (0.80-0.96) after risk adjustment. Postoperative NGAL alone and CVP alone only yielded moderate AUCs for detecting c-AKI (0.60 for NGAL and 0.68 for CVP).

Perioperative Changes in Biomarker Levels

Change in hs-cTnT levels between baseline and the postoperative period was associated with c-AKI (Tables E.2 and E.3). Δhs-cTnT alone yielded an AUC of 0.8 (0.64-0.96) for c-AKI detection, and was the only biomarker that significantly increased the AUC of the clinical model. Specifically, the AUC was 0.87 (0.76-0.99) when Δhs-cTnT was combined with baseline creatinine, 0.93 (0.88-0.99) when combined with diabetes status, and 0.94 (0.89-0.99) when combined with the full clinical model (Table E.3). The optimal cutoff of Δhs-cTnT for detecting c-AKI was > 730.9 pg/mL (sensitivity 82%, specificity 75%; Table E.4). In contrast, the ability of ΔCVP to detect c-AKI was no better than a coin toss (AUC 0.49, 95% CI 0.34-0.63).

Sample Size Calculation

A post-hoc sample size calculation was performed to validate our findings in light of the size of our cohort. An AUC of 0.70 for biomarker prediction of post cardiac surgery AKI has been deemed clinically meaningful[498]. We conservatively chose a null hypothesis AUC of 0.75. To detect an AUC of 0.93 in our Δhs-cTnT + diabetes model, our observed 18 c-AKI cases and 89 controls yielded a 86% power using a two-sided z-test at an alpha of 0.05.

Secondary Outcomes

Supplemental Table E.3 summarizes the AUCs of biomarkers and CVP in predicting non-congestive AKI and postoperative RVF. At baseline, all three biomarkers had moderate accuracy for predicting non-congestive AKI (AUC 0.67 to 0.70). Postoperatively, NT-proBNP detected non-congestive AKI with moderate accuracy (AUC 0.72). ΔBiomarker levels and ΔCVP detected non-congestive AKI poorly (AUC ranging from 0.44-0.57). In contrast, none of the parameters predicted or detected RVF well (AUC 0.48-0.62).

During follow up, 3 (1.7%) patients died (2 c-AKI and 1 control) and 3 patients (1.7%) developed severe AKI requiring renal replacement therapy (2 c-AKI and 1 non-congestive AKI). Compared to controls, patients who developed c-AKI had significantly longer hospitalization, ICU length of stay and duration of mechanical ventilation (Table E.1, Figure E.4). Non-congestive AKI was associated longer periods of ICU stay and mechanical ventilation compared to controls. In contrast, there were no differences in observed outcomes for patients who developed postoperative RVF alone (Figure E.4).

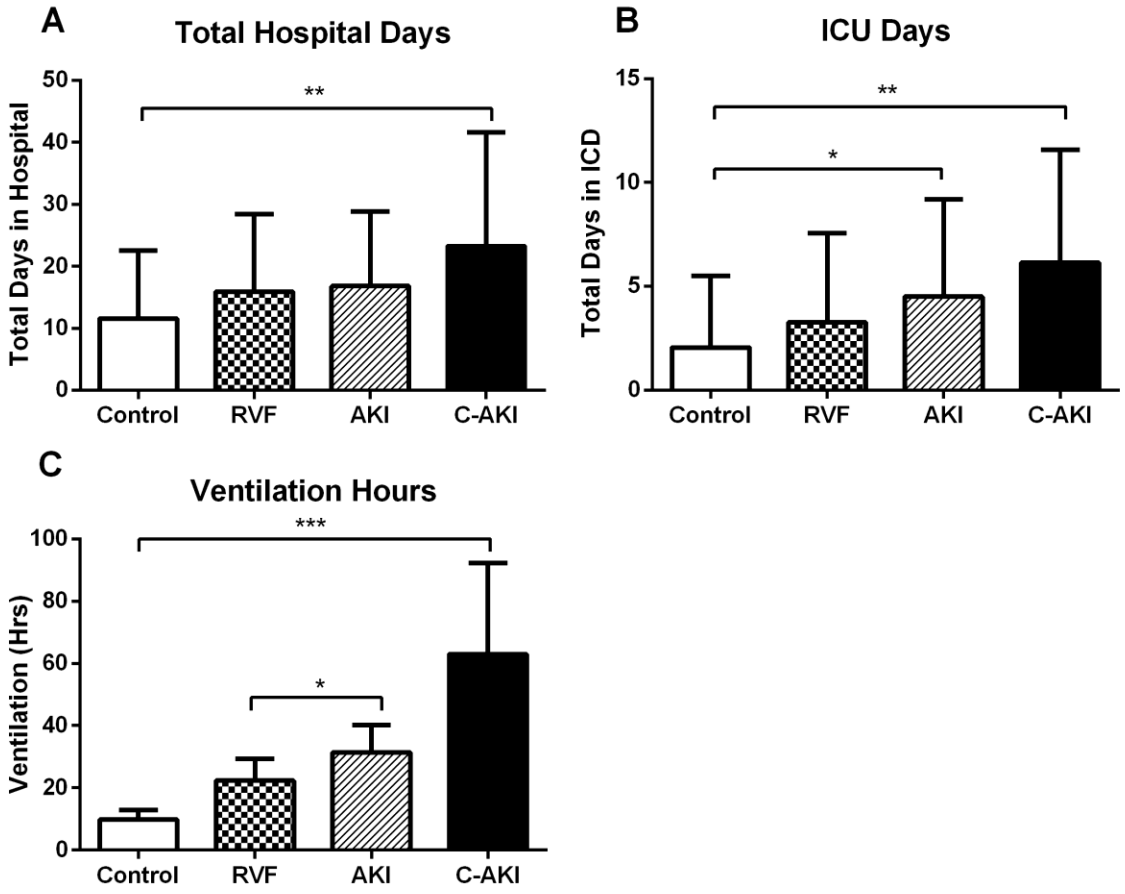

Figure E.4. Lengths of stay in hospital (A) and ICU (B) and duration of mechanical ventilation (C) in patients who developed postoperative acute kidney injury (AKI), right ventricular failure (RVF), congestive AKI (c-AKI) and controls. Data expressed mean +/- SD. *P<0.05, **P<0.01, ***P<0.001.

E.5.0 Discussion

This prospective nested case-control study found cardiac biomarkers hs-cTnT and NT-proBNP to be stronger predictors of c-AKI following cardiac surgery than the renal biomarker NGAL. Four major findings were derived from this study. 1) We identified the novel concept of c-AKI as a cardiorenal syndrome in the context of RVF. C-AKI was associated with prolonged mechanical ventilation and length of stay in hospital and ICU. 2) A single measurement of NT-proBNP or hs-cTnT predicted and detected c-AKI with higher accuracy than the traditional measure of venous congestion by CVP. Specifically, baseline and postoperative NT-proBNP yielded AUCs of 0.74 and 0.78, postoperative hs-cTnT yielded an AUC of 0.75, and baseline and postoperative CVP yielded AUCs of 0.64 and 0.68, respectively. 3) Δhs-cTnT alone yielded an AUC of 0.80 for c-AKI, and the addition of diabetes increased the AUC to 0.93. 4) Neither the cardiorenal biomarkers, clinical variables, nor CVP were able to predict postoperative RVF well.

A New AKI Phenotype

Our study is novel in our definition and characterization of a congestive subtype of AKI. We found that c-AKI was associated with a higher burden of postoperative morbidity and healthcare cost than non-congestive AKI or RVF alone. The etiology of cardiac surgery-associated AKI is multifactorial involving many non-modifiable risk factors such as ischemic-reperfusion injury, inflammation and oxidative stress[481]. Unlike other AKI subtypes, c-AKI is potentially preventable and treatable, although it is often difficult to detect at an early stage. Our findings offer new insights on the role of biomarkers in the prediction and early detection of c-AKI and represent a critical first step towards characterizing postoperative c-AKI. Determining whether a biomarker-

guided approach can complement current prediction, prevention and timely management strategies in the perioperative period is an important area for future investigation.

Venous Congestion and CVP

Our study is the first to prospectively characterize postoperative c-AKI with serial cardiac and renal biomarkers. Although several studies have evaluated the utility of similar biomarkers for AKI risk stratification in cardiac surgery cohorts[481,484,487,497,499], none has focused on c-AKI, which is truly a cardiorenal syndrome. AKI in the context of RVF results from a complex series of cardiorenal interactions. This interaction has been believed to be primarily due to renal hypoperfusion[500], but recent evidence suggests venous congestion as a primary contributor[239,482,501,502]. Transrenal perfusion pressure is calculated as the mean arterial pressure minus the CVP. Clinically, in patients with acute decompensated heart failure and volume overload, the combination of low systemic pressure with elevated CVP may impair renal perfusion[503,504]. In a study of 145 patients admitted with acute decompensated heart failure, and using CVP as a surrogate for systemic venous congestion, Mullens *et al* demonstrated that patients with low CVP (<8 mmHg) experienced significantly less decline in renal function compared to those with high CVP (>24 mmHg), independent of their cardiac index[239]. Similarly, we demonstrated that patients who developed postoperative c-AKI had elevated CVP at baseline that persisted into the postoperative period. In further support of a congestive etiology, those who developed c-AKI had LVEFs that were statistically similar to the controls and may benefit from perioperative decongestive strategies. The success of such strategies requires accurate and timely identification of venous congestion, as accumulating evidence suggests a poor correlation between CVP and circulating blood volume and an inability of CVP or ΔCVP to predict fluid

responsiveness (ROC AUC value of 0.56)[288,483]. Our study corroborates these findings. Specifically, CVP detected c-AKI poorly (AUC = 0.64 for baseline CVP and AUC = 0.49 for ΔCVP). In contrast, biomarkers of cardiac function and distention (NT-proBNP) and myocardial injury (hs-cTnT) were superior to CVP for predicting and detecting c-AKI.

Congestive AKI and Cardiorenal Biomarkers

NT-proBNP and hs-cTnT are well-established prognosticators in stable and acute decompensated heart failure. NT-proBNP is a prohormone secreted by the atria and ventricles in response to volume and pressure overload. In patients with pulmonary hypertension, NT-proBNP has been shown to increase in proportion to the degree of RV distension and wall stress; whereas hs-cTnT levels increase in proportion to the severity of RV dysfunction[489,490,505]. Several studies have evaluated whether baseline and postoperative BNP could predict cardiac surgery-associated AKI with mixed results (AUC range 0.60 to 0.86)[487,498,499]. To our knowledge, only two studies have evaluated the relationship between hs-cTnT and AKI in the perioperative setting.[497,498] One study reported similar hs-cTnT and NT-proBNP changes in a pediatric cohort to those observed in our adult cohort. In addition, these authors found baseline and postoperative biomarker levels were weakly predictive of AKI (AUC for hs-cTnT: baseline 0.57, post 0.62; AUC for NT-proBNP: pre 0.53, post 0.57)[498]. Our study adds to this knowledge by evaluating the same biomarkers to predict RVF, c-AKI and non-congestive AKI in adult patients. We demonstrate NT-proBNP and hs-cTnT as excellent potential biomarkers for postoperative c-AKI, but poor predictors of isolated RVF. This observation may be explained by two mechanisms. First, potential etiologies for perioperative RVF are diverse, including myocardial ischemia due to poor myocardial preservation[506], graft occlusion, or air emboli[507]. Some of these events are unanticipated complications of CPB and

surgery and cannot be predicted using biomarkers or conventional means[508,509]. Second, c-AKI is the end organ manifestation of longer and more severe episodes of perioperative RVF. In our study, there was a positive correlation between hs-cTnT and CPB duration ($r=0.44$, $p<0.0001$). Higher postoperative hs-cTnT levels (and thus higher Δhs-cTnT) were likely secondary to complex surgery requiring prolonged CPB with prolonged myocardial ischemia that was possibly compounded by suboptimal myocardial preservation. In addition, prolonged RV ischemia and infarction leading to end organ complications are more likely with complex cardiac procedures. Future studies are needed to fully elucidate mechanisms responsible for hs-cTnT release in c-AKI and congestive states.

Secondary Outcomes

In the cardiac surgical setting, elevated pre and postoperative NT-proBNP and hs-TnT levels have been shown to be associated with prolonged ICU length of stay, mechanical ventilation and postoperative inotropic support[499,510–513]. We showed higher preoperative hs-cTnT and postoperative NT-proBNP were associated with increased duration of mechanical ventilation, hospital and ICU stay.

Clinical Implications

Our findings have important implications for the optimization of patients who may be at high-risk for developing postoperative c-AKI. This is especially important, as unlike its non-congestive counterpart, c-AKI may improve with diuretic, vasodilator therapies and inotropic support[239,482]. Although both baseline and postoperative NT-proBNP levels were associated with c-AKI, baseline biomarker level may be of greater practical importance as it allows for a greater

window of opportunity for preoperative optimization by postponing non-emergent surgery for decongestive therapy. We in addition demonstrated a high AUC of 0.93 (95% CI 0.88-0.99) when combining Δhs-cTnT and diabetes for the early detection of c-AKI in the immediate postoperative period, days before the confirmation of c-AKI by serum creatinine using the traditional AKIN definition. When adjusted for diabetes, each 100 pg/ml increase in Δhs-cTnT is associated with a 23% increased odds of c-AKI (adjusted OR 1.23, 95% 1.10-1.38). In addition, 37% of diabetic patients who had Δhs-cTnT values above the cutoff developed c-AKI, where as none of the non-diabetic patients with Δhs-cTnT values below cutoff developed c-AKI. This simple model helps to efficiently identify a high-risk group that is most likely to benefit from future clinical trials of intensive perioperative monitoring and targeted therapy including fluid restriction, decongestion and inotropic support. The feasibility of these biomarker-guided trials is enhanced by the availability of NT-proBNP and hs-cTnT as accurate and affordable point of care assays that could be easily and rapidly implemented at the bedside or preoperative assessment clinics[514,515]. Significant progress has been made in the development of these point of care assays, with newer generations demonstrating comparable diagnostic accuracy as high sensitivity core-laboratory assays[514,515].

Study Limitations

This study has several limitations. Firstly, it is single center in nature. However, we recruited a representative sample of patients undergoing all major cardiac surgery, and our sample size was similar to that from other studies in the field. Secondly, c-AKI was a relatively rare event, and the small event rate limited our ability to explore the additive predictive value of biomarkers in more comprehensive clinical models. Thirdly, the number of patients experiencing dialysis or

death in our study was low, limiting our ability to evaluate the association of biomarkers with these outcomes.

Conclusions

Our study findings support hs-cTnT and NT-proBNP as potential biomarkers for prediction of a highly morbid subtype of postoperative AKI that occurs with RVF. Baseline and postoperative NT-proBNP, postoperative hs-cTnT and Δhs-cTnT had excellent AUCs for the prediction and early detection of c-AKI. Importantly, the addition of diabetes status to Δhs-cTnT further increased accuracy for detecting c-AKI. Our findings provide novel insights into cardiorenal physiology in the perioperative setting and may be used to monitor response to goal-directed decongestive therapy in clinical trials to mitigate c-AKI. In addition, the relatively rare incidence of postoperative c-AKI identified in our study highlights the importance of using biomarker models (i.e., Δhs-cTnT + diabetes) to identify high-risk patients for future interventional studies.

Author Contributions:

L.Y.S. and L.M.M designed the study; L.Y.S. acquired the data; J.G.E.Z and L.Y.S. analyzed the data and drafted the manuscript; all authors participated in data interpretation, critical revision and approval of the manuscript.

Sources of Funding: We acknowledge operating support from the Ottawa Region for Advanced Cardiovascular Research Excellence (Grant #4529) and in-kind support from the Division of Cardiac Anesthesiology, University of Ottawa Heart Institute. Jason Zelt is an MD/PhD student at the University of Ottawa Funded in part by Vanier Canada Graduate Scholarship and the University of Ottawa. Dr. Mielnicuk is supported by an award from the Heart and Stroke Foundation of Ontario. The funders do not have a role in the design and conduct of the study, in

the collection, analysis, and interpretation of the data, nor in the preparation, review, or approval of the manuscript.

Disclosures: none

E.6.0 Supplemental Material

Supplemental Table E.1. Diagnostic criteria for primary and secondary outcomes

Non-Congestive AKI	Right Ventricular Failure[493,494]	Congestive AKI
(AKIN) criteria: 1) >50% relative or >26 µmol/L absolute rise in serum creatinine above preoperative value within 48 hours of surgery	*C. Combined Clinical and Echocardiographic:* i. Difficult separation from CPB, characterized by 4. Concurrent use of ≥1 vasopressor and ≥1 inotrope or ≥1 pulmonary vasodilator (i.e. nitric oxide or epoprostenol); or 5. More than one CPB weaning attempt; or 6. Mechanical support device (i.e., RV assist device); and ii. >20% relative reduction in RV fractional area change measured by two-dimensional echocardiography.	Meets criteria for non-Congestive AKI and RVF
OR	AND/OR	
2) New onset dialysis within 48 hours of surgery	*D. Hemodynamic criteria:* i. CVP >18 mmHg or cardiac index < 1.8 L/min/m^2, in the absence of elevated left atrial and pulmonary capillary wedge pressure >18 mmHg, tamponade, ventricular arrhythmias or pneumothorax; and ii. RV stroke work index <4 $g.min^{-1}.m^2$. RVSWI = 0.136 x SVI x (mPAP – RAP).	

AKI, acute kidney injury; RVF, right ventricular failure; CVP, central venous pressure; RVSWI, right ventricle stroke work index; SVI, Stroke Volume Index (stroke volume/body surface area); mPAP, mean pulmonary artery pressure; RAP, right atrial pressure

Supplemental Table E.2. Characteristics of cases vs. controls.

	Control (n=89)	C-AKI (n=18)	AKI (n=35)	RHF (n=36)	P-Vale
Baseline Characteristics					
Male	61 (68.5%)	11 (61.1%)	25 (71.1%)	25 (69.4%)	0.89
Age (years)	66.0 (63.8-68.2)	67.1 (61.1-73.2)	68.5 (65.2—71.7)	67.4 (63.9-70.7)	0.69
Body Mass Index (kg/m^2)	28.5 (27.4-29.7)	30.5 (27.3-33.6)	33.0 (26.9-39.1)	29.6 (27.8- 31.5)	0.14
eGFR (mL/min/1.73m^2)	89.8 (83.4-96.1)	75.2 (60.6-89.7)	82.4 (71.4-93.4)	89.9 (76.0-103.7)	0.29
Serum Creatinine (μmol/L)	84.3 (79.5-89.1)	100.7 (87.3-114.1)	102.5 (86.8-118.3)	90.1 (80.0-100.2)	0.02
Cardiac Index (L/min/m^2)	2.18 (2.03-2.33)	1.93 (1.66- 2.19)	2.11 (1.93-2.28)	2.14 (1.92-2.36)	0.52
Central Venous Pressure (mmHg)	13.9 (12.9-14.9)	16.6 (14.1-19.1)	15.8 (14.1-17.5)	15.3 (14.0-16.6)	0.06
Left Ventricle Ejection Fraction (%)	53.1 (51.4-54.9)	49.6 (44.3-54.8)	50.4 (46.3-54.5)	51.4 (47.8-55.1)	0.37
Comorbidities					
Hypertension	57 (64%)	12 (67%)	27 (71%)	26 (72%)	0.55
Diabetes	20 (22%)	12 (67%)	18 (51%)	17 (47%)	0.0002
COPD	8 (9%)	1 (6%)	5 (14%)	6 (17%)	0.49
Pre-existing Right Heart Dysfunction	1 (1.1%)	1 (6%)	0 (0%)	1 (2.8%)	0.45
Coronary Artery Disease	57 (64%)	11 (61%)	22 (62%)	23 (64%)	0.99
Medications					
ASA	54 (61%)	11 (62%)	23 (66%)	26 (72%)	0.66
Beta Blocker	59 (66%)	11 (62%)	29 (83%)	25 (69%)	0.26
ACE Inhibitor	50 (56%)	8 (44%)	24 (69%)	19 (53%)	0.34
Lipid Lowering agents	55 (62%)	11 (62%)	26 (74%)	27 (75%)	0.36
Intraoperative Characteristics					
Surgery Type					
CABG	43 (48%)	5 (28%)	12 (34%)	11 (31%)	0.005
Single Valve	33 (37%)	3 (17%)	10 (29%)	11 (31%)	
Combined CABG/Valve/Other	13 (15%)	10 (56%)	13 (37%)	14 (39%)	
Cardiopulmonary Bypass Duration (min)	89.1 (82.1-96.0)	141.1 (114.5-167.7)	116.8 (99.7-133.9)	114.4 (100.5-128.3)	<0.0001
Aortic Cross Clamp Duration (min)	64.6 (58.4-70.8)	102.1 (78.8-125.4)	82.1 (69.2-95.0)	87.4 (74.3-100.4)	<0.0001

Postoperative characteristics					
Length of Hospital Stay (days)	11.8 (9.5-14.1)	23.3 (14.2-32.4)	17.4 (13.4-21.4)	16.1 (12.0-20.3)	0.002
Length of Intensive Care Unit Stay (days)	2.1 (1.3-2.8)	6.1 (3.4- 8.8)	4.7 (3.1-6.2)	3.3 (1.9-4.7)	0.0002
Mechanical Ventilation Duration (hours)	9.7 (3.6-15.7)	63.0 (1.23-124.7)	32.9 (15.0-50.9)	22.8 (8.7-36.8)	0.001

eGFR, estimated glomerular filtration rate; CABG, coronary artery bypass graft; COPD, chronic obstructive pulmonary disease; ASA, Acetysalicylic acid (Aspirin); ACE, angiotensin-converting-enzyme.

Supplemental Table E.3 ROC analysis: Area under the Receiver-Operating Characteristic curve values for the prediction of non-congestive acute kidney injury and right ventricular failure.

	Non-Congestive AKI AUC (95% CI)	Right Ventricular Failure AUC (95% CI)
Baseline		
NGAL	0.67 (0.56-0.78)	0.55 (0.43-0.66)
NT-proBNP	0.70 (0.58-0.82)	0.57 (0.45-0.69)
hs-cTnT	0.68 (0.56-0.79)	0.54 (0.43-0.65)
CVP	0.60 (0.48-0.71)	0.60 (0.49-0.70)
Postoperative		
NGAL	0.63 (0.53-0.74)	0.63 (0.52-0.74)
NT-proBNP	0.72 (0.60-0.84)	0.60 (0.44-0.69)
hs-cTnT	0.56 (0.45-0.67)	0.53 (0.41-0.64)
CVP	0.60 (0.49-0.71)	0.48 (0.37-0.59)
Change (Postoperative - Baseline)		
ΔNGAL	0.53 (0.41-0.66)	0.62 (0.51-0.74)
ΔNT-proBNP	0.44 (0.30-0.58)	0.53 (0.41-0.65)
Δhs-cTnT	0.57 (0.45-0.68)	0.52 (0.40-0.64)
ΔCVP	0.54 (0.42-0.65)	0.58 (0.48-0.68)

CVP, central venous pressure; neutrophil gelatinase-associated lipocalcin, NGAL; N-Terminal Pro-B-Type Natriuretic Peptide, NT-proBNP; hs-cTNT, high sensitivity cardiac troponin T

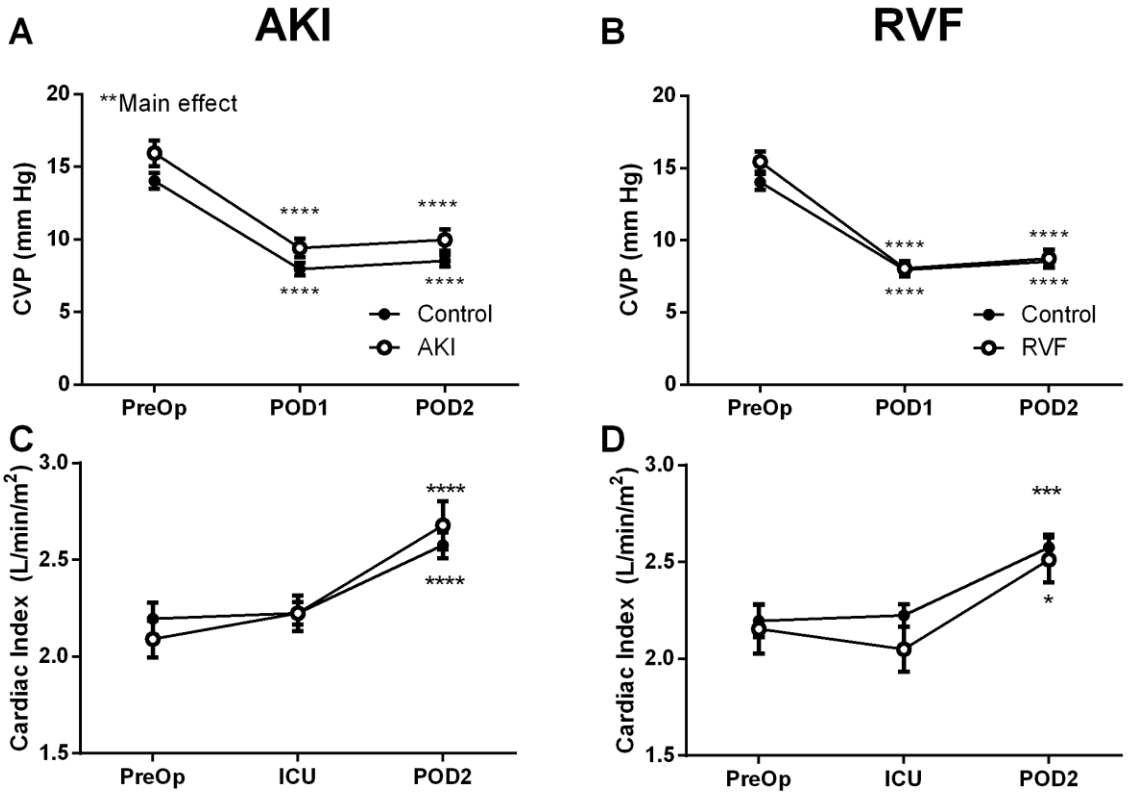

Supplemental Figure E.1. **Central venous pressure (A,B), and cardiac index (C/D), in patients who developed non-congestive acute kidney injury (AKI) or right ventricular failure (RVF) vs. controls.** Hemodynamic variables were assessed preoperatively, upon admission to ICU and on postoperative day two. * Significantly different than preoperative levels, P<0.05; **P<0.01; ***P<0.001; **** P<0.0001.

References

1. Vasan RS, Xanthakis V, Lyass A, Andersson C, Tsao C, Cheng S, Aragam J, Benjamin EJ, Larson MG. Epidemiology of Left Ventricular Systolic Dysfunction and Heart Failure in the Framingham Study: An Echocardiographic Study Over 3 Decades. *JACC Cardiovasc Imaging*. 2018;11:1–11.

2. van de Veerdonk MC, Kind T, Marcus JT, Mauritz G-J, Heymans MW, Bogaard H-J, Boonstra A, Marques KMJ, Westerhof N, Vonk-Noordegraaf A. Progressive Right Ventricular Dysfunction in Patients With Pulmonary Arterial Hypertension Responding to Therapy. *J Am Coll Cardiol*. 2011;58:2511–2519.

3. Srivastava D, Olson EN. A genetic blueprint for cardiac development. *Nature*. 2000;407:221–226.

4. Harvey RP. Organogenesis: Patterning the vertebrate heart. *Nat Rev Genet*. 2002;3:544–556.

5. Zaffran S, Kelly RG, Meilhac SM, Buckingham ME, Brown NA. Right Ventricular Myocardium Derives From the Anterior Heart Field. *Circ Res*. 2004;95:261–268.

6. Tan J, Silverman NH, Hoffman JI, Villegas M, Schmidt KG. Cardiac dimensions determined by cross-sectional echocardiography in the normal human fetus from 18 weeks to term. *Am J Cardiol*. 1992;70:1459–1467.

7. Firpo C, Hoffman JI, Silverman NH. Evaluation of fetal heart dimensions from 12 weeks to term. *Am J Cardiol*. 2001;87:594–600.

8. Hamill N, Yeo L, Romero R, Hassan SS, Myers SA, Mittal P, Kusanovic JP, Balasubramaniam M, Chaiworapongsa T, Vaisbuch E, Espinoza J, Gotsch F, Goncalves LF, Lee W. Fetal cardiac ventricular volume, cardiac output, and ejection fraction determined with 4-dimensional ultrasound using spatiotemporal image correlation and virtual organ computer-aided analysis. *Am J Obstet Gynecol*. 2011;205:76.e1-76.e10.

9. Hooper SB, te Pas AB, Lang J, van Vonderen JJ, Roehr CC, Kluckow M, Gill AW, Wallace EM, Polglase GR. Cardiovascular transition at birth: a physiological sequence. *Pediatr Res*. 2015;77:608–614.

10. Ryan JJ, Archer SL. The Right Ventricle in Pulmonary Arterial Hypertension: Disorders of Metabolism, Angiogenesis and Adrenergic Signaling in Right Ventricular Failure. *Circ Res*. 2014;115:176–188.

11. Ryan JJ, Huston J, Kutty S, Hatton ND, Bowman L, Tian L, Herr JE, Johri AM, Archer SL. Right ventricular adaptation and failure in pulmonary arterial hypertension. *Can J Cardiol*. 2015;31:391–406.

12. Kakouros NS, Kakouros SN. Clinical Assessment in Acute Heart Failure. *Hell J Cardiol HJC Hell Kardiologike Epitheorese*. 2015;56:285–301.

13. Benza R, Biederman R, Murali S, Gupta H. Role of Cardiac Magnetic Resonance Imaging in the Management of Patients With Pulmonary Arterial Hypertension. *J Am Coll Cardiol*. 2008;52:1683–1692.

14. Sanz J, Conroy J, Narula J. Imaging of the Right Ventricle. *Cardiol Clin*. 2012;30:189–203.

15. Forfia PR, Fisher MR, Mathai SC, Housten-Harris T, Hemnes AR, Borlaug BA, Chamera E, Corretti MC, Champion HC, Abraham TP, Girgis RE, Hassoun PM. Tricuspid annular displacement predicts survival in pulmonary hypertension. *Am J Respir Crit Care Med*. 2006;174:1034–1041.

16. Fijałkowska A, Torbicki A. Role of cardiac biomarkers in assessment of RV function and prognosis in chronic pulmonary hypertension. *Eur Heart J Suppl*. 2007;9:H41–H47.

17. Batkai S, Bär C, Thum T. MicroRNAs in right ventricular remodelling. *Cardiovasc Res*. 2017;113:1433–1440.

18. di Salvo TG, Yang K-C, Brittain E, Absi T, Maltais S, Hemnes A. Right ventricular myocardial biomarkers in human heart failure. *J Card Fail*. 2015;21:398–411.

19. Lewis GD, Ngo D, Hemnes AR, Farrell L, Domos C, Pappagianopoulos PP, Dhakal BP, Souza A, Shi X, Pugh ME, Beloiartsev A, Sinha S, Clish CB, Gerszten RE. Metabolic Profiling of Right Ventricular-Pulmonary Vascular Function Reveals Circulating Biomarkers of Pulmonary Hypertension. *J Am Coll Cardiol*. 2016;67:174–189.

20. Hoeper MM, Humbert M, Souza R, Idrees M, Kawut SM, Sliwa-Hahnle K, Jing Z-C, Gibbs JSR. A global view of pulmonary hypertension. *Lancet Respir Med*. 2016;4:306–322.

21. Hoeper MM, Bogaard HJ, Condliffe R, Frantz R, Khanna D, Kurzyna M, Langleben D, Manes A, Satoh T, Torres F, Wilkins MR, Badesch DB. Definitions and Diagnosis of Pulmonary Hypertension. *J Am Coll Cardiol*. 2013;62:D42–D50.

22. Assad TR, Maron BA, Robbins IM, Xu M, Huang S, Harrell FE, Farber-Eger EH, Wells QS, Choudhary G, Hemnes AR, Brittain EL. Prognostic Effect and Longitudinal Hemodynamic Assessment of Borderline Pulmonary Hypertension. *JAMA Cardiol*. 2017;2:1361.

23. Simonneau G, Robbins IM, Beghetti M, Channick RN, Delcroix M, Denton CP, Elliott CG, Gaine SP, Gladwin MT, Jing Z-C, Krowka MJ, Langleben D, Nakanishi N, Souza R. Updated Clinical Classification of Pulmonary Hypertension. *J Am Coll Cardiol*. 2009;54:S43–S54.

24. Simonneau G, Gatzoulis MA, Adatia I, Celermajer D, Denton C, Ghofrani A, Gomez Sanchez MA, Krishna Kumar R, Landzberg M, Machado RF, Olschewski H, Robbins IM, Souza R. Updated Clinical Classification of Pulmonary Hypertension. *J Am Coll Cardiol*. 2013;62:D34–D41.

25. Simonneau G, Montani D, Celermajer DS, Denton CP, Gatzoulis MA, Krowka M, Williams PG, Souza R. Haemodynamic definitions and updated clinical classification of pulmonary hypertension. *Eur Respir J*. 2019;53:1801913.

26. McLaughlin VV, Archer SL, Badesch DB, Barst RJ, Farber HW, Lindner JR, Mathier MA, McGoon MD, Park MH, Rosenson RS, Rubin LJ, Tapson VF, Varga J. ACCF/AHA 2009 Expert Consensus Document on Pulmonary Hypertension. *J Am Coll Cardiol*. 2009;53:1573–1619.

27. Farber HW, Miller DP, Poms AD, Badesch DB, Frost AE, Muros-Le Rouzic E, Romero AJ, Benton WW, Elliott CG, McGoon MD, Benza RL. Five-Year outcomes of patients enrolled in the REVEAL Registry. *Chest*. 2015;148:1043–1054.

28. Thenappan T, Shah SJ, Rich S, Tian L, Archer SL, Gomberg-Maitland M. Survival in pulmonary arterial hypertension: a reappraisal of the NIH risk stratification equation. *Eur Respir J*. 2010;35:1079–1087.

29. Benza RL, Gomberg-Maitland M, Miller DP, Frost A, Frantz RP, Foreman AJ, Badesch DB, McGoon MD. The REVEAL Registry risk score calculator in patients newly diagnosed with pulmonary arterial hypertension. *Chest*. 2012;141:354–362.

30. Humbert M, Morrell NW, Archer SL, Stenmark KR, MacLean MR, Lang IM, Christman BW, Weir EK, Eickelberg O, Voelkel NF, Rabinovitch M. Cellular and molecular pathobiology of pulmonary arterial hypertension. *J Am Coll Cardiol*. 2004;43:S13–S24.

31. Stacher E, Graham BB, Hunt JM, Gandjeva A, Groshong SD, McLaughlin VV, Jessup M, Grizzle WE, Aldred MA, Cool CD, Tuder RM. Modern Age Pathology of Pulmonary Arterial Hypertension. *Am J Respir Crit Care Med*. 2012;186:261–272.

32. Giaid A, Saleh D. Reduced expression of endothelial nitric oxide synthase in the lungs of patients with pulmonary hypertension. *N Engl J Med*. 1995;333:214–221.

33. Giaid A, Yanagisawa M, Langleben D, Michel RP, Levy R, Shennib H, Kimura S, Masaki T, Duguid WP, Stewart DJ. Expression of endothelin-1 in the lungs of patients with pulmonary hypertension. *N Engl J Med*. 1993;328:1732–1739.

34. Michelakis ED. Spatio-temporal diversity of apoptosis within the vascular wall in pulmonary arterial hypertension: heterogeneous BMP signaling may have therapeutic implications. *Circ Res*. 2006;98:172–175.

35. Zhao YD, Campbell AIM, Robb M, Ng D, Stewart DJ. Protective role of angiopoietin-1 in experimental pulmonary hypertension. *Circ Res*. 2003;92:984–991.

36. Kugathasan L, Dutly AE, Zhao YD, Deng Y, Robb MJ, Keshavjee S, Stewart DJ. Role of angiopoietin-1 in experimental and human pulmonary arterial hypertension. *Chest*. 2005;128:633S-642S.

37. Campbell AI, Zhao Y, Sandhu R, Stewart DJ. Cell-based gene transfer of vascular endothelial growth factor attenuates monocrotaline-induced pulmonary hypertension. *Circulation*. 2001;104:2242–2248.

38. Taraseviciene-Stewart L, Kasahara Y, Alger L, Hirth P, Mc Mahon G, Waltenberger J, Voelkel NF, Tuder RM. Inhibition of the VEGF receptor 2 combined with chronic hypoxia causes cell death-dependent pulmonary endothelial cell proliferation and severe pulmonary hypertension. *FASEB J Off Publ Fed Am Soc Exp Biol*. 2001;15:427–438.

39. Sakao S, Taraseviciene-Stewart L, Lee JD, Wood K, Cool CD, Voelkel NF. Initial apoptosis is followed by increased proliferation of apoptosis-resistant endothelial cells. *FASEB J Off Publ Fed Am Soc Exp Biol*. 2005;19:1178–1180.

40. Jones R, Jacobson M, Steudel W. alpha-smooth-muscle actin and microvascular precursor smooth-muscle cells in pulmonary hypertension. *Am J Respir Cell Mol Biol*. 1999;20:582–594.

41. Jeffery TK, Morrell NW. Molecular and cellular basis of pulmonary vascular remodeling in pulmonary hypertension. *Prog Cardiovasc Dis*. 2002;45:173–202.

42. Okada K, Tanaka Y, Bernstein M, Zhang W, Patterson GA, Botney MD. Pulmonary hemodynamics modify the rat pulmonary artery response to injury. A neointimal model of pulmonary hypertension. *Am J Pathol*. 1997;151:1019–1025.

43. Westöö C, Christian Norvik, Niccolò Peruzzi, Goran Lovric, Oscar van der Have, Ida Jeremiasen, Rajmund Mokso, Vinicio A De Jesus Perez, Hans Brunnström, Martin Bech, Csaba Galambos, Karin Tran-Lundmark. Distinct Types of Plexiform Lesions in Pulmonary Arterial Hypertension Identified by Synchrotron-Based Phase Contrast Micro-CT. *Circulation*. 2019;140:A15668.

44. Stenmark KR, Meyrick B, Galie N, Mooi WJ, McMurtry IF. Animal models of pulmonary arterial hypertension: the hope for etiological discovery and pharmacological cure. *AJP Lung Cell Mol Physiol*. 2009;297:L1013–L1032.

45. Nakayama Wong LS, Lamé MW, Jones AD, Wilson DW. Differential cellular responses to protein adducts of naphthoquinone and monocrotaline pyrrole. *Chem Res Toxicol*. 2010;23:1504–1513.

46. Kay JM, Harris P, Heath D. Pulmonary hypertension produced in rats by ingestion of Crotalaria spectabilis seeds. *Thorax*. 1967;22:176–179.

47. Huang J, Wolk JH, Gewitz MH, Mathew R. Progressive endothelial cell damage in an inflammatory model of pulmonary hypertension. *Exp Lung Res*. 2010;36:57–66.

48. Ramos M, Lamé MW, Segall HJ, Wilson DW. Monocrotaline pyrrole induces Smad nuclear accumulation and altered signaling expression in human pulmonary arterial endothelial cells. *Vascul Pharmacol*. 2007;46:439–448.

49. Urboniene D, Haber I, Fang Y-H, Thenappan T, Archer SL. Validation of high-resolution echocardiography and magnetic resonance imaging vs. high-fidelity catheterization in experimental pulmonary hypertension. *Am J Physiol Lung Cell Mol Physiol*. 2010;299:L401-412.

50. Wagner JG, Petry TW, Roth RA. Characterization of monocrotaline pyrrole-induced DNA cross-linking in pulmonary artery endothelium. *Am J Physiol*. 1993;264:L517-522.

51. Akhavein F, St-Michel EJ, Seifert E, Rohlicek CV. Decreased left ventricular function, myocarditis, and coronary arteriolar medial thickening following monocrotaline administration in adult rats. *J Appl Physiol Bethesda Md 1985*. 2007;103:287–295.

52. Gomez-Arroyo JG, Farkas L, Alhussaini AA, Farkas D, Kraskauskas D, Voelkel NF, Bogaard HJ. The monocrotaline model of pulmonary hypertension in perspective. *Am J Physiol Lung Cell Mol Physiol*. 2012;302:L363-369.

53. Handoko ML, de Man FS, Allaart CP, Paulus WJ, Westerhof N, Vonk-Noordegraaf A. Perspectives on novel therapeutic strategies for right heart failure in pulmonary arterial hypertension: lessons from the left heart. *Eur Respir Rev*. 2010;19:72–82.

54. van de Veerdonk MC, Kind T, Marcus JT, Mauritz G-J, Heymans MW, Bogaard H-J, Boonstra A, Marques KMJ, Westerhof N, Vonk-Noordegraaf A. Progressive Right Ventricular Dysfunction in Patients With Pulmonary Arterial Hypertension Responding to Therapy. *J Am Coll Cardiol*. 2011;58:2511–2519.

55. Clapp LH, Finney P, Turcato S, Tran S, Rubin LJ, Tinker A. Differential effects of stable prostacyclin analogs on smooth muscle proliferation and cyclic AMP generation in human pulmonary artery. *Am J Respir Cell Mol Biol*. 2002;26:194–201.

56. Tuder RM, Cool CD, Geraci MW, Wang J, Abman SH, Wright L, Badesch D, Voelkel NF. Prostacyclin synthase expression is decreased in lungs from patients with severe pulmonary hypertension. *Am J Respir Crit Care Med*. 1999;159:1925–1932.

57. Barst RJ, Rubin LJ, Long WA, McGoon MD, Rich S, Badesch DB, Groves BM, Tapson VF, Bourge RC, Brundage BH, Koerner SK, Langleben D, Keller CA, Murali S, Uretsky BF, Clayton LM, Jöbsis MM, Blackburn SD, Shortino D, Crow JW, Primary Pulmonary Hypertension Study Group. A comparison of continuous intravenous epoprostenol (prostacyclin) with conventional therapy for primary pulmonary hypertension. *N Engl J Med*. 1996;334:296–301.

58. McLaughlin VV, Benza RL, Rubin LJ, Channick RN, Voswinckel R, Tapson VF, Robbins IM, Olschewski H, Rubenfire M, Seeger W. Addition of inhaled treprostinil to oral therapy for pulmonary arterial hypertension: a randomized controlled clinical trial. *J Am Coll Cardiol*. 2010;55:1915–1922.

59. Tapson VF, Jing Z-C, Xu K-F, Pan L, Feldman J, Kiely DG, Kotlyar E, McSwain CS, Laliberte K, Arneson C, Rubin LJ, FREEDOM-C2 Study Team. Oral treprostinil for the treatment of pulmonary arterial hypertension in patients receiving background endothelin receptor antagonist and phosphodiesterase type 5 inhibitor therapy (the FREEDOM-C2 study): a randomized controlled trial. *Chest*. 2013;144:952–958.

60. Sitbon O, Channick R, Chin KM, Frey A, Gaine S, Galiè N, Ghofrani H-A, Hoeper MM, Lang IM, Preiss R, Rubin LJ, Di Scala L, Tapson V, Adzerikho I, Liu J, Moiseeva O, Zeng X, Simonneau G, McLaughlin VV. Selexipag for the Treatment of Pulmonary Arterial Hypertension. *N Engl J Med*. 2015;373:2522–2533.

61. Yanagisawa M, Kurihara H, Kimura S, Tomobe Y, Kobayashi M, Mitsui Y, Yazaki Y, Goto K, Masaki T. A novel potent vasoconstrictor peptide produced by vascular endothelial cells. *Nature*. 1988;332:411–415.

62. Rubin LJ, Badesch DB, Barst RJ, Galie N, Black CM, Keogh A, Pulido T, Frost A, Roux S, Leconte I, Landzberg M, Simonneau G. Bosentan therapy for pulmonary arterial hypertension. *N Engl J Med*. 2002;346:896–903.

63. Pulido T, Adzerikho I, Channick RN, Delcroix M, Galiè N, Ghofrani H-A, Jansa P, Jing Z-C, Le Brun F-O, Mehta S, Mittelholzer CM, Perchenet L, Sastry BKS, Sitbon O, Souza R, Torbicki A, Zeng X, Rubin LJ, Simonneau G, SERAPHIN Investigators. Macitentan and morbidity and mortality in pulmonary arterial hypertension. *N Engl J Med*. 2013;369:809–818.

64. Galiè N, Olschewski H, Oudiz RJ, Torres F, Frost A, Ghofrani HA, Badesch DB, McGoon MD, McLaughlin VV, Roecker EB, Gerber MJ, Dufton C, Wiens BL, Rubin LJ, Ambrisentan in Pulmonary Arterial Hypertension, Randomized, Double-Blind, Placebo-Controlled, Multicenter, Efficacy Studies (ARIES) Group. Ambrisentan for the treatment of pulmonary arterial hypertension: results of the ambrisentan in pulmonary arterial hypertension, randomized, double-blind, placebo-controlled, multicenter, efficacy (ARIES) study 1 and 2. *Circulation*. 2008;117:3010–3019.

65. Galiè N, Ghofrani HA, Torbicki A, Barst RJ, Rubin LJ, Badesch D, Fleming T, Parpia T, Burgess G, Branzi A, Grimminger F, Kurzyna M, Simonneau G, Sildenafil Use in Pulmonary Arterial Hypertension (SUPER) Study Group. Sildenafil citrate therapy for pulmonary arterial hypertension. *N Engl J Med*. 2005;353:2148–2157.

66. Galiè N, Brundage BH, Ghofrani HA, Oudiz RJ, Simonneau G, Safdar Z, Shapiro S, White RJ, Chan M, Beardsworth A, Frumkin L, Barst RJ, Pulmonary Arterial Hypertension and Response to Tadalafil (PHIRST) Study Group. Tadalafil therapy for pulmonary arterial hypertension. *Circulation*. 2009;119:2894–2903.

67. Ghofrani H-A, Galiè N, Grimminger F, Grünig E, Humbert M, Jing Z-C, Keogh AM, Langleben D, Kilama MO, Fritsch A, Neuser D, Rubin LJ, PATENT-1 Study Group. Riociguat for the treatment of pulmonary arterial hypertension. *N Engl J Med*. 2013;369:330–340.

68. Hoeper MM, Simonneau G, Corris PA, Ghofrani H-A, Klinger JR, Langleben D, Naeije R, Jansa P, Rosenkranz S, Scelsi L, Grünig E, Vizza CD, Chang M, Colorado P, Meier C, Busse D, Benza RL. RESPITE: switching to riociguat in pulmonary arterial hypertension patients with inadequate response to phosphodiesterase-5 inhibitors. *Eur Respir J*. 2017;50.

69. Fox BD, Shtraichman O, Langleben D, Shimony A, Kramer MR. Combination Therapy for Pulmonary Arterial Hypertension: A Systematic Review and Meta-analysis. *Can J Cardiol*. 2016;32:1520–1530.

70. Galiè N, Barberà JA, Frost AE, Ghofrani H-A, Hoeper MM, McLaughlin VV, Peacock AJ, Simonneau G, Vachiery J-L, Grünig E, Oudiz RJ, Vonk-Noordegraaf A, White RJ, Blair C, Gillies H, Miller KL, Harris JHN, Langley J, Rubin LJ, AMBITION Investigators. Initial Use of Ambrisentan plus Tadalafil in Pulmonary Arterial Hypertension. *N Engl J Med*. 2015;373:834–844.

71. Klinger JR, Elliott CG, Levine DJ, Bossone E, Duvall L, Fagan K, Frantsve-Hawley J, Kawut SM, Ryan JJ, Rosenzweig EB, Sederstrom N, Steen VD, Badesch DB. Therapy for Pulmonary Arterial Hypertension in Adults. *Chest*. 2019;155:565–586.

72. Sitbon O, Jaïs X, Savale L, Cottin V, Bergot E, Macari EA, Bouvaist H, Dauphin C, Picard F, Bulifon S, Montani D, Humbert M, Simonneau G. Upfront triple combination therapy in pulmonary arterial hypertension: a pilot study. *Eur Respir J*. 2014;43:1691–1697.

73. Chin KM, Sitbon O, Doelberg M, Gibbs JSSR, Hoeper MM, Martin N, Mathai SC, McLaughlin VV, Perchenet L, Simonneau G, Galiè N. Efficacy and Safety of Initial Triple Oral Versus Initial Double Oral Combination Therapy in Patients with Newly Diagnosed Pulmonary Arterial Hypertension (PAH): Results of the Randomized Controlled TRITON Study [Internet]. In: B27. UP-TO-DATE PAH ASSESSMENT AND MANAGEMENT. American Thoracic Society; 2020 [cited 2020 Jul 7]. p. A2928–

A2928.Available from: https://doi.org/10.1164/ajrccm-conference.2020.201.1_MeetingAbstracts.A2928

74. Zelt JGE, Chaudhary KR, Cadete VJ, Mielniczuk LM, Stewart DJ. Medical Therapy for Heart Failure Associated With Pulmonary Hypertension. *Circ Res*. 2019;124:1551–1567.

75. Galiè N, Humbert M, Vachiery J-L, Gibbs S, Lang I, Torbicki A, Simonneau G, Peacock A, Vonk Noordegraaf A, Beghetti M, Ghofrani A, Gomez Sanchez MA, Hansmann G, Klepetko W, Lancellotti P, Matucci M, McDonagh T, Pierard LA, Trindade PT, Zompatori M, Hoeper M. 2015 ESC/ERS Guidelines for the diagnosis and treatment of pulmonary hypertension: The Joint Task Force for the Diagnosis and Treatment of Pulmonary Hypertension of the European Society of Cardiology (ESC) and the European Respiratory Society (ERS)Endorsed by: Association for European Paediatric and Congenital Cardiology (AEPC), International Society for Heart and Lung Transplantation (ISHLT). *Eur Heart J*. 2016;37:67–119.

76. Galiè N, Channick RN, Frantz RP, Grünig E, Jing ZC, Moiseeva O, Preston IR, Pulido T, Safdar Z, Tamura Y, McLaughlin VV. Risk stratification and medical therapy of pulmonary arterial hypertension. *Eur Respir J*. 2019;53:1801889.

77. D'Alonzo GE. Survival in Patients with Primary Pulmonary Hypertension: Results from a National Prospective Registry. *Ann Intern Med*. 1991;115:343.

78. Benza RL, Miller DP, Gomberg-Maitland M, Frantz RP, Foreman AJ, Coffey CS, Frost A, Barst RJ, Badesch DB, Elliott CG, Liou TG, McGoon MD. Predicting Survival in Pulmonary Arterial Hypertension: Insights From the Registry to Evaluate Early and Long-Term Pulmonary Arterial Hypertension Disease Management (REVEAL). *Circulation*. 2010;122:164–172.

79. Sitbon O, Benza RL, Badesch DB, Barst RJ, Elliott CG, Gressin V, Lemarié J-C, Miller DP, Muros-Le Rouzic E, Simonneau G, Frost AE, Farber HW, Humbert M, McGoon MD. Validation of two predictive models for survival in pulmonary arterial hypertension. *Eur Respir J*. 2015;46:152–164.

80. Benza RL, Miller DP, Foreman AJ, Frost AE, Badesch DB, Benton WW, McGoon MD. Prognostic implications of serial risk score assessments in patients with pulmonary arterial hypertension: A Registry to Evaluate Early and Long-Term Pulmonary Arterial Hypertension Disease Management (REVEAL) analysis. *J Heart Lung Transplant*. 2015;34:356–361.

81. Benza RL, Gomberg-Maitland M, Elliott CG, Farber HW, Foreman AJ, Frost AE, McGoon MD, Pasta DJ, Selej M, Burger CD, Frantz RP. Predicting Survival in Patients with Pulmonary Arterial Hypertension: The REVEAL Risk Score Calculator 2.0 and Comparison With ESC/ERS-Based Risk Assessment Strategies. *Chest*. 2019;

82. Kylhammar D, Kjellström B, Hjalmarsson C, Jansson K, Nisell M, Söderberg S, Wikström G, Rådegran G. A comprehensive risk stratification at early follow-up determines prognosis in pulmonary arterial hypertension. *Eur Heart J*. 2018;39:4175–4181.

83. Hoeper MM, Kramer T, Pan Z, Eichstaedt CA, Spiesshoefer J, Benjamin N, Olsson KM, Meyer K, Vizza CD, Vonk-Noordegraaf A, Distler O, Opitz C, Gibbs JSR, Delcroix M, Ghofrani HA, Huscher D, Pittrow D, Rosenkranz S, Grünig E. Mortality in pulmonary arterial hypertension: prediction by the 2015 European pulmonary hypertension guidelines risk stratification model. *Eur Respir J*. 2017;50.

84. Nickel N, Golpon H, Greer M, Knudsen L, Olsson K, Westerkamp V, Welte T, Hoeper MM. The prognostic impact of follow-up assessments in patients with idiopathic pulmonary arterial hypertension. *Eur Respir J*. 2012;39:589–596.

85. Boucly A, Weatherald J, Savale L, Jaïs X, Cottin V, Prevot G, Picard F, de Groote P, Jevnikar M, Bergot E, Chaouat A, Chabanne C, Bourdin A, Parent F, Montani D, Simonneau G, Humbert M, Sitbon O. Risk assessment, prognosis and guideline implementation in pulmonary arterial hypertension. *Eur Respir J*. 2017;50:1700889.

86. Simons JE, Mann EB, Pierozynski A. Assessment of Risk of Disease Progression in Pulmonary Arterial Hypertension: Insights from an International Survey of Clinical Practice. *Adv Ther*. 2019;36:2351–2363.

87. Humbert M, Galiè N, McLaughlin VV, Rubin LJ, Simonneau G. An insider view on the World Symposium on Pulmonary Hypertension. *Lancet Respir Med* [Internet]. 2019 [cited 2019 Apr 16];Available from: https://linkinghub.elsevier.com/retrieve/pii/S2213260019301110

88. Guazzi M. Pulmonary hypertension in heart failure preserved ejection fraction: prevalence, pathophysiology, and clinical perspectives. *Circ Heart Fail*. 2014;7:367–377.

89. Vonk Noordegraaf A, Westerhof BE, Westerhof N. The Relationship Between the Right Ventricle and its Load in Pulmonary Hypertension. *J Am Coll Cardiol*. 2017;69:236–243.

90. Vonk Noordegraaf A, Chin KM, Haddad F, Hassoun PM, Hemnes AR, Hopkins SR, Kawut SM, Langleben D, Lumens J, Naeije R. Pathophysiology of the right ventricle and of the pulmonary circulation in pulmonary hypertension: an update. *Eur Respir J*. 2019;53:1801900.

91. Bogaard HJ, Natarajan R, Henderson SC, Long CS, Kraskauskas D, Smithson L, Ockaili R, McCord JM, Voelkel NF. Chronic pulmonary artery pressure elevation is insufficient to explain right heart failure. *Circulation*. 2009;120:1951–1960.

92. Ryan JJ, Archer SL. The Right Ventricle in Pulmonary Arterial Hypertension: Disorders of Metabolism, Angiogenesis and Adrenergic Signaling in Right Ventricular Failure. *Circ Res*. 2014;115:176–188.

93. Rich S, Pogoriler J, Husain AN, Toth PT, Gomberg-Maitland M, Archer SL. Long-term effects of epoprostenol on the pulmonary vasculature in idiopathic pulmonary arterial hypertension. *Chest*. 2010;138:1234–1239.

94. Hopkins WE, Waggoner AD. Severe pulmonary hypertension without right ventricular failure: the unique hearts of patients with Eisenmenger syndrome. *Am J Cardiol*. 2002;89:34–38.

95. Jiang B, Deng Y, Suen C, Taha M, Chaudhary KR, Courtman DW, Stewart DJ. Marked Strain-Specific Differences in the SU5416 Rat Model of Severe Pulmonary Arterial Hypertension. *Am J Respir Cell Mol Biol*. 2016;54:461–468.

96. Abdul-Ghani M, Suen C, Jiang B, Deng Y, Weldrick JJ, Putinski C, Brunette S, Fernando P, Lee TT, Flynn P, Leenen FHH, Burgon PG, Stewart DJ, Megeney LA. Cardiotrophin 1 stimulates beneficial myogenic and vascular remodeling of the heart. *Cell Res*. 2017;27:1195–1215.

97. Suen CM, Chaudhary KR, Deng Y, Jiang B, Stewart DJ. Fischer rats exhibit maladaptive structural and molecular right ventricular remodelling in severe pulmonary hypertension: a genetically prone model for right heart failure. *Cardiovasc Res*. 2018;

98. Frump AL, Goss KN, Vayl A, Albrecht M, Fisher A, Tursunova R, Fierst J, Whitson J, Cucci AR, Brown MB, Lahm T. Estradiol improves right ventricular function in rats with severe angioproliferative pulmonary hypertension: effects of endogenous and exogenous sex hormones. *Am J Physiol Lung Cell Mol Physiol*. 2015;308:L873-890.

99. Bogaard HJ, Natarajan R, Mizuno S, Abbate A, Chang PJ, Chau VQ, Hoke NN, Kraskauskas D, Kasper M, Salloum FN, Voelkel NF. Adrenergic Receptor Blockade Reverses Right Heart Remodeling and Dysfunction in Pulmonary Hypertensive Rats. *Am J Respir Crit Care Med*. 2010;182:652–660.

100. Westerhof BE, Saouti N, van der Laarse WJ, Westerhof N, Vonk Noordegraaf A. Treatment strategies for the right heart in pulmonary hypertension. *Cardiovasc Res*. 2017;113:1465–1473.

101. van Wolferen SA, Marcus JT, Westerhof N, Spreeuwenberg MD, Marques KMJ, Bronzwaer JGF, Henkens IR, Gan CT-J, Boonstra A, Postmus PE, Vonk-Noordegraaf A. Right coronary artery flow impairment in patients with pulmonary hypertension. *Eur Heart J*. 2008;29:120–127.

102. Potus F, Ruffenach G, Dahou A, Thebault C, Breuils-Bonnet S, Tremblay È, Nadeau V, Paradis R, Graydon C, Wong R, Johnson I, Paulin R, Lajoie AC, Perron J, Charbonneau E, Joubert P, Pibarot P, Michelakis ED, Provencher S, Bonnet S. Downregulation of

MicroRNA-126 Contributes to the Failing Right Ventricle in Pulmonary Arterial Hypertension. *Circulation*. 2015;132:932–943.

103. Piao L, Fang Y-H, Parikh K, Ryan JJ, Toth PT, Archer SL. Cardiac glutaminolysis: a maladaptive cancer metabolism pathway in the right ventricle in pulmonary hypertension. *J Mol Med*. 2013;91:1185–1197.

104. Bogaard HJ, Natarajan R, Henderson SC, Long CS, Kraskauskas D, Smithson L, Ockaili R, McCord JM, Voelkel NF. Chronic Pulmonary Artery Pressure Elevation Is Insufficient to Explain Right Heart Failure. *Circulation*. 2009;120:1951–1960.

105. Graham BB, Kumar R, Mickael C, Kassa B, Koyanagi D, Sanders L, Zhang L, Perez M, Hernandez-Saavedra D, Valencia C, Dixon K, Harral J, Loomis Z, Irwin D, Nemkov T, D'Alessandro A, Stenmark KR, Tuder RM. Vascular Adaptation of the Right Ventricle in Experimental Pulmonary Hypertension. *Am J Respir Cell Mol Biol*. 2018;

106. Sutendra G, Michelakis ED. The Metabolic Basis of Pulmonary Arterial Hypertension. *Cell Metab*. 2014;19:558–573.

107. Lowes BD, Minobe W, Abraham WT, Rizeq MN, Bohlmeyer TJ, Quaife RA, Roden RL, Dutcher DL, Robertson AD, Voelkel NF, Badesch DB, Groves BM, Gilbert EM, Bristow MR. Changes in gene expression in the intact human heart. Downregulation of alpha-myosin heavy chain in hypertrophied, failing ventricular myocardium. *J Clin Invest*. 1997;100:2315–2324.

108. Lopaschuk GD. Metabolic Modulators in Heart Disease: Past, Present, and Future. *Can J Cardiol*. 2017;33:838–849.

109. Neely JR, Morgan HE. Relationship between carbohydrate and lipid metabolism and the energy balance of heart muscle. *Annu Rev Physiol*. 1974;36:413–459.

110. Piao L, Sidhu VK, Fang Y-H, Ryan JJ, Parikh KS, Hong Z, Toth PT, Morrow E, Kutty S, Lopaschuk GD, Archer SL. FOXO1-mediated upregulation of pyruvate dehydrogenase kinase-4 (PDK4) decreases glucose oxidation and impairs right ventricular function in pulmonary hypertension: therapeutic benefits of dichloroacetate. *J Mol Med Berl Ger*. 2013;91:333–346.

111. Ohira H, deKemp R, Pena E, Davies RA, Stewart DJ, Chandy G, Contreras-Dominguez V, Dennie C, Mc Ardle B, Mc Klein R, Renaud JM, DaSilva JN, Pugliese C, Dunne R, Beanlands R, Mielniczuk LM. Shifts in myocardial fatty acid and glucose metabolism in pulmonary arterial hypertension: a potential mechanism for a maladaptive right ventricular response. *Eur Heart J Cardiovasc Imaging*. 2015;

112. Ohira H, deKemp R, Pena E, Davies RA, Stewart DJ, Chandy G, Contreras-Dominguez V, Dennie C, Mc Ardle B, Mc Klein R, Renaud JM, DaSilva JN, Pugliese C, Dunne R, Beanlands R, Mielniczuk LM. Shifts in myocardial fatty acid and glucose metabolism

in pulmonary arterial hypertension: a potential mechanism for a maladaptive right ventricular response. *Eur Heart J Cardiovasc Imaging*. 2016;17:1424–1431.

113. Fang Y-H, Piao L, Hong Z, Toth PT, Marsboom G, Bache-Wiig P, Rehman J, Archer SL. Therapeutic inhibition of fatty acid oxidation in right ventricular hypertrophy: exploiting Randle's cycle. *J Mol Med Berl Ger*. 2012;90:31–43.

114. Talati MH, Brittain EL, Fessel JP, Penner N, Atkinson J, Funke M, Grueter C, Jerome WG, Freeman M, Newman JH, West J, Hemnes AR. Mechanisms of Lipid Accumulation in the Bone Morphogenetic Protein Receptor Type 2 Mutant Right Ventricle. *Am J Respir Crit Care Med*. 2016;194:719–728.

115. Talati M, Hemnes A. Fatty acid metabolism in pulmonary arterial hypertension: role in right ventricular dysfunction and hypertrophy. *Pulm Circ*. 2015;5:269–278.

116. Legchenko E, Chouvarine P, Borchert P, Fernandez-Gonzalez A, Snay E, Meier M, Maegel L, Mitsialis SA, Rog-Zielinska EA, Kourembanas S, Jonigk D, Hansmann G. PPARγ agonist pioglitazone reverses pulmonary hypertension and prevents right heart failure via fatty acid oxidation. *Sci Transl Med*. 2018;10.

117. Gomez-Arroyo J, Mizuno S, Szczepanek K, Van Tassell B, Natarajan R, dos Remedios CG, Drake JI, Farkas L, Kraskauskas D, Wijesinghe DS, Chalfant CE, Bigbee J, Abbate A, Lesnefsky EJ, Bogaard HJ, Voelkel NF. Metabolic Gene Remodeling and Mitochondrial Dysfunction in Failing Right Ventricular Hypertrophy Secondary to Pulmonary Arterial Hypertension. *Circ Heart Fail*. 2013;6:136–144.

118. Lehman JJ, Boudina S, Banke NH, Sambandam N, Han X, Young DM, Leone TC, Gross RW, Lewandowski ED, Abel ED, Kelly DP. The transcriptional coactivator PGC-1alpha is essential for maximal and efficient cardiac mitochondrial fatty acid oxidation and lipid homeostasis. *Am J Physiol Heart Circ Physiol*. 2008;295:H185-196.

119. Archer SL, Marsboom G, Kim GH, Zhang HJ, Toth PT, Svensson EC, Dyck JRB, Gomberg-Maitland M, Thébaud B, Husain AN, Cipriani N, Rehman J. Epigenetic Attenuation of Mitochondrial Superoxide Dismutase 2 in Pulmonary Arterial Hypertension: A Basis for Excessive Cell Proliferation and a New Therapeutic Target. *Circulation*. 2010;121:2661–2671.

120. Jernigan NL, Naik JS, Weise-Cross L, Detweiler ND, Herbert LM, Yellowhair TR, Resta TC. Contribution of reactive oxygen species to the pathogenesis of pulmonary arterial hypertension. *PLOS ONE*. 2017;12:e0180455.

121. Tsutsui H, Kinugawa S, Matsushima S. Oxidative stress and heart failure. *Am J Physiol-Heart Circ Physiol*. 2011;301:H2181–H2190.

122. Ecarnot-Laubriet A, Rochette L, Vergely C, Sicard P, Teyssier J-R. The activation pattern of the antioxidant enzymes in the right ventricle of rat in response to pressure overload is of heart failure type. *Heart Dis Hagerstown Md*. 2003;5:308–312.

123. Redout EM, Wagner MJ, Zuidwijk MJ, Boer C, Musters RJP, van Hardeveld C, Paulus WJ, Simonides WS. Right-ventricular failure is associated with increased mitochondrial complex II activity and production of reactive oxygen species. *Cardiovasc Res*. 2007;75:770–781.

124. Freed BH, Gomberg-Maitland M, Chandra S, Mor-Avi V, Rich S, Archer SL, Jamison EB, Lang RM, Patel AR. Late gadolinium enhancement cardiovascular magnetic resonance predicts clinical worsening in patients with pulmonary hypertension. *J Cardiovasc Magn Reson Off J Soc Cardiovasc Magn Reson*. 2012;14:11.

125. Gomez-Arroyo J, Santos-Martinez LE, Aranda A, Pulido T, Beltran M, Muñoz-Castellanos L, Dominguez-Cano E, Sonnino C, Voelkel NF, Sandoval J. Differences in right ventricular remodeling secondary to pressure overload in patients with pulmonary hypertension. *Am J Respir Crit Care Med*. 2014;189:603–606.

126. Drake JI, Bogaard HJ, Mizuno S, Clifton B, Xie B, Gao Y, Dumur CI, Fawcett P, Voelkel NF, Natarajan R. Molecular signature of a right heart failure program in chronic severe pulmonary hypertension. *Am J Respir Cell Mol Biol*. 2011;45:1239–1247.

127. Heymans S, González A, Pizard A, Papageorgiou AP, López-Andrés N, Jaisser F, Thum T, Zannad F, Díez J. Searching for new mechanisms of myocardial fibrosis with diagnostic and/or therapeutic potential. *Eur J Heart Fail*. 2015;17:764–771.

128. Gorter TM, Verschuuren EAM, van Veldhuisen DJ, Hoendermis ES, Erasmus ME, Bogaard HJ, Vonk Noordegraaf A, Berger RMF, van Melle JP, Willems TP. Right ventricular recovery after bilateral lung transplantation for pulmonary arterial hypertension†. *Interact Cardiovasc Thorac Surg*. 2017;24:890–897.

129. Rain S, Andersen S, Najafi A, Gammelgaard Schultz J, da Silva Gonçalves Bós D, Handoko ML, Bogaard H-J, Vonk-Noordegraaf A, Andersen A, van der Velden J, Ottenheijm CAC, de Man FS. Right Ventricular Myocardial Stiffness in Experimental Pulmonary Arterial Hypertension: Relative Contribution of Fibrosis and Myofibril Stiffness. *Circ Heart Fail*. 2016;9.

130. Seta Y, Shan K, Bozkurt B, Oral H, Mann DL. Basic mechanisms in heart failure: the cytokine hypothesis. *J Card Fail*. 1996;2:243–249.

131. Perros F, Dorfmüller P, Montani D, Hammad H, Waelput W, Girerd B, Raymond N, Mercier O, Mussot S, Cohen-Kaminsky S, Humbert M, Lambrecht BN. Pulmonary lymphoid neogenesis in idiopathic pulmonary arterial hypertension. *Am J Respir Crit Care Med*. 2012;185:311–321.

132. Sydykov A, Mamazhakypov A, Petrovic A, Kosanovic D, Sarybaev AS, Weissmann N, Ghofrani HA, Schermuly RT. Inflammatory Mediators Drive Adverse Right Ventricular Remodeling and Dysfunction and Serve as Potential Biomarkers. *Front Physiol*

[Internet]. 2018 [cited 2018 Oct 3];9. Available from: https://www.frontiersin.org/article/10.3389/fphys.2018.00609/full

133. Tedford RJ, Mudd JO, Girgis RE, Mathai SC, Zaiman AL, Housten-Harris T, Boyce D, Kelemen BW, Bacher AC, Shah AA, Hummers LK, Wigley FM, Russell SD, Saggar R, Saggar R, Maughan WL, Hassoun PM, Kass DA. Right ventricular dysfunction in systemic sclerosis-associated pulmonary arterial hypertension. *Circ Heart Fail*. 2013;6:953–963.

134. Overbeek MJ, Mouchaers KTB, Niessen HM, Hadi AM, Kupreishvili K, Boonstra A, Voskuyl AE, Belien JAM, Smit EF, Dijkmans BC, Vonk-Noordegraaf A, Grünberg K. Characteristics of interstitial fibrosis and inflammatory cell infiltration in right ventricles of systemic sclerosis-associated pulmonary arterial hypertension. *Int J Rheumatol*. 2010;2010.

135. van Paassen P, Duijvestijn A, Debrus-Palmans L, Damoiseaux J, Vroomen M, Tervaert JWC. Induction of endothelial cell apoptosis by IgG antibodies from SLE patients with nephropathy: a potential role for anti-endothelial cell antibodies. *Ann N Y Acad Sci*. 2007;1108:147–156.

136. Yang T, Li Z-N, Chen G, Gu Q, Ni X-H, Zhao Z-H, Ye J, Meng X-M, Liu Z-H, Xiong C-M, He J-G. Increased levels of plasma CXC-Chemokine Ligand 10, 12 and 16 are associated with right ventricular function in patients with idiopathic pulmonary arterial hypertension. *Heart Lung J Crit Care*. 2014;43:322–327.

137. Soon E, Holmes AM, Treacy CM, Doughty NJ, Southgate L, Machado RD, Trembath RC, Jennings S, Barker L, Nicklin P, Walker C, Budd DC, Pepke-Zaba J, Morrell NW. Elevated Levels of Inflammatory Cytokines Predict Survival in Idiopathic and Familial Pulmonary Arterial Hypertension. *Circulation*. 2010;122:920–927.

138. Voelkel NF, Gomez-Arroyo J, Abbate A, Bogaard HJ, Nicolls MR. Pathobiology of pulmonary arterial hypertension and right ventricular failure. *Eur Respir J*. 2012;40:1555–1565.

139. Zhu M, Goetsch SC, Wang Z, Luo R, Hill JA, Schneider J, Morris SM, Liu Z-P. FoxO4 promotes early inflammatory response upon myocardial infarction via endothelial Arg1. *Circ Res*. 2015;117:967–977.

140. Murray DR, Prabhu SD, Chandrasekar B. Chronic beta-adrenergic stimulation induces myocardial proinflammatory cytokine expression. *Circulation*. 2000;101:2338–2341.

141. Sun X-Q, Abbate A, Bogaard H-J. Role of cardiac inflammation in right ventricular failure. *Cardiovasc Res*. 2017;113:1441–1452.

142. Wang Q, Zuo X, Wang Y, Xie W, Wang H, Zhang M. Monocrotaline-induced pulmonary arterial hypertension is attenuated by TNF-α antagonists via the suppression of TNF-α expression and NF-κB pathway in rats. *Vascul Pharmacol*. 2013;58:71–77.

143. Guihaire J, Deuse T, Fadel E, Reichenspurner H, Robbins RC, Schrepfer S. Macrophages Infiltration Is Associated with Maladaptive Remodeling of the Right Ventricle in an Experimental Model of Pulmonary Hypertension. *J Heart Lung Transplant*. 2014;33:S228.

144. Rakusan K, Sarkar K, Turek Z, Wicker P. Mast cells in the rat heart during normal growth and in cardiac hypertrophy. *Circ Res*. 1990;66:511–516.

145. Brown MB, Neves E, Long G, Graber J, Gladish B, Wiseman A, Owens M, Fisher AJ, Presson RG, Petrache I, Kline J, Lahm T. High-intensity interval training, but not continuous training, reverses right ventricular hypertrophy and dysfunction in a rat model of pulmonary hypertension. *Am J Physiol Regul Integr Comp Physiol*. 2017;312:R197–R210.

146. Kopcow HD, Karumanchi SA. Angiogenic factors and natural killer (NK) cells in the pathogenesis of preeclampsia. *J Reprod Immunol*. 2007;76:23–29.

147. Ormiston ML, Chang C, Long LL, Soon E, Jones D, Machado R, Treacy C, Toshner MR, Campbell K, Riding A, Southwood M, Pepke-Zaba J, Exley A, Trembath RC, Colucci F, Wills M, Trowsdale J, Morrell NW. Impaired natural killer cell phenotype and function in idiopathic and heritable pulmonary arterial hypertension. *Circulation*. 2012;126:1099–1109.

148. Ratsep MT, Moore SD, Jafri S, Mitchell M, Brady HJ, Mandelboim O, Southwood M, Morrell NW, Colucci F, Ormiston ML. Spontaneous pulmonary hypertension in genetic mouse models of natural killer cell deficiency. *Am J Physiol Lung Cell Mol Physiol*. 2018;

149. Ciarka A, Doan V, Velez-Roa S, Naeije R, van de Borne P. Prognostic significance of sympathetic nervous system activation in pulmonary arterial hypertension. *Am J Respir Crit Care Med*. 2010;181:1269–1275.

150. Goldsmith SR. Interactions between the sympathetic nervous system and the RAAS in heart failure. *Curr Heart Fail Rep*. 2004;1:45–50.

151. Kimura K, Ieda M, Kanazawa H, Yagi T, Tsunoda M, Ninomiya S -i., Kurosawa H, Yoshimi K, Mochizuki H, Yamazaki K, Ogawa S, Fukuda K. Cardiac Sympathetic Rejuvenation: A Link Between Nerve Function and Cardiac Hypertrophy. *Circ Res*. 2007;100:1755–1764.

152. Piao L, Fang Y-H, Parikh KS, Ryan JJ, D'Souza KM, Theccanat T, Toth PT, Pogoriler J, Paul J, Blaxall BC, others. GRK2-Mediated Inhibition of Adrenergic and Dopaminergic Signaling in Right Ventricular Hypertrophy Therapeutic Implications in Pulmonary Hypertension. *Circulation*. 2012;126:2859–2869.

153. Campo A, Mathai SC, Le Pavec J, Zaiman AL, Hummers LK, Boyce D, Housten T, Lechtzin N, Chami H, Girgis RE, Hassoun PM. Outcomes of hospitalisation for right heart failure in pulmonary arterial hypertension. *Eur Respir J*. 2011;38:359–367.

154. da Silva Gonçalves Bós D, Van Der Bruggen CEE, Kurakula K, Sun X-Q, Casali KR, Casali AG, Rol N, Szulcek R, dos Remedios C, Guignabert C, Tu L, Dorfmüller P, Humbert M, Wijnker PJM, Kuster DWD, van der Velden J, Goumans M-J, Bogaard H-J, Vonk-Noordegraaf A, de Man FS, Handoko ML. Contribution of Impaired Parasympathetic Activity to Right Ventricular Dysfunction and Pulmonary Vascular Remodeling in Pulmonary Arterial Hypertension. *Circulation*. 2018;137:910–924.

155. Safdar Z, Thakur A, Singh S, Ji Y, Guffey D, Minard CG, Entman ML. Circulating Aldosterone Levels and Disease Severity in Pulmonary Arterial Hypertension. *J Pulm Respir Med*. 2015;5.

156. Maron BA, Zhang Y-Y, White K, Chan SY, Handy DE, Mahoney CE, Loscalzo J, Leopold JA. Aldosterone Inactivates the Endothelin-B Receptor via a Cysteinyl Thiol Redox Switch to Decrease Pulmonary Endothelial Nitric Oxide Levels and Modulate Pulmonary Arterial HypertensionClinical Perspective. *Circulation*. 2012;126:963–974.

157. de Man FS, Tu L, Handoko ML, Rain S, Ruiter G, François C, Schalij I, Dorfmüller P, Simonneau G, Fadel E, Perros F, Boonstra A, Postmus PE, van der Velden J, Vonk-Noordegraaf A, Humbert M, Eddahibi S, Guignabert C. Dysregulated renin-angiotensin-aldosterone system contributes to pulmonary arterial hypertension. *Am J Respir Crit Care Med*. 2012;186:780–789.

158. Harrison A, Wilson BD, Ryan JJ. Exploring the Role of Aldosterone in Right Ventricular Function. *Can J Cardiol*. 2014;30:155–158.

159. Mizuno Y, Yoshimura M, Yasue H, Sakamoto T, Ogawa H, Kugiyama K, Harada E, Nakayama M, Nakamura S, Ito T, Shimasaki Y, Saito Y, Nakao K. Aldosterone production is activated in failing ventricle in humans. *Circulation*. 2001;103:72–77.

160. Triposkiadis F, Karayannis G, Giamouzis G, Skoularigis J, Louridas G, Butler J. The Sympathetic Nervous System in Heart Failure. *J Am Coll Cardiol*. 2009;54:1747–1762.

161. Gauthier C, Leblais V, Kobzik L, Trochu JN, Khandoudi N, Bril A, Balligand JL, Le Marec H. The negative inotropic effect of beta3-adrenoceptor stimulation is mediated by activation of a nitric oxide synthase pathway in human ventricle. *J Clin Invest*. 1998;102:1377–1384.

162. Schroeder C, Jordan J. Norepinephrine uptake mechanisms in cardiovascular disease deserve our attention: *J Cardiovasc Pharmacol*. 2011;1.

163. Eisenhofer G. The role of neuronal and extraneuronal plasma membrane transporters in the inactivation of peripheral catecholamines. *Pharmacol Ther*. 2001;91:35–62.

164. Slart RHJA, Tio RA, Elsinga PH, Schwaiger M, editors. Autonomic Innervation of the Heart [Internet]. Berlin, Heidelberg: Springer Berlin Heidelberg; 2015 [cited 2017 Jul 28]. Available from: http://link.springer.com/10.1007/978-3-662-45074-1

165. Link JM, Caldwell JH. Diagnostic and prognostic imaging of the cardiac sympathetic nervous system. *Nat Clin Pract Cardiovasc Med*. 2008;5 Suppl 2:S79-86.

166. Triposkiadis F, Karayannis G, Giamouzis G, Skoularigis J, Louridas G, Butler J. The sympathetic nervous system in heart failure physiology, pathophysiology, and clinical implications. *J Am Coll Cardiol*. 2009;54:1747–1762.

167. Fallavollita JA, Heavey BM, Luisi AJ, Michalek SM, Baldwa S, Mashtare TL, Hutson AD, Dekemp RA, Haka MS, Sajjad M, Cimato TR, Curtis AB, Cain ME, Canty JM. Regional myocardial sympathetic denervation predicts the risk of sudden cardiac arrest in ischemic cardiomyopathy. *J Am Coll Cardiol*. 2014;63:141–149.

168. Fallavollita JA, Canty JM. Dysinnervated but viable myocardium in ischemic heart disease. *J Nucl Cardiol Off Publ Am Soc Nucl Cardiol*. 2010;17:1107–1115.

169. Malhotra S, Fernandez SF, Fallavollita JA, Canty JM. Prognostic Significance of Imaging Myocardial Sympathetic Innervation. *Curr Cardiol Rep*. 2015;17:62.

170. Notarius CF, Floras JS. Limitations of the use of spectral analysis of heart rate variability for the estimation of cardiac sympathetic activity in heart failure. *Eur Eur Pacing Arrhythm Card Electrophysiol J Work Groups Card Pacing Arrhythm Card Cell Electrophysiol Eur Soc Cardiol*. 2001;3:29–38.

171. Cohn JN, Levine TB, Olivari MT, Garberg V, Lura D, Francis GS, Simon AB, Rector T. Plasma norepinephrine as a guide to prognosis in patients with chronic congestive heart failure. *N Engl J Med*. 1984;311:819–823.

172. Florea VG, Cohn JN. The Autonomic Nervous System and Heart Failure. *Circ Res*. 2014;114:1815–1826.

173. Jacobson AF, Senior R, Cerqueira MD, Wong ND, Thomas GS, Lopez VA, Agostini D, Weiland F, Chandna H, Narula J. Myocardial Iodine-123 Meta-Iodobenzylguanidine Imaging and Cardiac Events in Heart Failure. *J Am Coll Cardiol*. 2010;55:2212–2221.

174. Matteo Bauckneht, Gianmario Sambuceti, Elena Pomposelli, Francesco Fiz. Pathophysiological basis of myocardial innervation imaging in heart failure. *Clin Transl Imaging*. 2015;3:347–355.

175. Zelt JGE, Mielniczuk LM, Orlandi C, Robinson S, Hadizad T, Walter O, Garrard L, Beanlands RSB, deKemp RA. PET imaging of sympathetic innervation with [18F]Flurobenguan vs [11C]mHED in a patient with ischemic cardiomyopathy. *J Nucl Cardiol*. 2018;

176. Sinusas AJ, Lazewatsky J, Brunetti J, Heller G, Srivastava A, Liu Y-H, Sparks R, Puretskiy A, Lin S, Crane P, Carson RE, Lee LV. Biodistribution and radiation dosimetry of LMI1195: first-in-human study of a novel 18F-labeled tracer for imaging myocardial innervation. *J Nucl Med Off Publ Soc Nucl Med*. 2014;55:1445–1451.

177. Degrado TR, Zalutsky MR, Vaidyanathan G. Uptake mechanisms of meta-[123I]iodobenzylguanidine in isolated rat heart. *Nucl Med Biol*. 1995;22:1–12.

178. Dae MW, De Marco T, Botvinick EH, O'Connell JW, Hattner RS, Huberty JP, Yuen-Green MS. Scintigraphic assessment of MIBG uptake in globally denervated human and canine hearts--implications for clinical studies. *J Nucl Med Off Publ Soc Nucl Med*. 1992;33:1444–1450.

179. Agostini D, Nakajima K, Verberne HJ. Innervation of the Heart: Imaging Findings Using [123I]-MIBG Scintigraphy in Different Pathologies [Internet]. In: Marzullo P, Mariani G, editors. From Basic Cardiac Imaging to Image Fusion. Milano: Springer Milan; 2013 [cited 2017 Sep 22]. p. 51–70.Available from: http://link.springer.com/10.1007/978-88-470-2760-2_4

180. Rosenspire KC, Haka MS, Van Dort ME, Jewett DM, Gildersleeve DL, Schwaiger M, Wieland DM. Synthesis and preliminary evaluation of carbon-11-meta-hydroxyephedrine: a false transmitter agent for heart neuronal imaging. *J Nucl Med Off Publ Soc Nucl Med*. 1990;31:1328–1334.

181. DeGrado TR, Hutchins GD, Toorongian SA, Wieland DM, Schwaiger M. Myocardial kinetics of carbon-11-meta-hydroxyephedrine: retention mechanisms and effects of norepinephrine. *J Nucl Med Off Publ Soc Nucl Med*. 1993;34:1287–1293.

182. Raffel DM, Wieland DM. Assessment of cardiac sympathetic nerve integrity with positron emission tomography. *Nucl Med Biol*. 2001;28:541–559.

183. Werner RA, Rischpler C, Onthank D, Lapa C, Robinson S, Samnick S, Javadi M, Schwaiger M, Nekolla SG, Higuchi T. Retention Kinetics of the 18F-Labeled Sympathetic Nerve PET Tracer LMI1195: Comparison with 11C-Hydroxyephedrine and 123I-MIBG. *J Nucl Med*. 2015;56:1429–1433.

184. Tipre DN, Fox JJ, Holt DP, Green G, Yu J, Pomper M, Dannals RF, Bengel FM. In Vivo PET Imaging of Cardiac Presynaptic Sympathoneuronal Mechanisms in the Rat. *J Nucl Med*. 2008;49:1189–1195.

185. Nguyen NT, DeGrado TR, Chakraborty P, Wieland DM, Schwaiger M. Myocardial kinetics of carbon-11-epinephrine in the isolated working rat heart. *J Nucl Med Off Publ Soc Nucl Med*. 1997;38:780–785.

186. Raffel DM, Corbett JR, del Rosario RB, Mukhopadhyay SK, Gildersleeve DL, Rose P, Wieland DM. Sensitivity of [11C]phenylephrine kinetics to monoamine oxidase activity in normal human heart. *J Nucl Med Off Publ Soc Nucl Med*. 1999;40:232–238.

187. Simula S, Vanninen E, Viitanen L, Kareinen A, Lehto S, Pajunen P, Syvänne M, Kuikka J, Laakso M, Hartikainen J. Cardiac adrenergic innervation is affected in asymptomatic subjects with very early stage of coronary artery disease. *J Nucl Med*. 2002;43:1–7.

188. Luisi AJ, Suzuki G, Haka MS, Toorongian SA, Canty JM, Fallavollita JA, others. Regional 11C-hydroxyephedrine retention in hibernating myocardium: chronic inhomogeneity of sympathetic innervation in the absence of infarction. *J Nucl Med*. 2005;46:1368–1374.

189. Gutterman DD, Morgan DA, Miller FJ. Effect of brief myocardial ischemia on sympathetic coronary vasoconstriction. *Circ Res*. 1992;71:960–969.

190. Fernandez SF, Ovchinnikov V, Canty JM, Fallavollita JA. Hibernating myocardium results in partial sympathetic denervation and nerve sprouting. *AJP Heart Circ Physiol*. 2013;304:H318–H327.

191. Ciuffo AA, Ouyang P, Becker LC, Levin L, Weisfeldt ML. Reduction of sympathetic inotropic response after ischemia in dogs. Contributor to stunned myocardium. *J Clin Invest*. 1985;75:1504–1509.

192. Luisi AJ, Fallavollita JA, Suzuki G, Canty JM. Spatial Inhomogeneity of Sympathetic Nerve Function in Hibernating Myocardium. *Circulation*. 2002;106:779–781.

193. Dae MW, O'Connell JW, Botvinick EH, Chin MC. Acute and chronic effects of transient myocardial ischemia on sympathetic nerve activity, density, and norepinephrine content. *Cardiovasc Res*. 1995;30:270–280.

194. Fallavollita JA, Banas MD, Suzuki G, deKemp RA, Sajjad M, Canty JM. 11C-meta-hydroxyephedrine defects persist despite functional improvement in hibernating myocardium. *J Nucl Cardiol*. 2010;17:85–96.

195. Cao J-M, Fishbein MC, Han JB, Lai WW, Lai AC, Wu T-J, Czer L, Wolf PL, Denton TA, Shintaku IP, others. Relationship between regional cardiac hyperinnervation and ventricular arrhythmia. *Circulation*. 2000;101:1960–1969.

196. Dae MW, Herre JM, O'Connell JW, Botvinick EH, Newman D, Munoz L. Scintigraphic assessment of sympathetic innervation after transmural versus nontransmural myocardial infarction. *J Am Coll Cardiol*. 1991;17:1416–1423.

197. Barber MJ, Mueller TM, Henry DP, Felten SY, Zipes DP. Transmural myocardial infarction in the dog produces sympathectomy in noninfarcted myocardium. *Circulation*. 1983;67:787–796.

198. Lautamaki R, Sasano T, Higuchi T, Nekolla SG, Lardo AC, Holt DP, Dannals RF, Abraham MR, Bengel FM. Multiparametric Molecular Imaging Provides Mechanistic Insights into Sympathetic Innervation Impairment in the Viable Infarct Border Zone. *J Nucl Med*. 2015;56:457–463.

199. Li C-Y, Li Y-G. Cardiac Sympathetic Nerve Sprouting and Susceptibility to Ventricular Arrhythmias after Myocardial Infarction. *Cardiol Res Pract*. 2015;2015:1–8.

200. Parthenakis F. Segmental pattern of myocardial sympathetic denervation in idiopathic dilated cardiomyopathy: Relationship to regional wall motion and myocardial perfusion abnormalities. *J Nucl Cardiol*. 2002;9:15–22.

201. Hartmann F, Ziegler S, Nekolla S, Hadamitzky M, Seyfarth M, Richardt G, Schwaiger M. Regional patterns of myocardial sympathetic denervation in dilated cardiomyopathy: an analysis using carbon-11 hydroxyephedrine and positron emission tomography. *Heart Br Card Soc*. 1999;81:262–270.

202. Matsunari I, Aoki H, Nomura Y, Takeda N, Chen W-P, Taki J, Nakajima K, Nekolla SG, Kinuya S, Kajinami K. Iodine-123 metaiodobenzylguanidine imaging and carbon-11 hydroxyephedrine positron emission tomography compared in patients with left ventricular dysfunction. *Circ Cardiovasc Imaging*. 2010;3:595–603.

203. Hartmann F, Ziegler S, Nekolla S, Hadamitzky M, Seyfarth M, Richardt G, Schwaiger M. Regional patterns of myocardial sympathetic denervation in dilated cardiomyopathy: an analysis using carbon-11 hydroxyephedrine and positron emission tomography. *Heart*. 1999;81:262–270.

204. Thackeray JT, Renaud JM, Kordos M, Klein R, deKemp RA, Beanlands RSB, DaSilva JN. Test–retest repeatability of quantitative cardiac 11C-meta-hydroxyephedrine measurements in rats by small animal positron emission tomography. *Nucl Med Biol*. 2013;40:676–681.

205. Mardon K, Montagne O, Elbaz N, Malek Z, Syrota A, Dubois-Randé J-L, Meignan M, Merlet P. Uptake-1 carrier downregulates in parallel with the beta-adrenergic receptor desensitization in rat hearts chronically exposed to high levels of circulating norepinephrine: implications for cardiac neuroimaging in human cardiomyopathies. *J Nucl Med Off Publ Soc Nucl Med*. 2003;44:1459–1466.

206. Ungerer M, Hartmann F, Karoglan M, Chlistalla A, Ziegler S, Richardt G, Overbeck M, Meisner H, Schömig A, Schwaiger M. Regional in vivo and in vitro characterization of autonomic innervation in cardiomyopathic human heart. *Circulation*. 1998;97:174–180.

207. Oki H, Inoue S, Makishima N, Takeyama Y, Shiokawa A. Cardiac sympathetic innervation in patients with dilated cardiomyopathy: Immunohistochemical study using Anti-tyrosine hydroxylase antibody. *Jpn Circ J*. 1994;58:389–394.

208. Backs J, Haunstetter A, Gerber SH, Metz J, Borst MM, Strasser RH, Kübler W, Haass M. The Neuronal Norepinephrine Transporter in Experimental Heart Failure: Evidence for a Posttranscriptional Downregulation. *J Mol Cell Cardiol*. 2001;33:461–472.

209. Tiller D, Russ M, Greiser KH, Nuding S, Ebelt H, Kluttig A, Kors JA, Thiery J, Bruegel M, Haerting J, Werdan K. Prevalence of symptomatic heart failure with reduced and with normal ejection fraction in an elderly general population-the CARLA study. *PloS One*. 2013;8:e59225.

210. Tang ASL, Wells GA, Talajic M, Arnold MO, Sheldon R, Connolly S, Hohnloser SH, Nichol G, Birnie DH, Sapp JL, Yee R, Healey JS, Rouleau JL, Resynchronization-Defibrillation for Ambulatory Heart Failure Trial Investigators. Cardiac-resynchronization therapy for mild-to-moderate heart failure. *N Engl J Med*. 2010;363:2385–2395.

211. Wannamethee G, Shaper AG, Macfarlane PW, Walker M. Risk factors for sudden cardiac death in middle-aged British men. *Circulation*. 1995;91:1749–1756.

212. Exner DV, Kavanagh KM, Slawnych MP, Mitchell LB, Ramadan D, Aggarwal SG, Noullett C, Van Schaik A, Mitchell RT, Shibata MA, Gulamhussein S, McMeekin J, Tymchak W, Schnell G, Gillis AM, Sheldon RS, Fick GH, Duff HJ, REFINE Investigators. Noninvasive risk assessment early after a myocardial infarction the REFINE study. *J Am Coll Cardiol*. 2007;50:2275–2284.

213. Køber L, Thune JJ, Nielsen JC, Haarbo J, Videbæk L, Korup E, Jensen G, Hildebrandt P, Steffensen FH, Bruun NE, Eiskjær H, Brandes A, Thøgersen AM, Gustafsson F, Egstrup K, Videbæk R, Hassager C, Svendsen JH, Høfsten DE, Torp-Pedersen C, Pehrson S, DANISH Investigators. Defibrillator Implantation in Patients with Nonischemic Systolic Heart Failure. *N Engl J Med*. 2016;375:1221–1230.

214. Narula J, Gerson M, Thomas GS, Cerqueira MD, Jacobson AF. 123I-MIBG Imaging for Prediction of Mortality and Potentially Fatal Events in Heart Failure: The ADMIRE-HFX Study. *J Nucl Med*. 2015;56:1011–1018.

215. Wakabayashi T, Nakata T, Hashimoto A, Yuda S, Tsuchihashi K, Travin MI, Shimamoto K. Assessment of underlying etiology and cardiac sympathetic innervation to identify patients at high risk of cardiac death. *J Nucl Med Off Publ Soc Nucl Med*. 2001;42:1757–1767.

216. Verberne HJ, Brewster LM, Somsen GA, van Eck-Smit BLF. Prognostic value of myocardial 123I-metaiodobenzylguanidine (MIBG) parameters in patients with heart failure: a systematic review. *Eur Heart J*. 2008;29:1147–1159.

217. Kuwabara Y, Tamaki N, Nakata T, Yamashina S, Yamazaki J. Determination of the survival rate in patients with congestive heart failure stratified by ^{123}I-MIBG imaging: a meta-analysis from the studies performed in Japan. *Ann Nucl Med*. 2011;25:101–107.

218. Bax JJ, Kraft O, Buxton AE, Fjeld JG, Parizek P, Agostini D, Knuuti J, Flotats A, Arrighi J, Muxi A, Alibelli M-J, Banerjee G, Jacobson AF. 123I-mIBG Scintigraphy to Predict Inducibility of Ventricular Arrhythmias on Cardiac Electrophysiology Testing: A Prospective Multicenter Pilot Study. *Circ Cardiovasc Imaging*. 2008;1:131–140.

219. Kasama S, Toyama T, Kaneko Y, Iwasaki T, Sumino H, Kumakura H, Minami K, Ichikawa S, Matsumoto N, Sato Y, Kurabayashi M. Relationship between late ventricular potentials and myocardial 123I-metaiodobenzylguanidine scintigraphy in patients with dilated cardiomyopathy with mild to moderate heart failure: results of a prospective study of sudden death events. *Eur J Nucl Med Mol Imaging*. 2012;39:1056–1064.

220. Boogers MJ, Borleffs CJW, Henneman MM, van Bommel RJ, van Ramshorst J, Boersma E, Dibbets-Schneider P, Stokkel MP, van der Wall EE, Schalij MJ, Bax JJ. Cardiac sympathetic denervation assessed with 123-iodine metaiodobenzylguanidine imaging predicts ventricular arrhythmias in implantable cardioverter-defibrillator patients. *J Am Coll Cardiol*. 2010;55:2769–2777.

221. Nishisato K, Hashimoto A, Nakata T, Doi T, Yamamoto H, Nagahara D, Shimoshige S, Yuda S, Tsuchihashi K, Shimamoto K. Impaired Cardiac Sympathetic Innervation and Myocardial Perfusion Are Related to Lethal Arrhythmia: Quantification of Cardiac Tracers in Patients with ICDs. *J Nucl Med*. 2010;51:1241–1249.

222. Fallavollita JA, Dare JD, Carter RL, Baldwa S, Canty JM. Denervated Myocardium Is Preferentially Associated With Sudden Cardiac Arrest in Ischemic Cardiomyopathy: A Pilot Competing Risks Analysis of Cause-Specific Mortality. *Circ Cardiovasc Imaging*. 2017;10.

223. Cohen-Solal A, Rouzet F, Berdeaux A, Le Guludec D, Abergel E, Syrota A, Merlet P. Effects of carvedilol on myocardial sympathetic innervation in patients with chronic heart failure. *J Nucl Med Off Publ Soc Nucl Med*. 2005;46:1796–1803.

224. Hall AB, Ziadi MC, Leech JA, Chen S-Y, Burwash IG, Renaud J, deKemp RA, Haddad H, Mielniczuk LM, Yoshinaga K, Guo A, Chen L, Walter O, Garrard L, DaSilva JN, Floras JS, Beanlands RSB. Effects of Short-Term Continuous Positive Airway Pressure on Myocardial Sympathetic Nerve Function and Energetics in Patients With Heart Failure and Obstructive Sleep Apnea: A Randomized Study. *Circulation*. 2014;130:892–901.

225. Kasama S, Toyama T, Kumakura H, Takayama Y, Ichikawa S, Suzuki T, Kurabayashi M. Effect of spironolactone on cardiac sympathetic nerve activity and left ventricular

remodeling in patients with dilated cardiomyopathy. *J Am Coll Cardiol*. 2003;41:574–581.

226. Ohira H, Beanlands RS, Davies RA, Mielniczuk L. The role of nuclear imaging in pulmonary hypertension. *J Nucl Cardiol*. 2015;22:141–157.

227. Mak S, Witte KK, Al-Hesayen A, Granton JJ, Parker JD. Cardiac sympathetic activation in patients with pulmonary arterial hypertension. *AJP Regul Integr Comp Physiol*. 2012;302:R1153–R1157.

228. Velez-Roa S. Increased Sympathetic Nerve Activity in Pulmonary Artery Hypertension. *Circulation*. 2004;110:1308–1312.

229. Morimitsu T, Miyahara Y, Sinboku H, Ikeda S, others. Iodine-123-metaiodobenzyguanidine myocardial imaging in patients with right ventricular pressure overload. *J Nucl Med*. 1996;37:1343.

230. Morimitsu T, Miyahara Y, Sonoda K, Kohno S. Iodine-123 metaiodobenzylguanidine myocardial imaging in patients with pulmonary hypertension. *J Int Med Res*. 1997;25:53–61.

231. Sakamaki F, Satoh T, Nagaya N, Kyotani S, Oya H, Nakanishi N, Kuribayashi S, Ishida Y. Correlation between severity of pulmonary arterial hypertension and 123I-metaiodobenzylguanidine left ventricular imaging. *J Nucl Med*. 2000;41:1127–1133.

232. Mazzadi AN, Pineau J, Costes N, Le Bars D, Bonnefoi F, Croisille P, Porcher R, Chevalier P. Muscarinic Receptor Upregulation in Patients With Myocardial Infarction: A New Paradigm. *Circ Cardiovasc Imaging*. 2009;2:365–372.

233. Le Guludec D, Cohen-Solal A, Delforge J, Delahaye N, Syrota A, Merlet P. Increased Myocardial Muscarinic Receptor Density in Idiopathic Dilated Cardiomyopathy: An In Vivo PET Study. *Circulation*. 1997;96:3416–3422.

234. Konstam MA, Kiernan MS, Bernstein D, Bozkurt B, Jacob M, Kapur NK, Kociol RD, Lewis EF, Mehra MR, Pagani FD, Raval AN, Ward C, American Heart Association Council on Clinical Cardiology; Council on Cardiovascular Disease in the Young; and Council on Cardiovascular Surgery and Anesthesia. Evaluation and Management of Right-Sided Heart Failure: A Scientific Statement From the American Heart Association. *Circulation*. 2018;137:e578–e622.

235. Califf RM, Adams KF, McKenna WJ, Gheorghiade M, Uretsky BF, McNulty SE, Darius H, Schulman K, Zannad F, Handberg-Thurmond E, Harrell FE, Wheeler W, Soler-Soler J, Swedberg K. A randomized controlled trial of epoprostenol therapy for severe congestive heart failure: The Flolan International Randomized Survival Trial (FIRST). *Am Heart J*. 1997;134:44–54.

236. Redfield MM, Chen HH, Borlaug BA, Semigran MJ, Lee KL, Lewis G, LeWinter MM, Rouleau JL, Bull DA, Mann DL, Deswal A, Stevenson LW, Givertz MM, Ofili EO, O'Connor CM, Felker GM, Goldsmith SR, Bart BA, McNulty SE, Ibarra JC, Lin G, Oh JK, Patel MR, Kim RJ, Tracy RP, Velazquez EJ, Anstrom KJ, Hernandez AF, Mascette AM, Braunwald E, RELAX Trial for the. Effect of Phosphodiesterase-5 Inhibition on Exercise Capacity and Clinical Status in Heart Failure With Preserved Ejection Fraction: A Randomized Clinical Trial. *JAMA*. 2013;309:1268.

237. Koller B, Steringer-Mascherbauer R, Ebner CH, Weber Th, Ammer M, Eichinger J, Pretsch I, Herold M, Schwaiger J, Ulmer H, Grander W. Pilot Study of Endothelin Receptor Blockade in Heart Failure with Diastolic Dysfunction and Pulmonary Hypertension (BADDHY-Trial). *Heart Lung Circ*. 2017;26:433–441.

238. Abraham WT, Adamson PB, Bourge RC, Aaron MF, Costanzo MR, Stevenson LW, Strickland W, Neelagaru S, Raval N, Krueger S, Weiner S, Shavelle D, Jeffries B, Yadav JS. Wireless pulmonary artery haemodynamic monitoring in chronic heart failure: a randomised controlled trial. *The Lancet*. 2011;377:658–666.

239. Mullens W, Abrahams Z, Francis GS, Sokos G, Taylor DO, Starling RC, Young JB, Tang WHW. Importance of venous congestion for worsening of renal function in advanced decompensated heart failure. *J Am Coll Cardiol*. 2009;53:589–596.

240. Alajaji W, Baydoun A, Al-Kindi SG, Henry L, Hanna MA, Oliveira GH. Digoxin therapy for cor pulmonale: A systematic review. *Int J Cardiol*. 2016;223:320–324.

241. Packer M, Bristow MR, Cohn JN, Colucci WS, Fowler MB, Gilbert EM, Shusterman NH. The effect of carvedilol on morbidity and mortality in patients with chronic heart failure. U.S. Carvedilol Heart Failure Study Group. *N Engl J Med*. 1996;334:1349–1355.

242. Galiè N, Humbert M, Vachiery J-L, Gibbs S, Lang I, Torbicki A, Simonneau G, Peacock A, Vonk Noordegraaf A, Beghetti M, Ghofrani A, Gomez Sanchez MA, Hansmann G, Klepetko W, Lancellotti P, Matucci M, McDonagh T, Pierard LA, Trindade PT, Zompatori M, Hoeper M. 2015 ESC/ERS Guidelines for the diagnosis and treatment of pulmonary hypertension: The Joint Task Force for the Diagnosis and Treatment of Pulmonary Hypertension of the European Society of Cardiology (ESC) and the European Respiratory Society (ERS)Endorsed by: Association for European Paediatric and Congenital Cardiology (AEPC), International Society for Heart and Lung Transplantation (ISHLT). *Eur Heart J*. 2016;37:67–119.

243. de Man FS, Handoko ML, van Ballegoij JJM, Schalij I, Bogaards SJP, Postmus PE, van der Velden J, Westerhof N, Paulus WJ, Vonk-Noordegraaf A. Bisoprolol Delays Progression Towards Right Heart Failure in Experimental Pulmonary Hypertension. *Circ Heart Fail*. 2012;5:97–105.

244. Perros F, Frances S, Bogaard HJ, Antigny F, Simonneau G, Bonnet S, Provencher S, Galiè N, Humbert M. Use of β-Blockers in Pulmonary Hypertension. *Circ Heart Fail*. 2017;10:e003703.

245. Giardini A, Lovato L, Donti A, Formigari R, Gargiulo G, Picchio FM, Fattori R. A pilot study on the effects of carvedilol on right ventricular remodelling and exercise tolerance in patients with systemic right ventricle. *Int J Cardiol*. 2007;114:241–246.

246. van Campen JSJA, de Boer K, van de Veerdonk MC, van der Bruggen CEE, Allaart CP, Raijmakers PG, Heymans MW, Marcus JT, Harms HJ, Handoko ML, de Man FS, Vonk Noordegraaf A, Bogaard H-J. Bisoprolol in idiopathic pulmonary arterial hypertension: an explorative study. *Eur Respir J*. 2016;48:787–796.

247. Farha S, Saygin D, Park MM, Cheong HI, Asosingh K, Comhair SAA, Stephens OR, Roach EC, Sharp J, Highland KB, DiFilippo FP, Neumann DR, Tang WHW, Erzurum SC. Pulmonary arterial hypertension treatment with carvedilol for heart failure: a randomized controlled trial. *JCI Insight* [Internet]. 2017 [cited 2017 Nov 13];2. Available from: https://insight.jci.org/articles/view/95240

248. Yamamoto K, Origasa H, Hori M, J-DHF Investigators. Effects of carvedilol on heart failure with preserved ejection fraction: the Japanese Diastolic Heart Failure Study (J-DHF). *Eur J Heart Fail*. 2013;15:110–118.

249. Rothman AMK, Vachiery J-L, Howard LS, Mikhail GW, Lang IM, Jonas M, Kiely DG, Shav D, Shabtay O, Avriel A, Lewis GD, Rosenzweig EB, Kirtane AJ, Kim NH, Mahmud E, McLaughlain VV, Chetcuti S, Leon MB, Ben-Yehuda O, Rubin LJ. Intravascular Ultrasound Pulmonary Artery Denervation to Treat Pulmonary Arterial Hypertension (TROPHY1): Multicenter, Early Feasibility Study. *JACC Cardiovasc Interv*. 2020;13:989–999.

250. Chen S-L, Zhang F-F, Xu J, Xie D-J, Zhou L, Nguyen T, Stone GW. Pulmonary Artery Denervation to Treat Pulmonary Arterial Hypertension. *J Am Coll Cardiol*. 2013;62:1092–1100.

251. Liao S-Y, Zhen Z, Liu Y, Au K-W, Lai W-H, Tsang A, Tse H-F. Improvement of Myocardial Function Following Catheter-Based Renal Denervation in Heart Failure. *JACC Basic Transl Sci*. 2017;2:270–281.

252. Keimei Yoshida, Keita Saku, Kazuhiro Kamada, Mariko Tanaka, Takuya Akashi, Kohtaro Abe, Takuya Kishi, Kenji Sunagawa, Hiroyuki Tsutsui. Abstract 15401: Electrical Vagal Nerve Stimulation Significantly Redresses Autonomic Balance, Lowers Pulmonary Vascular Resistance and Improves Survival in Rats With Pulmonary Arterial Hypertension. *Circulation*. 2018;136:A15401.

253. Rich S, Martinez J, Lam W, Rosen KM. Captopril as treatment for patients with pulmonary hypertension. Problem of variability in assessing chronic drug treatment. *Br Heart J*. 1982;48:272–277.

254. Leier CV, Bambach D, Nelson S, Hermiller JB, Huss P, Magorien RD, Unverferth DV. Captopril in primary pulmonary hypertension. *Circulation*. 1983;67:155–161.

255. Dai H, Jiang L, Xiao Z, Guang X. ACE2-angiotensin-(1-7)-Mas axis might be a promising therapeutic target for pulmonary arterial hypertension. *Nat Rev Cardiol*. 2015;12:374.

256. Shenoy V, Kwon K-C, Rathinasabapathy A, Lin S, Jin G, Song C, Shil P, Nair A, Qi Y, Li Q, Francis J, Katovich MJ, Daniell H, Raizada MK. Oral delivery of Angiotensin-converting enzyme 2 and Angiotensin-(1-7) bioencapsulated in plant cells attenuates pulmonary hypertension. *Hypertens Dallas Tex 1979*. 2014;64:1248–1259.

257. Preston IR, Sagliani KD, Warburton RR, Hill NS, Fanburg BL, Jaffe IZ. Mineralocorticoid receptor antagonism attenuates experimental pulmonary hypertension. *AJP Lung Cell Mol Physiol*. 2013;304:L678–L688.

258. Borgdorff MA, Bartelds B, Dickinson MG, Steendijk P, Berger RMF. A cornerstone of heart failure treatment is not effective in experimental right ventricular failure. *Int J Cardiol*. 2013;169:183–189.

259. Maron BA, Waxman AB, Opotowsky AR, Gillies H, Blair C, Aghamohammadzadeh R, Loscalzo J, Leopold JA. Effectiveness of Spironolactone Plus Ambrisentan for Treatment of Pulmonary Arterial Hypertension (from the [ARIES] Study 1 and 2 Trials). *Am J Cardiol*. 2013;112:720–725.

260. Voelkel NF, Bogaard HJ, Al Husseini A, Farkas L, Gomez-Arroyo J, Natarajan R. Antioxidants for the treatment of patients with severe angioproliferative pulmonary hypertension? *Antioxid Redox Signal*. 2013;18:1810–1817.

261. Yet SF, Perrella MA, Layne MD, Hsieh CM, Maemura K, Kobzik L, Wiesel P, Christou H, Kourembanas S, Lee ME. Hypoxia induces severe right ventricular dilatation and infarction in heme oxygenase-1 null mice. *J Clin Invest*. 1999;103:R23-29.

262. Redout EM, van der Toorn A, Zuidwijk MJ, van de Kolk CWA, van Echteld CJA, Musters RJP, van Hardeveld C, Paulus WJ, Simonides WS. Antioxidant treatment attenuates pulmonary arterial hypertension-induced heart failure. *Am J Physiol-Heart Circ Physiol*. 2010;298:H1038–H1047.

263. Murakami K. New Components of the Renin-Angiotensin-Aldosterone System and Oxidative Stress. *J Hypertens Open Access* [Internet]. 2015 [cited 2018 Oct 24];04. Available from: http://www.omicsgroup.org/journals/new-components-of-the-reninangiotensinaldosterone-system-andoxidative-stress-2167-1095-1000211.php?aid=65565

264. Michelakis ED, McMurtry MS, Wu X-C, Dyck JRB, Moudgil R, Hopkins TA, Lopaschuk GD, Puttagunta L, Waite R, Archer SL. Dichloroacetate, a metabolic modulator, prevents and reverses chronic hypoxic pulmonary hypertension in rats: role of increased expression and activity of voltage-gated potassium channels. *Circulation*. 2002;105:244–250.

265. Michelakis ED, Gurtu V, Webster L, Barnes G, Watson G, Howard L, Cupitt J, Paterson I, Thompson RB, Chow K, O'Regan DP, Zhao L, Wharton J, Kiely DG, Kinnaird A, Boukouris AE, White C, Nagendran J, Freed DH, Wort SJ, Gibbs JSR, Wilkins MR. Inhibition of pyruvate dehydrogenase kinase improves pulmonary arterial hypertension in genetically susceptible patients. *Sci Transl Med*. 2017;9:eaao4583.

266. Khan SS, Cuttica MJ, Beussink-Nelson L, Kozyleva A, Sanchez C, Mkrdichian H, Selvaraj S, Dematte JE, Lee DC, Shah SJ. Effects of Ranolazine on Exercise Capacity, Right Ventricular Indices, and Hemodynamic Characteristics in Pulmonary Arterial Hypertension: A Pilot Study. *Pulm Circ*. 2015;5:547–556.

267. Maier LS, Layug B, Karwatowska-Prokopczuk E, Belardinelli L, Lee S, Sander J, Lang C, Wachter R, Edelmann F, Hasenfuss G, Jacobshagen C. RAnoLazIne for the Treatment of Diastolic Heart Failure in Patients With Preserved Ejection Fraction. *JACC Heart Fail*. 2013;1:115–122.

268. Frump AL, Bonnet S, de Jesus Perez VA, Lahm T. Emerging role of angiogenesis in adaptive and maladaptive right ventricular remodeling in pulmonary hypertension. *Am J Physiol Lung Cell Mol Physiol*. 2018;314:L443–L460.

269. Oka T, Akazawa H, Naito AT, Komuro I. Angiogenesis and cardiac hypertrophy: maintenance of cardiac function and causative roles in heart failure. *Circ Res*. 2014;114:565–571.

270. Suen CM, Mei SHJ, Kugathasan L, Stewart DJ. Targeted delivery of genes to endothelial cells and cell- and gene-based therapy in pulmonary vascular diseases. *Compr Physiol*. 2013;3:1749–1779.

271. Bristow MR, Long CS. Cardiotrophin-1 in Heart Failure. *Circulation*. 2002;106:1430–1432.

272. Hirota H, Chen J, Betz UA, Rajewsky K, Gu Y, Ross J, Müller W, Chien KR. Loss of a gp130 cardiac muscle cell survival pathway is a critical event in the onset of heart failure during biomechanical stress. *Cell*. 1999;97:189–198.

273. Ghiroldi A, Piccoli M, Cirillo F, Monasky MM, Ciconte G, Pappone C, Anastasia L. Cell-Based Therapies for Cardiac Regeneration: A Comprehensive Review of Past and Ongoing Strategies. *Int J Mol Sci*. 2018;19.

274. Loisel F, Provost B, Haddad F, Guihaire J, Amsallem M, Vrtovec B, Fadel E, Uzan G, Mercier O. Stem cell therapy targeting the right ventricle in pulmonary arterial

hypertension: is it a potential avenue of therapy? *Pulm Circ*. 2018;8:204589321875597.

275. Oommen S, Yamada S, Cantero Peral S, Campbell KA, Bruinsma ES, Terzic A, Nelson TJ. Human umbilical cord blood-derived mononuclear cells improve murine ventricular function upon intramyocardial delivery in right ventricular chronic pressure overload. *Stem Cell Res Ther* [Internet]. 2015 [cited 2018 Oct 16];6. Available from: http://stemcellres.com/content/6/1/50

276. Trac D, Xu C, Davis ME. Abstract 20115:Aggregation of Child Cardiac Progenitor Cells into Spheres Activates Notch Signaling and Improves Treatment of Right Ventricular Heart Failure. *Circulation*. 136:A20115.

277. Zhao YD, Courtman DW, Deng Y, Kugathasan L, Zhang Q, Stewart DJ. Rescue of monocrotaline-induced pulmonary arterial hypertension using bone marrow-derived endothelial-like progenitor cells: efficacy of combined cell and eNOS gene therapy in established disease. *Circ Res*. 2005;96:442–450.

278. Navaneethan SD, Wehbe E, Heresi GA, Gaur V, Minai OA, Arrigain S, Nally JV, Schold JD, Rahman M, Dweik RA. Presence and outcomes of kidney disease in patients with pulmonary hypertension. *Clin J Am Soc Nephrol CJASN*. 2014;9:855–863.

279. Nickel NP, O'Leary JM, Brittain EL, Fessel JP, Zamanian RT, West JD, Austin ED. Kidney dysfunction in patients with pulmonary arterial hypertension. *Pulm Circ*. 2017;7:38–54.

280. Weatherald J, Boucly A, Sitbon O. Risk stratification in pulmonary arterial hypertension: *Curr Opin Pulm Med*. 2018;24:407–415.

281. Weatherald J, Boucly A, Launay D, Cottin V, Prévot G, Bourlier D, Dauphin C, Chaouat A, Savale L, Jaïs X, Jevnikar M, Traclet J, De Groote P, Simonneau G, Hachulla E, Mouthon L, Montani D, Humbert M, Sitbon O. Haemodynamics and serial risk assessment in systemic sclerosis associated pulmonary arterial hypertension. *Eur Respir J*. 2018;52.

282. Weatherald J, Boucly A, Sahay S, Humbert M, Sitbon O. The Low-Risk Profile in Pulmonary Arterial Hypertension. Time for a Paradigm Shift to Goal-oriented Clinical Trial Endpoints? *Am J Respir Crit Care Med*. 2018;197:860–868.

283. National Kidney Foundation. K/DOQI clinical practice guidelines for chronic kidney disease: evaluation, classification, and stratification. *Am J Kidney Dis Off J Natl Kidney Found*. 2002;39:S1-266.

284. Chakinala MM, Coyne DW, Benza RL, Frost AE, McGoon MD, Hartline BK, Frantz RP, Selej M, Zhao C, Mink DR, Farber HW. Impact of declining renal function on outcomes in pulmonary arterial hypertension: A REVEAL registry analysis. *J Heart Lung Transplant*. 2018;37:696–705.

285. Persson F, Rossing P. Diagnosis of diabetic kidney disease: state of the art and future perspective. *Kidney Int Suppl*. 2018;8:2–7.

286. Rangaswami J, Bhalla V, Blair JEA, Chang TI, Costa S, Lentine KL, Lerma EV, Mezue K, Molitch M, Mullens W, Ronco C, Tang WHW, McCullough PA, On behalf of the American Heart Association Council on the Kidney in Cardiovascular Disease and Council on Clinical Cardiology. Cardiorenal Syndrome: Classification, Pathophysiology, Diagnosis, and Treatment Strategies: A Scientific Statement From the American Heart Association. *Circulation* [Internet]. 2019 [cited 2019 Jun 5];139. Available from: https://www.ahajournals.org/doi/10.1161/CIR.0000000000000664

287. Ronco C, Haapio M, House AA, Anavekar N, Bellomo R. Cardiorenal Syndrome. *J Am Coll Cardiol*. 2008;52:1527–1539.

288. Aronson D, Abassi Z, Allon E, Burger AJ. Fluid loss, venous congestion, and worsening renal function in acute decompensated heart failure. *Eur J Heart Fail*. 2013;15:637–643.

289. Zelt JGE, Mielniczuk LM, Liu PP, Dupuis J-Y, Chih S, Akbari A, Sun LY. Utility of Novel Cardiorenal Biomarkers in the Prediction and Early Detection of Congestive Kidney Injury Following Cardiac Surgery. *J Clin Med*. 2018;7.

290. Courand P-Y, Pina Jomir G, Khouatra C, Scheiber C, Turquier S, Glérant J-C, Mastroianni B, Gentil B, Blanchet-Legens A-S, Dib A, Derumeaux G, Humbert M, Mornex J-F, Cordier J-F, Cottin V. Prognostic value of right ventricular ejection fraction in pulmonary arterial hypertension. *Eur Respir J*. 2015;45:139–149.

291. van Wolferen SA, Marcus JT, Boonstra A, Marques KMJ, Bronzwaer JGF, Spreeuwenberg MD, Postmus PE, Vonk-Noordegraaf A. Prognostic value of right ventricular mass, volume, and function in idiopathic pulmonary arterial hypertension. *Eur Heart J*. 2007;28:1250–1257.

292. de Groote P, Millaire A, Foucher-Hossein C, Nugue O, Marchandise X, Ducloux G, Lablanche JM. Right ventricular ejection fraction is an independent predictor of survival in patients with moderate heart failure. *J Am Coll Cardiol*. 1998;32:948–954.

293. Ghio S, Gavazzi A, Campana C, Inserra C, Klersy C, Sebastiani R, Arbustini E, Recusani F, Tavazzi L. Independent and additive prognostic value of right ventricular systolic function and pulmonary artery pressure in patients with chronic heart failure. *J Am Coll Cardiol*. 2001;37:183–188.

294. Vonk-Noordegraaf A, Haddad F, Chin KM, Forfia PR, Kawut SM, Lumens J, Naeije R, Newman J, Oudiz RJ, Provencher S, Torbicki A, Voelkel NF, Hassoun PM. Right Heart Adaptation to Pulmonary Arterial Hypertension. *J Am Coll Cardiol*. 2013;62:D22–D33.

295. D'Alonzo GE, Barst RJ, Ayres SM, Bergofsky EH, Brundage BH, Detre KM, Fishman AP, Goldring RM, Groves BM, Kernis JT. Survival in patients with primary pulmonary

hypertension. Results from a national prospective registry. *Ann Intern Med*. 1991;115:343–349.

296. Ishikawa M, Sato N, Asai K, Takano T, Mizuno K. Effects of a pure α/β-adrenergic receptor blocker on monocrotaline-induced pulmonary arterial hypertension with right ventricular hypertrophy in rats. *Circ J*. 2009;73:2337–2341.

297. Provencher S, Herve P, Jais X, Lebrec D, Humbert M, Simonneau G, Sitbon O. Deleterious Effects of β-Blockers on Exercise Capacity and Hemodynamics in Patients With Portopulmonary Hypertension. *Gastroenterology*. 2006;130:120–126.

298. Rubin LJ. The adrenergic nervous system as a therapeutic target in pulmonary arterial hypertension: a cautionary tale. *Eur Respir J*. 2016;48:617–618.

299. Poole-Wilson PA, Swedberg K, Cleland JGF, Di Lenarda A, Hanrath P, Komajda M, Lubsen J, Lutiger B, Metra M, Remme WJ, Torp-Pedersen C, Scherhag A, Skene A, Carvedilol Or Metoprolol European Trial Investigators. Comparison of carvedilol and metoprolol on clinical outcomes in patients with chronic heart failure in the Carvedilol Or Metoprolol European Trial (COMET): randomised controlled trial. *Lancet Lond Engl*. 2003;362:7–13.

300. Lee W, Woo ER, Choi JS. Effects of myricetin on the bioavailability of carvedilol in rats. *Pharm Biol*. 2012;50:516–522.

301. Wang T, Wu KY, Miner RC, Renaud JM, Beanlands RSB, deKemp RA. Reproducible quantification of cardiac sympathetic innervation using graphical modeling of carbon-11-meta-hydroxyephedrine kinetics with dynamic PET-CT imaging. *EJNMMI Res*. 2018;8:63.

302. Harms HJ, de Haan S, Knaapen P, Allaart CP, Rijnierse MT, Schuit RC, Windhorst AD, Lammertsma AA, Huisman MC, Lubberink M. Quantification of [(11)C]-meta-hydroxyephedrine uptake in human myocardium. *EJNMMI Res*. 2014;4:52.

303. Sisson JC, Bolgos G, Johnson J. Measuring acute changes in adrenergic nerve activity of the heart in the living animal. *Am Heart J*. 1991;121:1119–1123.

304. Thackeray JT, deKemp RA, Beanlands RS, DaSilva JN. Early diabetes treatment does not prevent sympathetic dysinnervation in the streptozotocin diabetic rat heart. *J Nucl Cardiol Off Publ Am Soc Nucl Cardiol*. 2014;21:829–841.

305. Thackeray JT, Renaud JM, Kordos M, Klein R, deKemp RA, Beanlands RSB, DaSilva JN. Test–retest repeatability of quantitative cardiac 11C-meta-hydroxyephedrine measurements in rats by small animal positron emission tomography. *Nucl Med Biol*. 2013;40:676–681.

306. Matsunari I, Aoki H, Nomura Y, Takeda N, Chen W-P, Taki J, Nakajima K, Nekolla SG, Kinuya S, Kajinami K. Iodine-123 Metaiodobenzylguanidine Imaging and Carbon-11

Hydroxyephedrine Positron Emission Tomography Compared in Patients With Left Ventricular Dysfunction. *Circ Cardiovasc Imaging*. 2010;3:595–603.

307. Thackeray JT, Renaud JM, Kordos M, Klein R, Dekemp RA, Beanlands RSB, DaSilva JN. Test-retest repeatability of quantitative cardiac 11C-meta-hydroxyephedrine measurements in rats by small animal positron emission tomography. *Nucl Med Biol*. 2013;40:676–681.

308. van den Hoff J, Burchert W, Börner AR, Fricke H, Kühnel G, Meyer GJ, Otto D, Weckesser E, Wolpers HG, Knapp WH. [1-(11)C]Acetate as a quantitative perfusion tracer in myocardial PET. *J Nucl Med Off Publ Soc Nucl Med*. 2001;42:1174–1182.

309. Gomez O, Okumura K, Honjo O, Sun M, Ishii R, Bijnens B, Friedberg MK. Heart rate reduction improves biventricular function and interactions in experimental pulmonary hypertension. *Am J Physiol Heart Circ Physiol*. 2018;314:H542–H551.

310. Kaye DM, Lefkovits J, Jennings GL, Bergin P, Broughton A, Esler MD. Adverse consequences of high sympathetic nervous activity in the failing human heart. *J Am Coll Cardiol*. 1995;26:1257–1263.

311. Zelt JGE, deKemp RA, Rotstein BH, Nair GM, Narula J, Ahmadi A, Beanlands RS, Mielniczuk LM. Nuclear Imaging of the Cardiac Sympathetic Nervous System: A Disease-Specific Interpretation in Heart Failure. *JACC Cardiovasc Imaging*. 2019;

312. Yamazaki J, Muto H, Kabano T, Yamashina S, Nanjo S, Inoue A. Evaluation of beta-blocker therapy in patients with dilated cardiomyopathy--Clinical meaning of iodine 123-metaiodobenzylguanidine myocardial single-photon emission computed tomography. *Am Heart J*. 2001;141:645–652.

313. Fujimoto S, Inoue A, Hisatake S, Yamashina S, Yamashina H, Nakano H, Yamazaki J. Usefulness of 123I-metaiodobenzylguanidine myocardial scintigraphy for predicting the effectiveness of beta-blockers in patients with dilated cardiomyopathy from the standpoint of long-term prognosis. *Eur J Nucl Med Mol Imaging*. 2004;31:1356–1361.

314. Machado CR, Camargos ER, Guerra LB, Maria da Consolação VM. Cardiac autonomic denervation in congestive heart failure: comparison of Chagas' heart disease with other dilated cardiomyopathy. *Hum Pathol*. 2000;31:3–10.

315. Yoshida K, Saku K, Kamada K, Abe K, Tanaka-Ishikawa M, Tohyama T, Nishikawa T, Kishi T, Sunagawa K, Tsutsui H. Electrical Vagal Nerve Stimulation Ameliorates Pulmonary Vascular Remodeling and Improves Survival in Rats With Severe Pulmonary Arterial Hypertension. *JACC Basic Transl Sci*. 2018;3:657–671.

316. Suwa M, Otake Y, Moriguchi A, Ito T, Hirota Y, Kawamura K, Adachi I, Narabayashi I. Iodine-123 metaiodobenzylguanidine myocardial scintigraphy for prediction of response to beta-blocker therapy in patients with dilated cardiomyopathy. *Am Heart J*. 1997;133:353–358.

317. Blair JEA, Huffman M, Shah SJ. Heart Failure in North America. *Curr Cardiol Rev*. 2013;9:128–146.

318. Allman KC, Wieland DM, Muzik O, Degrado TR, Wolfe ER, Schwaiger M. Carbon-11 hydroxyephedrine with positron emission tomography for serial assessment of cardiac adrenergic neuronal function after acute myocardial infarction in humans. *J Am Coll Cardiol*. 1993;22:368–375.

319. Barber MJ, Mueller TM, Henry DP, Felten SY, Zipes DP. Transmural myocardial infarction in the dog produces sympathectomy in noninfarcted myocardium. *Circulation*. 1983;67:787–796.

320. Fallavollita JA, Heavey BM, Luisi AJ, Michalek SM, Baldwa S, Mashtare TL, Hutson AD, deKemp RA, Haka MS, Sajjad M, Cimato TR, Curtis AB, Cain ME, Canty JM. Regional Myocardial Sympathetic Denervation Predicts the Risk of Sudden Cardiac Arrest in Ischemic Cardiomyopathy. *J Am Coll Cardiol*. 2014;63:141–149.

321. Fallavollita JA, Canty JM. Dysinnervated but viable myocardium in ischemic heart disease. *J Nucl Cardiol*. 2010;17:1107–1115.

322. Yu M, Bozek J, Lamoy M, Guaraldi M, Silva P, Kagan M, Yalamanchili P, Onthank D, Mistry M, Lazewatsky J, Broekema M, Radeke H, Purohit A, Cdebaca M, Azure M, Cesati R, Casebier D, Robinson SP. Evaluation of LMI1195, a novel 18F-labeled cardiac neuronal PET imaging agent, in cells and animal models. *Circ Cardiovasc Imaging*. 2011;4:435–443.

323. Yu M, Bozek J, Lamoy M, Kagan M, Benites P, Onthank D, Robinson SP. LMI1195 PET imaging in evaluation of regional cardiac sympathetic denervation and its potential role in antiarrhythmic drug treatment. *Eur J Nucl Med Mol Imaging*. 2012;39:1910–1919.

324. Higuchi T, Yousefi BH, Kaiser F, Gärtner F, Rischpler C, Reder S, Yu M, Robinson S, Schwaiger M, Nekolla SG. Assessment of the 18F-labeled PET tracer LMI1195 for imaging norepinephrine handling in rat hearts. *J Nucl Med Off Publ Soc Nucl Med*. 2013;54:1142–1146.

325. Beanlands RSB, Ruddy TD, deKemp RA, Iwanochko RM, Coates G, Freeman M, Nahmias C, Hendry P, Burns RJ, Lamy A, Mickleborough L, Kostuk W, Fallen E, Nichol G, PARR Investigators. Positron emission tomography and recovery following revascularization (PARR-1): the importance of scar and the development of a prediction rule for the degree of recovery of left ventricular function. *J Am Coll Cardiol*. 2002;40:1735–1743.

326. O'Meara E, Mielniczuk LM, Wells GA, deKemp RA, Klein R, Coyle D, Mc Ardle B, Paterson I, White JA, Arnold M, Friedrich MG, Larose E, Dick A, Chow B, Dennie C, Haddad H, Ruddy T, Ukkonen H, Wisenberg G, Cantin B, Pibarot P, Freeman M,

Turcotte E, Connelly K, Clarke J, Williams K, Racine N, Garrard L, Tardif J-C, DaSilva J, Knuuti J, Beanlands R, IMAGE HF investigators. Alternative Imaging Modalities in Ischemic Heart Failure (AIMI-HF) IMAGE HF Project I-A: study protocol for a randomized controlled trial. *Trials*. 2013;14:218.

327. Beanlands R, Nichol G, Ruddy TD, deKemp RA, Hendry P, Humen D, Racine N, Ross H, Benard F, Coates G, Iwanochko RM, Fallen E, Wells G, Investigators P-2. Evaluation of outcome and cost-effectiveness using an FDG PET-guided approach to management of patients with coronary disease and severe left ventricular dysfunction (PARR-2): rationale, design, and methods. *Control Clin Trials*. 2003;24:776–794.

328. Dilsizian V, Bacharach SL, Beanlands RS, Bergmann SR, Delbeke D, Dorbala S, Gropler RJ, Knuuti J, Schelbert HR, Travin MI. ASNC imaging guidelines/SNMMI procedure standard for positron emission tomography (PET) nuclear cardiology procedures. *J Nucl Cardiol Off Publ Am Soc Nucl Cardiol*. 2016;23:1187–1226.

329. Thackeray JT, Beanlands RS, Dasilva JN. Presence of specific 11C-meta-Hydroxyephedrine retention in heart, lung, pancreas, and brown adipose tissue. *J Nucl Med Off Publ Soc Nucl Med*. 2007;48:1733–1740.

330. Yu M, Bozek J, Kagan M, Guaraldi M, Silva P, Azure M, Onthank D, Robinson SP. Cardiac retention of PET neuronal imaging agent LMI1195 in different species: impact of norepinephrine uptake-1 and -2 transporters. *Nucl Med Biol*. 2013;40:682–688.

331. Hall AB, Ziadi MC, Leech JA, Chen S-Y, Burwash IG, Renaud J, deKemp RA, Haddad H, Mielniczuk LM, Yoshinaga K, Guo A, Chen L, Walter O, Garrard L, DaSilva JN, Floras JS, Beanlands RSB. Effects of Short-Term Continuous Positive Airway Pressure on Myocardial Sympathetic Nerve Function and Energetics in Patients With Heart Failure and Obstructive Sleep Apnea: A Randomized Study. *Circulation*. 2014;130:892–901.

332. Jean Z. Wang, Jonathan B. Moody, Nicole Kaps, Deron Britt, Aaryn Lavallee, Jennifer M. Renaud, Jason G. E. Zelt, Kai Yi Wu, Rob S. Beanlands, James A. Fallavollita, John M. Canty, Robert A. deKemp. Reproducible Quantification of Regional Sympathetic Denervation with [11C]meta-Hydroxyephedrine PET Imaging. *J Nucl Cardiol*. 2020;

333. Wu KY, Zelt JGE, Wang T, Dinculescu V, Miner R, Lapierre C, Kaps N, Lavallee A, Renaud JM, Thackeray J, Mielniczuk LM, Chen S-Y, Burwash IG, DaSilva JN, Beanlands RSB, deKemp RA. Reliable quantification of myocardial sympathetic innervation and regional denervation using [11C]meta-hydroxyephedrine PET. *Eur J Nucl Med Mol Imaging*. 2019;

334. Innis RB, Cunningham VJ, Delforge J, Fujita M, Gjedde A, Gunn RN, Holden J, Houle S, Huang S-C, Ichise M. Consensus nomenclature for in vivo imaging of reversibly binding radioligands. *J Cereb Blood Flow Metab*. 2007;27:1533–1539.

335. DeGrado TR, Hutchins GD, Toorongian SA, Wieland DM, Schwaiger M. Myocardial kinetics of carbon-11-meta-hydroxyephedrine: retention mechanisms and effects of norepinephrine. *J Nucl Med*. 1993;34:1287–1293.

336. Thackeray JT, Beanlands RS, DaSilva JN. Presence of specific 11C-meta-hydroxyephedrine retention in heart, lung, pancreas, and brown adipose tissue. *J Nucl Med*. 2007;48:1733–1740.

337. Farber G, Boczar KE, Wiefels CC, Zelt JGE, Guler EC, deKemp RA, Beanlands RS, Rotstein BH. The Future of Cardiac Molecular Imaging. *Semin Nucl Med* [Internet]. 2020 [cited 2020 Apr 15];Available from: https://linkinghub.elsevier.com/retrieve/pii/S0001299820300064

338. Yoshinaga K, Ohira H, Tsujino I, Oyama-Manabe N, Mielniczuk L, Beanlands RSB, Katoh C, Kasai K, Manabe O, Sato T, Fujii S, Ito YM, Tomiyama Y, Nishimura M, Tamaki N. Attenuated right ventricular energetics evaluated using ^{11}C-acetate PET in patients with pulmonary hypertension. *Eur J Nucl Med Mol Imaging*. 2014;41:1240–1250.

339. Wong YY, Ruiter G, Lubberink M, Raijmakers PG, Knaapen P, Marcus JT, Boonstra A, Lammertsma AA, Westerhof N, van der Laarse WJ, Vonk-Noordegraaf A. Right ventricular failure in idiopathic pulmonary arterial hypertension is associated with inefficient myocardial oxygen utilization. *Circ Heart Fail*. 2011;4:700–706.

340. Ahmadi A, Renaud JM, Promislow S, Burwash IG, Dwivedi G, Klein R, Zelt JGE, deKemp RA, Beanlands RS, Mielniczuk LM. Increased myocardial oxygen consumption rates are associated with maladaptive right ventricular remodelling and decreased event-free survival in heart failure patients. *J Nucl Cardiol (In Press)*. 2020;

341. Cadete VJJ, Deschênes S, Cuillerier A, Brisebois F, Sugiura A, Vincent A, Turnbull D, Picard M, McBride HM, Burelle Y. Formation of mitochondrial-derived vesicles is an active and physiologically relevant mitochondrial quality control process in the cardiac system: Cardiac mitochondrial-derived vesicle formation. *J Physiol*. 2016;594:5343–5362.

342. Armbrecht JJ, Buxton DB, Schelbert HR. Validation of [1-11C]acetate as a tracer for noninvasive assessment of oxidative metabolism with positron emission tomography in normal, ischemic, postischemic, and hyperemic canine myocardium. *Circulation*. 1990;81:1594–1605.

343. Wu KY, Dinculescu V, Renaud JM, Chen S-Y, Burwash IG, Mielniczuk LM, Beanlands RSB, deKemp RA. Repeatable and reproducible measurements of myocardial oxidative metabolism, blood flow and external efficiency using 11C-acetate PET. *J Nucl Cardiol*. 2018;25:1912–1925.

344. Beanlands RS, Nahmias C, Gordon E, Coates G, deKemp R, Firnau G, Fallen E. The effects of beta(1)-blockade on oxidative metabolism and the metabolic cost of ventricular work in patients with left ventricular dysfunction: A double-blind, placebo-controlled, positron-emission tomography study. *Circulation*. 2000;102:2070–2075.

345. Beanlands RS, Bach DS, Raylman R, Armstrong WF, Wilson V, Montieth M, Moore CK, Bates E, Schwaiger M. Acute effects of dobutamine on myocardial oxygen consumption and cardiac efficiency measured using carbon-11 acetate kinetics in patients with dilated cardiomyopathy. *J Am Coll Cardiol*. 1993;22:1389–1398.

346. Lu W, Clasquin MF, Melamud E, Amador-Noguez D, Caudy AA, Rabinowitz JD. Metabolomic analysis via reversed-phase ion-pairing liquid chromatography coupled to a stand alone orbitrap mass spectrometer. *Anal Chem*. 2010;82:3212–3221.

347. Das S, Frisk C, Eriksson MJ, Walentinsson A, Corbascio M, Hage C, Kumar C, Asp M, Lundeberg J, Maret E, Persson H, Linde C, Persson B. Transcriptomics of cardiac biopsies reveals differences in patients with or without diagnostic parameters for heart failure with preserved ejection fraction. *Sci Rep* [Internet]. 2019 [cited 2020 Apr 13];9. Available from: http://www.nature.com/articles/s41598-019-39445-2

348. Dzeja PP, Chung S, Faustino RS, Behfar A, Terzic A. Developmental enhancement of adenylate kinase-AMPK metabolic signaling axis supports stem cell cardiac differentiation. *PloS One*. 2011;6:e19300.

349. Pucar D, Bast P, Gumina RJ, Lim L, Drahl C, Juranic N, Macura S, Janssen E, Wieringa B, Terzic A, Dzeja PP. Adenylate kinase AK1 knockout heart: energetics and functional performance under ischemia-reperfusion. *Am J Physiol-Heart Circ Physiol*. 2002;283:H776–H782.

350. Janssen E, Terzic A, Wieringa B, Dzeja PP. Impaired Intracellular Energetic Communication in Muscles from Creatine Kinase and Adenylate Kinase (M-CK/AK1) Double Knock-out Mice. *J Biol Chem*. 2003;278:30441–30449.

351. Dzeja PP, Vitkevicius KT, Redfield MM, Burnett JC, Terzic A. Adenylate Kinase–Catalyzed Phosphotransfer in the Myocardium: Increased Contribution in Heart Failure. *Circ Res*. 1999;84:1137–1143.

352. Pucar D, Dzeja PP, Bast P, Gumina RJ, Drahl C, Lim L, Juranic N, Macura S, Terzic A. Mapping hypoxia-induced bioenergetic rearrangements and metabolic signaling by 18O-assisted 31P NMR and 1H NMR spectroscopy. *Mol Cell Biochem*. 2004;256–257:281–289.

353. Weiss RG, Gerstenblith G, Bottomley PA. ATP flux through creatine kinase in the normal, stressed, and failing human heart. *Proc Natl Acad Sci*. 2005;102:808–813.

354. Oliff HS, Weber E, Miyazaki B, Marek P. Infarct volume varies with rat strain and vendor in focal cerebral ischemia induced by transcranial middle cerebral artery occlusion. *Brain Res*. 1995;699:329–331.

355. Sebkhi A, Zhao L, Lu L, Haley CS, Nunez DJ, Wilkins MR. Genetic determination of cardiac mass in normotensive rats: results from an F344xWKY cross. *Hypertens Dallas Tex 1979*. 1999;33:949–953.

356. Sitsapesan R, McGarry SJ, Williams AJ. Cyclic ADP-ribose competes with ATP for the adenine nucleotide binding site on the cardiac ryanodine receptor Ca(2+)-release channel. *Circ Res*. 1994;75:596–600.

357. Hancock CR, Janssen E, Terjung RL. Skeletal muscle contractile performance and ADP accumulation in adenylate kinase-deficient mice. *Am J Physiol-Cell Physiol*. 2005;288:C1287–C1297.

358. Lehman TJ, Allen JB, Plotz PH, Wilder RL. Lactobacillus casei cell wall-induced arthritis in rats: cell wall fragment distribution and persistence in chronic arthritis-susceptible LEW/N and -resistant F344/N rats. *Arthritis Rheum*. 1984;27:939–942.

359. Hajdu A, Rona G. Spontaneous thyroiditis in laboratory rats. *Experientia*. 1969;25:1325–1327.

360. Lee JY, Karen FA, Zhou C, Batten L, Cohen MV, Stevens T. EXPRESS: Biventricular diastolic dysfunction, thrombocytopenia and red blood cell macrocytosis in experimental pulmonary arterial hypertension. *Pulm Circ*. 2020;204589402090878.

361. Myerburg RJ, Kessler KM, Castellanos A. Sudden cardiac death: epidemiology, transient risk, and intervention assessment. *Ann Intern Med*. 1993;119:1187–1197.

362. Bennett M, Parkash R, Nery P, Sénéchal M, Mondesert B, Birnie D, Sterns LD, Rinne C, Exner D, Philippon F, Campbell D, Cox J, Dorian P, Essebag V, Krahn A, Manlucu J, Molin F, Slawnych M, Talajic M. Canadian Cardiovascular Society/Canadian Heart Rhythm Society 2016 Implantable Cardioverter-Defibrillator Guidelines. *Can J Cardiol*. 2017;33:174–188.

363. Moss AJ, Greenberg H, Case RB, Zareba W, Hall WJ, Brown MW, Daubert JP, McNitt S, Andrews ML, Elkin AD, Multicenter Automatic Defibrillator Implantation Trial-II (MADIT-II) Research Group. Long-term clinical course of patients after termination of ventricular tachyarrhythmia by an implanted defibrillator. *Circulation*. 2004;110:3760–3765.

364. Rijnierse MT, Allaart CP, de Haan S, Harms HJ, Huisman MC, Beek AM, Lammertsma AA, van Rossum AC, Knaapen P. Non-invasive imaging to identify susceptibility for ventricular arrhythmias in ischaemic left ventricular dysfunction. *Heart*. 2016;102:832–840.

365. Jacobson AF, Senior R, Cerqueira MD, Wong ND, Thomas GS, Lopez VA, Agostini D, Weiland F, Chandna H, Narula J. Myocardial Iodine-123 Meta-Iodobenzylguanidine Imaging and Cardiac Events in Heart Failure. *J Am Coll Cardiol*. 2010;55:2212–2221.

366. Imanli H, Ume KL, Jeudy J, Bob-Manuel T, Smith MF, Chen W, Abdulghani M, Ghzally Y, Mahat JB, Itah R, Restrepo A, See VY, Shorofsky S, Dilsizian V, Dickfeld T. Ventricular Tachycardia (VT) Substrate Characteristics: Insights from Multimodality Structural and Functional Imaging of the VT Substrate Using Cardiac MRI Scar, ^{123} I-Metaiodobenzylguanidine SPECT Innervation, and Bipolar Voltage. *J Nucl Med*. 2019;60:79–85.

367. Fallavollita JA, Heavey BM, Luisi AJ, Michalek SM, Baldwa S, Mashtare TL, Hutson AD, Haka MS, Sajjad M, Cimato TR. Regional myocardial sympathetic denervation predicts the risk of sudden cardiac arrest in ischemic cardiomyopathy. *J Am Coll Cardiol*. 2014;63:141–149.

368. Münch G, Nguyen NTB, Nekolla S, Ziegler S, Muzik O, Chakraborty P, Wieland DM, Schwaiger M. Evaluation of sympathetic nerve terminals with [11C] epinephrine and [11C] hydroxyephedrine and positron emission tomography. *Circulation*. 2000;101:516–523.

369. Raffel DM, Chen W, Sherman PS, Gildersleeve DL, Jung Y-W. Dependence of cardiac 11C-meta-hydroxyephedrine retention on norepinephrine transporter density. *J Nucl Med*. 2006;47:1490–1496.

370. Fricke E, Eckert S, Dongas A, Fricke H, Preuss R, Lindner O, Horstkotte D, Burchert W. Myocardial sympathetic innervation in patients with symptomatic coronary artery disease: Follow-up after 1 year with neurostimulation. *J Nucl Med*. 2008;49:1458–1464.

371. Harms HJ, de Haan S, Knaapen P, Allaart CP, Rijnierse MT, Schuit RC, Windhorst AD, Lammertsma AA, Huisman MC, Lubberink M. Quantification of [11 C]-meta-hydroxyephedrine uptake in human myocardium. *EJNMMI Res*. 2014;4:52.

372. Fallavollita JA, Luisi AJ, Michalek SM, Valverde AM, deKemp RA, Haka MS, Hutson AD, Canty JM. Prediction of arrhythmic events with positron emission tomography: PAREPET study design and methods. *Contemp Clin Trials*. 2006;27:374–388.

373. DeLong ER, DeLong DM, Clarke-Pearson DL. Comparing the areas under two or more correlated receiver operating characteristic curves: a nonparametric approach. *Biometrics*. 1988;44:837–845.

374. Pencina MJ, D'Agostino RB, D'Agostino RB, Vasan RS. Evaluating the added predictive ability of a new marker: from area under the ROC curve to reclassification and beyond. *Stat Med*. 2008;27:157–172; discussion 207-212.

375. Pizzuto MF, Valverde AM, Heavey BM, Banas MD, Michelakis N, Suzuki G, Fallavollita JA, Canty JM. Brief sympathetic activation precedes the development of ventricular tachycardia and ventricular fibrillation in hibernating myocardium. *J Electrocardiol*. 2006;39:S140–S145.

376. Fukuda K, Kanazawa H, Aizawa Y, Ardell JL, Shivkumar K. Cardiac Innervation and Sudden Cardiac Death. *Circ Res*. 2015;116:2005–2019.

377. Ungerer M, Hartmann F, Karoglan M, Chlistalla A, Ziegler S, Richardt G, Overbeck M, Meisner H, Schomig A, Schwaiger M. Regional In Vivo and In Vitro Characterization of Autonomic Innervation in Cardiomyopathic Human Heart. *Circulation*. 1998;97:174–180.

378. Fallavollita JA, Dare JD, Carter RL, Baldwa S, Canty JM. Denervated Myocardium Is Preferentially Associated With Sudden Cardiac Arrest in Ischemic Cardiomyopathy: A Pilot Competing Risks Analysis of Cause-Specific Mortality. *Circ Cardiovasc Imaging* [Internet]. 2017 [cited 2020 Apr 2];10. Available from: https://www.ahajournals.org/doi/10.1161/CIRCIMAGING.117.006446

379. Boogers MJ, Borleffs CJW, Henneman MM, van Bommel RJ, van Ramshorst J, Boersma E, Dibbets-Schneider P, Stokkel MP, van der Wall EE, Schalij MJ, Bax JJ. Cardiac sympathetic denervation assessed with 123-iodine metaiodobenzylguanidine imaging predicts ventricular arrhythmias in implantable cardioverter-defibrillator patients. *J Am Coll Cardiol*. 2010;55:2769–2777.

380. Moss AJ, Zareba W, Hall WJ, Klein H, Wilber DJ, Cannom DS, Daubert JP, Higgins SL, Brown MW, Andrews ML. Prophylactic Implantation of a Defibrillator in Patients with Myocardial Infarction and Reduced Ejection Fraction. *N Engl J Med*. 2002;346:877–883.

381. Singh V, Malhotra S, Canty J, Fallavollita J. The Volume of Denervated Myocardium Predicts Sudden Cardiac Death (SCD) and ICD Therapies for VF but not ICD Therapies for Slower Ventricular Tachyarrhythmia (VT): An Analysis of the Prediction of Arrhythmic Events with Positron Emission Tomography (PAREPET) Study. *J Am Coll Cardiol*. 2018;71.

382. Zelt JGE, DeKemp RA, Rotstein BH, Nair GM, Narula J, Ahmadi A, Beanlands RS, Mielniczuk LM. Nuclear Imaging of the Cardiac Sympathetic Nervous System: A Disease-Specific Interpretation in Heart Failure. *JACC Cardiovasc Imaging*. 2019;

383. Bristow MR, Ginsburg R, Minobe W, Cubicciotti RS, Sageman WS, Lurie K, Billingham ME, Harrison DC, Stinson EB. Decreased catecholamine sensitivity and β-adrenergic-receptor density in failing human hearts. *N Engl J Med*. 1982;307:205–211.

384. Fallavollita JA, Luisi AJ, Michalek SM, Valverde AM, Haka MS, Hutson AD, Canty JM. Prediction of arrhythmic events with positron emission tomography: PAREPET study design and methods. *Contemp Clin Trials*. 2006;27:374–388.

385. Bengel FM, Schwaiger M. Assessment of cardiac sympathetic neuronal function using PET imaging. *J Nucl Cardiol*. 2004;11:603–616.

386. Boschi S, Lodi F, Boschi L, Nanni C, Chondrogiannis S, Colletti PM, Rubello D, Fanti S. 11C-meta-hydroxyephedrine: a promising PET radiopharmaceutical for imaging the sympathetic nervous system. *Clin Nucl Med*. 2015;40:e96–e103.

387. Allman KC, Wieland DM, Muzik O, Degrado TR, Wolfe ER, Schwaiger M. Carbon-11 hydroxyephedrine with positron emission tomography for serial assessment of cardiac adrenergic neuronal function after acute myocardial infarction in humans. *J Am Coll Cardiol*. 1993;22:368–375.

388. Barber MJ, Mueller TM, Henry DP, Felten SY, Zipes DP. Transmural myocardial infarction in the dog produces sympathectomy in noninfarcted myocardium. *Circulation*. 1983;67:787–796.

389. Lautamaki R, Sasano T, Higuchi T, Nekolla SG, Lardo AC, Holt DP, Dannals RF, Abraham MR, Bengel FM. Multiparametric molecular imaging provides mechanistic insights into sympathetic innervation impairment in the viable infarct border zone. *J Nucl Med*. 2015;56:457–463.

390. Hiroshima Y, Manabe O, Naya M, Tomiyama Y, Magota K, Obara M, Aikawa T, Oyama-Manabe N, Yoshinaga K, Hirata K, Kroenke M, Tamaki N, Katoh C. Quantification of myocardial blood flow with 11C-hydroxyephedrine dynamic PET: comparison with 15O-H2O PET. *J Nucl Cardiol*. 2017;1–8.

391. Harms HJ, Lubberink M, de Haan S, Knaapen P, Huisman MC, Schuit RC, Windhorst AD, Allaart CP, Lammertsma AA. Use of a single 11C-meta-hydroxyephedrine scan for assessing flow–innervation mismatches in patients with ischemic cardiomyopathy. *J Nucl Med*. 2015;56:1706–1711.

392. Thackeray JT, Renaud JM, Kordos M, Klein R, Beanlands RSB, DaSilva JN. Test–retest repeatability of quantitative cardiac 11C-meta-hydroxyephedrine measurements in rats by small animal positron emission tomography. *Nucl Med Biol*. 2013;40:676–681.

393. Wang T, Wu KY, Miner RC, Renaud JM, Beanlands RSB. Reproducible quantification of cardiac sympathetic innervation using graphical modeling of carbon-11-meta-hydroxyephedrine kinetics with dynamic PET-CT imaging. *EJNMMI Res*. 2018;8:63.

394. Wu KY, Dinculescu V, Renaud JM, Chen S-Y, Burwash IG, Mielniczuk LM, Beanlands RSB, DeKemp RA. Repeatable and reproducible measurements of myocardial

oxidative metabolism, blood flow and external efficiency using 11 C-acetate PET. *J Nucl Cardiol*. 2018;1–14.

395. Rosenspire KC, Haka MS, Van Dort ME, Jewett DM, Gildersleeve DL, Schwaiger M, Wieland DM. Synthesis and preliminary evaluation of carbon-11-meta-hydroxyephedrine: a false transmitter agent for heart neuronal imaging. *J Nucl Med*. 1990;31:1328–1334.

396. Yoshinaga K, Burwash IG, Leech JA, Haddad H, Johnson CB, Garrard L, Chen L, Williams K, DaSilva JN, Beanlands RSB. The effects of continuous positive airway pressure on myocardial energetics in patients with heart failure and obstructive sleep apnea. *J Am Coll Cardiol*. 2007;49:450–458.

397. Klein R, Renaud JM, Ziadi MC, Thorn SL, Adler A, Beanlands RS. Intra-and inter-operator repeatability of myocardial blood flow and myocardial flow reserve measurements using rubidium-82 pet and a highly automated analysis program. *J Nucl Cardiol*. 2010;17:600–616.

398. Sander CY, Mandeville JB, Wey H-Y, Catana C, Hooker JM, Rosen BR. Effects of flow changes on radiotracer binding: Simultaneous measurement of neuroreceptor binding and cerebral blood flow modulation. *J Cereb Blood Flow Metab*. 2019;39:131–146.

399. Logan J, Volkow ND, Fowler JS, Wang G-J, Dewey SL, MacGregor R, Schlyer D, Gatley SJ, Pappas N, King P. Effects of blood flow on [11C] raclopride binding in the brain: model simulations and kinetic analysis of PET data. *J Cereb Blood Flow Metab*. 1994;14:995–1010.

400. Holthoff VA, Koeppe RA, Frey KA, Paradise AH, Kuhl DE. Differentiation of radioligand delivery and binding in the brain: validation of a two-compartment model for [11C] flumazenil. *J Cereb Blood Flow Metab*. 1991;11:745–752.

401. Lang RM, Badano LP, Mor-Avi V, Afilalo J, Armstrong A, Ernande L, Flachskampf FA, Foster E, Goldstein SA, Kuznetsova T. Recommendations for cardiac chamber quantification by echocardiography in adults: an update from the American Society of Echocardiography and the European Association of Cardiovascular Imaging. *J Am Soc Echocardiogr*. 2015;28:1–39.

402. Burwash IG, Forbes AD, Sadahiro M, Verrier ED, Pearlman AS, Thomas R, Kraft C, Otto CM. Echocardiographic volume flow and stenosis severity measures with changing flow rate in aortic stenosis. *Am J Physiol-Heart Circ Physiol*. 1993;265:H1734–H1743.

403. Shrout PE, Fleiss JL. Intraclass correlations: uses in assessing rater reliability. *Psychol Bull*. 1979;86:420.

404. Koo TK, Li MY. A guideline of selecting and reporting intraclass correlation coefficients for reliability research. *J Chiropr Med*. 2016;15:155–163.

405. Klein R, Ocneanu A, Renaud JM, Ziadi MC, Beanlands RSB. Consistent tracer administration profile improves test–retest repeatability of myocardial blood flow quantification with 82 Rb dynamic PET imaging. *J Nucl Cardiol*. 2016;1–13.

406. Bland JM, Altman DG. Statistical methods for assessing agreement between two methods of clinical measurement. *Int J Nurs Stud*. 2010;47:931–936.

407. Nordstokke DW, Zumbo BD. A new nonparametric Levene test for equal variances. *Psicológica*. 2010;31.

408. Bateman TM, Ananthasubramaniam K, Berman DS, Gerson M, Gropler R, Henzlova M, Mendoza F, Miyamoto M, Shah M, Weiland F. Reliability of the 123I-mIBG heart/mediastinum ratio: Results of a multicenter test–retest reproducibility study. *J Nucl Cardiol*. 2018;

409. van den Hoff J, Burchert W, Börner A-R, Fricke H, Kühnel G, Meyer GJ, Otto D, Weckesser E, Wolpers H-G, Knapp WH. [1-11C] Acetate as a quantitative perfusion tracer in myocardial PET. *J Nucl Med*. 2001;42:1174–1182.

410. Schäfers M, Dutka D, Rhodes CG, Lammertsma AA, Hermansen F, Schober O, Camici PG. Myocardial presynaptic and postsynaptic autonomic dysfunction in hypertrophic cardiomyopathy. *Circ Res*. 1998;82:57–62.

411. Thackeray JT, Beanlands RS, DaSilva JN. Insulin restores myocardial presynaptic sympathetic neuronal integrity in insulin-resistant diabetic rats. *J Nucl Cardiol*. 2013;20:845–856.

412. Thackeray JT, Radziuk J, Harper M-E, Suuronen EJ, Ascah KJ, Beanlands RS, DaSilva JN. Sympathetic nervous dysregulation in the absence of systolic left ventricular dysfunction in a rat model of insulin resistance with hyperglycemia. *Cardiovasc Diabetol*. 2011;10:75.

413. Hutchins GD, Caraher JM, Raylman RR. A region of interest strategy for minimizing resolution distortions in quantitative myocardial PET studies. *J Nucl Med*. 1992;33:1243–50.

414. Sasano T, Abraham MR, Chang KC, Ashikaga H, Mills KJ, Holt DP, Hilton J, Nekolla SG, Dong J, Lardo AC, Halperin H, Dannals RF, Marbán E, Bengel FM. Abnormal Sympathetic Innervation of Viable Myocardium and the Substrate of Ventricular Tachycardia After Myocardial Infarction. *J Am Coll Cardiol*. 2008;51:2266–2275.

415. Fallavollita JA, Dare JD, Carter RL, Baldwa S, Canty JM. Denervated Myocardium Is Preferentially Associated With Sudden Cardiac Arrest in Ischemic Cardiomyopathy. *Circ Cardiovasc Imaging*. 2017;10:e006446.

416. Aikawa T, Naya M, Obara M, Oyama-Manabe N, Manabe O, Magota K, Ito YM, Katoh C, Tamaki N. Regional interaction between myocardial sympathetic denervation,

contractile dysfunction, and fibrosis in heart failure with preserved ejection fraction: 11C-hydroxyephedrine PET study. *Eur J Nucl Med Mol Imaging*. 2017;44:1897–1905.

417. Zelt JGE, Mielniczuk LM, Orlandi C, Robinson S, Hadizad T, Walter O, Garrard L, Beanlands RSB, DeKemp RA. PET imaging of sympathetic innervation with [18F]Flurobenguan vs [11C]mHED in a patient with ischemic cardiomyopathy. *J Nucl Cardiol*. 2018;1–3.

418. Zelt J, Renaud J, Mielniczuk L, Garrard L, Orlandi C, Beanlands R, DeKemp R. Tracer Kinetics of Fluorine-18 LMI1195 Compared to Carbon-11 Hydroxyephedrine for PET Imaging of Sympathetic Innervation. *Can J Cardiol*. 2018;34:S117–S118.

419. Renkin EM. Transport of potassium-42 from blood to tissue in isolated mammalian skeletal muscles. *Am J Physiol-Leg Content*. 1959;197:1205–1210.

420. Crone C. The permeability of capillaries in various organs as determined by use of the 'indicator diffusion'method. *Acta Physiol*. 1963;58:292–305.

421. Hiroshima Y, Naya M, Aikawa T, Obara M, Yoshinaga K, Tomiyama Y, Magota K, Tamaki N, Katoh C. Quantification of Myocardial blood flow with 11C-hydroxyephedrine Dynamic PET: comparison with 15O-H2O PET. *J Nucl Med*. 2016;57:2703.

422. Katoh C, Yoshinaga K, Klein R, Kasai K, Tomiyama Y, Manabe O, Naya M, Sakakibara M, Tsutsui H, Tamaki N. Quantification of regional myocardial blood flow estimation with three-dimensional dynamic rubidium-82 PET and modified spillover correction model. *J Nucl Cardiol*. 2012;19:763–774.

423. Gheorghiade M, Sopko G, De Luca L, Velazquez EJ, Parker JD, Binkley PF, Sadowski Z, Golba KS, Prior DL, Rouleau JL, Bonow RO. Navigating the crossroads of coronary artery disease and heart failure. *Circulation*. 2006;114:1202–1213.

424. Rouleau JL, Bonow RO. An Approach to the Rational Use of Revascularization in Heart Failure Patients. *Can J Cardiol*. 2014;30:281–287.

425. Mielniczuk LM, Beanlands RS. Does imaging-guided selection of patients with ischemic heart failure for high risk revascularization improve identification of those with the highest clinical benefit?: Imaging-guided selection of patients with ischemic heart failure for high-risk revascularization improves identification of those with the highest clinical benefit. *Circ Cardiovasc Imaging*. 2012;5:262–270; discussion 270.

426. Velazquez EJ, Lee KL, Jones RH, Al-Khalidi HR, Hill JA, Panza JA, Michler RE, Bonow RO, Doenst T, Petrie MC, Oh JK, She L, Moore VL, Desvigne-Nickens P, Sopko G, Rouleau JL, STICHES Investigators. Coronary-Artery Bypass Surgery in Patients with Ischemic Cardiomyopathy. *N Engl J Med*. 2016;374:1511–1520.

427. Abraham A, Nichol G, Williams KA, Guo A, deKemp RA, Garrard L, Davies RA, Duchesne L, Haddad H, Chow B, DaSilva J, Beanlands RSB, PARR 2 Investigators. 18F-FDG PET imaging of myocardial viability in an experienced center with access to 18F-FDG and integration with clinical management teams: the Ottawa-FIVE substudy of the PARR 2 trial. *J Nucl Med Off Publ Soc Nucl Med*. 2010;51:567–574.

428. Schinkel AFL, Bax JJ, Poldermans D, Elhendy A, Ferrari R, Rahimtoola SH. Hibernating myocardium: diagnosis and patient outcomes. *Curr Probl Cardiol*. 2007;32:375–410.

429. Ling LF, Marwick TH, Flores DR, Jaber WA, Brunken RC, Cerqueira MD, Hachamovitch R. Identification of therapeutic benefit from revascularization in patients with left ventricular systolic dysfunction: inducible ischemia versus hibernating myocardium. *Circ Cardiovasc Imaging*. 2013;6:363–372.

430. Beanlands RSB, Nichol G, Huszti E, Humen D, Racine N, Freeman M, Gulenchyn KY, Garrard L, deKemp R, Guo A, Ruddy TD, Benard F, Lamy A, Iwanochko RM, PARR-2 Investigators. F-18-fluorodeoxyglucose positron emission tomography imaging-assisted management of patients with severe left ventricular dysfunction and suspected coronary disease: a randomized, controlled trial (PARR-2). *J Am Coll Cardiol*. 2007;50:2002–2012.

431. D'Egidio G, Nichol G, Williams KA, Guo A, Garrard L, deKemp R, Ruddy TD, DaSilva J, Humen D, Gulenchyn KY, Freeman M, Racine N, Benard F, Hendry P, Beanlands RSB, PARR-2 Investigators. Increasing benefit from revascularization is associated with increasing amounts of myocardial hibernation: a substudy of the PARR-2 trial. *JACC Cardiovasc Imaging*. 2009;2:1060–1068.

432. Mc Ardle B, Shukla T, Nichol G, deKemp RA, Bernick J, Guo A, Lim SP, Davies RA, Haddad H, Duchesne L, Hendry P, Masters R, Ross H, Freeman M, Gulenchyn K, Racine N, Humen D, Benard F, Ruddy TD, Chow BJ, Mielniczuk L, DaSilva JN, Garrard L, Wells GA, Beanlands RSB, PARR-2 Investigators. Long-Term Follow-Up of Outcomes With F-18-Fluorodeoxyglucose Positron Emission Tomography Imaging-Assisted Management of Patients With Severe Left Ventricular Dysfunction Secondary to Coronary Disease. *Circ Cardiovasc Imaging*. 2016;9.

433. Hachamovitch R, Rozanski A, Shaw LJ, Stone GW, Thomson LEJ, Friedman JD, Hayes SW, Cohen I, Germano G, Berman DS. Impact of ischaemia and scar on the therapeutic benefit derived from myocardial revascularization vs. medical therapy among patients undergoing stress-rest myocardial perfusion scintigraphy. *Eur Heart J*. 2011;32:1012–1024.

434. Gerber BL, Rousseau MF, Ahn SA, le Polain de Waroux J-B, Pouleur A-C, Phlips T, Vancraeynest D, Pasquet A, Vanoverschelde J-LJ. Prognostic value of myocardial viability by delayed-enhanced magnetic resonance in patients with coronary artery disease and low ejection fraction: impact of revascularization therapy. *J Am Coll Cardiol*. 2012;59:825–835.

435. Pagano D, Bonser RS, Townend JN, Ordoubadi F, Lorenzoni R, Camici PG. Predictive value of dobutamine echocardiography and positron emission tomography in identifying hibernating myocardium in patients with postischaemic heart failure. *Heart Br Card Soc*. 1998;79:281–288.

436. Di Carli MF, Davidson M, Little R, Khanna S, Mody FV, Brunken RC, Czernin J, Rokhsar S, Stevenson LW, Laks H. Value of metabolic imaging with positron emission tomography for evaluating prognosis in patients with coronary artery disease and left ventricular dysfunction. *Am J Cardiol*. 1994;73:527–533.

437. Allman KC, Shaw LJ, Hachamovitch R, Udelson JE. Myocardial viability testing and impact of revascularization on prognosis in patients with coronary artery disease and left ventricular dysfunction: a meta-analysis. *J Am Coll Cardiol*. 2002;39:1151–1158.

438. Bonow RO, Maurer G, Lee KL, Holly TA, Binkley PF, Desvigne-Nickens P, Drozdz J, Farsky PS, Feldman AM, Doenst T, Michler RE, Berman DS, Nicolau JC, Pellikka PA, Wrobel K, Alotti N, Asch FM, Favaloro LE, She L, Velazquez EJ, Jones RH, Panza JA, STICH Trial Investigators. Myocardial viability and survival in ischemic left ventricular dysfunction. *N Engl J Med*. 2011;364:1617–1625.

439. Panza JA, Holly TA, Asch FM, She L, Pellikka PA, Velazquez EJ, Lee KL, Borges-Neto S, Farsky PS, Jones RH, Berman DS, Bonow RO. Inducible myocardial ischemia and outcomes in patients with coronary artery disease and left ventricular dysfunction. *J Am Coll Cardiol*. 2013;61:1860–1870.

440. WRITING COMMITTEE MEMBERS, Yancy CW, Jessup M, Bozkurt B, Butler J, Casey DE, Drazner MH, Fonarow GC, Geraci SA, Horwich T, Januzzi JL, Johnson MR, Kasper EK, Levy WC, Masoudi FA, McBride PE, McMurray JJV, Mitchell JE, Peterson PN, Riegel B, Sam F, Stevenson LW, Tang WHW, Tsai EJ, Wilkoff BL, American College of Cardiology Foundation/American Heart Association Task Force on Practice Guidelines. 2013 ACCF/AHA guideline for the management of heart failure: a report of the American College of Cardiology Foundation/American Heart Association Task Force on practice guidelines. *Circulation*. 2013;128:e240-327.

441. Moe GW, Ezekowitz JA, O'Meara E, Lepage S, Howlett JG, Fremes S, Al-Hesayen A, Heckman GA, Abrams H, Ducharme A, Estrella-Holder E, Grzeslo A, Harkness K, Koshman SL, McDonald M, McKelvie R, Rajda M, Rao V, Swiggum E, Virani S, Zieroth S, Arnold JMO, Ashton T, D'Astous M, Chan M, De S, Dorian P, Giannetti N, Haddad H, Isaac DL, Kouz S, Leblanc M-H, Liu P, Ross HJ, Sussex B, White M, Canadian Cardiovascular Society. The 2014 Canadian Cardiovascular Society Heart Failure Management Guidelines Focus Update: anemia, biomarkers, and recent therapeutic trial implications. *Can J Cardiol*. 2015;31:3–16.

442. de Boer RA, Daniels LB, Maisel AS, Januzzi JL. State of the Art: Newer biomarkers in heart failure. *Eur J Heart Fail*. 2015;17:559–569.

443. Beaudoin J, Singh JP, Szymonifka J, Zhou Q, Levine RA, Januzzi JL, Truong QA. Novel Heart Failure Biomarkers Predict Improvement of Mitral Regurgitation in Patients Receiving Cardiac Resynchronization Therapy-The BIOCRT Study. *Can J Cardiol*. 2016;32:1478–1484.

444. Vitale GD, deKemp RA, Ruddy TD, Williams K, Beanlands RS. Myocardial glucose utilization and optimization of (18)F-FDG PET imaging in patients with non-insulin-dependent diabetes mellitus, coronary artery disease, and left ventricular dysfunction. *J Nucl Med Off Publ Soc Nucl Med*. 2001;42:1730–1736.

445. Klein R, Renaud JM, Ziadi MC, Thorn SL, Adler A, Beanlands RS, deKemp RA. Intra- and inter-operator repeatability of myocardial blood flow and myocardial flow reserve measurements using rubidium-82 pet and a highly automated analysis program. *J Nucl Cardiol Off Publ Am Soc Nucl Cardiol*. 2010;17:600–616.

446. Sanchis J, García-Blas S, Carratalá A, Valero E, Mollar A, Miñana G, Ruiz V, Balaguer JV, Roqué M, Bosch X, Núñez J. Clinical Evaluation Versus Undetectable High-Sensitivity Troponin for Assessment of Patients With Acute Chest Pain. *Am J Cardiol*. 2016;118:1631–1635.

447. Xu R-Y, Zhu X-F, Yang Y, Ye P. High-sensitive cardiac troponin T. *J Geriatr Cardiol JGC*. 2013;10:102–109.

448. Thygesen K, Alpert JS, Jaffe AS, Simoons ML, Chaitman BR, White HD, Joint ESC/ACCF/AHA/WHF Task Force for Universal Definition of Myocardial Infarction, Authors/Task Force Members Chairpersons, Thygesen K, Alpert JS, White HD, Biomarker Subcommittee, Jaffe AS, Katus HA, Apple FS, Lindahl B, Morrow DA, ECG Subcommittee, Chaitman BR, Clemmensen PM, Johanson P, Hod H, Imaging Subcommittee, Underwood R, Bax JJ, Bonow JJ, Pinto F, Gibbons RJ, Classification Subcommittee, Fox KA, Atar D, Newby LK, Galvani M, Hamm CW, Intervention Subcommittee, Uretsky BF, Steg PG, Wijns W, Bassand J-P, Menasche P, Ravkilde J, Trials & Registries Subcommittee, Ohman EM, Antman EM, Wallentin LC, Armstrong PW, Simoons ML, Trials & Registries Subcommittee, Januzzi JL, Nieminen MS, Gheorghiade M, Filippatos G, Trials & Registries Subcommittee, Luepker RV, Fortmann SP, Rosamond WD, Levy D, Wood D, Trials & Registries Subcommittee, Smith SC, Hu D, Lopez-Sendon J-L, Robertson RM, Weaver D, Tendera M, Bove AA, Parkhomenko AN, Vasilieva EJ, Mendis S, ESC Committee for Practice Guidelines (CPG), Bax JJ, Baumgartner H, Ceconi C, Dean V, Deaton C, Fagard R, Funck-Brentano C, Hasdai D, Hoes A, Kirchhof P, Knuuti J, Kolh P, McDonagh T, Moulin C, Popescu BA, Reiner Z, Sechtem U, Sirnes PA, Tendera M, Torbicki A, Vahanian A, Windecker S, Document Reviewers, Morais J, Aguiar C, Almahmeed W, Arnar DO, Barili F, et al. Third universal definition of myocardial infarction. *J Am Coll Cardiol*. 2012;60:1581–1598.

449. Januzzi JL, van Kimmenade R, Lainchbury J, Bayes-Genis A, Ordonez-Llanos J, Santalo-Bel M, Pinto YM, Richards M. NT-proBNP testing for diagnosis and short-term

prognosis in acute destabilized heart failure: an international pooled analysis of 1256 patients: the International Collaborative of NT-proBNP Study. *Eur Heart J*. 2006;27:330–337.

450. Ibrahim N, Januzzi JL. The potential role of natriuretic peptides and other biomarkers in heart failure diagnosis, prognosis and management. *Expert Rev Cardiovasc Ther*. 2015;13:1017–1030.

451. Gore MO, Seliger SL, Defilippi CR, Nambi V, Christenson RH, Hashim IA, Hoogeveen RC, Ayers CR, Sun W, McGuire DK, Ballantyne CM, de Lemos JA. Age- and sex-dependent upper reference limits for the high-sensitivity cardiac troponin T assay. *J Am Coll Cardiol*. 2014;63:1441–1448.

452. Redfield MM, Rodeheffer RJ, Jacobsen SJ, Mahoney DW, Bailey KR, Burnett JC. Plasma brain natriuretic peptide concentration: impact of age and gender. *J Am Coll Cardiol*. 2002;40:976–982.

453. Wang AY-M, Lai K-N. Use of cardiac biomarkers in end-stage renal disease. *J Am Soc Nephrol JASN*. 2008;19:1643–1652.

454. Wiley CL, Switzer SP, Berg RL, Glurich I, Dart RA. Association of B-type natriuretic Peptide levels with estimated glomerular filtration rate and congestive heart failure. *Clin Med Res*. 2010;8:7–12.

455. Braunwald E. Biomarkers in heart failure. *N Engl J Med*. 2008;358:2148–2159.

456. Jernberg T, Lindahl B, Siegbahn A, Andren B, Frostfeldt G, Lagerqvist B, Stridsberg M, Venge P, Wallentin L. N-terminal pro-brain natriuretic peptide in relation to inflammation, myocardial necrosis, and the effect of an invasive strategy in unstable coronary artery disease. *J Am Coll Cardiol*. 2003;42:1909–1916.

457. Omland T, Aakvaag A, Bonarjee VV, Caidahl K, Lie RT, Nilsen DW, Sundsfjord JA, Dickstein K. Plasma brain natriuretic peptide as an indicator of left ventricular systolic function and long-term survival after acute myocardial infarction. Comparison with plasma atrial natriuretic peptide and N-terminal proatrial natriuretic peptide. *Circulation*. 1996;93:1963–1969.

458. Nelson CA, Case C, McCrohon J, Marwick TH. Relationship of extent and nature of dysfunctional myocardium to brain natriuretic peptide in patients with ischemic left ventricular dysfunction. *Int J Cardiovasc Imaging*. 2005;21:295–300; discussion 301-302.

459. Aktas MK, Allen D, Jaber WA, Chuang H-H, Taylor DO, Yamani MH. Relation of brain natriuretic peptide level to extent of left ventricular scarring in patients with chronic heart failure secondary to ischemic cardiomyopathy. *Am J Cardiol*. 2009;103:243–245.

460. Nordenskjöld AM, Hammar P, Ahlström H, Bjerner T, Duvernoy O, Eggers KM, Fröbert O, Hadziosmanovic N, Lindahl B. Unrecognized myocardial infarctions detected by cardiac magnetic resonance imaging are associated with cardiac troponin I levels. *Clin Chim Acta Int J Clin Chem*. 2016;455:189–194.

461. Themudo RE, Lindahl B, Johansson L, Venge P, Ahlström H, Ebeling Barbier C, Eggers KM, Lind L, Bjerner T. Unrecognized myocardial scars detected by delayed-enhanced MRI are associated with increased levels of NT-proBNP. *Coron Artery Dis*. 2011;22:158–164.

462. Wu AH. Increased troponin in patients with sepsis and septic shock: myocardial necrosis or reversible myocardial depression? *Intensive Care Med*. 2001;27:959–961.

463. Narula J, Pandey P, Arbustini E, Haider N, Narula N, Kolodgie FD, Dal Bello B, Semigran MJ, Bielsa-Masdeu A, Dec GW, Israels S, Ballester M, Virmani R, Saxena S, Kharbanda S. Apoptosis in heart failure: release of cytochrome c from mitochondria and activation of caspase-3 in human cardiomyopathy. *Proc Natl Acad Sci U S A*. 1999;96:8144–8149.

464. Jhund PS, Claggett BL, Voors AA, Zile MR, Packer M, Pieske BM, Kraigher-Krainer E, Shah AM, Prescott MF, Shi V, Lefkowitz M, McMurray JJV, Solomon SD, PARAMOUNT Investigators. Elevation in high-sensitivity troponin T in heart failure and preserved ejection fraction and influence of treatment with the angiotensin receptor neprilysin inhibitor LCZ696. *Circ Heart Fail*. 2014;7:953–959.

465. Gravning J, Askevold ET, Nymo SH, Ueland T, Wikstrand J, McMurray JJV, Aukrust P, Gullestad L, Kjekshus J, CORONA Study Group. Prognostic effect of high-sensitive troponin T assessment in elderly patients with chronic heart failure: results from the CORONA trial. *Circ Heart Fail*. 2014;7:96–103.

466. Latini R, Masson S, Anand IS, Missov E, Carlson M, Vago T, Angelici L, Barlera S, Parrinello G, Maggioni AP, Tognoni G, Cohn JN, Val-HeFT Investigators. Prognostic value of very low plasma concentrations of troponin T in patients with stable chronic heart failure. *Circulation*. 2007;116:1242–1249.

467. Goetze JP, Christoffersen C, Perko M, Arendrup H, Rehfeld JF, Kastrup J, Nielsen LB. Increased cardiac BNP expression associated with myocardial ischemia. *FASEB J Off Publ Fed Am Soc Exp Biol*. 2003;17:1105–1107.

468. May D, Gilon D, Djonov V, Itin A, Lazarus A, Gordon O, Rosenberger C, Keshet E. Transgenic system for conditional induction and rescue of chronic myocardial hibernation provides insights into genomic programs of hibernation. *Proc Natl Acad Sci U S A*. 2008;105:282–287.

469. Skhiri M, Hunt SA, Denault AY, Haddad F. [Evidence-based management of right heart failure: a systematic review of an empiric field]. *Rev Esp Cardiol*. 2010;63:451–471.

470. Gambardella I, Gaudino M, Ronco C, Lau C, Ivascu N, Girardi LN. Congestive kidney failure in cardiac surgery: the relationship between central venous pressure and acute kidney injury. *Interact Cardiovasc Thorac Surg*. 2016;23:800–805.

471. Costachescu T, Denault A, Guimond J-G, Couture P, Carignan S, Sheridan P, Hellou G, Blair L, Normandin L, Babin D, Allard M, Harel F, Buithieu J. The hemodynamically unstable patient in the intensive care unit: hemodynamic vs. transesophageal echocardiographic monitoring. *Crit Care Med*. 2002;30:1214–1223.

472. Denault AY, Haddad F, Jacobsohn E, Deschamps A. Perioperative right ventricular dysfunction. *Curr Opin Anaesthesiol*. 2013;26:71–81.

473. Maslow AD, Regan MM, Panzica P, Heindel S, Mashikian J, Comunale ME. Precardiopulmonary bypass right ventricular function is associated with poor outcome after coronary artery bypass grafting in patients with severe left ventricular systolic dysfunction. *Anesth Analg*. 2002;95:1507–1518, table of contents.

474. Haddad F, Denault AY, Couture P, Cartier R, Pellerin M, Levesque S, Lambert J, Tardif J-C. Right ventricular myocardial performance index predicts perioperative mortality or circulatory failure in high-risk valvular surgery. *J Am Soc Echocardiogr Off Publ Am Soc Echocardiogr*. 2007;20:1065–1072.

475. Thiele RH, Isbell JM, Rosner MH. AKI associated with cardiac surgery. *Clin J Am Soc Nephrol CJASN*. 2015;10:500–514.

476. Karkouti K, Wijeysundera DN, Yau TM, Callum JL, Cheng DC, Crowther M, Dupuis J-Y, Fremes SE, Kent B, Laflamme C, Lamy A, Legare J-F, Mazer CD, McCluskey SA, Rubens FD, Sawchuk C, Beattie WS. Acute kidney injury after cardiac surgery: focus on modifiable risk factors. *Circulation*. 2009;119:495–502.

477. Thomson R, Meeran H, Valencia O, Al-Subaie N. Goal-directed therapy after cardiac surgery and the incidence of acute kidney injury. *J Crit Care*. 2014;29:997–1000.

478. Pearse R, Dawson D, Fawcett J, Rhodes A, Grounds RM, Bennett ED. Early goal-directed therapy after major surgery reduces complications and duration of hospital stay. A randomised, controlled trial [ISRCTN38797445]. *Crit Care Lond Engl*. 2005;9:R687-693.

479. Waikar SS, Bonventre JV. Creatinine kinetics and the definition of acute kidney injury. *J Am Soc Nephrol JASN*. 2009;20:672–679.

480. Shiao C-C, Wu V-C, Li W-Y, Lin Y-F, Hu F-C, Young G-H, Kuo C-C, Kao T-W, Huang D-M, Chen Y-M, Tsai P-R, Lin S-L, Chou N-K, Lin T-H, Yeh Y-C, Wang C-H, Chou A, Ko W-J, Wu K-D, National Taiwan University Surgical Intensive Care Unit-Associated Renal Failure Study Group. Late initiation of renal replacement therapy is associated with worse outcomes in acute kidney injury after major abdominal surgery. *Crit Care Lond Engl*. 2009;13:R171.

481. Devarajan P. Neutrophil gelatinase-associated lipocalin: a promising biomarker for human acute kidney injury. *Biomark Med*. 2010;4:265–280.

482. Aronson D, Abassi Z, Allon E, Burger AJ. Fluid loss, venous congestion, and worsening renal function in acute decompensated heart failure. *Eur J Heart Fail*. 2013;15:637–643.

483. Marik PE, Baram M, Vahid B. Does central venous pressure predict fluid responsiveness? A systematic review of the literature and the tale of seven mares. *Chest*. 2008;134:172–178.

484. Bulluck H, Maiti R, Chakraborty B, Candilio L, Clayton T, Evans R, Jenkins DP, Kolvekar S, Kunst G, Laing C, Nicholas J, Pepper J, Yellon DM, Hausenloy DJ. Neutrophil gelatinase-associated lipocalin prior to cardiac surgery predicts acute kidney injury and mortality. *Heart Br Card Soc*. 2017;

485. Daniels LB, Barrett-Connor E, Clopton P, Laughlin GA, Ix JH, Maisel AS. Plasma neutrophil gelatinase-associated lipocalin is independently associated with cardiovascular disease and mortality in community-dwelling older adults: The Rancho Bernardo Study. *J Am Coll Cardiol*. 2012;59:1101–1109.

486. Lindberg S, Pedersen SH, Mogelvang R, Jensen JS, Flyvbjerg A, Galatius S, Magnusson NE. Prognostic utility of neutrophil gelatinase-associated lipocalin in predicting mortality and cardiovascular events in patients with ST-segment elevation myocardial infarction treated with primary percutaneous coronary intervention. *J Am Coll Cardiol*. 2012;60:339–345.

487. Patel UD, Garg AX, Krumholz HM, Shlipak MG, Coca SG, Sint K, Thiessen-Philbrook H, Koyner JL, Swaminathan M, Passik CS, Parikh CR, Translational Research Investigating Biomarker Endpoints in Acute Kidney Injury (TRIBE-AKI) Consortium. Preoperative serum brain natriuretic peptide and risk of acute kidney injury after cardiac surgery. *Circulation*. 2012;125:1347–1355.

488. Song D, de Zoysa JR, Ng A, Chiu W. Troponins in acute kidney injury. *Ren Fail*. 2012;34:35–39.

489. Blyth KG, Groenning BA, Mark PB, Martin TN, Foster JE, Steedman T, Morton JJ, Dargie HJ, Peacock AJ. NT-proBNP can be used to detect right ventricular systolic dysfunction in pulmonary hypertension. *Eur Respir J*. 2007;29:737–744.

490. Nagaya N, Nishikimi T, Okano Y, Uematsu M, Satoh T, Kyotani S, Kuribayashi S, Hamada S, Kakishita M, Nakanishi N, Takamiya M, Kunieda T, Matsuo H, Kangawa K. Plasma brain natriuretic peptide levels increase in proportion to the extent of right ventricular dysfunction in pulmonary hypertension. *J Am Coll Cardiol*. 1998;31:202–208.

491. Ricci Z, Cruz DN, Ronco C. Classification and staging of acute kidney injury: beyond the RIFLE and AKIN criteria. *Nat Rev Nephrol*. 2011;7:201–208.

492. Holman WL. Interagency Registry for Mechanically Assisted Circulatory Support (INTERMACS): what have we learned and what will we learn? *Circulation*. 2012;126:1401–1406.

493. Denault AY, Bussières JS, Arellano R, Finegan B, Gavra P, Haddad F, Nguyen AQN, Varin F, Fortier A, Levesque S, Shi Y, Elmi-Sarabi M, Tardif J-C, Perrault LP, Lambert J. A multicentre randomized-controlled trial of inhaled milrinone in high-risk cardiac surgical patients. *Can J Anaesth J Can Anesth*. 2016;63:1140–1153.

494. Rudski LG, Lai WW, Afilalo J, Hua L, Handschumacher MD, Chandrasekaran K, Solomon SD, Louie EK, Schiller NB. Guidelines for the echocardiographic assessment of the right heart in adults: a report from the American Society of Echocardiography endorsed by the European Association of Echocardiography, a registered branch of the European Society of Cardiology, and the Canadian Society of Echocardiography. *J Am Soc Echocardiogr Off Publ Am Soc Echocardiogr*. 2010;23:685–713; quiz 786–788.

495. Giannitsis E, Kurz K, Hallermayer K, Jarausch J, Jaffe AS, Katus HA. Analytical validation of a high-sensitivity cardiac troponin T assay. *Clin Chem*. 2010;56:254–261.

496. Bolignano D, Lacquaniti A, Coppolino G, Donato V, Campo S, Fazio MR, Nicocia G, Buemi M. Neutrophil gelatinase-associated lipocalin (NGAL) and progression of chronic kidney disease. *Clin J Am Soc Nephrol CJASN*. 2009;4:337–344.

497. Omar AS, Mahmoud K, Hanoura S, Osman H, Sivadasan P, Sudarsanan S, Shouman Y, Singh R, AlKhulaifi A. Acute kidney injury induces high-sensitivity troponin measurement changes after cardiac surgery. *BMC Anesthesiol* [Internet]. 2017 [cited 2018 Feb 25];17. Available from: http://bmcanesthesiol.biomedcentral.com/articles/10.1186/s12871-017-0307-5

498. Bucholz EM, Whitlock RP, Zappitelli M, Devarajan P, Eikelboom J, Garg AX, Philbrook HT, Devereaux PJ, Krawczeski CD, Kavsak P, Shortt C, Parikh CR, TRIBE-AKI Consortium. Cardiac biomarkers and acute kidney injury after cardiac surgery. *Pediatrics*. 2015;135:e945-956.

499. Elíasdóttir SB, Klemenzson G, Torfason B, Valsson F. Brain natriuretic peptide is a good predictor for outcome in cardiac surgery. *Acta Anaesthesiol Scand*. 2008;52:182–187.

500. Schrier RW, Bansal S. Pulmonary hypertension, right ventricular failure, and kidney: different from left ventricular failure? *Clin J Am Soc Nephrol CJASN*. 2008;3:1232–1237.

501. Firth JD, Raine AE, Ledingham JG. Raised venous pressure: a direct cause of renal sodium retention in oedema? *Lancet Lond Engl*. 1988;1:1033–1035.

502. Gambardella I, Gaudino M, Ronco C, Lau C, Ivascu N, Girardi LN. Congestive kidney failure in cardiac surgery: the relationship between central venous pressure and acute kidney injury. *Interact Cardiovasc Thorac Surg*. 2016;23:800–805.

503. Liang KV, Williams AW, Greene EL, Redfield MM. Acute decompensated heart failure and the cardiorenal syndrome. *Crit Care Med*. 2008;36:S75-88.

504. Liu PP. Cardiorenal syndrome in heart failure: a cardiologist's perspective. *Can J Cardiol*. 2008;24 Suppl B:25B–9B.

505. Daquarti G, March Vecchio N, Mitrione CS, Furmento J, Ametrano MC, Dominguez Pace MP, Costabel JP. High-sensitivity troponin and right ventricular function in acute pulmonary embolism. *Am J Emerg Med*. 2016;34:1579–1582.

506. Allen BS, Winkelmann JW, Hanafy H, Hartz RS, Bolling KS, Ham J, Feinstein S. Retrograde cardioplegia does not adequately perfuse the right ventricle. *J Thorac Cardiovasc Surg*. 1995;109:1116–1124; discussion 1124-1126.

507. Kevin LG, Barnard M. Right ventricular failure. *Contin Educ Anaesth Crit Care Pain*. 2007;7:89–94.

508. Aissaoui N, Salem J-E, Paluszkiewicz L, Morshuis M, Guerot E, Gorria GM, Fagon J-Y, Gummert J, Diebold B. Assessment of right ventricular dysfunction predictors before the implantation of a left ventricular assist device in end-stage heart failure patients using echocardiographic measures (ARVADE): Combination of left and right ventricular echocardiographic variables. *Arch Cardiovasc Dis*. 2015;108:300–309.

509. Matthews JC, Koelling TM, Pagani FD, Aaronson KD. The right ventricular failure risk score a pre-operative tool for assessing the risk of right ventricular failure in left ventricular assist device candidates. *J Am Coll Cardiol*. 2008;51:2163–2172.

510. Brynildsen J, Petäjä L, Pettilä V, Nygård S, Vaara ST, Linko R, Okkonen M, Hagve T-A, Soininen L, Suojaranta-Ylinen R, Lyngbakken MN, Omland T, Røsjø H. The predictive value of NT-proBNP and hs-TnT for risk of death in cardiac surgical patients. *Clin Biochem*. 2018;

511. Cuthbertson BH, Croal BL, Rae D, Gibson PH, McNeilly JD, Jeffrey RR, Smith WC, Prescott GJ, Buchan KG, El-Shafei H, Gibson GA, Hillis GS. N-terminal pro-B-type natriuretic peptide levels and early outcome after cardiac surgery: a prospective cohort study. *Br J Anaesth*. 2009;103:647–653.

512. Domanski MJ, Mahaffey K, Hasselblad V, Brener SJ, Smith PK, Hillis G, Engoren M, Alexander JH, Levy JH, Chaitman BR, Broderick S, Mack MJ, Pieper KS, Farkouh ME.

Association of myocardial enzyme elevation and survival following coronary artery bypass graft surgery. *JAMA*. 2011;305:585–591.

513. Mohammed AA, Agnihotri AK, van Kimmenade RRJ, Martinez-Rumayor A, Green SM, Quiroz R, Januzzi JL. Prospective, comprehensive assessment of cardiac troponin T testing after coronary artery bypass graft surgery. *Circulation*. 2009;120:843–850.

514. Wilke P, Masuch A, Fahron O, Zylla S, Leipold T, Petersmann A. Diagnostic performance of point-of-care and central laboratory cardiac troponin assays in an emergency department. *PloS One*. 2017;12:e0188706.

515. Fellner S, Hentze S, Kempin U, Richter E, Rocktäschel J, Langer B. Analytical evaluation of a BNP assay on the new point-of-care platform respons®IQ. *Pract Lab Med*. 2015;2:15–21.